DEVELOPMENT OF DESIGN GUIDELINES

FOR SOIL EMBEDDED POST SYSTEMS

USING WIDE-FLANGE I-BEAMS TO CONTAIN TRUCK IMPACT

A Dissertation

by

SEOK GYU LIM

Submitted to the Office of Graduate Studies of
Texas A&M University
in partial fulfillment of the requirements for the degree of

DOCTOR OF PHILOSOPHY

May 2011

Major Subject: Civil Engineering

Development of Design Guidelines

for Soil Embedded Post Systems

Using Wide-Flange I-Beams to Contain Truck Impact

DEVELOPMENT OF DESIGN GUIDELINES

FOR SOIL EMBEDDED POST SYSTEMS

USING WIDE-FLANGE I-BEAMS TO CONTAIN TRUCK IMPACT

A Dissertation

by

SEOK GYU LIM

Submitted to the Office of Graduate Studies of
Texas A&M University
in partial fulfillment of the requirements for the degree of

DOCTOR OF PHILOSOPHY

Approved by:

Chair of Committee,	Jean-Louis Briaud
Committee Members,	Charles Aubeny
	Rashid Abu Al-Rub
	Mark Everett
	Akram Y Abu-Odeh
Head of Department,	John Niedzwecki

May 2011

Major Subject: Civil Engineering

ABSTRACT

Development of Design Guidelines for Soil Embedded Post Systems

Using Wide-Flange I-Beams to Contain Truck Impact. (May 2011)

Seok Gyu Lim, B.Eng.; M.Eng., Chung-Ang University

Chair of Advisory Committee: Dr. Jean-Louis Briaud

Anti ram perimeter barriers are part of the protection of important facilities such as power plants, air ports and embassies against unrestricted vehicle access. Many different systems can be used to achieve the containment goal. One of these systems makes use of soil embedded posts either single posts if the soil is hard enough, or groups of soil embedded posts tied together by beams if the soil is not hard enough for a single post to stop the in-coming truck. The design of these soil embedded posts needs to take account of a number of influencing factors, which include the soil strength and stiffness, the post strength and stiffness, the mass of the vehicle and its approach velocity.

This dissertation describes the work done to develop a set of design recommendations to select the embedment of a single post or group of posts. The post is a steel beam with an H shape cross section: W14X109 for the single post system and W14X90 for the group system with a double beam made of square hollow steel section HSS8X8X1/2. The spacing of the posts for the group includes 2.44 m, 4.88 m, and 7.32 m. The soil strength varies from loose sand and soft clay to very dense sand and very

hard clay. The vehicle has a mass of 6800 kg, and the velocities include 80 km/h, 65 km/h, and 50 km/h.

The design guidelines presented here are based on 10 medium scale pendulum impact tests, 2 medium scale bogie impact tests, 1 full scale impact test on a single post, 1 full scale impact test on a group of 8 side by side posts with a 5.2 m spacing and connected with two beams, approximately 150 4-D numerical simulations of full scale impact tests using LS-DYNA, as well as fundamental theoretical concepts.

DEDICATION

To my parents:

Byungwoo Lim and Kyoungsook Lee

My son and daughter:

Sunwoo Lim and Jiwoo Rachel Lim

And my wife:

Eunjoo Kim

ACKNOWLEDGEMENTS

First of all, I would like to thank my committee chair, Dr. Jean-Louis Briaud for his exceptional guidance and support throughout this study. My committee members, Dr. Charles Aubeny, Dr. Rashid K. Abu Al-Rub and Dr. Mark Everett deserve to thanks for their guidance. I want to extend my sincere thanks to my special appointment, Dr. Akram Abu-Odeh for his guidance and help in numerical simulation.

I would like to thank the United States Department of State, Bureau of Diplomatic Security, Physical Security Division and Sandia National Laboratories which sponsored the project and provided the support for my research studies. I also want to extend my gratitude to Dr. Dean Alberson, Dr. Roger Bligh, Mr. Gary Gerke, Mr. Dusty Arrington and other members at Texas Transportation Institute for their support and help in impact testing and in-situ soil testing.

I also want to extend my gratitude to my friends and colleagues and the department faculty and staff for making my time at Texas A&M University a great experience. Thanks go to Kangmi Kim, Jennifer Nicks, Ok-Youn Yu, Ozzy Bravo, Deeyvid Saez and Bradley Smith for their help in numerical simulation and soil testing. Thanks also go to Michelle Lee Bernhardt for her comprehensive proofreading of my dissertation.

Finally, thanks to my parents, parents-in-law and my brother for their unconditional support and love and to my wife, my son and my daughter for their patience, encouragement and love.

TABLE OF CONTENTS

LIST OF FIGURES

Page

Page

Page

LIST OF TABLES

Page

1. INTRODUCTION

1.1 Background

Lateral loads applied to a single post or group of posts systems can be classified in two categories: static load, and dynamic load. Lateral loads from vibrations, earthquake, and impact can be considered as dynamic lateral loads. A number of research projects have been performed on analyzing the behavior of piles under static lateral loads, vibration, and earthquake. For example, Brinch Hansen (1961), Broms (1964a; 1964b), Matlock and Reese (1960), Poulos (1971a; 1971b), and Briaud (1997) proposed design methods or analytical solutions for pile foundations under static lateral loads. Several methods to analyze response of pile under horizontal load and moment due to vibration and earthquake have been introduced by Tucker (1964), Novak (1974), Prakash and Chandrasekaran (1973) and others.

Dewey et al. (1983) and Eggers and Hirsch (1986) compared static and dynamic lateral resistances of single posts and Brown (2007) analyzed lateral dynamic interaction between pile and soil using Statnamic tests. However, the behavior of a post under lateral dynamic impact has not been studied as much. The piles of harbor structures, bridge piers, guardrails, and perimeter barriers are often subjected to lateral impact loads due to of ships or vehicles. Anti-ram vehicle barriers are the typical example of the single post or group of posts system under the lateral impact loads.

_____

This dissertation follows the style of the *Journal of Geotechnical and Geoenvironmental Engineering.*

In order to prevent unrestricted vehicle access to important facilities such as embassies, industrial facilities, power plants, airports, military bases, public venue, and governmental assets, anti-ram perimeter barriers are in use. These barriers protect employee and facilities from both the intended or unintended impact of vehicle traveling at a high speed including a vehicle with explosive or hazardous material. Many different systems can be used to achieve the containment goal. One of these systems makes use of soil embedded posts either single posts if the soil is hard enough or groups of soil embedded posts tied together by beams if the soil is not hard enough for a single post to stop the in-coming vehicle.

1.2 Problems

According to *Diplomatic security (DS) certified anti-ram vehicle barriers* (U.S. Department of State 2008), most of the anti-ram barrier systems are embedded in large continuous reinforced concrete footing. Anti-ram bollard and plinth wall needs to be fully embedded into a large concrete strip foundation with several feet deep to resist the impact of a vehicle (FEMA 2003). However, it is often difficult to install continuous reinforced concrete footing for perimeter barriers because of extensive underground utilities and limited space, especially in urban area. Federal Emergency Management Agency (FEMA) also stated that existing ground utilities and limit of property line may cause a problem on installing the foundation of barrier system. Thus a design method for security perimeter barrier founded on piles directly embedded in soil is needed to resolve the problems due to the continuous or massive concrete foundations. The design of these

soil embedded posts needs to take account a number of influencing factors which include the soil strength and stiffness, the post strength and stiffness, the mass of the truck and its approach velocity. Indeed single piles and a row of piles will minimize the space requirement.

1.3 Research objectives

The main goal of this study is to develop design guidelines for soil embedded post systems using wide-flange I-beam to contain truck impact. ASTM F2656-07, *Standard Test Methods for Vehicle Crash Testing of Perimeter Barrier* (2007) provides a range of test condition and penetration designations. The proposed design guideline was established to meet all criteria for M50/P1, M40/P1 and M30/P1 (test condition designation/ penetration designation). The single post or group of posts system directly embedded in sand or clay designed by the proposed design guideline is capable of arresting a 6,810 kg (15,000 lb) truck traveling at 80 km/h (50 mph), 65 km/h (40 mph) or 50km/h (30 mph) within 1.0 m (3.3 ft) of vehicle partial penetration.

In particular, the following objectives are addressed:

Objective 1: Develop soil strength categories for sand and clay

The soil strength classification system developed for sand and clay was used not only for numerical simulations performed to develop the design guidelines but will also be part of the proposed design method.

Objective 2: Investigate the lateral resistance of a single post and group of posts system under static and dynamic impact loads

Compare the static and dynamic lateral resistances of a single post and group of posts systems from measured and simulated forces from the proposed experiments and finite element analysis the four dimensional numerical simulations using LS-DYNA, as well as fundamental theoretical concepts.

Objective 3: Develop design charts for a single post in sand and clay

Develop design charts for anti-ram single posts embedded in sand and clay to arrest a vehicle having a mass of 6800 kg and velocities include 80 km/h, 65 km/h and 50 km/h using finite element analysis based on the proposed experiments and fundamental theoretical concepts.

Objective 4: Develop design charts for a group of posts system in sand and clay

Develop design charts for anti-ram group of posts system embedded in sand and clay to arrest a vehicle having a mass of 6800 kg and velocities include 80 km/h, 65 km/h and 50 km/h using finite element analysis based on the proposed experiments and fundamental theoretical concepts.

Objective 5: Develop design guidelines for post systems embedded in sand and clay

Develop design guidelines for anti-ram post system directly embedded in sand and clay to arrest a vehicle having a mass of 6800 kg and velocities include 80 km/h, 65 km/h and 50 km/h based on the proposed design charts.

1.4 Organization of dissertation

This dissertation describes the work done to develop a set of design recommendations to select the embedment of a single post or group of posts and to investigate post behaviors under a lateral impact load. This dissertation consists of five parts: previous work and background, experiments, numerical simulations, the proposed design guidelines and conclusions and recommendations.

2. LITERATURE REVIEW

2.1 Soil strength classifications

Terzaghi et al. (1996) proposed the relation between consistency of clay, SPT (Standard Penetration Test) blow count (N) and unconfined compression strength (q_u) as shown in Table 2.1. In the table, clay can be divided into five according to standard penetration test blow count or unconfined compressive strength.

Table 2.1. Relation of consistency of clay, number of blows N_{60} on sampling spoon, and unconfined compressive strength (Terzaghi et al. 1996)

Consistency	q_u (kPa)					
	Very soft	Soft	Medium	Stiff	Very Stiff	Hard
N_{60}	<2	2-4	4-8	8-15	15-30	>30
q_u	<25	25-50	50-100	100-200	200-400	>400

Typical values of dry unit weights (γ_d) of natural soil and drained friction angles (φ) for sands and silts were published by Das (1998). Dry unit weight and saturated moisture content of typical soils including sands and clays are shown in Table 2.2. Saturated unit weight of soil can be obtained from saturated moisture contents and dry unit weight. Range of unit weight of typical soils can be estimated as dry unit weight to saturated unit weight. Drained angle of friction for sands and silts are shown in Table 2.3. Friction angle of sands and silts are ranging from 27 degrees to 48 degrees.

Table 2.2. Void ratio, moisture content and dry unit weight for some typical soils in a natural state (Das 1998)

Type of soil	Void ratio, e	Natural moisture content in a saturated state (%)	Dry Unit Weight, γ_d	
			lb/ft^3	kN/m^3
Loose uniform sand	0.8	30	92	14.5
Dense uniform sand	0.45	16	115	18
Loose angular-grained silty sand	0.65	25	102	16
Dense angular-grained silty sand	0.4	15	121	19
Stiff Clay	0.6	21	108	17
Soft Clay	0.9-1.4	30-50	73-93	11.5-14.5
Loess	0.9	25	86	13.5
Soft organic clay	2.5-3.2	90-120	38-51	6-8
Glacial till	0.3	10	134	21

Table 2.3. Typical values of drained angle of friction for sands and silts (Das 1998)

Soil Type	φ (deg)
Sand: Rounded grains	
Loose	27-30
Medium	30-35
Dense	35-38
Sand: Angular grains	
Loose	30-35
Medium	35-40
Dense	40-45
Gravel with some sand	34-48
Silts	26-35

Briaud (1992) introduced a correlation between various soil properties for sand and clay including the pressuremeter initial elastic modulus (E_0), pressuremeter reload elastic modulus (E_r), pressuremeter limit pressure (P_L), tip resistance and sleeve friction

resistance (q_u and f_s) from cone penetrometer test (CPT), blow count (N) of standard

penetration test (SPT) and undrained shear strength of clay (S_u) as shown in Table 2.4

and Table 2.5. In Table 2.5, additional row and column were added for blow count of

standard penetration test according to Terzaghi et al. (1996).

Table 2.4. Correlation results for sand (Column A = number in table x row B) (Briaud 1992)

	B	E_0	E_R	P_L	q_c	f_s	N
A		(kPa)	(kPa)	(kPa)	(kPa)	(kPa)	(bpf)
E_0	(kPa)	1	0.125	8	1.15	57.5	383
E_R	(kPa)	8	1	64	6.25	312.5	2174
P_L	(kPa)	0.125	0.0156	1	0.11	5.5	47.9
q_c	(kPa)	0.87	0.16	9	1	50	479
f_s	(kPa)	0.0174	0.0032	0.182	0.02	1	9.58
N	(bpf)	0.0026	0.00046	0.021	0.0021	0.104	1

Table 2.5. Correlation results for clay (Column A = number in table x row B) (After Briaud 1992; Terzaghi et al. 1996)

	B	E_0	E_R	P_L	q_c	f_s	S_u	*N*
A		(kPa)	(kPa)	(kPa)	(kPa)	(kPa)	(kPa)	*(bpf)*
E_0	(kPa)	1	0.278	14	2.5	56	100	*1300*
E_R	(kPa)	3.6	1	50	13	260	300	*3900*
P_L	(kPa)	0.071	0.02	1	0.2	4	7.5	*97.5*
q_c	(kPa)	0.40	0.077	5	1	20	27	*351*
f_s	(kPa)	0.079	0.0038	0.25	0.05	1	1.6	*20.8*
S_u	(kPa)	0.010	0.0033	0.133	0.037	0.625	1	*13*
N	*(bpf)*	*0.0078*	*0.0026*	*0.1037*	*0.0288*	*0.4875*	*0.78*	*1*

A simple soil classification by using pressuremeter parameters was also proposed

by Briaud (1992) as shown in Table 2.6 and Table 2.7. The method using either limit

pressure or initial elastic modulus can classify sand and clay as five and four classes, respectively.

Table 2.6. Clay classification based on pressuremeter parameter (Briaud 1992)

	Clay				
Soil type	Soft	Medium	Stiff	Very Stiff	Hard
P_L (kPa)	0-200	200-400	400-800	800-1600	>1600
E_0 (kPa)	0-2500	2500-5000	5000-12000	12000-25000	>25000

Table 2.7. Sand classification based on pressuremeter parameter (Briaud 1992)

	Sand			
Soil type	Loose	Compact	Dense	Very dense
P_L (kPa)	0-500	500-1500	1500-2500	>2500
E_0 (kPa)	0-3500	3500-12000	12000-22500	>22500

2.2 The dilatancy effect in soils

When anything is done to disturb the arrangement of the soil particles by distorting the boundary of the soil sample, rearrangement will be accompanied by some change in the volumetric packing (Wood 2001). Dilatancy is the soil behavior of volumetric change during shearing. According to Rowe (1962), dense sands expand during shear to failure whereas loose sands contract during shearing.

When loosely packed soil particles is sheared, the particles in each row move over the particles in the row below and fall into gaps between particles of lower row. As the results of the particle movement, volume of the soil reduces. On the contrary, one

layer is displaced sideways and forced to climb over the particles in the lower layer in densely packed soil particles. The volume of dense soil increases during shearing. A simple illustration of the dilatancy is shown in Figure 2.1.

Loose   Dense
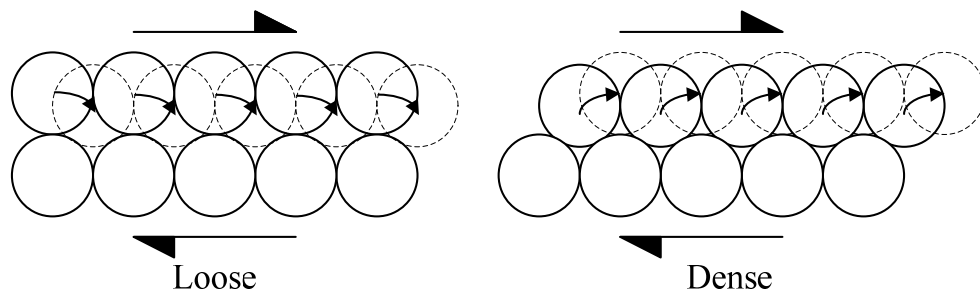
Figure 2.1. Movement of particles during shearing (After Wood 2001)

Dilation behavior of granular soil during shearing is illustrated as an inclined shear surface in Figure 2.2. Soil particles slide sideways along with planes inclined at a dilation angle (ψ) with respect to the horizontal plane. The ratio between shear load and vertical load is indicated as mobilized angle of shearing resistance (φ_m) (Wood 2001). Critical state angel of shearing resistance (φ_{crit}) corresponds to constant volume shearing.
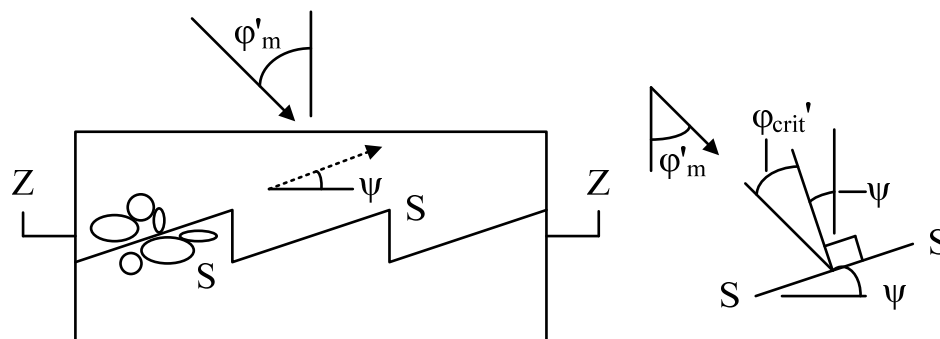
Figure 2.2. Inclined shear surface and mobilized friction (After Bolton 1986)

The relationship among dilation angle, mobilized angle of shearing resistance and critical state angle of shearing can be expressed as

$$\phi_m = \phi_{crit} + \psi \qquad (2\text{-}1)$$

where, ϕ_m = mobilized angle of shearing resistance

ϕ_{crit} = critical state angle of shearing resistance

ψ = angle of dilatancy

The concept of dilation angle in a plane strain deformation can be applied to the case of the direct shear test as shown in Figure 2.3.when rigid block of non-failing soil are assumed to bound the thin uniformly straining rupture zone ZZ, the zone ZZ is a zero extension line (Bolton 1986). The following relationship can be expressed as

$$d\gamma_{yz} = \frac{dz}{y} \qquad (2\text{-}2)$$

$$d\varepsilon_y = -\frac{dy}{y} \qquad (2\text{-}3)$$

Therefore,

$$\tan\psi = -\frac{d\varepsilon_y}{d\gamma_{yz}} = \frac{dy}{dz} \qquad (2\text{-}4)$$

where, γ_{yz} = shear strain

ε_y = vertical strain

ψ = angle of dilatancy

According to Bolton (1986), the dilation angle can be considered to be equal to the instantaneous angle of motion of the sliding blocks relative to the rupture surface as shown in Figure 2.4.
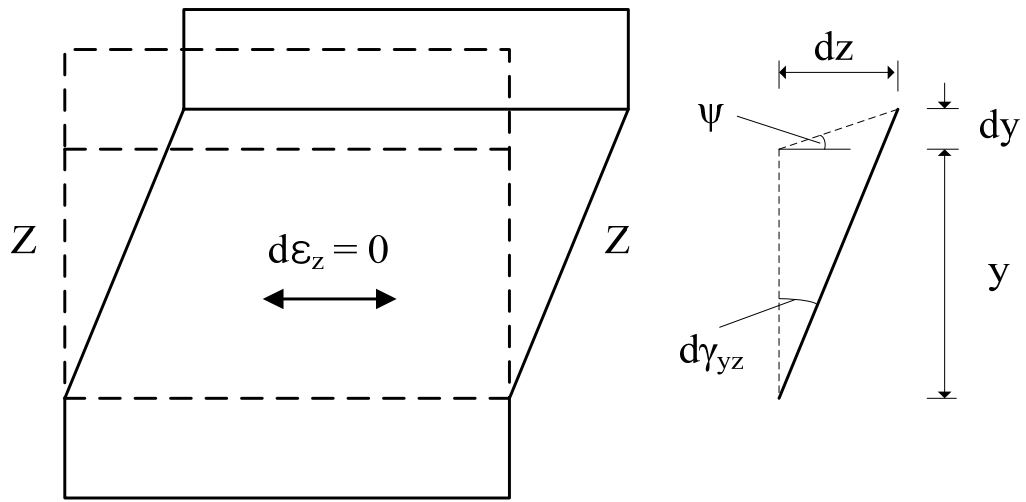
Figure 2.3. Dilation angle ψ in plane shear (After Bolton 1986)
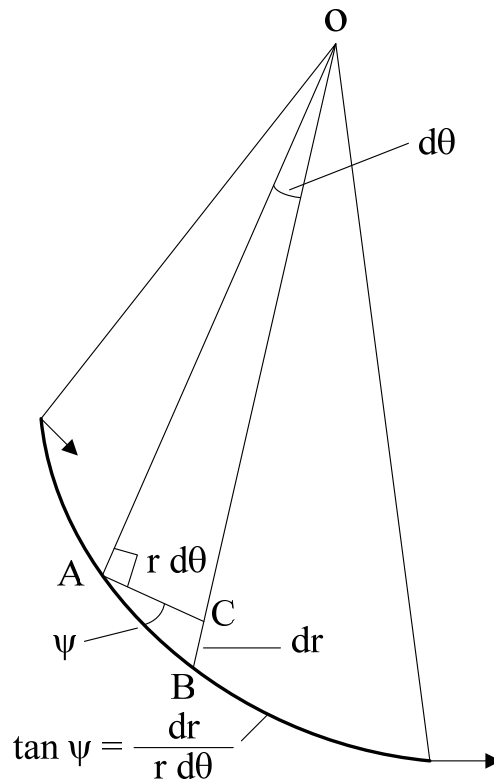
Figure 2.4. Schematic drawing of dilation angle (After Bolton 1986)

The dilatancy of sand depends on both the density and on the friction angle. The order of magnitude of dilation angle of quarts sand is lower than angle of friction by 30 degrees. In most cases, the angle of dilatancy is zero for sand having less than 30 degrees of friction angle. According to Plaxis version 8 Reference manual (2002), a small negative value for dilation angle is realistic for extremely loose sands.

2.3 Laterally loaded pile

Piles are often subjected to lateral loads and overturning moments due to wind loads, seismic loads, vehicle impact, etc. The lateral capacity of piles under lateral load are required to be checked both soil resistance and pile capacity. Not only the piles should have enough lateral soil bearing capacity to resist the lateral loads but also the horizontal deflection of the pile should be within an allowable limit.

The problem is one of laterally loaded piles under impact loading. The problem of laterally loaded piles under static lateral loads is well known with work by engineers such as Broms, Matlock, Reese and others. The ability to predict the behavior of piles and pile groups under cyclic and vibratory loads is lagging behind the ability to predict the behavior under static loads. The behavior of piles under impact lateral loads is lagging even further.

2.3.1 Static load

A number of studies on static lateral load-deformation behavior have been conducted. For instance, Broms (1964a; 1964b) proposed ultimate soil resistance for cohesion soils

and cohesionless soils as shown in Figure 2.5. Poulos (1971a; 1971b) proposed elastic continuum model for single and group of posts under lateral loading. Generalized solution for laterally loaded piles using p-y curve was developed by Matlock and Reese (1960).
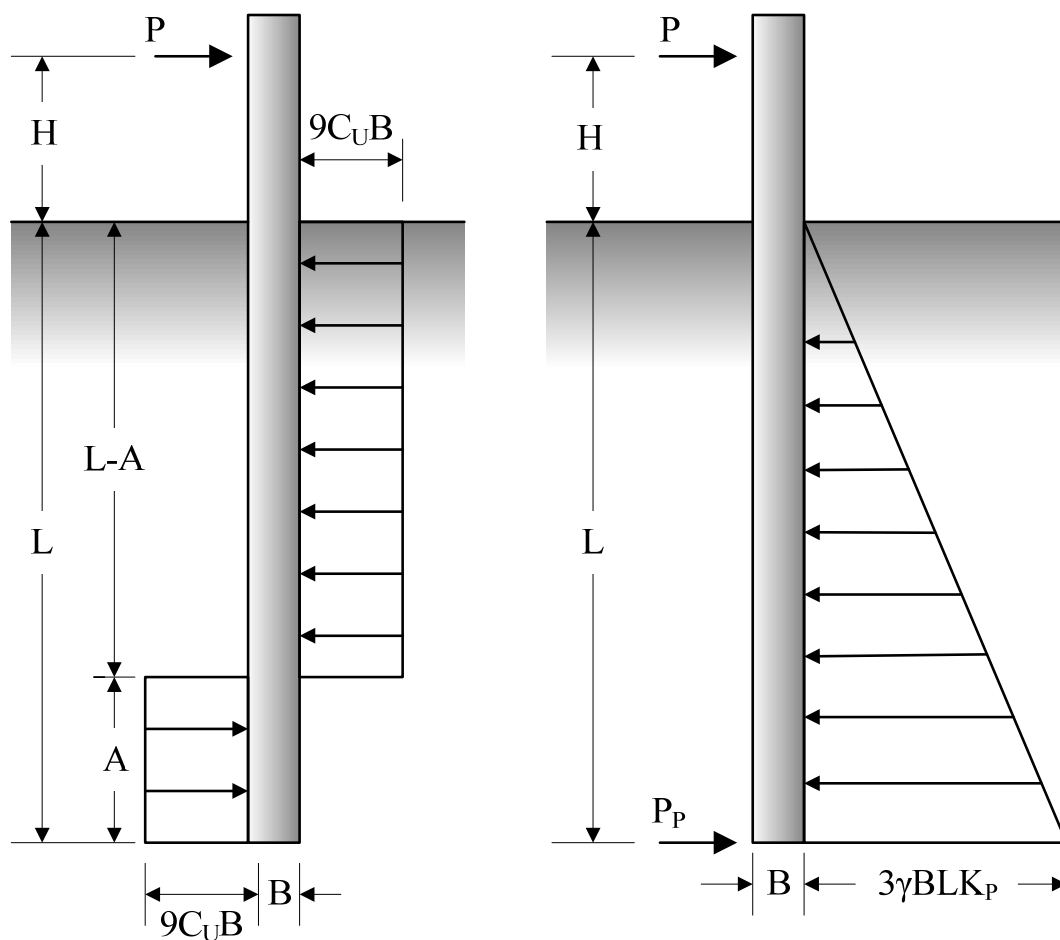
Figure 2.5. Ultimate lateral resistance of cohesive and cohesionless soils
(After Broms 1964a; 1964b)

Briaud (1997) proposed SALLOP method, a semi-empirical method to analysis load-deformation behavior of piles under lateral loading. Results of pressuremeter tests including the pressuremeter initial elastic modulus and pressuremeter limit pressure are required. The pressuremeter test consists of lowering a cylindrical probe in an open borehole and inflating it while recording the increase in volume and pressure of the probe. As described in the previous section, Briaud also proposed a correlation between various soil properties for sand and clay from various soil tests including Pressuremeter test and Standard Penetration test.

The methods for performing lateral capacity analyses are determined depending on the connection type between the pile and structure as shown in Figure 2.6. Free head condition is that connection between pile and structure allows both lateral movements and rotations. Fixed head condition is that connection between pile and structure allows only lateral movements but does not allow rotations of the pile head.

The zero-shear depth, D_v can be obtained using the transfer length. The transfer length is indicates the relative stiffness between the pile and the soil in unit length. The transfer length can be computed as

$$l_0 = \left(\frac{4EI}{K_s} \right)^{\frac{1}{4}}$$

(2-5)

where, l_0 = transfer length

EI = bending stiffness of pile

K_s = spring constant of soil
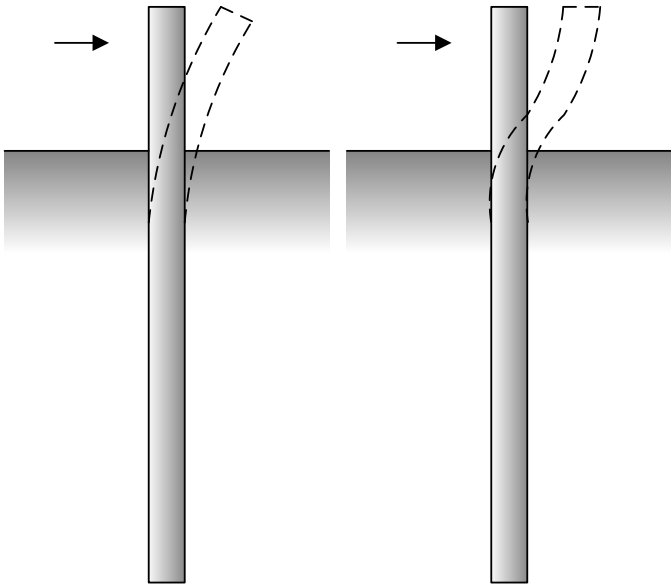
Figure 2.6. Free head and fixed head piles under lateral loading
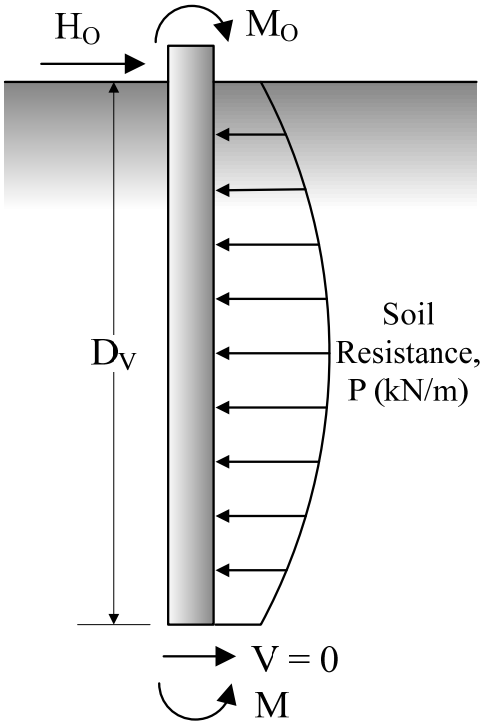
Figure 2.7. Free body diagram of pile down to zero-shear depth (After Briaud 1997)

The spring constant, K_s is the ratio of the lateral resistance of the soil per unit length of a pile to the lateral displacement of the pile (Briaud 1997). The spring constant is proposed as

$$K_s = 2.3E_0 \tag{2-6}$$

where, E_0 = initial or first elastic modulus measured from pressuremeter test

The zero-shear depth, D_v can be computed by setting V=0.

For long flexible piles ($L \geq 3l_0$),

$$D_v = l_0 \tan^{-1}\left(\frac{1}{1+\dfrac{2M_0}{l_0 H_0}}\right) \tag{2-7}$$

For short rigid piles ($L < l_0$),

$$D_v = \frac{H_0 L^2}{3(H_0 L + 2M_0)} \tag{2-8}$$

where, D_v = zero-shear depth

L = pile embedment length
M_0 = applied moment at the ground level
H_0 = applied lateral load at the ground level
l_0 = transfer length

If the pile length is between the criteria of long flexible pile and short rigid pile, a linear interpolation between two values will be used (Briaud 1997).

The ultimate lateral capacity of the pile with respect to soil capacity, H_{ou} is computed as

$$H_{ou} = 0.75P_L B D_v \tag{2-9}$$

where, P_L = limit pressure of soil measured from pressuremeter test

B = width of pile

Korean National Railroad (KNR 1999) expended SALLOP method for maximum bending moments of pile, displacement of pile head and at the ground level. The deflection of a long flexible pile at the ground level and at the pile head can be calculated as

$$y_0 = \frac{(1+h/l_0)H_0 l_0^3}{2EI} \qquad (2\text{-}10)$$

$$y_h = \frac{\left((1+h/l_0)^3 + 0.5\right)H_0 l_0^3}{3EI} \qquad (2\text{-}11)$$

where, H_0 = applied lateral load at the ground level

y_0 = pile deflection at the ground level

y_h = pile deflection at the pile head

h = height of the pile above the ground level

The maximum bending moment in the pile, M_{max} for a flexible pile can be computed as (KNR 1999)

$$M_{max} = \frac{H_0 l_0}{2} \sqrt{(1+2h/l_0)^2 + 1} \cdot e^{-(D_v/l_0)} \qquad (2\text{-}12)$$

The zero-shear depth for fixed head condition can be computed (KNR 1999).
For long flexible piles ($L \geq 3l_0$),

$$D_v = l_0 \tan^{-1}\left(\frac{l_0}{h}\right) \qquad (2\text{-}13)$$

where, D_v = zero-shear depth

h = height of the pile above the ground level

l_0 = transfer length

The deflection of a long flexible pile at the ground level and at the pile head for fixed head condition can be calculated as

$$y_0 = \frac{(1 + h/l_0)H_0 l_0^3}{4EI} \tag{2-14}$$

$$y_h = \frac{\left((1 + h/l_0)^3 + 2\right)H_0 l_0^3}{12EI} \tag{2-15}$$

where, H_0 = applied lateral load at the ground level

y_0 = pile deflection at the ground level

y_h = pile deflection at the pile head

h = height of the pile above the ground level

The maximum bending moment, M_{max} in the pile for a flexible pile can be computed as

$$M_{max} = \frac{H_0 l_0}{2} e^{-(D_v/l_0)} \sqrt{1 + (h/l_0)^2} \tag{2-16}$$

2.3.2 Lateral statnamic tests

The statnamic test is a load test using pyrotechnical loading system. The statnamic device is usually composed of a reaction mass, a piston and a connection to the test foundation including load cells. When fuel in the piston is ignited, expanding gasses push the reaction mass away from the foundation and apply an equal and opposite thrust on the foundation (Brown 2007).

Lateral statnamic test can be considered as a dynamic load test. El Naggar (1998) analyzed the lateral statnamic test results based on Winkler hypothesis, a pile in nonlinear spring and dashpot system. Brown (2007) proposed a simple analysis on the

lateral statnamic tests on the basis of single degree of freedom model. The force acting

on the foundation can be expressed as

$$F_{meas} = F_{inertia} + F_{damping} + F_{static} \qquad (2\text{-}17)$$

where, F_{meas} = measured force on the load cell

$F_{inertia}$ = inertial resistance from effective mass of the foundation

$F_{damping}$ = effective viscous damping resistance

F_{static} = effective static soil resistance

Figure 2.8. Lateral statnamic tests (Applied Foundation Tesing 2010)

Rollins and Sparks (2002) conducted a study on lateral statnamic test and analysis of a pile group. Also the soil reaction is considered as a sum of inertia resistance, damping resistance and static resistance. The measured dynamic resistance was 30 to 80% higher than the static resistance (Rollins and Sparks 2002).

2.3.3 Impact tests

Texas Transportation Institute has performed almost 2,000 full-scale crash tests at the TTI Proving Grounds Research Facility (TTI 2010). The crash tests on a variety of safety devices including guardrails, mechanically stabilized wall and barrier systems have been conducted with a various vehicles from subcompacts to tractor trailer. According to Reid et al. (2009), numerous studies on behavior of guardrail posts under impact load using experiments and numerical simulations have been conducted by Southwest Research Institute, Texas Transportation Institute and Midwest Roadside Safety Facility.

Dewey Jr. et al. (1983) and Eggers and Hirsch (1986) conducted a series of static load tests and impact tests using a bogie traveling at 27 km/h on two kinds of guardrail posts. The post was 0.97 m embedded in either cohesionless or cohesive soil. The maximum static lateral resistances and impact forces are shown in Table 2.8. In the last column of the table, the dynamic factors, the ratio of the maximum impact force and the maximum static resistance, are indicated. Average dynamic factor of these tests is 5.

Table 2.8. Static and impact test on guardrail posts (After Eggers and Hirsch 1986)

Post Type	Soil Type	Static test (kN)	Impact test (kN)	Dynamic factor
Wood	Cohesive	16.5	72.5	4.4
Steel	Cohesive	14.7	75.6	5.1
Wood	Cohesionless	14.2	59.2	4.2
Steel	Cohesionless	14.7	99.5	6.8

Beason and Hirsch (1989) measured and compared vehicle impact forces using an instrumented wall and accelerometer attached on vehicle. The test vehicles were ranging from sedan, pickup truck to three tractor trailer rigs. As the results of the research, the product of 50ms average deceleration and vehicle mass was well matched with the measured impact force using the instrumented wall.

The standards used to evaluate the performance of an anti-ram barrier are ASTM F 2656-07 - *Standard Test Method for Vehicle Crash Testing of Perimeter Barriers* (2007) and SD-STD-02.01, Revision A –*Test Method for Vehicle Crash Testing of Perimeter Barriers and Gates* (2003). The impact condition designations of ASTM F 2656-07 are shown in Table 2.9. According to ASTM F 2656-07, the condition designation M50 is an impact with a medium duty truck weighting 6800 kg (1500 lb) at a speed of 80 km/h (50 mph). The same truck with a speed of 65 km/h (40 mph) and 50 km/h (30 mph) are called M40 and M30 respectively.

The test criteria to evaluate the performance of barrier system are dynamic penetration rating as shown in Table 2.10. For medium duty truck (M), the

maximum measured penetration the leading lower edge of the cargo bed on the truck and location of barrier system is defined as a dynamic penetration.

Table 2.9. Impact condition designations (ASTM F2656-07)

Test vehicle/Minimum Test Inertia Vehicle kg (lbs)	Nominal Minimum Test Velocity km/h (mph)	Permissible Speed Range km/h (mph)	Kinetic Energy kJ (ft-kips)	Condition Designation
Small passenger car (C)	65 (40)	60.1-75.0 (38.0-46.9)	179 (131)	C40
1,100 (2,430)	80 (50)	75.1-90.0 (47.0-56.9)	271 (205)	C50
	100 (60)	90.1-above (57.0-above)	424 (295)	C60
Pickup truck (P)	65 (40)	60.1-75.0 (38.0-46.9)	375 (273)	PU40
2,300 (5,070)	80 (50)	75.1-90.0 (47.0-56.9)	568 (426)	PU50
	100 (60)	90.1-above (57.0-above)	887 (613)	PU60
Medium-duty truck (M)	50 (30)	45.0-60.0 (28.0-37.9)	656 (451)	M30
6,800 (15,000)	65 (40)	60.1-75.0 (38.0-46.9)	1,110 (802)	M40
	80 (50)	75.1-above (47.0-above)	1,680 (1,250)	M50
Heavy goods vehicle (H)	50 (30)	45.0-60.0 (28.0-37.9)	2,850 (1,950)	H30
29,500 (65,000)	65 (40)	60.1-75.0 (38.0-46.9)	4,810 (3,470)	H40
	80 (50)	75.1-above (47.0-above)	7,280 (5,430)	H50

According to SD-STD-02.01, Revision A, M50, M40 and M30 of ASTM F 2656-07 are defined as K12, K8 and K4, respectively as shown in Table 2.11. The impact performance is evaluated depending on the dynamic penetration. To pass, the dynamic penetration has to be less than one meter.

Table 2.10. Penetration Ratings (ASTM F2656-07)

Designation	Dynamic Penetration Rating
P1	≤ 1 m (3.3 ft)
P2	1.01 to 7 m (3.31 to 23.0 ft)
P3	7.01 to 30 m (23.1 to 98.4 ft)
P4	30 m (98 ft) or greater

Table 2.11. Impact condition designations for a gross vehicle weight of 6,800kg (SD-STD-02.01)

Nominal impact speed	Permissible impact speed range	Kinetic energy	Designation
80 km/h	75.0 - above km/h	1,695,000 J	K12
50 mph	47.0 - 56.9 mph	1,250,000 ft-lb	
65 km/h	60.1 - 75.0 km/h	1,085,000 J	K8
40 mph	38.0 - 46.9 mph	800,000 ft-lb	
50 km/h	45.0 - 60.0 km/h	610,000 J	K4
30 mph	28.0 - 37.9 mph	450,000 ft-lb	

2.4 Soil model

In numerical modeling, the constitutive response that is the link between stress change and strain change is required as well as equilibrium, kinematics and compatibility (Wood

2001). Most of geotechnical problems including laterally loaded pile and impact behaviors are related to plasticity. Isotropic elastic plastic model using Von Mises yield criteria and Drucker-Prager model are generally used in handling geotechnical problems.

2.4.1 Isotropic elastic plastic model using Von Mises yield criteria

As shown in Figure 2.9, the Tresca yield surface has corners. These corners can cause difficulties in numerical analysis (Potts and Zdravkovic 1999). Due to the analytical difficulties in using Tresca criterion, simplified yield function as a circular shape, Von Mises criterion is generally used in solving geotechnical problems.
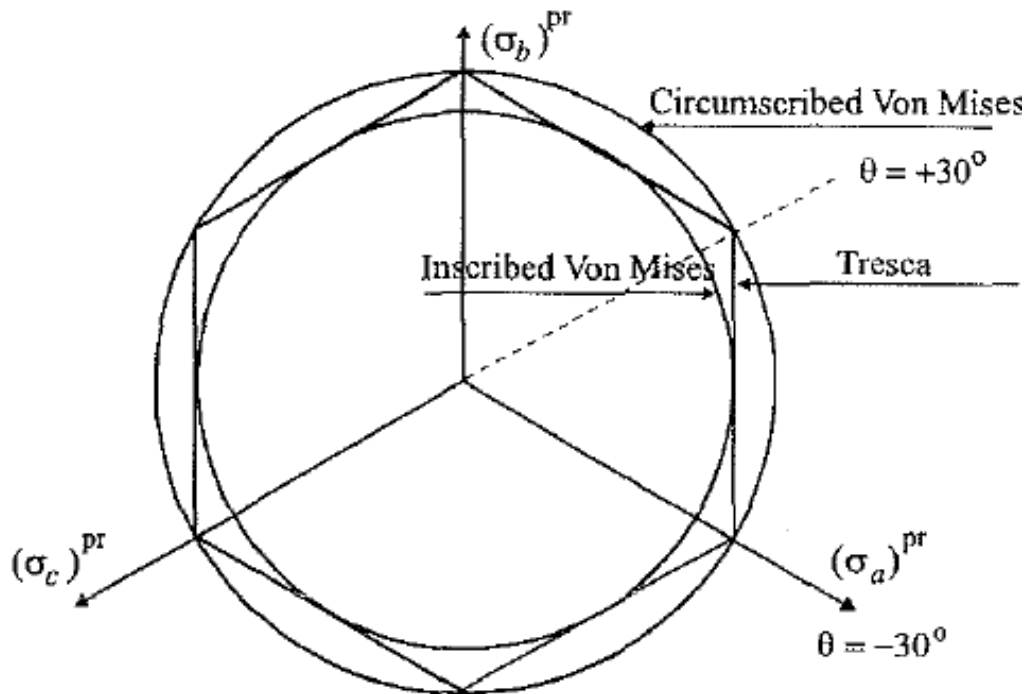
Figure 2.9. Comparison of Tresca and Von Mises criterion
(Potts and Zdravkovic 1999)

Isotropic Elastic Plastic model supported in LS-DYNA follows Von Mises yield criteria. The pre-yielding behavior is modeled as linear elastic using Hook's law. Von Mises yield surface in principal stress space is shown in Figure 2.10. The Von Mises yield condition is given by:

$$f(J_2) = J_2 - \frac{\sigma_y^2}{3}$$ (2-18)

where, J_2 = second stress invariant

σ_y = yield stress

The second stress invariant is defined in terms of the deviatoric stress component as

$$J_2 = \frac{1}{2} s_{ij} s_{ij}$$ (2-19)

where, S_{ij} = deviator stress tensor
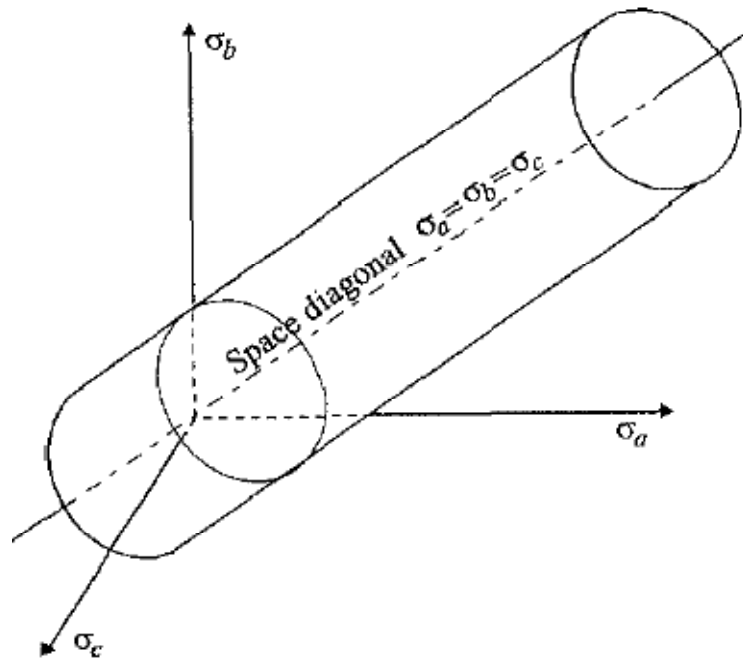
Figure 2.10. Von Mises yield surface (Potts and Zdravkovic 1999)

The yield stress, σ_y, is a function of the effective plastic strain, ε_{eff}^p, and the plastic hardening modulus, E_P:

$$\sigma_y = \sigma_0 + E_p \varepsilon_{eff}^p \qquad (2\text{-}20)$$

The effective plastic strain is defined as:

$$\varepsilon_{eff}^p = \int_0^t d\varepsilon_{eff}^p \qquad (2\text{-}21)$$

where, $d\varepsilon_{eff}^p = \sqrt{\dfrac{2}{3} d\varepsilon_{ij}^p d\varepsilon_{ij}^p}$

The plastic tangent modulus is defined in terms of the input tangent modulus, E_t, as

$$E_p = \frac{E E_t}{E - E_t} \qquad (2\text{-}22)$$

Pressure is given by the expression

$$p^{n+1} = K\left(\frac{1}{V^{n+1}} - 1\right) \qquad (2\text{-}23)$$

where, K = bulk modulus

In case of uniaxial compression, $\sigma_1 \neq 0$ and $\sigma_2 = \sigma_3 = 0$, the Von Mises criterion reduces to

$$\sigma_1 = \sigma_y \qquad (2\text{-}24)$$

This model may be the most cost effective plasticity model. Only on history variable , ε_{eff}^p, is stored with this model (LS-DYNA 2006). Isotropic Elastic plastic with

Failure model is available in LS-DYNA. This model is basically same with Isotropic Elastic Plastic model except failure. Failure initially assumed to occur when either cases of Eq.2-25 or Eq. 2-26.

$$p^{n+1} < p_{min} \tag{2-25}$$

$$\varepsilon_{eff}^{p} > \varepsilon_{max}^{p} \tag{2-26}$$

where, p_{min} = failure pressure

ε_{max}^{p} = plastic failure strain

The failure pressure and plastic failure strain is user-defined parameters. Once failure has occurred, pressure may never be negative and the deviatoric components are set to zero:

$$s_{ij} = 0 \tag{2-27}$$

For all time, The failed element can only carry loads in compression (LS-DYNA 2006).

2.4.2 Drucker-Prager model

The original Drucker-Prager model was developed as a perfectly plastic model. In numerical simulations, an idealized material which behaves elastically up to some state of stresses at which slip or yielding occurs, replaces the soil (Drucker and Prager 1952). Similar to Von Mises yield criteria, Drucker-Prager yield criteria has its advantage in computation effort to Mohr-Coulomn yield criteria having corners as shown in Figure 2.11 (Potts and Zdravkovic 1999).
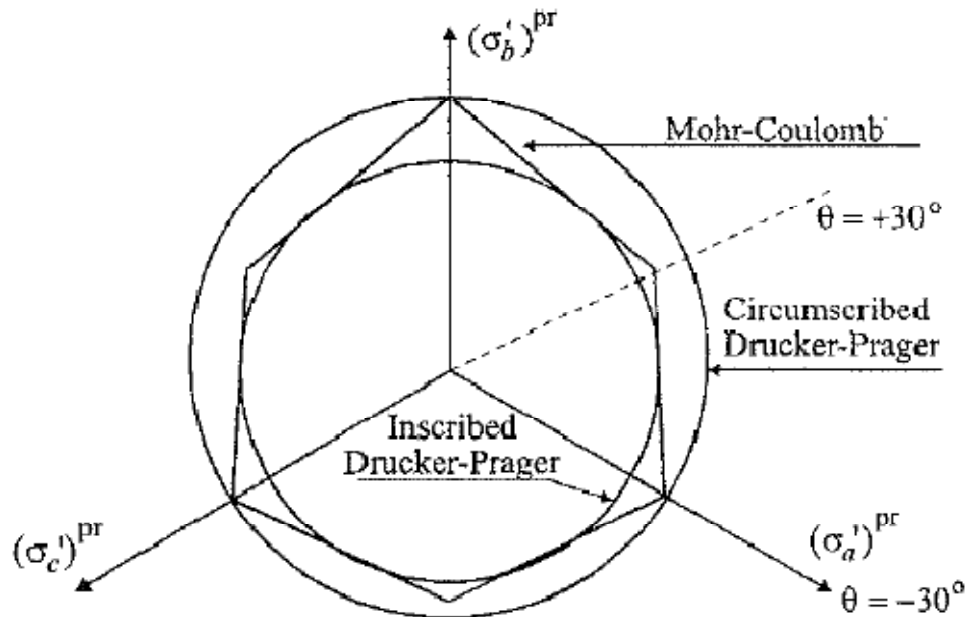
Figure 2.11. Comparison of Mohr-Coulomb and Drucker-Prager criterion (Potts and Zdravkovic 1999)

The pre-yield behavior of the soil is assumed to be linear elastic using Hooke's law. Drucker-Prager yield surface in principal stress space is shown in Figure 2.12. Drucker-Prager yield criterion can be expressed as

$$f(I_1, J_2) = \alpha I_1 + \sqrt{J_2} - k = 0 \qquad (2\text{-}28)$$

where, I_1 = the first invariant of stress tensor

J_2 = the second invariant of the deviatoric stress

α and k = positive constants at each point of the material

If the yield function is less than zero, the material behaves as an elastic material and no volume change is recorded. Yielding occurs and material begins behaving as a plastic material when the yield function is zero. When the yield function is bigger than

zero, the stresses are moved on the yield surface. The stress state is not permitted but numerically it can be happen.
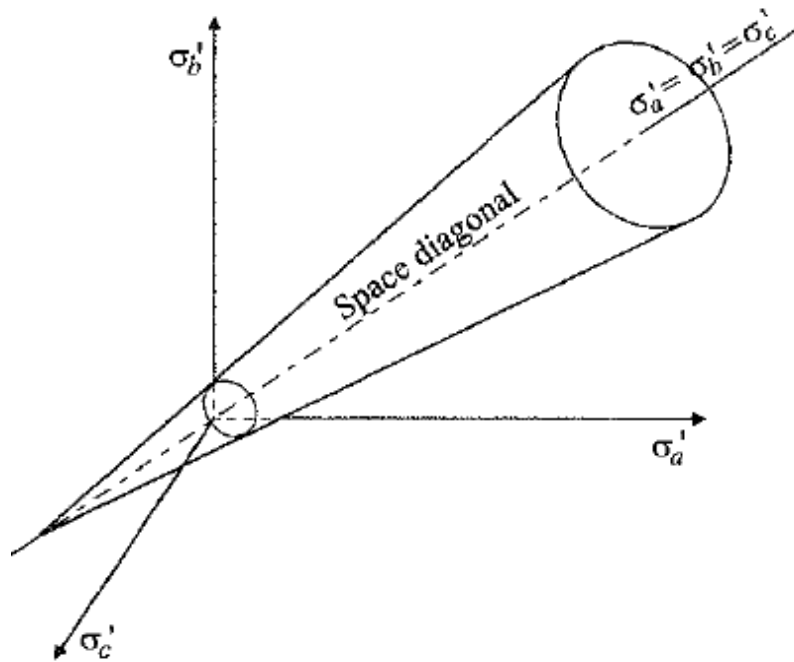
Figure 2.12. Drucker-Prager yield surface (Potts and Zdravkovic 1999)

Plastic strain will occur if the current stress state is on the yield surface. If the plastic-strain increment is considered as a vector in the plastic-strain space superimposed on the stress space, can be written as

$$d\varepsilon_{ij}^{p} = d\lambda \frac{\partial g(\sigma_{ij})}{\partial \sigma_{ij}}$$
(2-29)

where, $d\varepsilon_{ij}^{p}$ = the plastic-strain increment

$d\lambda$ = a non-negative scalar

$g(\sigma_{ij})$ = plastic potential function, for associate flow rule $g = f$

The total strain increment is then given by

$$d\varepsilon_{ij} = d\varepsilon_{ij}^e + d\varepsilon_{ij}^p \qquad (2\text{-}30)$$

where, $d\varepsilon_{ij}$ = the total strain increment

$d\varepsilon_{ij}^e$ = the elastic strain increment

The direction of the plastic strain increment is determined by the gradient vector $\partial g(\sigma_{ij})/\partial \sigma_{ij}$ and $d\lambda$ defines the magnitude of the plastic strain increment.

Since the Drucker-Prager model implemented in LS-DYNA is elastic perfectly plastic material, there is no hardening. Also the original Drucker-Prager model has a fixed yield surface.

3. EXPERIMENTS

To fulfill the proposed objectives, extensive experiments including site investigations, impact tests using pendulums and a bogie and full-scale impact tests were conducted. All the experiments took place at the Texas Transportation Institute (TTI) Proving Ground located 16 km northwest of the main campus of Texas A&M University, College Station

A series of small-scale impact tests using either a pendulum or a bogie were designed and performed for three kinds of soil conditions: medium dense crushed limestone, loose sand and hard clay. Also two full-scale impact tests with condition designation M50 were conducted in accordance with ASTM F 2656-07. The first one was an impact test on a single post embedded in very dense crushed limestone and the other was an impact test on a group of posts embedded in loose sand. For each test, soil tests including standard penetration test, pressuremeter test and index properties were performed according to ASTM Standards.

3.1 Properties of the soils tested

A site investigation for the four kinds of soil conditions was performed to prepare and design impact tests including pendulum tests, bogie tests and full-scale impact tests for single post systems and group of posts systems. The four soil conditions were loose sand, medium dense crushed limestone, very dense crushed limestone and stiff clay at the Texas Transportation Institute (TTI) Proving Ground. There were two kinds of loose sand conditions which were one for the pendulum tests and the other one for the full-

scale impact test on a group of posts system. The results of the soil tests were also used to calibrate the proposed soil strength category matrix to develop the design guidelines.

The three soil conditions: the loose sand for the pendulum tests, the medium dense crushed limestone and the very dense crushed limestone can be considered as fairly homogeneous since these soil deposits were constructed in a certain trench or pit, whereas the stiff clay was an existing intact soil next to the main taxiway at the TTI Proving Ground. The loose sand and medium dense crushed limestone were placed and compacted in a 1.5m wide, 3.0m long and 1.8m deep rectangular pit for the pendulum test. Separately from the pendulum tests pit, there was a trapezoidal ditch of very dense crushed limestone that is 5.5m wide at the top, 1.2m wide at the bottom and 2.1m deep.

Figure 3.1. TEXAM Pressuremeter (http://www.roctest.com/)

Standard penetration test (SPT), pressuremeter test (PMT) and soil classification using Unified Soil Classification System (USCS) were performed for all of the soil conditions. Direct shear tests, Tri-axial tests, Hand vane tests, unconfined compress tests, pocket penetrometer tests and sieve analysis were carried out whenever necessary, according to ASTM Standards. Two kinds of pressuremeter units were used. One was the TEXAM pressuremeter (Figure 3.1) and the other was the PENCEL pressuremeter. The PENCEL pressuremeter unit and the boring machine for the SPT can be found in Figure 3.2.
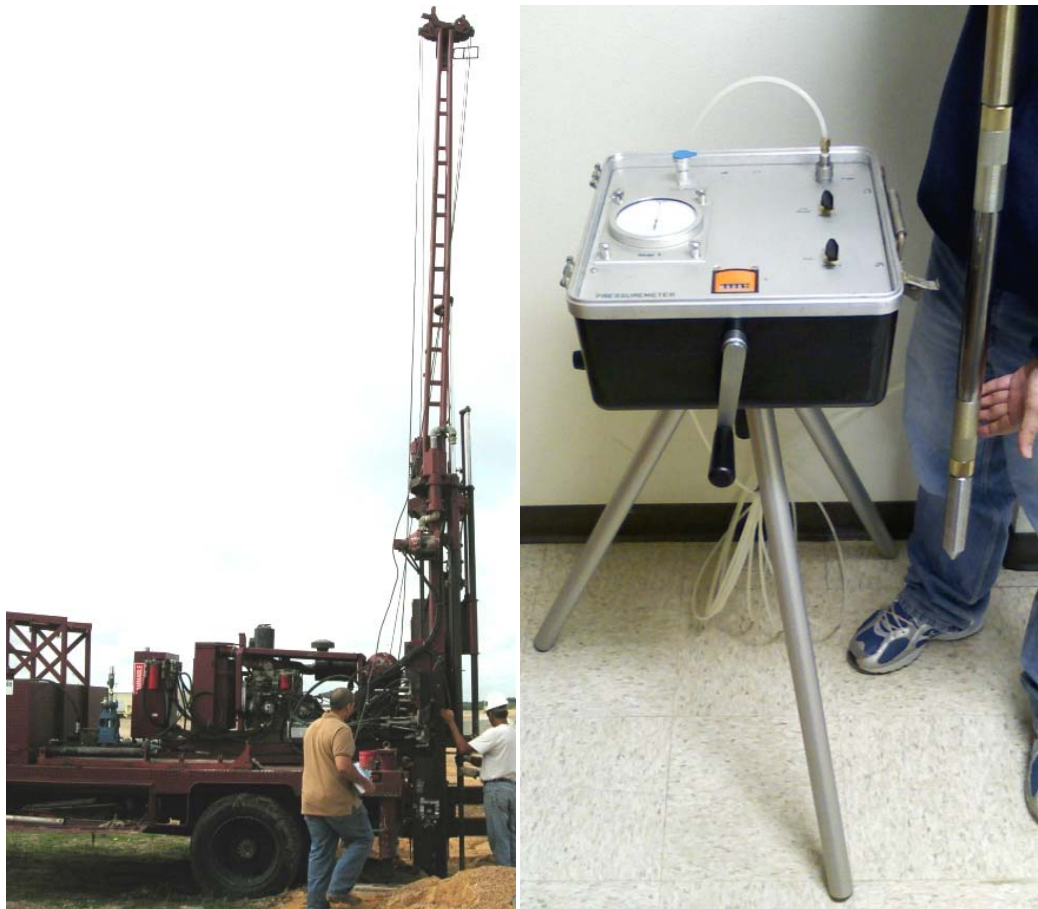
Figure 3.2. Standard penetration test (SPT) and PENCEL Pressuremeter

3.1.1 Very dense crushed limestone

In order to design a single post directly embedded in very dense crushed limestone, a site investigation on the proposed ditch located next to the runway of the TTI Proving ground was carried out. The trench was filled and compacted with crushed limestone. The soil seemed very hard and cemented since the crushed limestone had been in place for more than a year before the first soil test. Indeed the cementitious characteristics of the limestone increased the stiffness and strength as function of time.
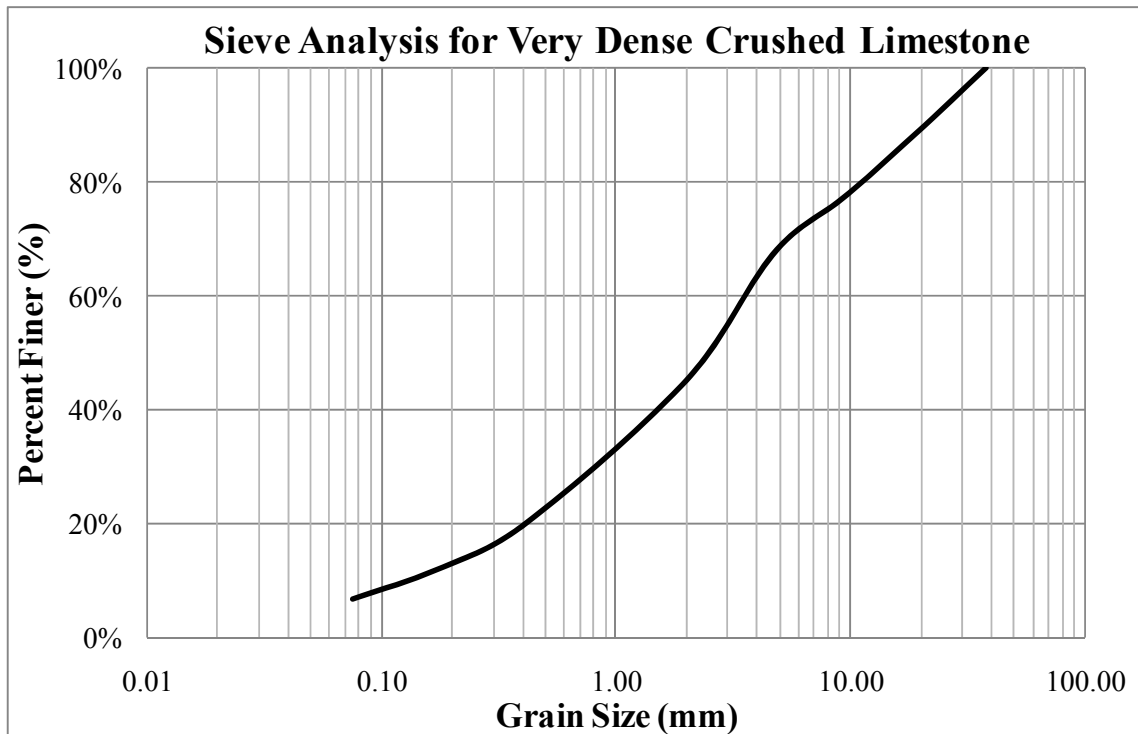
Figure 3.3. Particle size distribution curve for the very dense crushed limestone

A pressuremeter test using the TEXAM pressuremeter unit was conducted before the design of the post. After the impact test, a detailed soil investigation was performed

including sieve analysis, PENCEL pressuremeter test and standard penetration test (SPT). The soil can be classified as poorly graded sand with silt and gravel (SP-SM) by USCS. The particle-size distribution curve in accordance with the designation ASTM D2217 is shown in Figure 3.3. The size of the largest particle is around 25mm (1 inch).
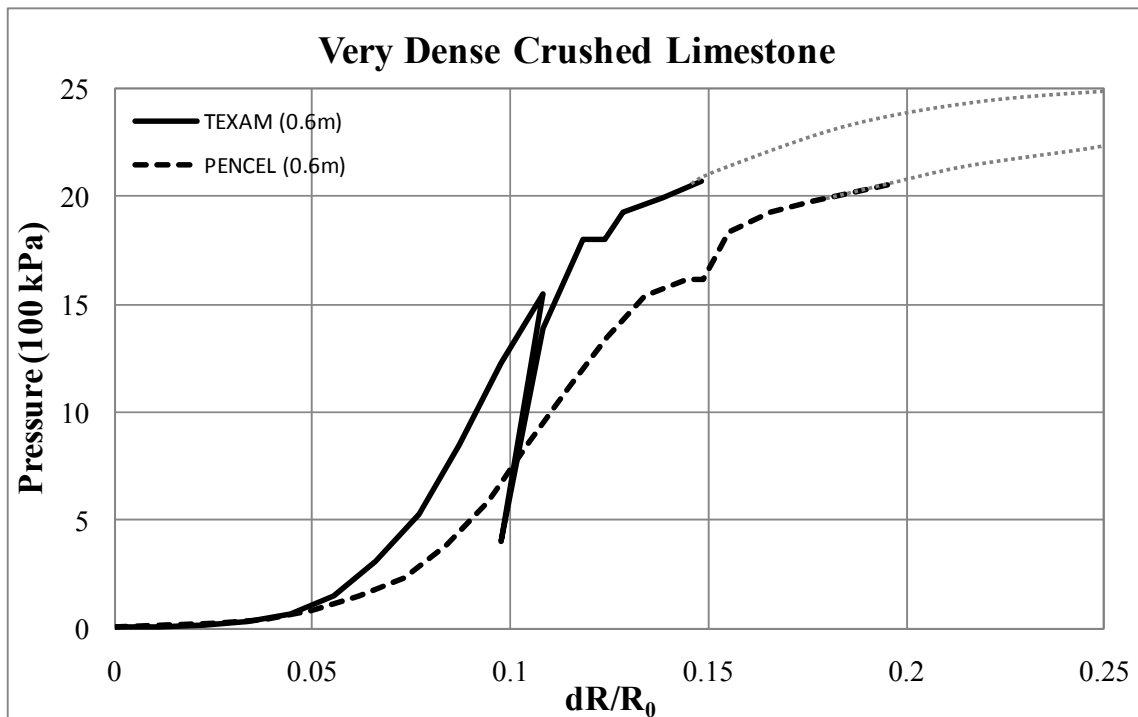
Figure 3.4. Pressuremeter test results for the very dense crushed limestone

The pressuremeter elastic modulus (E) and pressuremeter limit pressure (P_L) of the soil were measured as 46.7 MPa and 2,500 kPa using the TEXAM pressuremeter unit. Those values were also measured as 25.0 MPa and 2,250 kPa using the PENCEL pressuremeter unit (Figure 3.4). There is some difference between the two measured elastic modulus whereas the limit pressures are similar with each other. It can be because

those two tests were take place in pre-bored holes. Though the diameters of the hand auger for drilling a pre-bored hole is smaller than the diameters of pressuremeter probe, the actual diameter of the prepared hole was similar with the size of probe and the soil around the pre-bored hole is disturbed. Since the TEXAM has bigger probe and also allow the bigger displacement that reduce the effect of disturbed soil and bad sitting of probe than the PENCEL pressuremeter, the results from the TEXAM pressuremeter are more reliable.

Table 3.1. Summary of soil testing for very dense crushed limestone

TEXAM PMT - 0.6m		PENCEL PMT - 0.6m		SPT (N)		Water	Unit weight
P_L	E	P_L	E	0 - 2.1m	USCS	Contents	of soil
(kPa)	(kPa)	(kPa)	(kPa)	(blow/ft)		(%)	(kN/m^3)
2,500	46,700	2,250	25,000	50	SP-SM	3.0	24

The unit weight of the soil and the dry unit weight of the soil were measured as 24 kN/m^3 and 23.1 kN/m^3 by Saez Barrios (2010). Using triaxial tests, the friction angle of the material was measured as 45 degrees (Saez Barrios 2010). The blow count of Standard Penetration Test (N) was 50 (blow/ft). The summary of the tests results is shown in Table 3.1. In the table, pressuremeter limit pressure and pressuremeter elastic modulus is notated as P_L and E, respectively. The details of standard penetration test results can be found in Appendix A.

3.1.2 Medium dense crushed limestone

A medium dense crushed limestone pit was constructed at the pendulum test facility, the TTI Proving Ground. The same material with the previous very dense crushed limestone was filled and compacted. The differences from the previous one are the level of compaction and the cementation that increase the strength and stiffness of the soil. Due to the cementation, the particles of very dense crushed limestone in the ditch were bonded each other. Whereas the particles of this soil were not boned since the soil was newly constructed for the proposed pendulum tests.
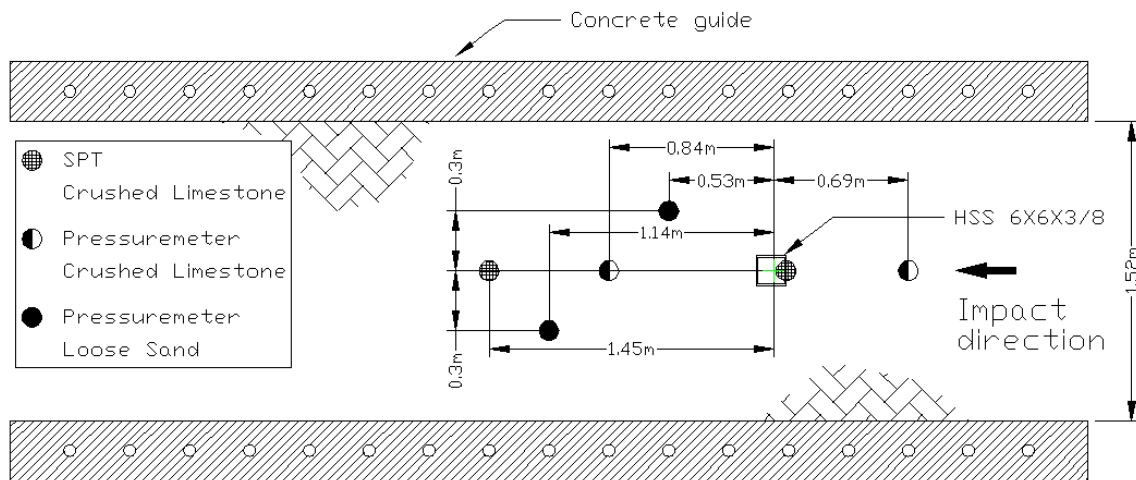
Figure 3.5. Soil testing locations in the pendulum pit

Standard Penetration tests (SPT), pressuremeter test using PENCEL and sieve analysis were conducted. The locations of the soil testing are shown in Figure 3.5. Figure 3.6 shows the particle size distributions of very dense crushed limestone of the ditch for

the full-scale impact test on a single post and medium dense crushed limestone from the pendulum pit. This soil can be classified as silty gravel with sand (GM) by USCS.

Sieve Analysis for Crushed Limestone
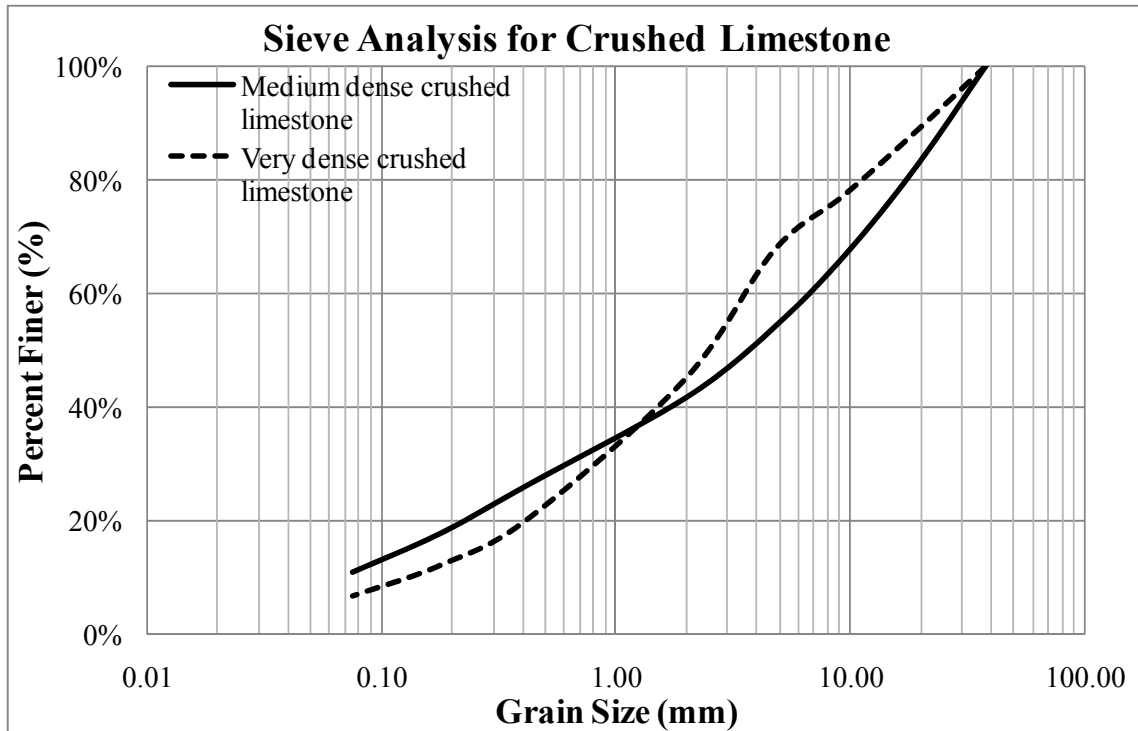
Figure 3.6. Particle size distribution curve for the very dense and medium dense crushed limestone

The results of pressuremeter tests are shown in Figure 3.7. The measurement of pressuremeter elastic modulus (E) and pressuremeter limit pressure (P_L) of the soil at 0.6m and 1.2m depth are shown in Table 3.2. The measured limit pressures and pressuremeter elastic moduli were measured as 6.0 MPa and 710 kPa using the PENCEL pressuremeter unit. The blow counts of SPT (N) were 11.5 (blow/ft) and 7.5 (blow/ft) at 0.6m and 1.2m, respectively. The above soil properties were measured within a week

before the test. Soil testing after the pendulum test was impossible due to the test schedule. The medium dense crushed limestone was removed just after the pendulum tests since the pendulum tests for post systems embedded in loose sand was scheduled immediately after the test.
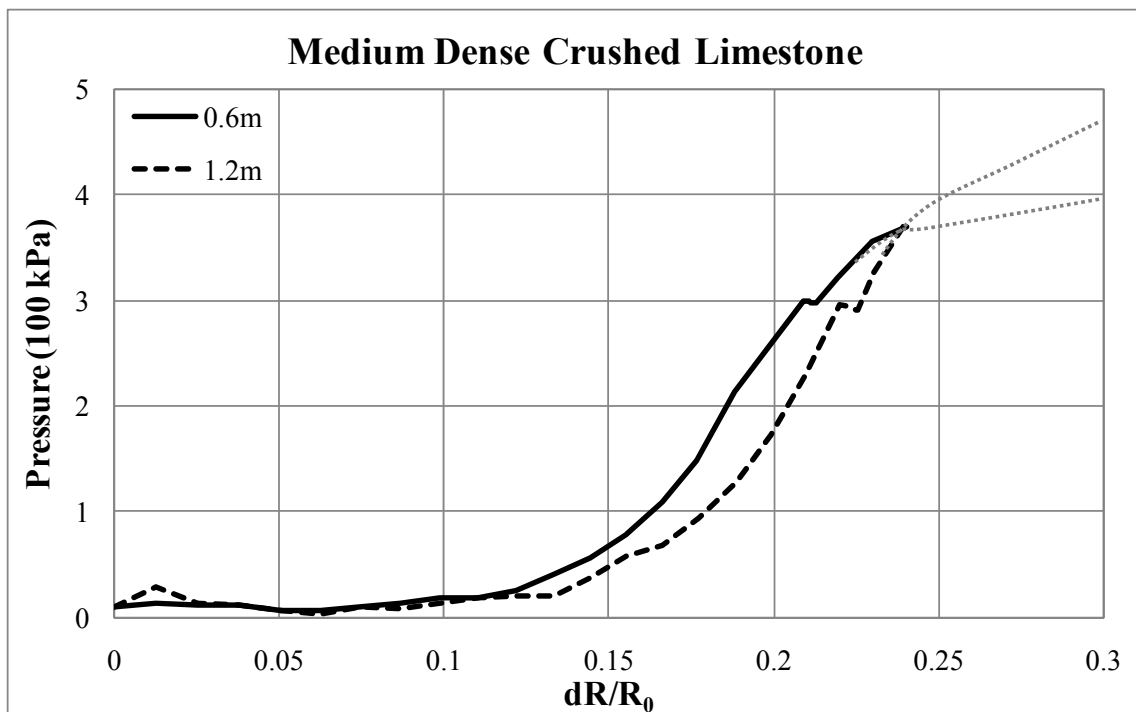
Figure 3.7. Pressuremeter test results for the very dense crushed limestone

Table 3.2. Summary of test results for medium dense crushed limestone

Depth (m)	P_L (kPa)	E (kPa)	SPT (N) (blow/ft)	USCS	Water Contents (%)	Unit weight of soil (kN/m^3)
0.6	720	6000	11.5	GM	1.0	23.1
1.2	700	5950	7.5	GM	1.0	23.1

The unit weight of the soil was measured as 23.1 kN/m^3 by Saez Barrios (2010). The summary of the tests results is shown in Table 3.2. In the table, pressuremeter limit pressure and pressuremeter elastic modulus is notated as P_L and E, respectively. The details of standard penetration test results from Terracon can be found in Appendix A.

3.1.3 Loose sand

Two kinds of loose sands were used and tested in this study. The one is for the proposed pendulum tests and the other is for the full-scale impact test on group of posts system described in Section 3.5. Those two soils were filled and compacted in the pendulum pit and a excavated ditch. Thus both of soil conditions can be considered as fairly homogeneous and uniform one since they were not intact or existing soil.

3.1.3.1 Loose sand for the pendulum test

The pendulum pit at the TTI Proving Ground was filled and compacted just after the pendulum tests with the medium dense crushed limestone. A loose sand pit with the same material for the pendulum pit was located next to the pendulum pit. A series of soil testing including standard penetration test, PENCEL pressuremeter test, and soil classification was conducted before and after the pendulum tests.

Sieve analysis also conducted for particle size distribution curve of the soil and soil classification before and after the pendulum tests. The particle size distribution curves of this soil are shown in Figure 3.8. This soil was classified as poorly graded sand according to Unified Soil Classification System (USCS).

Sieve Analysis for Loose Sand
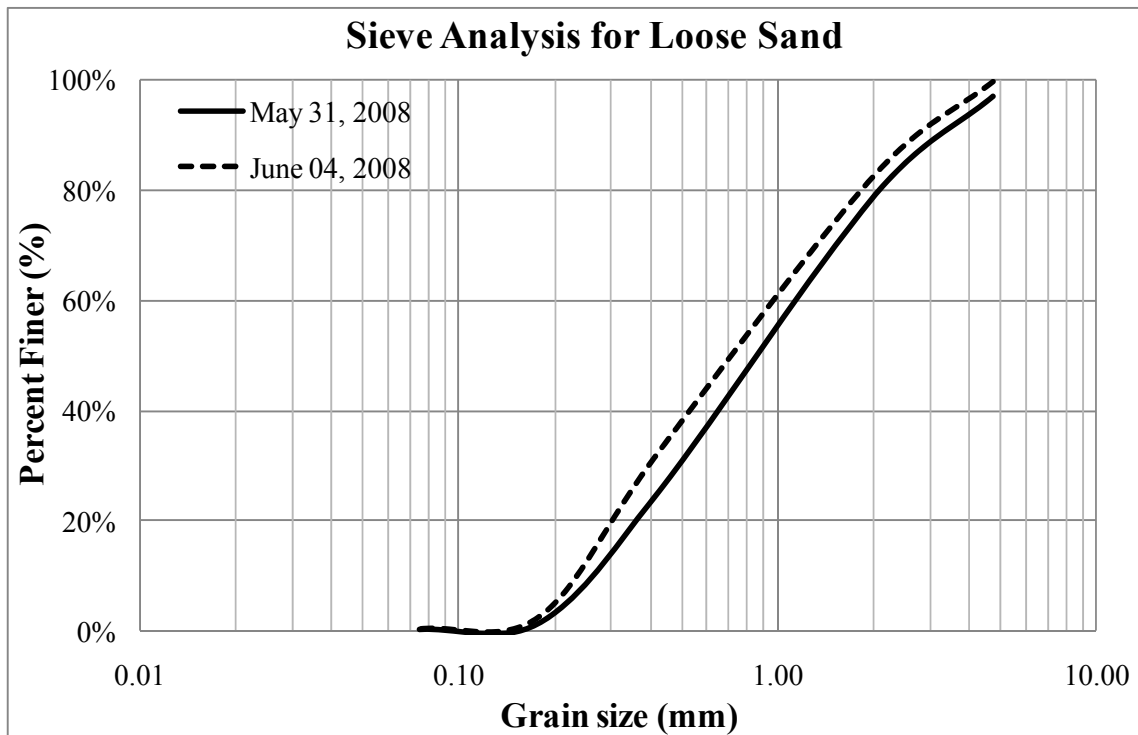
Figure 3.8. Particle size distribution curve for loose sand for pendulum tests

Terracon Consultants, Inc. performed the Standard Penetration Tests (Figure 3.9) and the average blow count was measured as 1 (blow/ft). The blow count of the soil with moisture content of 3.4% at 0.6m depth was W.O.H (weight of hammer) which means the split spoon sampler was advanced one foot depth due to the self-weight of the hammer without any single blow.

Saez Barrios (2010) conducted soil tests for the identical sand including density measurements, direct share tests and compaction tests. The dry unit weight of this soil was 17.28 kN/m^3 and the friction angle of the remolded sand was 34 to 36 degrees from direct shear tests and triaxial tests which can be different from the in-situ condition.

Figure 3.9. Standard penetration test (SPT) on loose sand and split spoon sampler

Figure 3.10. PENCEL pressuremeter test on the loose sand

A series of pressuremeter tests using the PENCEL unit were done before and
after the pendulum tests (Figure 3.10). The biggest difference of soil condition was water
contents of the soil. After the pendulum test, the average value of moisture contents was
measured as 8.4%, whereas it was 3.4% before the pendulum tests. As shown in Figure
3.11, the difference in moisture contents makes the later one with higher moisture
content stronger than the other in terms of the measured limit pressure and elastic
modulus. The reason might be the apparent cohesion from the suction of soil and the
surface tension of the water in the void of the soil particles. The detail locations of
Standard Penetration Tests and pressuremeter tests are indicated in Figure 3.5. The tests
results are summarized in Table 3.3.
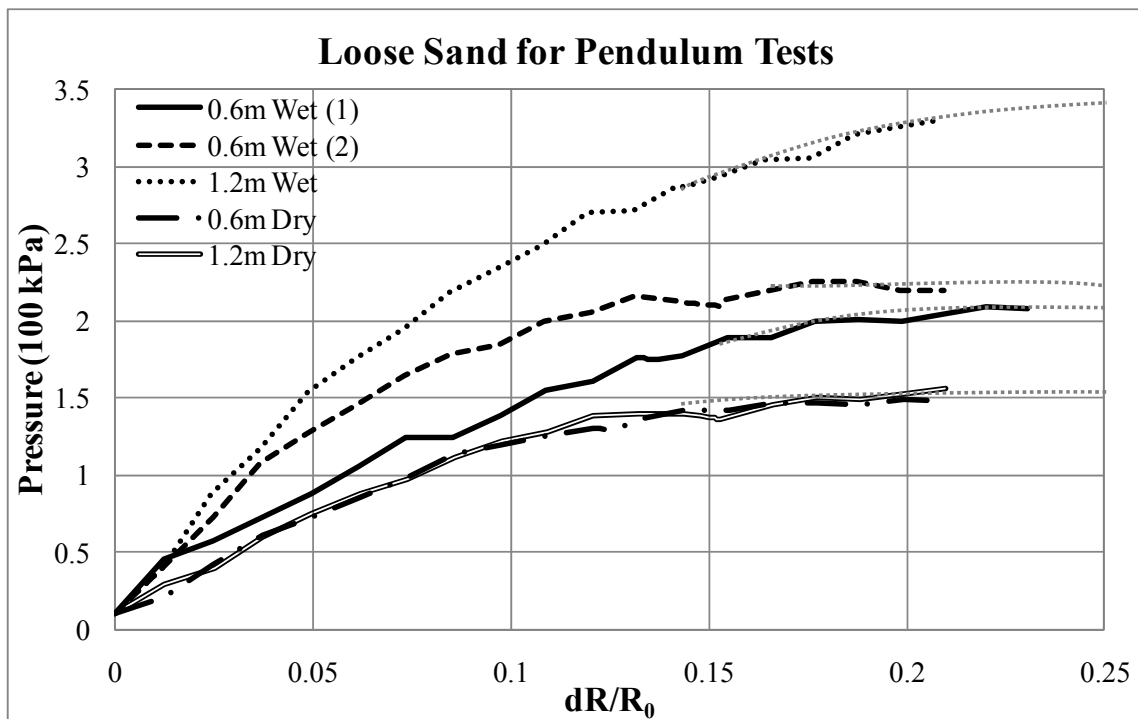
Figure 3.11. Pressuremeter test result for loose sand for pendulum tests

Table 3.3. Summary of the soil testing of loose sand for pendulum tests

Depth (m)	P_L (kPa)	E (kPa)	SPT N (blow/ft)	USCS	Water Contents (%)
0.6	150	1200	W.O.H.[*]	SP	3.4
1.2	160	1150	1		
0.6	215	1800	1	SP	8.4
1.2	340	2450	1		

* W.O.H : weight of hammer

3.1.3.2 Loose sand for the full-scale impact test on group of posts system

Bravo de los Rios (2010) conducted in-situ and laboratory tests for the loose sand for the full-scale impact test on group of posts system including index properties, pressuremeter tests, Standard Penetration Tests and direct shear tests. The ditch was excavated and filled with clean sand without any compaction. The soil condition seemed very loose and clean sand. The detail locations for the Standard Penetration Tests and the pressuremeter tests are shown in Figure 3.12.
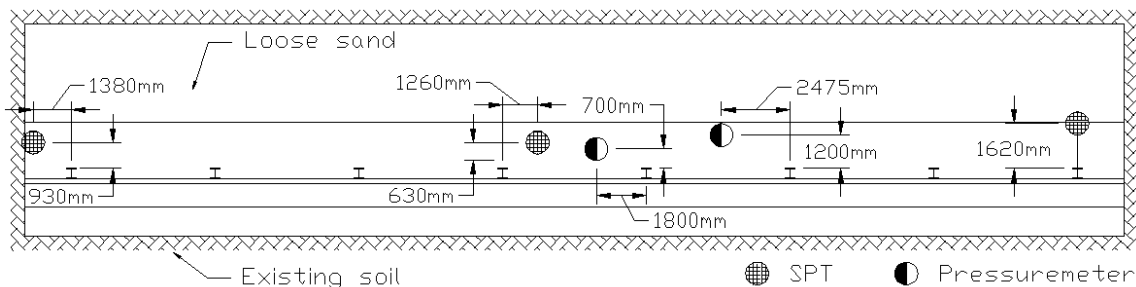
Figure 3.12. Soil testing locations for full-scale impact test
(After Bravo de los Rios 2010)

The average unit weight and dry unit weight of the soil using the sand cone method were measured as 17.6 kN/m^3 and 16.8 kN/m^3, respectively. The particle size analyses were performed in accordance with ASTM D 422-98 designation. According to the Unified Soil Classification System, the sand was classified as poorly graded sand (SP) (Figure 3.13).
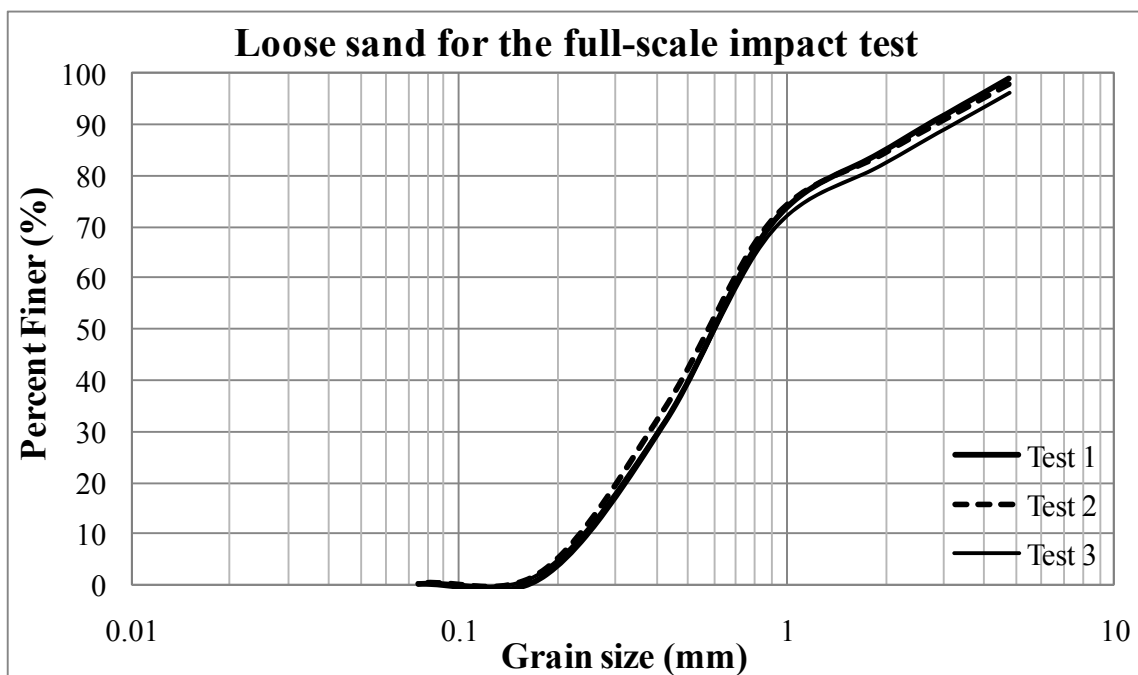
Figure 3.13. Particle size distribution curve for loose sand for full-scale impact test (After Bravo de los Rios 2010)

From the direct shear tests, the friction angle of the soil was measured as 29 degrees. The dilation angles were estimated as tangent, secant and small strain dilation angle. The averages of those are 4.3, 0.6 and -8.1 degrees, respectively. Since the phenomena of impact against the soil imbedded posts system is take place approximately

within 0.5 sec, the dilation angle for small strain may be the reasonable estimation for analyzing the impact. Though the phenomenon is a large-strain, loose sands under the impact tend to contract rather than dilate. Moreover, the soil particles near the post around the ground level are dispersed at the impact. Thus it seems that the dilation angle for small strain can be the reasonable value on this problem.
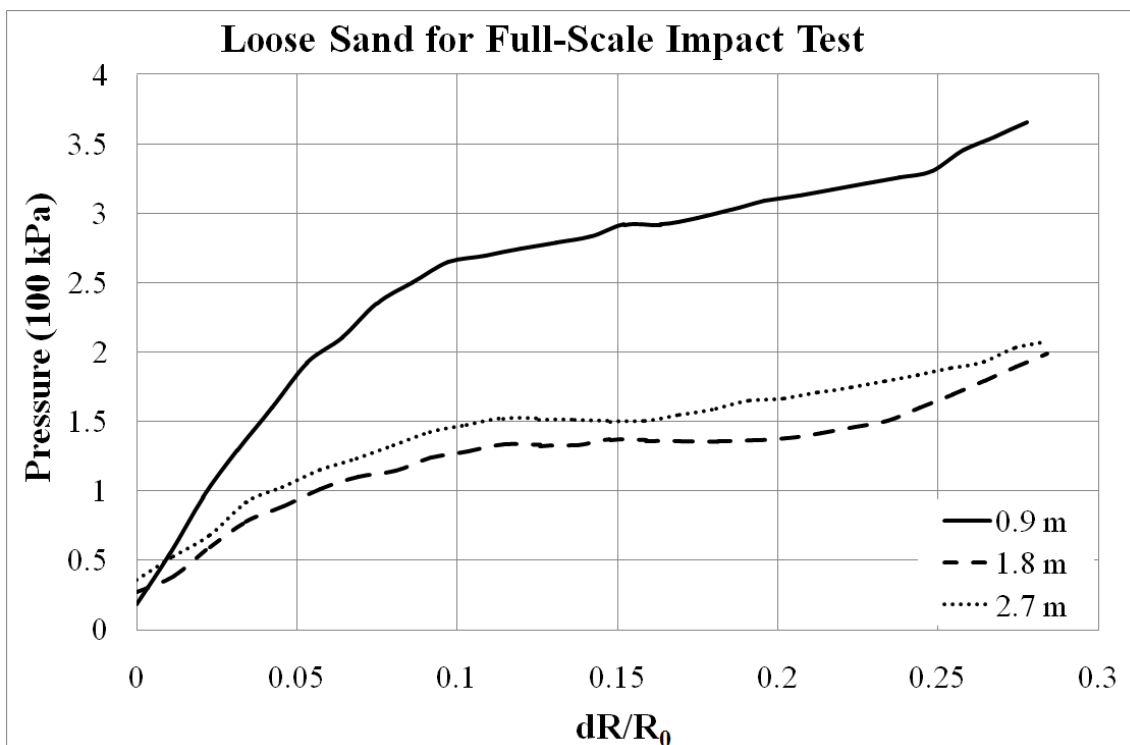
Figure 3.14. Pressuremeter tests results of loose sand for full-scale impact test (After Bravo de los Rios 2010)

The results of the pressuremeter tests using the PENCEL pressuremeter are shown in Figure 3.14 and Table 3.4. The results of Standard Penetration Tests (SPT)

conducted by Terracon Consultants, Inc are summarized in Table 3.4. From the results, the soil strength at ground level to 1.0 m depth is higher than the strength at the deeper locations. The reasons are that the top portion of soil was more compacted and the soil near the ground level was desiccated due to exposal. The soil was dumped and filled without compaction. However, the top part of soil was compacted by the walking and moving of people and the construction equipments. As described in the previous Section, the strength of the desiccated soil increased due to the suction.

Table 3.4. Summary of the soil testing of the loose sand for full-scale impact test (After Bravo de los Rios 2010)

Depth (m)	P_L (kPa)	E (kPa)	SPT (N) (blow/ft)	Water Contents (%)
1.0	295	2800	1.5	3.5
2.0	190	1300	W.O.H*	5.0
3.0	175	1500	W.O.H*	5.5

* W.O.H : weight of hammer

3.1.4 Hard clay

The proposed bogie tests were conducted at the next to the main taxiway of the TTI Proving Ground. Since it is somewhat difficult to construct a clay pit in a short period, the tests were taken place using the existing hard clay instead of a man-made clay pit. This is the reason that a bogie was used as a mean of impact mass instead of a pendulum.

The existing hard clay was made an around 4 m wide flat level to insure the drivability of the bogie. Then the single post and the group of posts system were driven.

Terracon Consultant, Inc. drilled four boreholes for Standard Penetration Tests and Shelby tube sampling. The PENCEL pressuremeter tests were conducted (Figure 3.15). The locations of post systems, boreholes and pressuremeter tests are shown in Figure 3.16.

Figure 3.15. Pressuremeter test for hard clay for the bogie tests

The dry unit weight of hard clay and the unit weight of hard clay were measured as 16.9 kN/m^3 and 19.5 kN/m^3. According to the Unified soil classification system, the soil was classified as lean clay (CL) or fat clay (CH). From the two sample using Shelby tube were subjected to test the unconfined compressive strength by a pocket type soil penetrometer (Figure 3.17) and undrained shear strength by a hand held shear vane tester (Figure 3.18). Though those two soil testing methods give not an exact soil strength parameter but an approximate one, these methods give an idea to classify cohesive soils

in terms of consistency. Also soil tests for index properties and unconfined compress test were performed using the Shelby tube samples by Terracon Consultant, Inc. The logs of boring including SPT and Shelby tube sampling can be found in Appendix A.
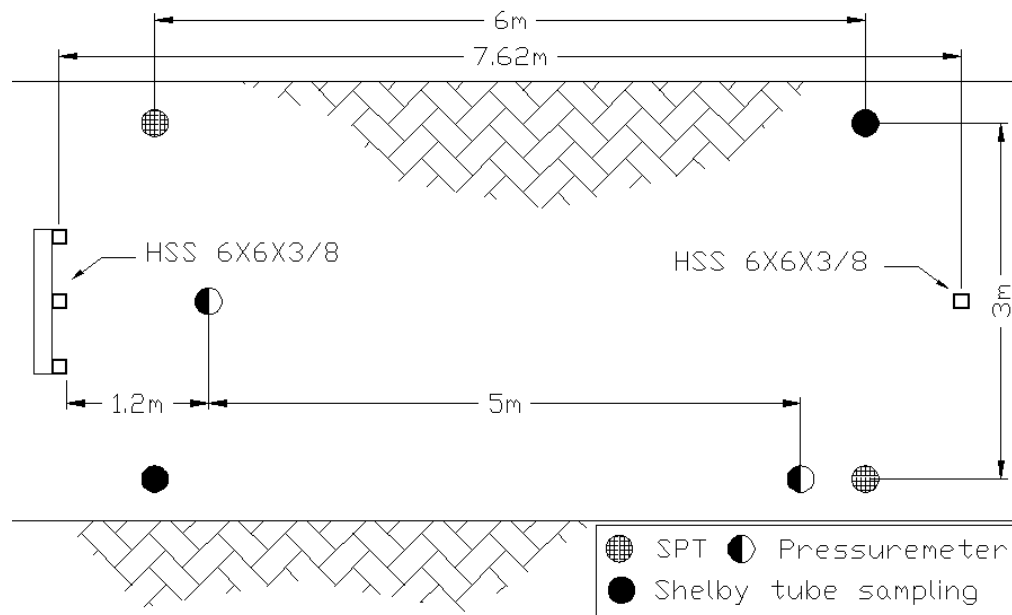
Figure 3.16. Soil testing locations of hard clay for the bogie tests

Figure 3.17. Pocket type soil penetrometer

Figure 3.18. Hand held shear vane tester
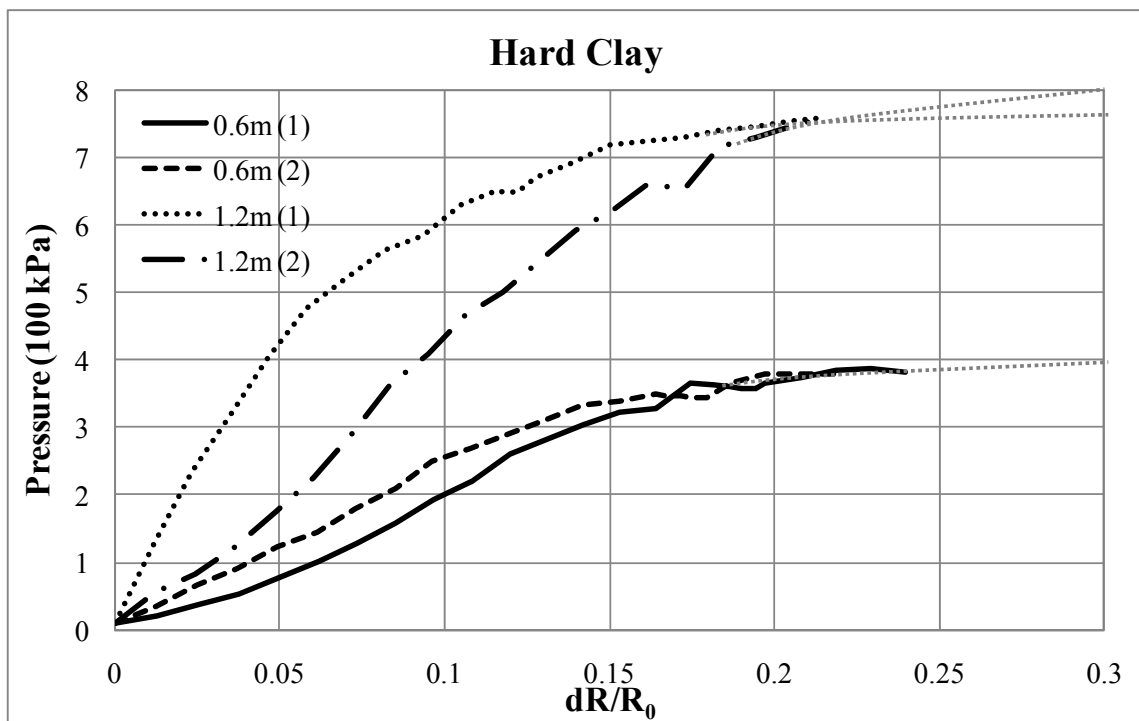
Figure 3.19. Pressuremeter tests results of the hard clay for the bogie tests

The results of pressuremeter tests and summary of the test results are shown in Figure 3.19 and Table 3.5, respectively. The hand vane measured the undrained shear strength (S_u) and the pocket penetrometer and the unconfined compression test measured compressive strength (q_u). The compressive strength of cohesive soil is twice of the undrained shear strength. The comparison of the measured undrained shear strength using the three methods is shown in Table 3.6.

Table 3.5. Summary of the soil testing of hard clay for the bogie tests

Depth (m)	P_L (kPa)	E (kPa)	SPT N (blow/ft)	Hand Vane S_u (kPa)	Pocket Penetrometer q_u (kPa)	Water Contents w (%)	Compressive Strength q_u (kPa)	USCS
0.6	390	2400	7.5	107	335	17	290	CL
1.2	785	6300	13.5	140 +	470	17	430	CH

Table 3.6. Comparison of the measured undrained shear strength (kPa)

Depth (m)	Hand vane	Pocket penetrometer	Unconfined compression test
0.6	107	163	145
1.2	140 +	235	215

3.1.5 Soil strength category matrix

To develop the proposed design guideline, a soil strength category and the typical values of physical and engineering properties of each strength category were required for the numerical simulation purpose. The proposed soil strength categories allow classifying

soils in terms of the soil strength. The category consists of seven strength classes with the range of physical and engineering soil properties for sand and clay. The mean values of the range of soil properties in each category were determined as the representative values of the each strength class. The proposed soil strength category matrix is shown in Table 3.7.

The proposed soil strength category was used as a mean of developing the design guidelines for the anti-ram post system directly embedded in soil. The typical strength parameters including elastic modulus (E), unit weight of soil (γ), friction angle (φ), dilation angle (ψ), cohesion (c), undrained shear strength (S_u), limit pressure from pressuremeter (P_L), and Standard Penetration Test (SPT) blow count (N) were used for the proposed numerical simulations. The soil strength category is not only a important means of achieving the object of this work but also a simple soil strength classification method using the results of either SPT or pressuremeter test. In addition, this work may be a helpful method to give an idea about general soil strength properties to the engineers and contractors who may work in unfavorable conditions including the use of unsophisticated equipment.

For the proposed study, the soil strength category was developed by using numerical simulations with LS-DYNA, literature reviews and the previous soil tests. The preliminary soil strength category was developed based on mainly the literatures of Terzaghi et al. (1996), Das (1998), and Briaud (1992) stated in Section 2.1. The preliminary one covered most of soil properties except the dilation angle of sandy soil.

Table 3.7. Soil strength category matrix

Sand:

Number	Strength	Representative values for Numerical simulation							Range of values		
		E (MPa)	γ (kN/m³)	φ (Degrees)	ψ (Degrees)	c (kPa)	P_L (kPa)	N (bpf)	E (Mpa)	N (bpf)	P_L (kPa)
1	Loose	2	17	27	-10	1	200	1	0-3	0-5	0-250
1.5	Medium/Loose	4	17.3	29	-8	1.3	500	10	3-6	5-15	250-750
2	Medium	8	18	33	-5	2	1000	20	6-10	15-25	750-1250
2.5	Dense/Medium	12	19.1	35	1	2.5	1500	30	10-14	25-35	1250-1750
3	Dense	16	20	36	5	3	2000	40	14-18	35-45	1750-2250
3.5	V.Dense/Dense	20	20.6	37	7	3.3	2500	50	18-26	45-50	2250-2500
4	Very Dense	32	22	40	10	4	2500+	50+	>26	> 50	> 2500

Clay:

Number	Strength	Representative values for Numerical simulation					Range of values			
		E (Mpa)	γ (kN/m³)	S_u (kPa)	N (bpf)	P_L (kPa)	S_u (kPa)	E (Mpa)	N (bpf)	P_L (kPa)
1	Soft	1.5	17	11	0	50	0-21	0-2.5	0-3	0-100
1.5	Medium/Soft	3.5	17.5	30	4	200	21-40	2.5-4.8	3-5	100-260
2	Medium	6	18	50	6	320	40-72.5	4.8-8.8	5-9	260-460
2.5	Hard/Medium	11.5	19.1	95	11	600	72.5-116	8.8-14.3	9-15	460-775
3	Hard	17	20	137.5	18	950	116-166	14.3-21.3	15-24	775-1225
3.5	V.Hard/Hard	25.5	21.1	195	30	1500	195-166	21.3-25	24-30	1225-1500
4	Very Hard	34	22	250	30+	>1500	> 200	> 25	> 30	> 1500

E	Elastic modulus	c	Cohesion
γ	Unit weight	P_L	Limit pressure
φ	Friction angle	N	SPT blow count
ψ	Dilation angle	S_u	Undrained shear strength

For numerical modeling purpose, dilation angles of sand were needed. Since the dilation angle of soil can be changed by soil density, stress state, and so on, the dilation angles of each soil were obtained by back calculations from the numerical simulations of the pendulum tests and the full-scale test on a single post and the direct shear tests. It is because dilation angle of soil is changing along with shearing process. On the contrary to the actual behavior, dilation angle of Drucker-Prager model in LS-DYNA is a constant value. Thus dilation angles for numerical simulations have to be determined depending on the soil behavior of simulated phenomena.

3.2 Full-scale impact test – July 2007

As stated in introduction, most of vehicle barriers are embedded in large reinforced concrete foundations. However, vehicle barriers directly embedded in soil are needed for occasion demands, especially in an urban area. Therefore the development of the design method for a single post embedded in soil was proposed by the results of the experiments and the numerical simulations.

The full-scale impact test on a single post in the very dense crushed limestone was performed in accordance with designation SD-STD-02.01, Revision A. on July 18, 2007 at the Texas Transportation Institute (TTI) Proving Ground. The test vehicle and the single post are shown in Figure 3.20. The impact condition designation was K-12 that is identical to the impact condition designation M50 and the penetration designation P1 of ASTM F 2656-07. The objective of this test is to arrest a 6,800 kg vehicle at 80 km/h with less than one meter of dynamic penetration.

Figure 3.20. Full-scale M50 impact test on single post (Alberson et al. 2007)

3.2.1 Design of experiment

In order to design a single post system capable to contain the impact of the condition designation M50, a pressuremeter test using the TEXAM pressuremeter unit was conducted. Since there was no design procedure for the first test, the post was designed using SALLOP: Simple Approach for Lateral Loads on Piles (Briaud 1997) with the assumptions based on literatures. The design consisted of using the peak dynamic force measured in the previous impact tests on a post, dividing it by a dynamic amplification factor assumed to be equal to 5 based on experience. This brought the design back to a pile subjected to a static lateral load.

The post was designed to resist 250 kN of static lateral load within 25 mm of lateral displacement at the impact level using SALLOP method. The behind of this design was that an approximated peak impact force during the M50 test was 1,250 kN. Dynamic amplification factor, DF is defined as the ratio of the peak dynamic force, $F_{Dynamic}$ of a single post and the maximum static resistance, F_{Static}. The dynamic amplification factor assumed as 5 based on Dewey Jr. et al. (1983) and Eggers and Hirsch (1986). Thus the design static resistance was determined as 250 kN by Eq. (3-2).

$$DF = \frac{F_{Dynamic}}{F_{Static}} \qquad (3\text{-}1)$$

$$\left(F_{Static}\right)_{Design} = \frac{F_{Dynamic}}{DF} = \frac{1250\,\text{kN}}{5} = 250\,\text{kN} \qquad (3\text{-}2)$$

where, DF= Dynamic amplification factor

F_{Static} = Static resistance

$(F_{Static})_{Design}$ = Equivalent design static load

$F_{Dynamic}$ = Peak dynamic force

The detailed calculation using SALLOP method for design of the single post can be found on Appendix B. The Standard Penetration Test blow count (N) was measured as 50 (blow/ft). The pressuremeter elastic modulus and limit pressure from the TEXAM pressuremeter test were 46.7 MPa and 2,500 kPa, respectively.

3.2.2 Test set up

As stated in the previous section, the soil condition was the aged very dense crushed limestone. The post embedment was designed 3 m whereas the depth of the crushed

limestone ditch was 2.13 m (Figure 3.21). Thus a drilled hole with diameter of 9.14 m was augured to 3.05 m below the ground surface to allow the design post embedment as shown in Figure 3.22. After placing a 4m long wide flange I beam in the pre-drilled hole, the hole was filled with the same material, the crushed limestone and compacted using a mechanical tamper. Details of the installation are shown in Figure 3.21 through Figure 3.24. The post was a wide flange I beam W14x109 (14 inches wide and weighing 109 lbs/ft of length).
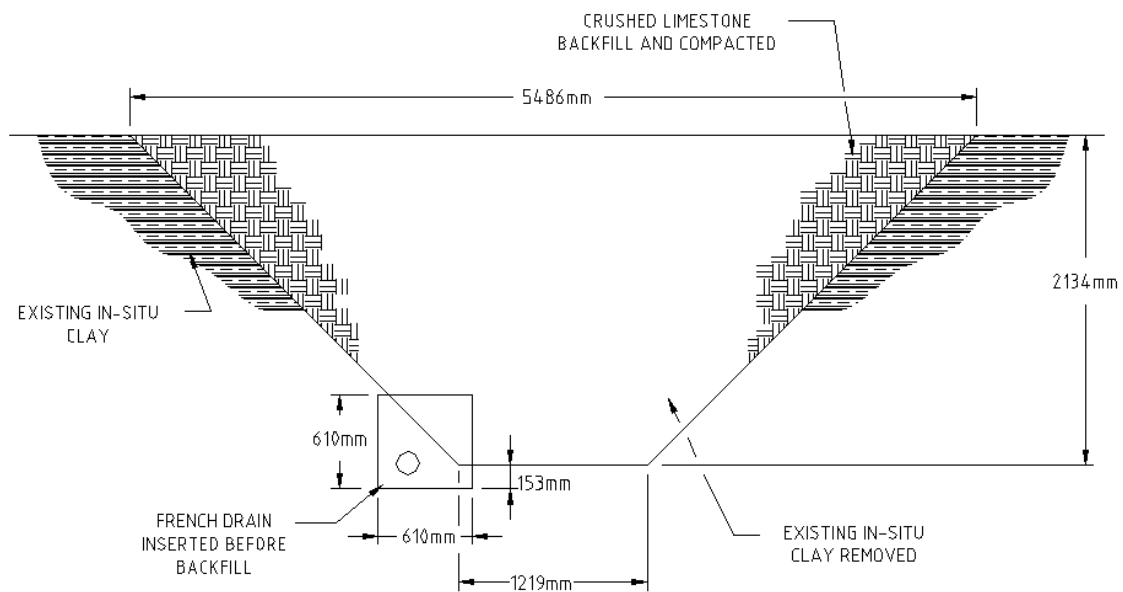
Figure 3.21. The existing crushed limestone ditch (After Alberson et al. 2007)
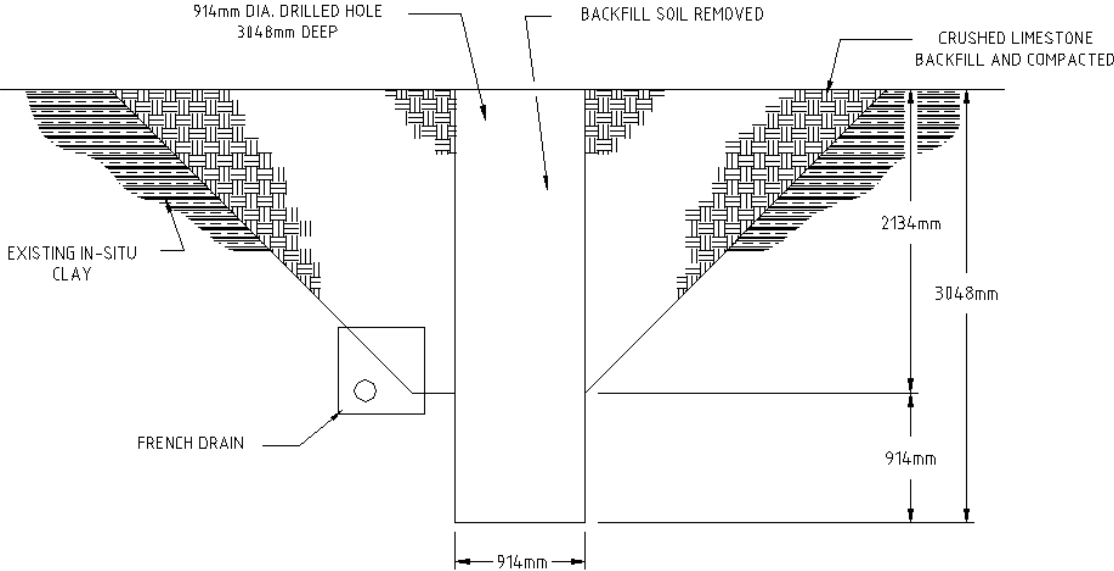
Figure 3.22. Drilled hole for post installation (After Alberson et al. 2007)
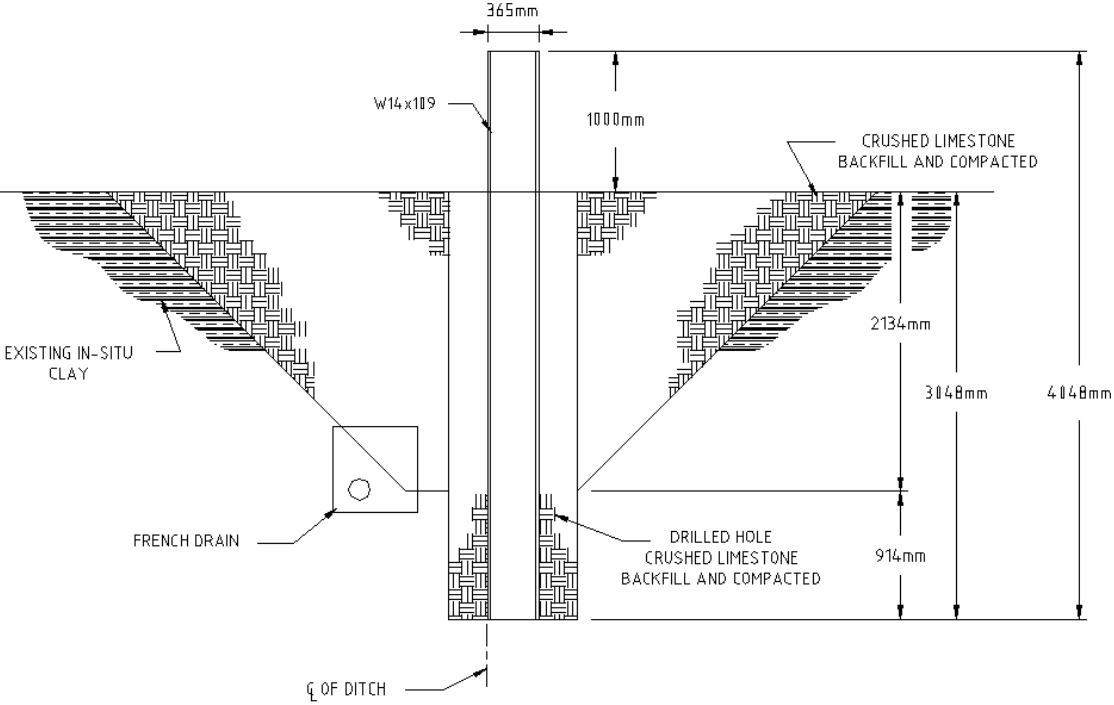
Figure 3.23. Detail of the direct embedded single post (After Alberson et al. 2007)
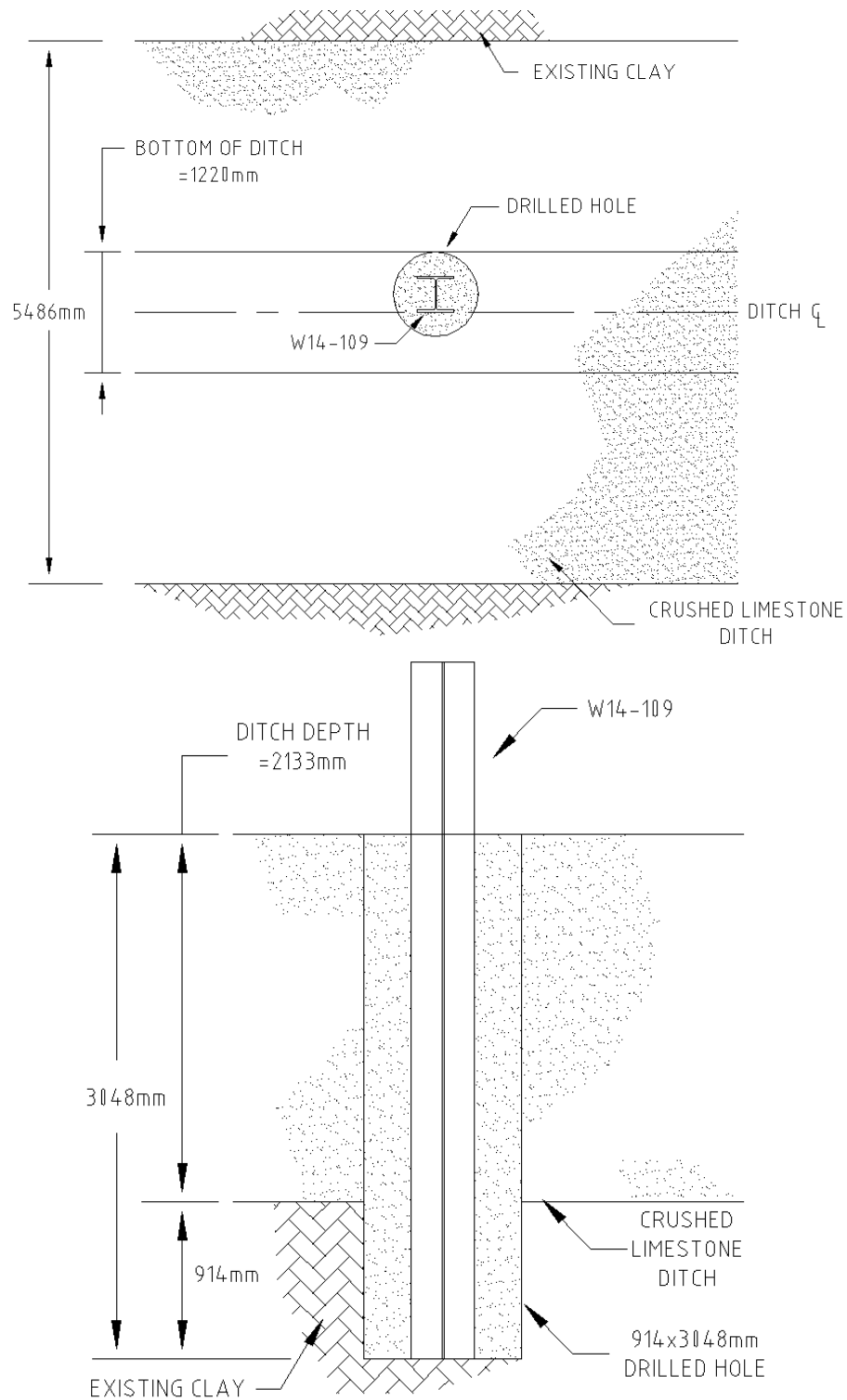
Figure 3.24. Plan and front elevation view of installed single post

For the full-scale impact test on a single post, a 1998 Navi-Star 4700 single-unit flatbed truck was used as a test vehicle (Figure 3.25). Test inertia weight of the truck was measured as 6,813 kg. The height to the lower edge of the truck front bumper was 51 cm, and the height to the upper edge of the front bumper was 80 cm. The additional dimensions and information on the truck are shown in Appendix B. The truck was guided into the installed single post using the cable reverse tow and guidance system, and was released to be free-wheeling and unrestrained just before the impact. (Alberson et al. 2007).

Figure 3.25. Vehicle used for the impact test (Alberson et al. 2007)

Two triaxial accelerometers were installed on the flatbed of the vehicle at the center of mass of the vehicle and the location of rear axle. Accelerometers on the behind

of the post and soil behind the post were placed to measure the accelerations of the post and soil during the impact. Details of accelerometers installation on the post and the soil are shown in Figure 3.26. The accelerometer on the behind of post was attached at the ground level and those for the soil was placed 152mm beneath the ground surface. In order to measure the dynamic displacement of the targets attached on the vehicle and the post, films were captured using three high-speed cameras.
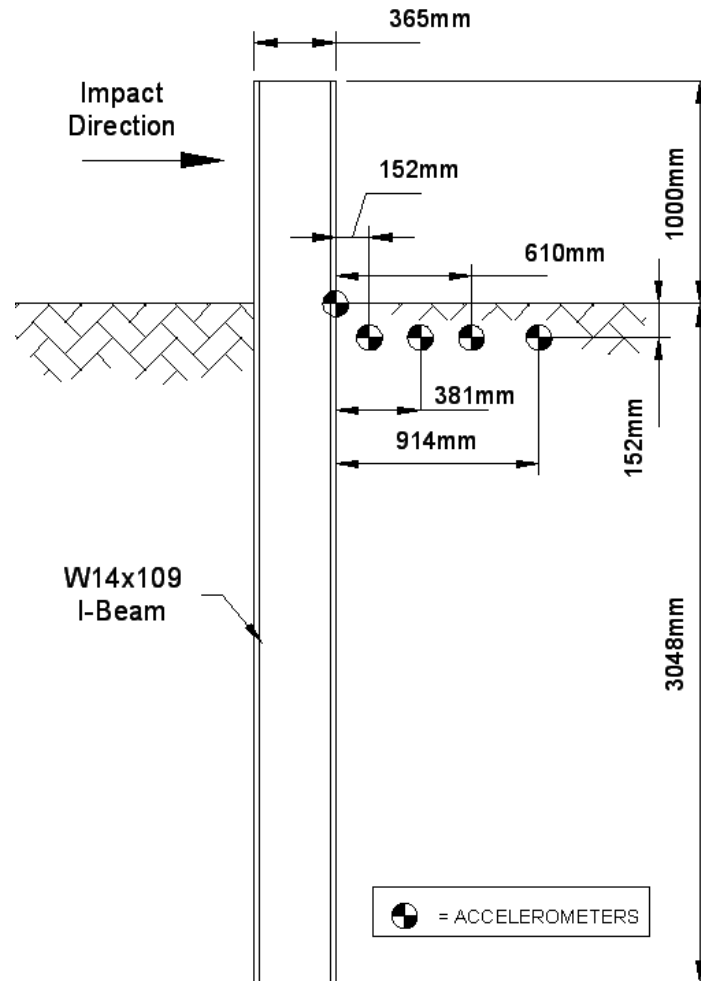
Figure 3.26. Installed accelerometers behind the post and the soil

3.2.3 Test results

The single-unit flatbed truck, traveling at an impact speed of 78.5 km/h, impacted the single post direct embedded in the very dense crushed limestone. The single post brought the truck to a complete stop with 0.04 m of the dynamic penetration. According to ASTM F 2656-07, the dynamic penetration of the vehicle is measured as from the inside edge of the post to the maximum dynamic penetration point of the leading lower bed edge of the vehicle. The dynamic penetration versus time history from the film analysis is shown in Figure 3.27.
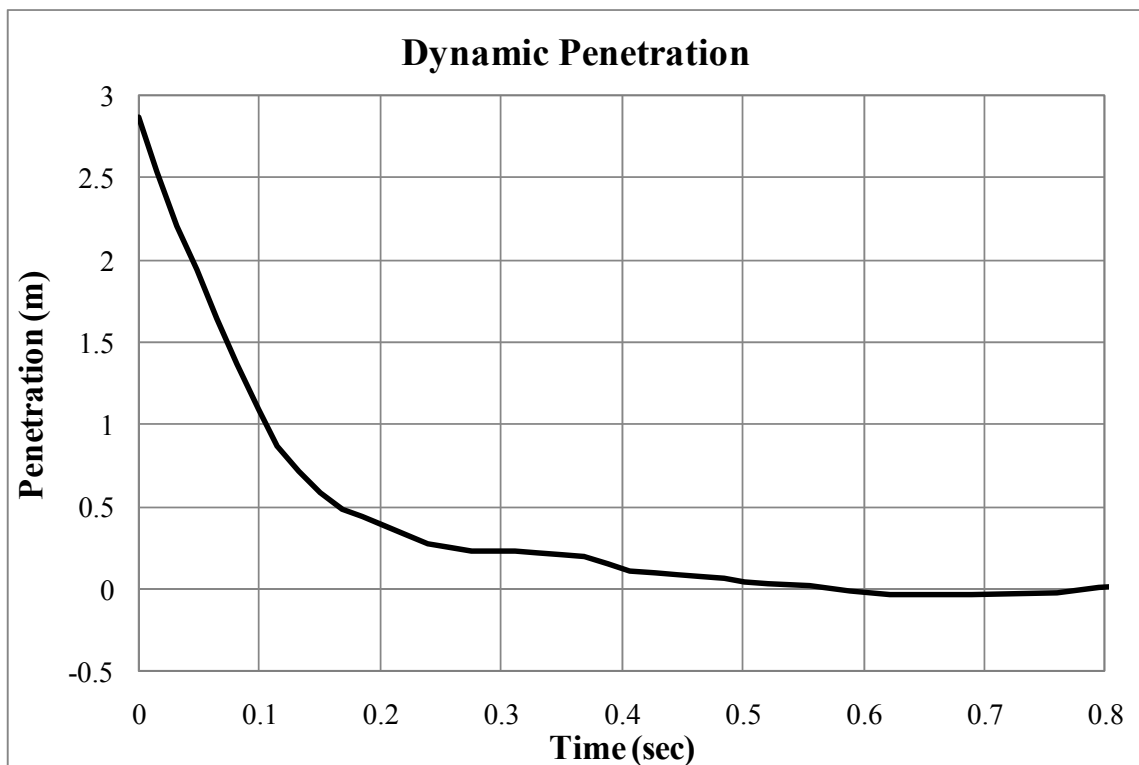
Figure 3.27. Dynamic penetration history of the full-scale test on a single post

At the beginning of the impact, the front bumper began to wrap around the post and the post began to deflect toward the inside at 0.005 s after impact. The front axle contacted the pier at 0.055 s. The cargo bed began to rise at 0.153 s and forward motion of the cargo ended with the cargo bed having penetrated 0.04 m beyond the inside edge of the post at 0.206 s. The vehicle rebounded and came to rest 0.68m forward of the inside edge of the post. Sequential photographs of the test period can be found in Appendix B.

The post and vehicle after the impact are shown in Figure 3.28 and Figure 3.29. The post rotated 9 degrees away from the impact. The post deflection on the impact side was measured as 127 mm and the depth of a gap between the post and soil was 610 mm. On the opposite side, the deflection was 41 mm and the depth of a gap was 450 mm.

The soil heaving was observed for a distance of 3 m toward the inside from the impact face of the post and 1.7 m on either side of centerline of the post. Soil movement at the surface as observed on the overhead high-speed film extended approximately 2.54 m longitudinally behind the post. The wedge of soil was measured to be approximately 107.4 degrees from the rear flange of the post, almost symmetric about the center line of the post. The displaced soil dimensions are shown in Figure 3.30 (Alberson et al. 2007).

Though three high speed cameras captured films of the impact, the post displacement could not be obtained from the films. The reason is that the front side of the vehicle wrapped around the post. Hence the wrapped front side of the vehicle hided the target attached on the side of the post from the angle of camera.

Figure 3.28. The single post after the impact (Alberson et al. 2007)

Figure 3.29. Vehicle after the impact (Alberson et al. 2007)
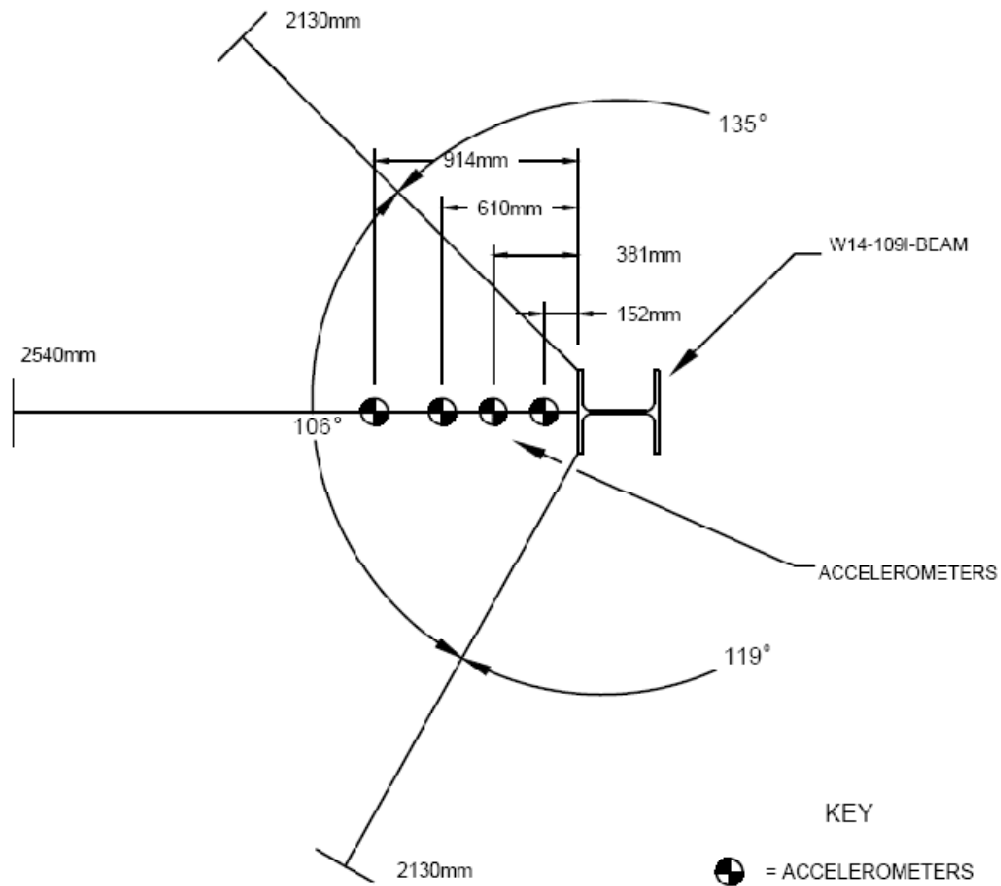
Figure 3.30. Extent of surface soil displacement (After Alberson et al. 2007)

The three-directional accelerations of vehicle at the C.G. (center of gravity) and the rear of the vehicle were measured. The rear one was attached on the flatbed above the rear axle. In this section, the longitudinal accelerations are mainly stated and analyzed rather than the lateral and vertical accelerations. The reason is that the longitudinal behavior is the most dominant in this particular test, especially in the post system and the soil.

Peak longitudinal decelerations of the vehicle at the C.G and the rear were 42g at 0.095s, and 36g at 0.12 s, respectively. The maximum 50-msec average acceleration of vehicle at the C.G. and the rear were 21g and 20g. The raw and 50-msec average acceleration histories of vehicle measured at the C.G. and the rear of truck are shown in Figure 3.31 and Figure 3.32. The rear accelerometer was installed as a back-up of the on at the C.G. of vehicle. Since the acceleration histories of those two shown in Figure 3.33 are similar, the measured vehicle accelerations can be considered as creditable.
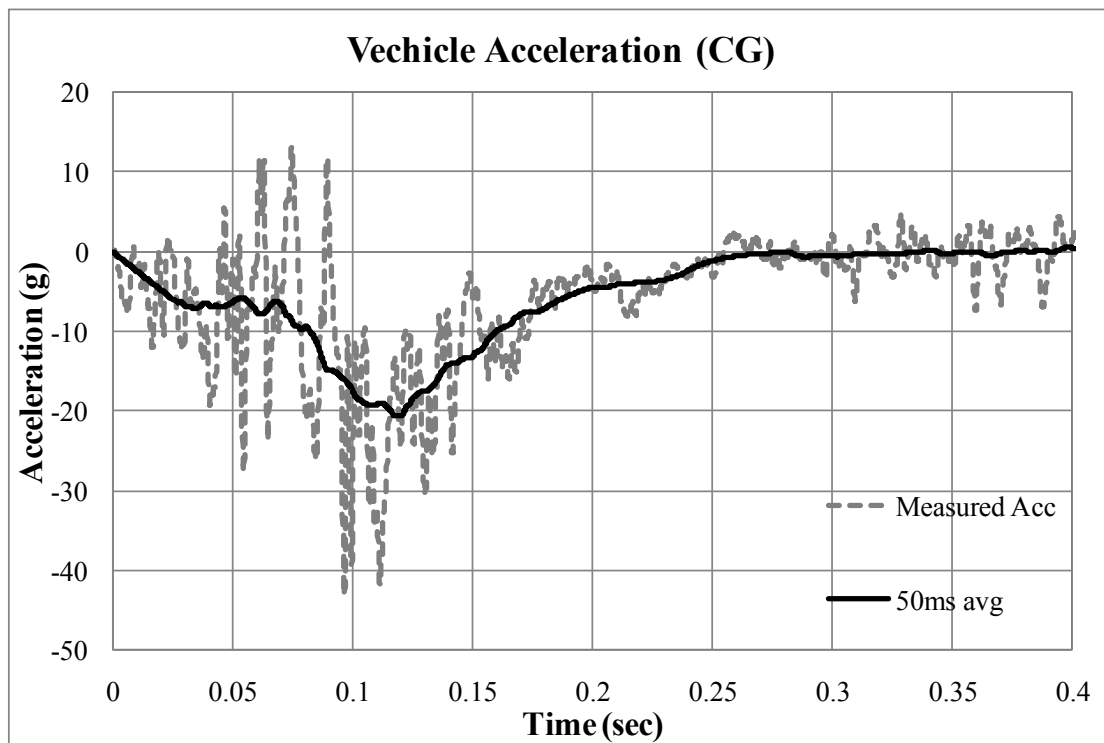
Figure 3.31. Raw and 50msec average acceleration of vehicle measure at the C.G.
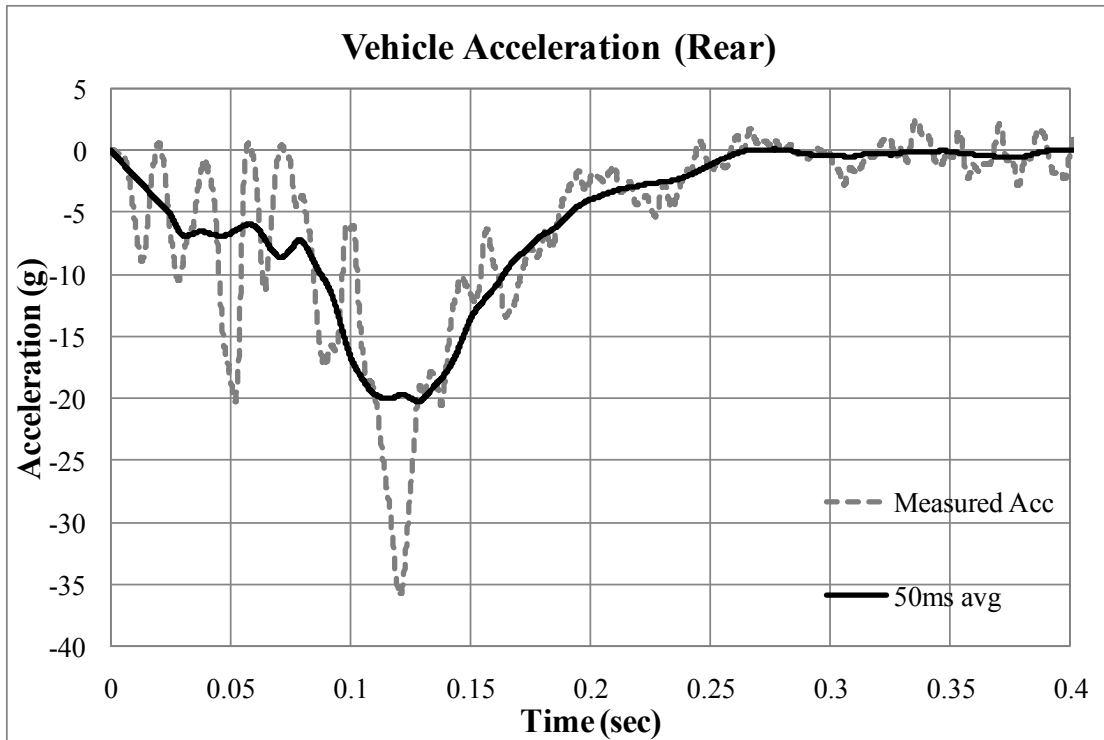
Figure 3.32. Raw and 50msec average acceleration of vehicle measure at the rear

As shown in Figure 3.33, as soon as the impact, the deceleration of vehicle increased. At 0.25 sec to 0.75 sec, the deceleration stayed constant and began increasing at 0.75 sec. At first, the bumper and the surface of truck contacted with the post and at 0.75 sec the front axle and the frame of the truck began contacting to the post. Between the time 0.25 sec and 0.75 sec, there was no significant increment of resistance that is the reason of deceleration, since there was some crushable area between the bumper and the engine, axle or main frame of the truck.
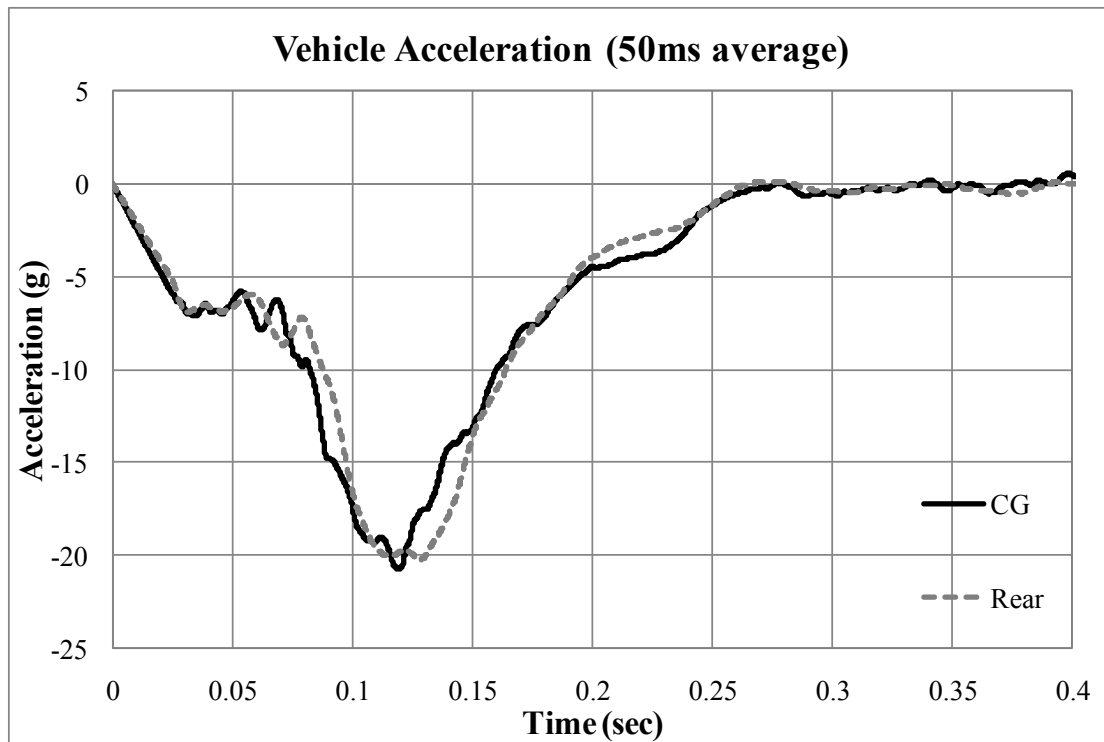
Figure 3.33. 50msec average acceleration of vehicle measure at the C.G and the rear

The impact force acting on the post can be calculated using Newton's second law that force is equal to change in momentum over time. Since there was negligible change in mass of vehicle during the test, the longitudinal impact force is obtained from the mass of vehicle times the acceleration of vehicle at certain time (Eq 3-3). Thus 50-msec average impact force history shown in Figure 3.34 was obtained. The peak impact force was 1,350 kN at 1.20 sec.

$$F(t) = M(t) \times a(t) \qquad (3\text{-}3)$$

where, $F(t)$ = impact force at time, t

$\quad M(t)$ = mass of vehicle at time, t

$\quad a(t)$ = acceleration of vehicle at time, t
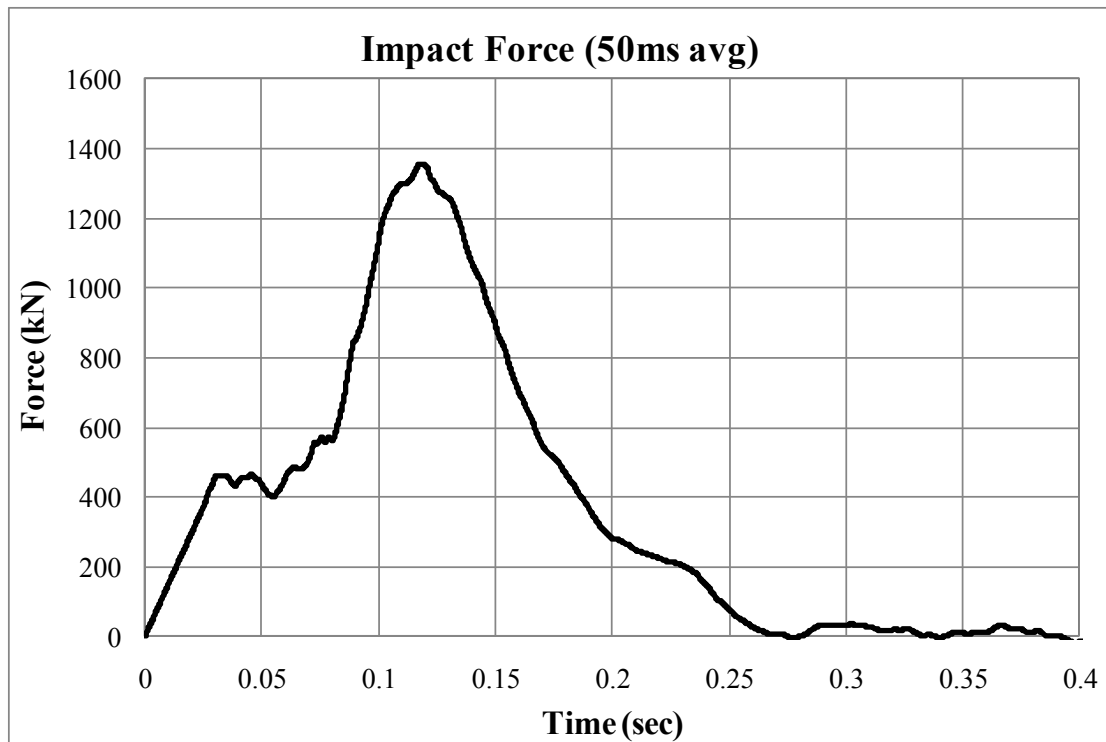
Figure 3.34. Impact force during the M50 test on the single post

The histories of vehicle velocity-time and displacement-time can be obtained by integration and double integration of the vehicle acceleration data. The initial velocity of vehicle was 78.5 km/h and the initial displacement was zero. The vehicle velocity and the displacement histories are shown in Figure 3.35 and Figure 3.36. The truck began rebound at 0.25 sec according to the vehicle velocity history. The maximum displacement of the vehicle measured at the C.G was 2.5 m.
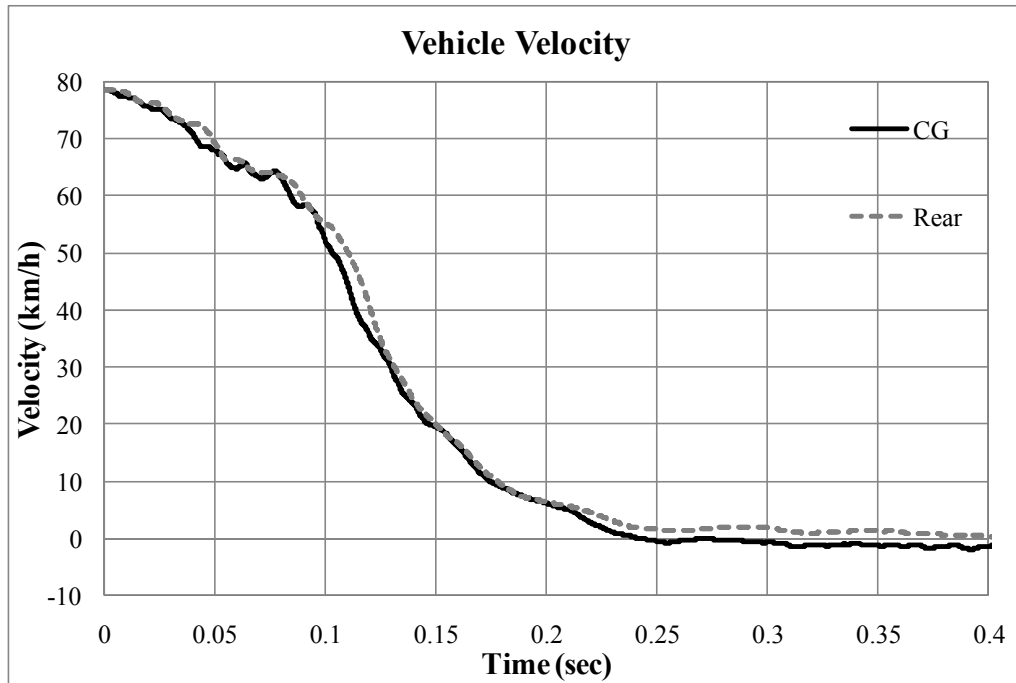
Figure 3.35. Vehicle velocity from the measured acceleration data
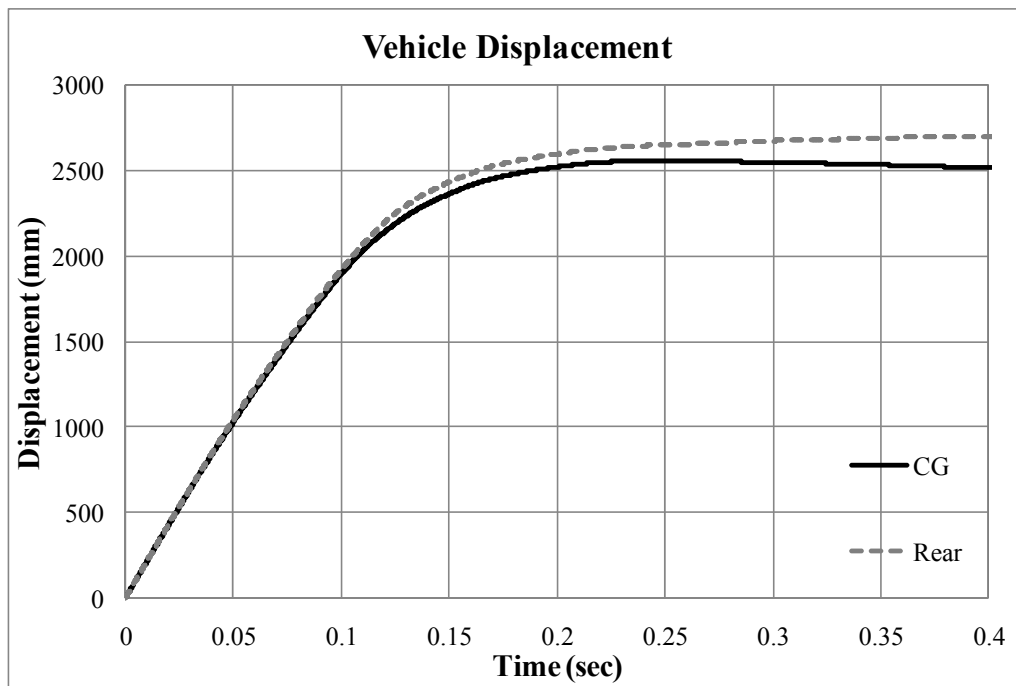
Figure 3.36. Vehicle displacement from the measured acceleration data

The acceleration-time histories of the post and the soil are shown in Figure 3.37. Peak 50-msec average accelerations in the soil at incremental distances of 152mm, 381 mm, 610 mm, and 914 mm were 4 g, 4 g, 3g and 2.5g, respectively. The maximum 50-msec average acceleration of post was 5.5g. Figure 3.38 and Figure 3.39 show the velocity-time histories and displacement-time histories calculated by integration and double integration of the acceleration data. The velocity and displacement histories of the soil at distance of 381mm seem unrealistic. It can be caused either the noise of the raw data or the failure of accelerometer due to the impact. The maximum velocity and displacement of post at the ground level were 4.3 m/sec and 0.36 m, respectively.
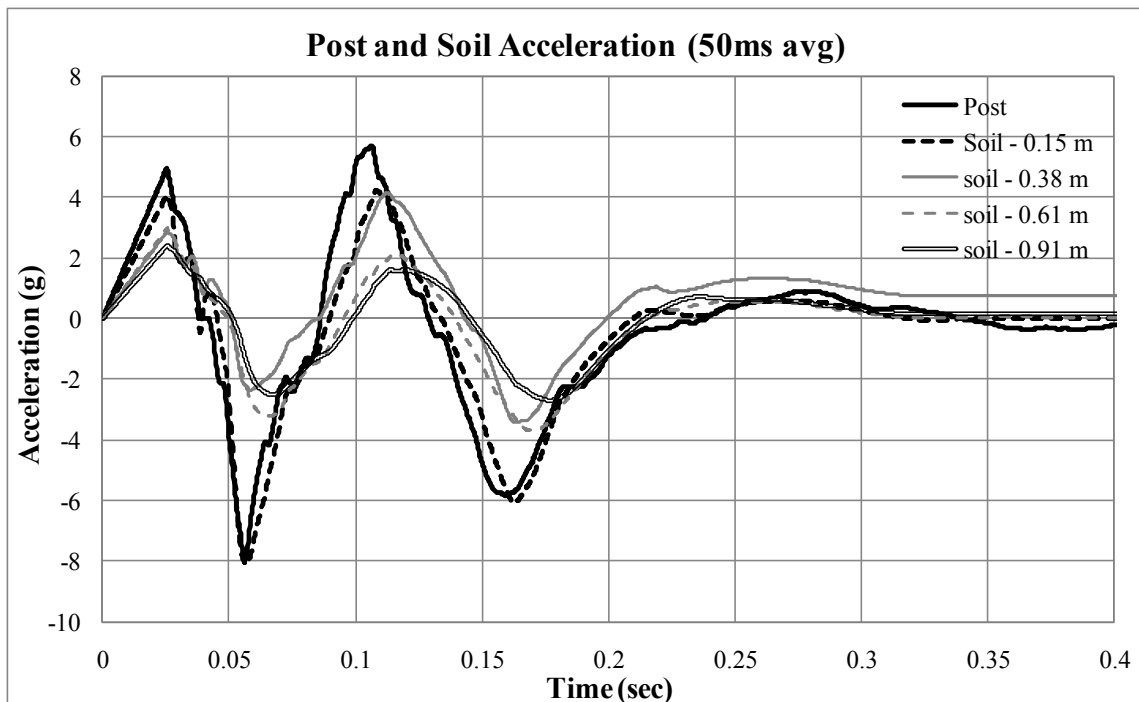
Figure 3.37. Acceleration histories of the post and the soil
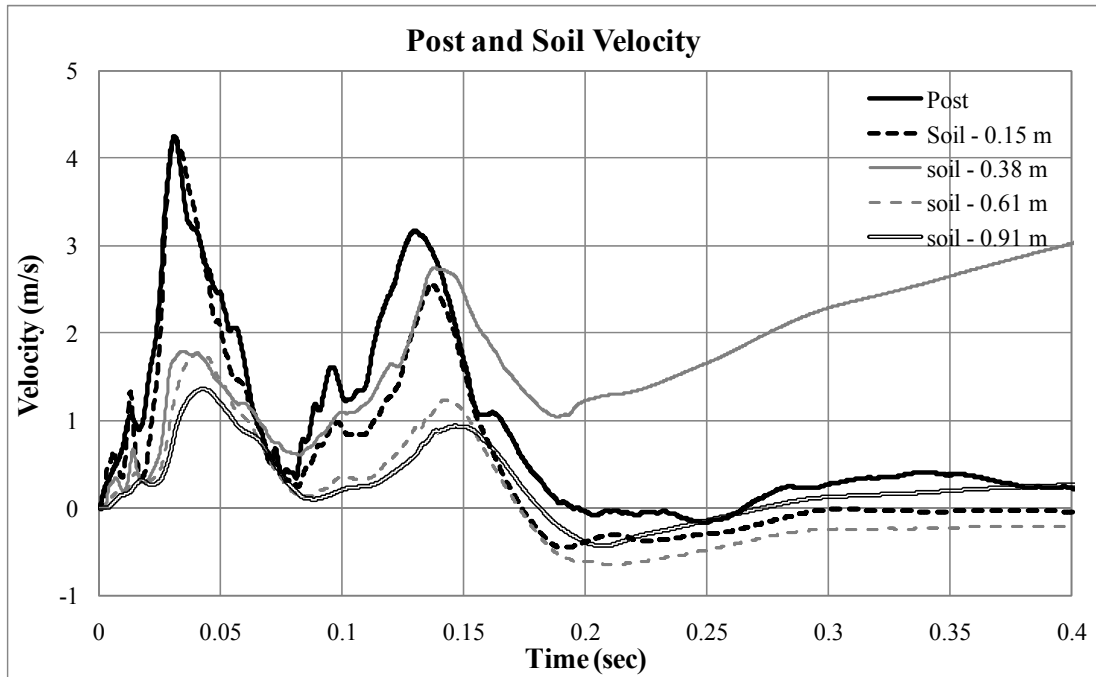
Figure 3.38. Velocity histories of the post and the soil
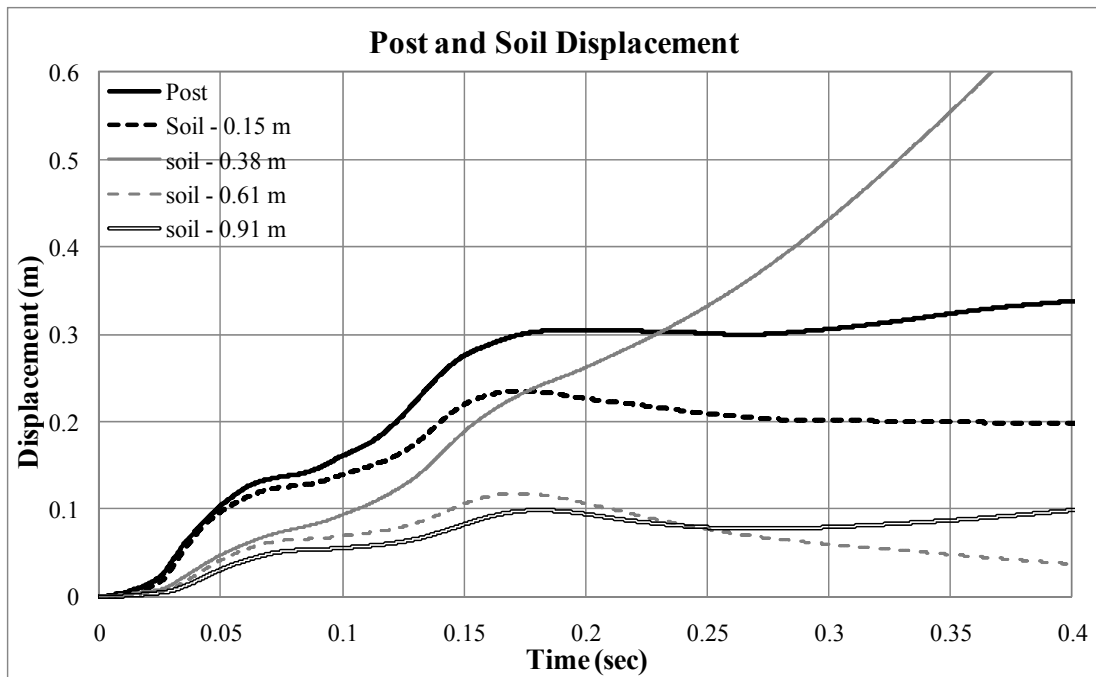
Figure 3.39. Displacement histories of the post and the soil

3.2.4 Data analysis

If the soil just behind the post accelerated at the same level with the post and the acceleration of the soil at the distance of 2,540mm and further was negligible as shown in Figure 3.30, the trend of decay of the soil acceleration as a function of distance from the post would be obtained as shown in Figure 3.40. There were the four main inflection points on the acceleration-histories of the post and the soil behind the post shown in Figure 3.37. The data points in Figure 3.40 was picked from those four inflection points in the acceleration-histories of the post and the soil and normalized.
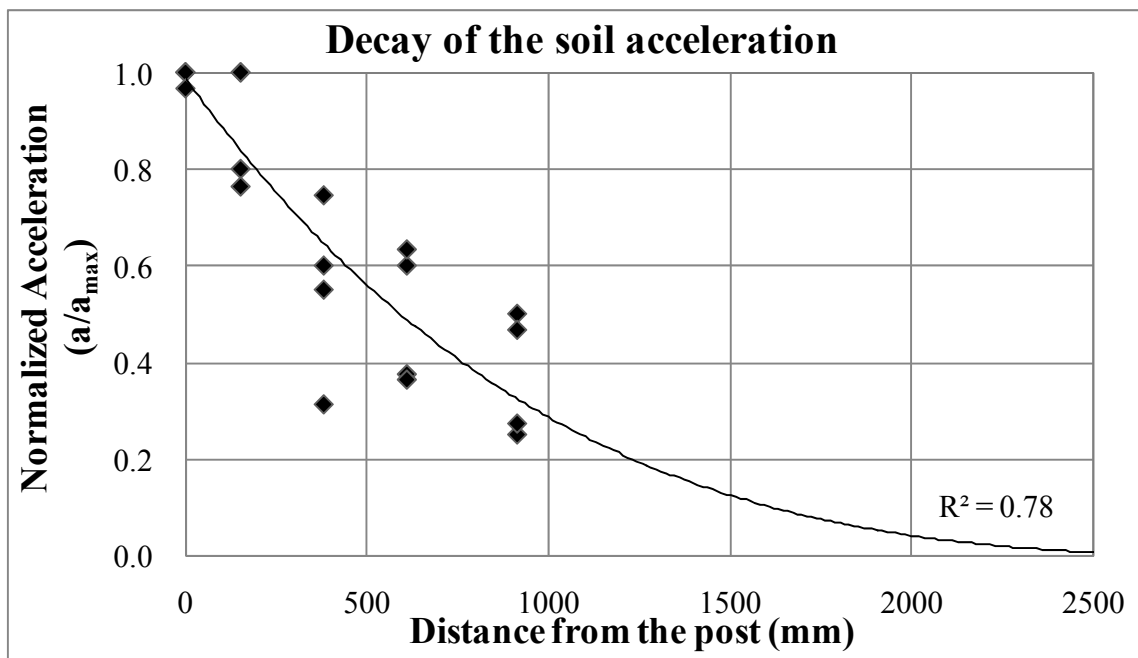
Figure 3.40. Decay of the soil acceleration as a function of distance from the post
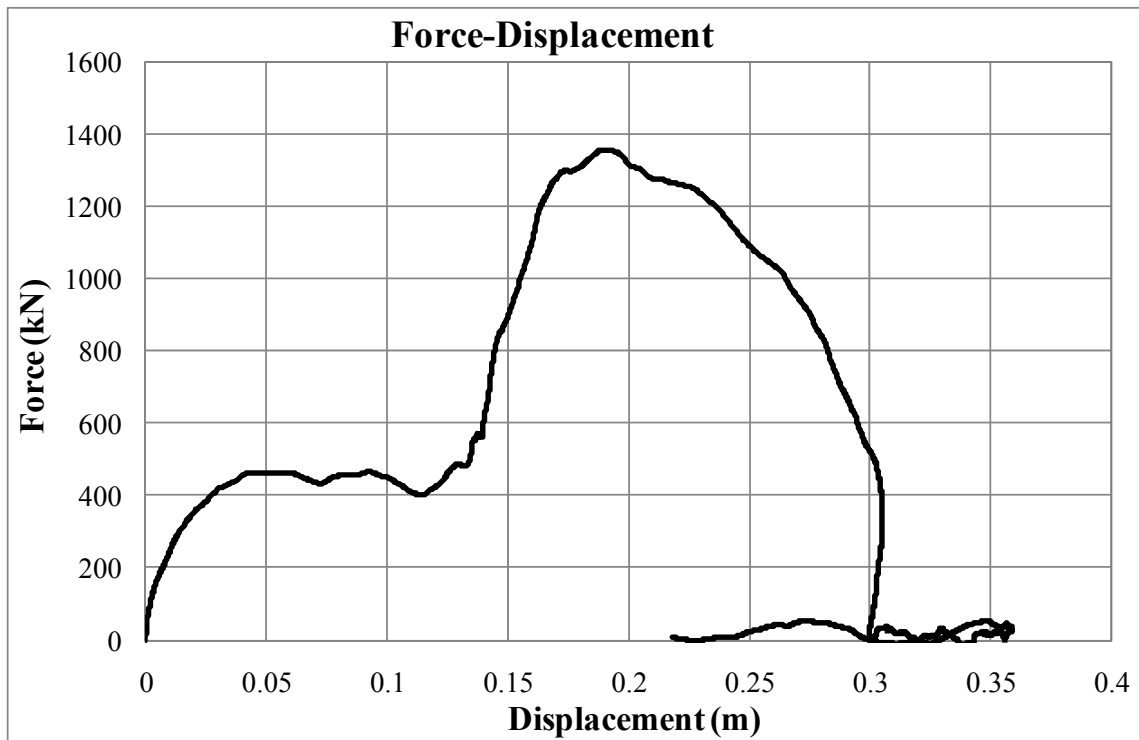
Figure 3.41. Impact force versus displacement

The impact force versus displacement is shown in Figure 3.41. As stated in the previous, the impact force is calculated using Newton's second law and the displacement of the post is calculated by double integration of the post acceleration data. Note that the displacement measured not that at the impact point but at the ground level. Thus the real displacement at the impact location would be bigger than the displacement shown in Figure 3.41.

In this test, the dynamic amplification factor, DF is the ratio of the maximum dynamic force, 1,350 kN and static resistance, 250 kN. Hence, dynamic amplification factor, DF was calculated as 5.4 that is 8% bigger than the design assumption of 5.

3.2.5 Conclusions

The single post embedded in the very dense crushed limestone met the requirements for condition designation M50 and penetration rating P1 in accordance ASTM F2656-07. The 4m-long W14X109 post 3m embedded in the very dense crushed limestone brought the vehicle to a complete stop with 0.04m of dynamic penetration. The actual impact speed was 78.5 km/h and the mass of vehicle was 6813 kg.

The peak impact force from the acceleration data was 1,350 kN. Dynamic amplification factor was 5.4. The accelerations of the soil behind the post decreased to zero at the 2,500 mm of distance from the post. However, dynamic factor and size of mobilized soil wedge may be changed as a functions of impact velocity, mass of truck, soil stiffness and strength, post stiffness and strength, post embedment depth, post cross section, etc.

3.3 Pendulum tests – June 2008

Though full-scale impact testing is the best way to predict the behavior of post and soil under lateral impact loads, it is very difficult to conduct lots of cases due to restrictions such as cost and time. Thus a set of miniature impact tests using pendulums were performed on June 2 through 6, 2008 in two different soil conditions: the loose sand and the medium dense crushed limestone at a pendulum test facility located at the Texas Transportation Institute (TTI) Proving Ground shown in Figure 3.42. The pendulum tests were designed based on the dimensional analysis in Section 3.3.1.
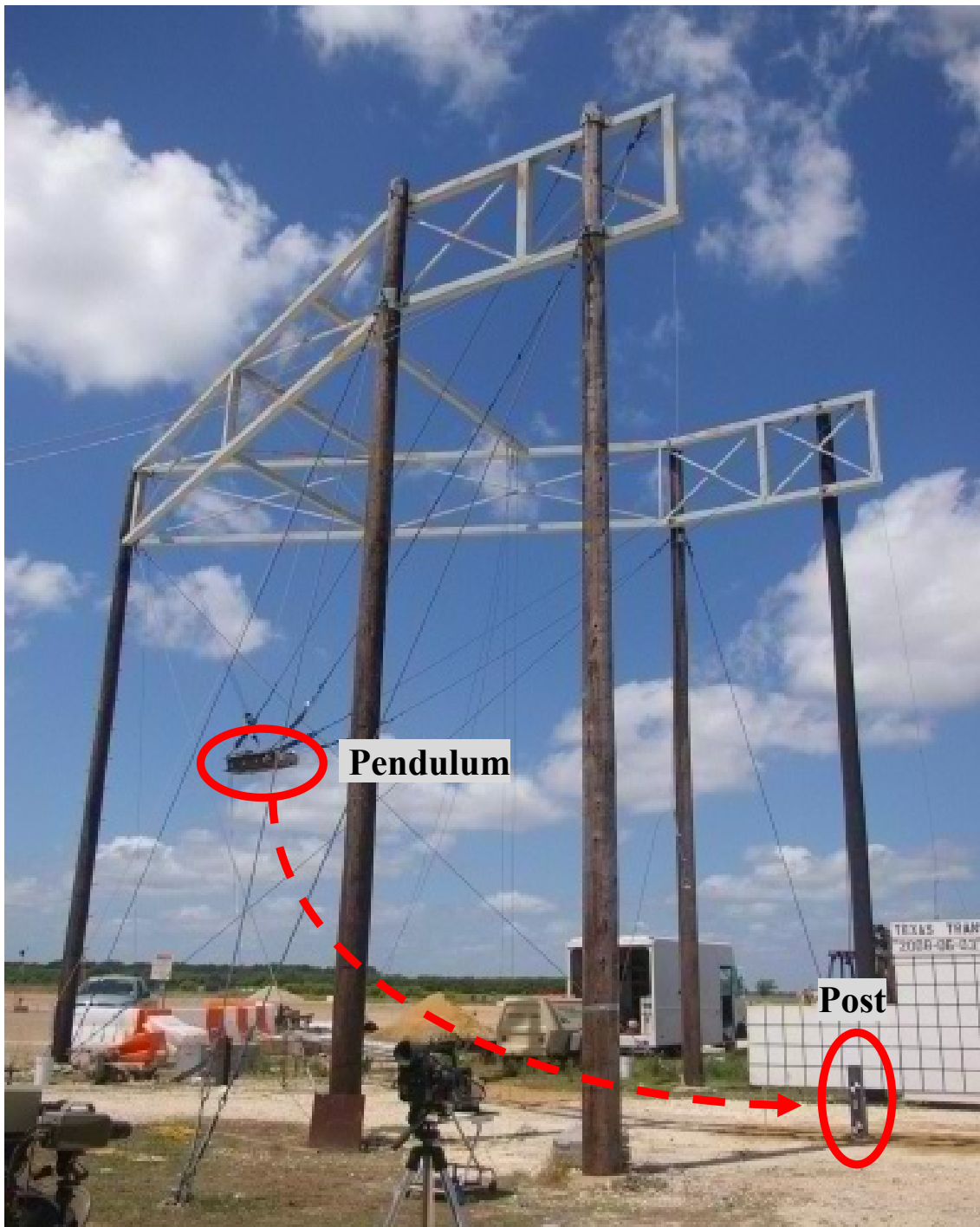
Figure 3.42. Pendulum test facility at Texas transportation Institute Proving Ground

Figure 3.43. Model test using a pendulum with 860 kg of mass

Two pendulums with 250 kg (550 lb) and 860 kg (1900 lb) of mass were used for the impact tests in the loose sand and the medium dense crushed limestone. A pendulum test with 860 kg mass is shown in Figure 3.43. The impact speeds of the pendulum were 8 km/h (5 mph), 16 km/h (10 mph) and 36 km/h (22.5 mph). According to the law of conservation of energy, the impact velocity can be controlled by changing the drop height of the pendulum. Accelerometers were installed on both the post systems and the pendulums to capture the motion of the post and to estimate the impact force. In order to measure the deflection of the posts, the films from a high-speed camera were analyzed.
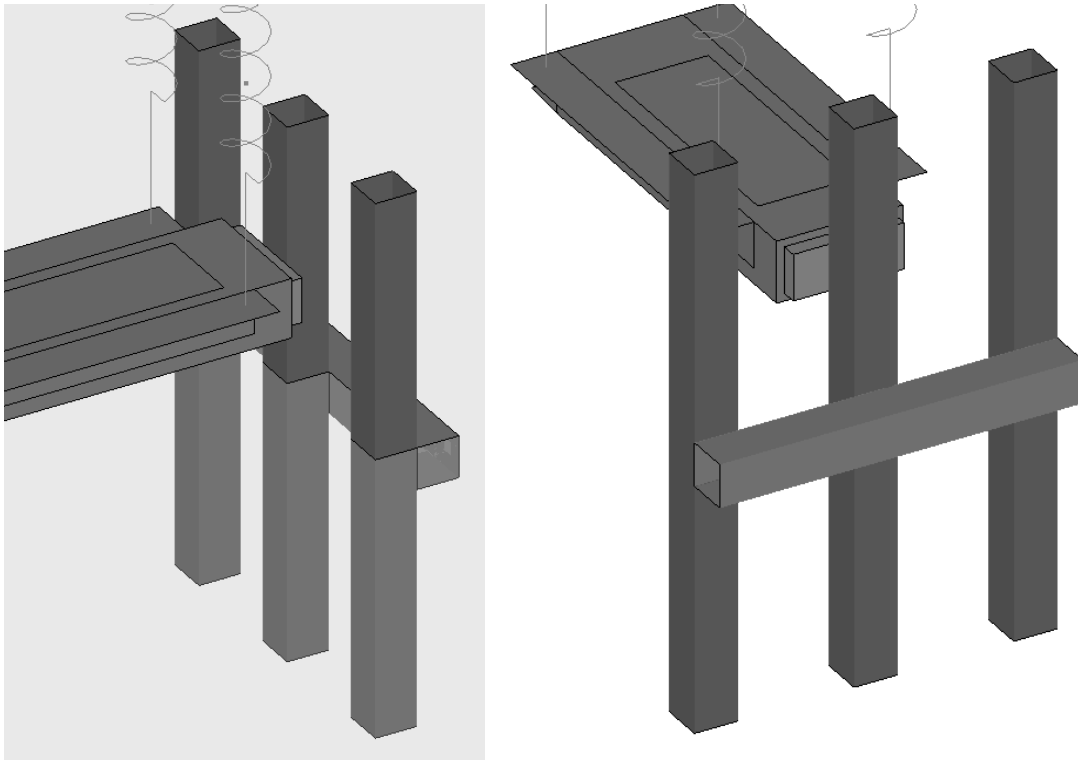
Figure 3.44. A row of three posts with a beam (three side by side posts)

In order to evaluate the group effect, three kinds of post systems were tested for the loose sand. As stated in the previous section, if the soil is strong enough, a single post directly embedded in soil can resist against a truck impact within the allowable penetration of vehicle. However, in the most of soil conditions including loose sands and soft clays, a single post system is not capable to contain truck impact. Thus evaluating the group effect was needed to complete the proposed design method.

Two kinds of group of posts systems were designed. The one is a row of three posts (three side by side posts) connected with a beam at the ground level shown

in Figure 3.44. The other is two rows of six posts (3 by 2 group of posts) connected with beams shown in Figure 3.45.

Also static load tests were take place prior to the impact tests to compare the static resistance and the dynamic resistance of each post system including single posts and group of posts systems.
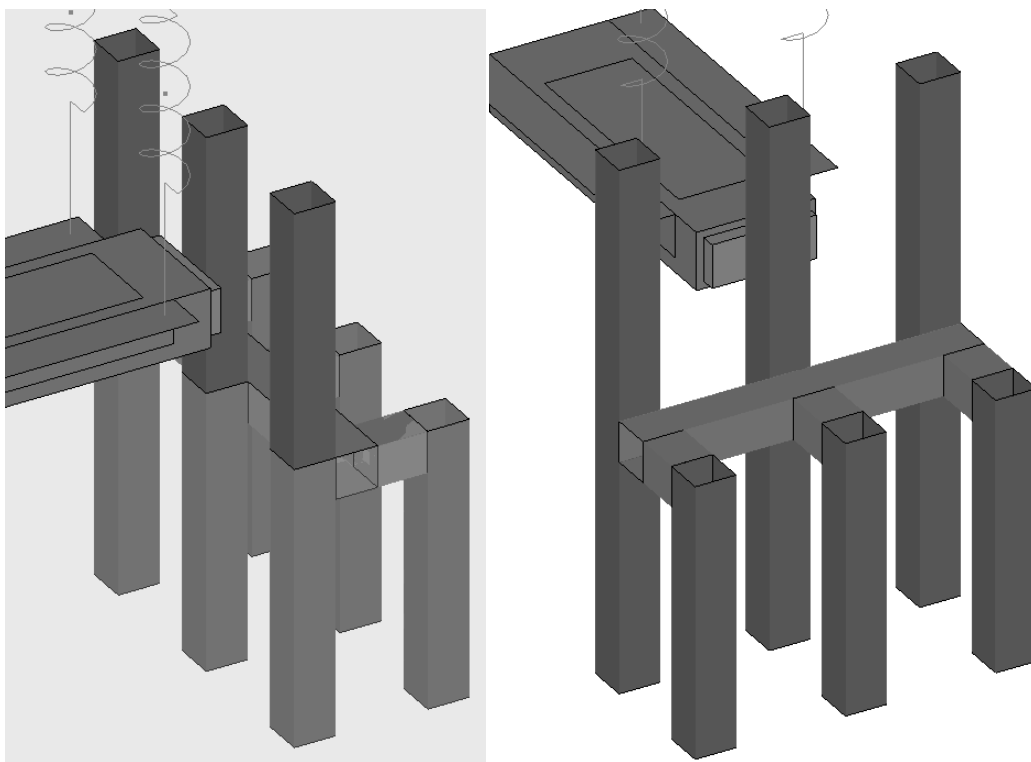
Figure 3.45. Two rows of six posts with beams (3 by 2 posts)

A model test matrix for the post system in medium dense crushed limestone and loose sand is shown in Table 3.8. A typical test sequence is stated as follows:

1. Prepare the pendulum pit

2. Install post system by either driving or backfilling

3. Static lateral load test on the opposite direction to the impact direction

4. Rearrange the post position

5. Model impact tests with the intermediate velocity (5 m/s) for single post or the maximum velocity (10 m/s) for group of posts systems

6. Remove the post system and reinstall with the same method of step 2

7. Model impact test with the minimum velocity (2.5 m/s) for single post

8. Rearrange the post position

9. Model impact test with the maximum velocity (10 m/s) for single post

Table 3.8. Test matrix of pendulum tests

Test number	Test type	Post system	Mass of pendulum (kg)	Impact velocity (m/s)	Remarks
S1	Static	Single Post			Backfilled
P1	Pendulum	Single Post	862	4.65	Backfilled
P2	Pendulum	Single Post	862	2.41	Backfilled
P3	Pendulum	Single Post	862	9.97	Backfilled
S2	Static	Single Post			Driven
P4	Pendulum	Single Post	250	4.94	Driven
P5	Pendulum	Single Post	250	2.50	Driven
P6	Pendulum	Single Post	250	10.10	Driven
S3	Static	Group of Posts (a row)	250		Backfilled
P7	Pendulum	Group of Posts (a row)	250	10.01	Backfilled
P8	Pendulum	Group of Posts (a row)	250	10.21	Backfilled
S4	Static	Group of Posts (two rows)			Backfilled
P9	Pendulum	Group of Posts (two rows)	250	9.83	Backfilled
S5	Static	Single Post			Backfilled
P10	Pendulum	Single Post	250	9.83	Backfilled

A duplicated group of posts with a row of three posts (P8) test was performed due to the problem on reading of the accelerations of the posts (P7). To compare the group effect for the impact loadings, a backfilled single post was installed and tested for both the static (S5) and the impact (P10).

3.3.1 Dimensional analysis

A basis for direct scaling of model tests to prototype prediction can be achieved based on dimensional analysis. The theory of dimensional analysis is based on Buckingham's theorem: *If an equation is dimensionally homogeneous, it can be reduced to a relationship among a complete set of dimensionless products* (Wood 2001).

Primary units are the minimum number of units required to describe the relationship among the variables. For mechanical system these are generally length [L], time [T] and either mass [M] or force [F] which come from the fundamental balance laws such as conservation of mass, conservation of energy, etc. In this study, length [L], Time [T] and force [F] was selected as the primary units for the dimensional analysis. A schematics drawing of full-scale impact test and model test using either a pendulum or a bogie can be found in Figure 3.46.

According to Munson et al. (1998), the steps to be followed in performing a dimensional analysis using the method of repeating variables are as follows:

1. List all the variables involved in the problem
2. Express each of the variables in terms of primary dimensions
3. Determine the required number of pi terms

4. Select a number of repeating variable. (usually the same as the number of primary units)

5. Form a pi term by multiplying one of the non repeating variables by the product of repeating variables each raised to an exponent that will make the combination dimensionless

6. Repeat Step 5 for each of the remaining repeating variables

7. Check all the resulting pi terms to make sure they are dimensionless

8. Express the final form as a relationship among the pi terms and think about what it means
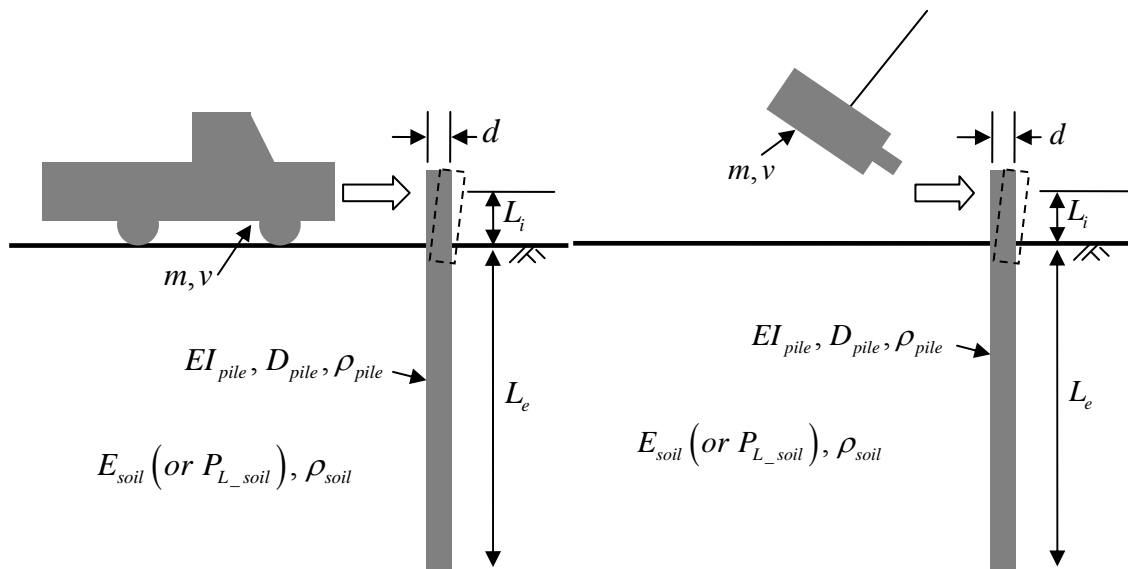
Figure 3.46. Schematics drawings of full-scale impact test and model test using pendulum

Ten variables shown in Figure 3.46 that are involved in this problem are listed as follows:

$$M, V, L_i, L_e, d, D_{Post}, E_{soil}, \rho_{post}, \rho_{soil}, EI_{Post}$$

where, M = mass of pendulum or bogie.

V = impact velocity of pendulum or bogie.

L_i = distance of the ground level and impact location

L_e = post embedment

d = post displacement at the impact location

D_{Post} = width of post

E_{soil} = Young's modulus of soil

ρ_{post} = density of post

ρ_{soil} = density of soil

EI_{Post} = bending stiffness of post

Three primary dimensions are listed as follows:

$$[L], [F], [T]$$

where, $[L]$ = length.

$[F] = [MLT^{-2}]$ = force.

$[T]$ = time.

$[M]$ = mass.

The dimensions of the variables using the primary units are

$$M\left[\frac{F \cdot T^2}{L}\right], V\left[\frac{L}{T}\right], L_i, L_e, d, D_{Post}[L], E_{soil}\left[\frac{F}{L^2}\right], \rho_{post}, \rho_{soil}\left[\frac{F \cdot T^2}{L^4}\right], EI_{Post}[F \cdot L^2]$$

The relationship between these parameters is formulated in Eq. 3-4.

$$d = f\left(M, V, L_i, L_e, D_{post}, E_{soil}, \rho_{soil}, \rho_{post}, EI_{post}\right) \tag{3-4}$$

There are ten variables and three primary dimensions. Thus the number of dimensionless pi terms is seven that is calculated ten subtract three. The selected repeating variables are D_{post}, EI_{post}, M .

The dimensionless pi terms are listed in Eq. 3-5.

$$\therefore \pi_i = \left(\frac{d}{D_{post}}, \frac{L_e}{D_{post}}, \frac{L_i}{D_{post}}, \frac{\rho_{soil} \cdot D_{post}^3}{M}, \frac{\rho_{post} \cdot D_{post}^3}{M}, \frac{E_{soil} \cdot D_{post}^4}{EI_{post}}, \frac{M \cdot V^2 \cdot D_{post}}{EI_{post}} \right) \qquad (3\text{-}5)$$

After the dimensional analysis, the following relationship is obtained (Eq. 3-6):

$$\frac{d}{D_{post}} = f \left(\frac{L_e}{D_{post}}, \frac{L_i}{D_{post}}, \frac{\rho_{soil} \cdot D_{post}^3}{M}, \frac{\rho_{post} \cdot D_{post}^3}{M}, \frac{E_{soil} \cdot D_{post}^4}{EI_{post}}, \frac{M \cdot V^2 \cdot D_{post}}{EI_{post}} \right) \qquad (3\text{-}6)$$

In order to properly design model so that the model and prototype will behave in a similar fashion, similitude has to be considered using dimensionless pi terms. The properly designed model and prototype satisfy Eq. 3-7.

$$\left(\pi_i \right)_{Prototype} = \left(\pi_i \right)_{Model} \qquad (3\text{-}7)$$

Assume that the material properties of post and soil for model test are same with those of prototype.

$$(E_{post}, \rho_{post}, E_{soil}, \rho_{soil})_{Model} = (E_{post}, \rho_{post}, E_{soil}, \rho_{soil})_{Prototype}$$

Substitute the pi terms from Eq. 3-5 into Eq. 3-7:

i.   From i=1 to 3, Eq. 3-7 can be expressed as:

$$\left(\pi_1\right)_{Model} = \left(\frac{d/n}{D_{post}/n}\right) = \left(\frac{d}{D_{post}}\right) = \left(\pi_1\right)_{Prototype} \tag{3-8}$$

ii.   From i=4 to 5, Eq. 3-7 can be expressed as:

$$\left(\pi_4\right)_{Model} = \left(\frac{\rho_{soil} \cdot (D_{post}/n)^3}{M/n_m}\right) = \left(\frac{\rho_{soil} \cdot D_{post}^3}{M}\right) \cdot \left(\frac{n^3}{n_m}\right) = \left(\pi_4\right)_{Prototype} \tag{3-9}$$

$$\therefore n^3 = n_m$$

iii.   For i=6, Eq. 3-7 can be expressed as:

$$\pi_6 = \frac{E_{soil} \cdot D_{post}^4}{EI_{post}}$$

$$\left(\pi_6\right)_{Model} = \left(\frac{E_{soil} \cdot (D_{post}/n)^4}{EI_{post}/n^4}\right) = \left(\frac{E_{soil} \cdot D_{post}^4}{EI_{post}}\right) = \left(\pi_6\right)_{Prototype} \tag{3-10}$$

iv.   For i=6, Eq. 3-7 can be expressed as:

$$\pi_7 = \frac{M \cdot V^2 \cdot D_{post}}{EI_{post}}$$

$$\left(\pi_7\right)_{Model} = \left(\frac{M/n_m \cdot (V/n_v)^2 \cdot D_{post}/n}{EI_{post}/n^4}\right) = \left(\frac{M \cdot V^2 \cdot D_{post}}{EI_{post}}\right)\left(\frac{n^3}{n_m \cdot n_v}\right) = \left(\pi_7\right)_{Prototype} \tag{3-11}$$

$$\therefore n_v = 1 \ \ (\because n^3 = n_m \text{ from Eq. 3-9})$$

Therefore the properly scaled model should satisfy the followings:

$$\left(Length\right)_{Model} = \frac{1}{n}\left(Length\right)_{Prototype}$$

$$\left(Mass\right)_{Model} = \frac{1}{n^3}\left(Mass\right)_{Prototype}$$

$$\left(Velocity\right)_{Model} = \left(Velocity\right)_{Prototype}$$

According to the dimensional analysis, it turned out that mass and length can be scaled down but even miniature test, the impact velocity have to same with a full-scale test to satisfy the similitude. Though the proposed miniature test cannot be a scaled down test for actual full-scale test, the results can be used for calibrations of finite element analysis and analysis of the dynamic load factors which is defined as the ratio between the maximum static resistance and the maximum dynamic resistance. The pendulum tests and bogie test were designed by scaling down the full-scale test on single post described in the previous section.

3.3.2 Pendulum tests in medium dense crushed limestone

On June 2, 2008, Impact tests on single post embedded in the medium dense crushed limestone were performed using a pendulum with 862 kg (1,900 lbs) of mass (Figure 3.47). A 1.83m (72 inches) long hollow square section HSS 6X6X3/8 steel post (6 inches wide, 6 inches high, and 3/8 inches wall thickness) was embedded 1.01m (40 inches). The impact velocities were 2.41 m/s (5.4 mph), 4.65 m/s (10.4 mph) and 9.97 m/s (22.3 mph). The impact location is at 356 mm (14 inches) above the ground surface.

3.3.2.3 Test set up

The single post was placed in a pre-bored hole in medium dense crushed limestone in a 1.5 m wide, 3.0 m long and 1.8 m deep rectangular pit. Then the drilled hole was filled with crushed limestone and compacted using a mechanical tamper as shown in Figure

3.48. Figure 3.49 shows the post after the installation in the 1.5 m wide pit filled with the medium dense crushed limestone.

Figure 3.47. Pendulum with mass of 862 kg

Figure 3.48. Soil compaction during the post installation using a mechanical tamper

Figure 3.49. Post after the installation

Figure 3.50. Pulling system for static lateral load test

Prior to the impact tests using the pendulum, a static load test to estimate the lateral load capacity of the single post was conducted in the opposite direction of the impact. On the impact side of the post was connected to a hydraulic jack and the other side was connected to a displacement transducer (Figure 3.50 and Figure 3.51). The lateral static force was measured with a pressure transducer.

Figure 3.51. Displacement measuring system for static load test

The impact speeds were controlled by changing the drop height of the pendulum. After the static load test and the first pendulum impact test with the medium velocity (4.65 m/s) shown in Figure 3.52, the post was removed and reinstalled for the pendulum impact test with the different velocities. After the static load test and the impact test with

the slow velocity (2.41 m/s), the post was rearranged to the initial post position without reinstallation since the displacement of the post from those two tests were relatively small.

Figure 3.52. Set-up of a pendulum test

Three accelerometers were attached in the opposite side of the impact at the impact level, the middle and bottom of the post. As shown in Figure 3.53, the accelerations at the impact level, the middle and the bottom of the post were measured. To measure the accelerations of the pendulum, an accelerometer was attached on the center of gravity (C.G) of pendulum. High speed cameras captured films to analyze the displacement of the two targets attached on the side of the post. The geometry of two targets on the single post is shown in Figure 3.54.

93
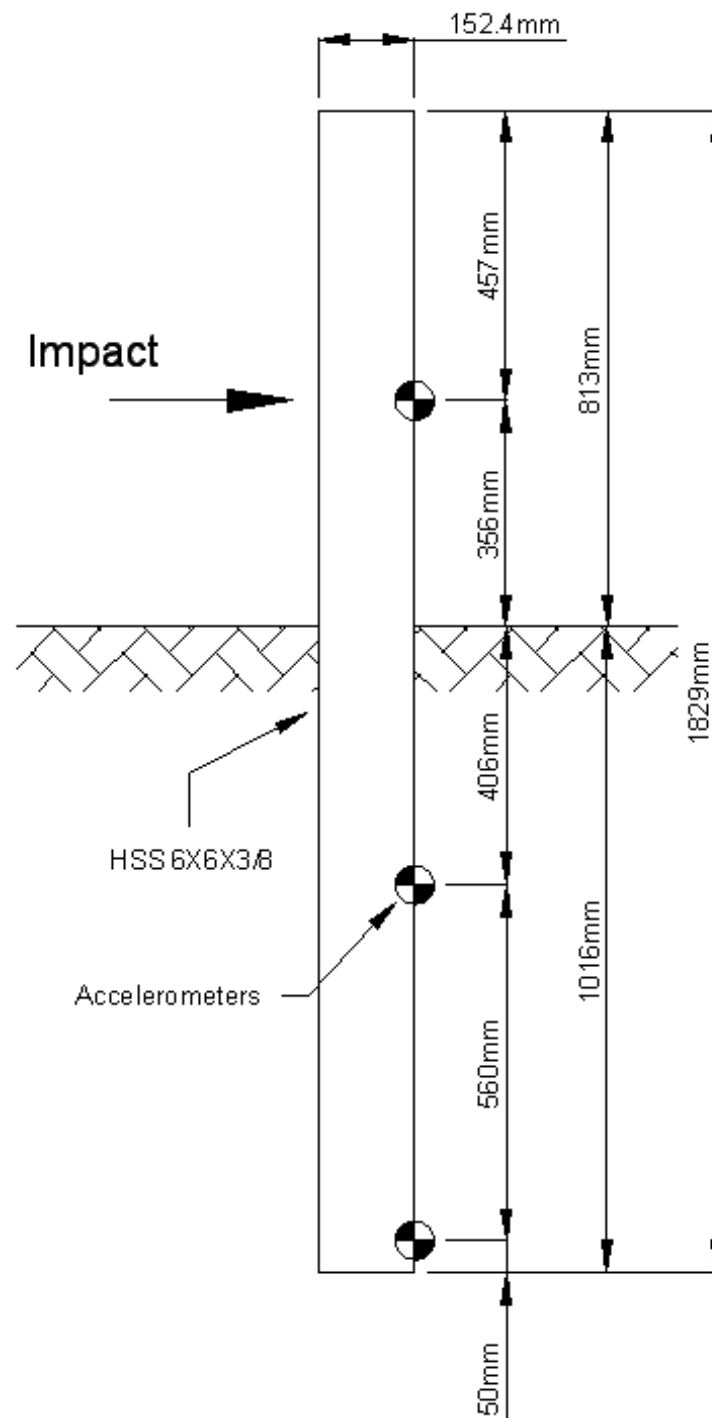
Figure 3.53. Single post for pendulum tests with accelerometers
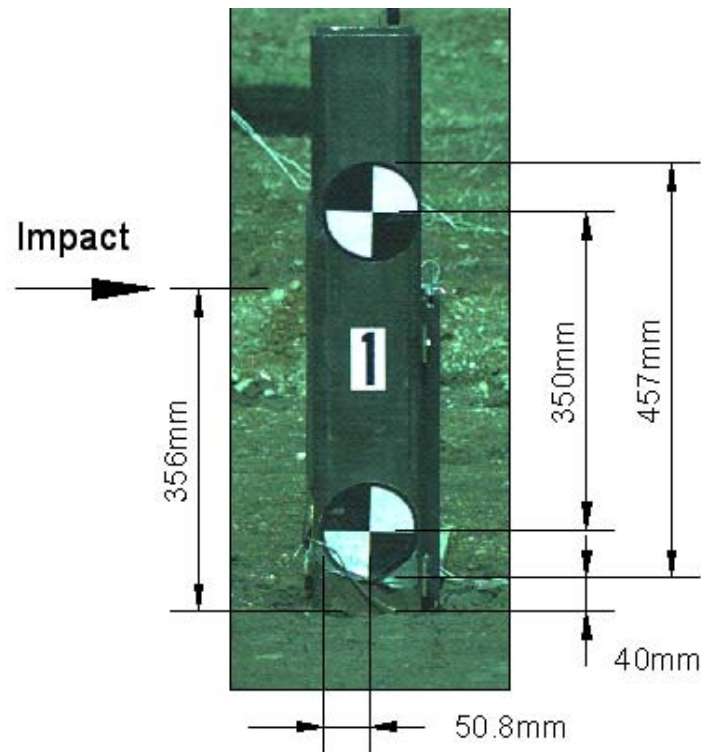
Figure 3.54. Geometry of the two targets on the post for film analysis

3.3.2.4 Test results

Accelerations of the pendulum and the post at the impact level, at the middle and the bottom of the post were measured. Also the films taken using high speed camera were analyzed to capture the motion of the targets on the post.

Prior to the impact tests, static lateral capacity of single post was conducted. The post was pulled at 356 mm above the ground level that is the impact location of the pendulum. The force-displacement result is shown in Figure 3.55. Peak force during the test was 23 kN at the displacement of 43 mm. Loading speed was 0.6 mm/s and the lateral loading had lasted for 70 sec.
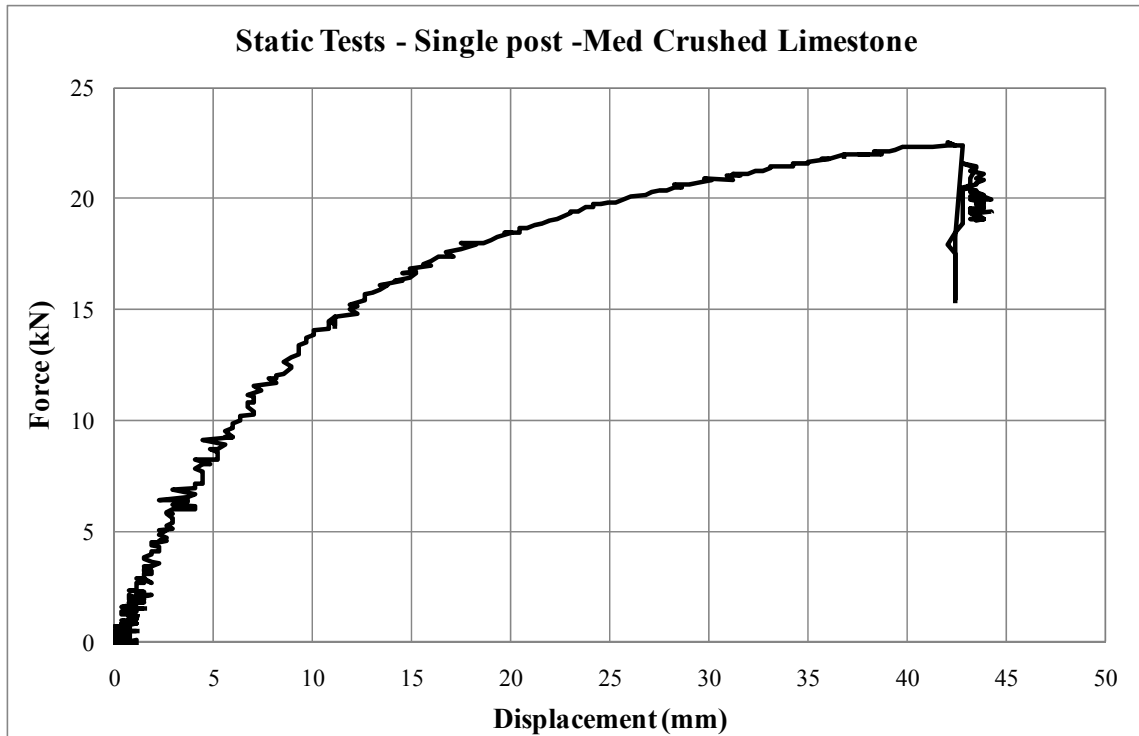
Figure 3.55. Static force-displacement of single post in medium dense crushed limestone

Single post pendulum test with 4.65 m/sec of impact velocity (P1)

Peak longitudinal 50ms-average deceleration of the pendulum was 7.5 g at 0.025 sec. The impact force-history is shown in Figure 3.56. The maximum impact force was 65 kN.

Figure 3.57 shows the post acceleration at the impact level (0.36 m above the ground level) the middle (0.41 m below the ground level) and the bottom (0.96m below the ground level) of the post. Also the velocity-time and displacement-time histories of the post were obtained by integration of the acceleration data as shown in Figure 3.57.

Film analysis was conducted to obtain the post displacement history. The film from high speed camera is analyzed to obtain more reliable displacement history.
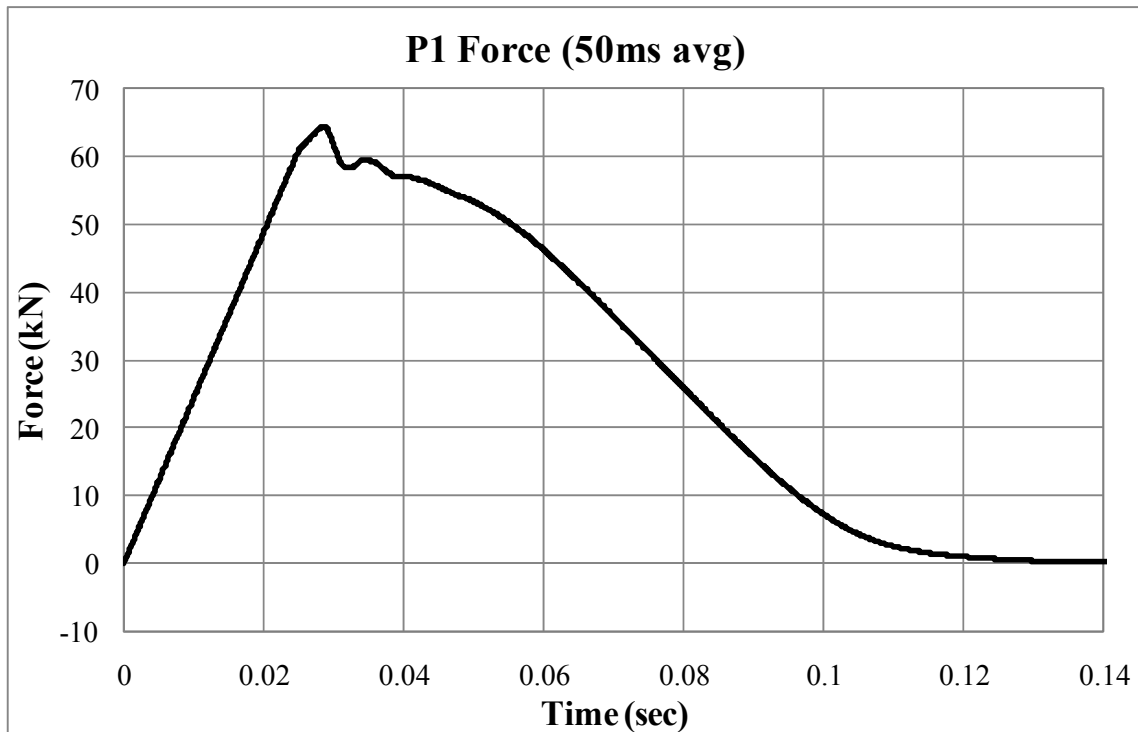
Figure 3.56. 50msec average impact force-time history (P1)

The maximum longitudinal displacement of the post at impact location was 0.125 m at 0.075 sec using film analysis. The permanent displacement at the location was 0.08 m. The tracers of two targets attached on the post shown in Figure 3.58. In Figure 3.58, x1and y1 are the x-direction displacement (longitudinal) and the y-direction displacement (vertical) of the upper target. Also the x2 and y2 are the longitudinal and vertical displacement of the lower target. The target locations are shown in Figure 3.54. To obtain the longitudinal and vertical displacement of the post at the impact location, a

simple mathematical calculation using proportionality based on the assumption that the post did not bend and keep straight. The calculated displacement at the impact location is indicated as X-disp and Y-disp for the longitudinal and vertical displacement in Figure 3.58. After the test, the permanent rotation of the post was measured as 6 degrees.
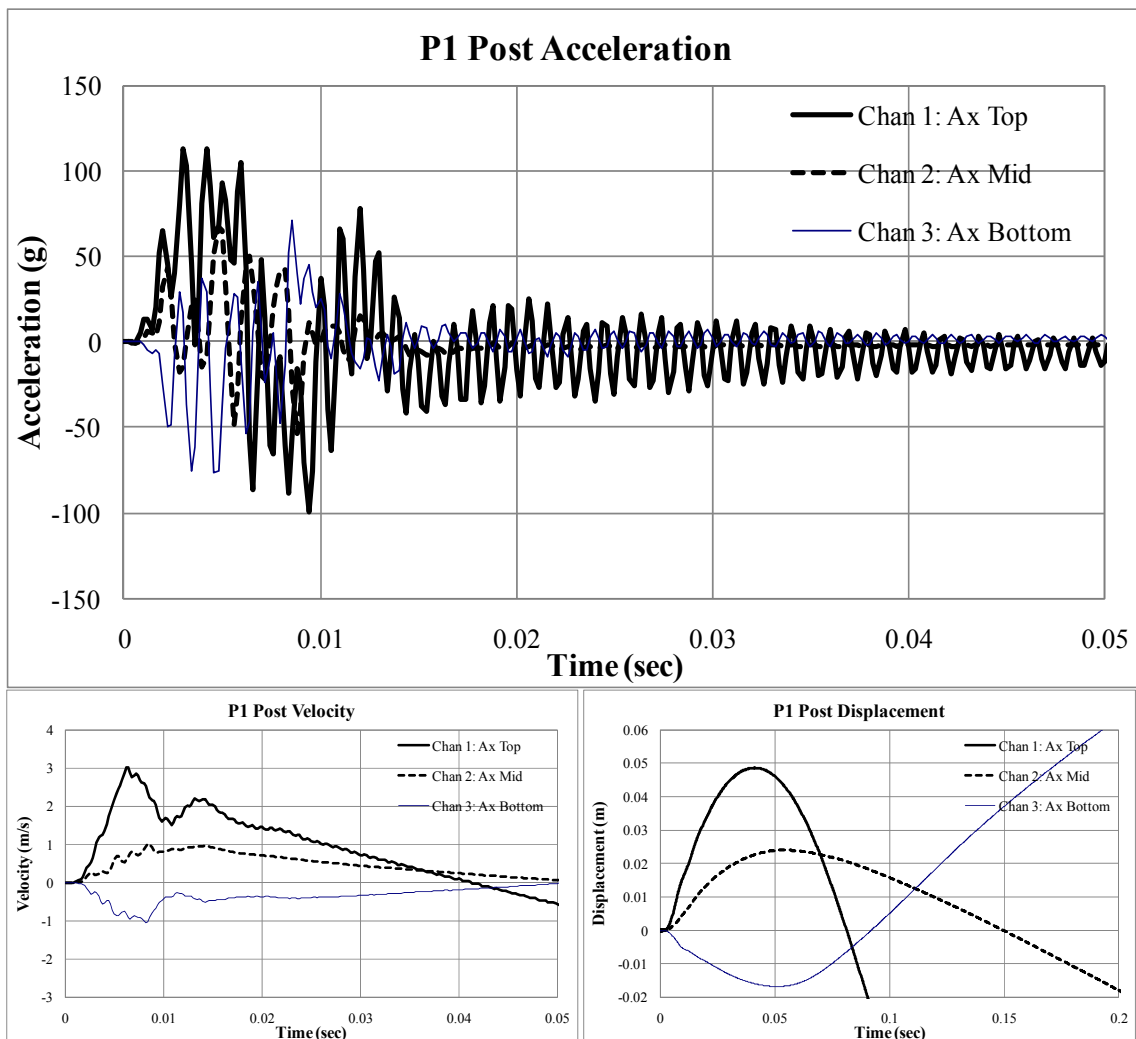
Figure 3.57. Acceleration, velocity and displacement of post history from acceleration data (P1)
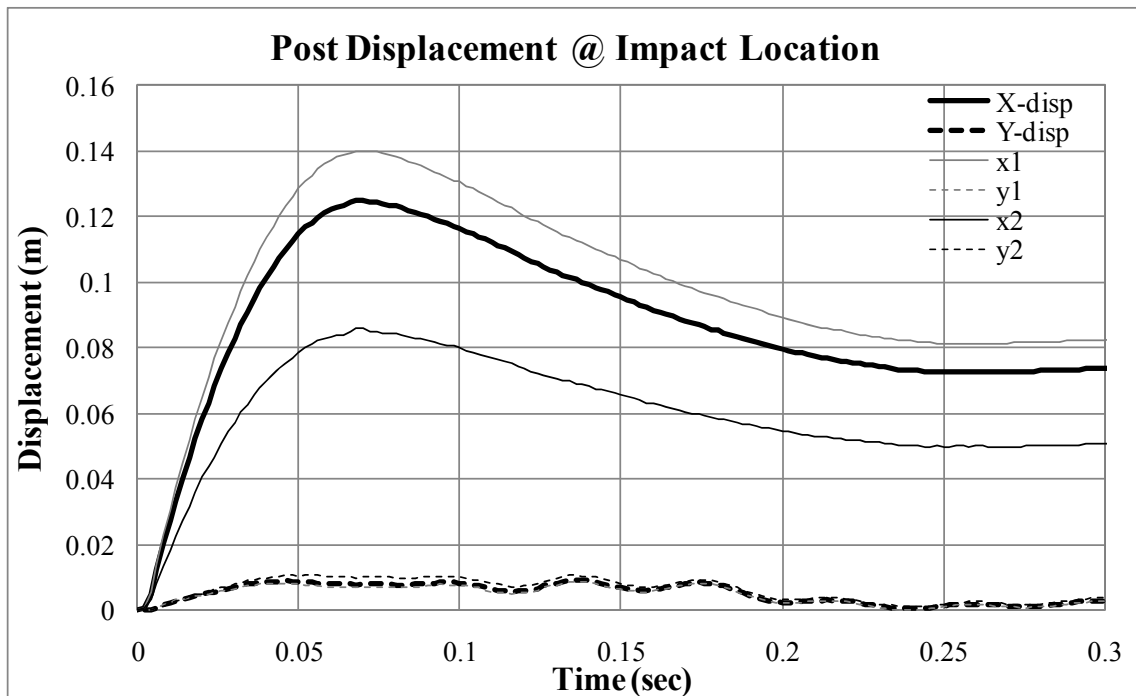
Figure 3.58. Post displacement history from film analysis (P1)

Single post pendulum test with 2.41 m/sec of impact velocity (P2)

Peak longitudinal 50ms-average deceleration of the pendulum was 5.5 g at 0.025 sec.

The maximum impact force was 50 kN as shown in Figure 3.59.

Figure 3.60 shows the post acceleration at the impact level (0.36 m above the

ground level) the middle (0.41 m below the ground level) and the bottom (0.96m below

the ground level) of the post. Also the velocity-time and displacement-time histories of

the post were obtained by integration of the acceleration data as shown in Figure 3.60.
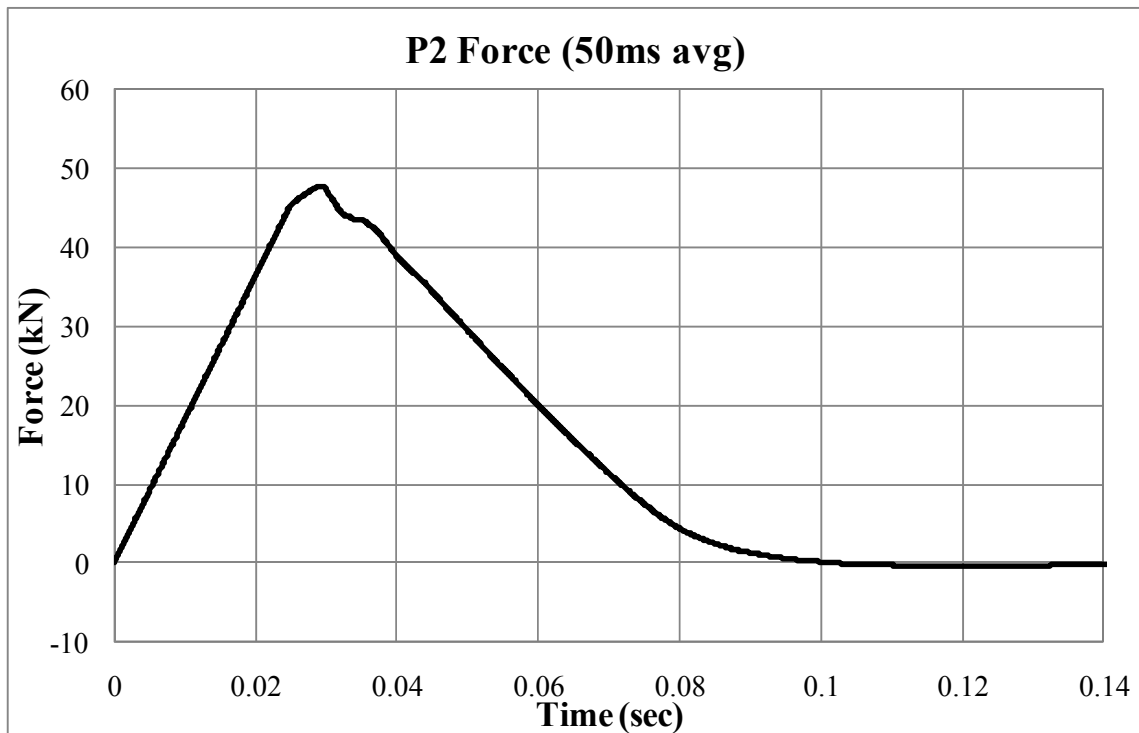
Figure 3.59. 50msec average impact force-time history (P2)

The maximum longitudinal displacement of the post at impact location was obtained as 0.047 m at 0.045 sec using film analysis. The permanent displacement at the location was 0.025m. Film analysis results for this test (P2) were shown in Figure 3.61. The displacement at the impact location is indicated as X-disp and Y-disp for the longitudinal and vertical displacement. After the test, the permanent rotation of the post was measured as 1.5 degrees.
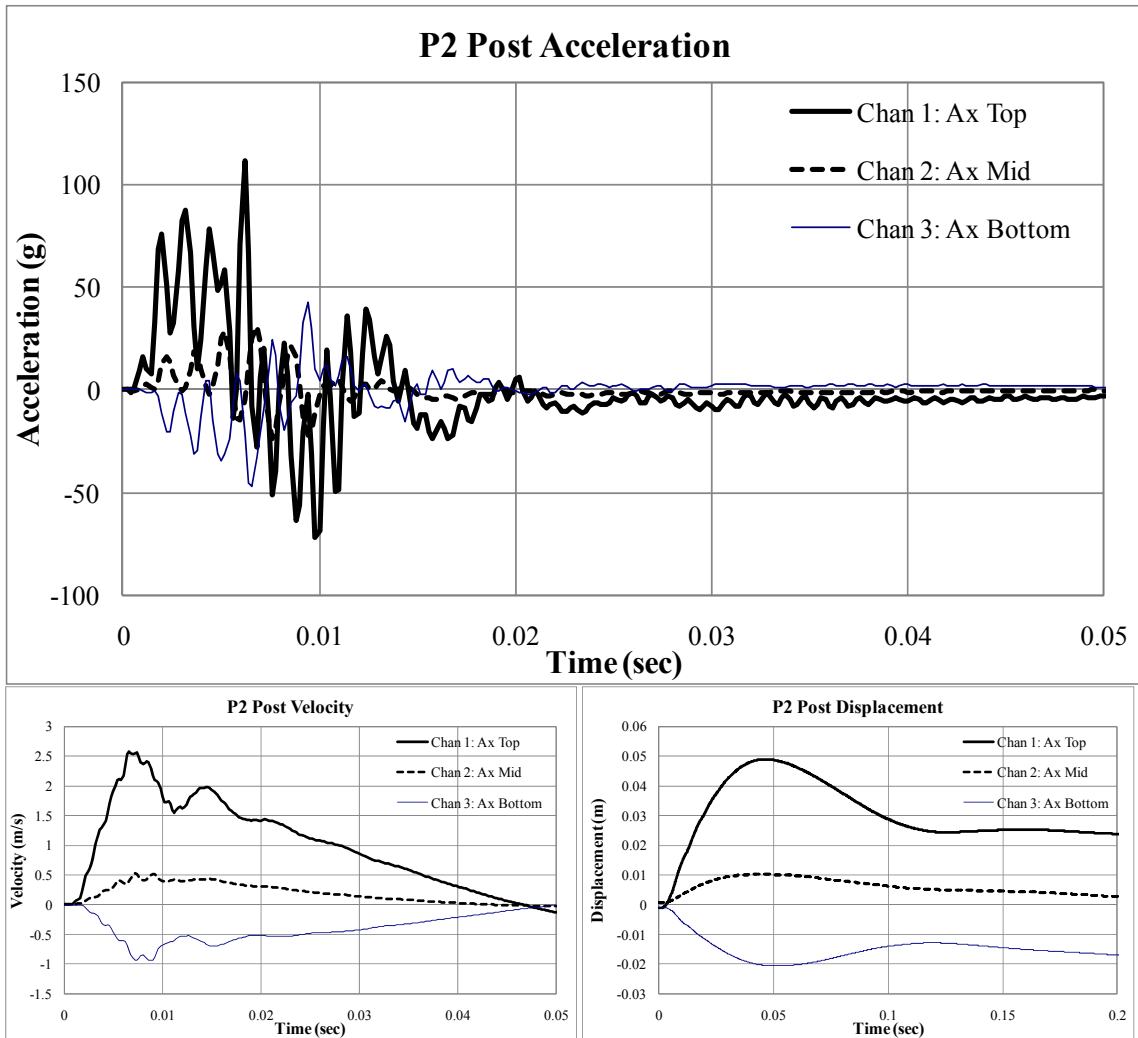
Figure 3.60. Acceleration, velocity and displacement of post history from acceleration data (P2)
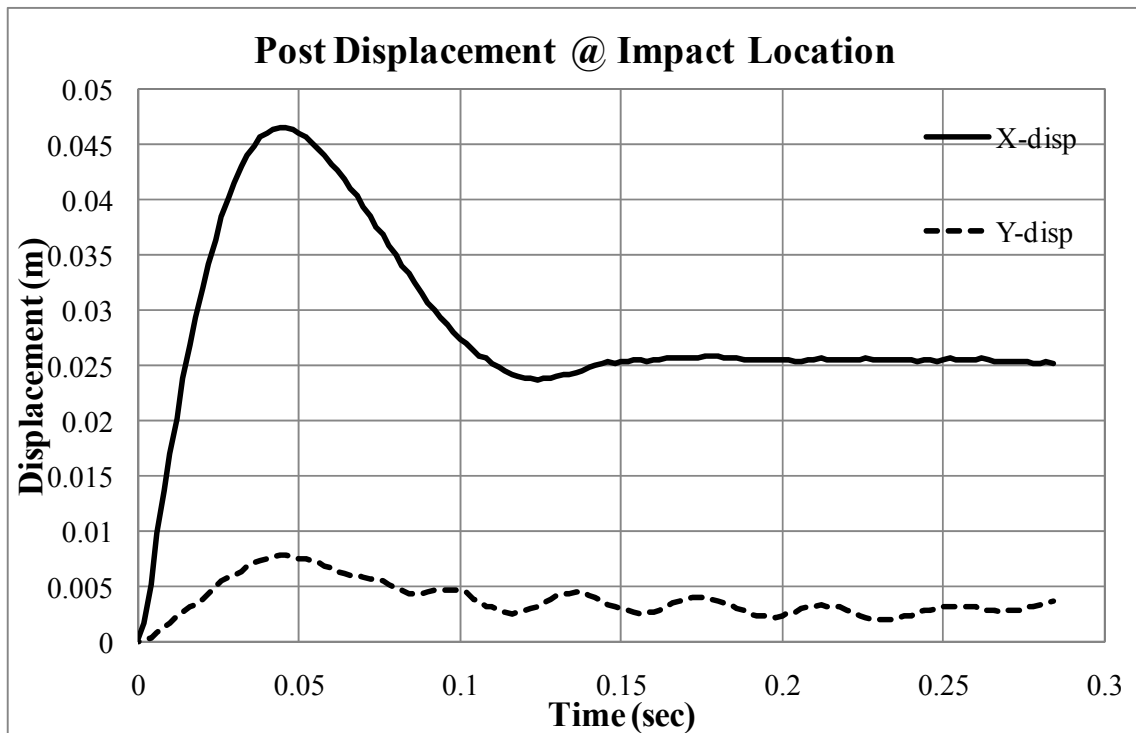
Figure 3.61. Post displacement history at the impact location from film analysis (P2)

Single post pendulum test with 9.97 m/sec of impact velocity (P3)

The deformed post and the pendulum just after the impact with 9.97 m/sec of velocity (P3) are shown in Figure 3.62. After the test, the permanent rotation of the post was measured as 28.5 degrees. The pendulum impacted twice against the post. Peak longitudinal 50ms-average acceleration of the pendulum was 11 g at 0.027 sec. The impact force-history is shown in Figure 3.63. The maximum impact force was 86 kN.

The maximum longitudinal 50ms-average deceleration of the pendulum was 10.5 g at 0.024 sec. The maximum impact force was 85 kN as shown in Figure 3.63. The post acceleration at the impact level (0.36 m above the ground level) the middle (0.41 m below the ground level) and the bottom (0.96m below the ground level) of the post are

shown in Figure 3.64. Also the velocity-time and displacement-time histories of the post

were obtained by integration of the acceleration data as shown in Figure 3.64.

Figure 3.62. Deformed single post after pendulum test (P3)
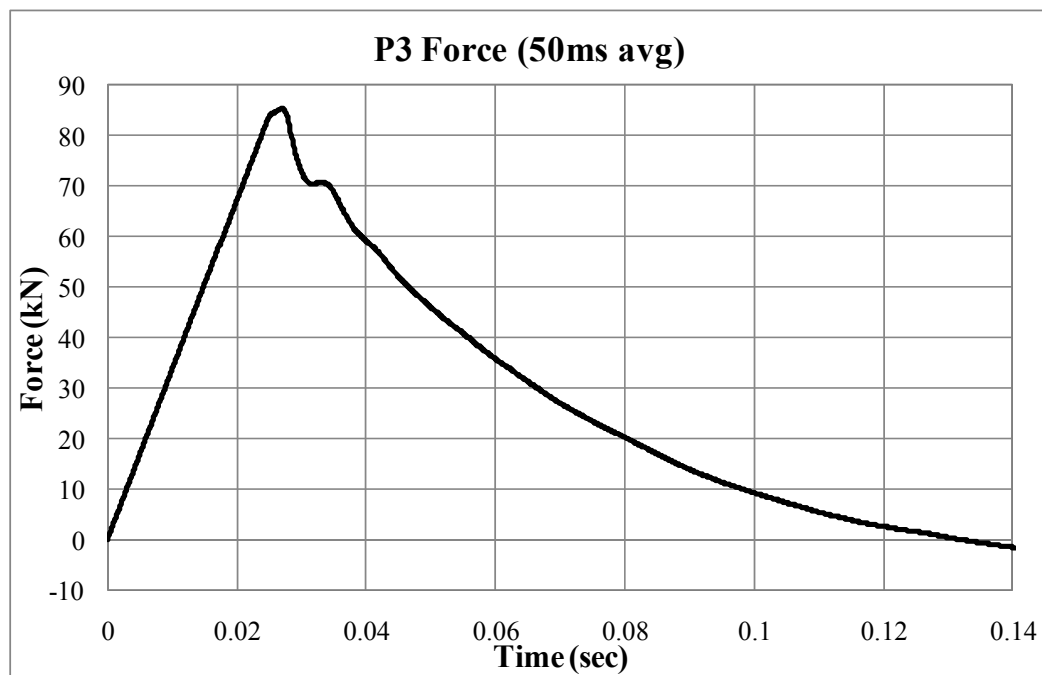
Figure 3.63. 50msec average impact force-time history (P3)
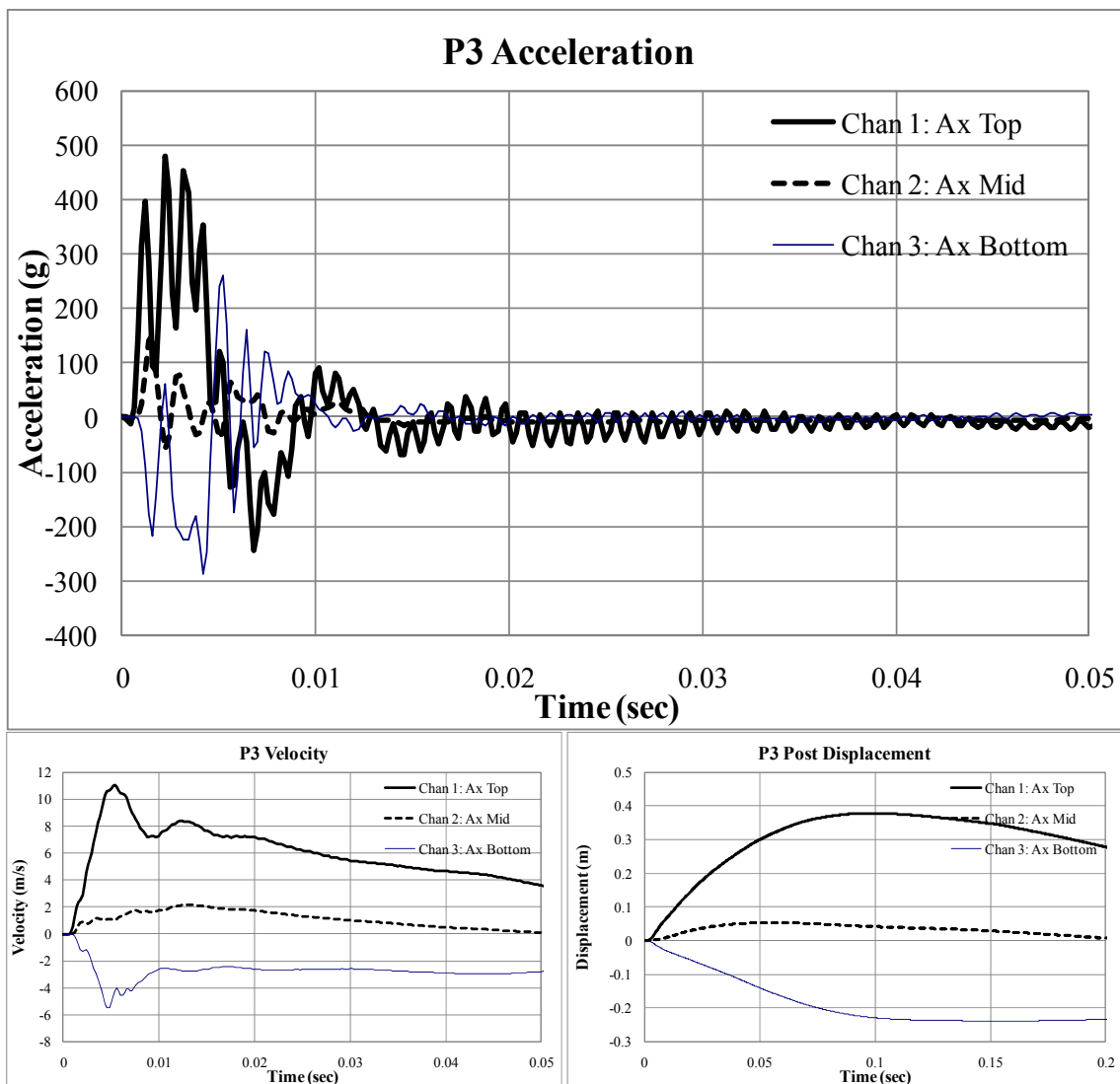
Figure 3.64. Acceleration, velocity and displacement of post history from acceleration data (P3)

The maximum longitudinal displacement of the post at impact location was obtained as 0.38 m at 0.10 sec using film analysis. Film analysis results for this test (P2) were shown in Figure 3.65. The displacement at the impact location is indicated as X-disp and Y-disp for the longitudinal and vertical displacement.
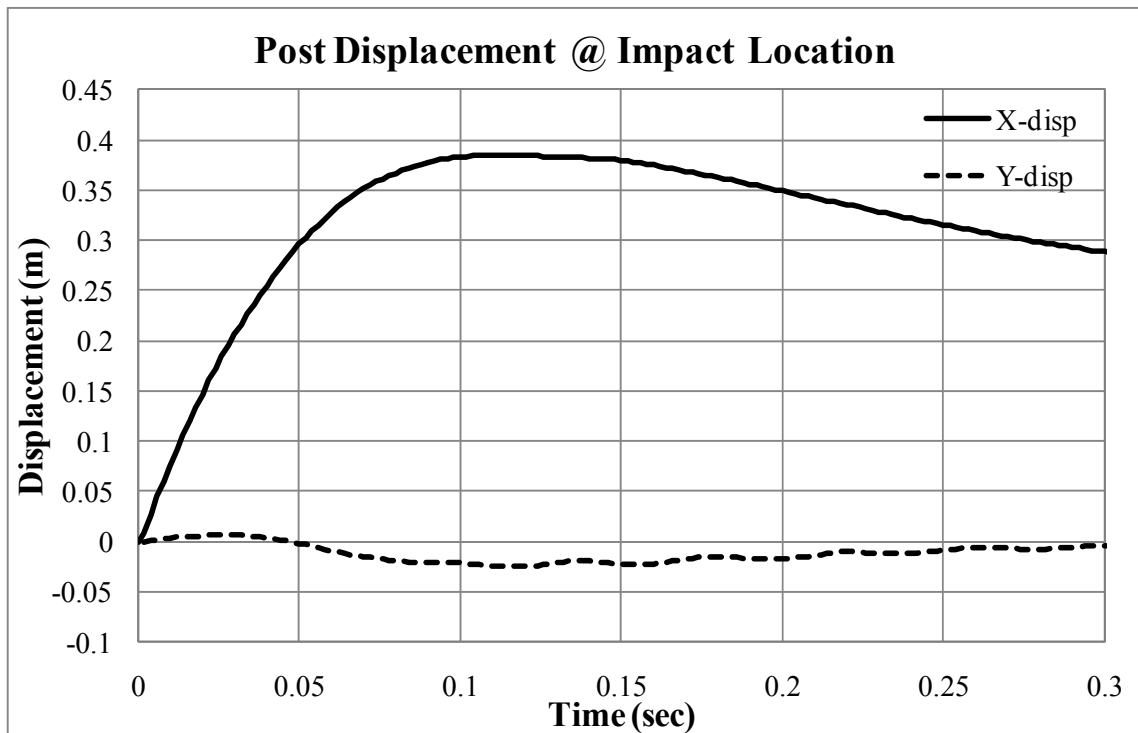
Figure 3.65. Post displacement history at the impact location from film analysis (P3)

3.3.2.5 Data analysis

The post displacement from film analysis and that from integration of acceleration data were compared and shown in Figure 3.66, Figure 3.67 and Figure 3.68. The displacement history of P1 test seems unrealistic due to the noise of the raw acceleration data (Figure 3.66). According to film analysis, the motion of the post came to stop at 0.3 sec whereas the displacement history from the integration did not stop.

The displacement from film analysis is generally more reliable than that from integration of acceleration data. The film analysis is capable to capture the geometry directly whereas the accuracy of double-integration of acceleration can be determined from the quality of raw data.
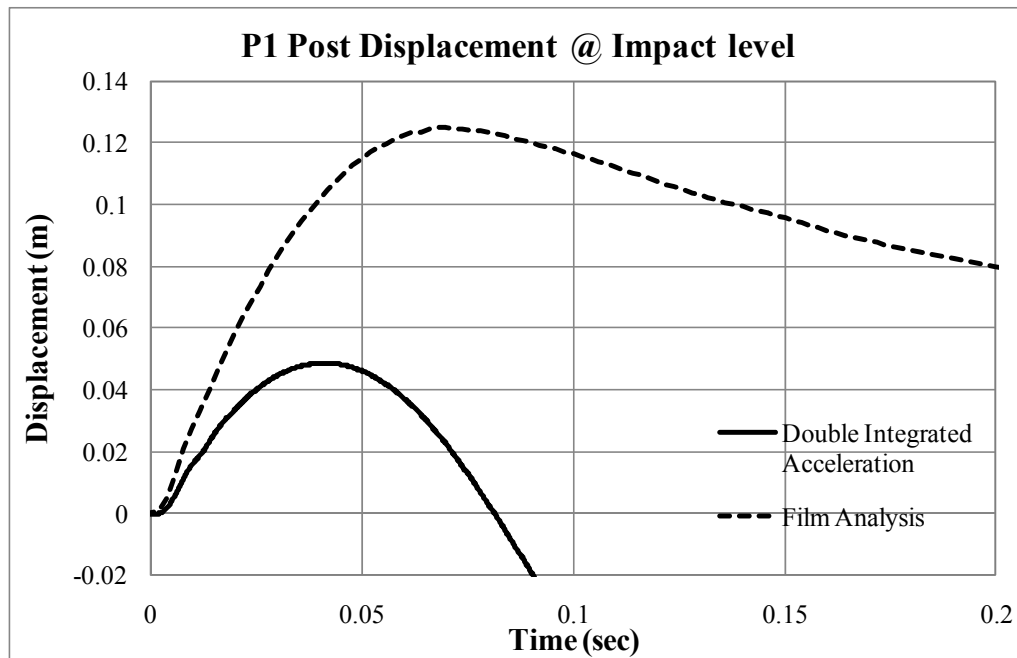
Figure 3.66. Post displacement comparison (P1)
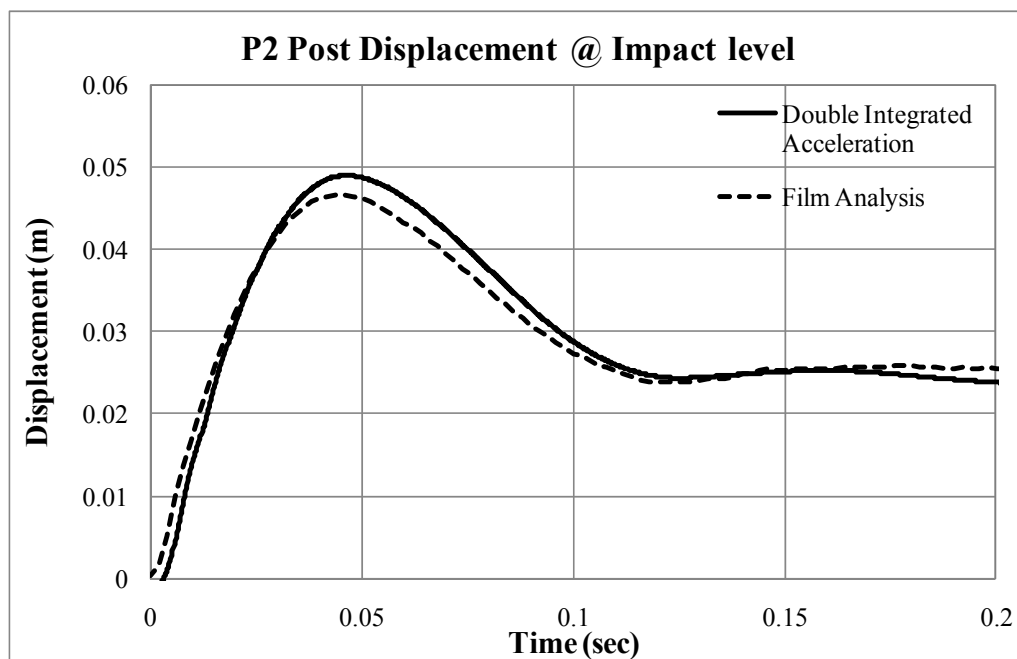
Figure 3.67. Post displacement comparison (P2)

P3 Post Displacement @ Impact level
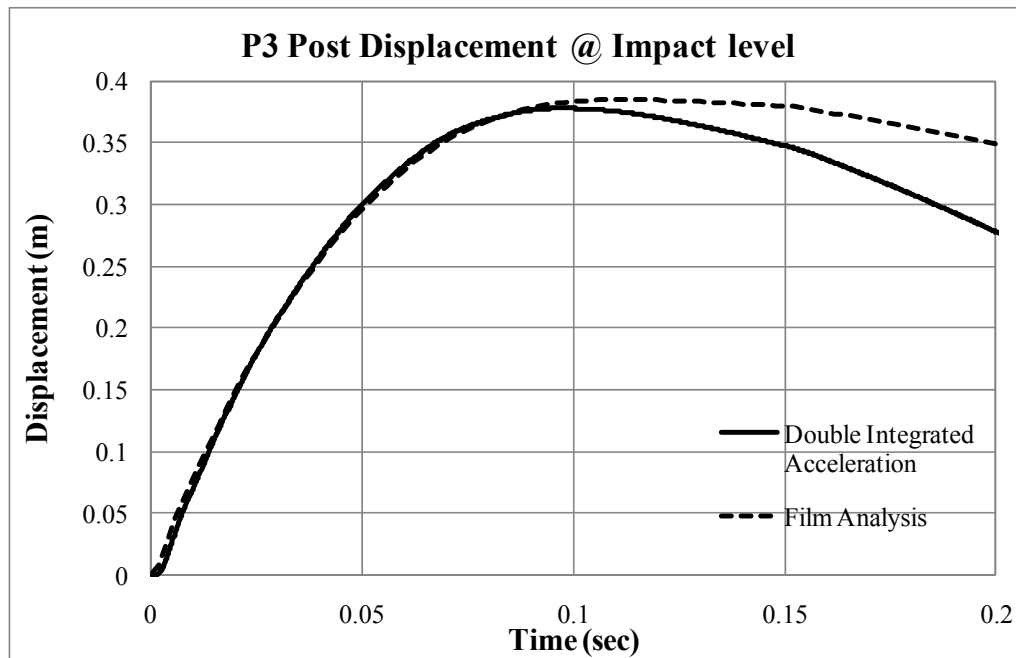
Figure 3.68. Post displacement comparison (P3)

Based on the post displacement history and the impact force history, the force versus displacement relationship was obtained (Figure 3.69). Since the loading speed of the static test was approximately 0.6 mm/sec, the speed of static test can be considered as zero. The forces of impact test were last around 0.2 sec whereas that of the static test was last 70 sec.

The maximum forces versus impact velocities are plotted in Figure 3.70. According to this, dynamic factor, DF is a function of impact velocity. The maximum force increase and the increment of force decrease as the impact velocity increase. It may have a certain critical point or limit. Hence the maximum force may stop increase at a critical impact velocity. This data is analyzed in Section 3.4.3 with the tests data from other model tests.
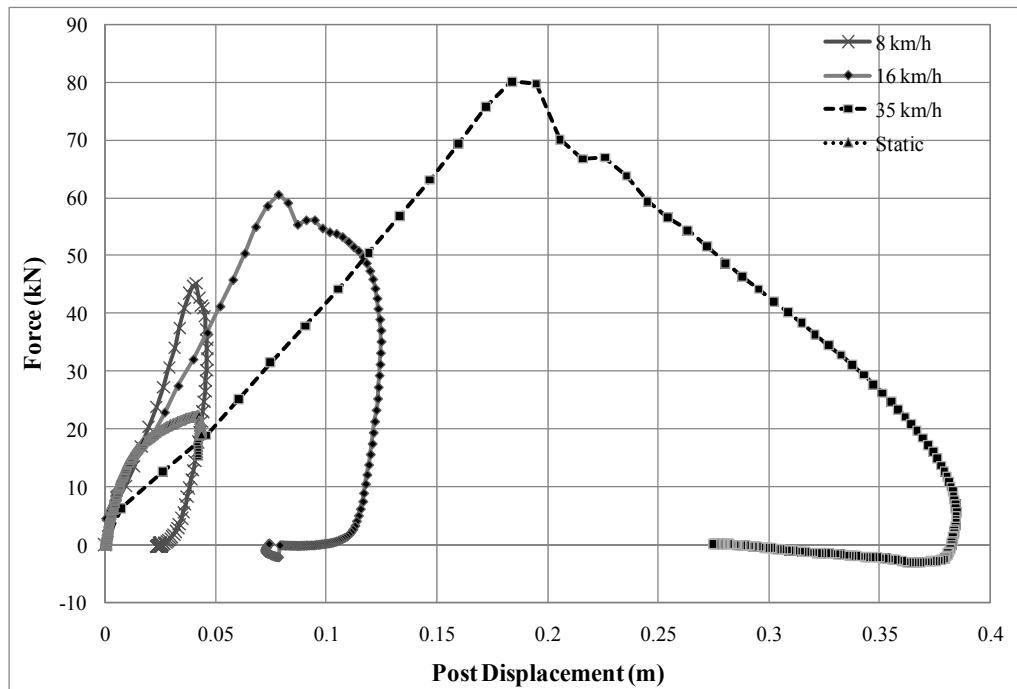
Figure 3.69. Force-displacement of single post in medium dense crushed limestone
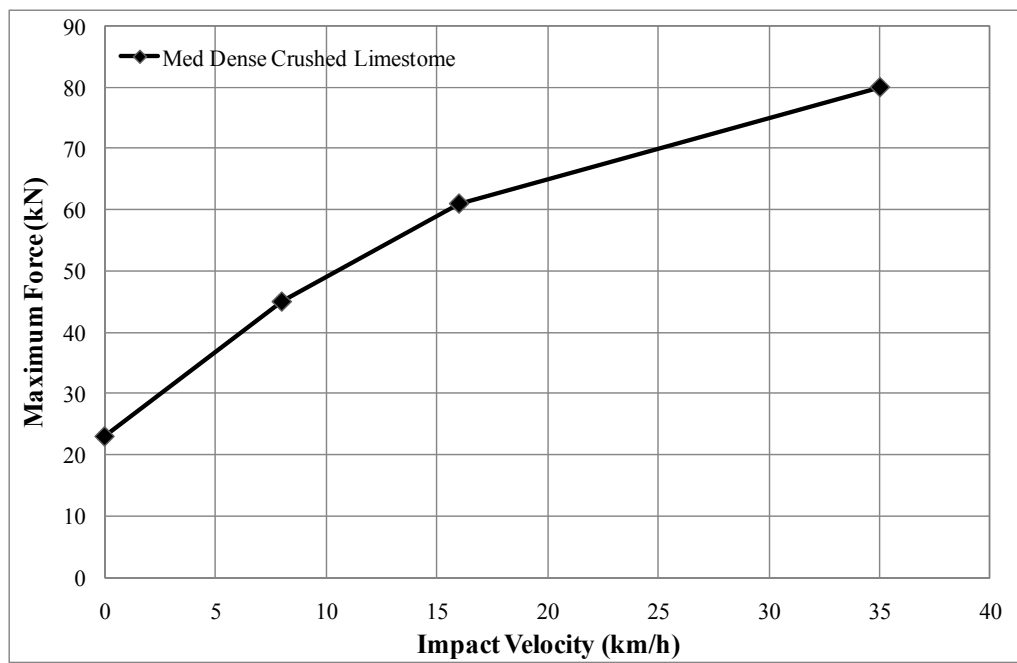
Figure 3.70. The maximum force-impact velocity for medium dense crushed limestone

3.3.3 Pendulum test in loose sand

Impact tests on post systems embedded in the loose sand were performed using a pendulum with 250 kg (550 lbs) of mass shown in Figure 3.71. 1.83m (72 inches) long hollow square section HSS 6X6X3/8 steel posts (6 inches wide, 6 inches high, and 3/8 inches wall thickness) were embedded 1.01m (40 inches) for the test of single posts. The impact velocities were 2.41 m/s (5.4 mph), 4.65 m/s (10.4 mph) and 9.97 m/s (22.3 mph).

In order to investigate the group effects, pendulum tests and static tests on two kinds of group of posts system (Figure 3.44 and Figure 3.45) were conducted with impact velocity of 10 m/s (22 mph). HSS 6X6X3/8 beam was used as posts and beams of the group of posts systems. The group of posts systems and one of the single posts are backfilled. The other single post was driven into the loose sand pit.

Figure 3.71. Small pendulum test on single post embedded in crushed limestone

3.3.3.6 Test set up

The pendulum pit filled with clean loose sand was prepared. Clean sand was dumped into the excavated pendulum pit and to construct loose sand condition, there was only little compaction effort like tamping with a rake or feet shown in Figure 3.73. Two single posts and two kinds of group of posts system were installed in the loose sand pit. The one of the single post was driven and the other was backfilled to compare to the results of the impact test using group of posts systems. Figure 3.72 and Figure 3.73 show installation of post systems. The backfilled post system was placed in the excavated loose sand pit and the ditch was filled and compacted.

Figure 3.72. Excavation of the loose sand pit to install the posts system

Figure 3.73. Installation of a group of posts system with two by three group of posts

Figure 3.74. Instrumentations of the lateral static test (S3)

Static load tests for the lateral load capacity were conducted in the opposite direction of the impact, prior to the impact test using the pendulum. On the impact side of the post was connected to a hydraulic jack and the other side was connected to a displacement transducer (Figure 3.74). The lateral static force was measured with a pressure transducer.

The impact speeds were controlled by changing the drop height of the pendulum. From the test number P4 to P6, the single post was driven into the loose sand. After the static load test and the first pendulum impact test with the medium velocity (4.65 m/s), the post was removed and reinstalled for the pendulum test with the different velocities. After the static load test and the impact test with the slow velocity (2.41 m/s), the post was rearranged to the initial post position without reinstallation since the displacement of the post from those two tests were relatively small. The impact test on post systems in loose sand except the driven single post were backfilled and subject to static load test and pendulum test with the velocity of 10 m/s (22 mph).

Three accelerometers were attached on the single posts (P4, P5, P6 and P10) in the opposite side of the impact at locations as shown in Figure 3.53. The accelerations at the impact level, the middle and the bottom of the post were measured. Also three accelerometers were installed on the each posts of the group of posts systems with a row of three posts (P7 and P8) at the ground level. The group of posts system with two rows of six posts (P9) test conducted without accelerometers. To measure the accelerations of pendulum, an accelerometer was attached on the center of gravity (C.G) of pendulum (Figure 3.75).

Figure 3.75. Pendulum test on group of posts system embedded in loose sand (P8)

High speed camera captured films to analyze the displacement of the two targets attached on the side of the post for all of the impact tests in the loose sand. The two target locations on the posts are shown in Figure 3.54.

Details of the geometry of the group of posts system with a three posts (side by side posts) along with the locations of accelerometers are shown in Figure 3.76 and Figure 3.77. And the details of the geometry of group of posts system with two rows of six posts (three by two) are shown in Figure 3.78 and Figure 3.79.
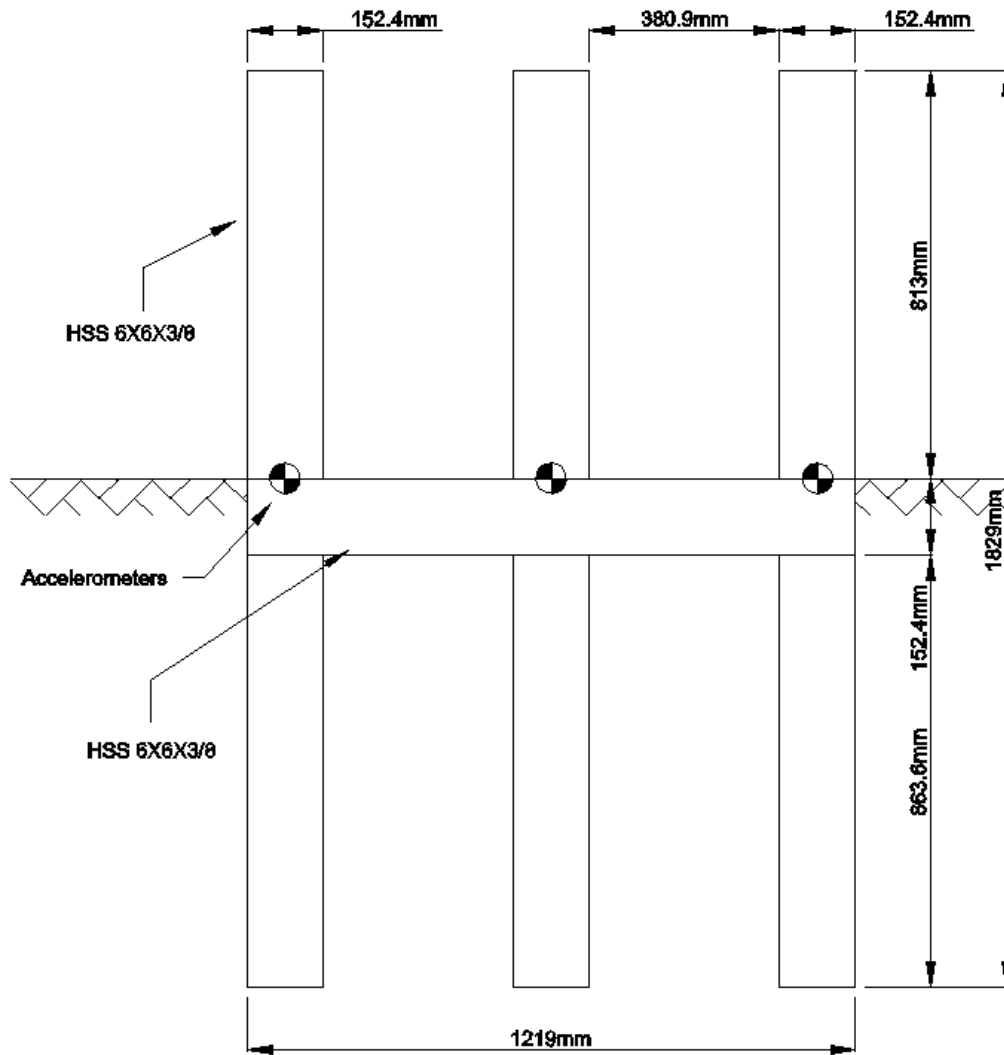
Figure 3.76. Rear elevation view of the three side by side posts
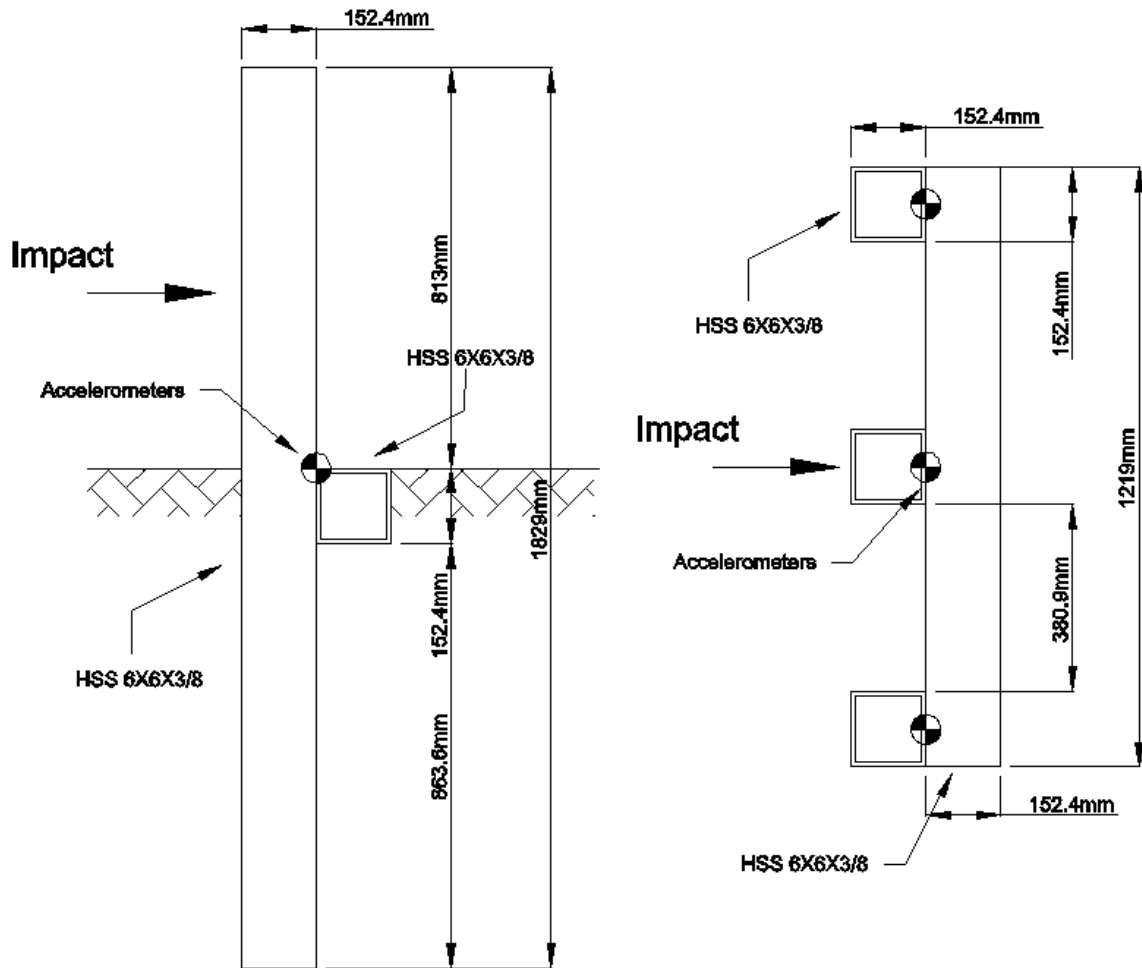
Figure 3.77. Side elevation and plan view of the three side by side posts
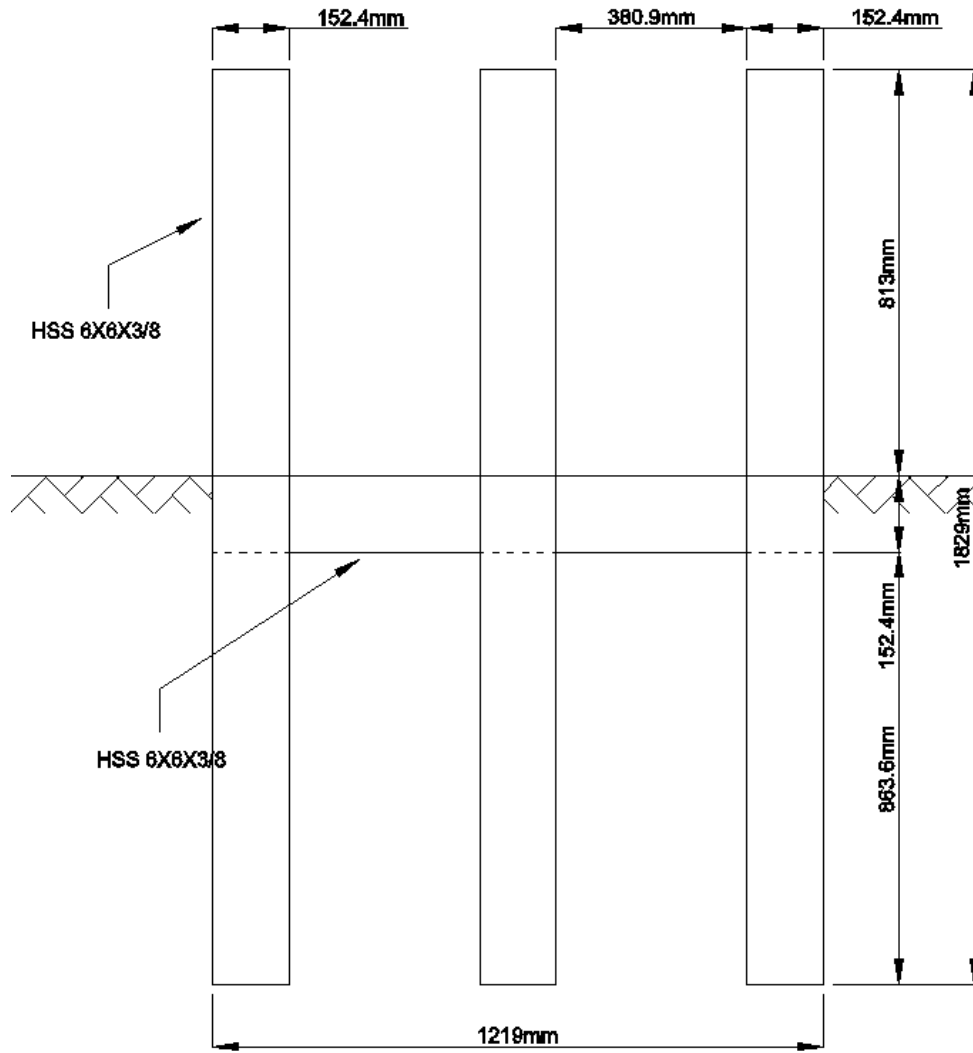
Figure 3.78. Front elevation view of the six three by two posts
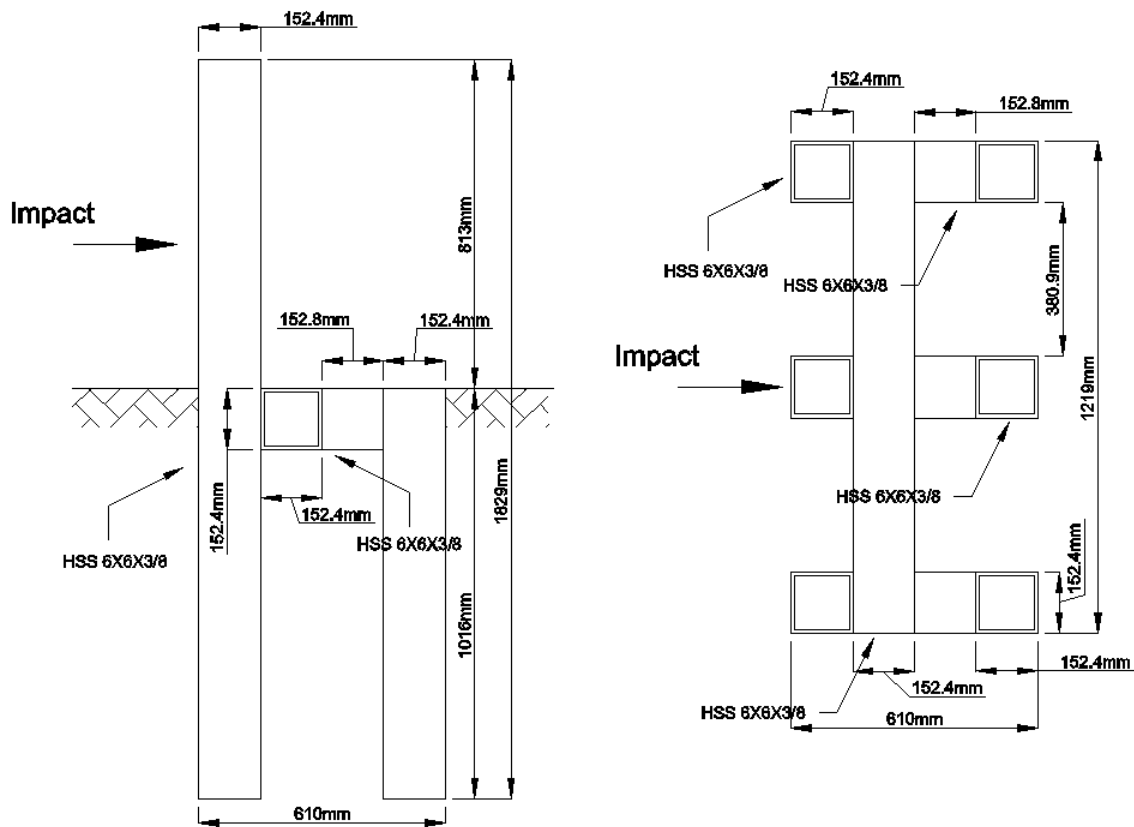
Figure 3.79. Side elevation and plan view of the six three by two posts

3.3.3.7 Test results

Accelerations of the pendulum and the post at the impact level, at the middle and the bottom of the posts were measured. Also the films taken using high speed camera were analyzed to capture the motion of the two targets.

Prior to the impact tests, static lateral capacities of all of the post systems embedded in loose sand were tested. The post was pulled at 356 mm above the ground level that is the impact location of pendulum. The force-displacement results are shown in Figure 3.80. The groups of posts with a row of three posts (Figure 3.44) and with two

rows of six posts (Figure 3.45) are indicated as Group and Framed, respectively in Figure 3.80. Peak force of the backfilled single post was 3.2 kN at the displacement of 34 mm. The peak lateral resistance of the one row of three posts and two rows of six posts were 11.8 kN and 12.3 kN at the displacement of 42 mm and 38 mm, respectively. Note that the displacements were measured at the location where pendulum impacted.
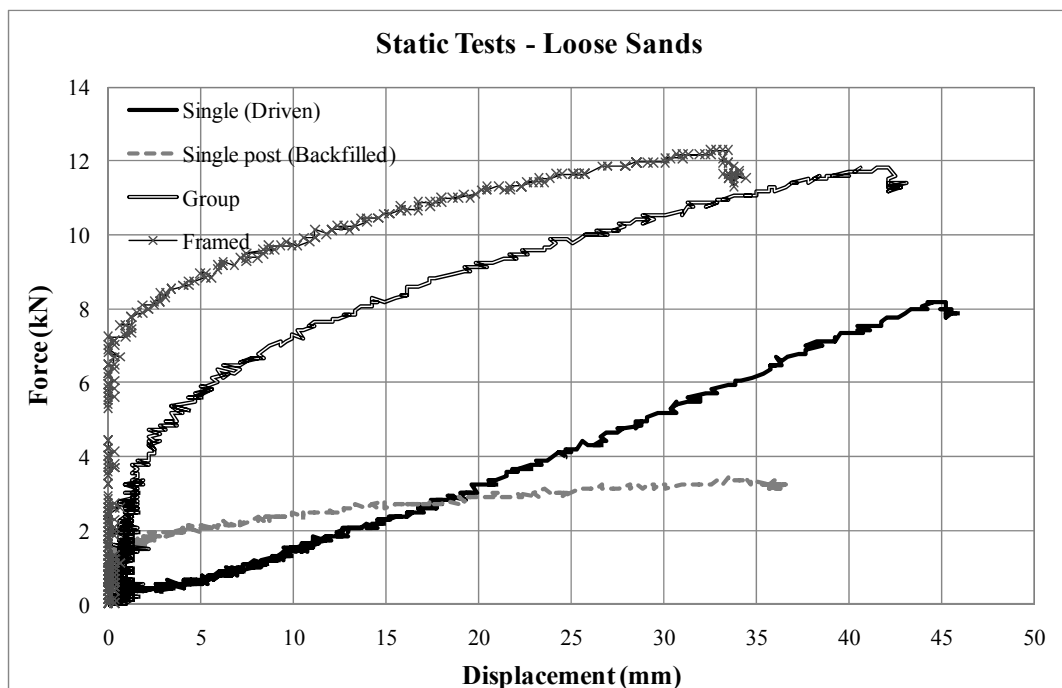
Figure 3.80. Static load test results of post system embedded in loose sand

The force-displacement behavior of the driven post seems somewhat controversial. Since driven pile is generally stronger than backfilled pile in cohesionless soil due to densification of soil, the maximum resistance was measure 8.2 kN that is

more than twice of the resistance of the backfilled one (3.2 kN). However, there is no distinct yielding up to 45 mm of displacement (around 30% of width of the post).

Single post pendulum test with 4.94 m/sec of impact velocity (P4)

Peak longitudinal 50ms-average deceleration of the pendulum was 5.2 g at 0.038 sec. The impact force-history is shown in Figure 3.81. The maximum impact force was 12.6 kN.

The post acceleration at the impact level (0.36 m above the ground level) the middle (0.41 m below the ground level) and the bottom (0.96m below the ground level) of the post are shown in Figure 3.82. Also the velocity-time and displacement-time histories of the post were obtained by integration of the acceleration data as shown in Figure 3.82.
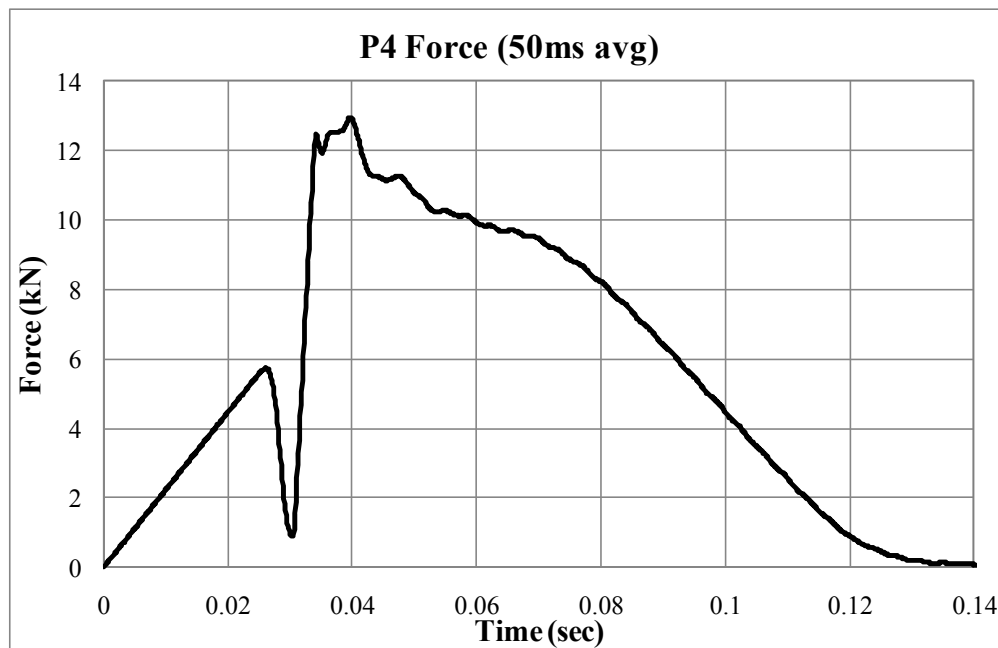
Figure 3.81. 50msec average impact force-time history (P4)
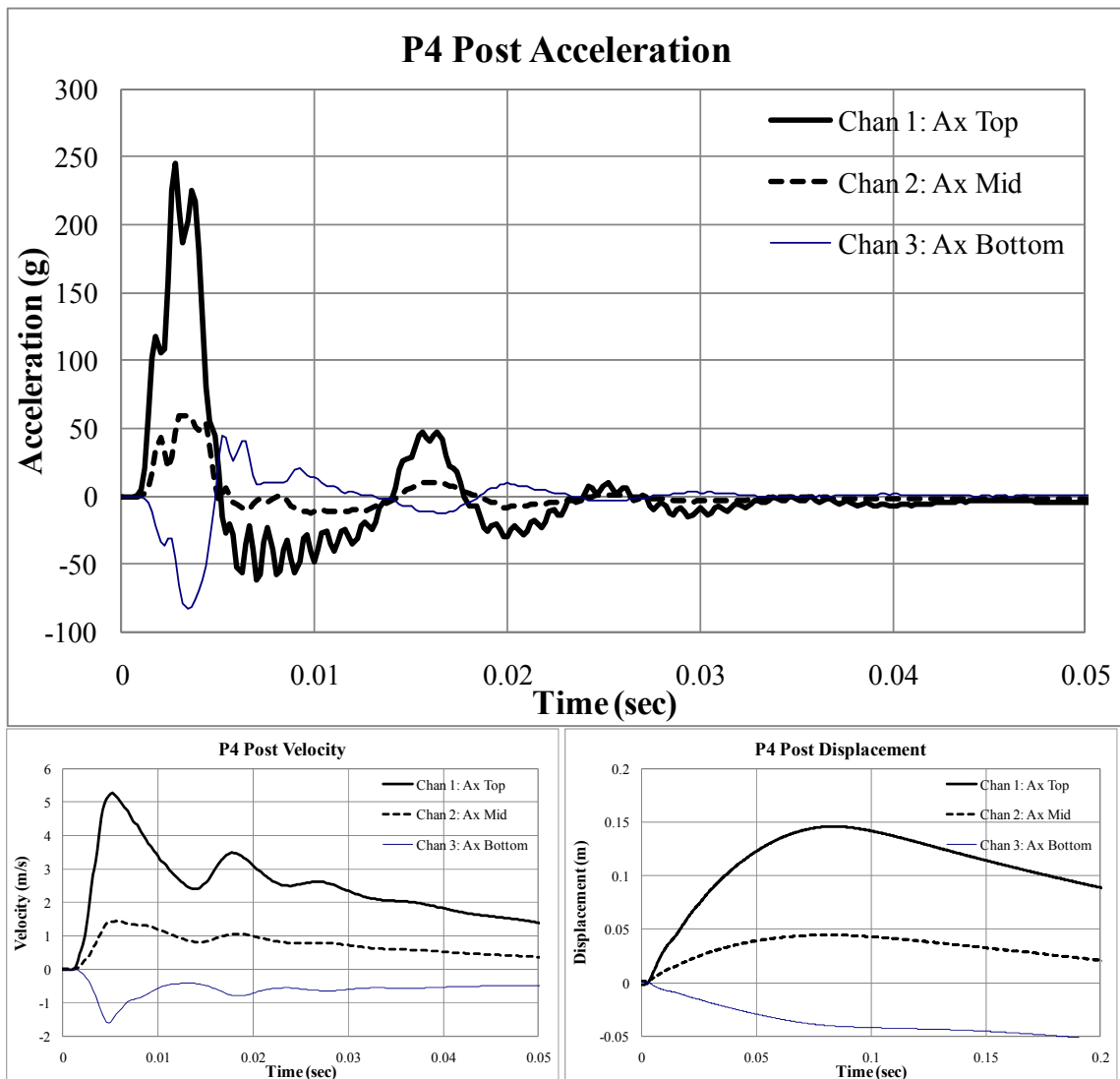
Figure 3.82. Acceleration, velocity and displacement of post history from acceleration data (P4)

Film analysis was conducted to obtain the post displacement history. The film from high speed camera is analyzed to obtain more reliable displacement history. The maximum longitudinal displacement of the post at impact location was 0.142 m at 0.080

sec using film analysis. The permanent displacement at the location was 0.118 m. The displacements at the impact location are indicated as X-disp and Y-disp for the longitudinal and vertical displacement in Figure 3.83. After the test, the permanent rotation of the post was measured as 6.5 degrees.
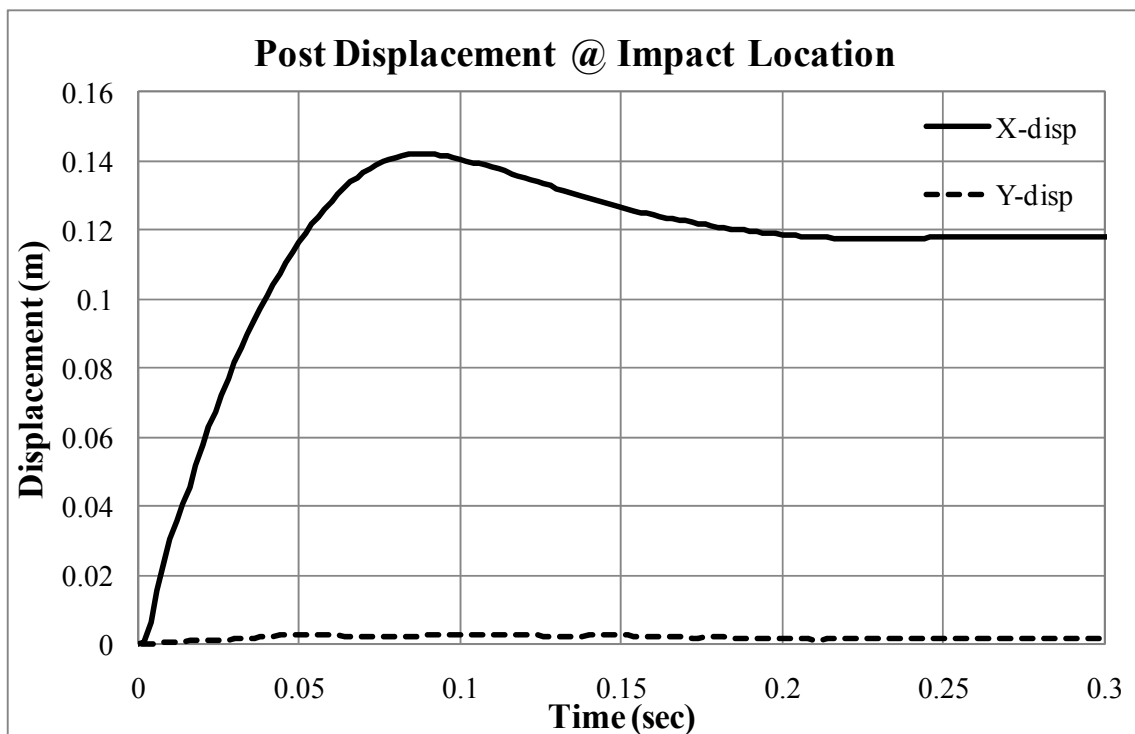
Figure 3.83. Post displacement history from film analysis (P4)

Single post pendulum test with 2.50 m/sec of impact velocity (P5)

Peak longitudinal 50ms-average deceleration of the pendulum was 3.72 g at 0.054 sec. The impact force-history is shown in Figure 3.84. The maximum impact force was 9.1 kN.

The post acceleration at the impact level (0.36 m above the ground level) the middle (0.41 m below the ground level) and the bottom (0.96m below the ground level) of the post are shown in Figure 3.85. Also the velocity-time and displacement-time histories of the post were obtained by integration of the acceleration data as shown in Figure 3.85.

Figure 3.84. 50msec average impact force-time history (P5)

Film analysis was conducted to obtain the post displacement history. The film from high speed camera is analyzed to obtain more reliable displacement history. The maximum longitudinal displacement of the post at impact location was 0.11 m at 0.09 sec using film analysis. The permanent displacement at the location could not be

obtained since the original film was not in a good shape. However, the minimum number of data points in longitudinal direction was manually obtained. The longitudinal displacements at the impact location are shown in Figure 3.86. After the test, the permanent rotation of the post was measured as 4 degrees.
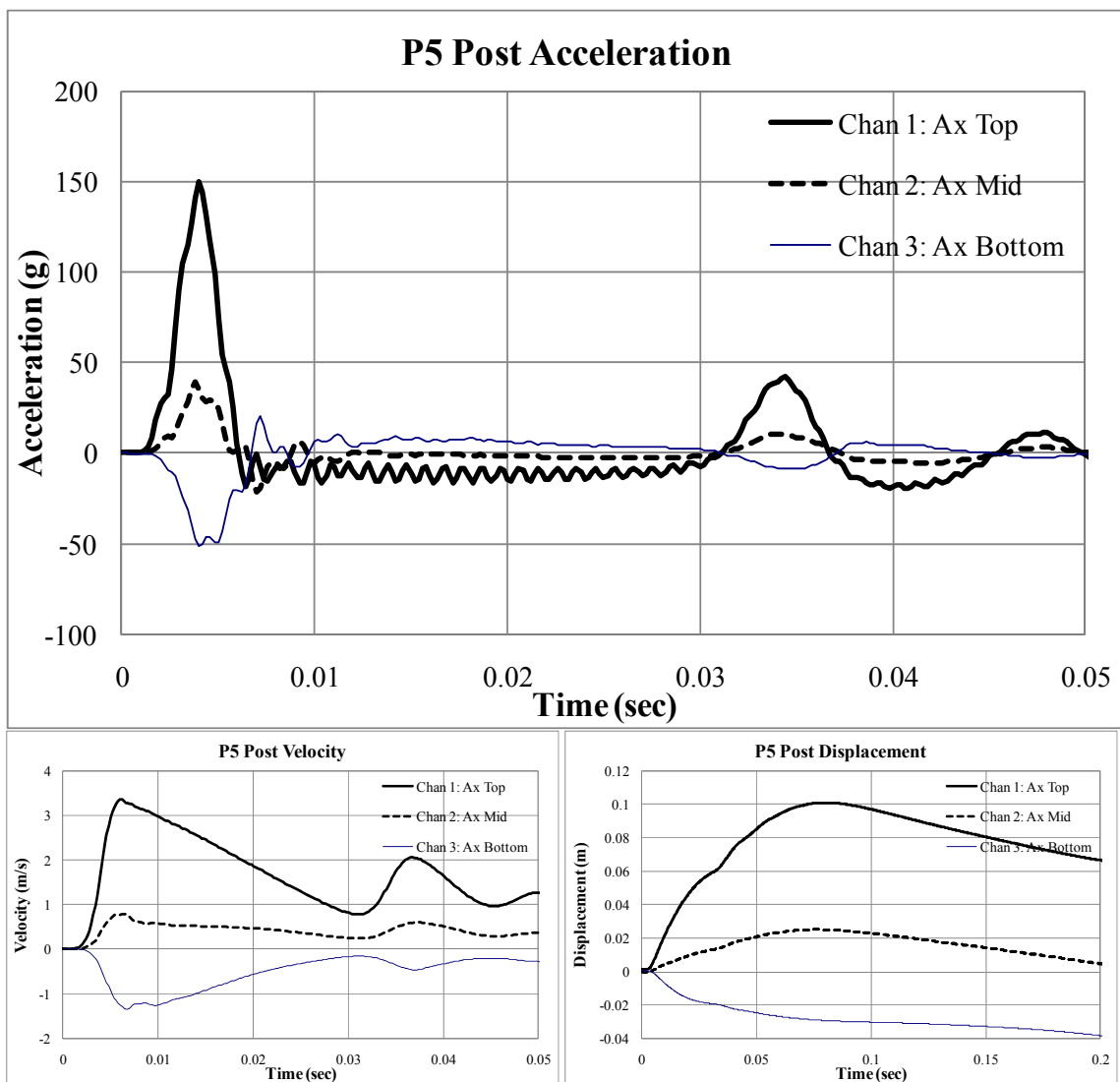
Figure 3.85. Acceleration, velocity and displacement of post history from acceleration data (P5)
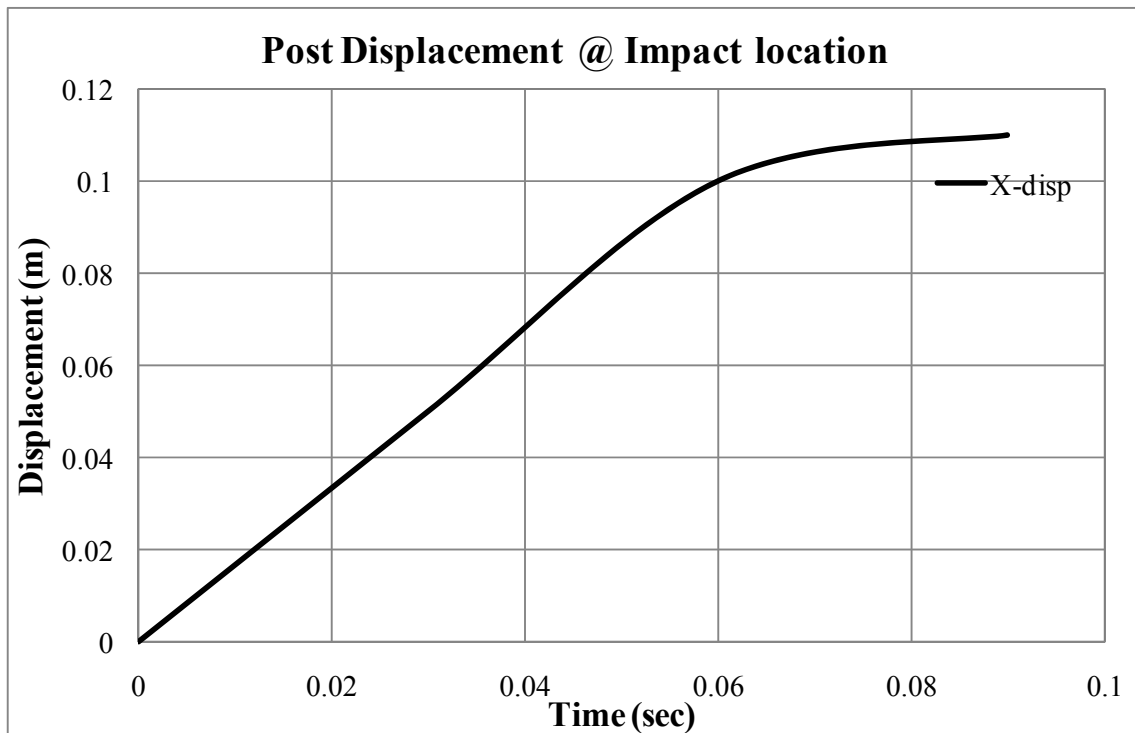
Figure 3.86. Post displacement history from film analysis (P5)

Single post pendulum test with 10.10 m/sec of impact velocity (P6)

The post and pendulum at the moment of the impact with 10.10 m/sec of velocity (P6) are shown in Figure 3.87. There were two impacts between the post and pendulum. As shown in the figure, the soil particles behind the post were dispersed and covered the ground surface behind the post. The range of the mobilized soil seems smaller than the range of the previous test using the medium crushed limestone. It can be evidence that the size of mobilized soil wedge increases as the strength of soil increase. The deformed post and the pendulum just after the impact with are shown in Figure 3.88. The permanent rotation of the post was measured as 33.5 degrees.

Figure 3.87. Pendulum test on single post embedded in loose sand (P6)

Figure 3.88. Displaced single post embedded in loose sand after impact test (P6)

Peak longitudinal 50ms-average deceleration of the pendulum was 8.8 g at 0.024 sec. The impact force-history is shown in Figure 3.89. The maximum impact force was 21.3 kN.

The post acceleration at the impact level (0.36 m above the ground level) the middle (0.41 m below the ground level) and the bottom (0.96m below the ground level) of the post are shown in Figure 3.90. Also the velocity-time and displacement-time histories of the post were obtained by integration of the acceleration data as shown in Figure 3.90.
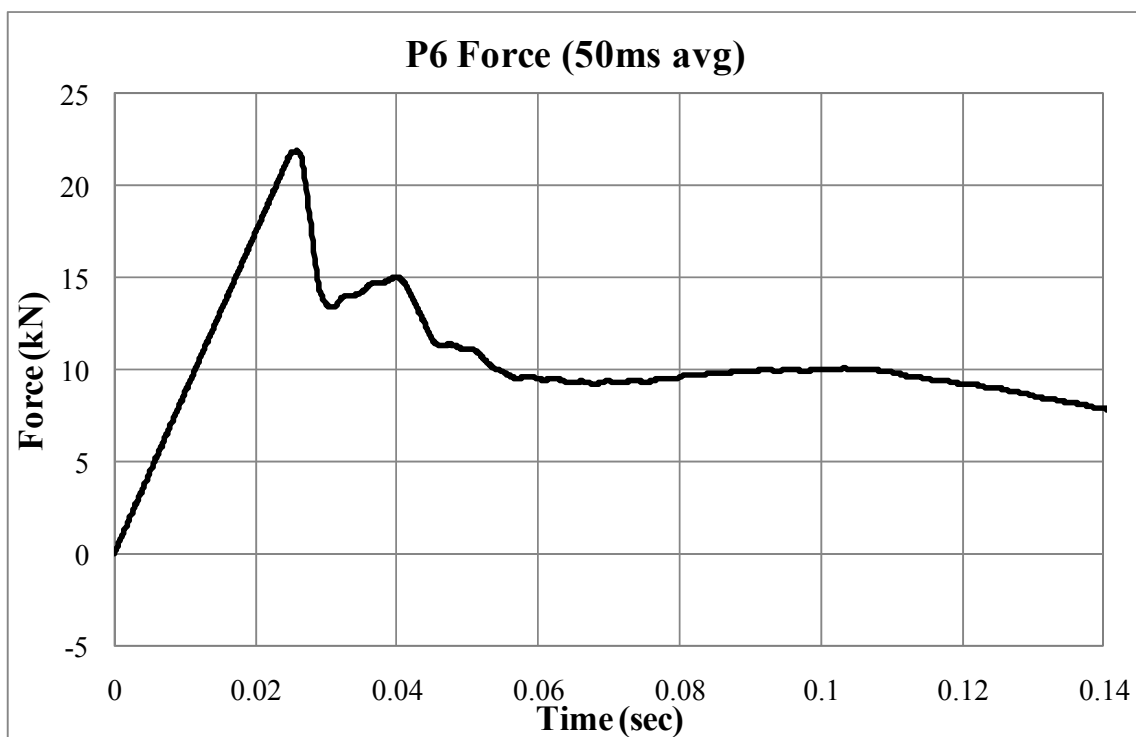
Figure 3.89. 50msec average impact force-time history (P6)
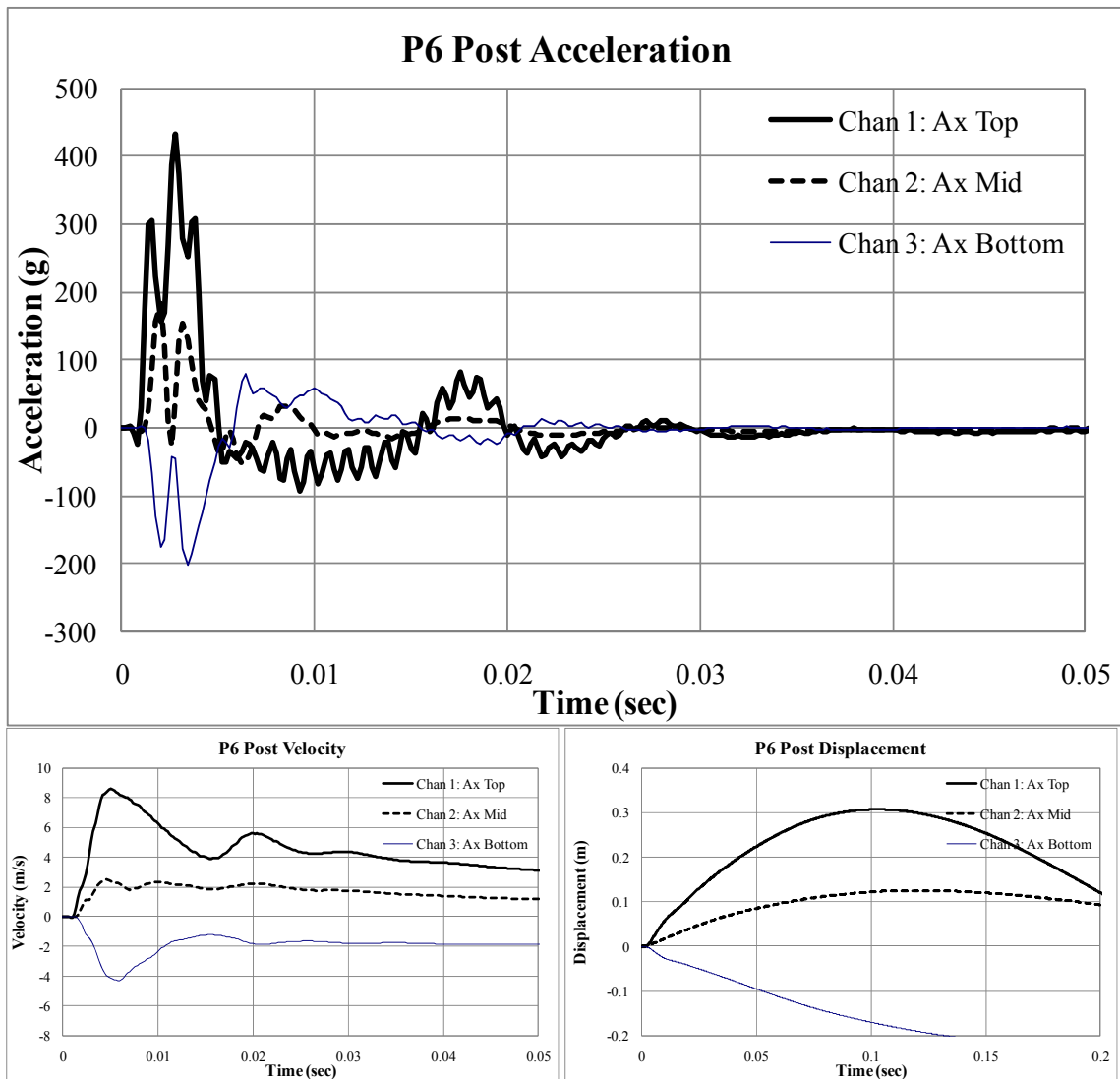
Figure 3.90. Acceleration, velocity and displacement of post history from acceleration data (P6)

Film analysis was conducted to obtain the post displacement history. The film from high speed camera is analyzed to obtain more reliable displacement history than that from integration of acceleration data. The maximum longitudinal displacement of the post at impact location was 0.55 m at 0.015 sec using film analysis. The permanent

displacement at the location was 0.54 m. The displacements at the impact location are indicated as X-disp and Y-disp for the longitudinal and vertical displacement in Figure 3.91.
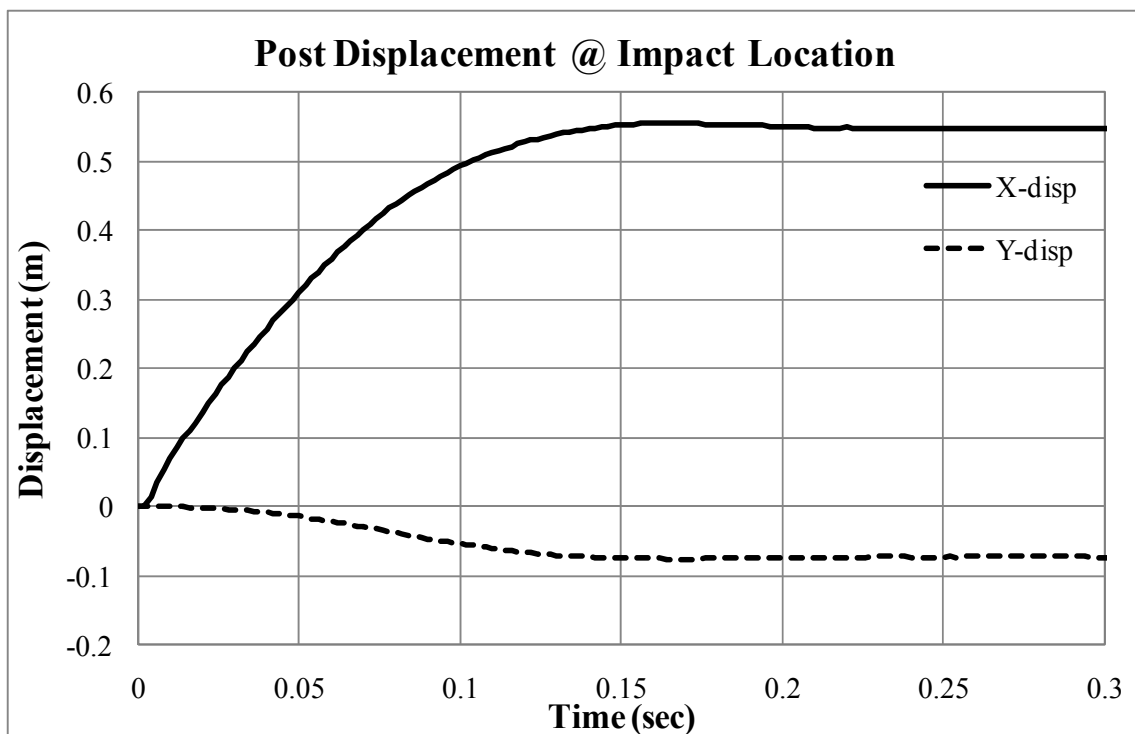
Figure 3.91. Post displacement history from film analysis (P6)

Group of three posts in a row pendulum test with 10.01 m/sec of impact velocity (P7)

The permanent rotation of the post was measured as 19 degrees. The center post deflected 3 mm more than the other two side posts at the ground level.

The post system and pendulum at the moment of the impact with 10.01 m/sec of velocity (P7) are shown in Figure 3.92. As shown in the figure, the soil particles behind

the post were dispersed and covered the ground surface behind the post. The deformed post and the pendulum just after the impact with are shown in Figure 3.93.

The accelerations of the pendulum exceeded the range set for the accelerometer. Some portion of signal representing the peak acceleration of pendulum was truncated. Thus, the maximum 50 ms-average acceleration and force provides lower values than the actual acceleration and impact force. Peak longitudinal 50ms-average deceleration of the pendulum was 8.3 g at 0.028 sec. The impact force-history is shown in Figure 3.94. The maximum impact force was 20.65 kN.

Figure 3.92. Pendulum test on group of posts system embedded in loose sand (P7)

Figure 3.93. Displaced group of posts system embedded in loose sand after impact test (P7)
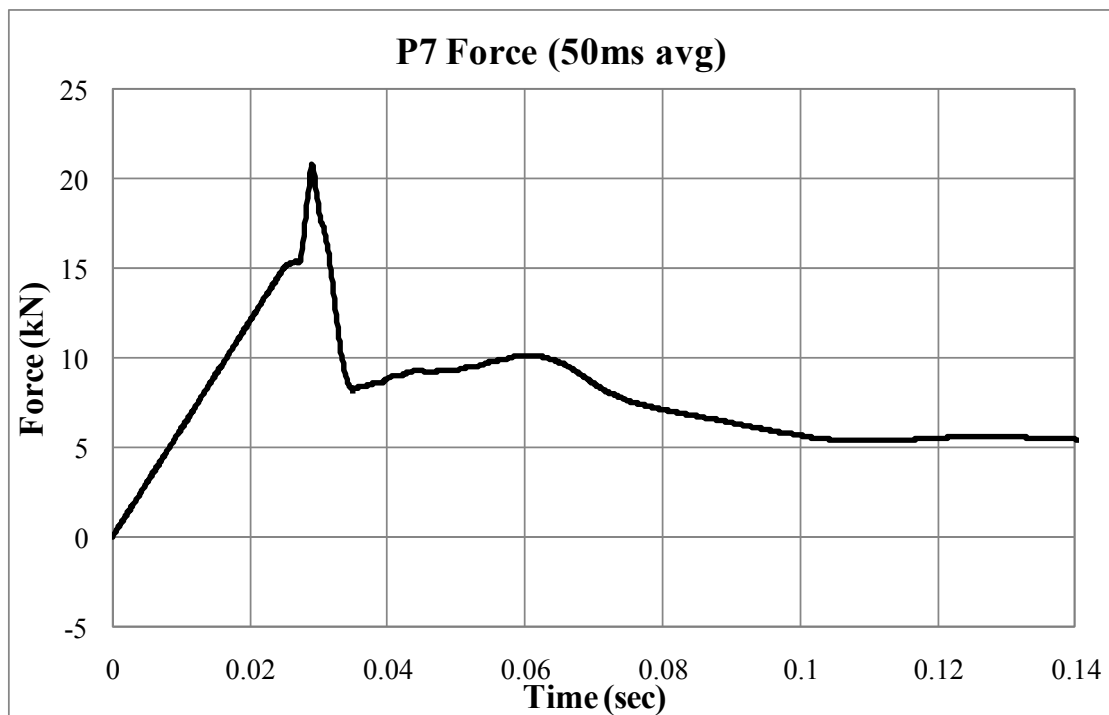
Figure 3.94. 50msec average impact force-time history (P7)

The accelerations at the ground level of the three posts are shown in Figure 3.95. Also the velocity-time and displacement-time histories of the posts were obtained by integration of the acceleration data as shown in Figure 3.95.
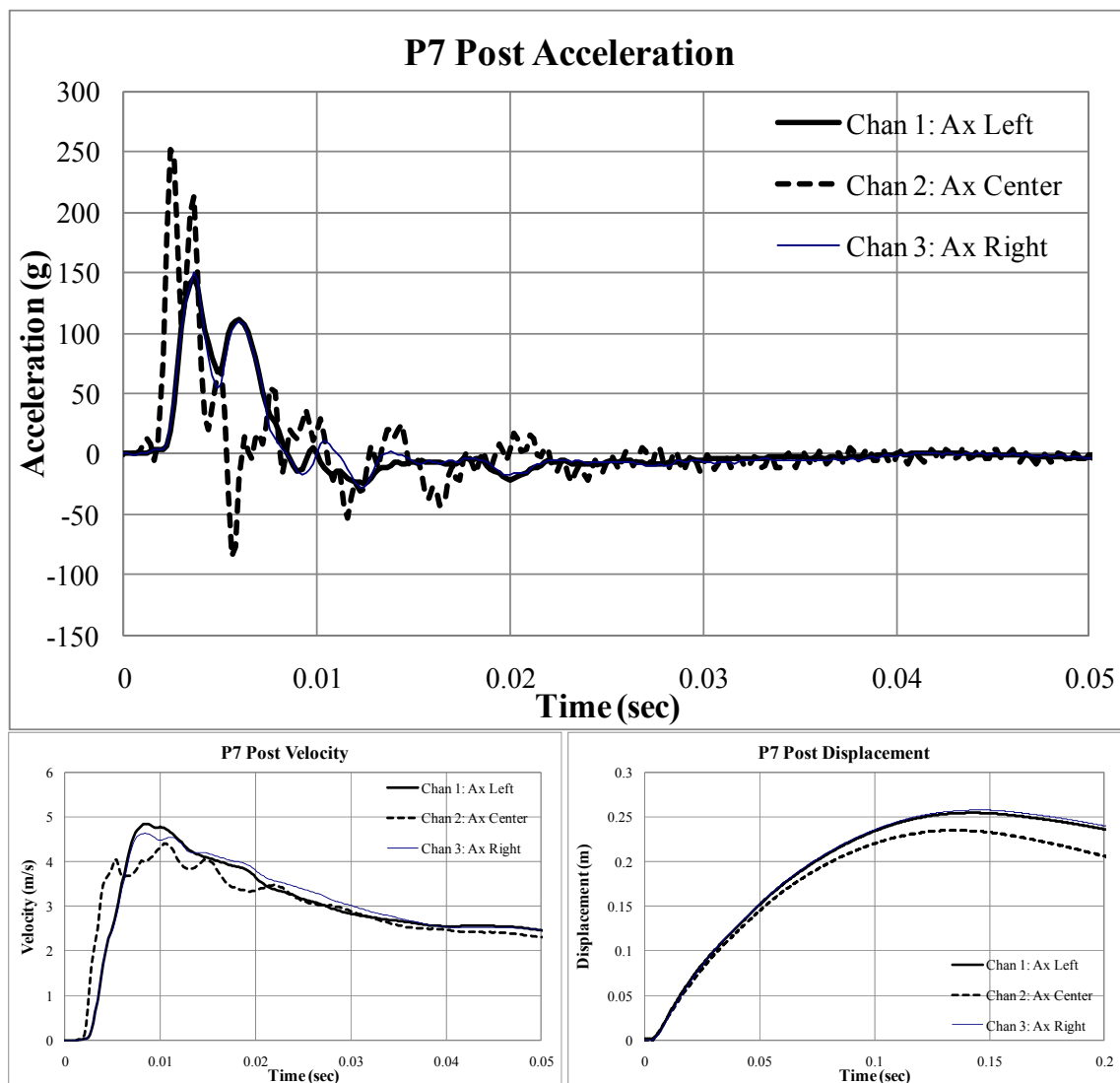
Figure 3.95. Acceleration, velocity and displacement of post history from acceleration data (P7)

Film analysis was conducted to obtain the post displacement history. The targets were attached on the right side post not on the center one, since the center post was obscured by the side posts. According to film analysis and measurement after test, the difference in displacement of the center posts and the other two was around 0.005 mm at the impact location (356 mm above the ground level).

The maximum longitudinal displacement of the post at impact location was 0.37 m at 0.15 sec using film analysis. The permanent displacement at the location was 0.35 m. The displacements at the impact location are indicated as X-disp and Y-disp for the longitudinal and vertical displacement in Figure 3.96.
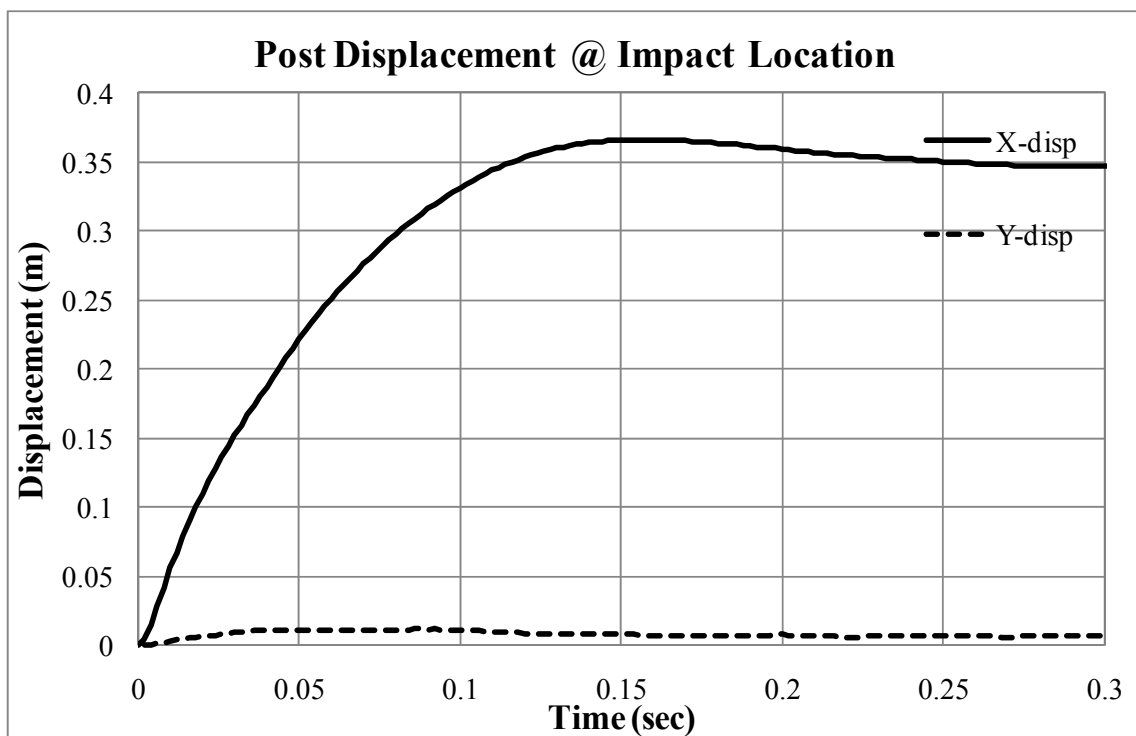
Figure 3.96. Post displacement history from film analysis (P7)

Pendulum test with 10.21 m/sec of impact velocity (P8)

As stated in the previous paragraph, the some portion of acceleration of pendulum of P7 was truncated. Therefore, P8, the identical test of P7 was conducted. The actual impact velocity of P8 was 0.2 m/sec higher than that of P7. The post system used for P7 was used again but reinstalled. Before the test, the center posts was placed 4 mm behind the other two posts. After the test the permanent rotation of the post was measured as 24 degrees. The center post deflected 4 mm more than the other two side posts at the ground level. The difference in deflection of the center post and the others stayed same before and after the impact.

The displaced soil behind the test is shown in Figure 3.97. The heaving of soil behind the post extended up to 690 mm behind the post. Since the particles of soil behind the post were dispersed and covered the soil surface, the measurement was not indicated the actual size of the mobilized soil.

Figure 3.97. Displaced soil after impact test (P8)

Peak longitudinal 50ms-average deceleration of the pendulum was 12 g at 0.025 sec. The impact force-history is shown in Figure 3.98. The maximum impact force was 30 kN. The maximum impact force of the previous test (P7) was 20.65 kN that was lower than actual value, since the raw acceleration of P7 was truncated.

P8 Force (50ms avg)
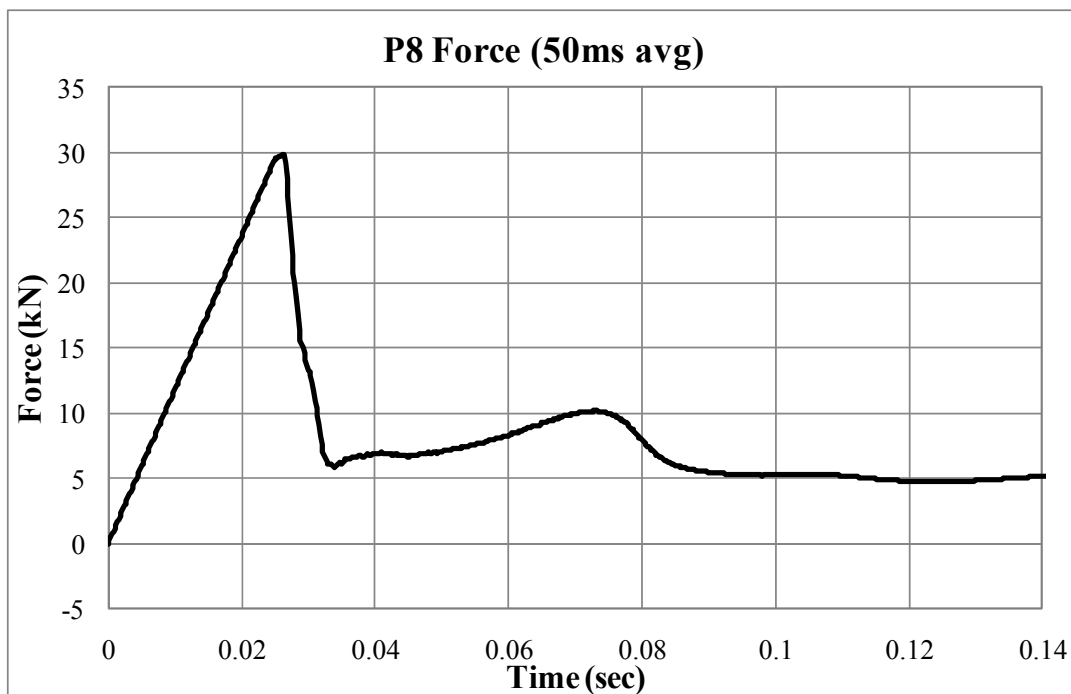
Figure 3.98. 50msec average impact force-time history (P8)

The post acceleration at the impact level (0.36 m above the ground level) the middle (0.41 m below the ground level) and the bottom (0.96m below the ground level) of the post are shown in Figure 3.99. Also the velocity-time and displacement-time histories of the post were obtained by integration of the acceleration data as shown in Figure 3.99.
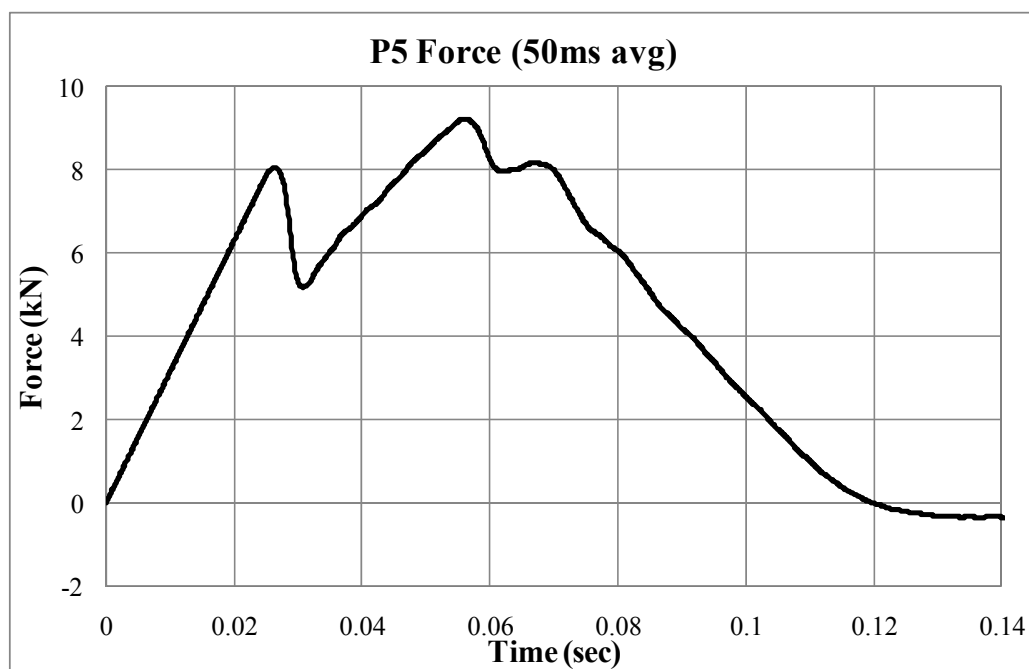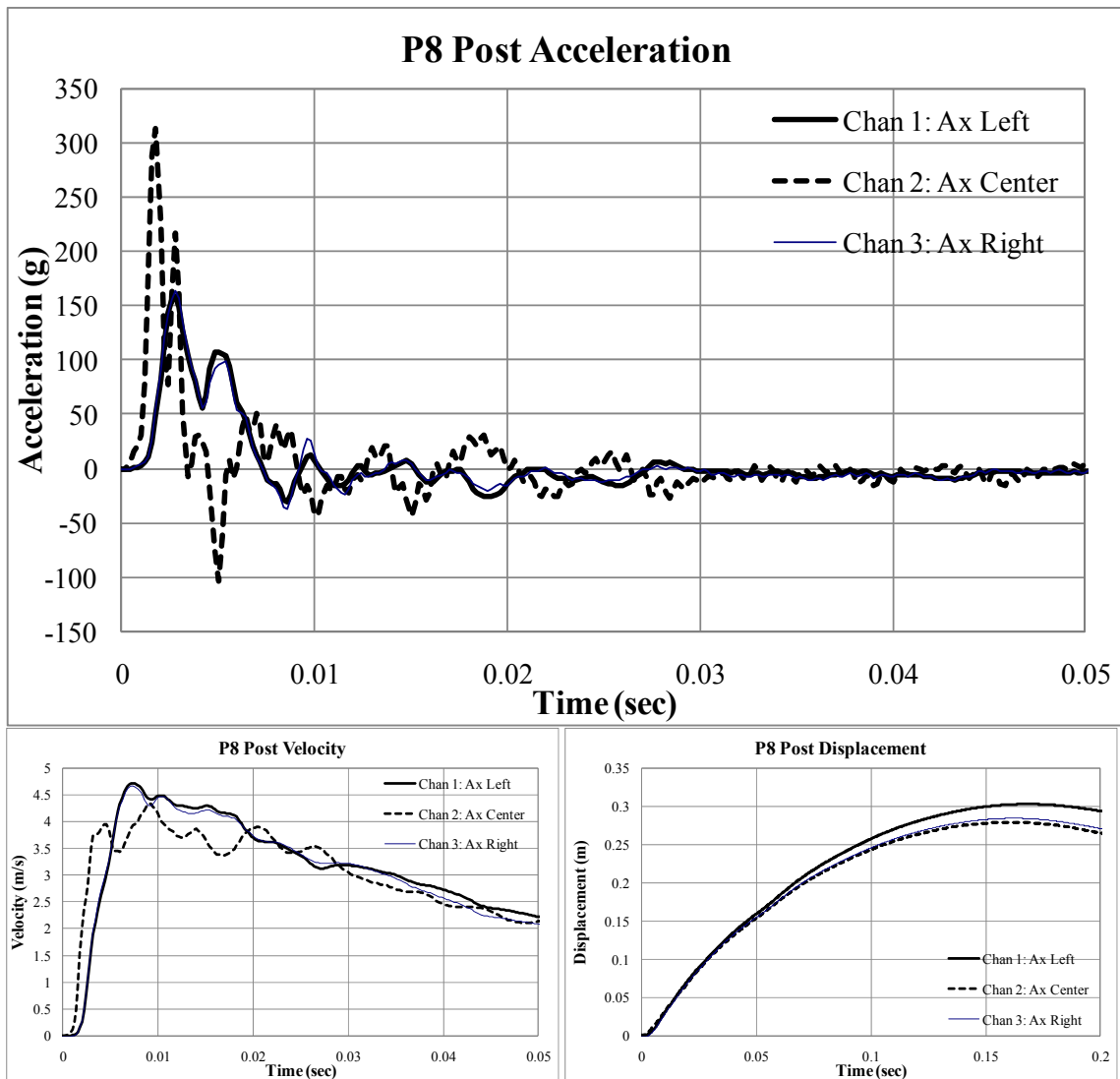
Figure 3.99. Acceleration, velocity and displacement of post history from acceleration data (P8)

Film analysis was conducted to obtain the post displacement history. The maximum longitudinal displacement of the post at impact location was 0.445 m at 0.18 sec using film analysis. The permanent displacement at the location was 0.43 m. The

displacements at the impact location are indicated as X-disp and Y-disp for the longitudinal and vertical displacement in Figure 3.100.
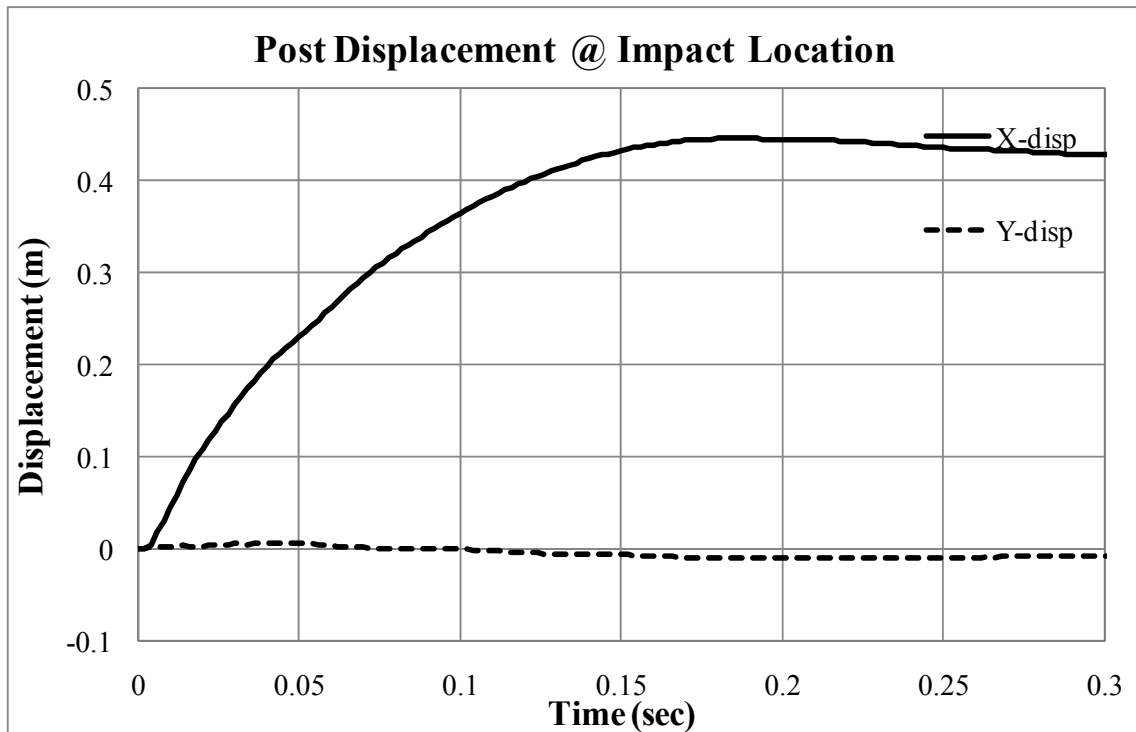
Figure 3.100. Post displacement history from film analysis (P8)

Group of six posts in two rows pendulum test with 9.83 m/sec of impact velocity (P9)

The permanent rotation of the post was measured as 16.5 degrees after the impact. The center post of the first row deflected 3 mm more than the other two side posts at the ground level.

The post system and pendulum at the moment of the impact with 9.83 m/sec of velocity (P9) are shown in Figure 3.101. As shown in the figure, the soil particles behind

the post were dispersed and covered the ground surface behind the post. The deformed post and the pendulum just after the impact with are shown in Figure 3.102.

Peak longitudinal 50ms-average deceleration of the pendulum was 14.6 g at 0.0246 sec. The impact force-history is shown in Figure 3.103. The maximum impact force was 35.7 kN. The acceleration of post system was not measured.

Film analysis was conducted to obtain the post displacement history. The targets were attached on the right side post in the first row not on the center one, since the center post was obscured by the side posts. According to film analysis and measurement after test, the difference in displacement of the center posts and the other two was around 0.005 mm at the impact location (356 mm above the ground level).

Figure 3.101. Pendulum test on group of posts system embedded in loose sand (P9)

Figure 3.102. Displaced group of posts system embedded in loose sand after impact test (P9)
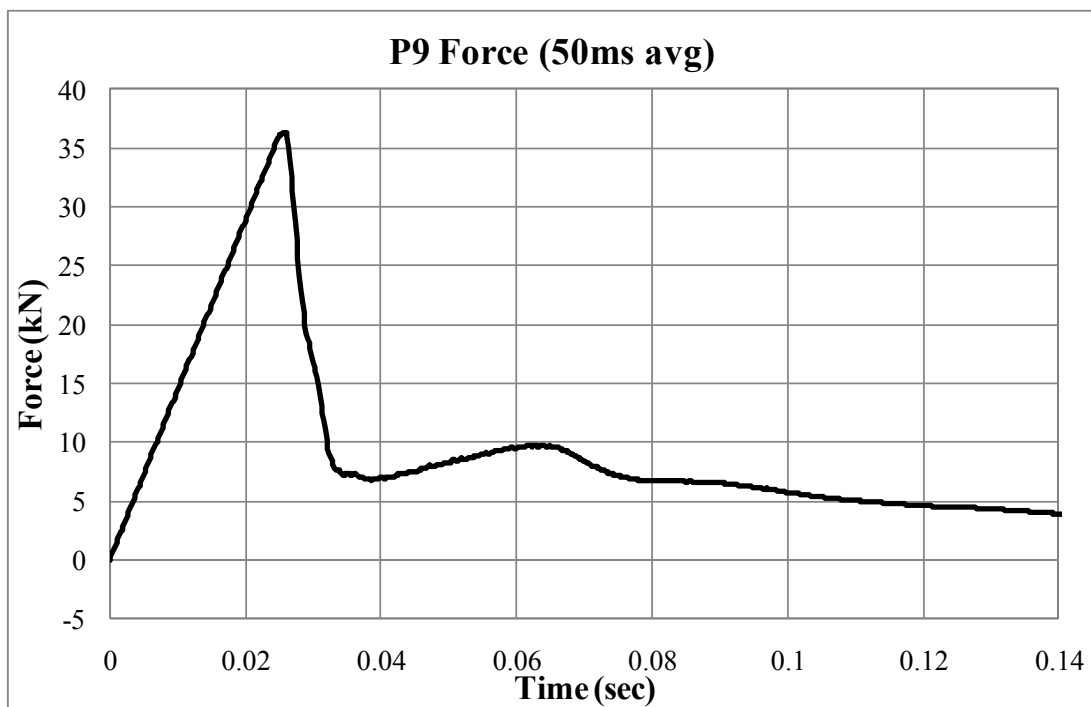
Figure 3.103. 50msec average impact force-time history (P9)

The maximum longitudinal displacement of the post at impact location was 0.345m at 0.15 sec using film analysis. The permanent displacement at the location was 0.31 m. The displacements at the impact location are indicated as X-disp and Y-disp for the longitudinal and vertical displacement in Figure 3.104.
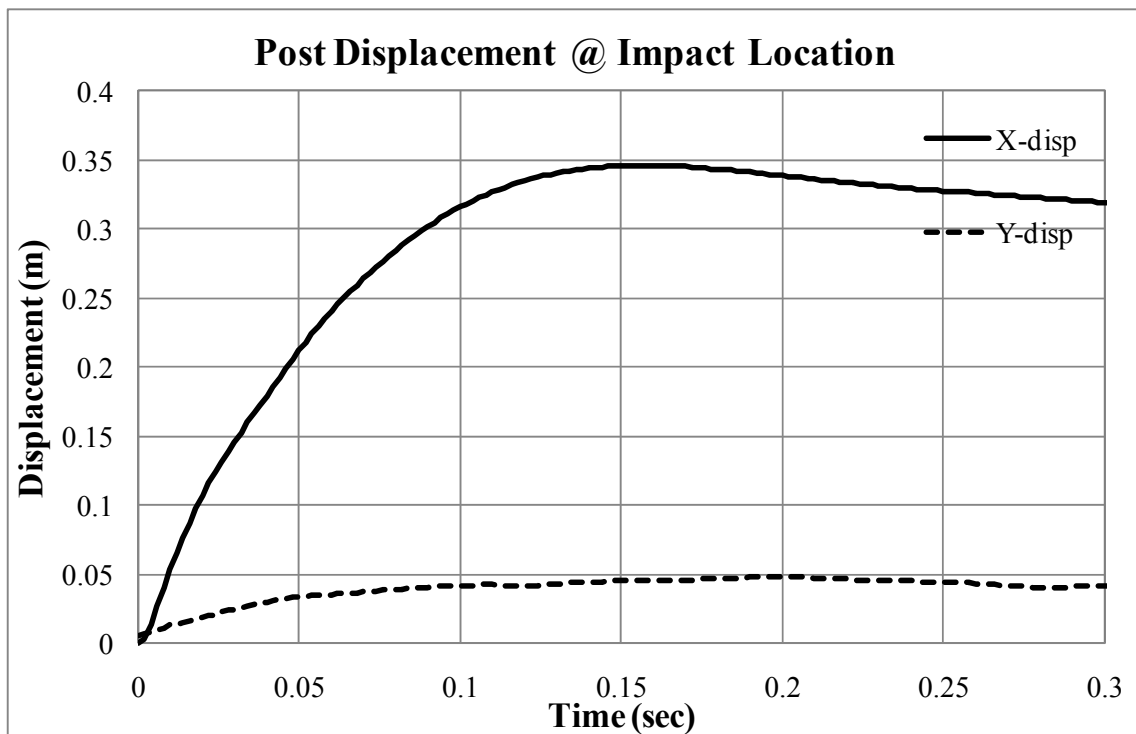
Figure 3.104. Post displacement history from film analysis (P9)

Single post pendulum test with 9.83 m/sec of impact velocity (P10)

The single post pendulum test (P10) was the identical test of (P6) except the installation of post. The post of P10 was backfilled whereas the post of P6 was driven. Since the group of posts system was backfilled in loose sand, backfilled single post test (P10) was

performed. Peak longitudinal 50ms-average deceleration of the pendulum was 5.6 g at 0.026 sec. The impact force-history is shown in Figure 3.105. The maximum impact force was 14 kN.
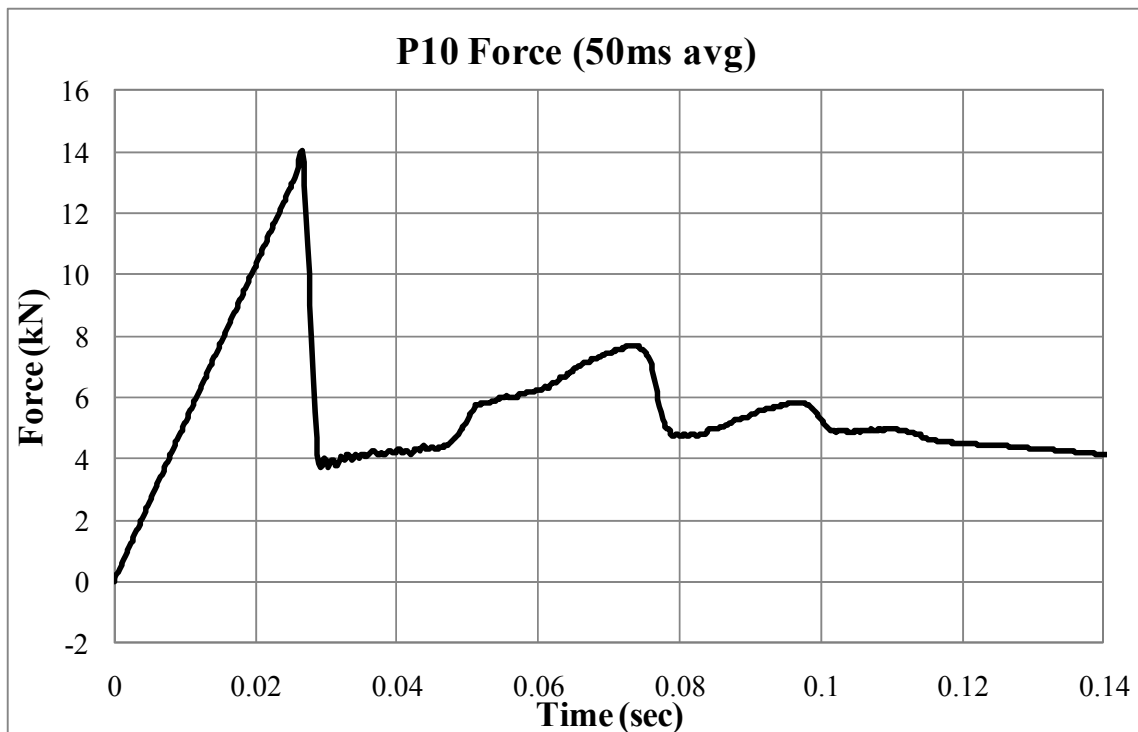
Figure 3.105. 50msec average impact force-time history (P10)

The post acceleration at the impact level (0.36 m above the ground level) the middle (0.41 m below the ground level) and the bottom (0.96m below the ground level) of the post are shown in Figure 3.106. Also the velocity-time and displacement-time histories of the post were obtained by integration of the acceleration data as shown in Figure 3.106.
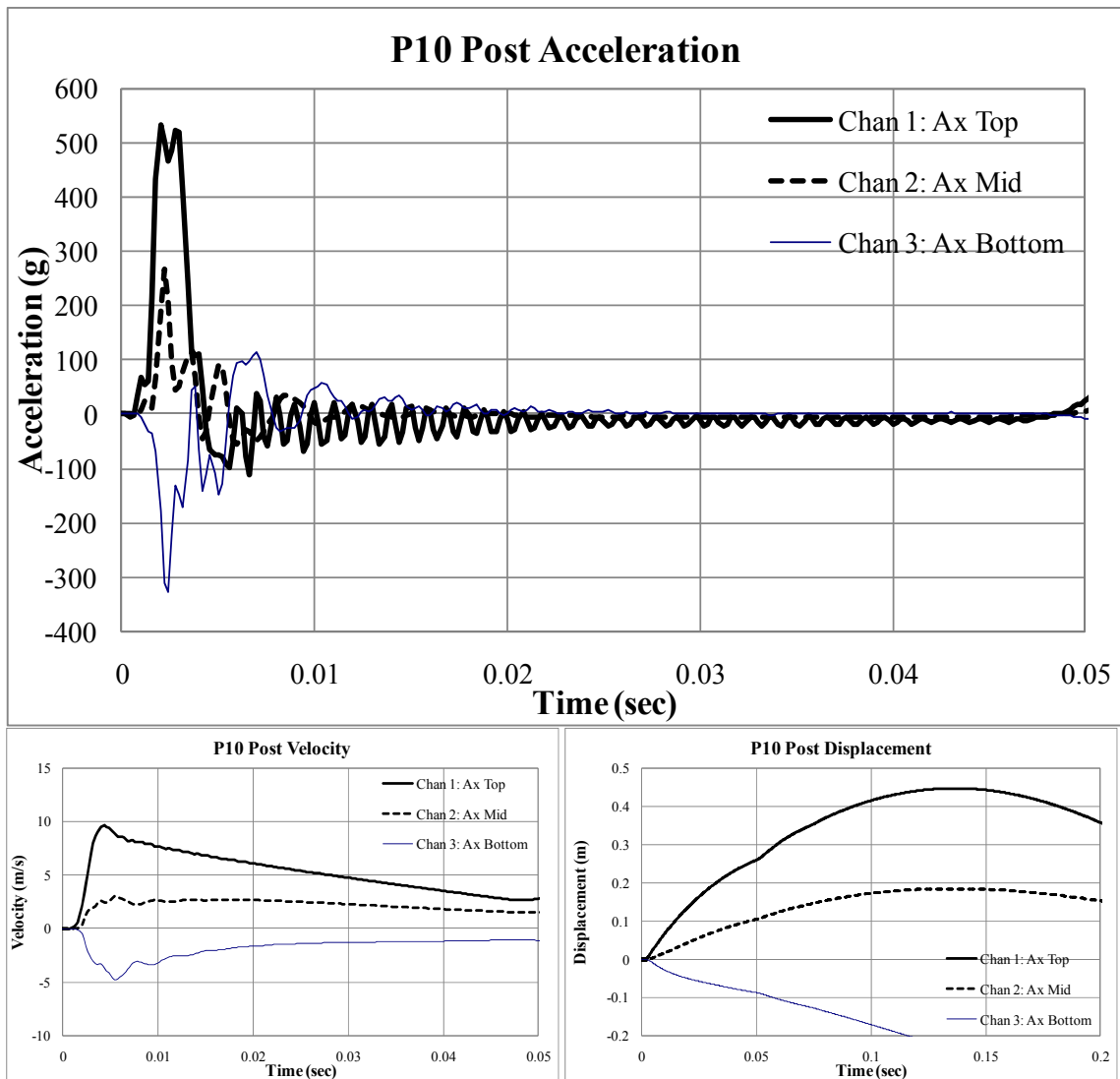
Figure 3.106. Acceleration, velocity and displacement of post history from acceleration data (P10)

Film analysis was conducted to obtain the post displacement history. Since the dispersed soil particles obscured the targets after 0.18 sec, the displacement data could not be obtained. The maximum longitudinal displacement of the post at impact location was 0.78 m at 0.018 sec using film analysis. The displacements at the impact location

are indicated as X-disp and Y-disp for the longitudinal and vertical displacement in Figure 3.107.

Post Displacement @ Impact Location
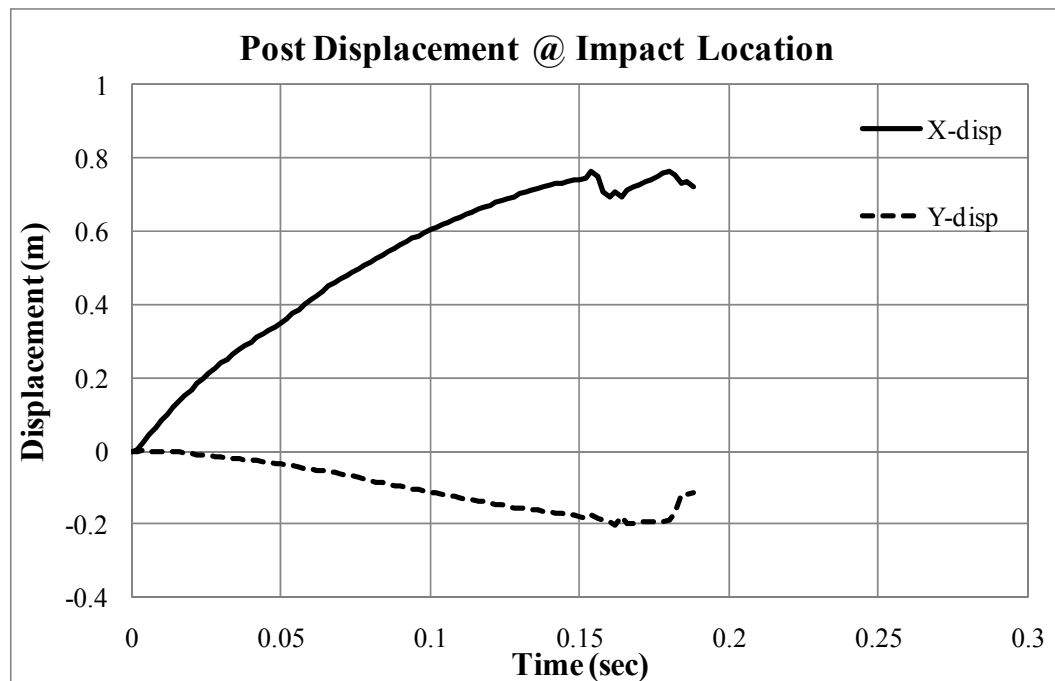
Figure 3.107. Post displacement history from film analysis (P10)

3.3.3.8 Data analysis

The post displacement from film analysis and that from integration of acceleration data were compared and shown in Figure 3.108 through Figure 3.113. The displacement histories of P6 and P10 tests seem unrealistic due to the noise of the raw acceleration data (Figure 3.110 and Figure 3.113). The displacements of group of posts system at the ground level not at the impact location were compared because the accelerometers of group of posts were installed at the ground level.
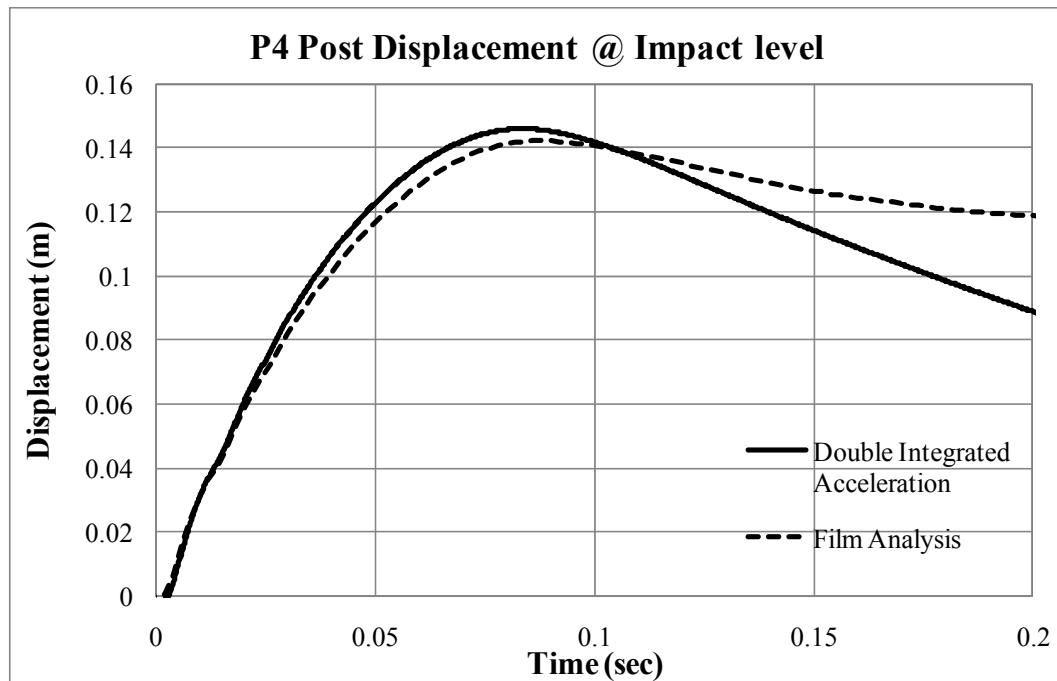
Figure 3.108. Post displacement comparison (P4)
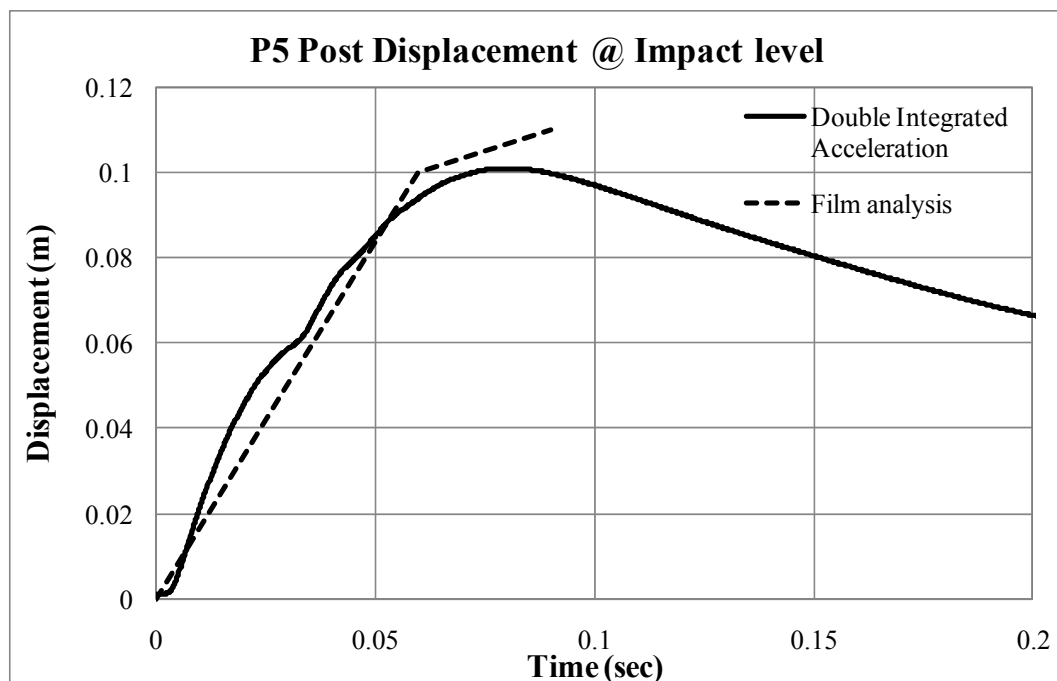
Figure 3.109. Post displacement comparison (P5)
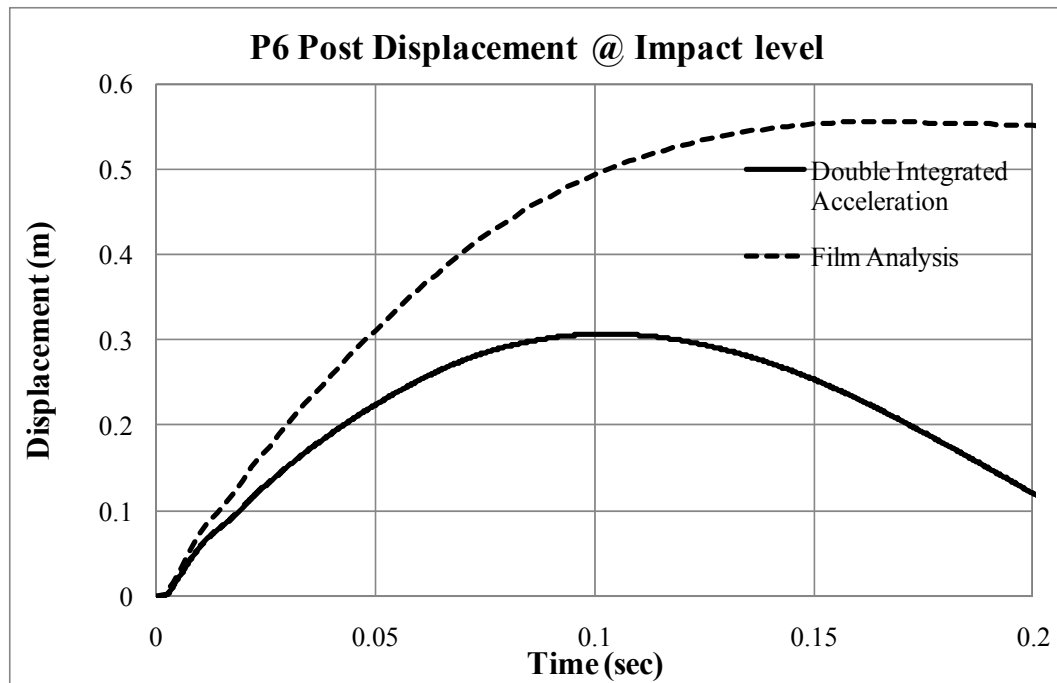
Figure 3.110. Post displacement comparison (P6)
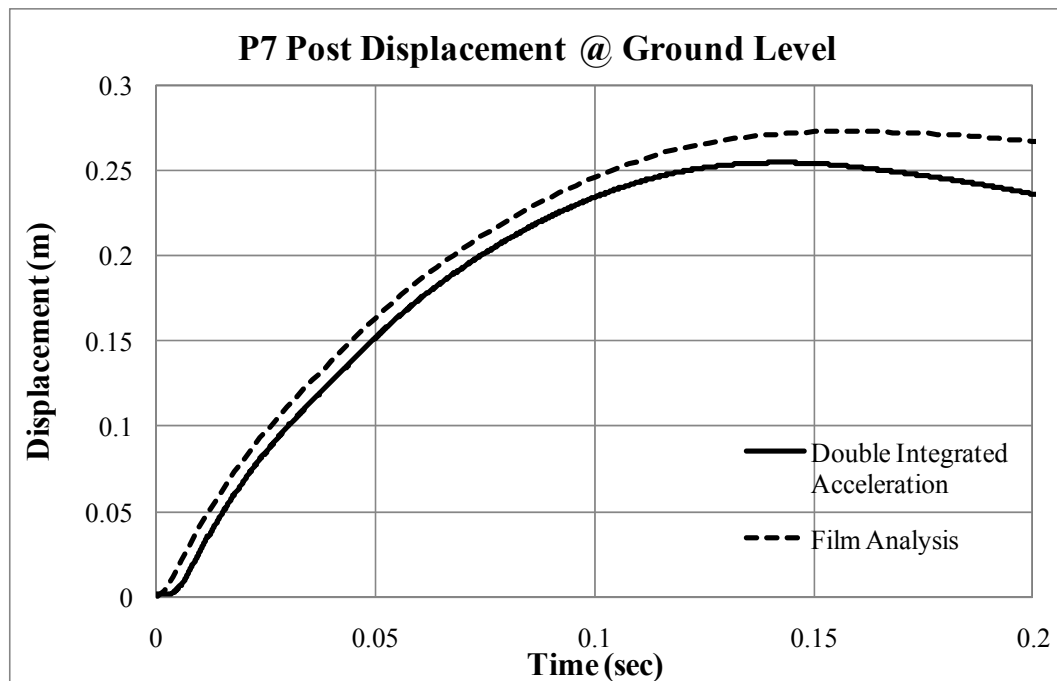
Figure 3.111. Post displacement comparison (P7)
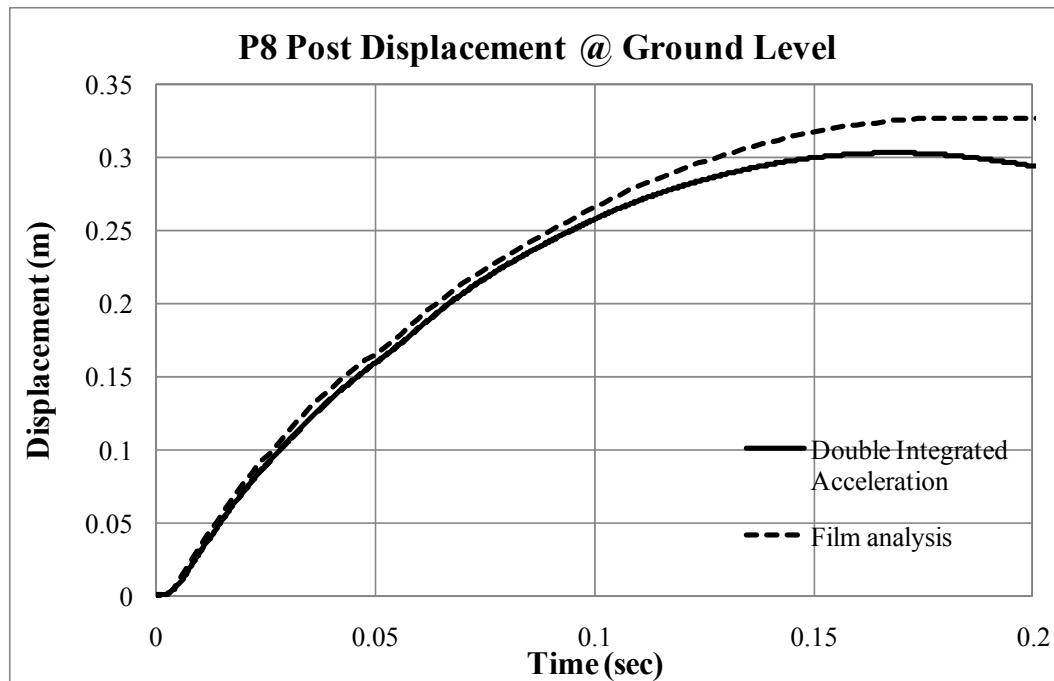
Figure 3.112. Post displacement comparison (P7)
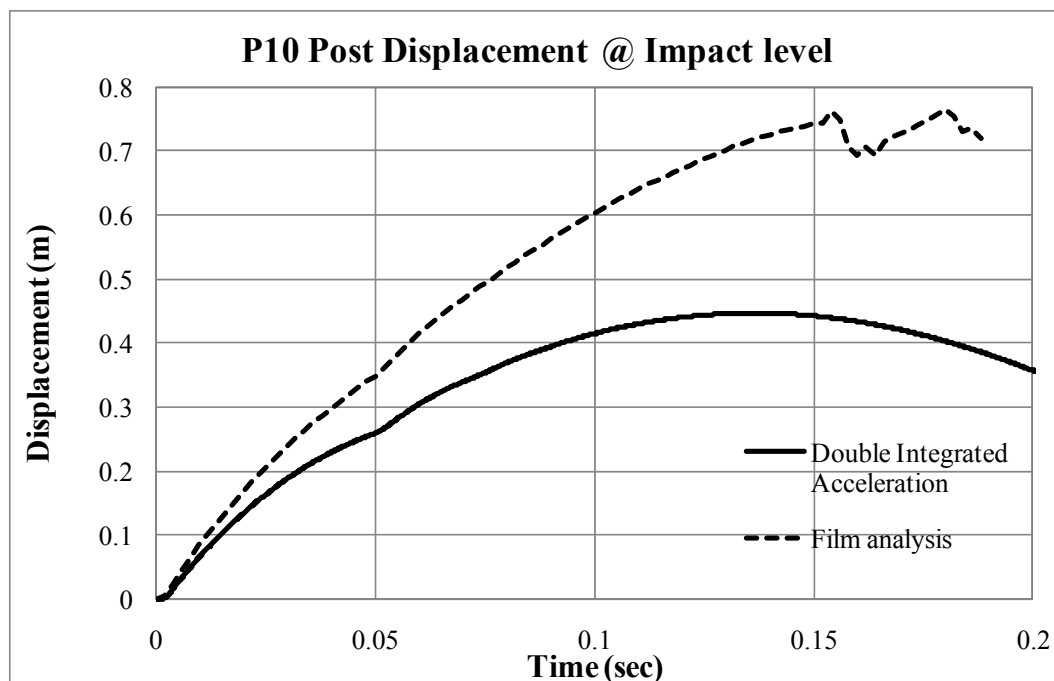
Figure 3.113. Post displacement comparison (P10)

Based on the post displacement history and the impact force history, the force versus displacement relationship was obtained (Figure 3.114). Since the loading speed of the static test was approximately 0.6 mm/sec, the speed of static test can be considered as zero. The forces of impact test were last around 0.2 sec whereas that of the static test was last 70 sec.
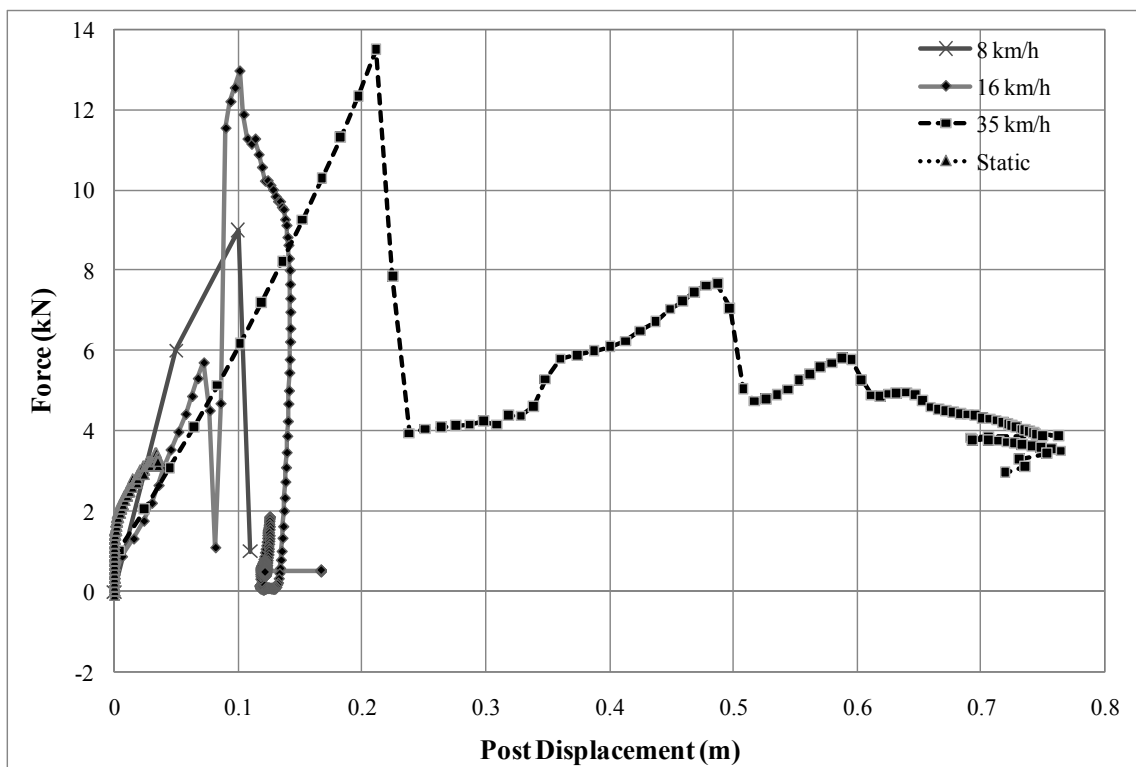
Figure 3.114. Force-displacement of single post in loose sand

The maximum forces versus impact velocities are plotted in Figure 3.115. According to this, dynamic factor, DF is a function of impact velocity. The maximum force increase and the increment of force decrease as the impact velocity increase. It may

have a certain critical point or limit. Hence the maximum force may stop increase at a critical impact velocity. In this particular test with single post in loose sand, the limit velocity and limit force are 16 km/s and 13 kN, respectively. This data is analyzed in Section 3.4.3 with the tests data from other model tests.
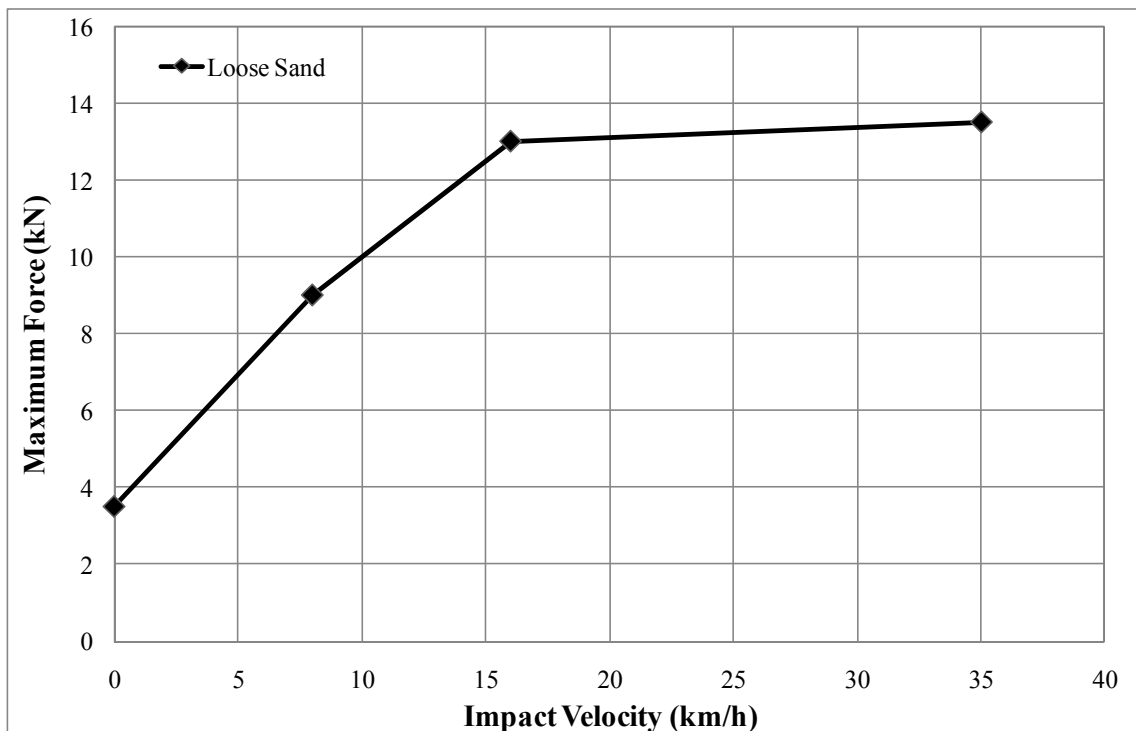
Figure 3.115. The maximum force-impact velocity for loose sand

The maximum force versus impact relationship for all single post pendulum tests is shown in Figure 3.116. The magnitude of increment of the maximum forces of single posts in medium dense crushed limestone for higher velocity impact tests is bigger than that of the tests in loose sand. The maximum forces for loose sand converged to a critical

or limit value whereas that for medium dense crushed limestone increased as impact velocity increased, though the increment was decreased.

The phenomena can be simplified using Single degree of freedom (SDOF) model with soil mass damper and spring as shown in Figure 3.117. The model can be expressed as:

$$M_T \cdot a_T = M_S \cdot \ddot{x} + C \cdot \dot{x} + k \cdot x \qquad (3\text{-}12)$$

where, M_T = mass of vehicle, pendulum or bogie.

a_T = deceleration of vehicle, pendulum or bogie.

M_S = mobilized mass of soil and post system

C = damping of the system

k = spring constant of system

$\ddot{x}$ = Acceleration of the system

$\dot{x}$ = velocity of the system

x = displacement of the system

The static resistance can be considered as spring constant times displacement of system, $k \cdot x$. The other components, soil inertia, $M_S \cdot \ddot{x}$ and damping, $C \cdot \dot{x}$ can be caused due to dynamic effects. Figure 3.118, Figure 3.119 and Figure 3.120 are obtained using the above assumption. Damping such as rate effect can be negligible for sand or cohesionless material. Then the dynamic effect is largely from the inertia effect.
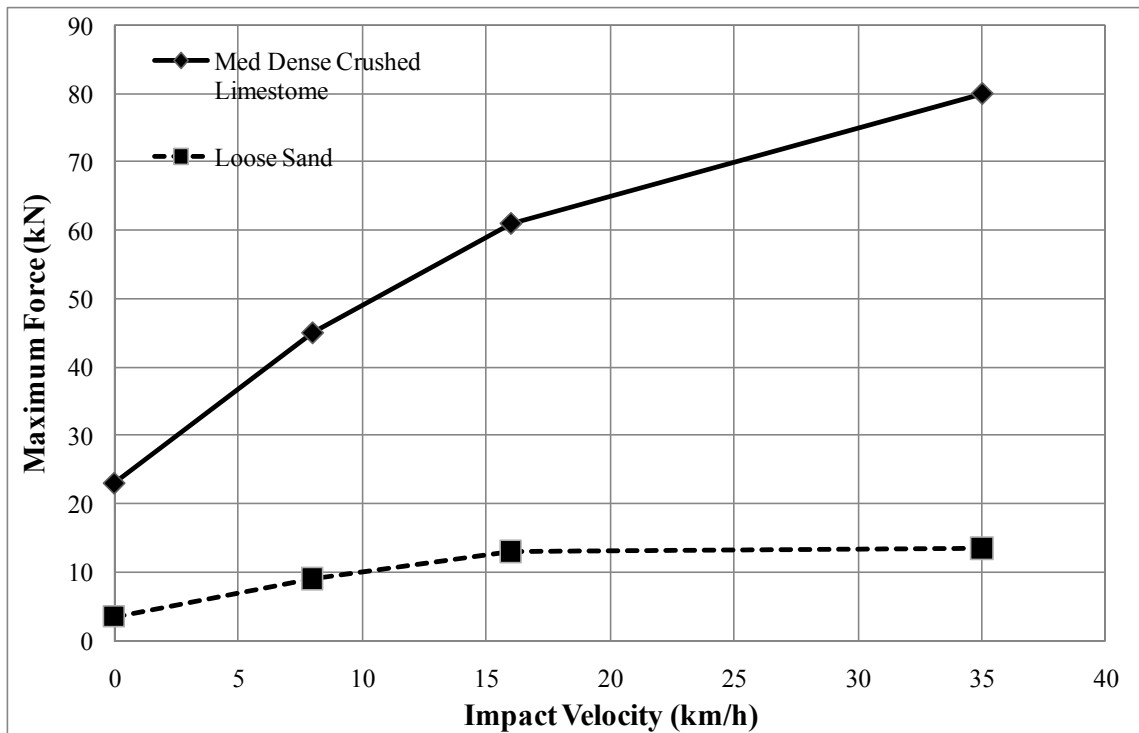
Figure 3.116. The maximum force-impact velocity relationship for pendulum tests
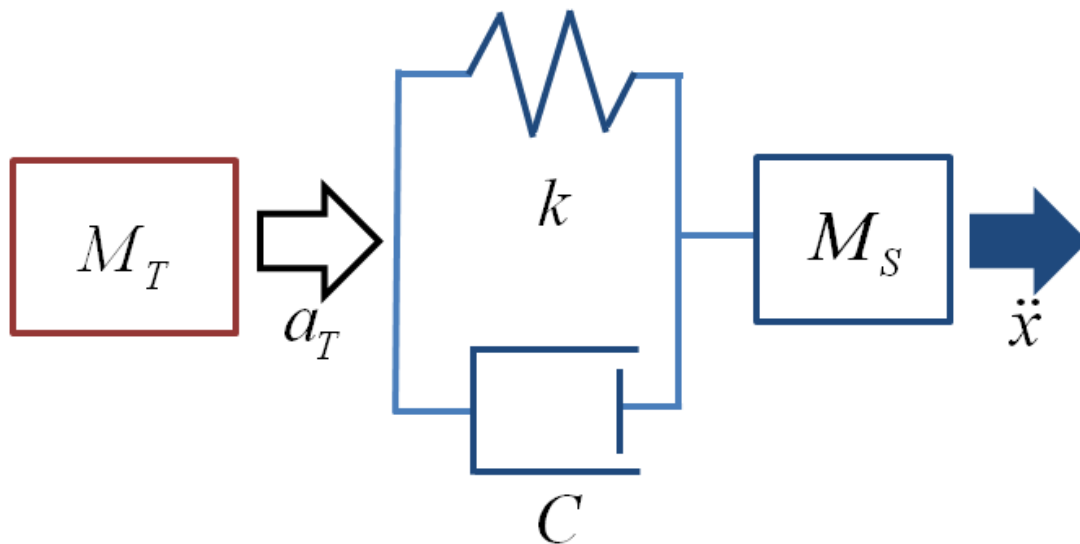
Figure 3.117. Single degree of freedom model
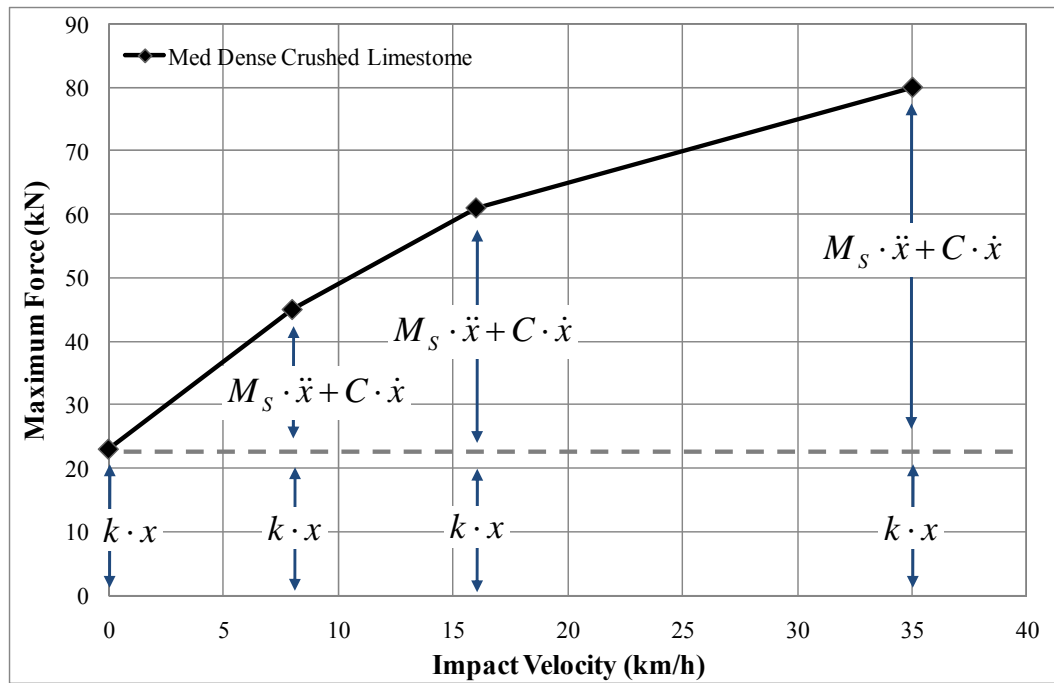
Figure 3.118. The max. force-impact velocity for medium dense crushed limestone (SDOF)
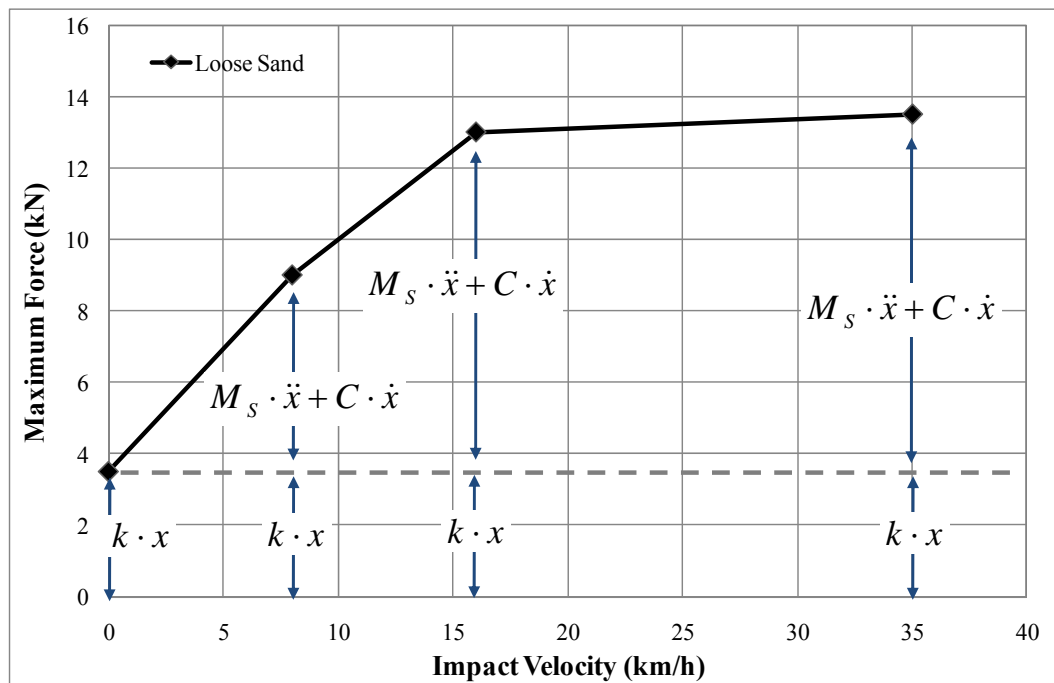
Figure 3.119. The max. force-impact velocity for loose sand (SDOF)
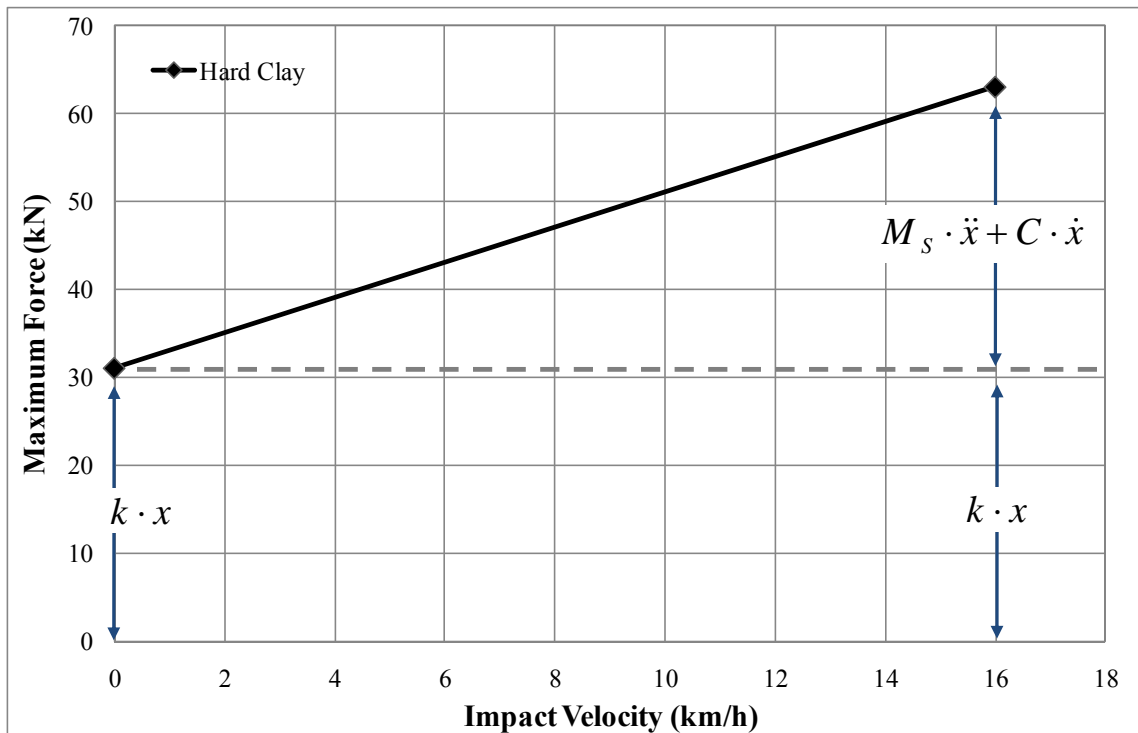
Figure 3.120. The max. force-impact velocity for hard clay (SDOF)

During the impact, the mass of mobilized post and soil wedge was accelerated in the same direction of the impact. According to Newton's second law, the product of the acceleration and the mass is the force. The inertia effect is the resistance against the impact from the mobilized soil and post mass. The mobilized mass of post and soil is determined depending on the soil stiffness and strength and the post stiffness and strength. The size of the mobilized soil wedge increases as the strength of the soil increases.

The normalized maximum force is defined as the ratio of the maximum force and static resistance. The definition of normalized maximum force is same with dynamic

amplification factor for a specific velocity. The normalized maximum force or dynamic factor versus impact velocity relationship is shown in Figure 3.121. The critical dynamic factor for loose sand was 3.8. The dynamic factor for medium dense crushed limestone was 3.5 at the impact velocity of 35 km/h.

The critical dynamic factor for loose sand was 3.8. The dynamic factors for medium dense crushed limestone were 1.9, 2.7 and 3.5 at the impact velocity of 7.6 km/h, 16 km/h and 35 km/h, respectively. The dynamic factor for hard clay was 2.0 at the impact velocity of 16 km/h. At the same velocity of 16 km/h, the magnitude of peak force increases and the dynamic factors decreases, as the strength of soil increases.

From Figure 3.121 and the conclusions in Section 3.2.5, the following statements can be obtained:

- There is a certain limit dynamic factor for a single post.

- Limit dynamic factor can be determined by strength of soil. Magnitude of dynamic factor increases as strength of soil increases.

- Limit impact velocity corresponding to limit dynamic factor also increase as strength of soil increase.

- The dynamic effect was largely from the inertia effect
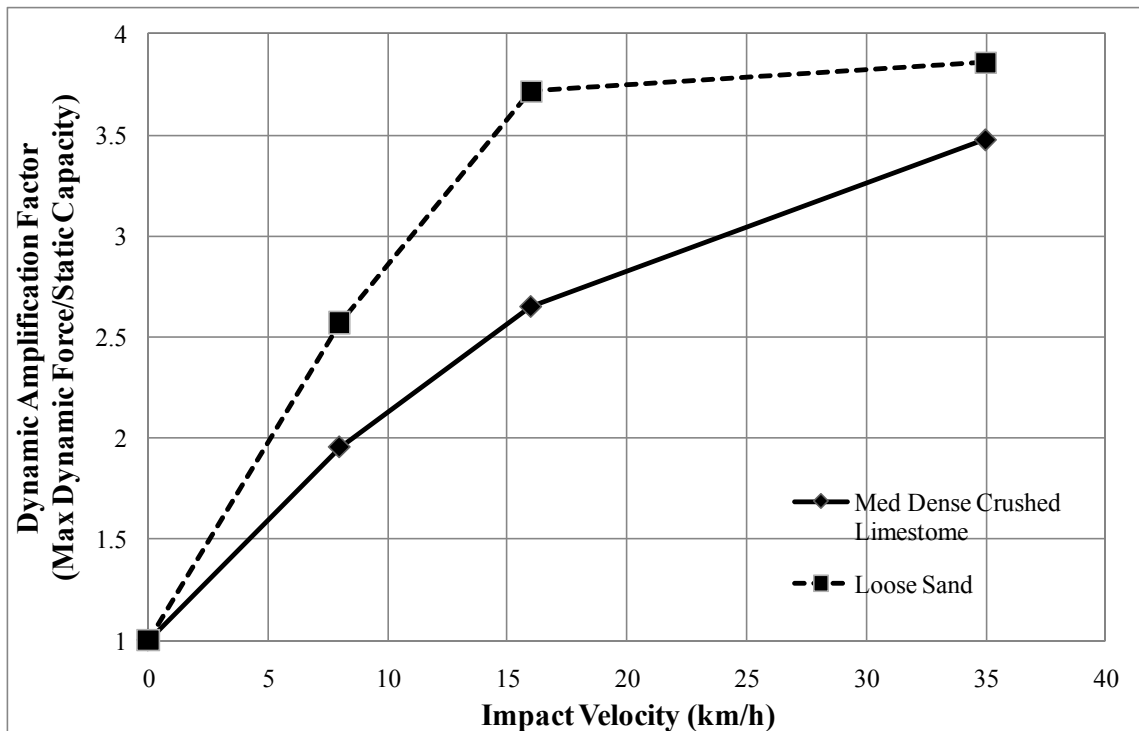
Figure 3.121. Dynamic amplification factor for pendulum tests

In order to investigate the group effect of posts system embedded in loose sand, the forces versus displacements of post systems at impact location were compared in Figure 3.122. The normalized force versus corresponding number of posts for static tests (Figure 3.80) and dynamic impact tests are shown in Figure 3.123. The normalized force is the ratio of the maximum force and the resistance of single post test. Three and six of the abscissa represent three posts in a row and six posts in two rows.
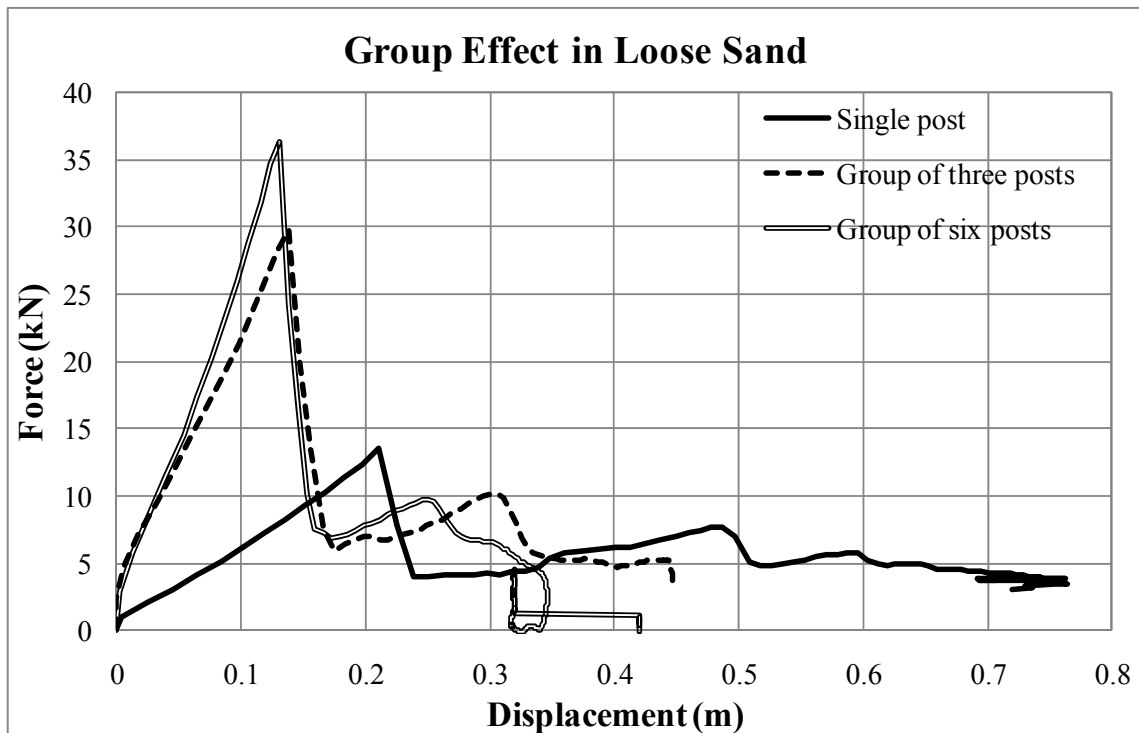
Figure 3.122. Force-displacement of post systems in loose sand

According to Figure 3.123, the group efficient for static tests that is defined as ratio of normalized force and number of posts was 96 % and 64 % for three posts in a row and six posts in two rows, respectively. And the dynamic group efficient was 75% and 45 % for three posts and six posts. The efficient of group decreases as the number of posts increase, though the configurations of two post systems were different. Dynamic group efficient is approximately 75 % of static group efficient for these particular tests.
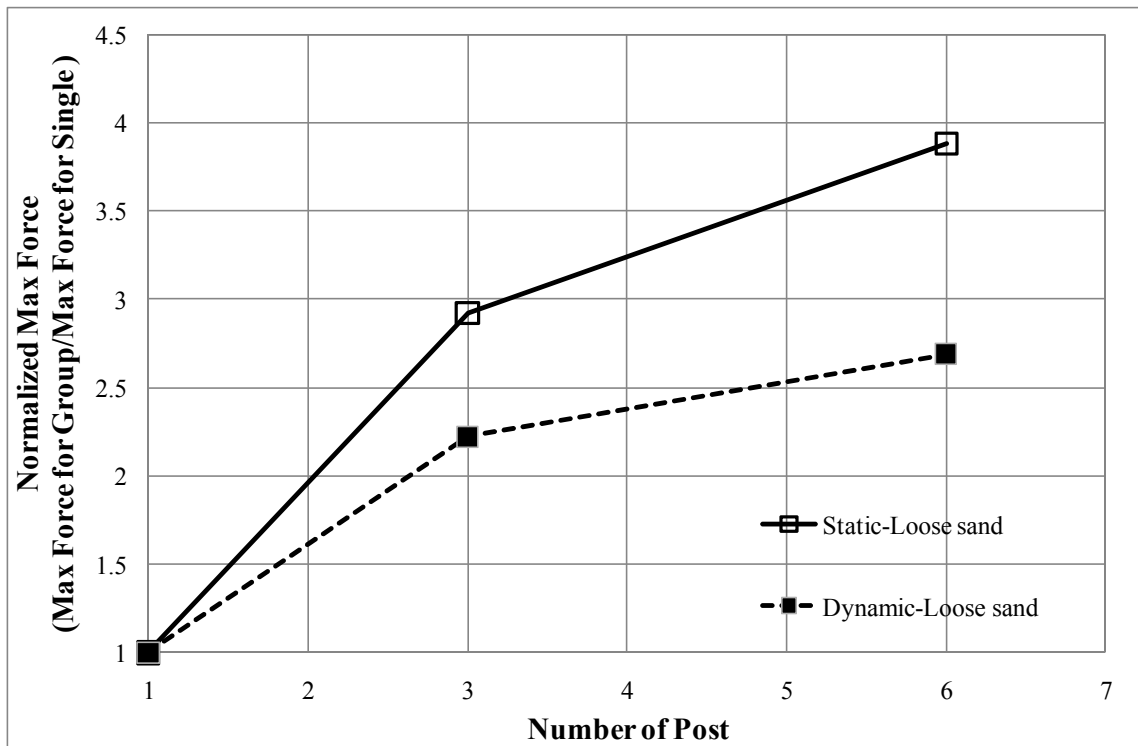
Figure 3.123. Normalized force-number of posts relationship for post systems in loose sand

3.3.4 Conclusions

A series of static and pendulum tests in either the medium dense crushed limestone or the loose sand was conducted at the TTI Proving Ground in June, 2008. The post systems including single post, group of post system were designed using the result of the dimensional analysis.

Single posts directly embedded in soil may have a certain limit dynamic amplification factor. There is a limit dynamic amplification factor for a single post pendulum test embedded in the loose sand. Also the single post in the medium dense crushed limestone has a trend to converge.

Limit dynamic amplification factor can be determined by strength of soil. Dynamic amplification factor increases as strength of soil increases. The dynamic amplification factor of the full-scale impact test on the single post, July 2007 was 5.4 and the limit dynamic amplification factor of the single post in the loose sand was 3.8.

The limit impact velocity corresponding to the limit dynamic amplification factor also increase as strength of soil increase. The limit impact velocity of the single post tests in loose sand was 16 km/h, whereas the limit impact velocity of the single post tests may be higher than 35 km/h.

The dynamic group efficient was approximately 75 % of the static group efficient from the static and impact tests in the loose sand. The group efficient of posts system under static and impact load decreases as number of posts increases.

According to simple single degree of freedom analysis, the dynamic effect was largely from the inertia effect. Also the size of mobilized soil mass increases, as the soil strength increases.

3.4 Bogie tests – June 2008

A set of miniature impact tests using a bogie was performed in existing hard clay. For all the post systems, static load tests were conducted prior to the impact. The impact speeds of bogie were 16 km/h (10 mph) for both the single post and the group of posts system. Accelerometers were installed on both post and the bogie to calculate impact force, velocity and displacement. In order to measure the deflection of the post, the films from

a high-speed camera were analyzed. The test matrix of the bogie tests is shown in Table

3.9.

Table 3.9. Test Matrix for bogie tests

Test number	Test type	Post system	Mass of bogie (kg)	Impact velocity (m/s)	Remark
S6	Static	Single Post			Driven
B1	Bogie	Single Post	900	4.56	Driven
S7	Static	Group of Posts (a row)			Driven
B2	Bogie	Group of Posts (a row)	900	4.65	Driven

1.83m (72 inches) long hollow square section HSS 6X6X3/8 steel posts (6 inches

wide, 6 inches high, and 3/8 inches wall thickness) were embedded 1.01m (40 inches)

for the test of single post. In order to investigate the group effects, impact tests and static

tests on a group of posts system with three posts in a row (Figure 3.44) were conducted

with impact velocity of 16 km/h (10 mph). The group of posts system consisted of long

hollow square section (HSS 6" X 3/8") beams. The group of posts system and a single

post are driven into the existing hard clay.

The bogie tests were designed using a bogie instead of a pendulum, because

constructing a hard clay pit at the pendulum test facility is much more difficult and

inefficient in terms of cost and time than using the existing clay. Bogie tests can be

conducted where there is enough space to accelerate the bogie to design impact velocity,

whereas pendulum test can be conducted only where the pendulum facility is newly

constructed or moved.

3.4.1 Test set up

The existing hard clay next to the runway of the TTI Proving Ground was selected for the location of the proposed bogie tests. Since the location is just next to the runway, there was enough space to accelerate bogie to the design velocity. A Bogie with 900 kg (1990 lb) of mass shown in Figure 3.124 was used.

Both a single post and a group of posts system with three posts in a row (three side by side posts) were driven into the existing hard clay prior to the tests as shown in Figure 3.125. The distance between two posts system was 7.62 m (25 feet) and the locations are shown in Figure 3.16. The clay surface was leveled to obtain drivability of bogie. The soil tests described in Section 3.1.4 were conducted prior to the static and impact tests.

Figure 3.124. Bogie test with 900 kg (1990 lb) of mass used for the proposed tests

Figure 3.125. Single post and group of posts system embedded in hard clay

The heights of plugged soil inside the post were measured as shown in Figure 3.126. When driving an open end pile, soil is allowed to enter the bottom of the pile or tube. The measurements are 756 mm and 813 mm for single post and group of posts, respectively.

Static load test for the lateral load capacity was conducted in the opposite direction of the impact prior to the impact test using pendulum. On the impact side of the post was connected to a hydraulic jack and the other side was connected to a displacement transducer as shown in Figure 3.127. The lateral static force was measured with a pressure transducer. After the each static load tests, the post and group of posts were rearranged to the initial post position without reinstallation.
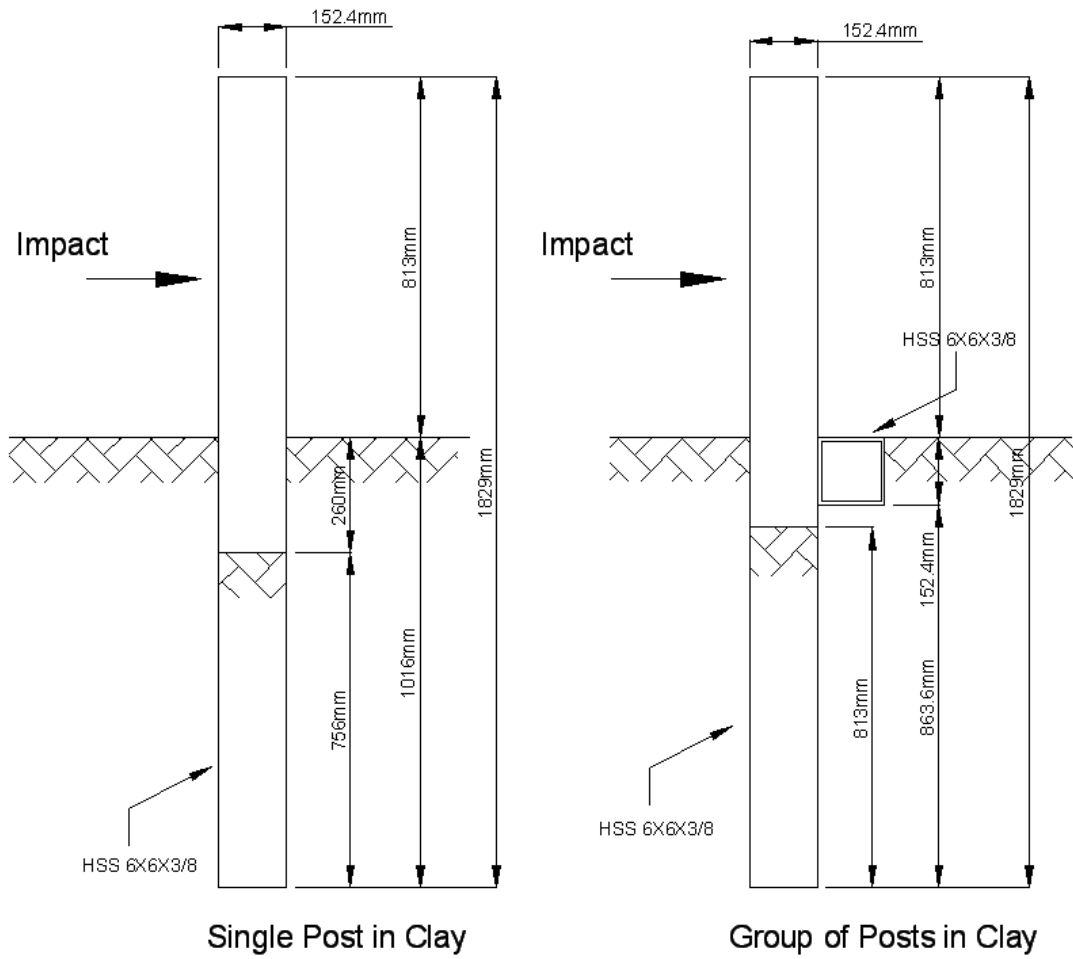
Figure 3.126. Plugged hard clay inside the post due to driving

Figure 3.127. Static load test on group of posts system embedded in hard clay

The bogie was towed into the test installation using a steel cable guidance and reverse tow system. The bogie guidance system is shown in Figure 3.128. As the towing vehicle is accelerated, the bogie is accelerated at the same rate to design impact velocity. The connection between the bogie and vehicle was released just before the impact. The bogie remained free-wheeling until the impact.

Figure 3.128. Bogie guidance system

Two accelerometers were attached on the single post (B1) in the opposite side of the impact at the impact level and the middle of the post (Figure 3.53). Also three accelerometers were installed on the each posts of the group of posts system with a row of three posts (B2) at the ground level. Details of the geometry of group of posts system with a three posts along with the locations of accelerometer are shown in Figure 3.76 and Figure 3.77. To measure the accelerations of bogie, an accelerometer was attached on the center of gravity (C.G) of bogie (Figure 3.124).

High speed camera captured films to analyze the displacement of the targets attached on the side of the post for all of the impact tests in loose sand. The target locations on the posts are shown in Figure 3.54.

3.4.2 Test results

Prior to the impact tests, the static lateral capacities of all of the post systems embedded in the hard clay were tested. The post was pulled at 356 mm (14 inches) above the ground level that is the impact location of bogie. The impact location of bogie was the height of the center of bogie nose from the ground surface.
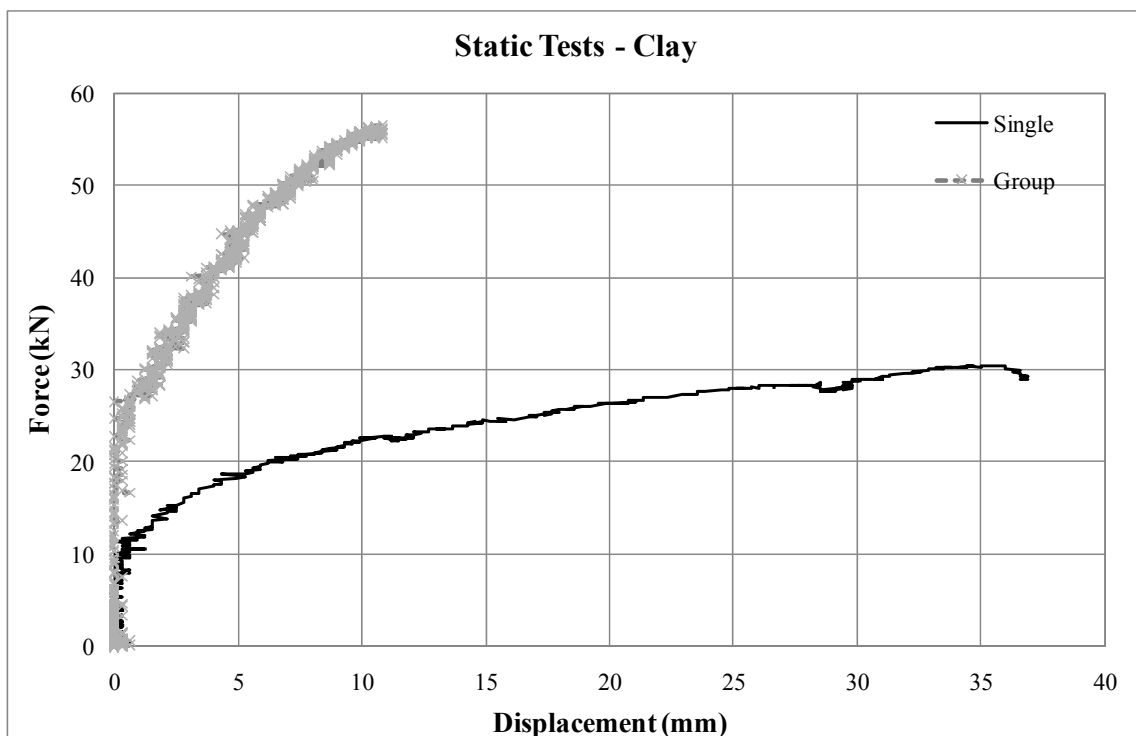
Figure 3.129.Static load test results of post system embedded in hard clay

The force-displacement results of the two static load test on the single posts and the group of posts are shown in Figure 3.129. Peak force of the single post in the hard was 30 kN at the displacement of 35 mm. The peak lateral resistance of the one row of three posts (three side by side posts) was 56 kN at the displacement of 12 mm. Note that the displacements were measured at the location where bogie impacted.

Single post bogie test with 4.56 m/sec of impact velocity (B1)

The post and bogie at the moment of the impact with 4.56 m/sec of velocity (B1) are shown in Figure 3.130. The deformed post and the bogie after the impact with are shown in Figure 3.131. The length of the gap behind the post shown in Figure 3.131 was 20 mm. The permanent rotation of the post was measured as 7 degrees.

Figure 3.130. Bogie test on single post embedded in stiff clay (B1)

Figure 3.131. Displaced single post embedded in hard clay after impact test (B1)

Figure 3.132. Single post and bogie after the impact (B1)
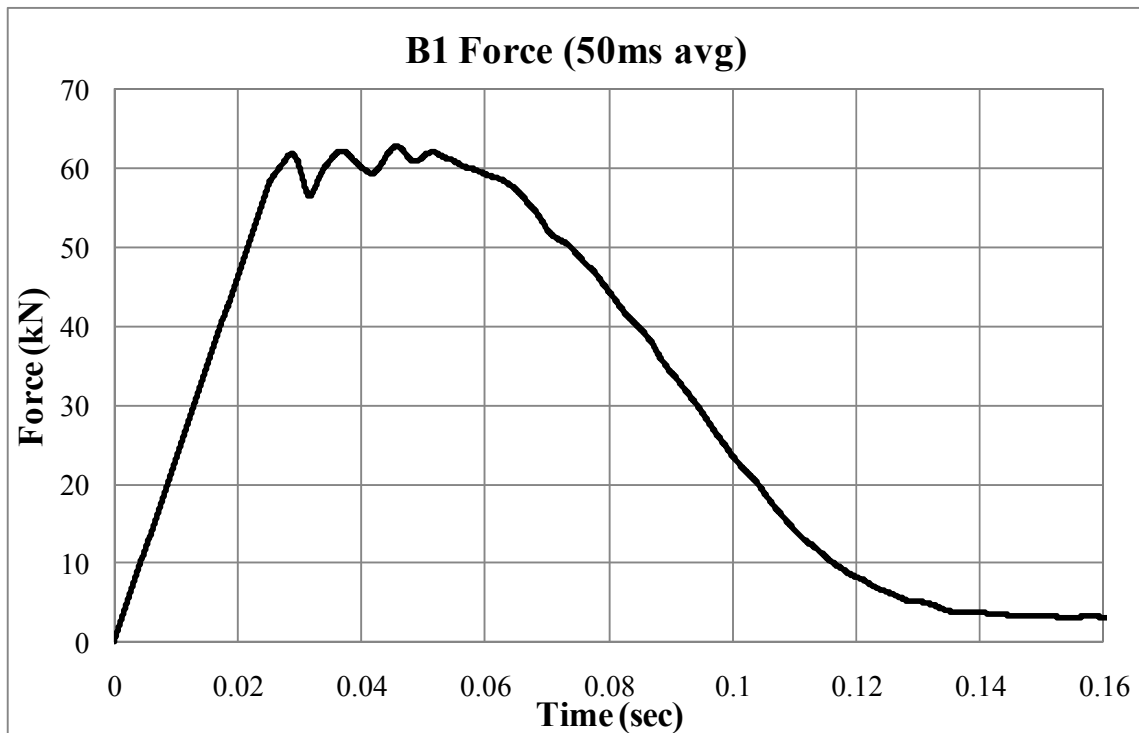
Figure 3.133. 50msec average impact force-time history (B1)

Peak longitudinal 50ms-average deceleration of the bogie was 7.1 g at 0.044 sec. The impact force-history is shown in Figure 3.133. The maximum impact force was 62 kN.

The post acceleration at the impact level (0.36 m above the ground level) and the middle (0.41 m below the ground level) of the post are shown in Figure 3.134. Also the velocity-time and displacement-time histories of the post were obtained by integration and double integration of the acceleration data as shown in Figure 3.134.
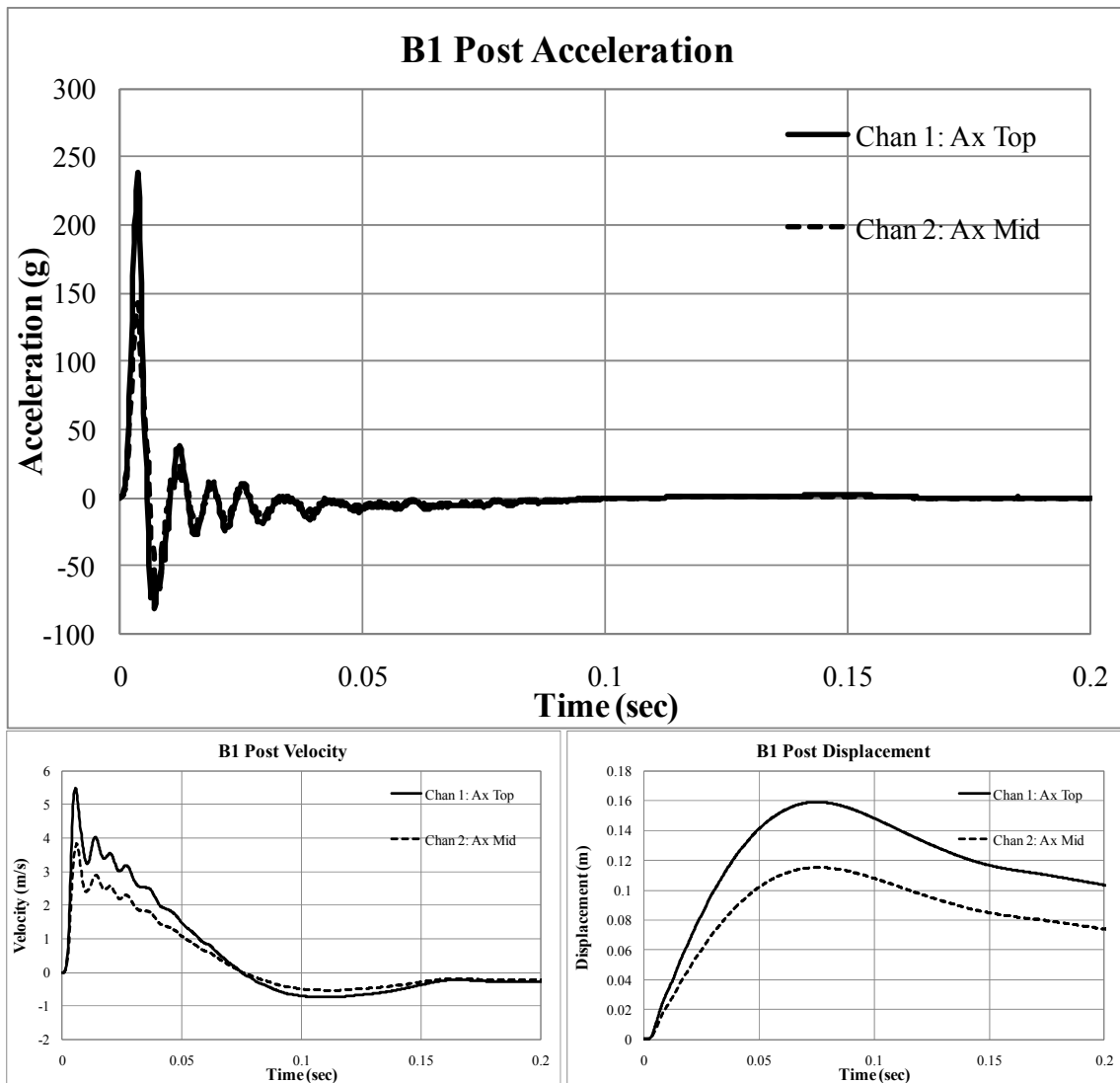
Figure 3.134. Acceleration, velocity and displacement of post history from acceleration data (B1)

Film analysis was conducted to obtain the post displacement history. The film from high speed camera is analyzed to obtain more reliable displacement history than that from integration of acceleration data. The maximum longitudinal displacement of the post at impact location was 14 m at 0.075 sec using film analysis. The permanent

displacement at the location was 0.116 m. The displacements at the impact location are indicated as X-disp and Y-disp for the longitudinal and vertical displacement in Figure 3.135.
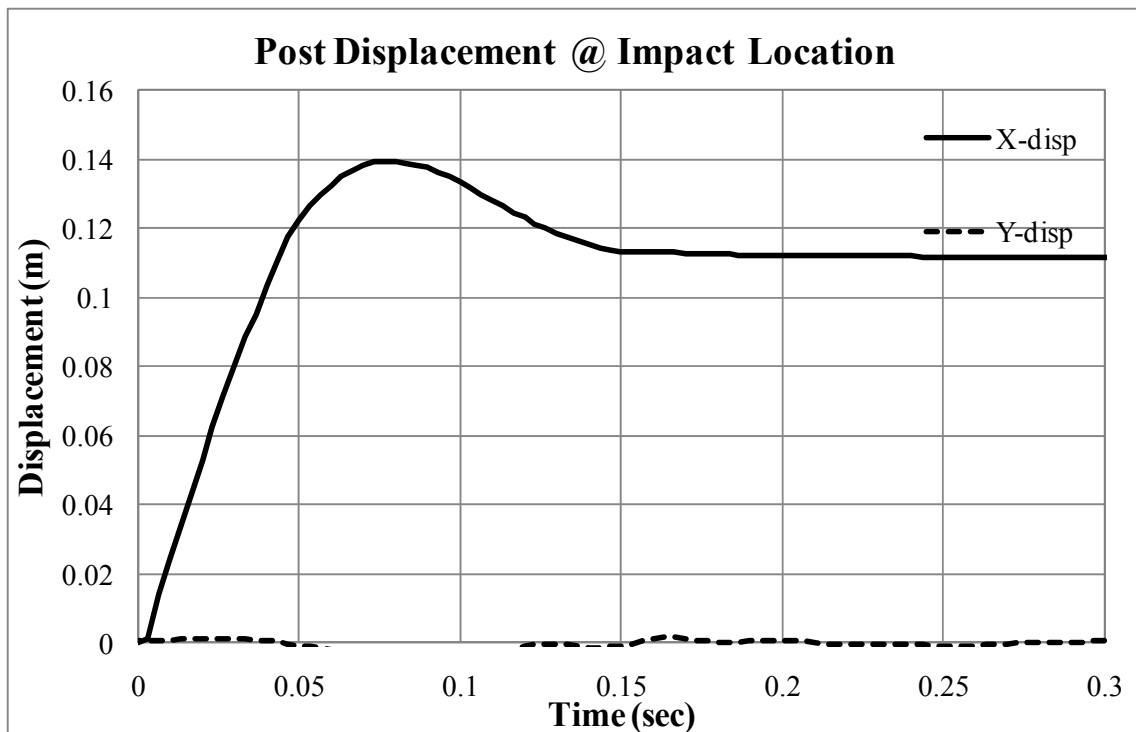
Figure 3.135. Post displacement history from film analysis (B1)

Group of posts bogie test with 4.65 m/sec of impact velocity (B2)

The three side by side posts system in the hard clay and bogie at the moment of the impact with 4.65 m/sec of velocity (B2) are shown in Figure 3.136. The length of the gap in front and behind the post was 10 mm and 12 mm, respectively. The permanent rotation of the post was measured as one degree.

Figure 3.136. Bogie test on group of posts system embedded in stiff clay (B2)
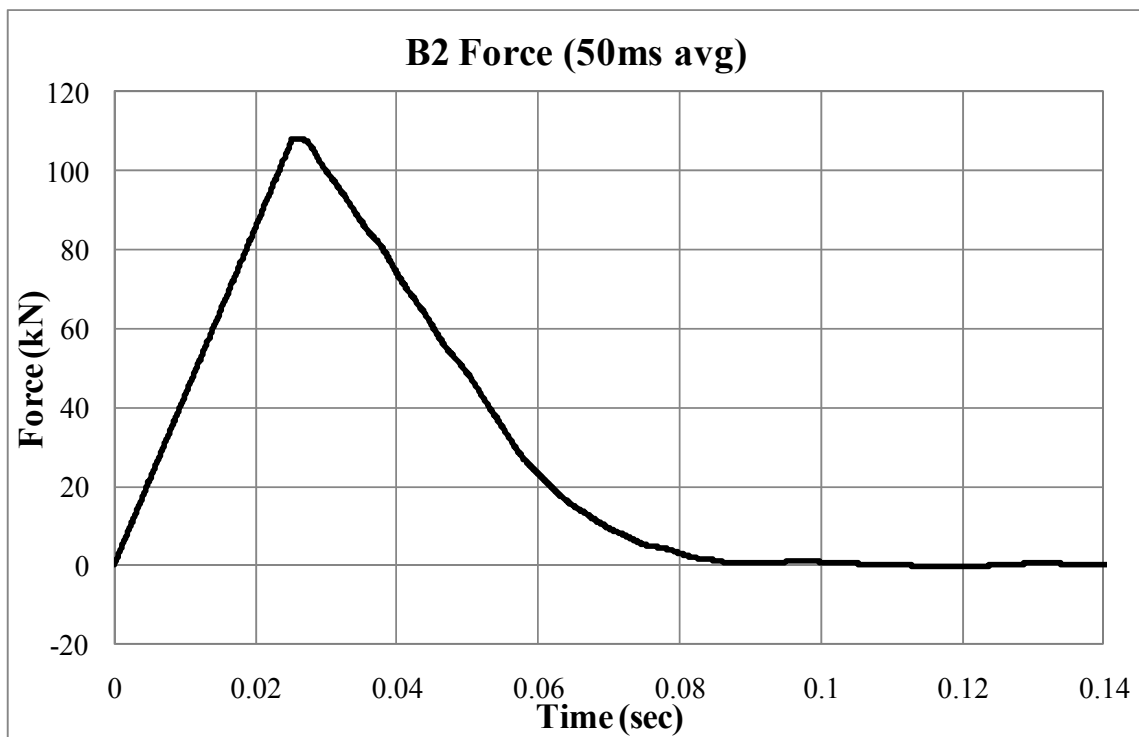
Figure 3.137. 50msec average impact force-time history (B2)

Peak longitudinal 50ms-average deceleration of the bogie was 12.1 g at 0.025 sec. The impact force-history is shown in Figure 3.137. The maximum impact force was 108 kN. The accelerations at the ground level of the three posts are shown in Figure 3.138. Also the velocity-time and displacement-time histories of the posts were obtained by integration of the acceleration data as shown in Figure 3.138.
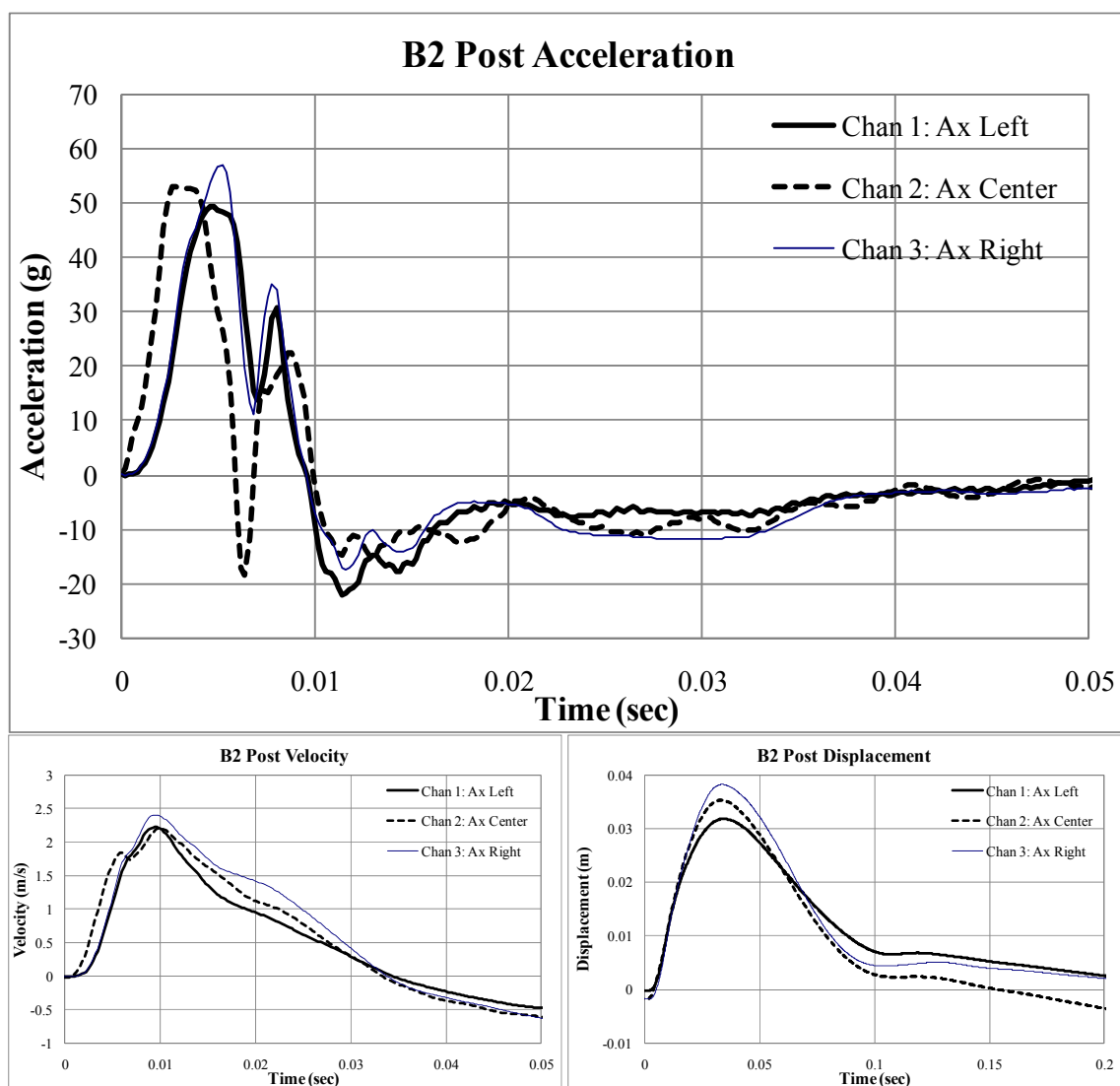
Figure 3.138. Acceleration, velocity and displacement of post history from acceleration data (B2)

Film analysis was conducted to obtain the post displacement history. The maximum longitudinal displacement of the post at impact location was 0.048 m at 0.03 sec using film analysis. The permanent displacement at the location was 0.012 m. The displacements at the impact location are indicated as X-disp and Y-disp for the longitudinal and vertical displacement in Figure 3.139.
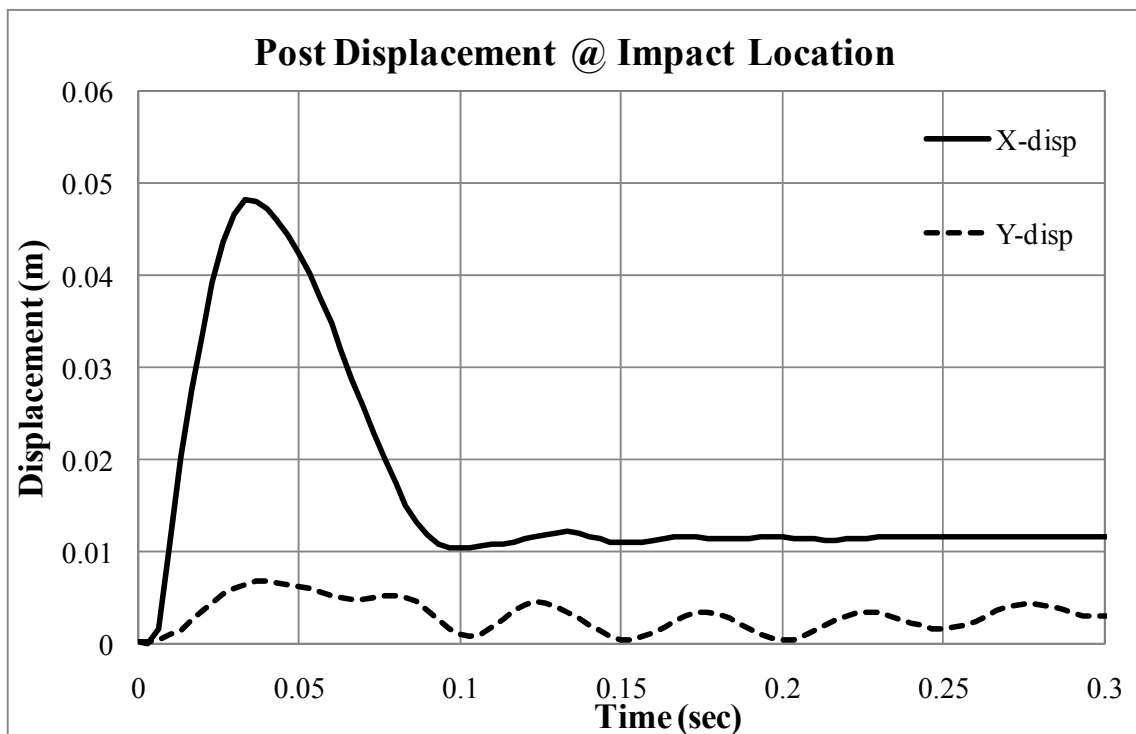
Figure 3.139. Post displacement history from film analysis (B2)

3.4.3 Data analysis

The results of single post embedded in soil including medium dense crushed limestone, loose sand and hard clay are shown in Figure 3.140. The displacements at the

displacement of 15 mm that is 10% of the post width were 2.5 kN, 17 kN and 24 kN for medium dense crushed limestone and loose sand and hard clay, respectively.
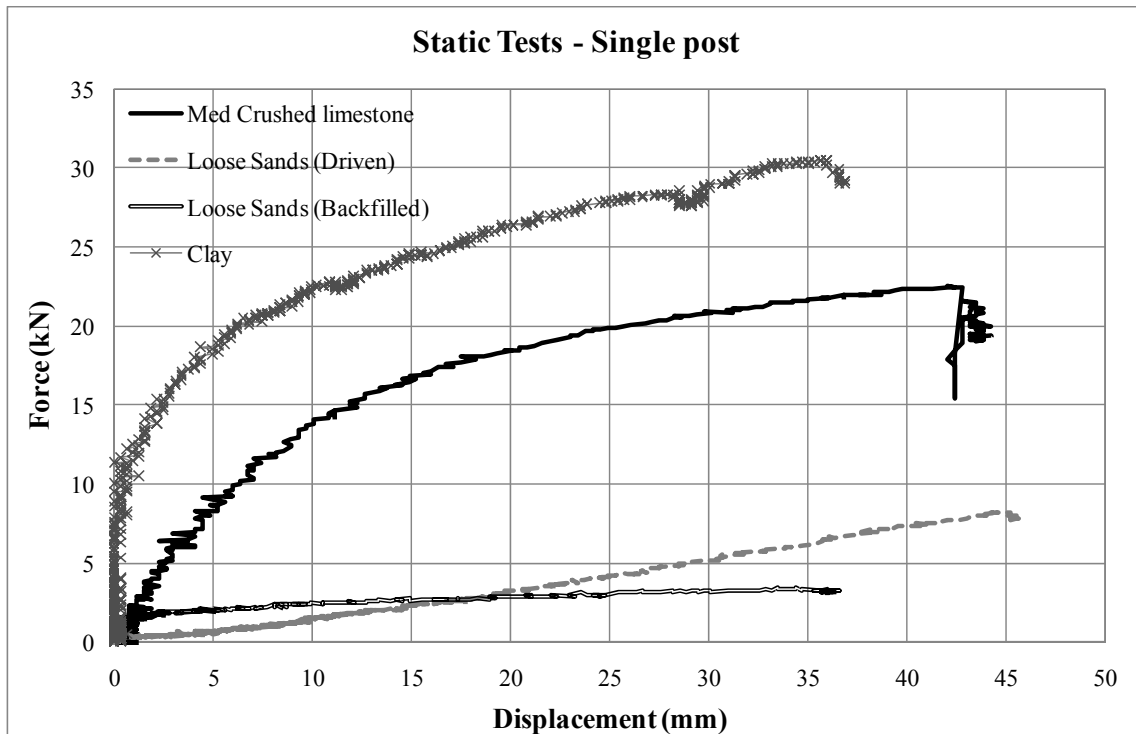
Figure 3.140. Static load test results of single post

The post displacement from film analysis and that from integration of acceleration data were compared and shown in Figure 3.141 and Figure 3.142. The displacements of group of post system (B2) at the ground level not at the impact location were compared because the accelerometers of group of posts were installed at the ground level.
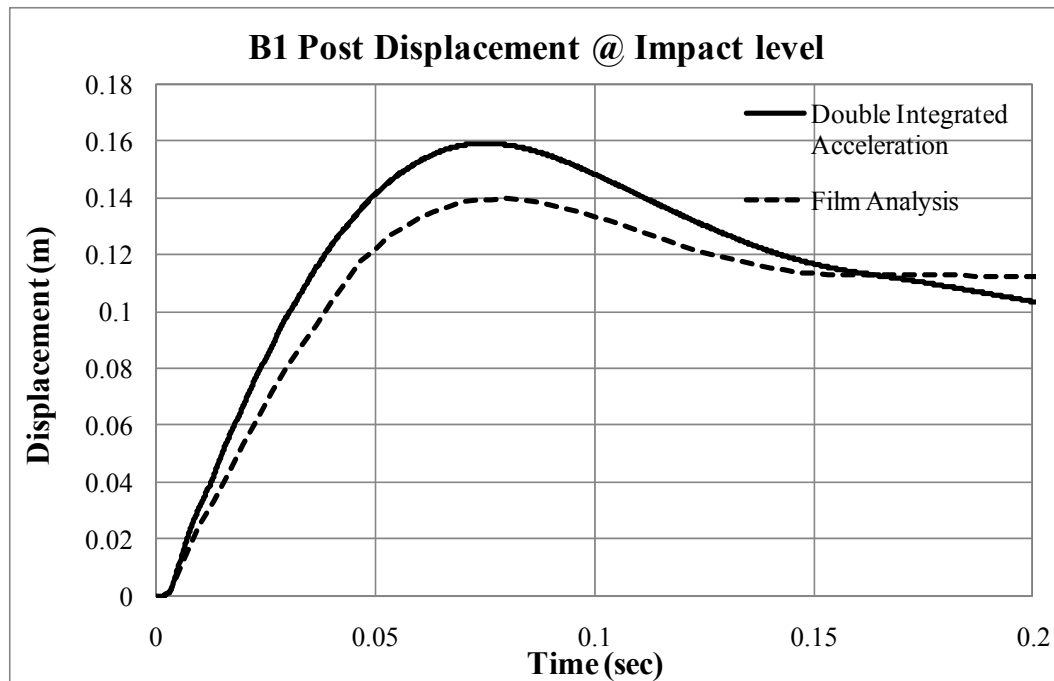
Figure 3.141. Post displacement comparison (B1)
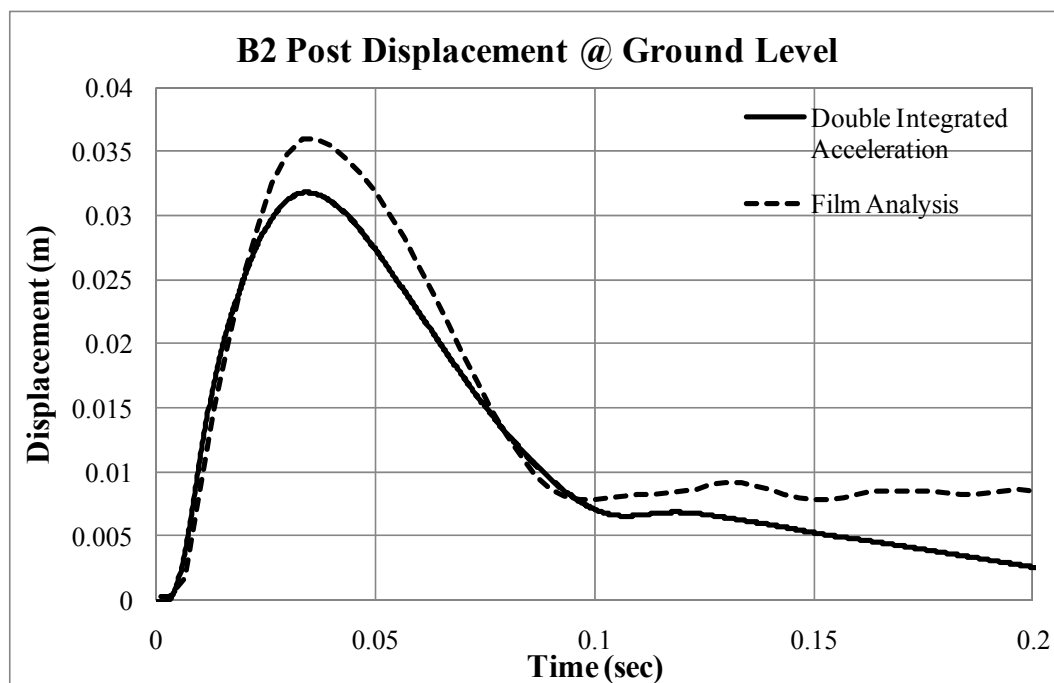
Figure 3.142. Post displacement comparison (B2)

Based on the post displacement history and the impact force history, the force versus displacement relationship of single post was obtained as shown in Figure 3.143. Since the loading speed of the static test was approximately 0.6 mm/sec, the speed of static test can be considered as zero. The forces of impact test were last around 0.1 sec whereas that of the static test was last 70 sec.

The maximum forces versus impact velocities are plotted in Figure 3.144. According to this, dynamic factor, DF was 2 for this specific test. The maximum force under dynamic impact was twice of the static resistance. The displacement of impact test was more than three times of that of the static test.
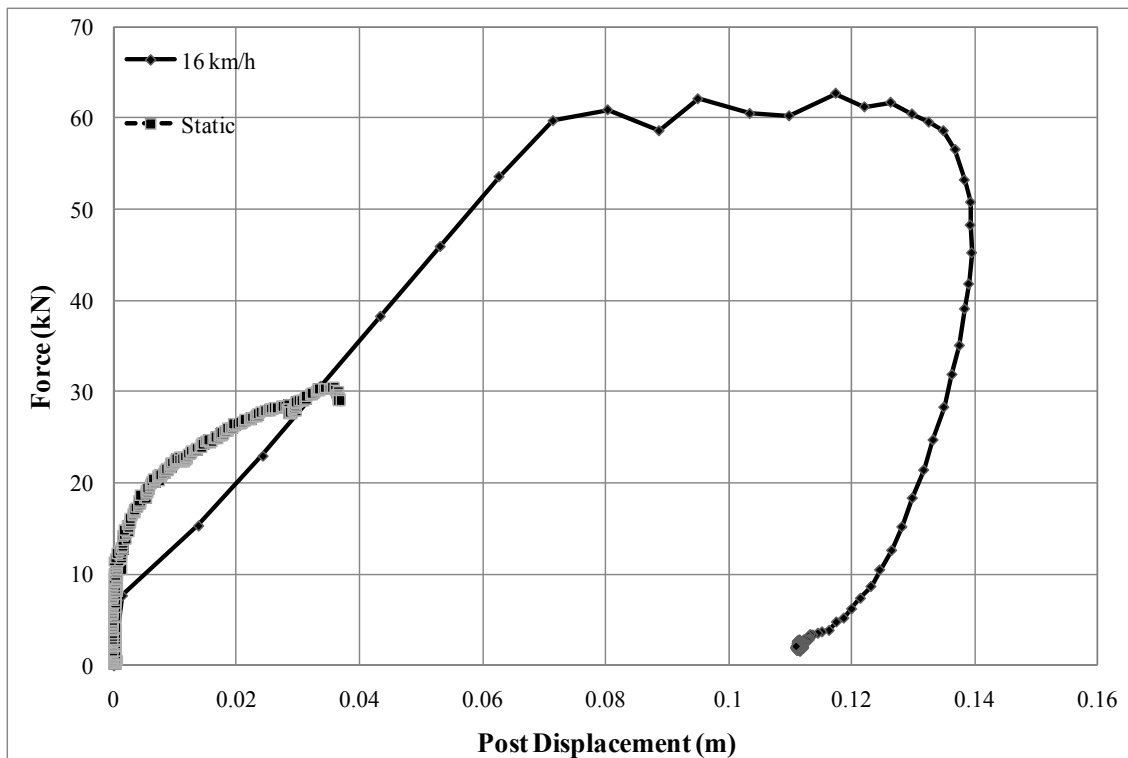
Figure 3.143. Force-displacement of single posts in hard clay
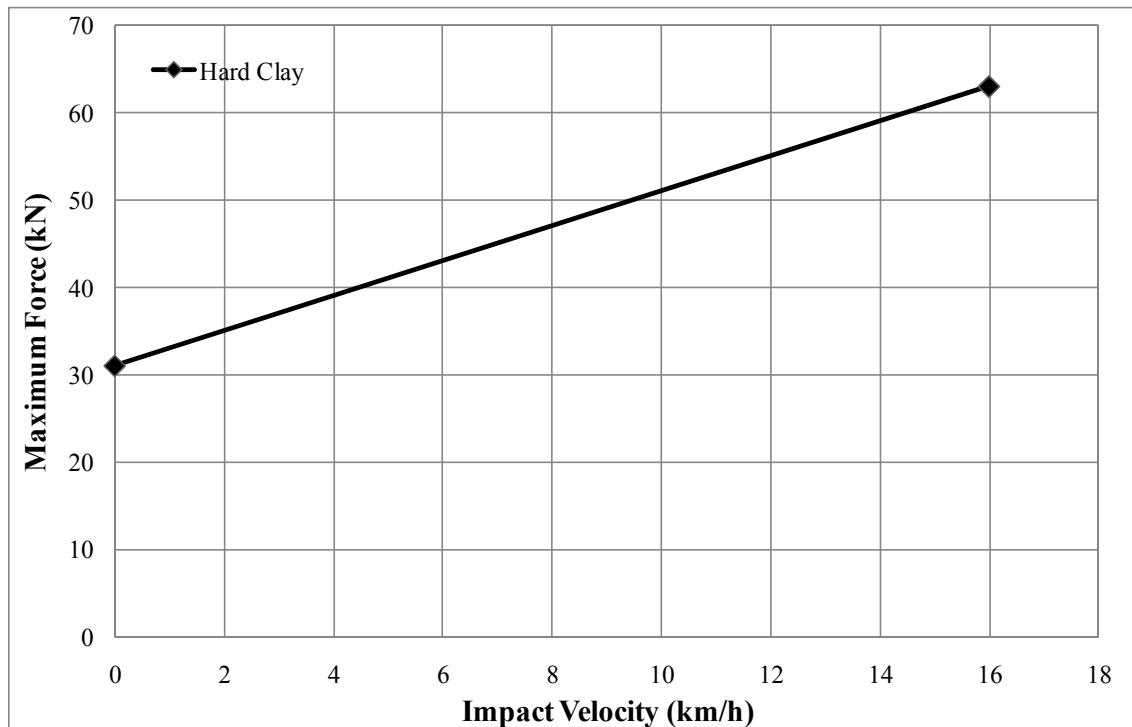
Figure 3.144.The maximum force-impact velocity for hard clay

The maximum force versus impact relationship for all single post model tests is shown in Figure 3.145. The magnitudes of increment of the maximum forces of single posts in medium dense crushed limestone and hard clay for higher velocity impact tests are bigger than that of the tests in loose sand. As stated the previous section, the maximum forces for loose sand converged to a critical or limit value whereas that for medium dense crushed limestone and hard clay increased as impact velocity increased, though the increment was decreased.

From Figure 3.146 and the conclusions in Section 3.2.5, the following statements can be obtained:

- There is a certain limit dynamic factor for a single post.

- Limit dynamic factor can be determined by strength of soil. Magnitude of dynamic factor increases as either strength of soil or impact velocity increase.

- Limit impact velocity corresponding to limit dynamic factor also increase as strength of soil increase.

- At the same velocity, the magnitude of peak force increases and the dynamic factors decreases, as the strength of soil increases.
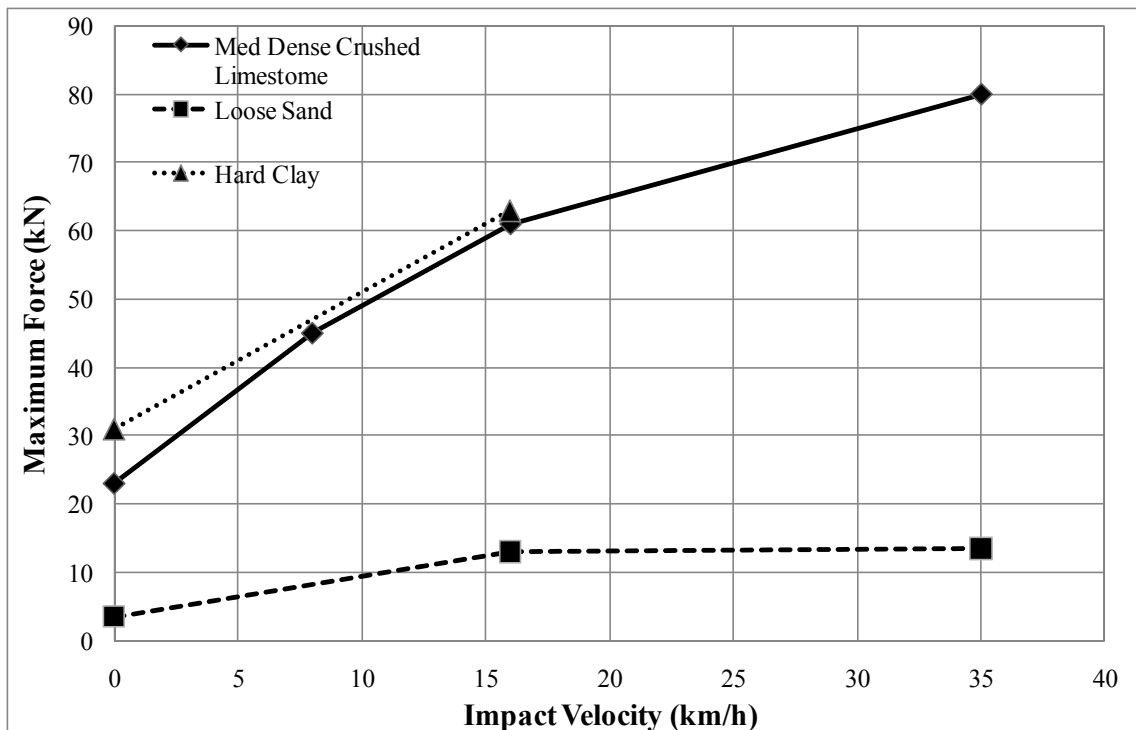
Figure 3.145. The maximum force-impact velocity relationship for the model tests
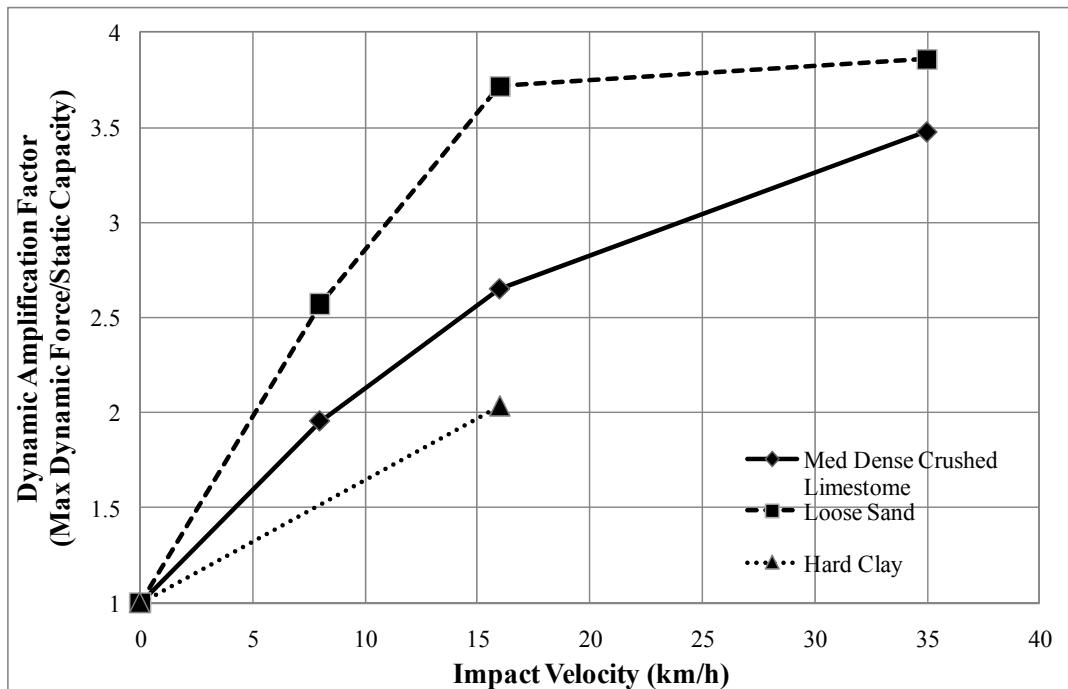
Figure 3.146. Dynamic amplification factor for the model tests
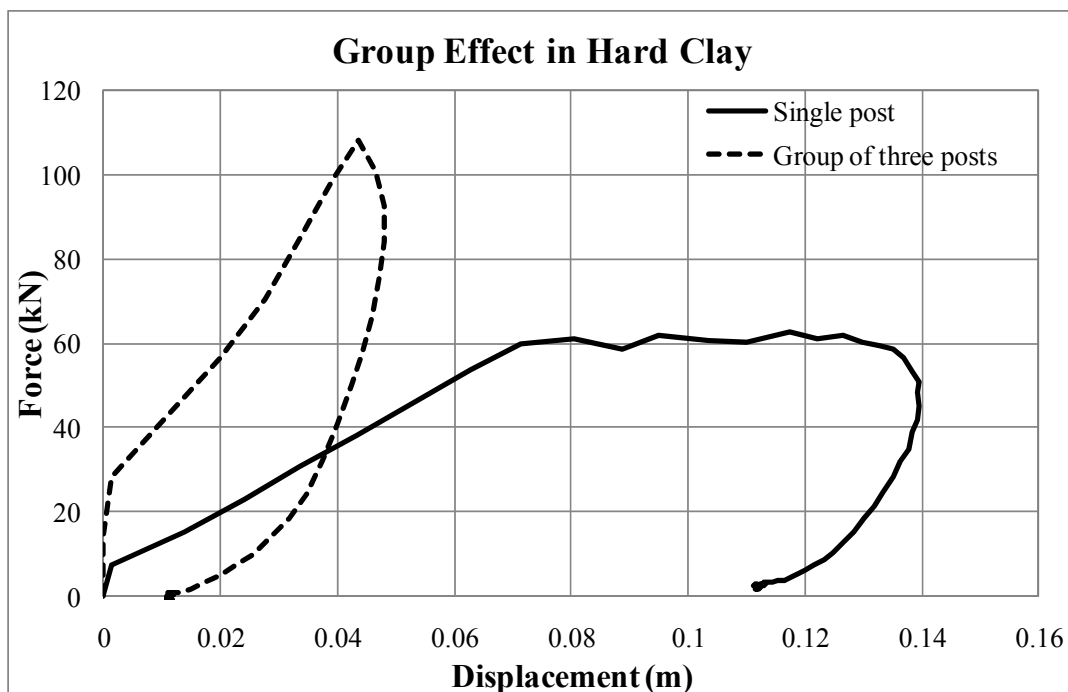
Figure 3.147. Force-displacement of post systems in hard clay

To investigate the group effect of posts system embedded in hard clay, the forces versus displacements of post systems at impact location were compared in Figure 3.147. The normalized force versus corresponding number of posts for static tests (Figure 3.129) and dynamic impact tests are shown in Figure 3.148. The normalized force is the ratio of the maximum force and the resistance of single post test. Three and six of the abscissa represent three posts in a row and six posts in two rows.
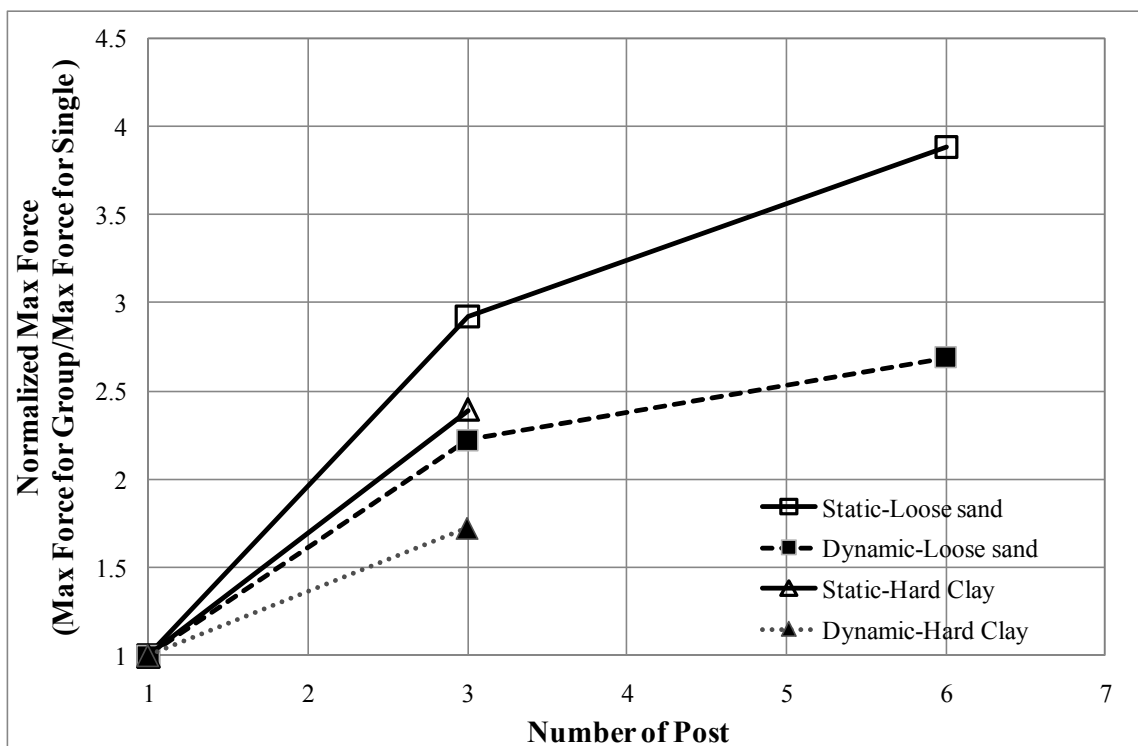
Figure 3.148. Normalized force-number of posts relationship for the post systems

According to Figure 3.148, the group efficient for static tests that is defined as ratio of normalized force and number of posts was 96 % and 64 % for three posts in a

row and six posts in two rows in loose sand, respectively. The static group efficient of post system in hard clay was 80 %. Also the dynamic group efficient was 75% and 45 % for three posts and six posts in loose sand. The dynamic group efficient was 56%. The efficient of group decreases as the number of posts increase, though the configurations of two post systems were different. Dynamic group efficient is approximately ranging from 70 % to 78 % of the static group efficient for these particular tests.

3.4.4 Conclusions

A series of static and bogie tests in the existing hard clay was conducted at TTI Proving Ground in June, 2008. Post systems including single post, group of post system were designed using the result of the dimensional analysis. The test results were compared with the results of the pendulum tests in medium dense crushed limestone and loose sand. Most of conclusions of the previous section were confirmed.

The dynamic factor for hard clay was 2.0 at the impact velocity of 16 km/h. At the same velocity, the magnitude of peak force increases and the dynamic factors decreases, as the strength of soil increases.

Dynamic group efficient was ranging from approximately 70 % to 78% of the static group efficient for the impact tests. Group efficient of posts system under static and impact load decreases as number of posts increases.

3.5 Full-scale impact test – May 2010

Because it was deemed economically unreasonable to arrest a 6800kg truck at 80kph with a single post in a weak soil, group effect was considered as a useful alternative. In order to verify the proposed design guidelines described in Section 5, a full scale impact test was performed on a group of post system embedded in loose sand at the runway of the Texas Transportation Institute (TTI) Proving Ground on May 27, 2010. According to ASTM F2656-07, the test was designed to meet all the requirements for the condition designation M50 and penetration rating P1 using the proposed design guideline and the finite element analysis. The impact test was also conducted in accordance with ASTM F2656-07. Accelerometers and strain gages were installed on the vehicle and the posts system, respectively. In order to measure the deflection of the post, the films from a high-speed camera were analyzed. Soil tests including laboratory tests and field tests were carried out before and after the impact test.

3.5.1 Design of experiments

The group of posts system was designed based on a series of numerical simulations in Section 4.2 and the proposed design chart for group of posts in Section 4.4.3. The posts configurations and geometry of loose sand ditch are shown in Figure 3.149 and Figure 3.150. Also the dimensions of loose sand ditch were determined from the result of numerical simulations.

The design of the group of posts was started by simulating various groups of using LS-DYNA in a weak soil. The weak soil was a loose sand because it would be

much easier to build a loose sand deposit than a soft clay deposit. After a few iterations, the final system was a group of 8 side by side posts embedded 3m into the loose sand. The original design from numerical simulations consisted of eight of W14X90 pile with a HSS 10X10X1/2 horizontal beam. The design was modified using two HSS 8X8X1/2 horizontal beams instead of single horizontal beam by Dusty Arrington, Engineering Research Associate of Roadside Safety program, Texas Transportation Institute. Also the connection between post and horizontal beams were designed by Arrington. Details of group of posts design can be found on the TTI Test Report No. 400951-SNL24 (Arrington et al. 2010).
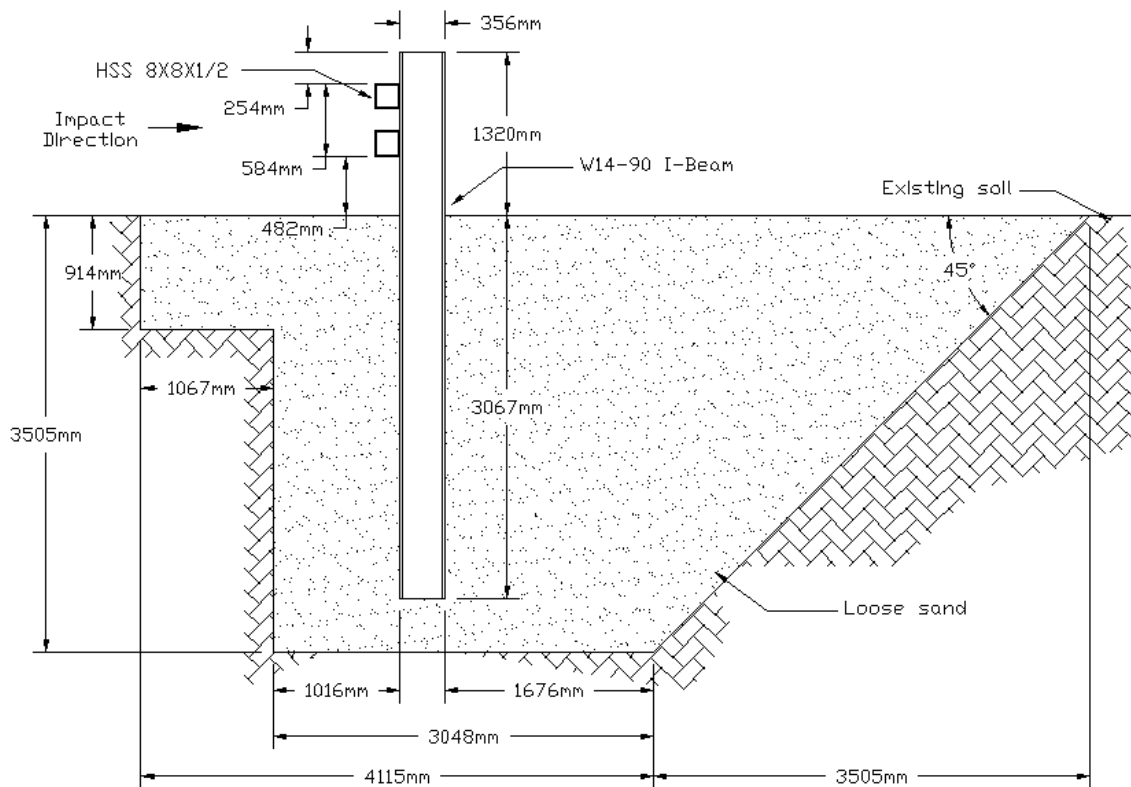
Figure 3.149. Side elevation of the group of posts system in the loose sand
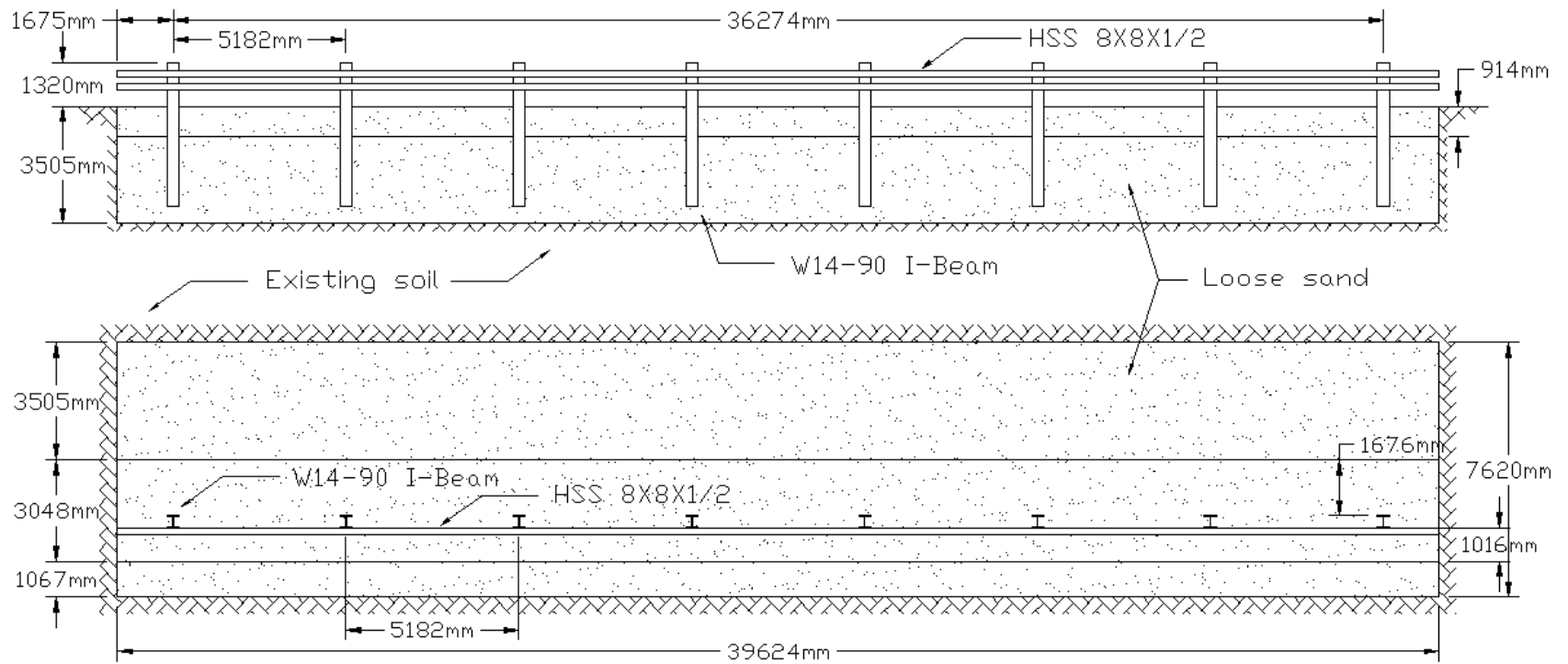
Figure 3.150. Plan and front elevation of the group of posts system in the loose sand

3.5.2 Test set up

A loose sand ditch with dimensions of 40 m long and 3.5 m deep was constructed for the proposed impact test on the group of posts system. Details of the loose sand ditch are shown in Figure 3.149 and Figure 3.150. The existing hard clay was located next to the main runway of the TTI Proving Ground.

Figure 3.151. Loose sand ditch construction

The excavated trench was filled with clean sand without compaction (Figure 3.151). The front side which is the impact side was excavated vertically with a 1.1 m wide and 0.9 m deep step at the ground level. The other side of ditch was excavated with 45 degrees of slope (1:1 slope). The width of the ditch at the ground level and the width of bottom of the ditch were 7.6 m and 3.1 m, respectively.

Figure 3.152. Pile driving rig and pile driving into the loose sand ditch

Eight W14X90 posts were driven to 3.05 m embedment with an evenly distributed spacing, 5.18 m center to center. The pile driving rig and a photograph of driving a post are shown in Figure 3.152. Two hollow square section HSS 8X8X1/2 steel tubes were used as the horizontal beams. The beams were attached to the posts using four 0.25 m diameter steel rods. The completed installation is shown in Figure 3.153. The details of the posts system can be found on the TTI Test Report No. 400951-SNL24 (Arrington et al. 2010).

Figure 3.153. Group of posts system for the proposed impact test

After driving the posts, a static load test to estimate the lateral load capacity of single post in the loose sand was conducted in the opposite direction of the impact prior to attach beams. On the impact side of the post was connected to a hydraulic jack and the other side was connected to a displacement transducer as shown in Figure 3.154. The lateral static force was measured with a pressure transducer. The lateral load was applied at 127 mm above the ground level. After the static test, the post was pushed back to the original position.

Figure 3.154. Static test on the single driven in loose sand ditch

For the crash test, a 2001 International 4700 single-unit flatbed truck (Figure 3.155) was used. The mass of the truck was measured as 6,835 kg. The height to the lower edge of the truck front bumper and the height to the upper edge of the front bumper were also measured as 520 mm and 800 mm, respectively. The additional dimensions and information of the test truck is shown in Appendix D.

Figure 3.155. Test vehicle for the M50 impact on the group of posts system

As shown in Figure 3.156, a vehicle guidance system was installed in front of the posts system. The guidance system consisted of pulleys and steel cable on a concrete foundation. The system directed the test vehicle into the group of posts system and a towing vehicle towed the test vehicle in the opposite direction of the impact with the

same velocity of the impact velocity. The system released the test truck to be free-wheeling and unrestrained just before the impact.

Figure 3.156. Vehicle guidance system for the full-scale test on group of posts

Figure 3.157. Accelerometers and data transmitter installed on the test vehicle

Two triaxial accelerometers (Figure 3.157) were installed on the flatbed of the vehicle at the center of mass of the vehicle and the location of rear axle. Eight strain gages were attached on the four of posts as two strain gages on the front and back side on each post at the ground level (Figure 3.158). The bending strains of the four posts in the right half to the impact direction were measured. In addition to the accelerometers and strain gages, films were captured using three high-speed cameras to measure the dynamic displacement of the targets attached on the vehicle and the post.

Figure 3.158. Strain gage attached on the post

3.5.3 Test results

Prior to the impact tests, static lateral capacity of single post was tested. The post was pulled at 127 mm above the ground level. The force-displacement result is shown in Figure 3.159. Peak force during the test was 61 kN at the displacement of 65 mm. The comparison between static resistance of single post and the dynamic force acting on each post during the impact is shown in Section 4.3.4.
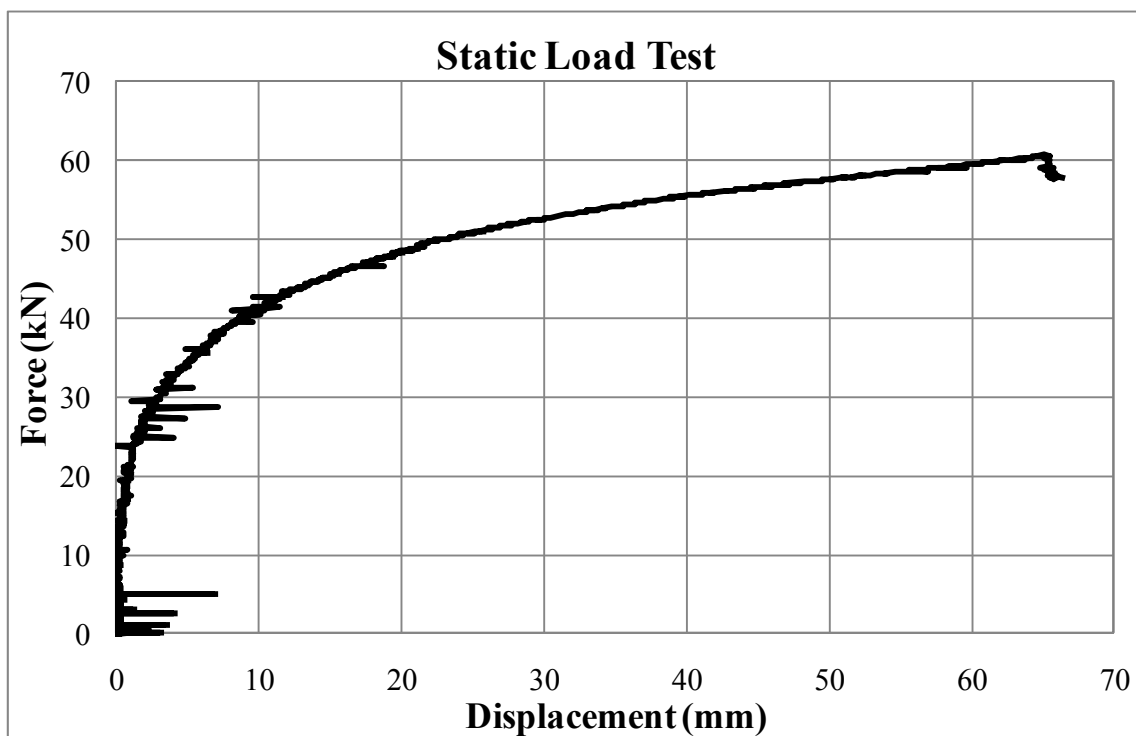
Figure 3.159. Static force-displacement of the single post in the loose sand

The single-unit flatbed truck which was traveling at an impact speed of 80.3 km/h, impacted the group of posts system direct embedded in loose sand. The post

system brought the truck to a complete stop with 0.274 m of the dynamic penetration. According to ASTM F 2656-07, the dynamic penetration of the vehicle is measured as from the inside edge of the post to the maximum dynamic penetration point of the leading lower bed edge of the vehicle. The dynamic penetration versus time history from the film analysis is shown in Figure 3.160.
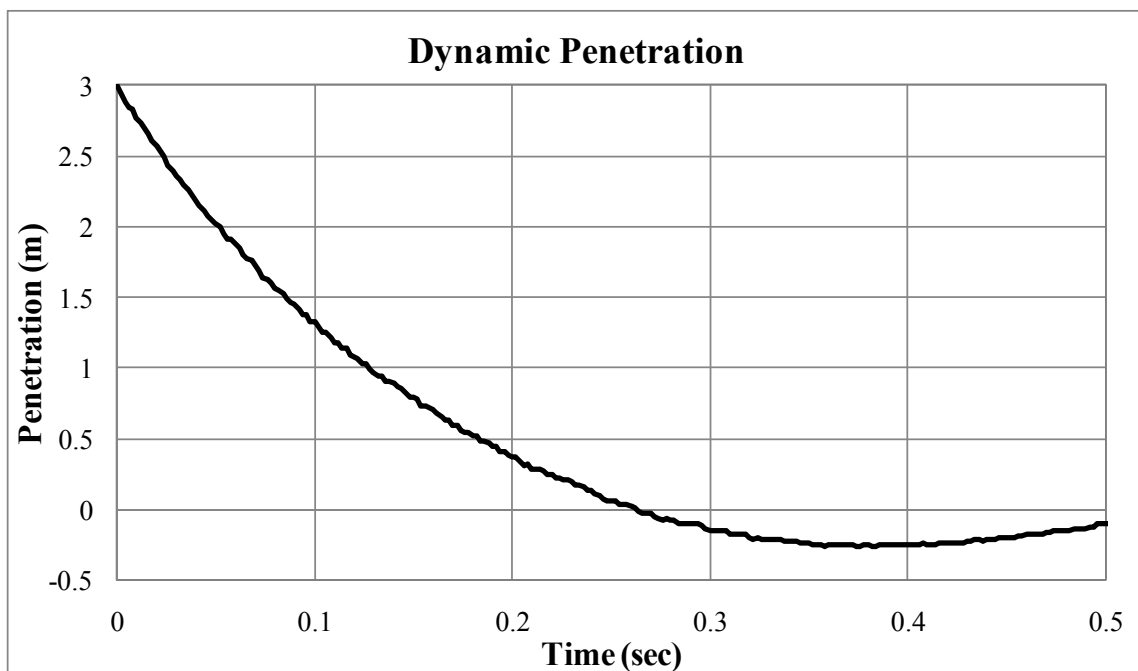
Figure 3.160. Dynamic penetration history of the full-scale test on a group of posts

The horizontal beams began to deflect toward the direction of the impact as soon as the truck impacted. At 0.010 s, the post to the left of the vehicle began to deflect, and at 0.012 s, the post to the right of the vehicle began to deflect. The hood released from the vehicle near the cab at 0.039 s, and the end post to the left of the vehicle began to

deflect toward the impact direction at 0.086 s. At 0.181 s, the rear wheels left the ground surface, and at 0.341 s, forward motion of the vehicle ended. The vehicle began to rebound at 0.405 s, and the rear of the vehicle reached its highest pitch at 0.563 s. The rear wheels touched ground again at 1.112 s. At 5.398 s, rebound ended and the vehicle began to move forward slightly and came to a complete stop at 5.719 s. Sequential photographs of the test period are shown in Appendix D (Arrington et al. 2010).

Figure 3.161. Test vehicle and the group of posts after the impact

The post and vehicle after the impact are shown in Figure 3.161. The posts rotated from 2.2 to 38.1 degrees toward the impact side. The measured permanent rotation and displacement of the posts are shown in Table 3.10. The post number is assigned left to right, i.e. post 1 is located at the end of left side and post 4 is the fourth

post from the left end. All the posts leaned toward the impact direction and also toward the impact location laterally. The permanent posts location is shown in Figure 3.162. As shown in Figure 3.162 and Table 3.10, the behaviors of posts were almost symmetry along the centerline of the group of posts.

The deformed group of posts system after the test is shown in Figure 3.163 and Figure 3.164. All four bolts that tied the beam to the posts, of the two center posts were broken as shown in Figure 3.164. The degree of damage of the test vehicle for this test was less severe than that of the full-scale test on single posts embedded in very dense crushed limestone (Figure 3.29). The damaged test vehicle for this test is shown in Figure 3.165.

Table 3.10. Permanent rotation and displacement of posts (Arrington et al. 2010)

Post No.	Permanent Rotation (degrees)		Permanent Post displacement at the ground level (mm)
	The impact direction	Lateral	
1	2.2	2.3	76
2	8.6	2.5	333
3	17.7	7.5	775
4	38.1	6.4	1543
5	36.0	6.8	1492
6	18.1	3.5	845
7	9.9	3.3	400
8	3.3	2.3	135
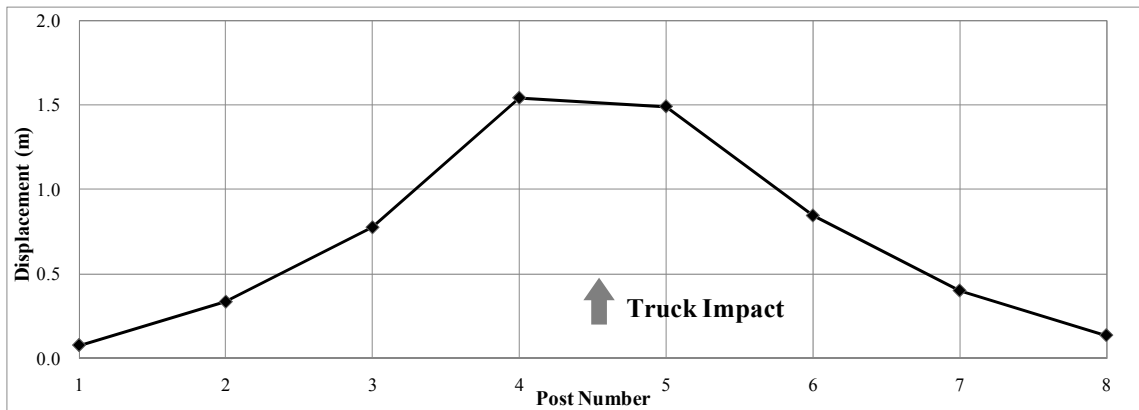
Figure 3.162. Permanent post locations after the impact

Figure 3.163. Deformed group of posts system after the impact

Figure 3.164. Broken connection of the two center posts

Figure 3.165. Deformed vehicle after the impact on the group of posts system

The three-directional accelerations of vehicle at the C.G. (center of gravity) and the rear of the vehicle were measured. The rear one was attached on the flatbed above the rear axle as a back-up of the accelerometer at the C.G. In this section, the longitudinal accelerations is mainly analyzed rather than the lateral and vertical accelerations. The reason is that the longitudinal behavior is the most dominant in this particular test, especially in the post system and the soil.

The accelerometer installed at the center of gravity of the vehicle might be defected during the impact. The reasons are that the peak acceleration was way too high and the velocity and the displacement histories were unrealistic. The acceleration data from the C.G. of the vehicle is shown in Figure 3.166. Peak longitudinal decelerations of the vehicle at the C.G were truncated around 190g. The maximum 50-msec average deceleration of vehicle at the C.G. was 115g. The impact force from the 50-msec average acceleration data can be calculated as 7,560 kN according to Newton's second law. The velocity and displacement histories of vehicle are also unrealistic as shown in Figure 3.166. The velocity and displacement of the vehicle at 0.5 sec was obtained as -320 km/h and -32m, respectively. Thus the acceleration data from the rear of the vehicle was analyzed instead of that from the C.G. of vehicle.
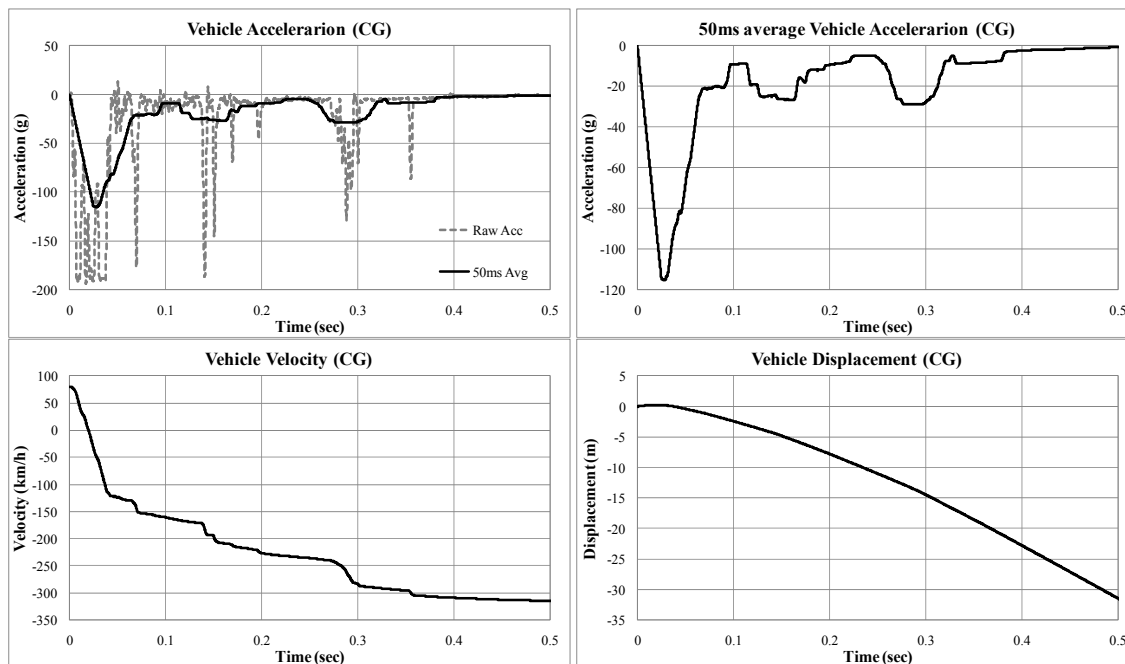
Figure 3.166. Accelerations, velocity and displacement of the vehicle at the center of gravity

The acceleration data from the rear of the vehicle is shown in Figure 3.167. Peak longitudinal deceleration of the vehicle at the rear was measured as 40g. The maximum 50-msec average deceleration of vehicle at the rear was 14g. The velocity and displacement histories of vehicle were obtained using integration of the acceleration data as shown in Figure 3.167. According to the figure, the forward movement of the truck ended and began to rebound at 0.40 sec and the rear of the vehicle displaced 3.3 m from time, 0 sec to 0.4 sec.
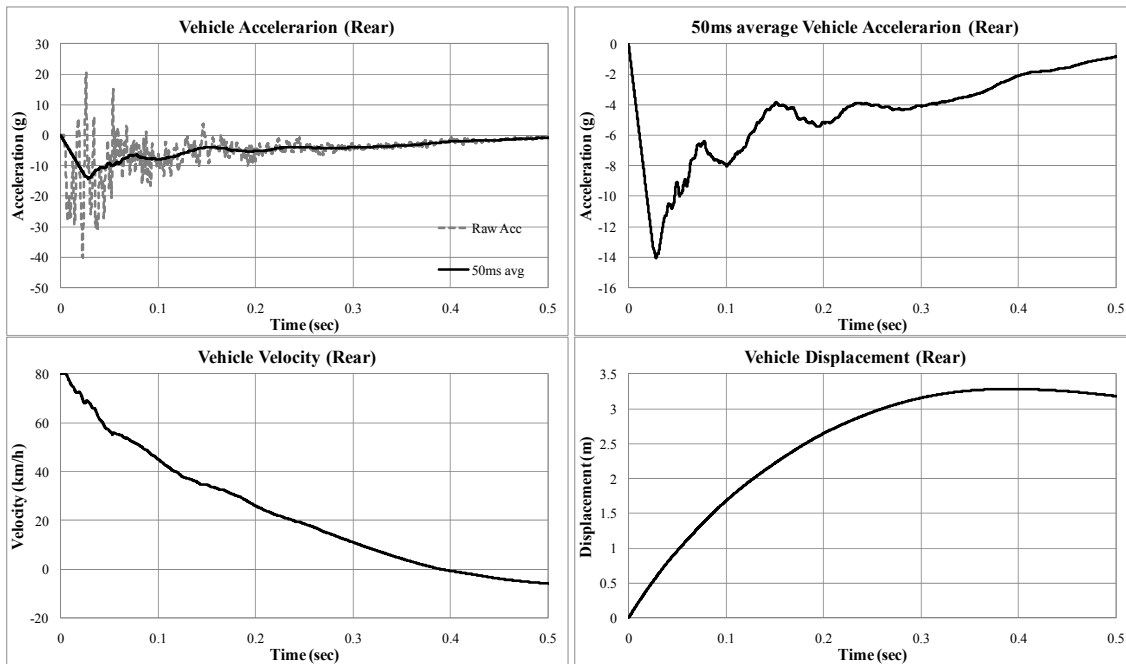
Figure 3.167. Accelerations, velocity and displacement of the vehicle at the rear

As mentioned in Section 3.2.3, the impact force acting on the post can be calculated using Newton's second law that force is equal to change in momentum over time. Since there was negligible change in mass of vehicle during the test, the longitudinal impact force is obtained from the mass of vehicle times the acceleration of vehicle at certain time (Eq 3-3). Thus 50-msec average impact force history shown in Figure 3.168 was obtained. The peak impact force was 925 kN at 0.027 sec.
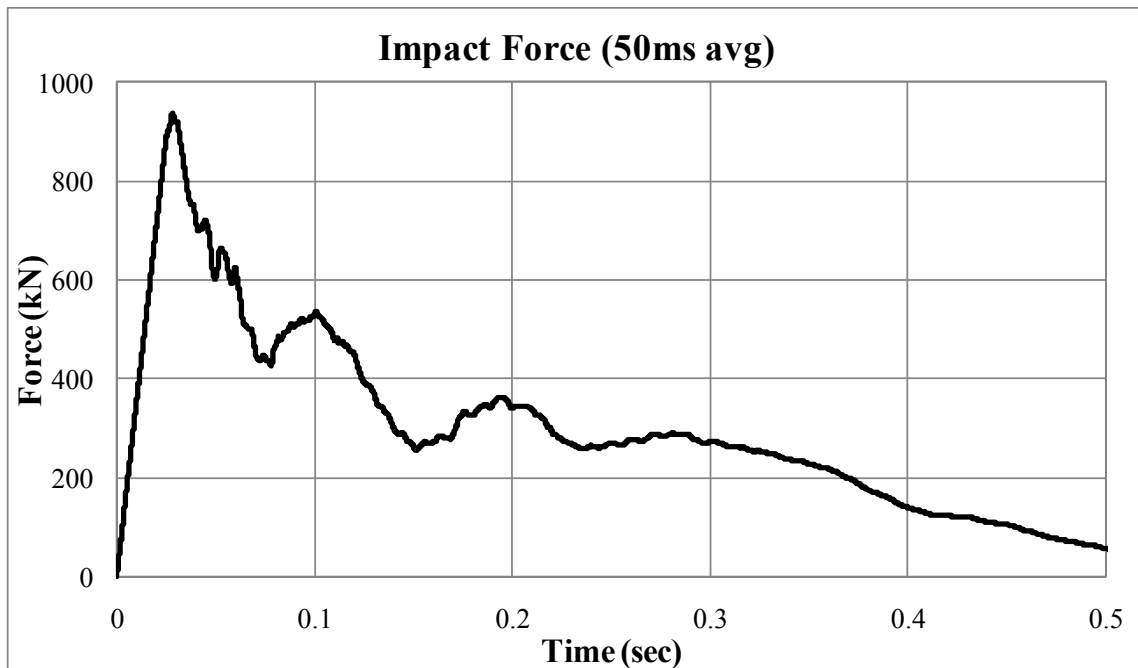
Figure 3.168. Impact force history of group of posts system

Displacement history at the 1.5m above the ground level was obtained and can be found in Figure 3.169. Three high speed cameras captured the motion of the targets attached on the side of the post 1 through 4 (Figure 3.164). Since the behaviors of the posts were almost symmetry, displacement histories of the other half of posts can be considered as same with Figure 3.169. The displacement histories for Post 3 and Post 4 could not be obtained continuously. The targets on the two posts sometimes hided by the dispersing sand particles or the other posts. Bravo de los Rios (2010) manually obtained some missing displacement data points of Post 4 from the original films. The maximum and permanent displacements of Post 4 were 2.8 m and 2.3 m, respectively. The peak displacements of Post 1, Post 2 and Post 3 were 1.4 m, 0.75 m and 0.25 m, respectively.

The strains of the posts located in the left half of the system were measured. The average strain histories of Post 1, Post 2 and Post 4 are shown in Figure 3.170. The strain gages attached on Post 3 were not obtained. Peak strains of Post 4 was 400 micro strain at 0.02 sec then drastically decreased and reached -340 micro strain at 0.13 sec, increased to 210 micro strain at 0.14 sec and decreased toward zero. The strain of Post 2 increased to 340 micro strains at 0.12 sec and decreased toward zero. The strain of Post 8 began to increase at 0.09 sec, increased to 420 micro strains at 0.31 sec and decreased toward 160 micro strains.
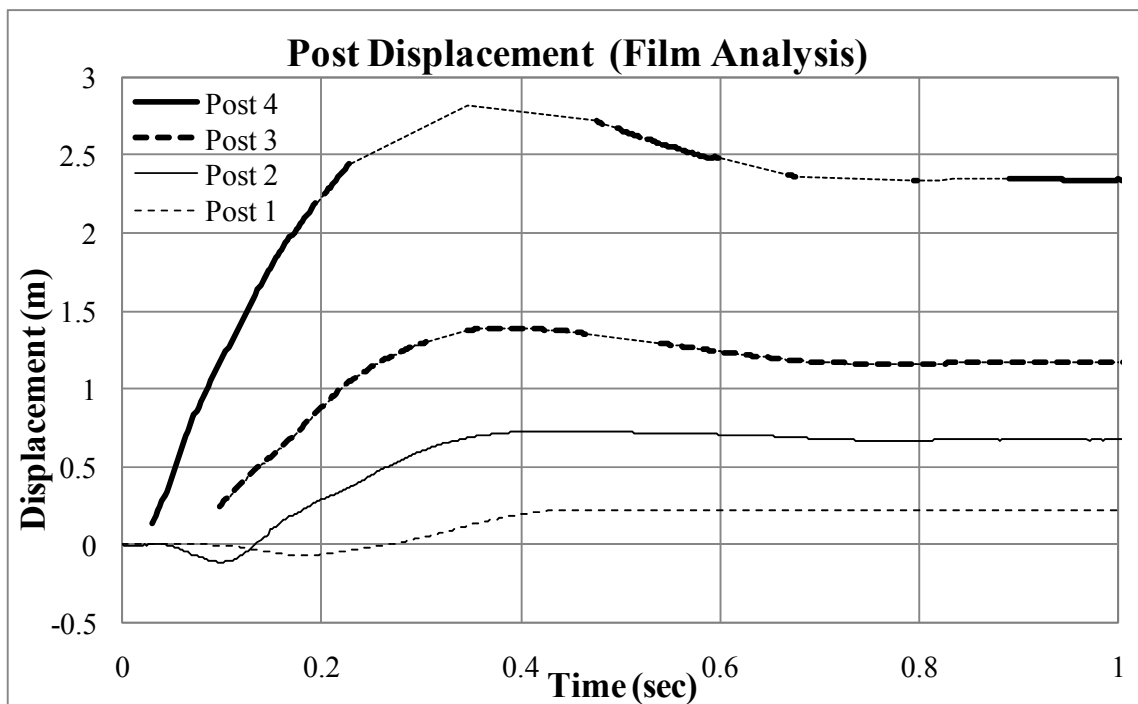
Figure 3.169. Post displacement history at 1.5 m above the ground level
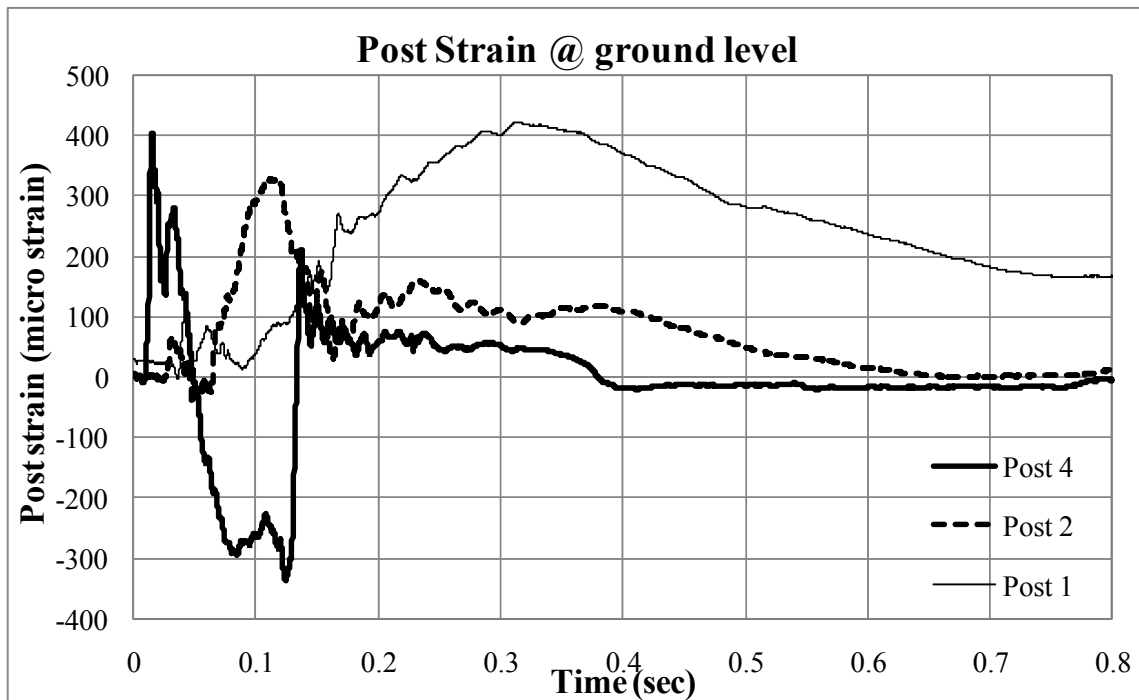
Figure 3.170. Average strain history of the posts at the ground level

3.5.4 Data analysis

The damage of the test vehicle of this test was less severe than the damage of the test vehicle for the full-scale single post test. In addition, the impact force of the test for group of posts system, 925 kN was 68 % of the impact force of the test for the single post, 1,350 kN as shown in Figure 3.171. The impact force of group of posts system lasted longer than that of single post. The reason is that the group of posts system was more flexible system than the single post embedded in very dense crushed limestone in terms of the soil strength and the flexibility of whole system. Also the group of posts

system allowed more deformations. As flexibility of system increases, degree of damage of vehicle and impact force decreases, deformation of post system increases.
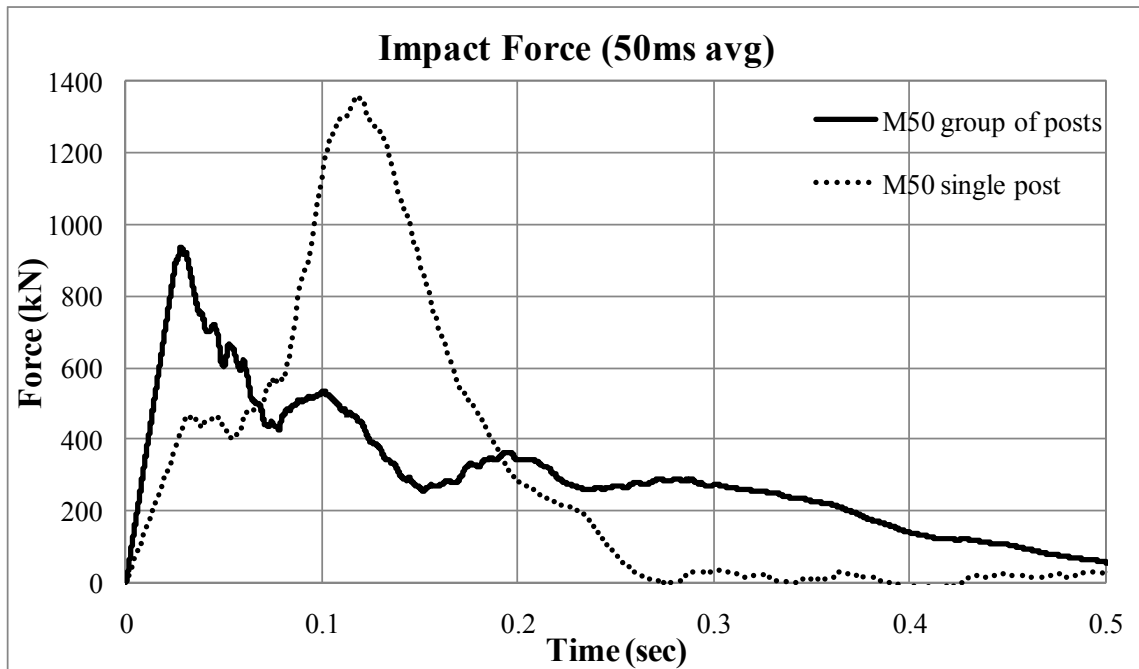
Figure 3.171. Impact force histories of the M50 tests

According to Figure 3.169, Post 1 and Post 2 moved backward to the direction of the impact at the beginning of the impact. The Post 1 and Post 2 were tied with two horizontal beams. Upon the impact, the beams deflected toward the direction of impact. As results of the deflection of beams, the two outside posts were pulled to the opposite direction of the impact. Then the posts were pushed toward the direction of the impact when the inner posts and the beams displaced enough.

In this test, the longitudinal force acting on each post at the ground level could not be calculated from the strain data. The reason is that not only the assumptions of elastic equations were not valid in this case in terms of strain level but also the measured strain was from both the moment from the impact force and the torsion of the beams.

After the test, there were some features that make the elastic assumption invalid. The phenomena were large strain of system, large permanent displacement, failure of the bolts on Post 4 and Post 5. The two horizontal beams stayed somewhat vertically whereas the posts were inclined. Torsion was applied on the posts, since both the beams and posts were tied together with steel bolts. Moreover, the failure of the bolts on Post 4 and Post 5 and residual strain on Post 8 makes the problem more difficult. Due to the reasons listed above, the force acting on each post could not be obtained.

The test data was compared with the results of finite element analysis. The detail analysis of this test including dynamic factor can be found in Section 4.3.4.

3.5.5 Conclusions

The group of posts system met the requirements for condition designation M50 and penetration rating P1 in accordance ASTM F2656-07. The eight 4.5 m long W14X90 posts 3m embedded in loose sand with two HSS 8X8X1/2 horizontal beams brought the vehicle to a complete stop with 0.274 m of dynamic penetration. The actual impact speed was 80.3 km/h and the mass of vehicle was 6,835 kg.

The peak impact force from the acceleration data was 925 kN. As flexibility of system increases, degree of damage of vehicle and impact force decreases, deformation

of post system increases, according to the comparison with the previous M50 test on single post embedded in very dense crushed limestone.

The force acting on each post could not be calculated from the strain data. However, the strain history was used as a mean of validating the result of finite element analysis described in Section 4.3.4. Also dynamic factor could not be obtained from the test data due to lack of data. Dynamic factor was estimated using both the result of experiment data and numerical simulation in Section 4.3.4.

4. NUMERICAL SIMULATIONS

4.1 Finite element analysis

In order to analyze an impact test, an explicit finite element analysis tool was required. LS-DYNA was selected as a mean of numerical simulation for this research. The software package selected for the simulation was LS-DYNA because of previous experience and success with this package. The advantages of LS-DYNA in this study are that test truck and post system including post and soil can be modeled and analyzed and limited but applicable plastic soil models are supported.

4.1.1 LS-DYNA

LS-DYNA is a general purpose transient dynamic finite element program which is capable of simulating complex non linear phenomena (LS-DYNA 2006). LS-DYNA works with either implicit or explicit solver for analyzing the large deformation static and dynamic response of structures including automotive crashworthiness and occupant safety, aerospace applications, earthquake analysis and civil and mechanical engineering applications. Also LS-DYNA allows solving a complex problem with the massively parallel processing (MPP) that can result in a reduction in time and cost.

In this study, HyperMesh, a finite element pro-processor supporting ABAQUS, ANSYS, LS-DYNA, etc. and LS-Prepost, a pre and post processor for LS-DYNA was used as a mean of modeling and post-process. LS-DYNA version 971 was used for implicit and explicit solver.

4.1.2 Soil model

In this research, two soil models were used as a mean of modeling soil. The one was Jointed Rock model that is modified from Drucker-Prager model for sand. The other was Isotropic Elastic-Plastic with Failure model for clay. The input parameters for sand were the unit weight, the modulus of elasticity, the Poisson's ratio, the cohesion intercept, the friction angle, the dilation angle. The input parameters for the clay were the unit weight, the modulus of elasticity, the Poisson's ratio, and the undrained shear strength. The values of the parameters were selected to represent a range of stiffness and strength of the soils corresponding to a range of expected values for the SPT blow count and the pressuremeter modulus and limit pressure.

4.1.2.1 Isotropic elastic–plastic with failure

Isotropic Elastic-Plastic model is one of simple and cost-effective plasticity material models for solids. Isotropic Elastic-Plastic with Failure model is a non-iterative plasticity with simple plastic strain failure model. When the effective plastic strain reaches the failure strain or when the pressure reaches the failure pressure, the element loses its ability to carry tension and the deviatoric stress are set to zero, i.e., the material behaves like a fluid (LS-DYNA Keyword User's Manual Verosion 971 2007).

Material card for this model is shown in Table 4.1. The explanations of the abbreviations for the variables in Table 4.1 are shown in Table 4.2. Details of input parameters can be found in the following section.

Table 4.1. Material cards for Isotropic Elastic-Plastic with Failure (LS-DYNA 2007)

CARD 1	1	2	3	4	5	6
Variable	MID	RO	G	SIGY	ETAN	BULK
Default	none	none	none	none	0.0	none
CARD 2	1	2	3	4	5	6
Variable	EPF	PRF	REM	TREM		
Default	none	0.0	0.0	0.0		

Table 4.2. Variables on Isotropic Elastic-Plastic with Failure (LS-DYNA 2007)

Variable	Description
MID	Material identification
RO	Mass density
G	Shear modulus
SIGY	Yield stress
ETAN	Plastic hardening modulus
BULK	Bulk modulus
EPF	Plastic failure strain
PRF	Failure pressure ($<= 0.0$)
REM	Element erosion option
TREM	dt for element removal

4.1.2.2 Jointed Rock model

Sand model was basically modeled using Drucker-Prager model. However, the behavior
of the Drucker-Prager material model in LS-DYNA version 971 was unstable with the
explicit solver. Hence Jointed Pock material card was used instead of Drucker-Prager

material card. By adding zero joint as an input, the Jointed Rock model becomes Drucker-Prager model. Drucker-Prager model is widely used in geotechnical field and enables soil to be modeled effectively since the parameters used to define the yield surface are familiar geotechnical parameters, i.e. friction angle and dilation angle. The modified Drucker-Prager yield surface is used in this material model enabling the shape of the surface to be distorted into a more realistic definition for soils (LS-DYNA Keyword User's Manual Verosion 971 2007).

Jointed Rock model was developed based on Drucker-Prager model. The main elastic-plastic behavior of Jointed Rock model is same with Drucker-Prager model since the matrix behavior is modified Drucker-Prager. The difference between these two is that Jointed Rock model is capable of considering some physical and engineering properties of rocks including dip, joint plane and joint properties. If the variables of Jointed Rock material card that are related to rock properties are modified, Jointed Rock model will be exactly same with Drucker-Prager model.

Material cards for Drucker-Prager model and Jointed Rock model are shown in Table 4.3 and Table 4.4, respectively. The explanations of the abbreviation for the variables on the material cards are shown in Table 4.5. The different variables and the explanations that represent the properties of rock are printed as italic letters in those tables. Details of input parameters can be found in the following section.

Table 4.3. Material cards for Drucker-Prager model (LS-DYNA 2007)

CARD 1	1	2	3	4	5	6	7	8
Variable	MID	RO	GMOD	RNU	RKF	PHI	CVAL	PSI
Default					1.0			0.0
CARD 2	1	2	3	4	5	6	7	8
Variable	STR_LIM							
Default	0.005							
CARD 3	1	2	3	4	5	6	7	8
Variable	GMODDP	PHIDP	CVALDP	PSIDP	GMODGR	PHIGR	CVALGR	PSIGR
Default	0.0	0.0	0.0	0.0	0.0	0.0	0.0	0.0

Table 4.4. Material cards for Jointed Rock model (LS-DYNA 2007)

CARD 1	1	2	3	4	5	6	7	8
Variable	MID	RO	GMOD	RNU	RKF	PHI	CVAL	PSI
Default					1.0			0.0
CARD 2	1	2	3	4	5	6	7	8
Variable	STR_LIM	*NPLANES*	*ELASTIC*	*LCCPDR*	*LCCPT*	*LCCJDR*	*LCCJT*	*LCSFAC*
Default	0.005	*0*	*0*	*0*	*0*	*0*	*0*	*0*
CARD 3	1	2	3	4	5	6	7	8
Variable	GMODDP	PHIDP	CVALDP	PSIDP	GMODGR	PHIGR	CVALGR	PSIGR
Default	0.0	0.0	0.0	0.0	0.0	0.0	0.0	0.0
CARD 4	*1*	*2*	*3*	*4*	*5*	*6*	*7*	*8*
Variable	*DIP*	*STRIKE*	*CPLANE*	*FRPLANE*	*TPLANE*	*SHRMAX*	*LOCAL*	
Default	*0.0*	*0.0*	*0.0*	*0.0*	*0.0*	*1.0e+20*	*0.0*	

Repeat Card 4 for each plane (maximum 3 planes):

Table 4.5. Variables on Drucker-Prager and Jointed Rock model (LS-DYNA 2007)

Variable	Description
MID	Material identification
RO	Mass density
GMOD	Shear modulus
RNU	Poisson's ratio
RKF	Failure surface shape parameter
PHI	Angle of friction (radians)
CVAL	Cohesion
PSI	Dilation angle (radians)
STR_LIM	Minimum shear strength of material is given by STR_LIM*CVAL
NPLANES	*Number of joint planes (maximum 3)*
ELASTIC	*Flag = 1 for elastic behavior only*
LCCPDR	*Load curve for extra cohesion for parent material (dynamic relaxation)*
LCCPT	*Load curve for extra cohesion for parent material (transient)*
LCCJDR	*Load curve for extra cohesion for joints (dynamic relaxation)*
LCCJT	*Load curve for extra cohesion for joints (transient)*
LCSFAC	*Load curve giving factor on strength vs time*
GMODDP	Depth at which shear modulus is correct
PHIDP	Depth at which angle of friction is correct
CVALDP	Depth at which cohesion is correct
PSIDP	Depth at which dilation angle is correct
GMODGR	Gradient at which shear modulus increases with depth
PHIGR	Gradient at which angle of friction increases with depth
CVALGR	Gradient at which cohesion increases with depth
PSIGR	Gradient at which dilation angle increases with depth
DIP	*Angle of the plane in degrees below the horizontal*
DIPANG	*Plan view angle (degrees) of downhill vector drawn on the plane*
CPLANE	*Cohesion for shear behavior on plane*
PHPLANE	*Friction angle for shear behavior on plane (degrees)*
TPLANE	*Tensile strength across plane (generally zero or very small)*
SHRMAX	*Max shear stress on plane (upper limit, independent of compression)*
LOCAL	*DIP and DIPANG are with respect to the global or local axes*

4.1.3 Soil properties

Input soil properties for the proposed numerical simulations were determined using either the proposed soil strength category (Table 3.7) or the measured properties described in Section 3.1.

In order to complete the proposed design chart, soil properties from the soil strength categories were used. Soil properties required for Jointed Rock model are soil density, shear modulus, Poisson's ratio, friction angle, cohesion intercept and dilation angle. For example, a Jointed Rock material card for sand with strength 1, loose sand is shown in Table 4.6. The unit of friction and dilation angle was radians. Shear modulus was obtained using Elastic modulus and Poisson's ratio (Eq. 4-1).

$$G = \frac{E}{2(1-\upsilon)} \tag{4-1}$$

where, G = Shear modulus
E = Elastic modulus (Young's modulus)
υ = Poisson's ratio

Also, soil properties required for Isotropic Elastic-Plastic with Failure model are soil density, shear modulus, yield stress, plastic hardening modulus, bulk modulus and failure pressure. For example, a Isotropic Elastic-Plastic with Failure material card for clay with strength 1, soft clay is shown in Table 4.7. Element erosion option (REM) was selected as 1.0. In other words, the failed elements due to tension do not be eroded and removed from the model. Cohesion was used as failure pressure (PRF).

Table 4.6. Example of Jointed Rock material card for loose sand

CARD 1	1	2	3	4	5	6	7	8
Variable	MID	RO	GMOD	RNU	RKF	PHI	CVAL	PSI
Default	*2000002*	*1.700E-9*	*0.740741*	*0.35000*	1.0000	*0.471239*	*0.0010*	*-0.17453*
CARD 2	1	2	3	4	5	6	7	8
Variable	STR_LIM	NPLANES	ELASTIC	LCCPDR	LCCPT	LCCJDR	LCCJT	LCSFAC
Default	0.005	0	0	0	0	0	0	0
CARD 3	1	2	3	4	5	6	7	8
Variable	GMODDP	PHIDP	CVALDP	PSIDP	GMODGR	PHIGR	CVALGR	PSIGR
Default	0.0	0.0	0.0	0.0	0.0	0.0	0.0	0.0
CARD 4	1	2	3	4	5	6	7	8
Variable	DIP	STRIKE	CPLANE	FRPLANE	TPLANE	SHRMAX	LOCAL	
Default	0.0	0.0	0.0	0.0	0.0	1.0e+20	0.0	

Table 4.7. Example of Isotropic Elastic-Plastic with Failure Material card for soft clay

CARD 1	1	2	3	4	5	6
Variable	MID	RO	G	SIGY	ETAN	BULK
Default	*2000002*	*1.7000E-9*	*0.555556*	*0.022000*	*0.0*	*1.666667*
CARD 2	1	2	3	4	5	6
Variable	EPF	PRF	REM	TREM		
Default	none	*-0.011000*	*1.0*	0.0		

Shear modulus and Bulk modulus were obtained using Elastic modulus and Poisson's ratio (Eq. 4-1 and Eq. 4-2).

$$K = \frac{E}{3(1-2\upsilon)}$$
(4-2)

where, K = Bulk modulus

E = Elastic modulus (Young's modulus)

υ = Poisson's ratio

The yield criterion of Isotropic Elastic-Plastic with Failure is Von Mises yield criterion. Yield stress (SIGY) can be obtained using undrained compression strength of clay. The yield function is expressed as:

$$\phi = J_2 - \frac{\sigma_y^2}{3}$$

(4-3)

where, ϕ = yield function

$J_2 = \frac{1}{2} S_{ij} S_{ij}$ = the Second deviatoric stress invariant

σ_y = yield stress

In the case of uniaxial stress that is same with undrained compression, $\sigma_1 \neq 0$, $\sigma_2 = \sigma_3 = 0$, Eq (4-3) reduces to

$$\sigma_1 = \sigma_y$$

(4-4)

where, σ_y = yield stress

σ_1 = major principle stress = undrained compression strength

Therefore, undrained compression strength is same with the yield stress of Isotropic Elastic-Plastic with Failure model.

4.1.4 Vehicle and post system models

Akram Abu-Odeh, a Research scientist of Roadside Safety program, Texas Transportation Institute, modeled the initial M50 test for single post embedded in the very dense crushed limestone.

The single unit single-unit flatbed truck with test inertia weight of 6,800 kg and the vehicle model for finite element analysis are shown in Figure 4.1. Throughout the numerical simulations, some features of the original vehicle were modified including

change of thickness of main frame of vehicle per measurement, contact properties and meshes.

Figure 4.1. Vehicle for M50 impact test and vehicle model for numerical simulation

The pendulum and bogie model for the proposed numerical simulations were prepared. An accelerometer was placed at the C. G of bogie and pendulums model similar to the actual bogie and pendulums. Though the model was simplified, the mass and contact properties were modeled as similar as possible. The actual test bogie and pendulums and those models are shown in Figure 4.2, Figure 4.3 and Figure 4.4.
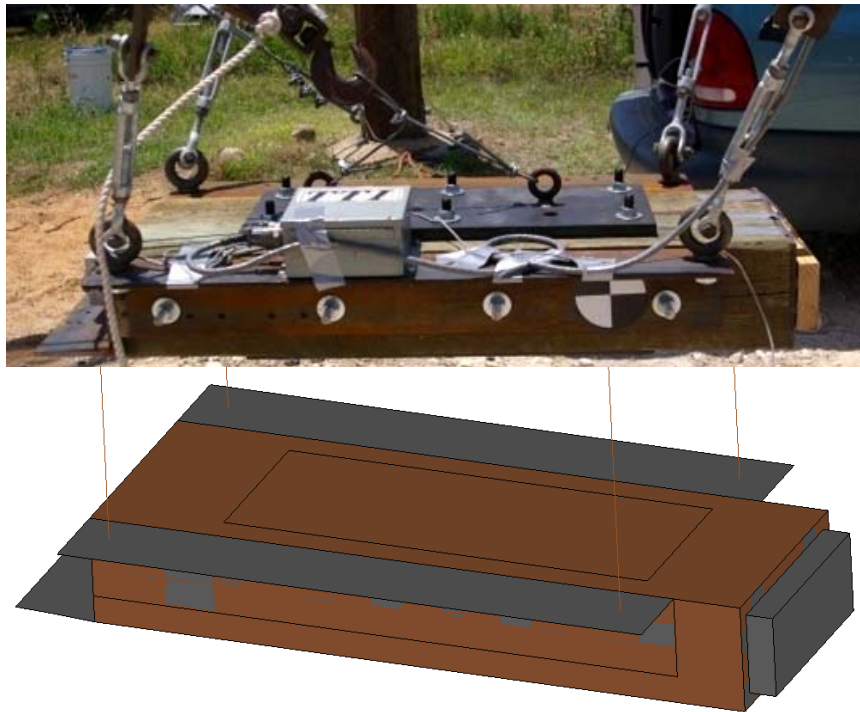
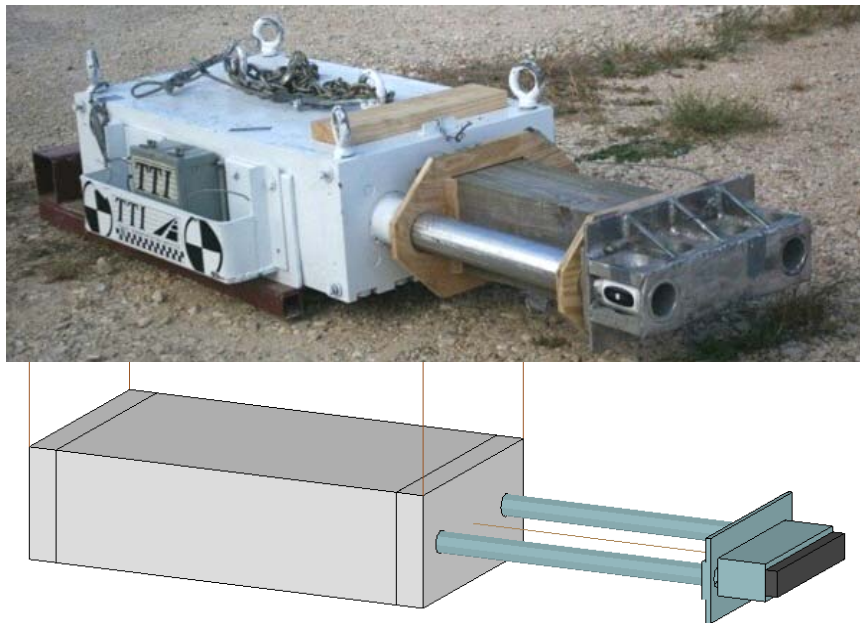**Figure 4.2. Pendulum for impact test in loose sand and the model**

Figure 4.3. Pendulum for impact test in medium dense crushed limestone and the model
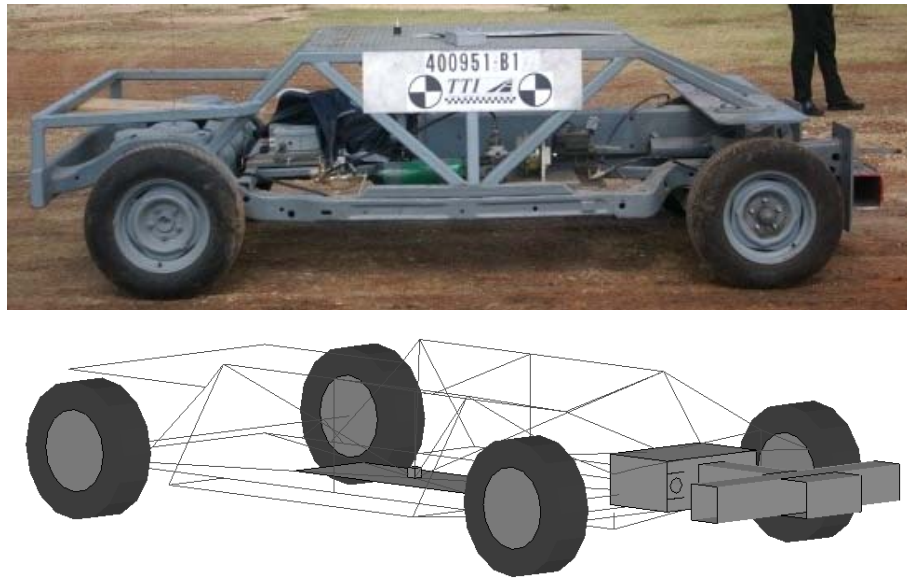
Figure 4.4. Bogie for impact test in hard clay and the model

The post system and soil was modeled with a number of solid and shell elements. Soil was modeled as a continuum model with solid elements. The soil meshes near the post system were modeled with finer meshes than the others. The post and beams were made of shell elements.

The contact between the post system and the soil was merged instead of using a contact. However, the behavior of post and soil was reasonable and realistic, since Jointed Rock model and Isotropic Elastic-Plastic with Failure model, have tensile limit such as cohesion and failure pressure (PRF). If tensile stress of an element reaches the tensile strength, the soil element cannot carry the tensile stress but carry compressive stress only. This behavior is similar to actual behavior of soil.

The post system and soil model was initialized for gravitational loading. Soil pressure due to the self weight of soil should be considered. Moreover, the stress states

determine the plasticity behavior of soil models. Therefore, the initialization with gravitational loading has to be performed prior to impact simulation. A initialized model for post system and soil is shown in Figure 4.5. The initializations were performed using either implicit solver or explicit solver. Poisson's ratio of soil was assumed as 0.35.
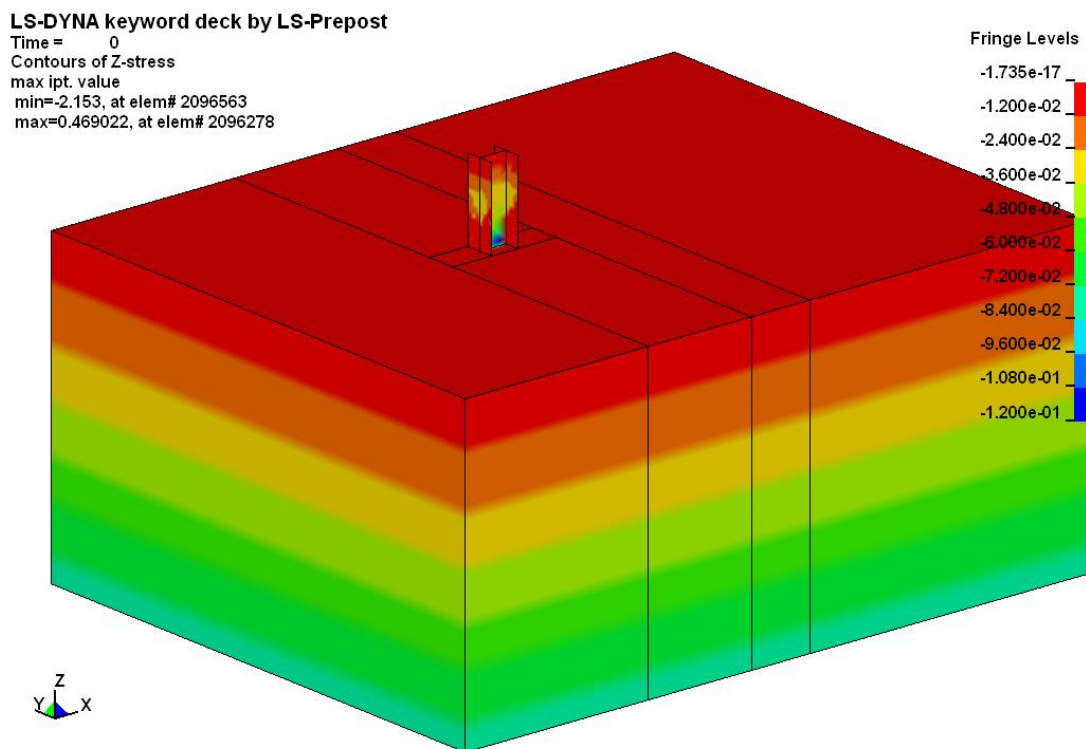

Figure 4.5. Initialized model of single post embedded in soil

4.2 Design of group of posts system

After the M50 impact test on single post embedded in very dense crushed limestone, design of group of posts system embedded in loose sand was started. The soil strength of the very dense crushed limestone is one of the strongest conditions. However, most of

soil conditions are weaker than the soil. Group of posts systems are required to contain M50 level truck impact for those soil conditions especially for loose sand or soft clay. Also there can be some special needs for continuous barrier systems.

3.4 m embedded seventeen posts with a beam at the ground level in loose sand

The first design of posts system was shown in Figure 4.6. The system consisted of seventeen of 4.9m long W14X109 posts with 1.22 m clearances and a HSS 16X16X5/8 steel tube as a horizontal beam at the ground level. The posts were embedded 3.4 m in loose sand. Vehicle with 6,800 kg of mass traveling 80 km/h against the posts system was simulated using LS-DYNA.

Captured simulation results at the beginning and at 0.25 sec are shown in Figure 4.7. As results of this simulation, the system could not bring a complete stop of vehicle at 0.26 sec. Also the dynamic penetration was more than 1 m. Simulated vehicle velocity for this case and two other cases described later in this section, are shown in Figure 4.8.

The impact load on the center post was not transferred to the other sixteen posts. The reasons is that the center post was deflected but the other posts did not well engaged with the center one as shown in Figure 4.8 and Figure 4.9. Post 1 is located at the right end of the row and Post 9 is the center post that contact with the vehicle.
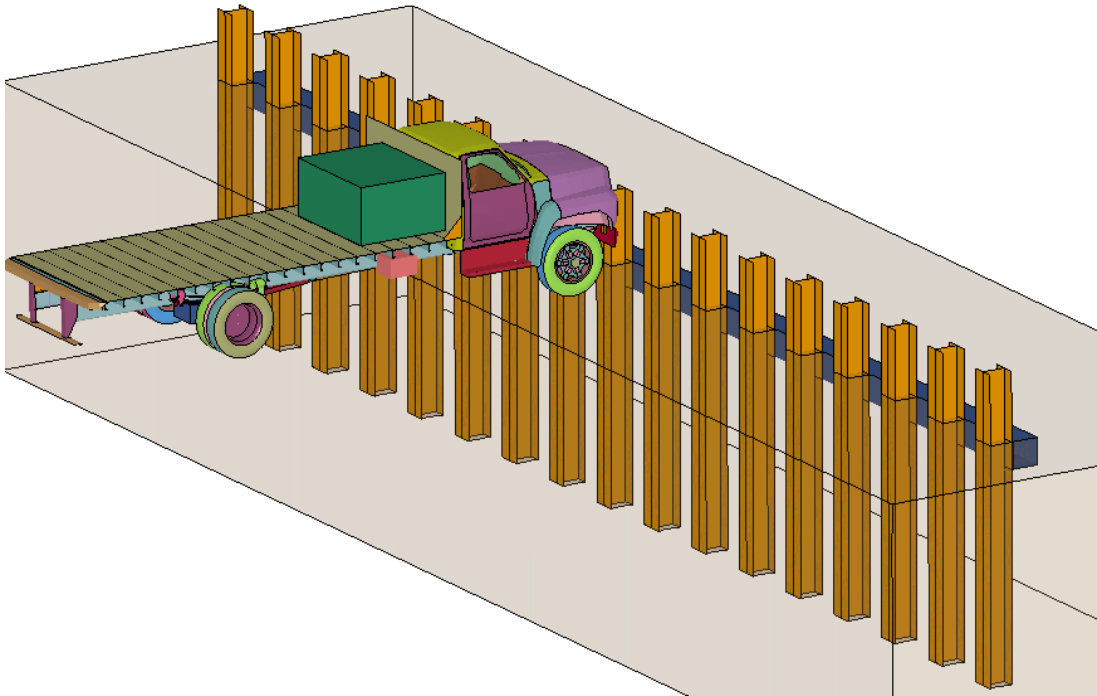
Figure 4.6. Impact simulation for seventeen posts with a beam at the ground level

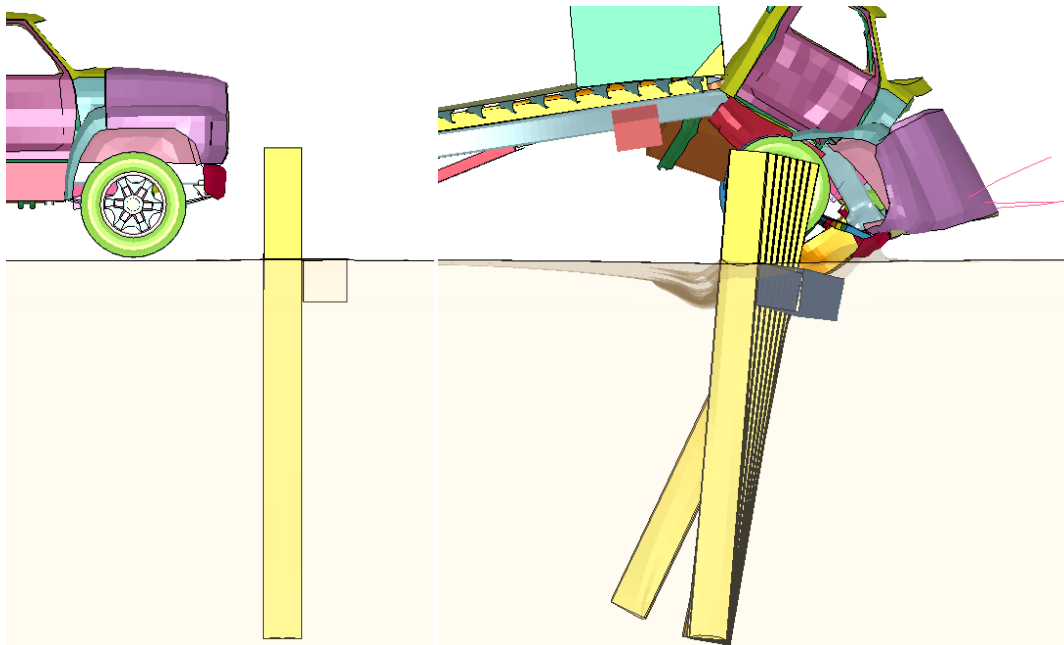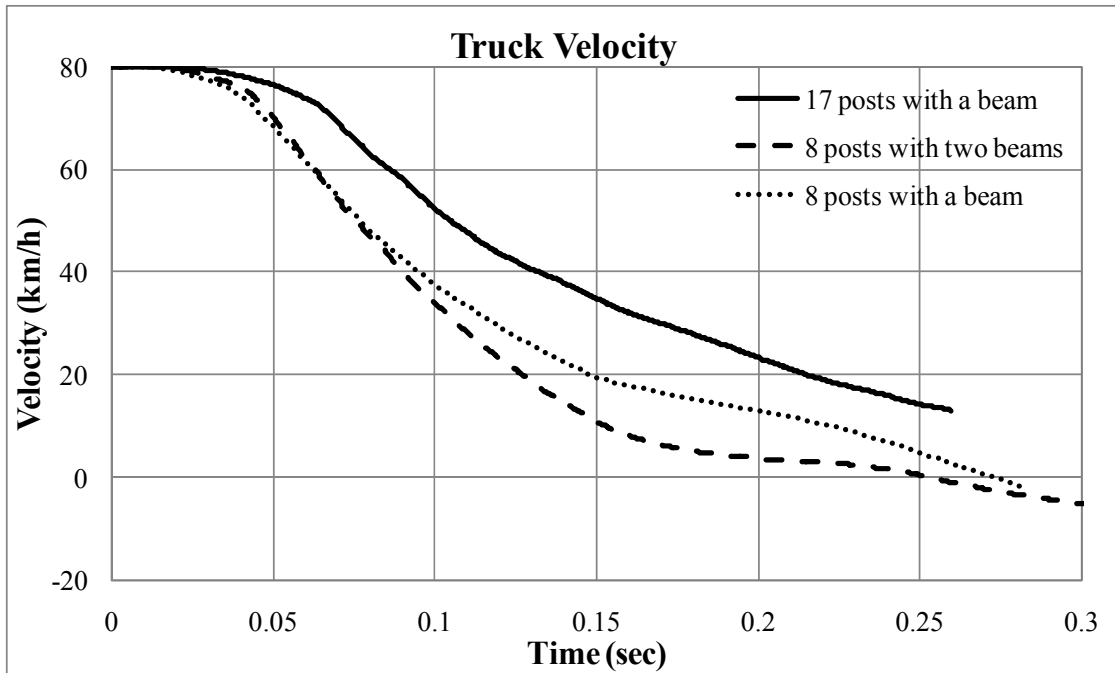**Figure 4.7. Simulation results of seventeen posts with a beam**

Truck Velocity

Figure 4.8. Vehicle velocity of group of posts for design
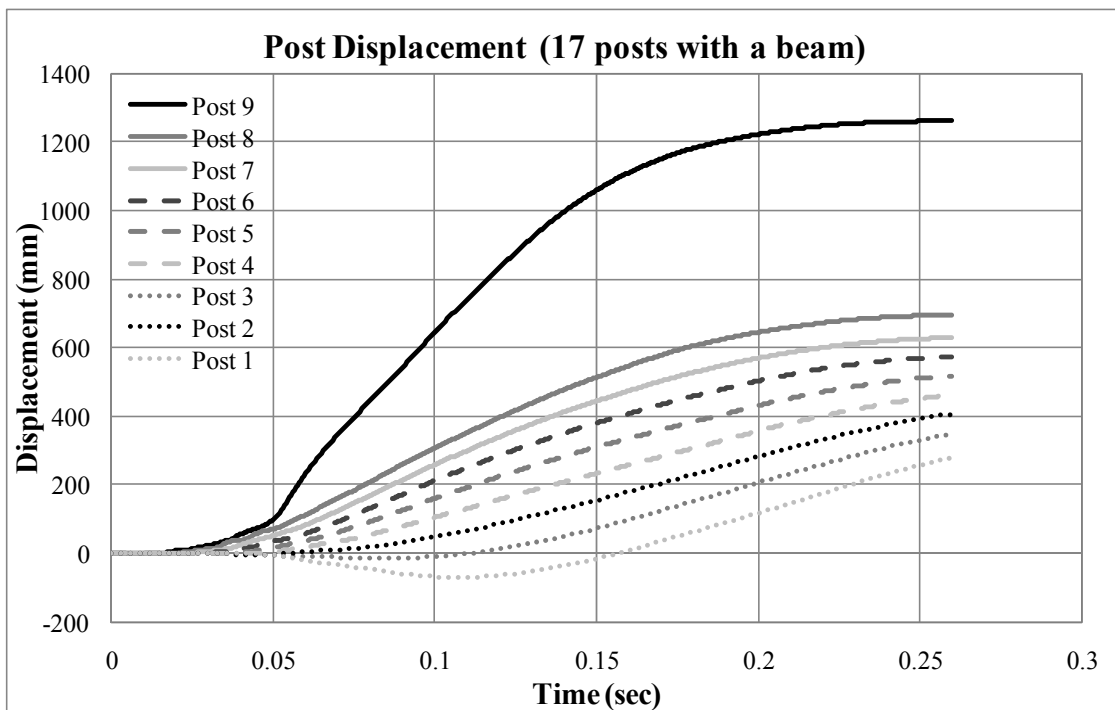
Post Displacement (17 posts with a beam)

Figure 4.9. Post displacement for seventeen posts with a beam simulation

6 m embedded eight posts with two beams in loose sand

The second design of posts system was shown in Figure 4.10. The system consisted of eight of 7.5m long W14X109 posts with 4.88 m clearances and two HSS 16X16X5/8 steel tubes as horizontal beams at the ground level and at the impact level. The posts were embedded 6 m in loose sand. Vehicle with 6,800 kg of mass traveling 80 km/h against the posts system was simulated.
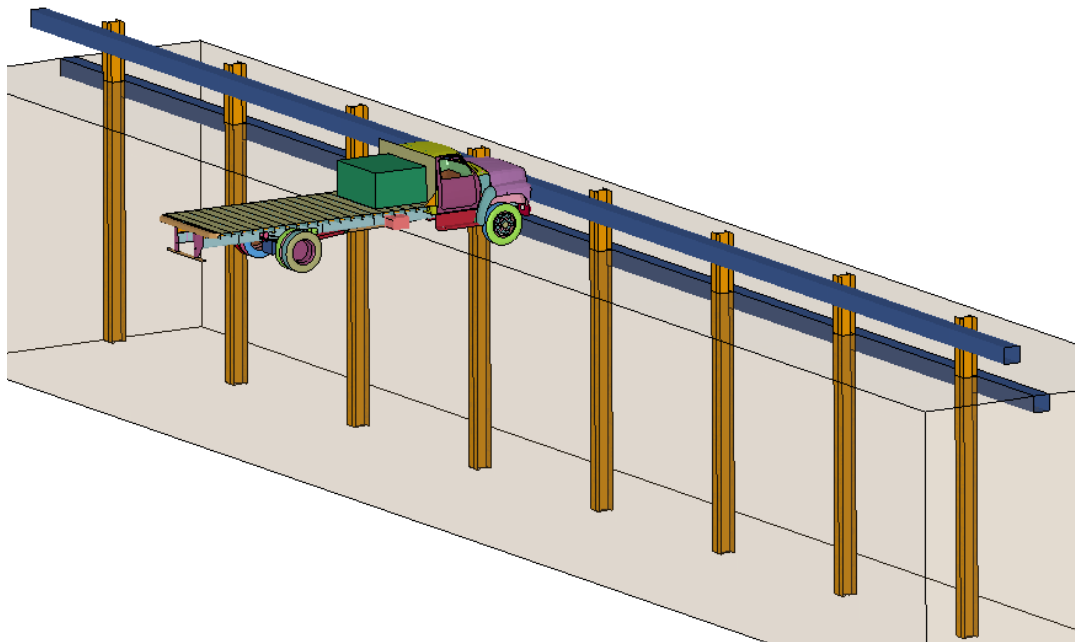
Figure 4.10. Impact simulation for eight posts with a two beams

Captured simulation results at the beginning and at 0.25 sec are shown in Figure 4.11. As results of this simulation, the system brought a complete stop of vehicle at 0.25 sec. as shown in Figure 4.8. The system allowed 0.95 m of peak post deflection at the impact level and did not allow dynamic penetration.

Figure 4.11. Simulation result of eight posts with two beams

Figure 4.12. Post displacement for eight posts with two beams simulation

The impact load was well transferred to all the posts through the two beams. The posts were deflected almost together shown in Figure 4.11 and Figure 4.12. In Figure 4.12, Post 1 is located at the right end of the row and Post 4 is the center post that is the nearest post to the vehicle impact. The upper beam transferred the impact load and the lower beam confined the post displacement at the ground level.

6 m embedded eight posts with a beam at the impact level in loose sand

The final design of posts system was shown in Figure 4.13. The system consisted of eight of 7.5m long W14X109 posts with 4.88 m clearances and a HSS 16X16X5/8 steel tubes as a horizontal beam at the impact level. The posts were embedded 6 m in loose sand. The system was identical to the previous posts system with eight posts and two beams except the horizontal beam at the ground level. The impact condition followed the condition designation M50 of ASTM F2656-07.

Captured simulation results at the beginning and at 0.25 sec are shown in Figure 4.14. As results of this simulation, the system brought a complete stop of vehicle at 0.275 sec. as shown in Figure 4.8. The system allowed 1.37 m of peak post deflection at the impact level and did not allow dynamic penetration.
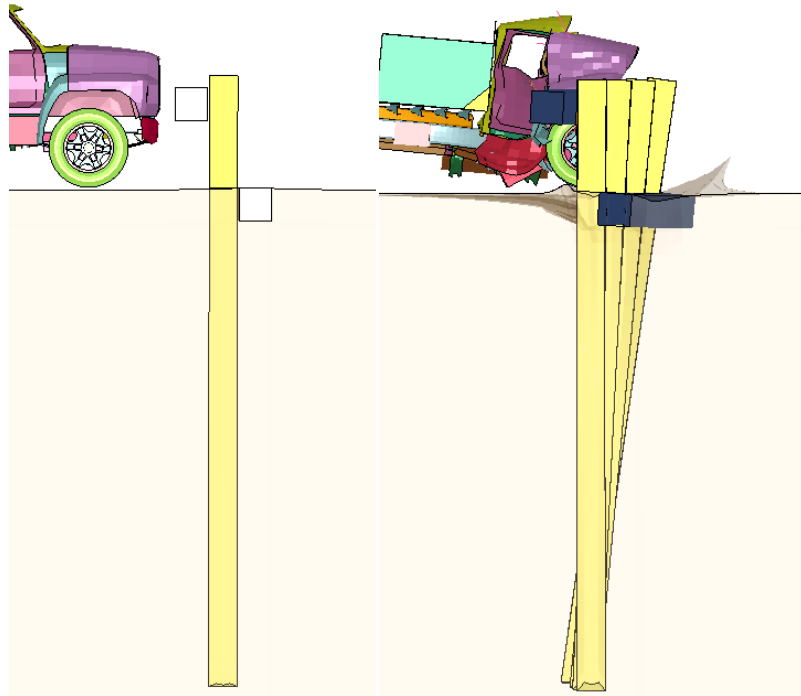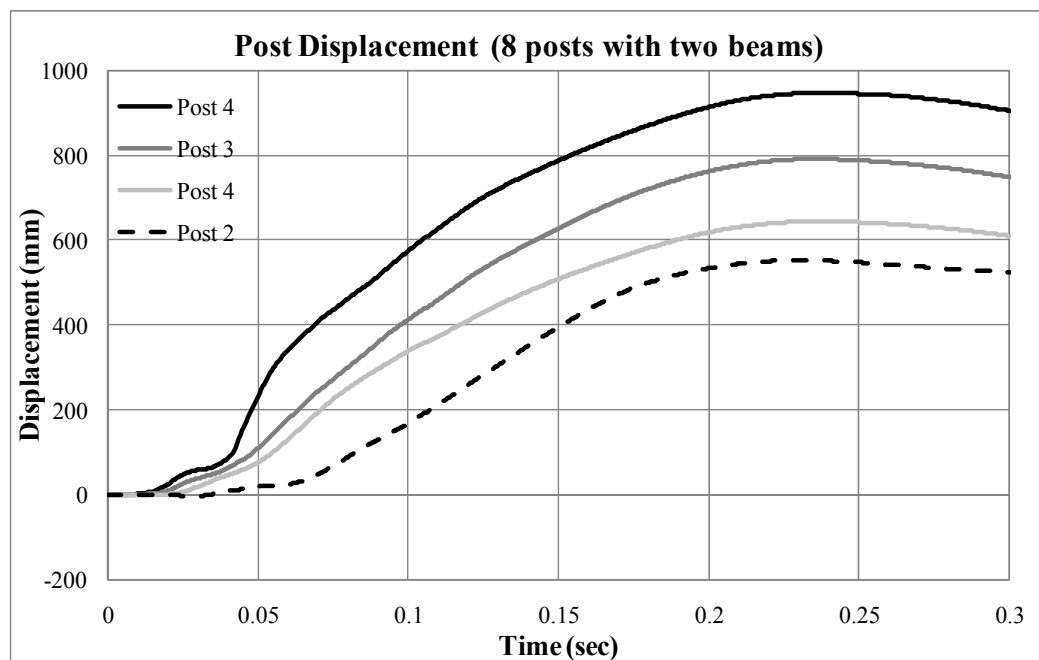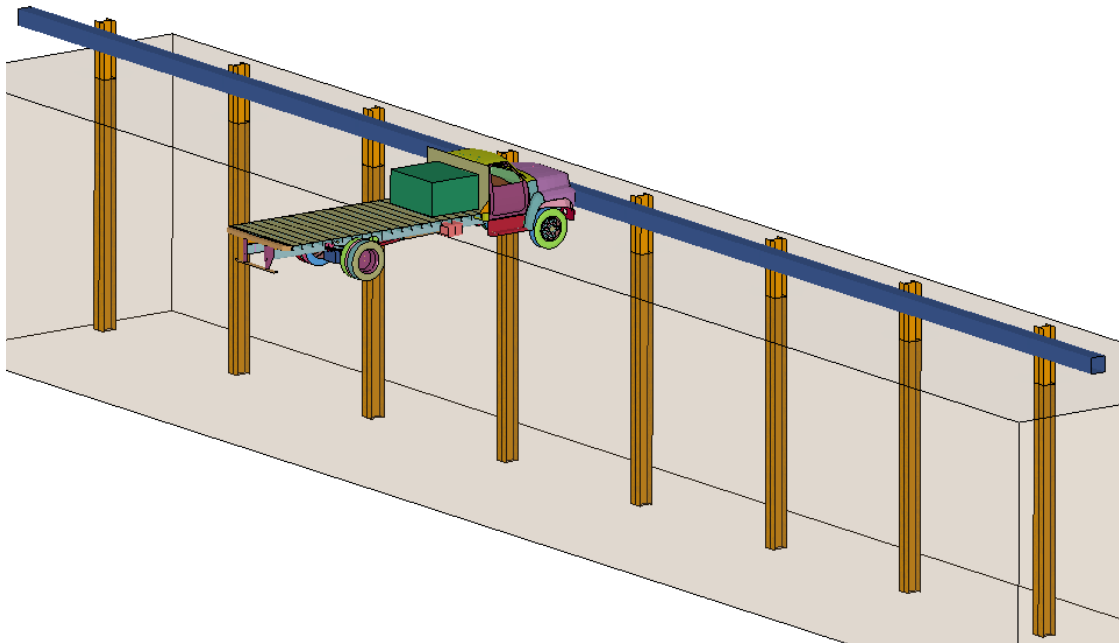
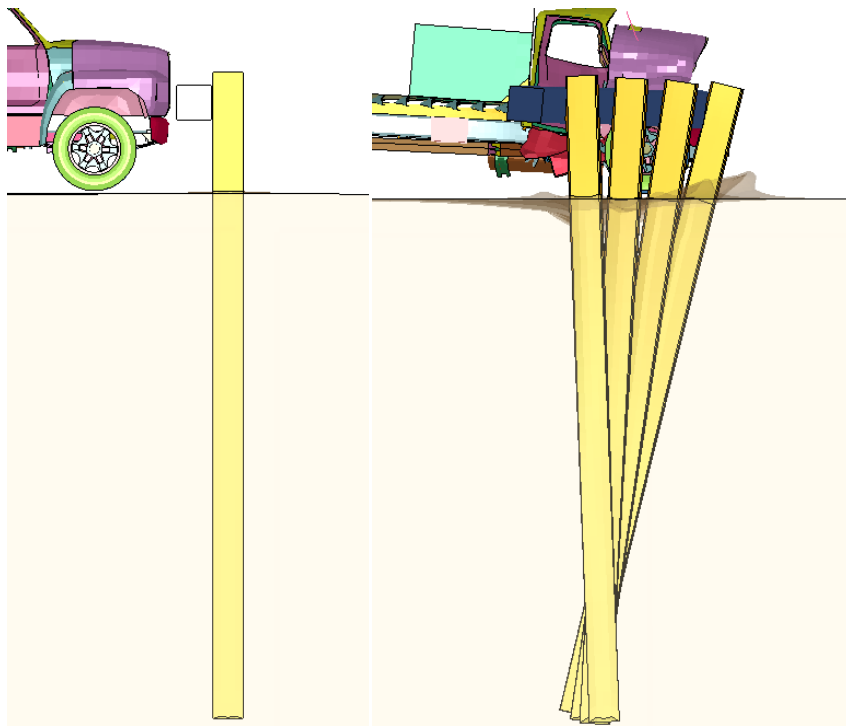**Figure 4.13. Impact simulation for eight posts with a beam at the impact level**

Figure 4.14. Simulation results of eight posts with a beam at impact level
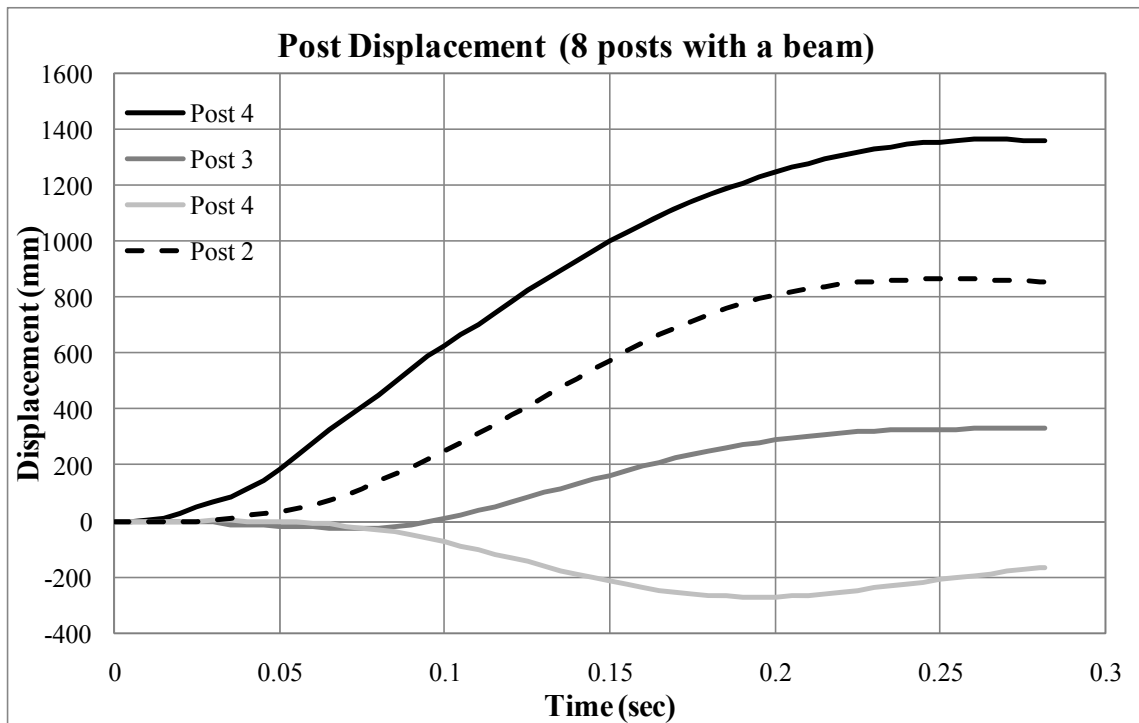
Figure 4.15. Post displacement for eight posts with a beam simulation

The impact load was also well transferred to all the posts through the horizontal beam. The six posts near the center were deflected toward same direction as shown in Figure 4.8 and Figure 4.15. In Figure 4.15, Post 1 is located at the right end of the row and Post 4 is the center post that is the nearest post to the vehicle impact. The outer two posts deflected to the opposite direction of the impact direction due to the bending of the horizontal beam to 0.20 sec. As result of the bending of the beam towards the protected side, the end of beams displaced to the opposite direction. The outer two posts began move toward the same directions of the other posts deflection at 0.2 sec.

In the previous design with two beams, the upper beam transferred the impact load and the lower beam confined the post displacement at the ground level. In this case,

the impact load was well distributed despite of the absent of the lower beam. Though the confining effect was less than that with the beam, the soil resistance around the ground level confined the deflection of posts. The confining effect from soil resistance increases as soil strength increases. In this study, design of group of posts system was determined as a row of posts with a beam at the impact level.

Mesh sensitivity

Mesh size sensitivity of the finite element analysis using LS-DYNA was checked to obtain reasonable accuracy. As shown in Figure 4.16, loose or weak material with coarse mesh can behave stronger than its real strength.

Loose or Weak Material   Dense or Strong Material
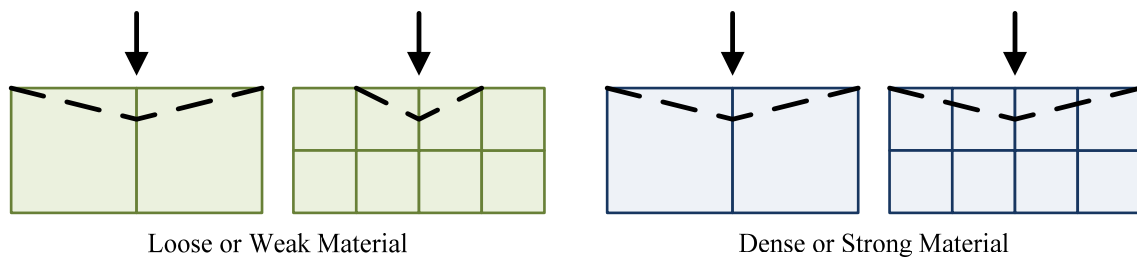
Figure 4.16. Mesh size sensitivity

The original design post system was modeled with finer soil mesh. As a result, number of soil elements was increased from 0.4 million to 1.2 millions. Results from two simulations with different mesh size were compared in Figure 4.18, Figure 4.19 and Figure 4.20. Thus the mesh size of numerical simulations for the proposed design chart is finer enough.

Figure 4.17. 0.4 millions of elements versus 1.2 millions of elements
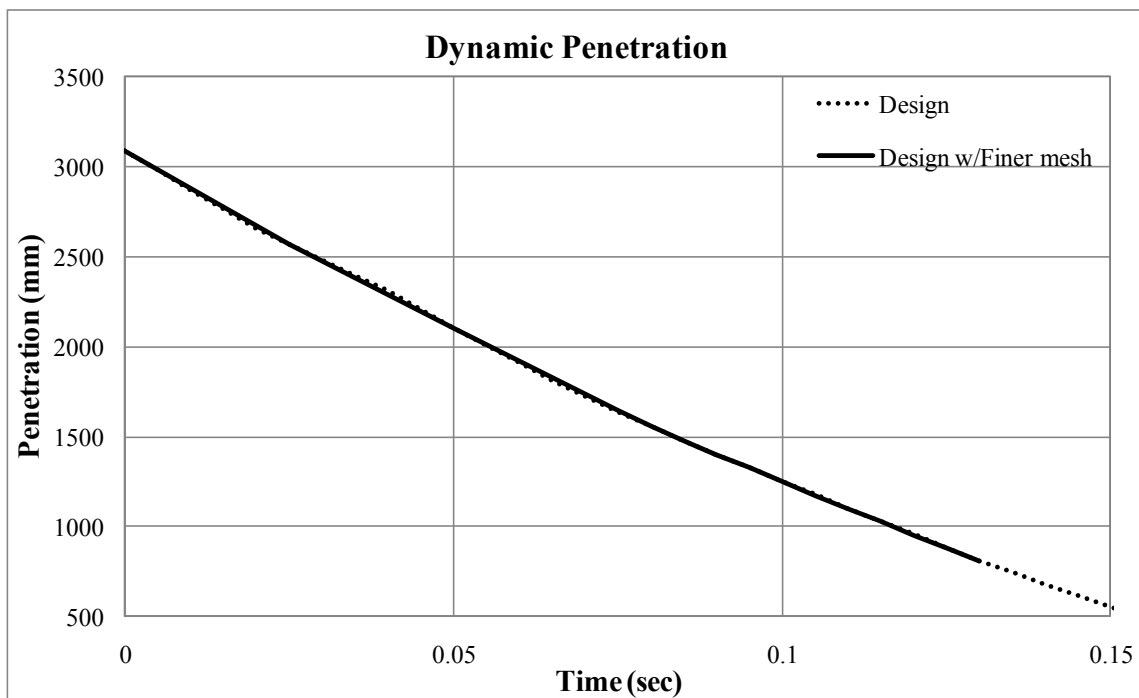
Figure 4.18. Simulated dynamic penetration for mesh size sensitivity
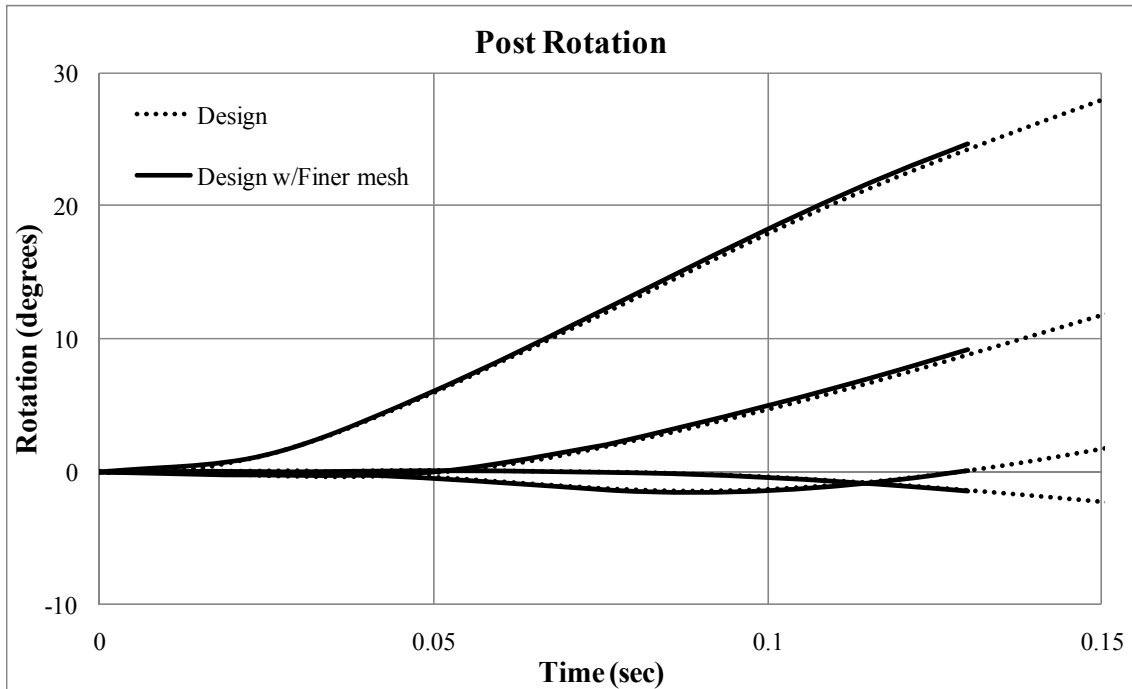
Post Rotation

Figure 4.19. Simulated post rotation for mesh size sensitivity

Contact Force
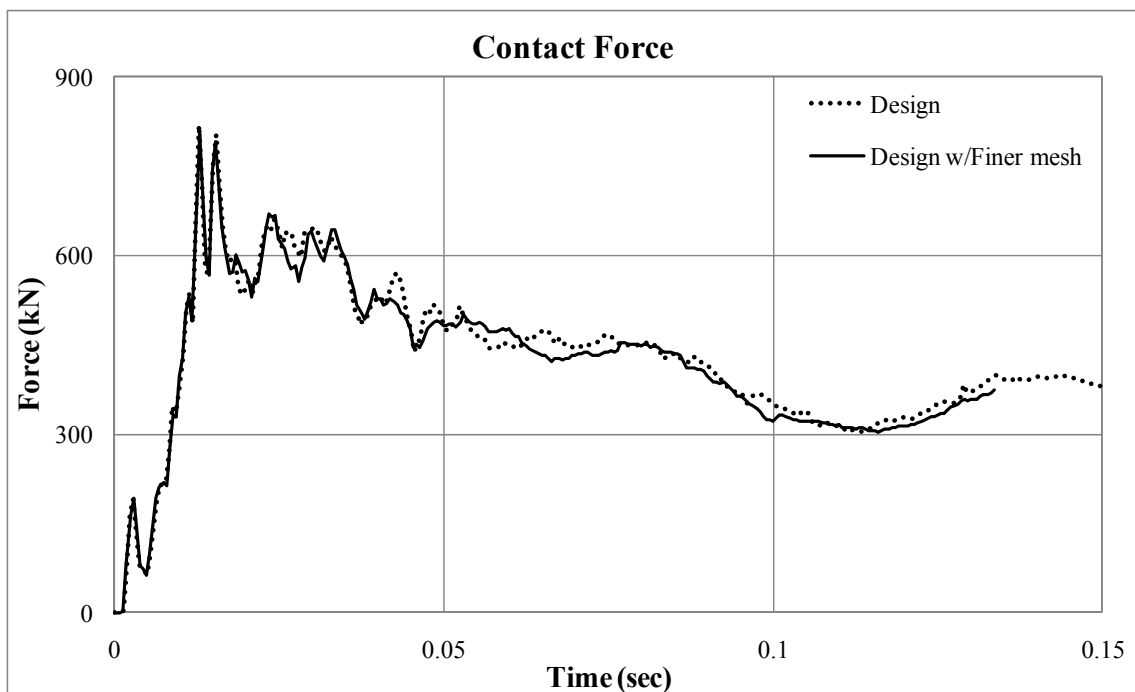
Figure 4.20. Simulated impact force for mesh size sensitivity

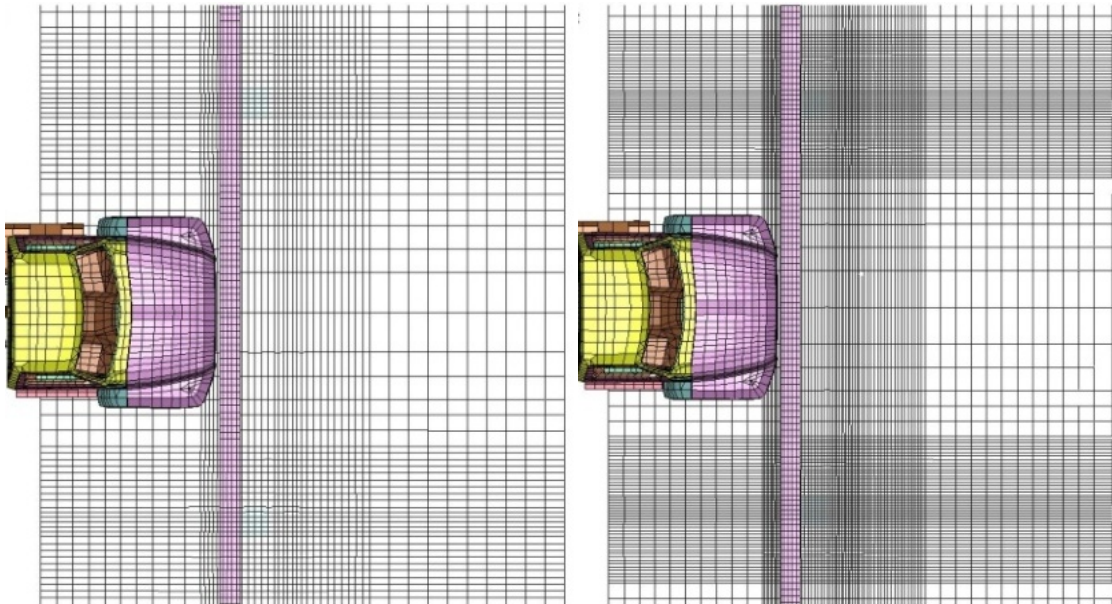*Number of posts in a row*

Four finite elements models were simulated to determine the minimum number of posts in a row. During the simulations, the number of posts was increased from six posts to sixteen posts. The other test conditions including soil strength, impact condition and post section were same for all four tests. Finite element model for six posts, ten posts and sixteen posts are shown in Figure 4.21.
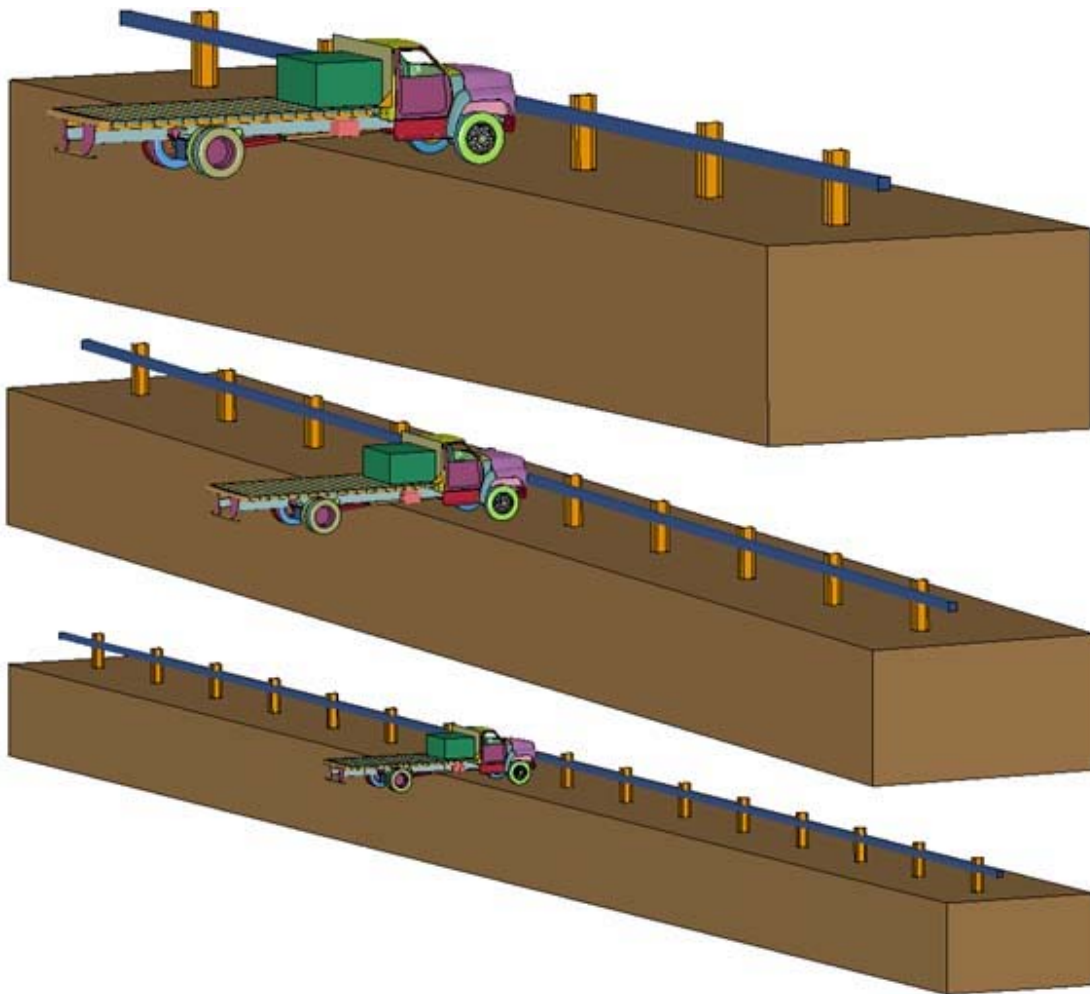
Figure 4.21. Group of posts system models with 6, 10 and 16 posts

Comparisons of simulated vehicle velocity and dynamic penetration are shown in Figure 4.22 and Figure 4.23. Except the posts system with six posts, all systems met ASTM requirements, M50 and P1. Though dynamic penetration decreases as number of posts increases, the decrease rate was very small. The reason is that even the number posts increased, load transfer length is limited depends on stiffness of horizontal beam.
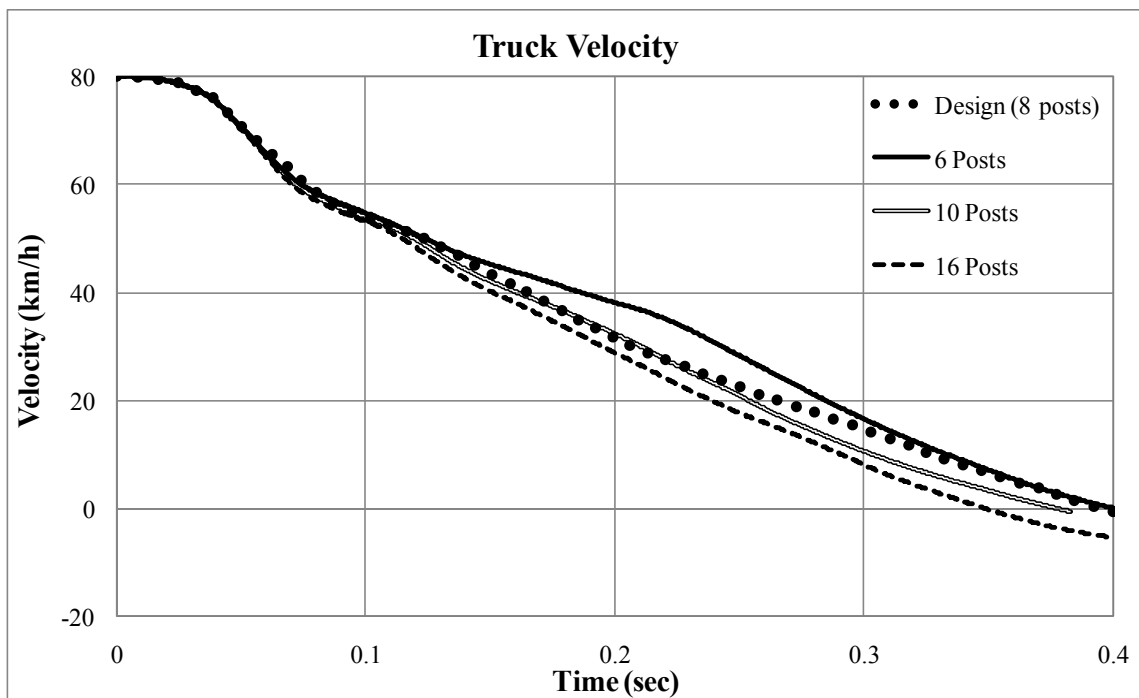
Figure 4.22. Vehicle velocity of group of posts system with 6, 10 and 16 posts
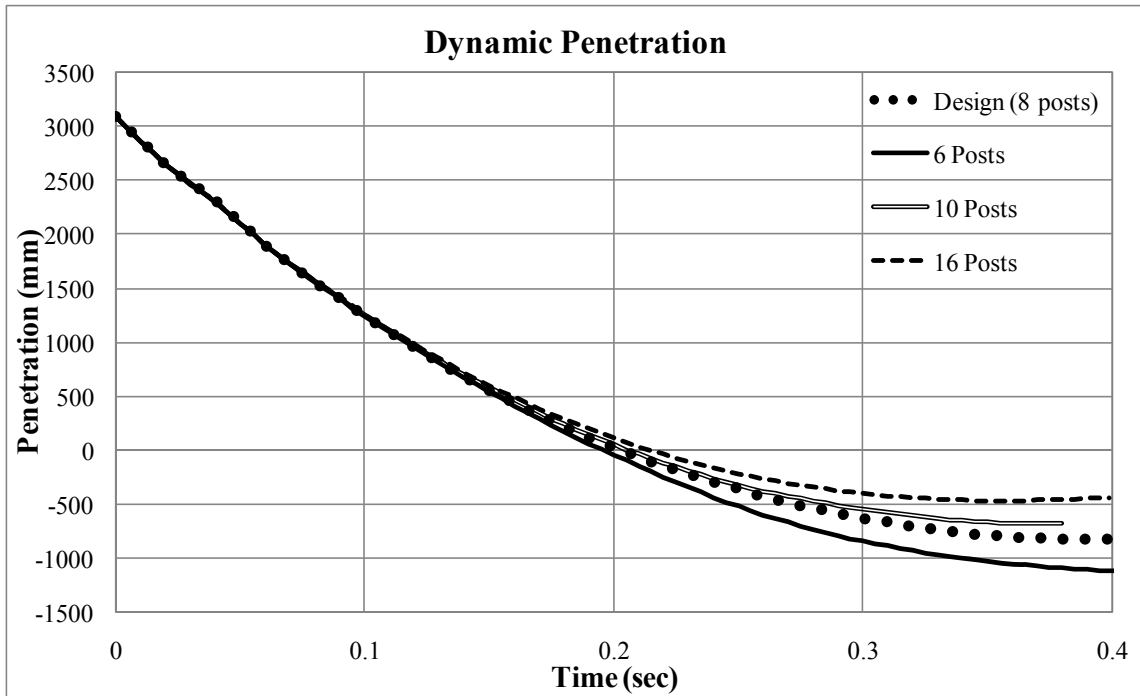
Figure 4.23. Dynamic penetration of group of posts system with 6, 10 and 16 posts
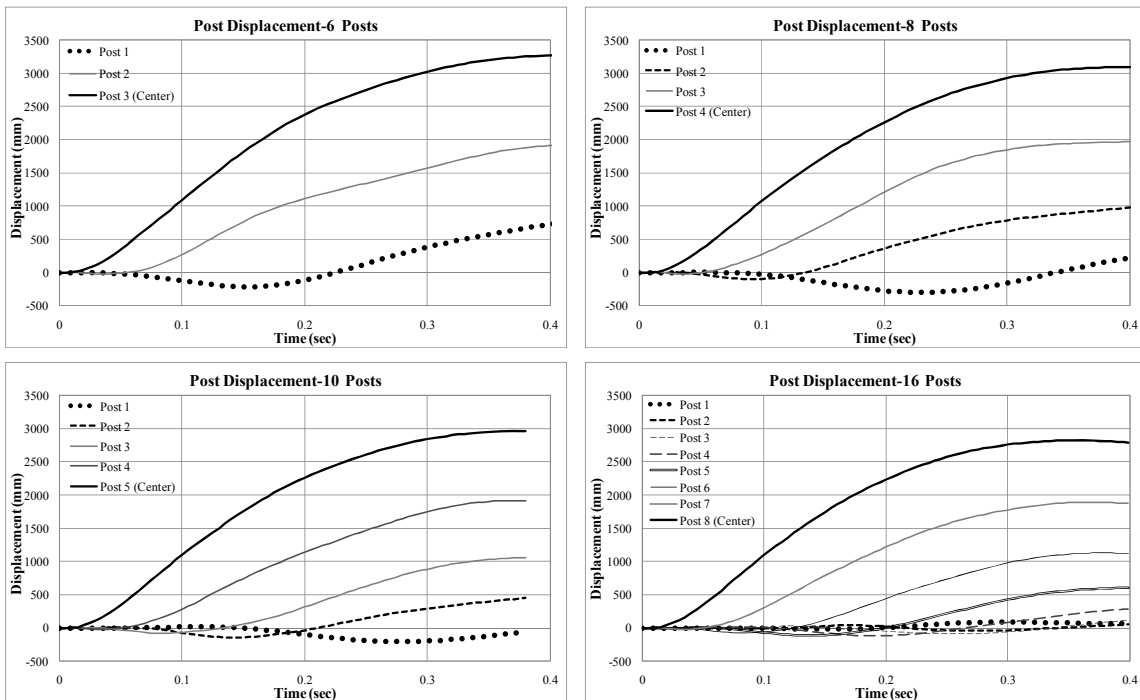
Figure 4.24. Post displacement of group of posts system with 6, 10 and 16 posts

Impact location

A finite element analysis that vehicle impact at one of center posts not in between the two posts was simulated to double check the minimum required number of posts as shown in Figure 4.25.
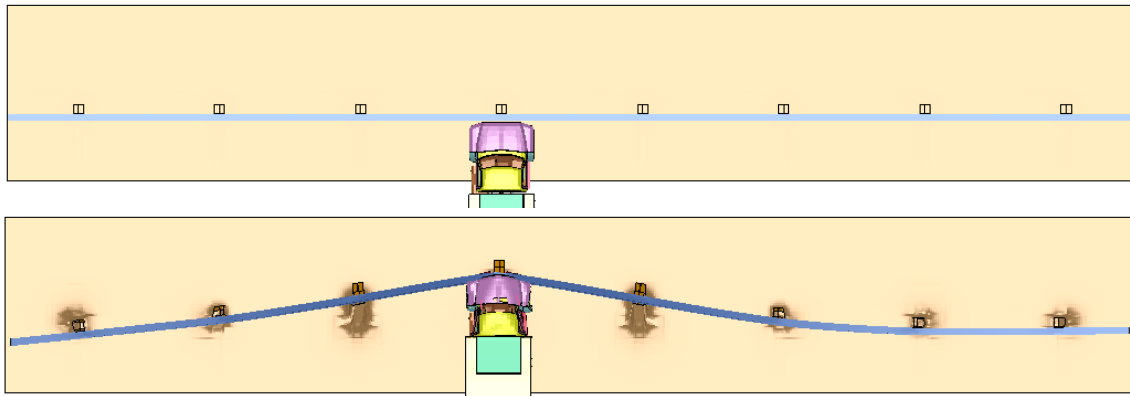
Figure 4.25. Simulation of vehicle impact against a center posts

According to this result and group of six posts simulation, at least four or more posts on each side of impact are required to meet the requirements of ASTM. As shown in Figure 4.26 and Figure 4.27, the behaviors of post system are almost same. Hence group of posts system of the proposed design chart was developed under the assumption that number of posts is more than eight and vehicle impact within two of center posts.
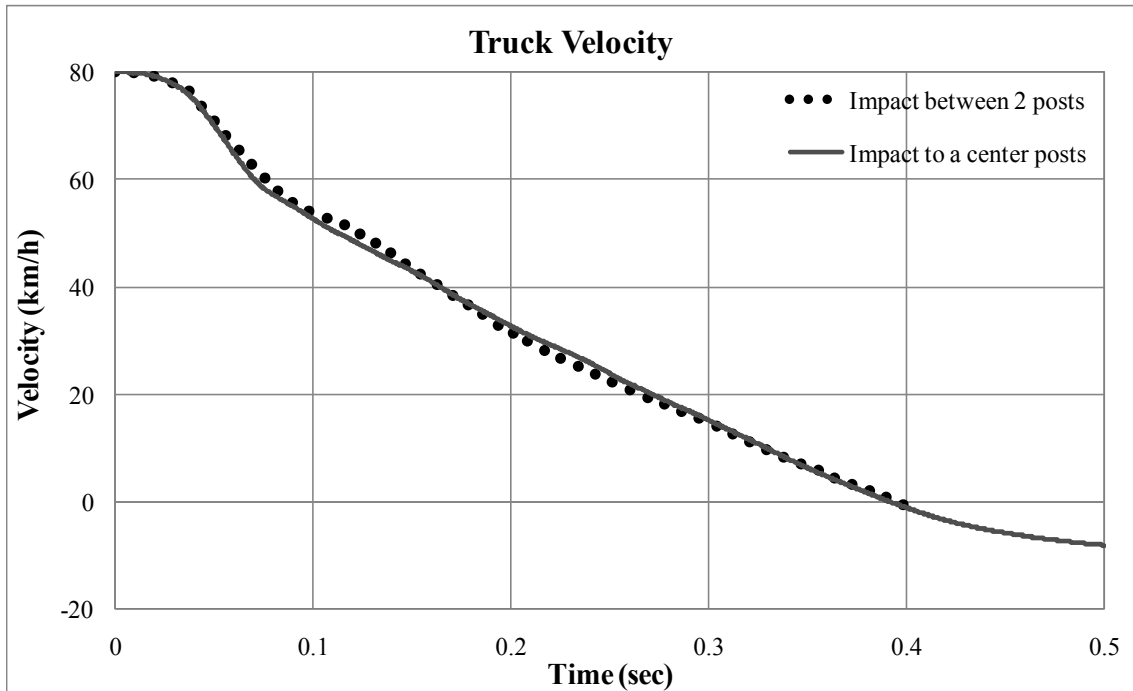
Figure 4.26. Vehicle velocity for impact locations
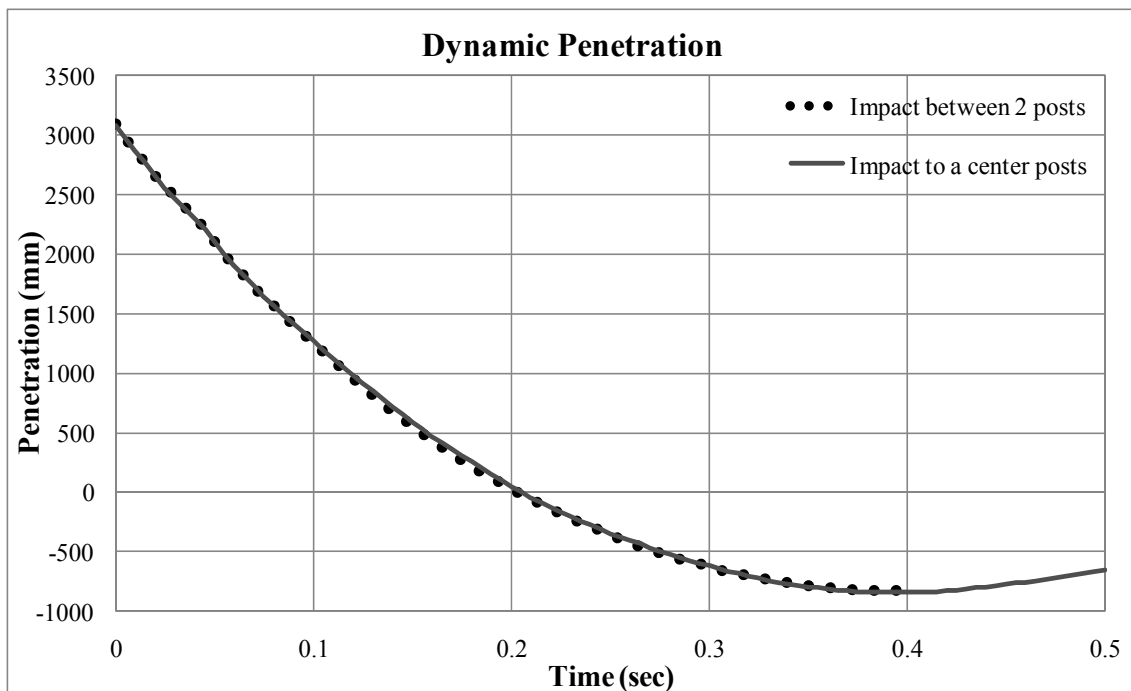
Figure 4.27. Dynamic penetration for impact locations

Number of beams

The design chart for group of posts system was developed for a system consisting of eight posts connected using a beam. As stated in the previous section, the section of post and beam are W14-90 beam and HSS 10X10X1/2 tube, respectively. Beam and posts can be substituted using post and beam having equivalent or bigger bending stiffness and width. Since the posts of the full-scale experiment were connected using two HSS 8X8X1/2 beams instead of a HSS 10X10X1/2 beam. Two posts system with one beam and two beams shown in Figure 4.28 and Figure 4.29 were simulated and compared.
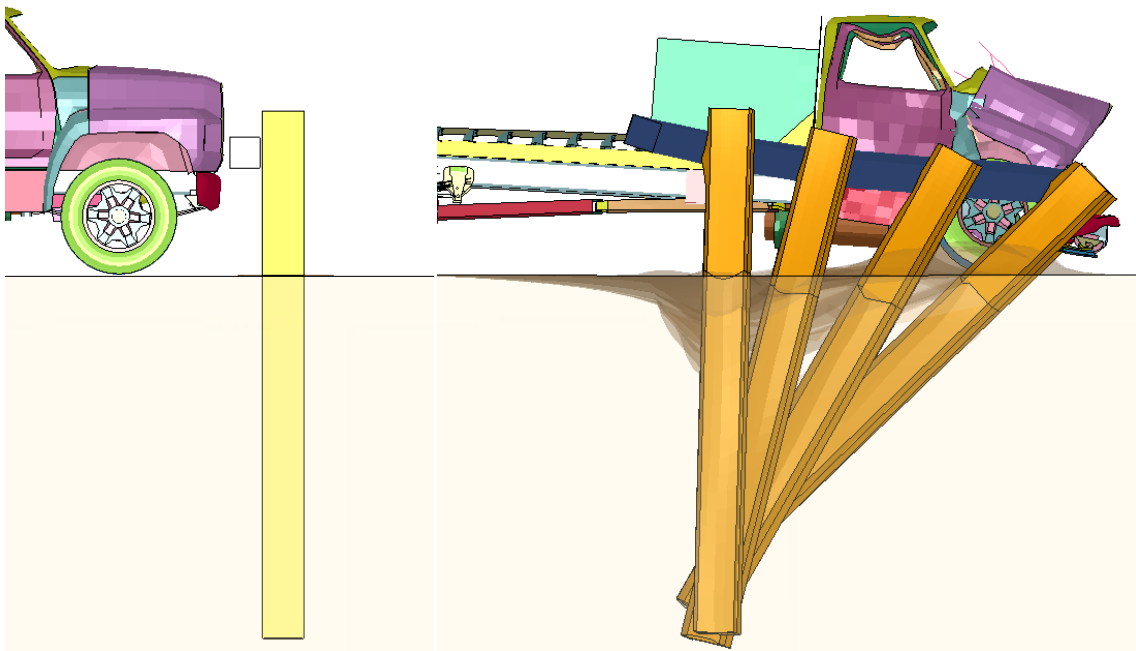
Figure 4.28. Simulation of group of posts system with a beam
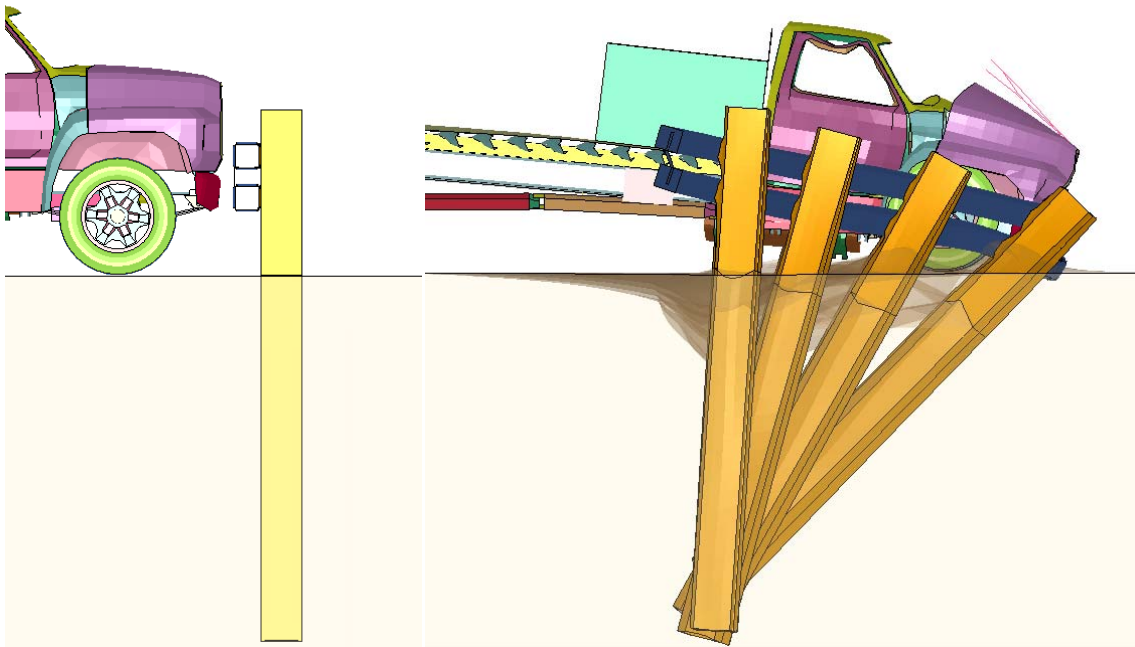
Figure 4.29. Simulation of group of posts system with two beams

The simulated results of these cases are compared in Figure 4.30 and Figure 4.31. The system with a single horizontal beam brought the stop of vehicle a bit faster than the system with two beams. The system with two horizontal beams seems more flexible than the single beam system, since impact load transferred more slowly than the other. Performance of two systems can be considered same in terms of dynamic penetration of vehicle, 0.8 m.
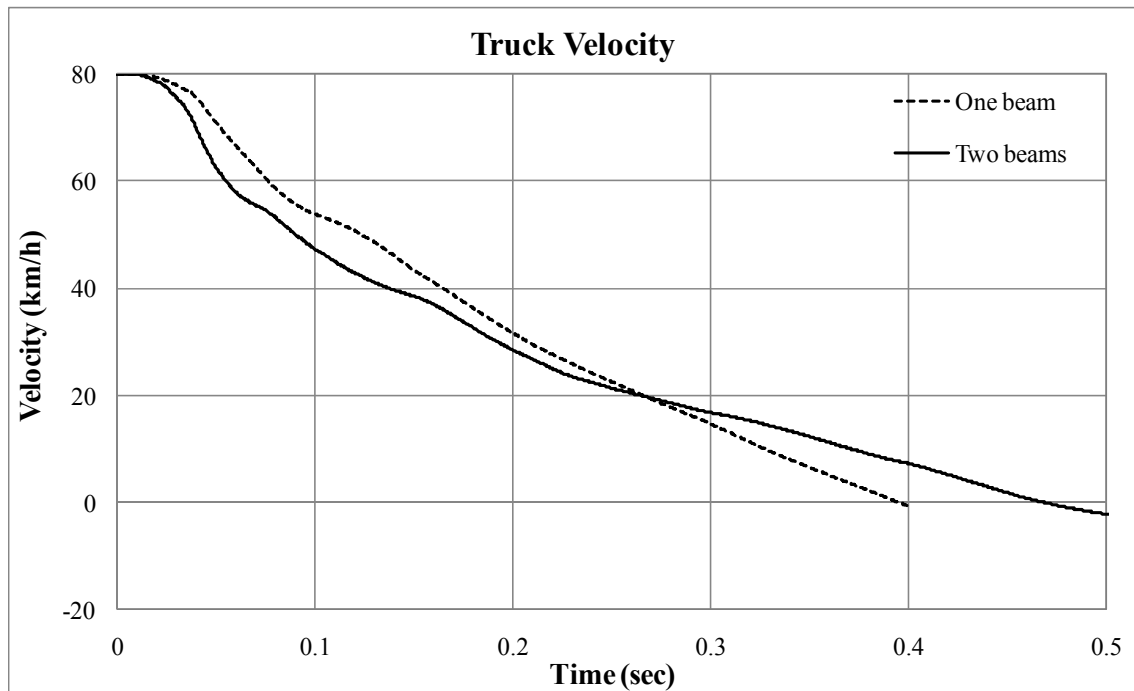
Figure 4.30. Vehicle velocity of posts system with a beam and two beams
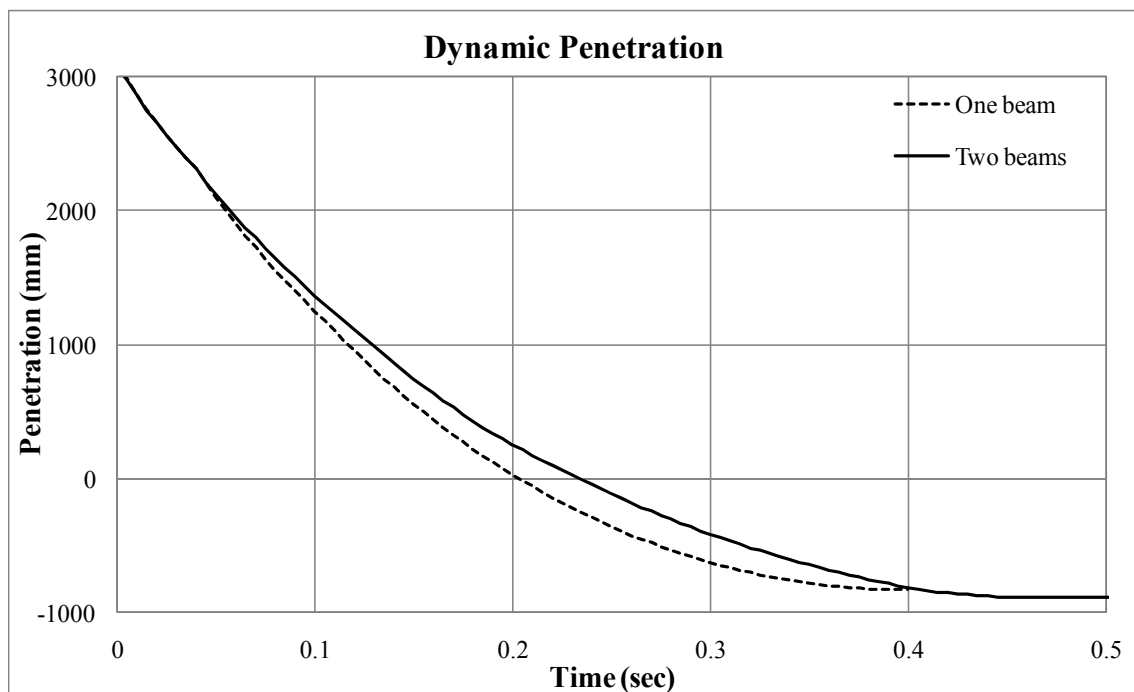
Figure 4.31. Dynamic penetration of posts system with a beam and two beams

Design of group of posts system for full-scale M50 impact test in loose sand

The design charts for group of posts system with a beam are shown in Section 5. According to the chart, 2.5 m embedded eight of W14-90 posts connected using a HSS 10X10X1/2 horizontal beam to contain truck impact of M50 designation with P1 penetrating rate in loose sand. However, the minimum required embedment of post was 3 m when the full-scale impact test on group of posts system in loose sand was designing. The horizontal beam can be not only a HSS 10X10X1/2 steel tube but also steel beam or beams having equal or stiffer section properties. Also W14-90 posts can be substituted to posts with equivalent or bigger post width (D) and bending stiffness (EI).For instance, two of HSS 8X8X1/2 steel tubes was used instead of one HSS 10X10X1/2 steel tube.

4.3 Calibrations against experiment results

In order to calibrate the finite element model and input parameters such as soil properties, a series of numerical simulations was performed for the full-scale test on the single post and the pendulum and bogie tests against single post using LS-DYNA. The initial input parameters including soil properties, material properties and impact velocity were from the measured values from those tests. The measured and simulated deformations of post and vehicle and the accelerations of vehicle were compared to validate the result of finite element analysis. The calibration of the soil models consisted of comparing the predicted response with the measured response in the pendulum tests, the bogie tests, the full scale test on the single post in the very dense crushed rock, and the full scale test on the group of posts in the loose sand. These comparisons included

deceleration of the truck, acceleration of the barrier, impact force history, velocity history, and displacement history.

4.3.1 Full-scale M50 single post test

The full-scale impact test on single post embedded in very dense crushed limestone in 2007 was modeled and numerically simulated using finite element analysis technique. A series of numerical simulations using LS-DYNA was performed in order to validate the soil and post model. The validated soil and post model was used to complete the proposed post system design chart under impact.

Finite element model of the full-scale impact test is shown in Figure 4.32. Crushed limestone was modeled using Jointed Rock material that is identical to Drucker-Prager model in this model.
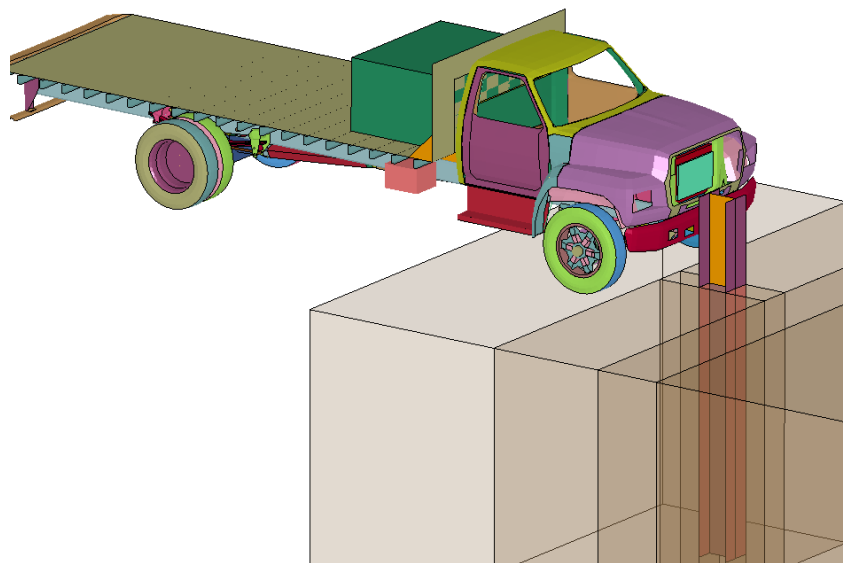

Figure 4.32 Test model for M50 test for single post in very dense crushed limestone

Prior to detail soil tests, the prototype finite element model consisting of vehicle, post and soil was modeled by Akram Abu-Odeh, a Research scientist of Roadside Safety program, Texas Transportation Institute. Numerical simulation matrix for the full-scale impact test on single post is shown in Table 4.8. In the matrix, simulation 1 is the input soil properties of the prototype simulation before the soil tests except TEXAM pressuremeter test.

Though the overall result of simulation was well matched to the measured test result, there were some problems including elements tangling. Element tangling means that numerically two or more elements are tangled each other and consequently tangled elements stick together. In this simulation, elements of vehicle bumper tangled with elements of post. As the result, vehicle pulled post vertically instead of sliding. Also soil properties were not measured value except the elastic modulus.

Table 4.8. Numerical simulation matrix for the full-scale impact test on single post

Number	Unit weight, γ (kN/m^3)	Elastic modulus, E (MPa)	Shear modulus, G (MPa)	Cohesion, c (kPa)	Friction angle, φ (degrees)	Dilation angle, Ψ (degrees)
1	21	50	18.5	20	40	15
2	23	47	17.4	80	45	10
3	23	47	17.4	20	45	10
4	23	45	16.7	15	45	10
5	23	45	16.7	15	45	5
6	23	45	16.7	10	45	5
7	23	45	16.7	5	45	10

The initial model was modified on several features including size of meshes, extended boundary and contact properties to obtain better result. In order to remove the element tangling, the mesh size of post was reduced and virtual thickness of contact was increased. Also size of mesh near the post was decreased to get precise result. The size of soil boundary was extended to minimize the effect of boundary.

After each simulation, the results including acceleration of vehicle and velocity were compared with the measurement of the experiment until obtaining result with reasonable accuracy. The result of simulation 7 (Figure 4.33) is the best estimation among those tests in the matrix. The behavior of vehicle from the numerical simulation and the experiment are compared in Figure 4.34, Figure 4.35 and Figure 4.36.

The simulated vehicle acceleration could not catch the trend that the deceleration stayed constant from time 0.025 sec to 0.08 sec. The inflection point of simulated deceleration curve at 0.04 sec might have the same physical meaning that the post began contact with the engine and main frame of vehicle.

Peak decelerations and trend of acceleration curves were similar as shown in Figure 4.34. The velocity and displacement histories of vehicle were even similar as shown in Figure 4.35 and Figure 4.36.
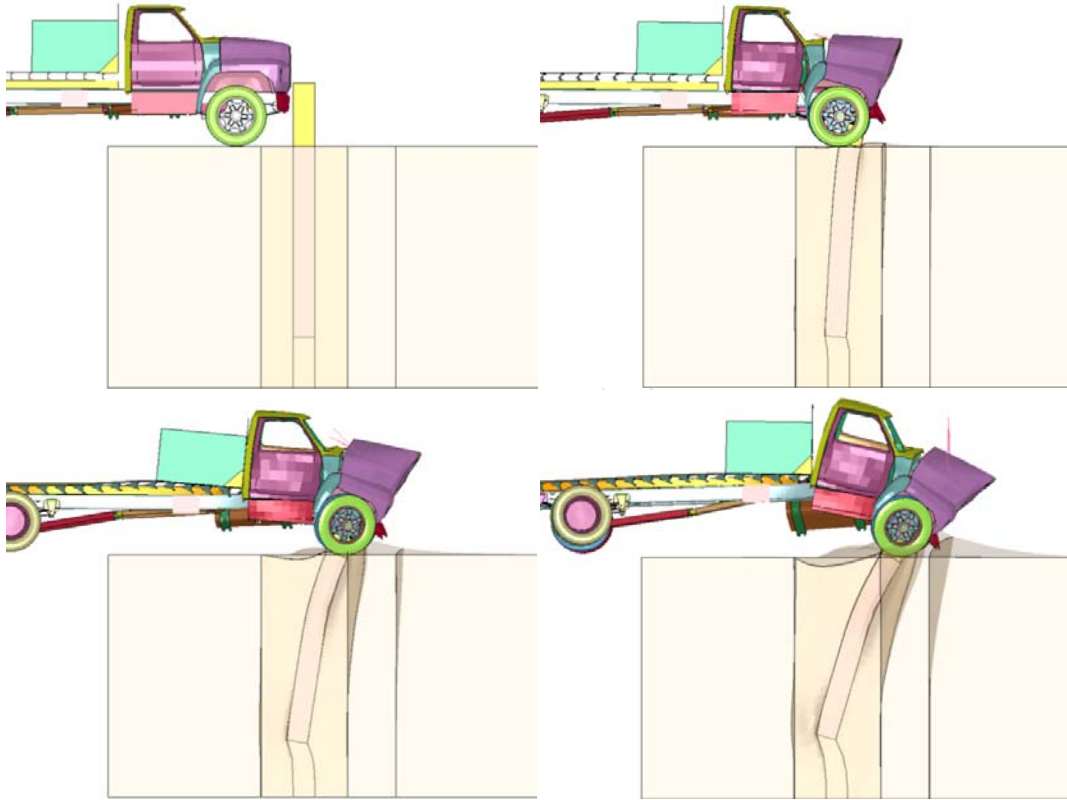
Figure 4.33. Simulated sequential figures of the full-scale impact test on single post
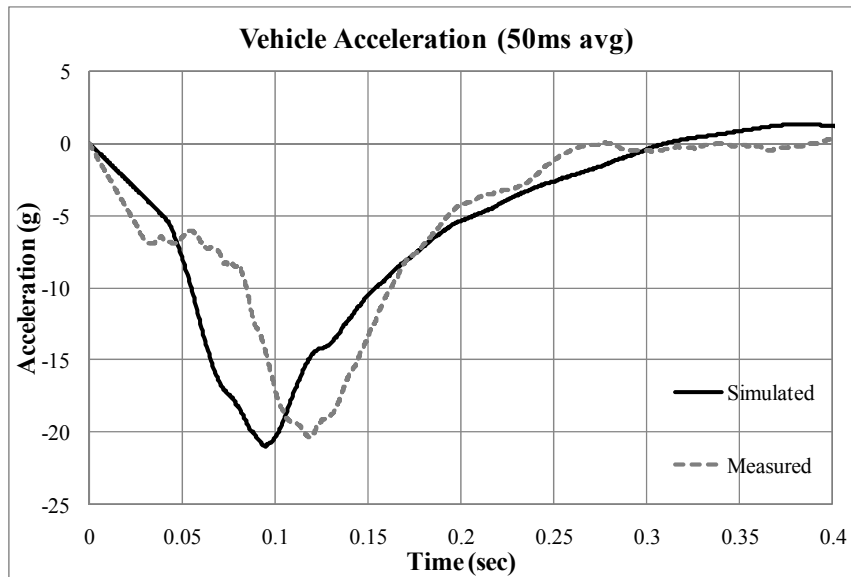

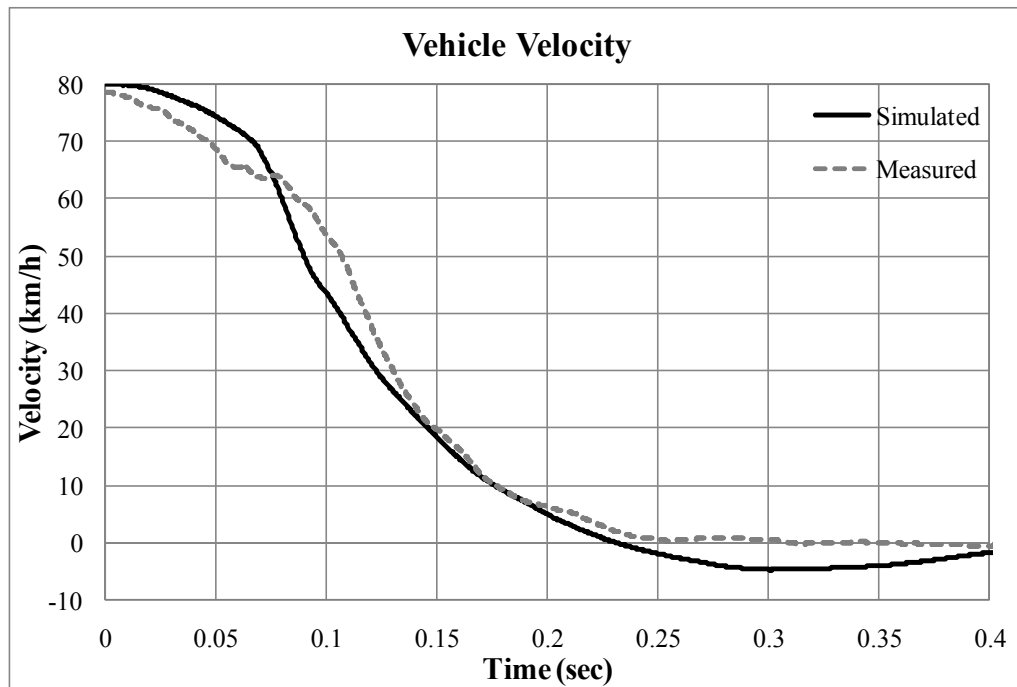**Figure 4.34. Comparison of vehicle acceleration (M50 single post)**

Figure 4.35. Comparison of vehicle velocity (M50 single post)
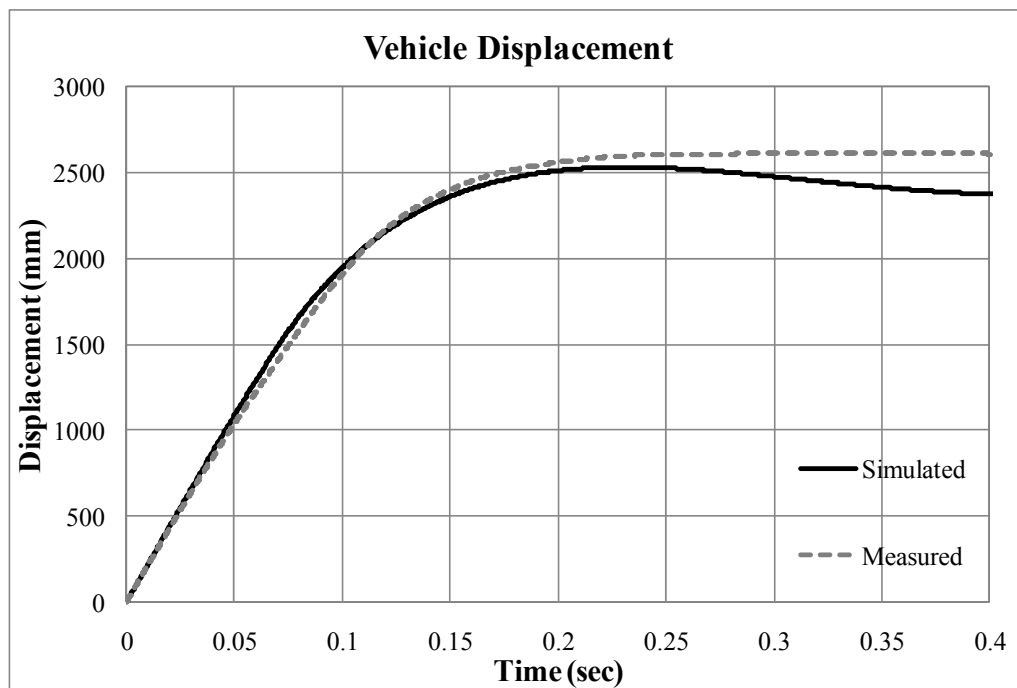

Figure 4.36. Comparison of vehicle displacement (M50 single post)

Impact forces were compared as well in Figure 4.37. As shown the figure, measured impact force is around 30% higher than the simulated impact force. The reasons are that the test vehicle was not rigid and acceleration at the C.G of vehicle was not always same with accelerations of other point of the vehicle. The simulated impact force was calculated using the forces acting on the contact between vehicle and post whereas the measure impact force was calculated using Newton's second law, mass times acceleration.

Due to crushing of vehicle, the front part of the vehicle was decelerated faster than the C.G of vehicle. In other words, the measured acceleration at the C.G was lower than the average acceleration of the vehicle. The deceleration of a rigid body is higher than the deceleration of a flexible body. However the measured deceleration may be the values between the deceleration of a rigid body and a flexible body, since the front part of vehicle was only crushed. This can be one reason that the measured impact force was smaller than the simulated contact force though both have similar acceleration histories.

The accelerometer at the C.G. of the vehicle was installed on the flat bed of the truck. The front part of vehicle was crushed and moved upward along with the deflection of the post whereas the flat bed mainly moved in the longitudinal direction (Figure 4.38). The calculated impact force form the measured acceleration of the vehicle was transferred in the front part of vehicle and separated in longitudinal and vertical forces.

Due to these two reasons, the measured impact force was higher by 30 % than the simulated impact force. The analysis using linear momentum and conservation of energy are shown in Appendix E.
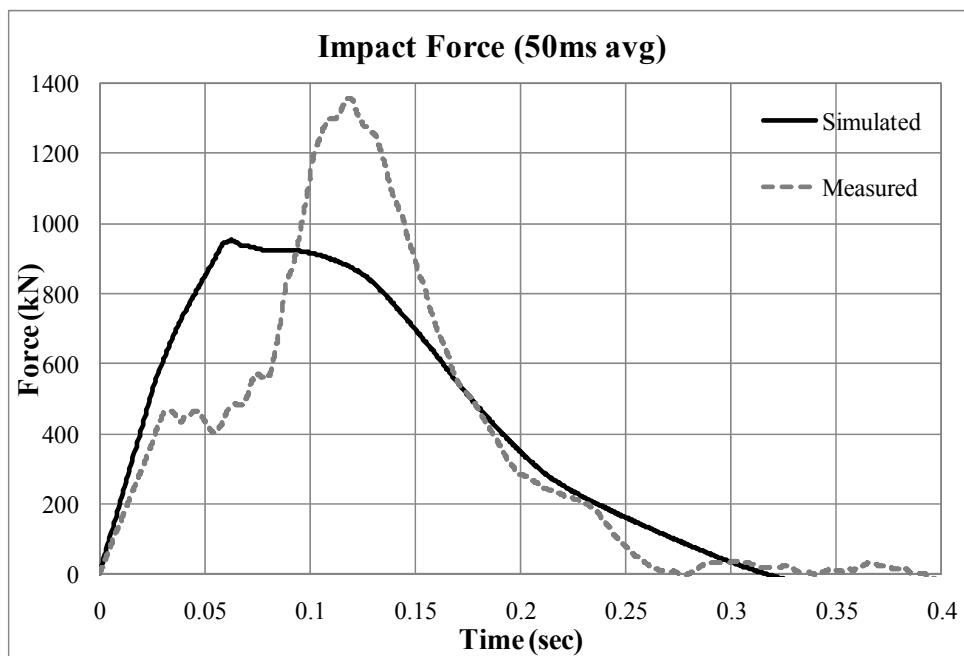
Figure 4.37. Comparison of impact force (M50 single post)
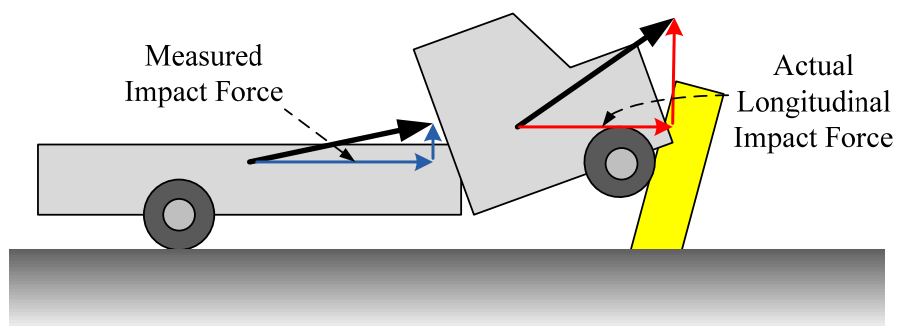
Figure 4.38. Comparison of the actual and the measured longitudinal impact forces

The dynamic penetration is defined as the distance between the initial position of the post and the maximum penetration of the leading edge of the flat bed of the truck. The measured and simulated dynamic penetrations are shown in Figure 4.39 along with the dynamic penetration rating, P1 from ASTM F2656-07.
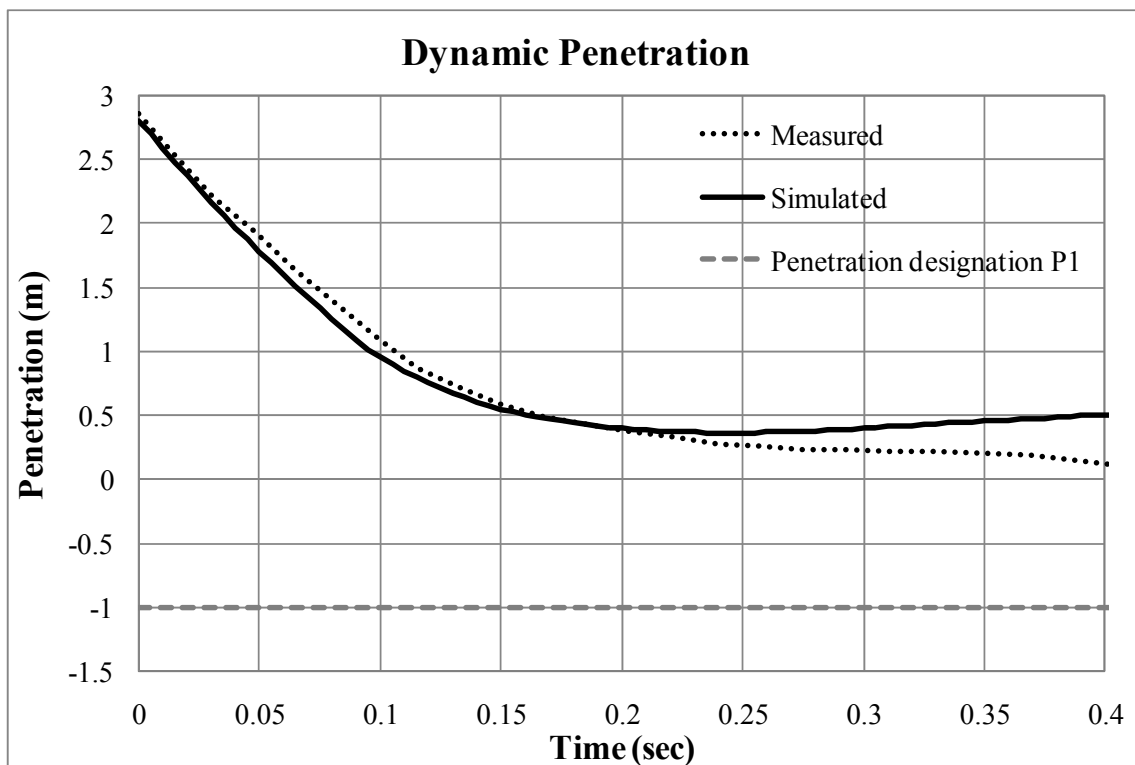
Figure 4.39. Simulated dynamic penetration (M50 single post)

4.3.2 Pendulum tests

The main purpose of numerical simulations of the pendulum tests were to calibrate the model for soil and post system under impact loading condition and to modify the proposed soil strength category. The pendulum impact tests on single post embedded in

the medium dense crushed limestone and the loose sand were modeled and simulated. The soil properties from the result of soil tests in the previous section were used for the initial trial. Then the input soil properties were modified and applied to soil model according to previous simulation results. Dilation angle of soils for the proposed soil strength category could not be determined from the literature review as described in Section 2.2. The initial dilation angle from direct shear test was selected for the first trial value.

Pendulum test on single post backfilled in crushed limestone (P1, P2 and P3)

The finite element model for the pendulum and the single post embedded in the medium dense crushed limestone is shown in Figure 4.40. The soil was modeled using Jointed Rock material with the measured soil properties. Mass of pendulum was 862 kg. The pendulum had initial velocity that was same with the impact velocity instead of dropping pendulum at certain height like the real test. Since the single posts were backfilled in the soil, soil plugging was not considered. In other words, Inside of the post below the ground level was empty though the post had an open end.

Matrix of finite element analysis is shown in Table 4.9. From the simulations 1 to 6, the input parameters were based on the actual soil tests. Each simulation case in the table consisted of three tests with different impact velocities, 16.7 km/h, 8.7 km/h and 35.9 km/h. The results from the numerical simulations with the measured soil properties overestimated displacement of post for all three cases (P1, P2 and P3). Addition to

displacement, the simulated impact force from the first numerical simulations was underestimated.

The post displacement is inversely proportional to the unit weight of soil, elastic modulus, cohesion, friction angle and dilation angle according. The impact force is proportional to the soil strength. For the followed numerical simulations, each input parameters for soil strength was increased until getting similar post displacement as shown in the numerical simulation matrix (simulation 6 to 15).

Table 4.9. Numerical simulation matrix for the pendulum test in crushed limestone

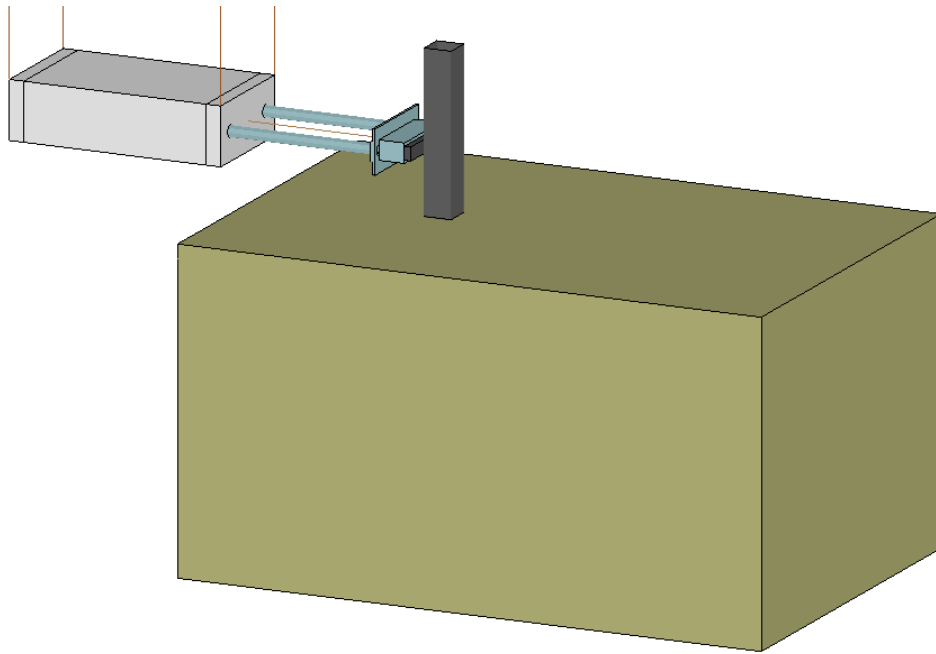| Number	Unit weight, γ (kN/m^3)	Elastic modulus, E (MPa)	Shear modulus, G (MPa)	Cohesion, c (kPa)	Friction angle, φ (degrees)	Dilation angle, Ψ (degrees)
1	18.0	6	2.2	2	33	-5
2	18.0	6	2.2	2	33	0
3	20.0	6	2.2	2	33	0
4	20.0	8	3.0	2	35	0
5	**20.0**	**8**	**3.0**	**2**	**35**	**1**
6	19.1	12	4.4	2	35	1
7	20.0	16	5.9	3	36	5
8	21.0	20	7.4	3	37	5
9	22.0	25	9.3	3	37	5
10	22.0	34	12.6	4	40	10
11	23.0	45	16.7	4	40	10
12	23.0	45	16.7	4	45	10
13	23.0	45	16.7	15	45	10
14	23.0	50	18.5	20	45	10
15	**23.0**	**60**	**22.2**	**20**	**45**	**10**

Figure 4.40. Finite element model of single post in medium dense crushed limestone

The post displacements and impact forces from numerical simulation 5, 15 and the measurement for the pendulum tests, P1, P2 and P3 are shown in from Figure 4.41 to Figure 4.46. As stated in the previous paragraph, the results from simulation 5 and actual measurement were not well matched. On the contrary, the input soil properties of simulation 15 are much higher than the results from the soil testing. The input soil properties of simulation 15 were stronger than the measured soil properties of the full-scale test, very dense crushed limestone in terms of soil strength. However, the displacement history and impact force history of simulation 15 is almost same with actual measurement. The force-time graph shows a loss of contact for the simulation which is not observed in the measurements; this may be due to the fact that the nose of the simulated pendulum was too rigid and created a bouncing effect at the contact.
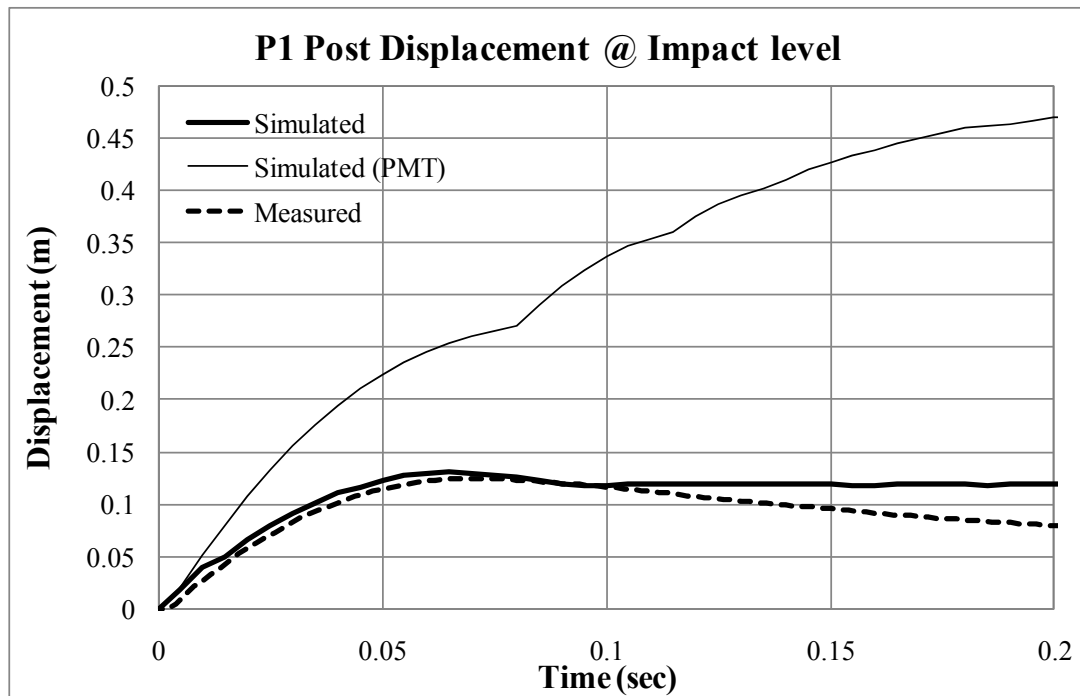
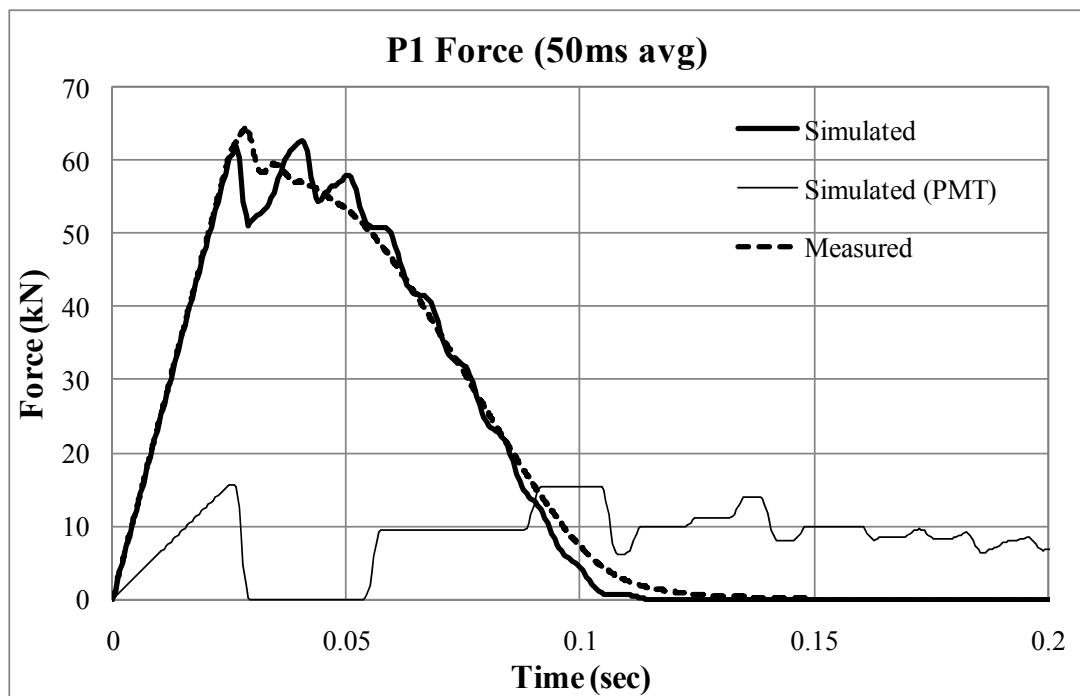**Figure 4.41. Comparison of post displacement (P1)**

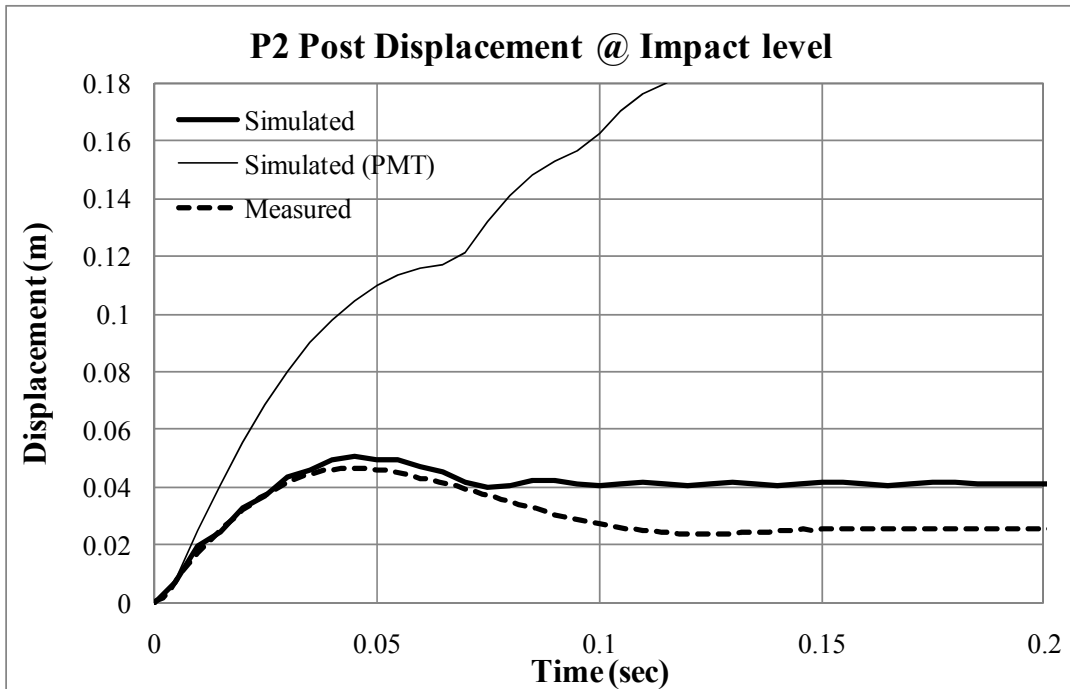**Figure 4.42. Comparison of impact force (P1)**
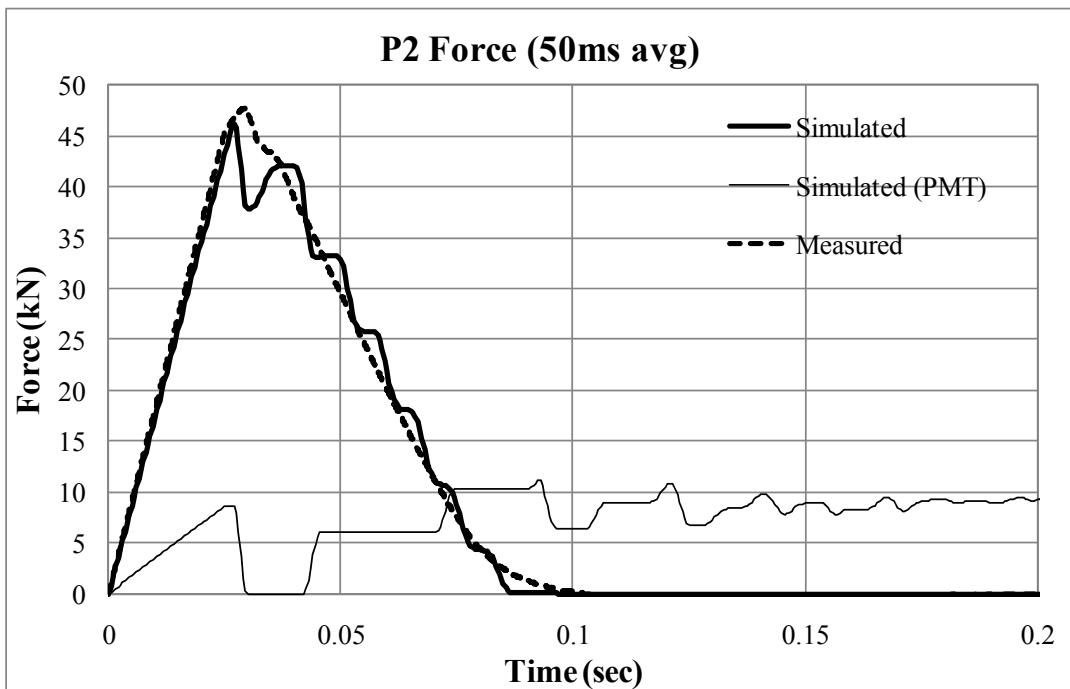
Figure 4.43. Comparison of post displacement (P2)

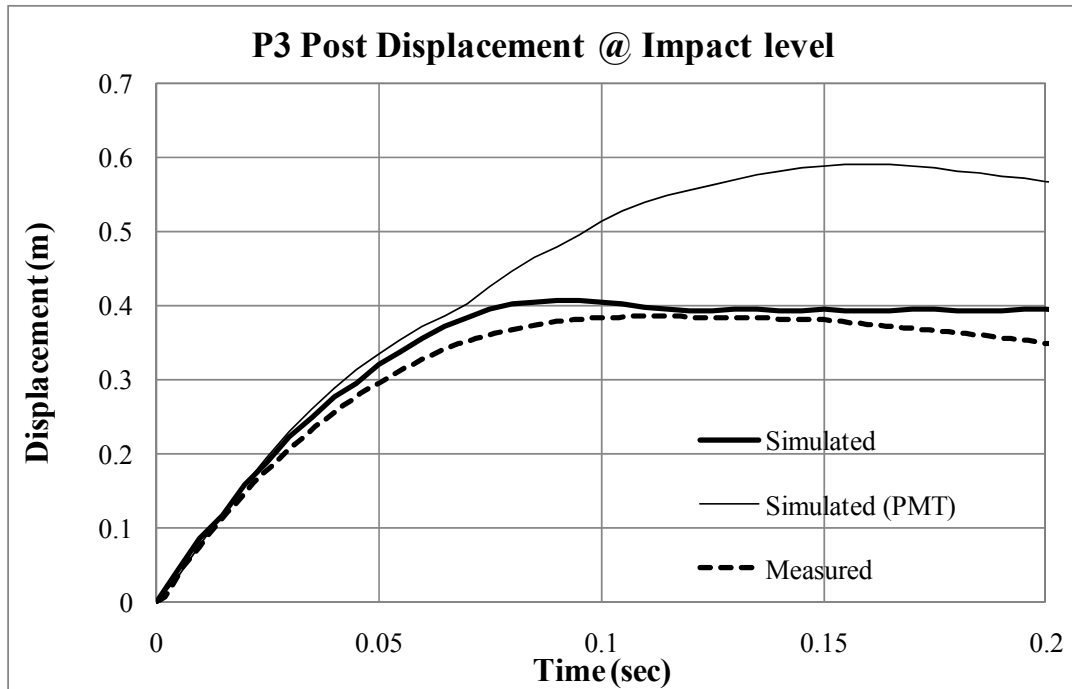

Figure 4.44. Comparison of impact force (P2)

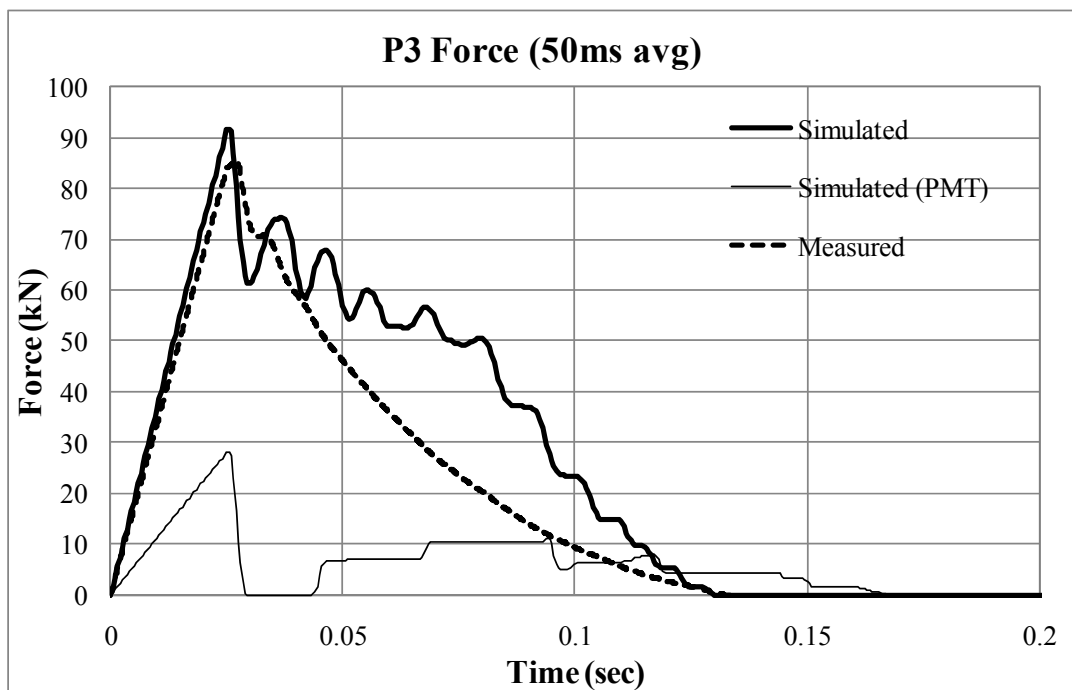**Figure 4.45. Comparison of post displacement (P3)**

Figure 4.46. Comparison of impact force (P3)

The soil condition of the pendulum pit was medium dense crushed limestone. Since the soil was not well compacted, there might have some distance between the large particles. According to the previous sieve analysis, soil particles of 33 % by weight has diameter of 10 mm to 30 mm. These large particles might not be well contacted and engaged with each other during the small displacement soil tests such as Standard penetration test and Pressuremeter test. For instance, the maximum radial displacement of soil during PENCEL pressuremeter test is 3.84 mm. However, the displacement at the ground level was approximately 30 to 400 mm during the pendulum tests. During the impact test, due to the large deformation, the large particles were contacted with each other and can behave like rock. Therefore, the post embedded in medium dense crushed limestone behaved as if it was embedded in rock in terms of soil strength under impact load.

Though the full-scale M50 test on single post in very dense crushed limestone had similar particle size distribution with the pendulum test, the very dense crushed limestone ditch was not only cemented due to aging effect but also the ratio of largest particle size and post size was smaller than the pendulum tests. The behavior cemented crushed limestone is similar with continuum model rather than discrete model. The post size of the pendulum tests was scaled down to one third whereas the particle size of soil was same with the full-scale test.

In this particular test condition, size of soil particle has to be considered in dimensional analysis and similitude analysis when planning model test. Also discrete soil model has to be used instead of continuum model in finite element analysis.

Pendulum test on single post driven in loose sand (P4, P5 and P6)

Model of pendulum and single post embedded in loose sand is shown in Figure 4.47. The soil was modeled using Jointed Rock material with the measured soil properties. Mass of pendulum was 250 kg. The pendulum had initial velocity that was same with the impact velocity instead of dropping pendulum at certain height like the real test.

The single posts of the pendulum test P4 through P6 were driven into loose sand. Driving pile into loose sand allows densifying the soil around the driven pile. Densifying sand generally causes the increase of unit weight of soil, elastic modulus, friction angle and dilation angle. Thus the soil properties for the tests P4 to P6 were somewhat higher than the measurement.
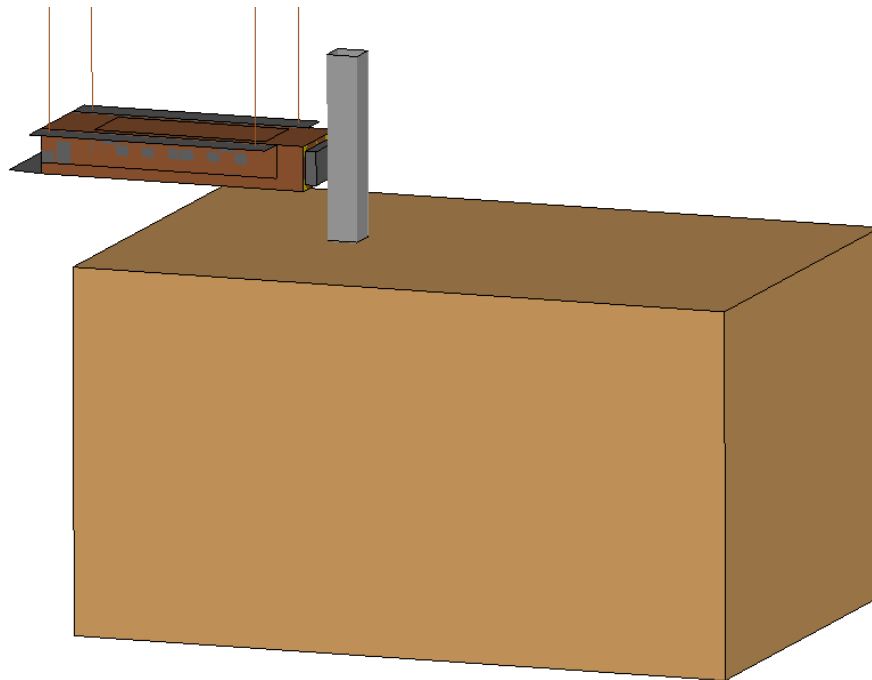

Figure 4.47. Finite element model of pendulum test for single post in loose sand

Since the single posts of P4, P5 and P6 were driven into the soil, soil plugging was considered. Plugged soil inside the post was modeled with the same material card and merged mesh to the other soil mesh.

Matrix of finite element analysis is shown in Table 4.10. Each simulation case in the table consisted of three tests with different impact velocities, 17.8 km/h, 9.0 km/h and 36.4 km/h. In the table, soil plugging is the plugged soil height from the bottom of the post.

Table 4.10. Numerical simulation matrix for the pendulum test in loose sand (P4-P6)

Number	Unit weight, γ (kN/m^3)	Elastic modulus, E (MPa)	Shear modulus, G (MPa)	Cohesion, c (kPa)	Friction angle, φ (degrees)	Dilation angle, Ψ (degrees)	Soil plugging (mm)
1	17.0	2.5	0.9	1.0	30	0	600
2	17.0	3.0	1.1	1.0	30	0	600
3	17.0	2.5	0.9	1.0	33	0	600
4	17.5	2.5	0.9	1.0	30	0	600
5	17.5	3.0	1.1	1.0	30	0	600
6	17.5	3.0	1.1	1.0	30	0	860
7	18.0	3.0	1.1	1.0	30	0	860
8	18.0	3.0	1.1	1.0	33	0	860
9	18.0	3.0	1.1	1.0	35	1	860
10	18.0	3.0	1.1	1.0	35	5	860
11	**18.5**	**3.5**	**1.3**	**1.5**	**36**	**5**	**860**

The post displacements and impact forces from numerical simulation 11 and the measurement for the pendulum tests, P4, P5 and P6 are shown in from Figure 4.48 to Figure 4.53. The simulated result was similar to the measurement from the real test except the displacement history of P4.
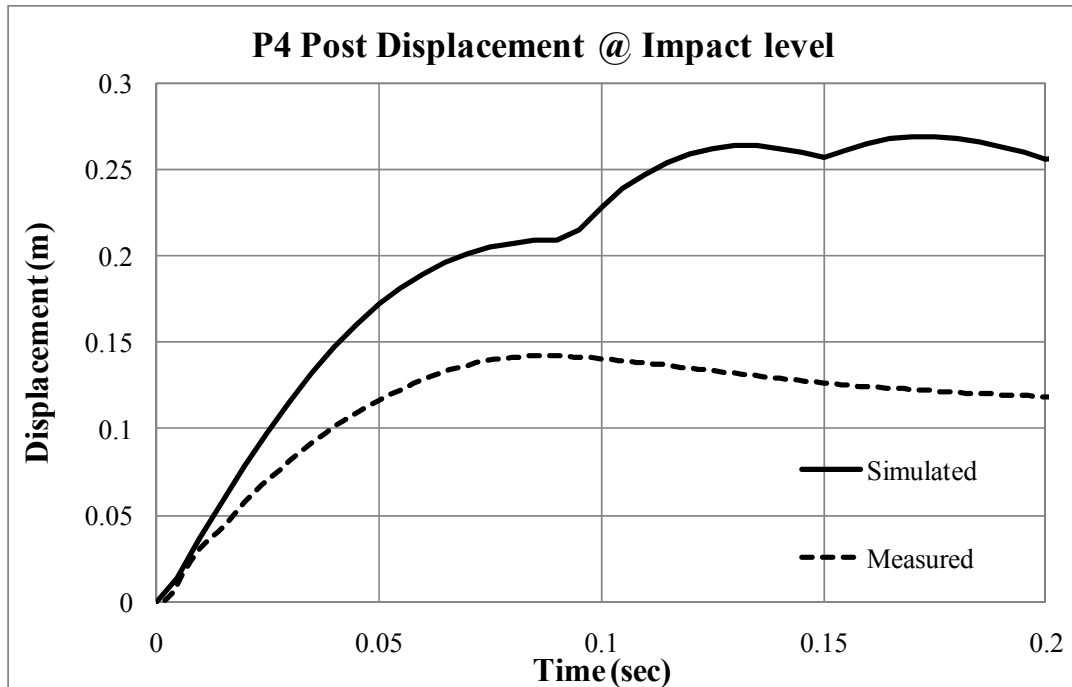
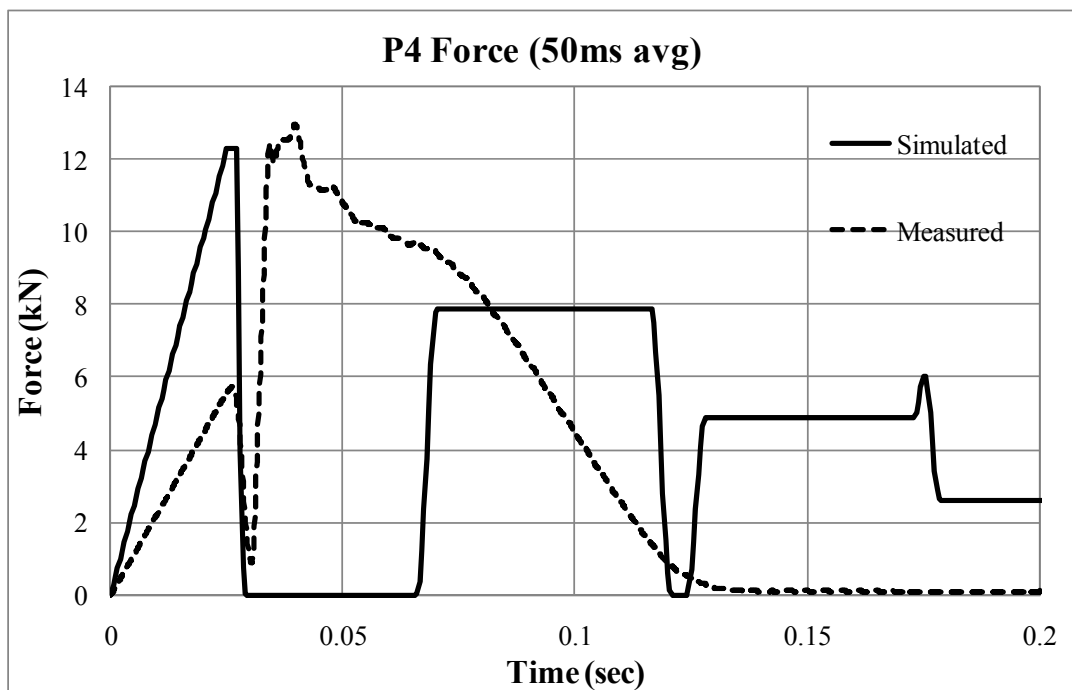**Figure 4.48. Comparison of post displacement (P4)**

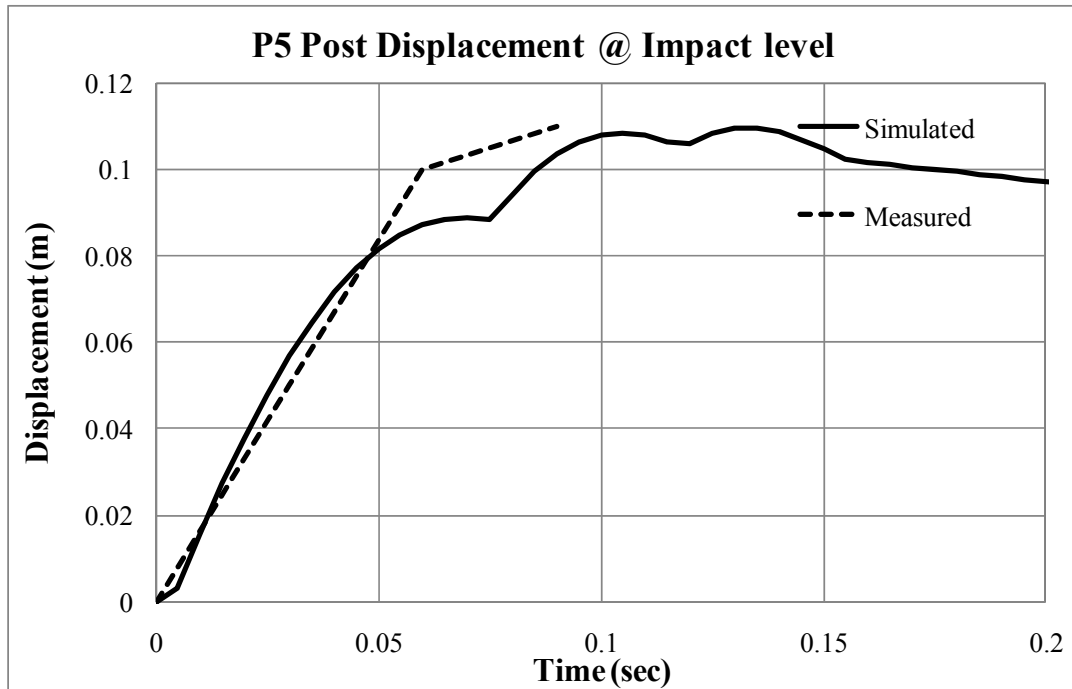**Figure 4.49. Comparison of impact force (P4)**
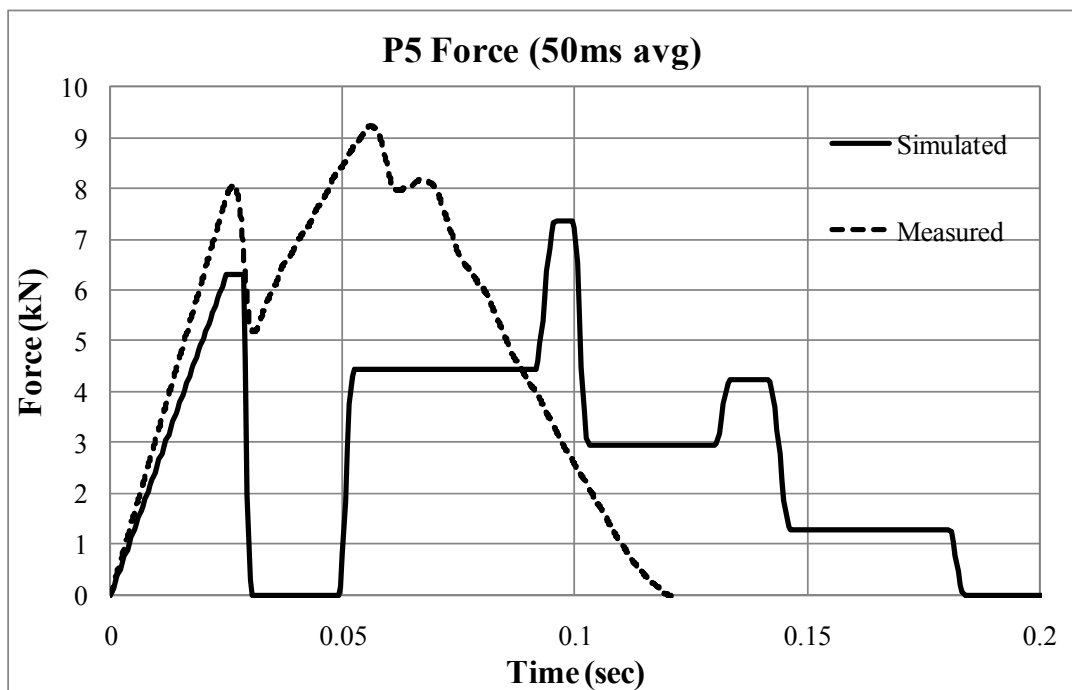
Figure 4.50. Comparison of post displacement (P5)

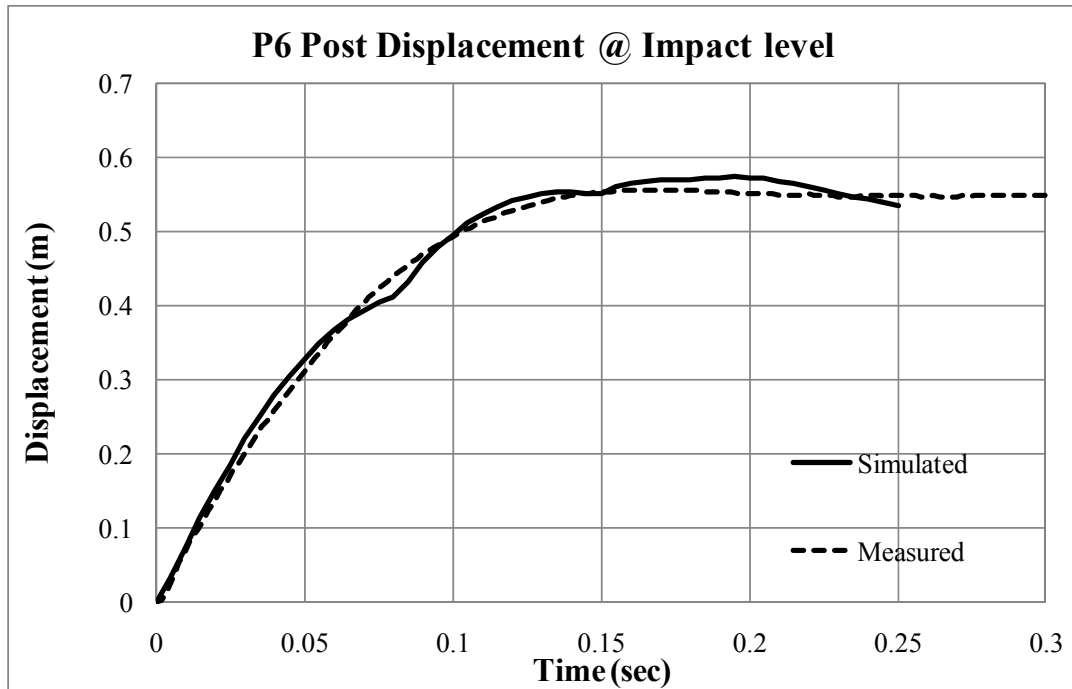

Figure 4.51. Comparison of impact force (P5)

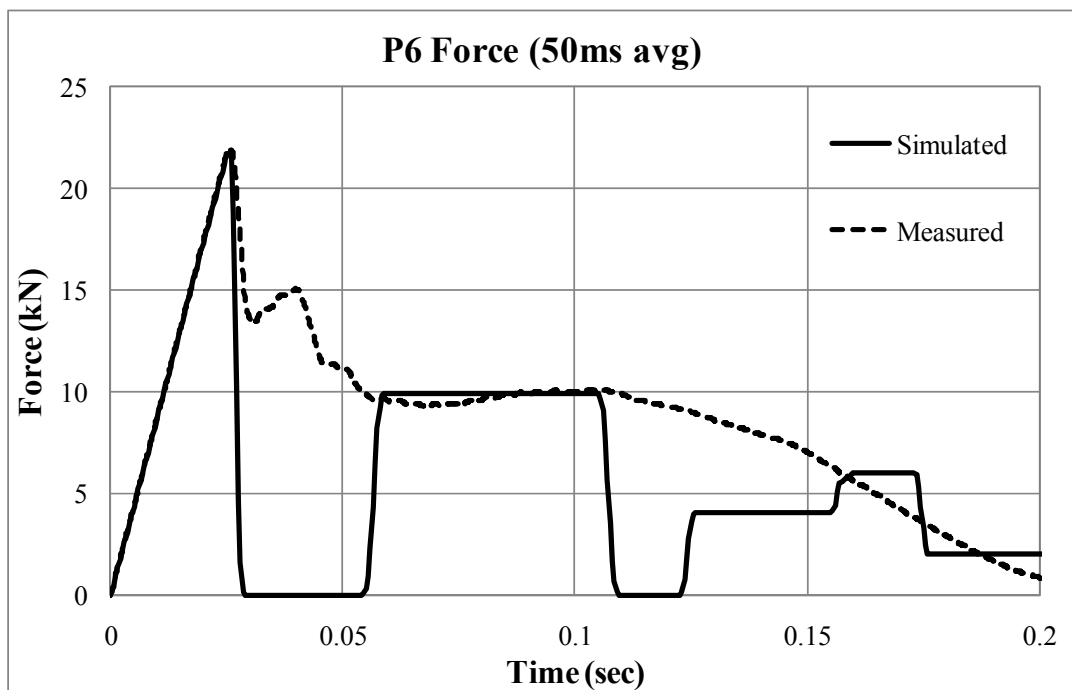**Figure 4.52. Comparison of post displacement (P6)**

Figure 4.53. Comparison of impact force (P6)

The Displacement history of simulation 11 and actual measurement were not well matched. The reason can be that the soil condition for the single post, P4 might be different from other tests. The pendulum test was performed after static load test. After the static load test, the position of the post was rearranged to its original position and compacted. It can be compacted more than other cases since the compaction process was manually performed, tamping with a rake or stepping by foot.

Pendulum test on single post backfilled in loose sand (P10)

Model of pendulum and single post embedded in loose sand is same with the previous simulation for P4 to P6, except the soil plugging. Since the single posts were backfilled in the soil, soil plugging was not considered. The soil was modeled using Jointed Rock material with the measured soil properties. Mass of pendulum was 250 kg. The pendulum had initial velocity that was same with the impact velocity instead of dropping pendulum at certain height like the real test. Matrix of finite element analysis is shown in Table 4.11. The impact velocity of the simulations was 35.4 km/h.

Table 4.11. Numerical simulation matrix for the pendulum test in loose sand (P10)

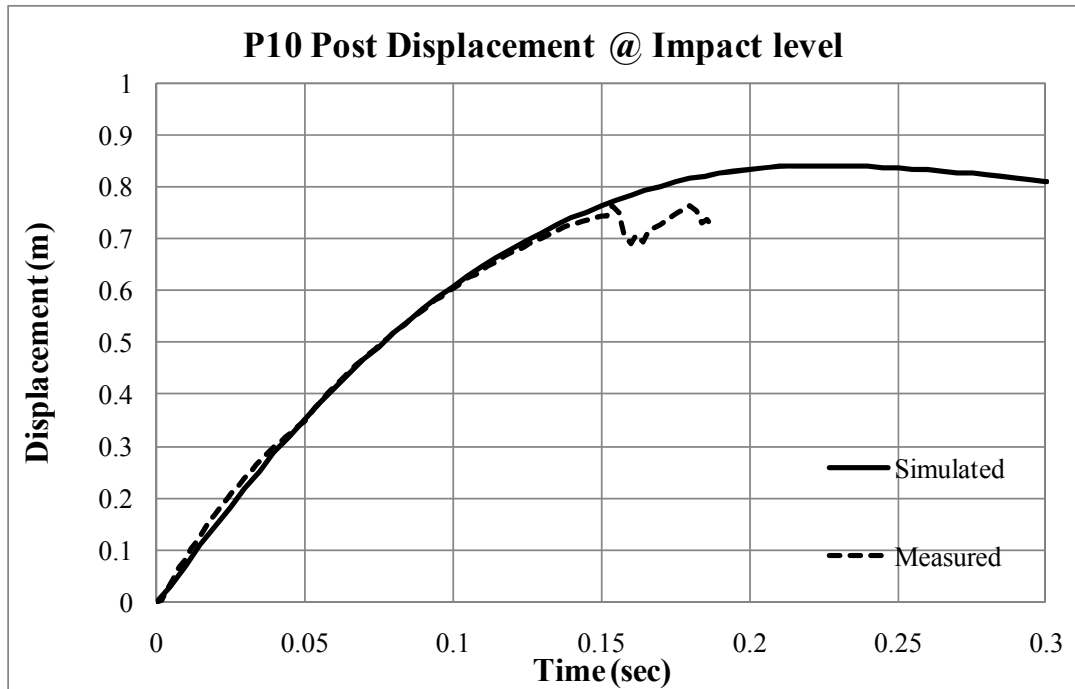| Number	Unit weight, γ (kN/m^3)	Elastic modulus, E (MPa)	Shear modulus, G (MPa)	Cohesion, c (kPa)	Friction angle, φ (degrees)	Dilation angle, Ψ (degrees)
1	17	1.8	0.67	0	27	-10
2	17	2.0	0.74	1	27	-10
3	17	2.0	0.74	1	27	-5
4	17	2.5	0.93	1	27	-5
5	17	2.0	0.74	1	30	-10
6	**17**	**2.5**	**0.93**	**1**	**27**	**-10**

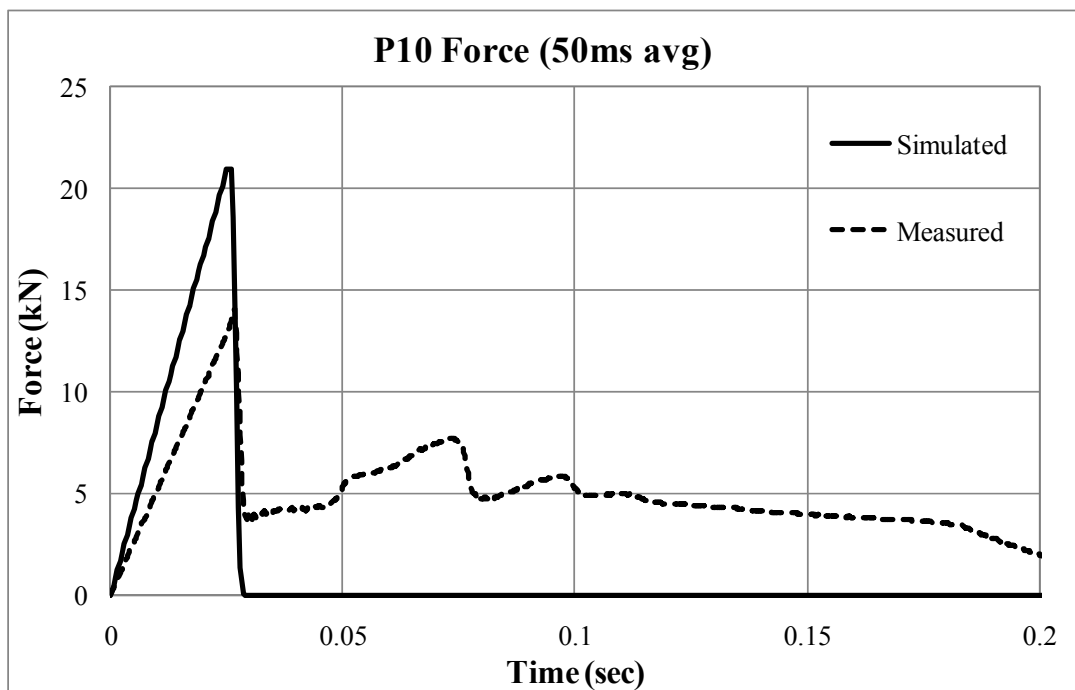**Figure 4.54. Comparison of post displacement (P10)**

Figure 4.55. Comparison of impact force (P10)

The post displacements and impact forces from numerical simulation 6 and the measurement for the pendulum tests, P10 are shown in Figure 4.54 and Figure 4.55. The simulated result was similar to the measurement from the real test.

Dilation angle of loose sand under the impact loading was assumed as the same with the initial dilation angle called small strain dilation angle. According to the validated simulation result, the assumption can be reasonable in the impact condition.

4.3.3 Bogie tests

Bogie and single post embedded in hard clay is shown in Figure 4.56. The soil was modeled using Isotropic Elastic-Plastic with Failure material with the measured soil properties. Mass of bogie was 900 kg. The bogie had initial velocity that was same with the impact velocity, 16.4 km/h.
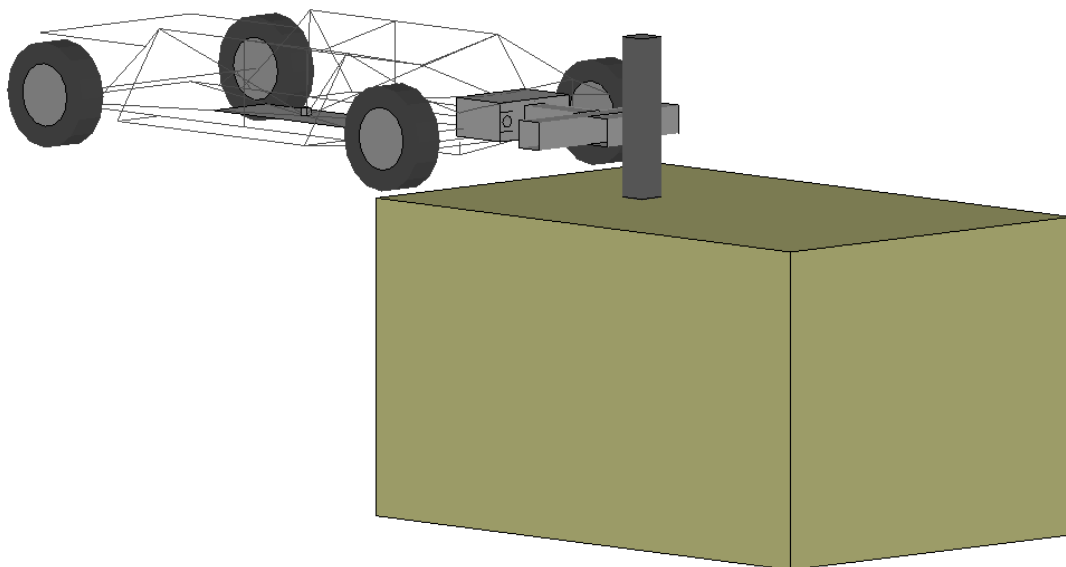

Figure 4.56. Finite element model of bogie test for single post in hard clay

Since the single post of the bogie test, B1 was driven into hard clay, soil plugging was considered. Plugged soil inside the post was modeled with the same material card and merged mesh to the other soil mesh. Matrix of finite element analysis is shown in Table 4.12. In the table, soil plugging is the plugged soil height from the bottom of the post.

According to the proposed soil strength category, the soil can be classified as medium clay and hard-medium clay using the result of PENCEL pressuremeter test and standard penetration test, respectively. Thus the input soil properties were selected from medium clay to hard-medium clay in the soil strength category. The displacement and impact force histories of simulation 2 and 9 were shown in Figure 4.57 and Figure 4.58.

Table 4.12. Numerical simulation matrix for the bogie test in hard clay

| Number	Unit weight, γ (kN/m^3)	Elastic modulus, E (MPa)	Shear modulus, G (MPa)	Bulk modulus, K (MPa)	Cohesion , c (kPa)	Yield stress, σ_y (degrees)	Soil plugging (mm)
1	19.0	11.5	4.3	12.8	0.095	0.190	600
2	**19.5**	**6.5**	**2.4**	**7.2**	**0.150**	**0.300**	**600**
3	19.5	11.5	4.3	12.8	0.150	0.300	600
4	19.5	12.0	4.4	13.3	0.175	0.350	760
5	20.0	12.0	4.4	13.3	0.175	0.350	760
6	20.0	12.0	4.4	13.3	0.200	0.400	760
7	20.0	17.0	6.3	18.9	0.138	0.275	760
8	19.5	12.0	4.4	13.3	0.190	0.380	760
9	**20.0**	**12.0**	**4.4**	**13.3**	**0.190**	**0.380**	**760**
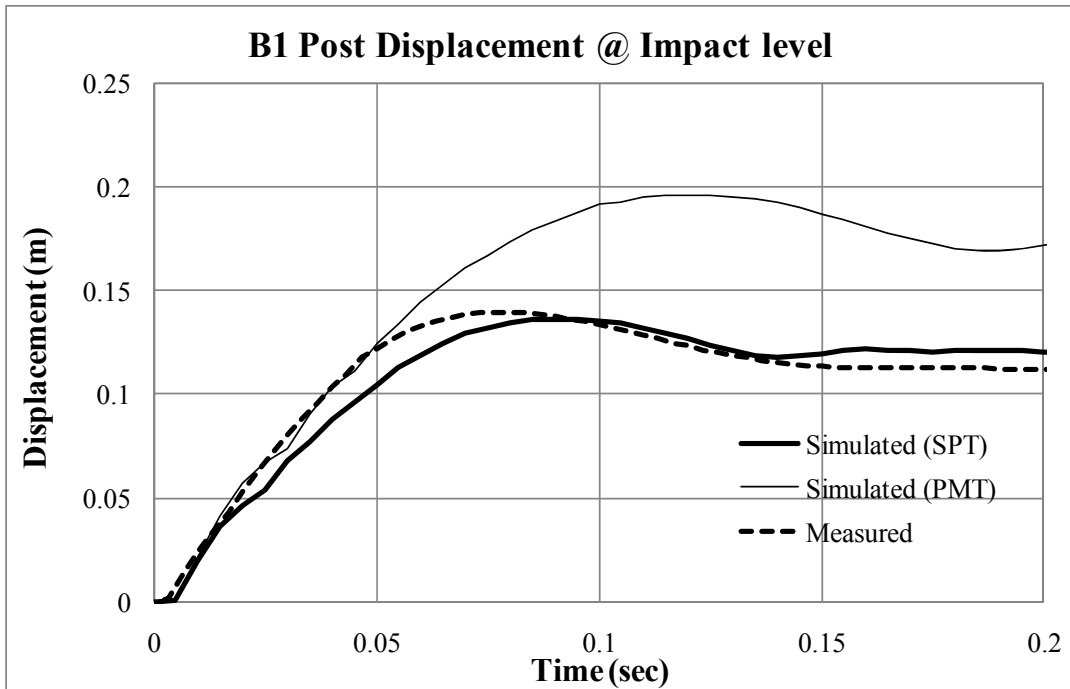
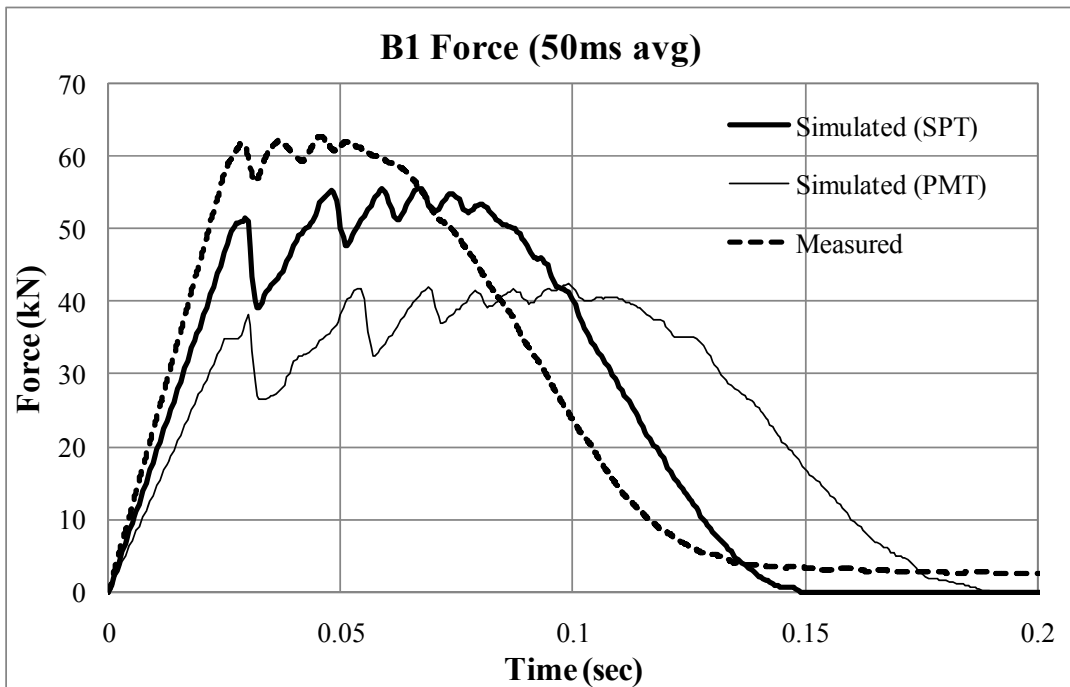**Figure 4.57. Comparison of post displacement (B1)**

Figure 4.58. Comparison of impact force (B1)

The soil properties of simulation 2 and simulation 9 were selected based on the soil tests, pressuremeter test and standard penetration test, respectively. As shown in Figure 4.57 and Figure 4.58, the soil strength of simulation 2 was underestimated, whereas that of simulation 9 was similar with the actual soil strength. The difference of the two simulations was the sources of the soil properties: standard penetration test and pressuremeter test.

The measured soil properties using PENCEL pressuremeter can be underestimated. During the pressuremeter test, it was challenging to advance the pre-bored hole to insert the pressuremeter probe due to the cohesion of clay. Hence, the pre-bored hole was a bit larger than the diameter of the hand auger and the clay around the pre-borehole was disturbed. As stated in section 4.3.2, the displacement range of PENCEL pressuremeter is within 3.84 mm. If the pre-bored hole and pressuremeter probe were not well contacted each other, measured strength of soil can be underestimated. Also disturbance of clay around the hole can be the reason of underestimation. In addition, the numerical simulations did not include the damping effect of soil. Thus the soil properties from SPT are more suitable in this case.

4.3.4 Full-scale M50 group of posts test

The full-scale impact test on group of posts system embedded in loose sand in 2010 was modeled and numerically simulated. A series of finite element analysis with measured soil properties was simulated in order to validate the results from the numerical simulations including the proposed design method. Though the full-scale test was

designed based on numerical simulations, input soil properties were not same with the measured soil properties.

To validate the results of numerical simulations, the effect of soil boundary size and ditch was checked using a series simulation shown in Table 4.13. Model of original soil boundary, extended soil boundary and extended soil boundary with sand ditch are shown in Figure 4.59. Distance from post and the end of soil boundary was extended 3.7 m to 5.4 m. Sand ditch was modeled for both the original soil boundary and the extended soil boundary. Dimensions of modeled sand ditch were same with the full-scale experiment. Outside of the sand ditch was modeled very dense crushed limestone as shown in Figure 4.60. Though the existing hard clay was weaker than the very dense crushed limestone, the outer soil was modeled with stronger soil model to check the size of sand ditch.

Table 4.13. Numerical simulation matrix for the full-scale impact test on group of posts

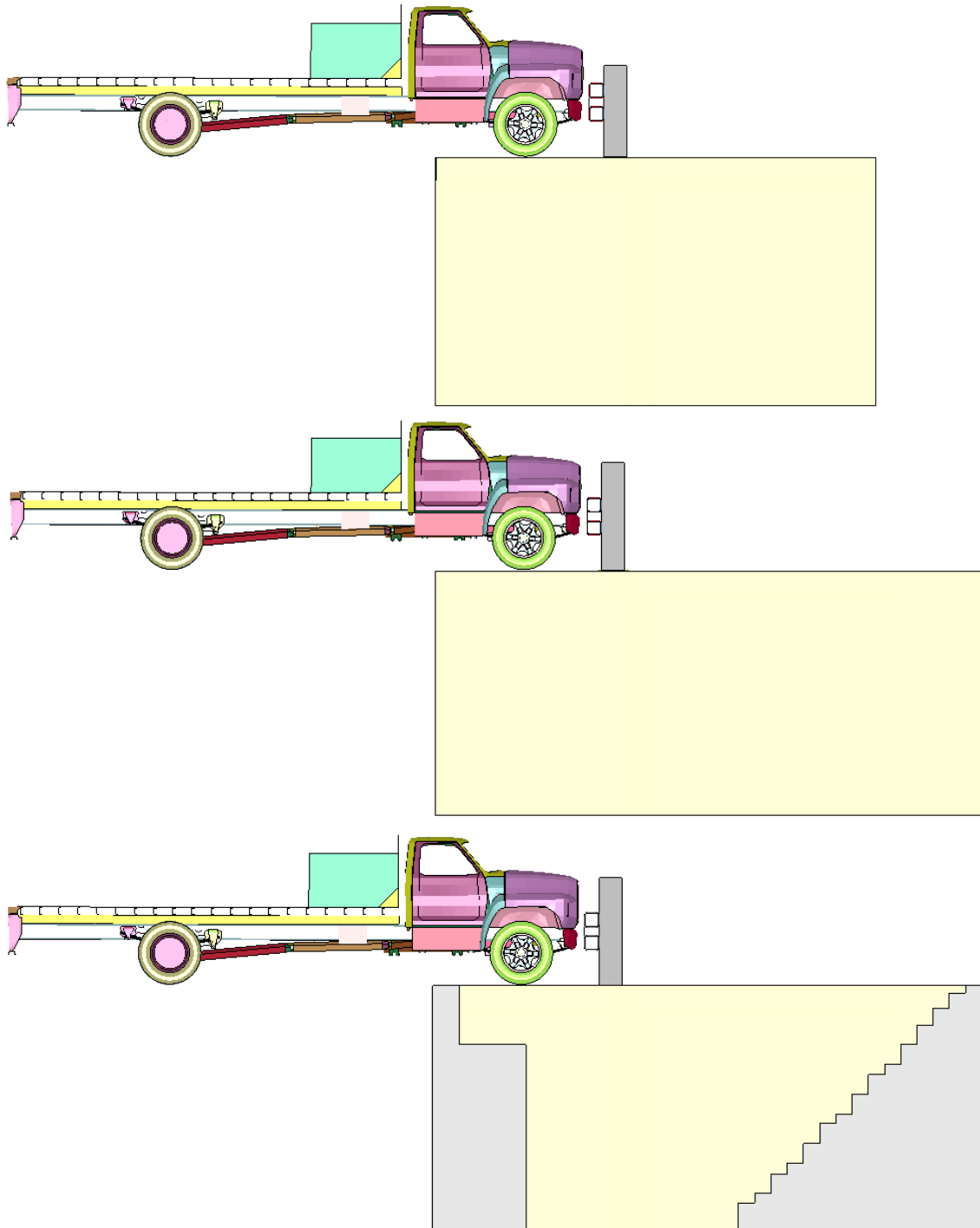| Number	Unit weight (kN/m^3)	Elastic modulus (MPa)	Shear modulus (MPa)	Cohesion (kPa)	Friction angle (degrees)	Dilation angle (degrees)	Extended soil boundary	Sand ditch model
1	17	2	0.74	1	27	-10	X	X
2	17	2	0.74	1	27	-10	X	O
3	17	2	0.74	1	27	-10	O	O
4	17	2	0.74	1	27	-10	O	X
5	17	3	1.11	1	30	0	O	X
6	**17.5**	**2.5**	**0.93**	**1**	**27**	**-5**	**O**	**X**
7	17.5	2.5	0.93	1	27	-10	O	X

Figure 4.59. Boundaries for design chart, extended soil and extended soil with ditch
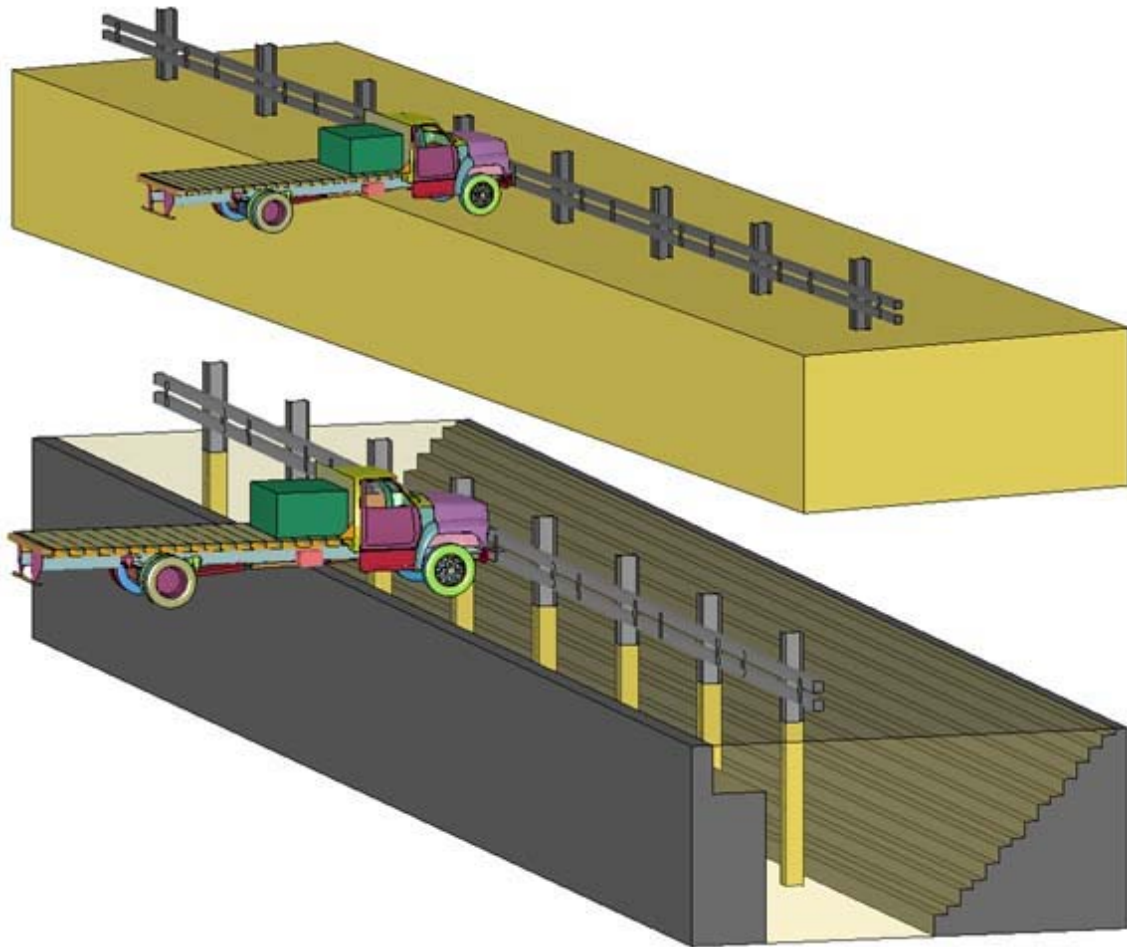
Figure 4.60. Homogenous soil model and soil model with sand ditch

The size of designed sand ditch for full-scale experiment and the size of initial soil boundary for numerical simulations for design chart were large enough, since the behaviors of vehicle and the posts systems were same for all four cases. Comparison of simulated vehicle velocity and dynamic penetration histories of the simulations are shown in Figure 4.61 and Figure 4.62.
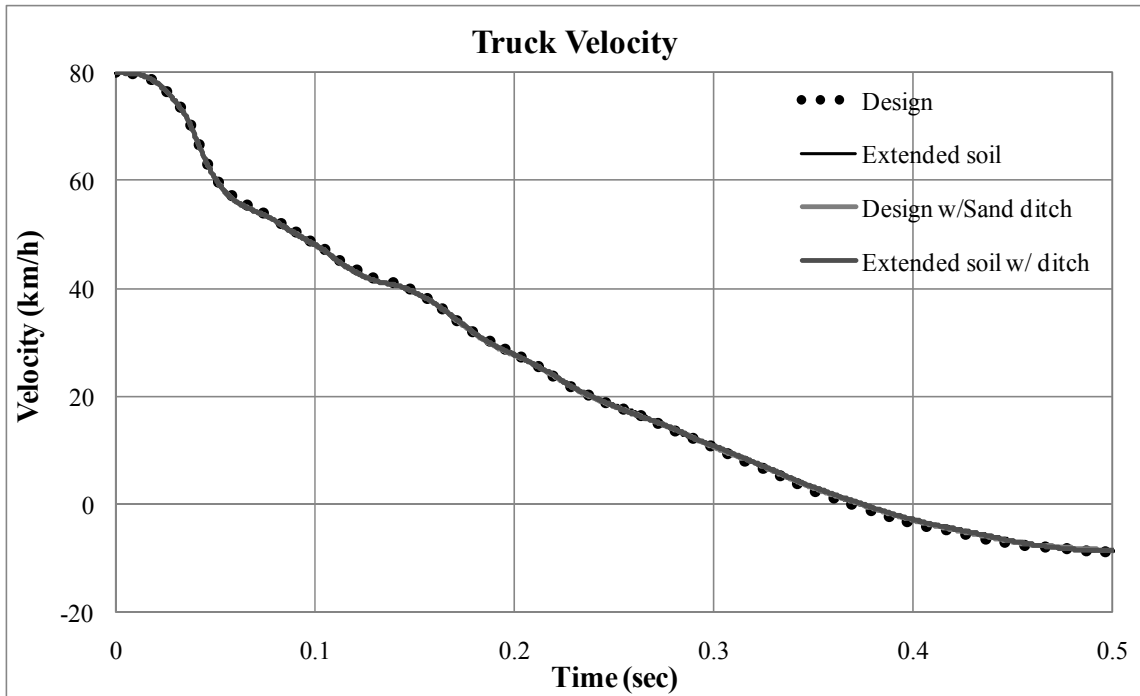
Figure 4.61. Simulated vehicle velocity for various soil boundaries
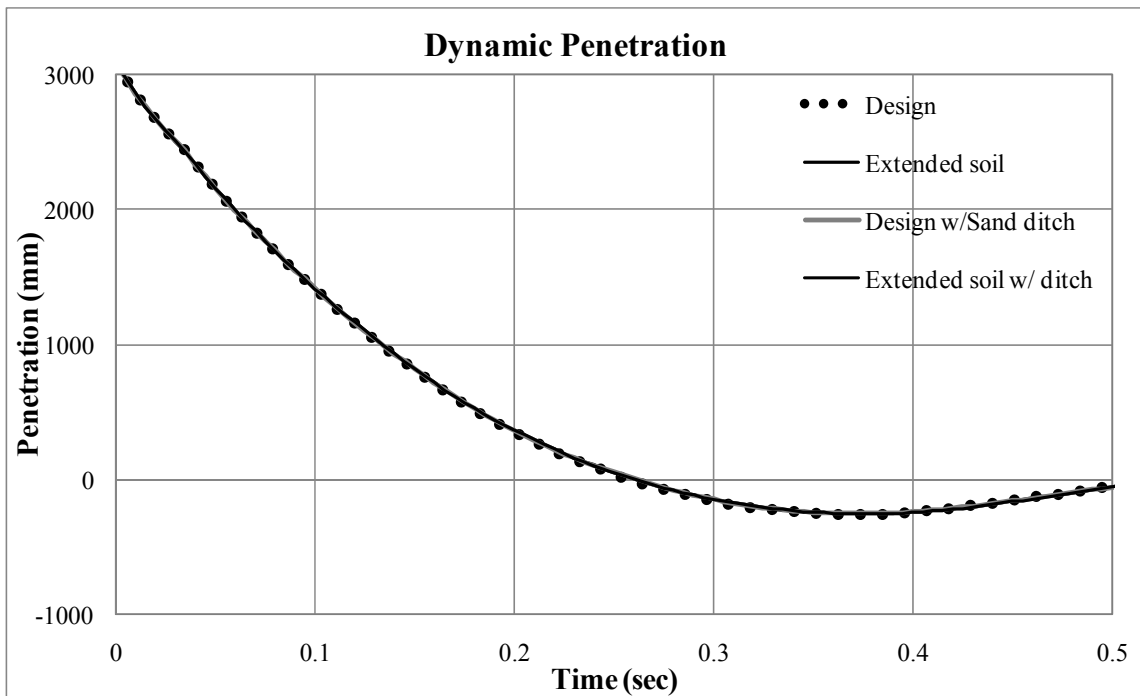
Figure 4.62. Simulated dynamic penetration for various soil boundaries

After the full-scale experiment, the group of posts models was modified with the measured soil properties. Loose sand near the ground level in the ditch was compacted due to the installation of posts system including pile driving. Hence the input soil properties were bit higher than those used for design as shown in finite element analysis matrix (Table 4.13).
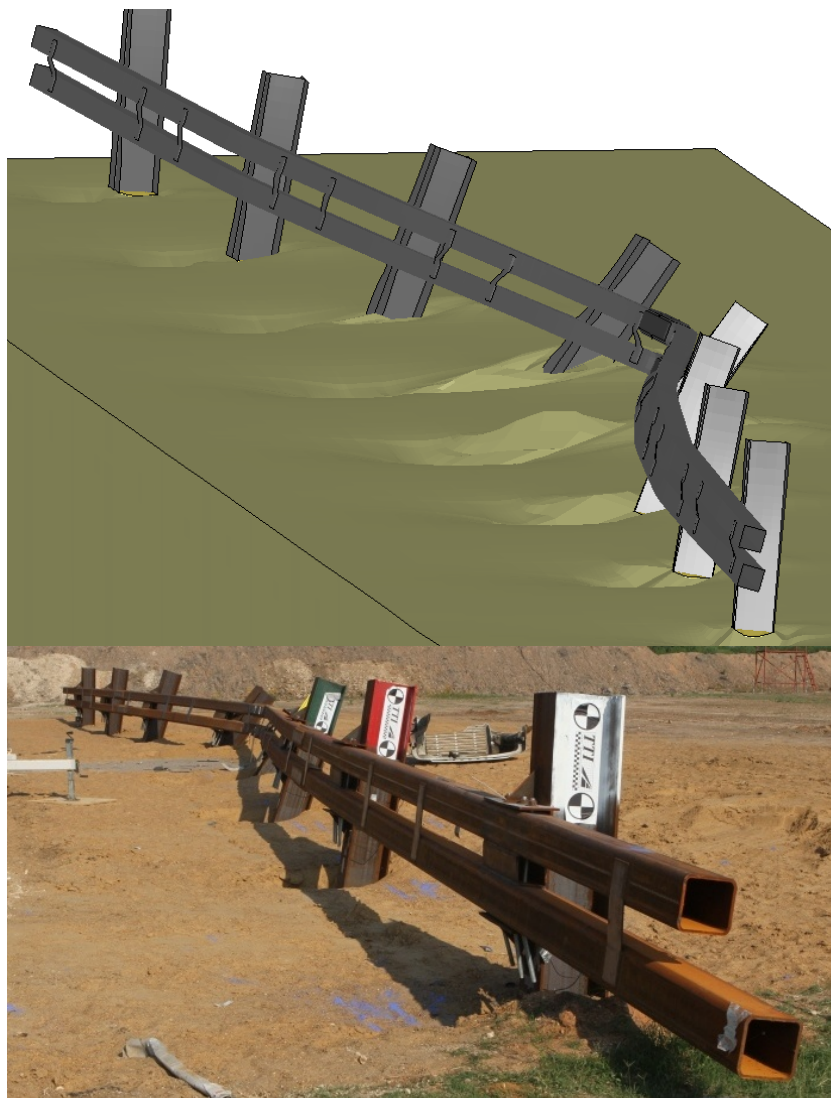
Figure 4.63. Simulated and actual deformed group of posts after impact

Simulation 6 in Table 4.13 was selected as the best estimation for the full-scale experiment. Simulated vehicle and post system after impact and sequential figures of simulated impact are shown in Appendix E. The measured and simulated deformed shapes of group of posts system are shown in Figure 4.63.

Since the acceleration signal at the C.G of vehicle was defected during the experiment, the behaviors of vehicle observed at the rear of vehicle were compared to the simulated results. Compared 50ms average acceleration, velocity and displacement of vehicle are shown in Figure 4.64, Figure 4.65 and Figure 4.66. Peak decelerations of vehicle were 14g for both the experiment and the simulations. As shown in Figure 4.66, the maximum vehicle displacements measured from the impact were 3.2 and 3.3 m for the experiment and the simulations. The analysis using linear momentum is shown in Appendix E.
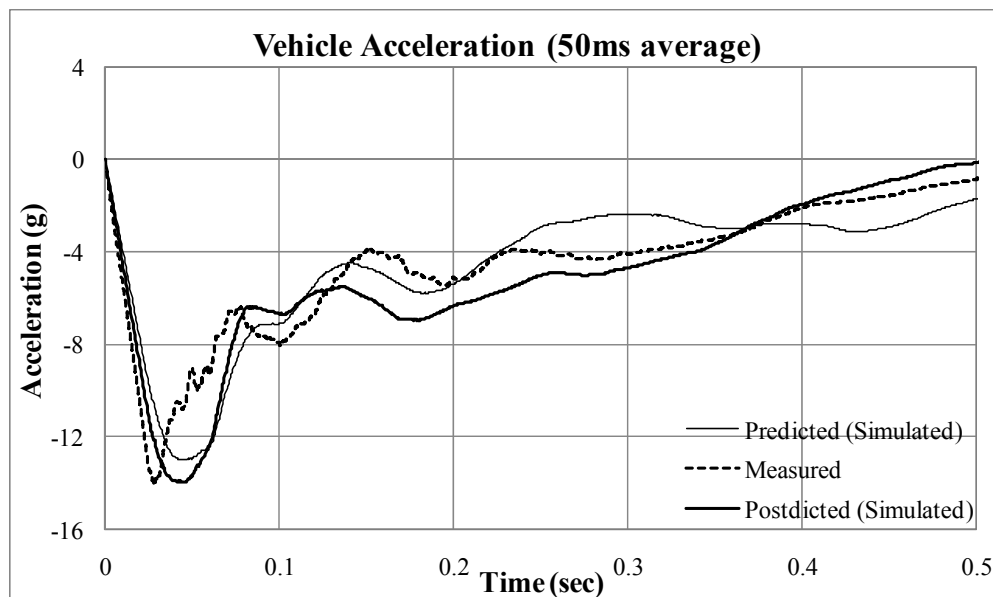

Figure 4.64. Comparison of vehicle acceleration (M50 Group of posts system)
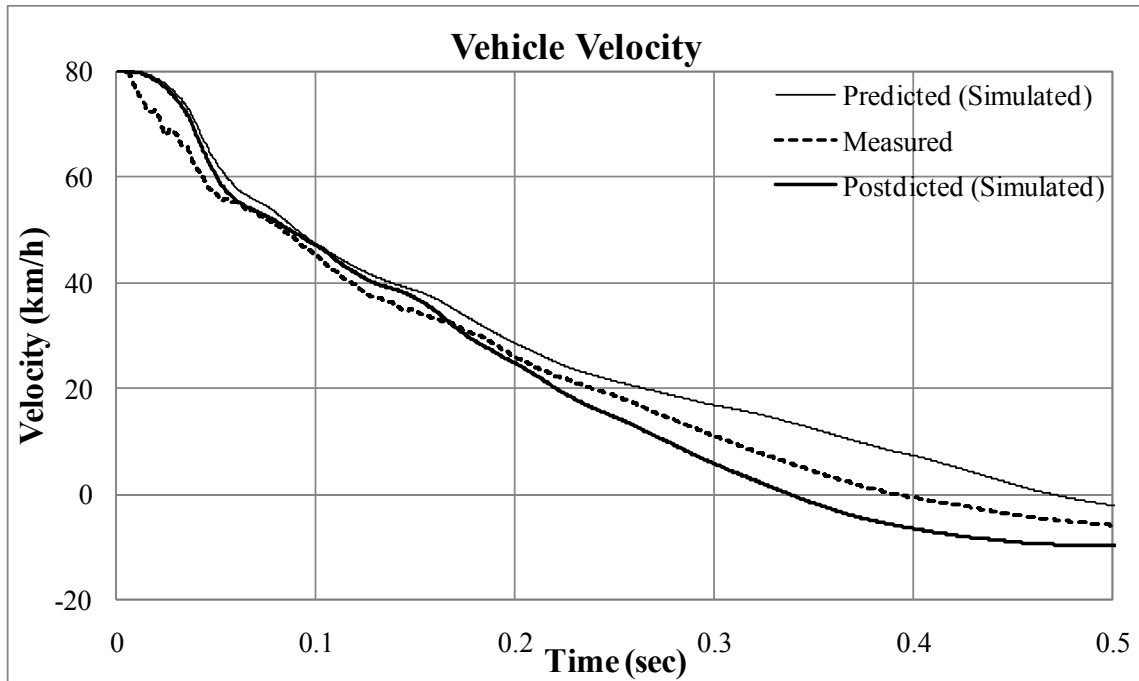
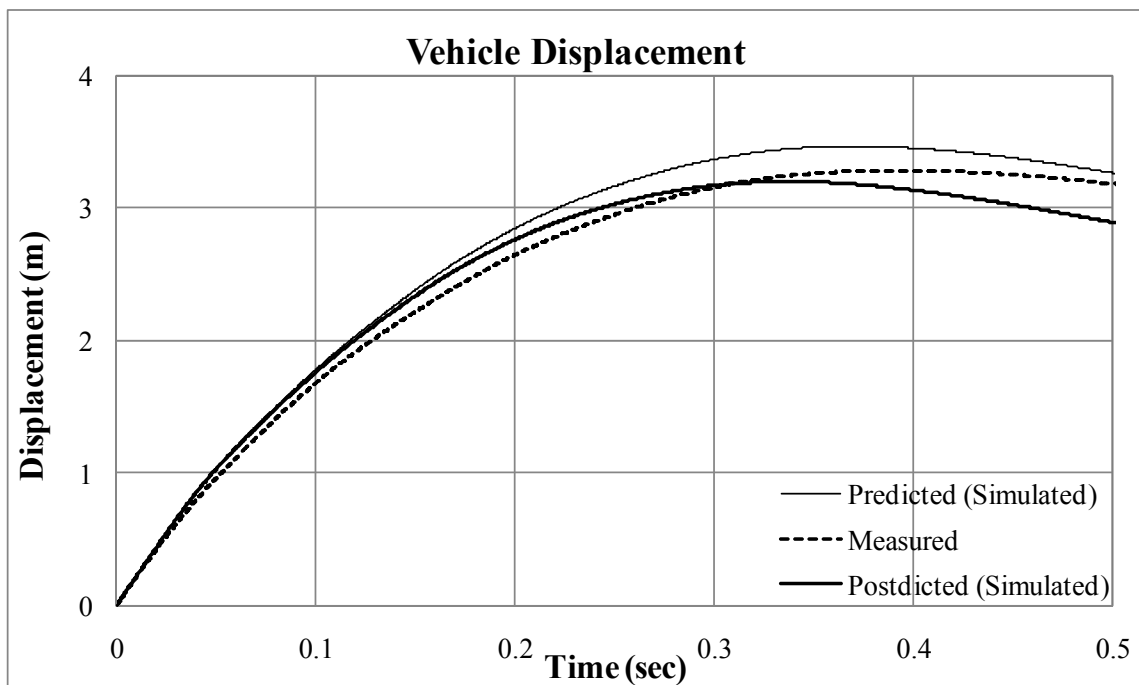**Figure 4.65. Comparison of vehicle velocity (M50 Group of posts system)**

Figure 4.66. Comparison of vehicle displacement (M50 Group of posts system)

The measured impact force that was calculated using the product of 50ms average acceleration and vehicle mass was compared with the simulated contact force between the post system and test truck in Figure 4.67. Peak impact forces were 925 kN and 850 kN for the experiment and the finite element analysis. The reason of difference in impact forces is due to the characteristics of vehicle model. The modeled vehicle can be deformed but not allow the failure of connections that causes change in mass. Also the simulated overall deformation of vehicle was less severe than the experiment.

Simulated rotation of the center post was underestimated and those of the other posts were overestimated as shown in Figure 4.68. Another major difference between the experiment and finite element analysis was connection between posts and beams. The beams are attached to posts using steel bolts in the experiment, whereas the beams and posts were tied together with Nodal-rigid body contact that does not allow fracture. During the experiment, the bolt connections on two center posts that located near the impact were broken.

The dynamic penetration is defined as the distance between the initial position of the post and the maximum penetration of the leading edge of the flat bed of the truck. The measured and simulated dynamic penetrations of the test are shown in Figure 4.70 .
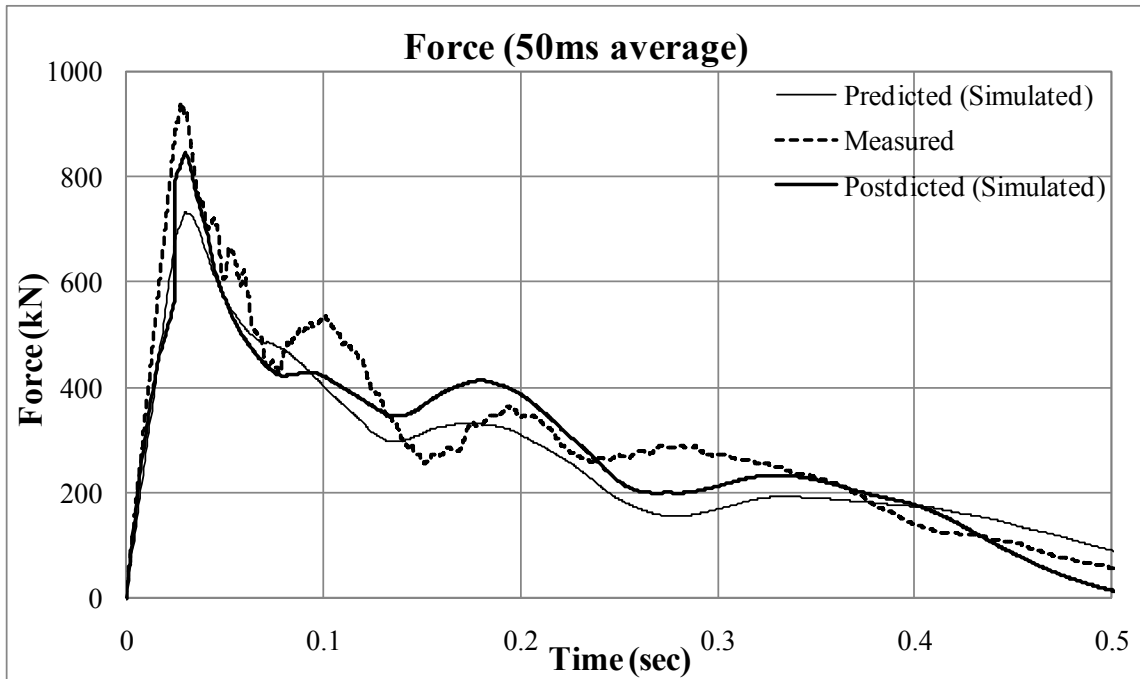
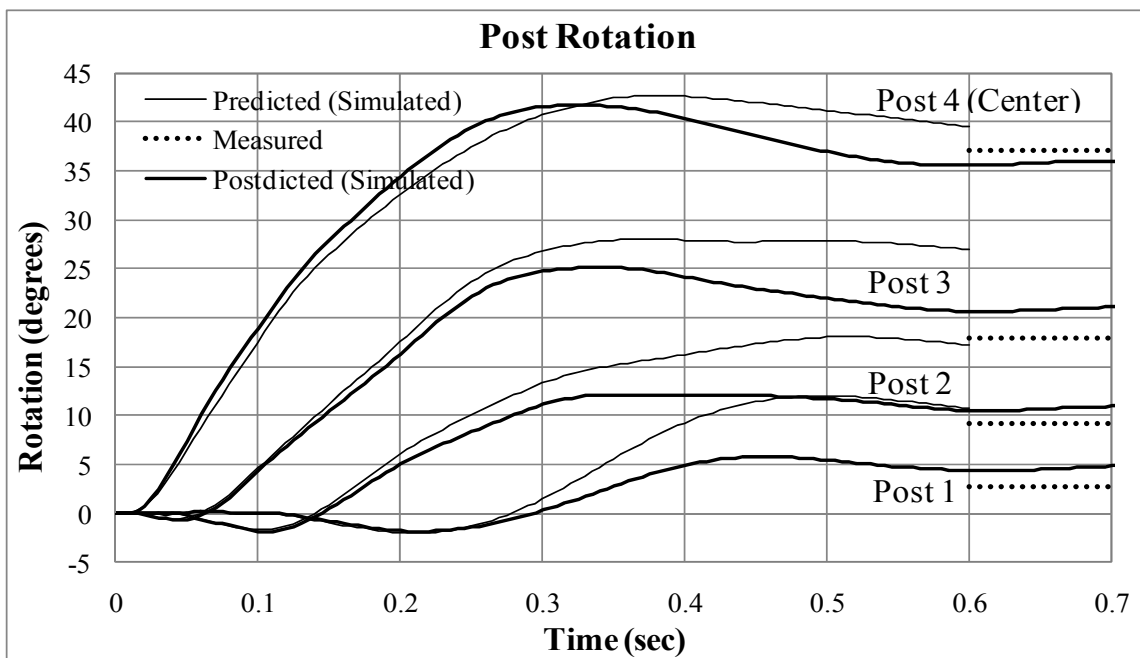**Figure 4.67. Comparison of impact force (M50 Group of posts system)**

Figure 4.68. Comparison of post rotation (M50 Group of posts system)
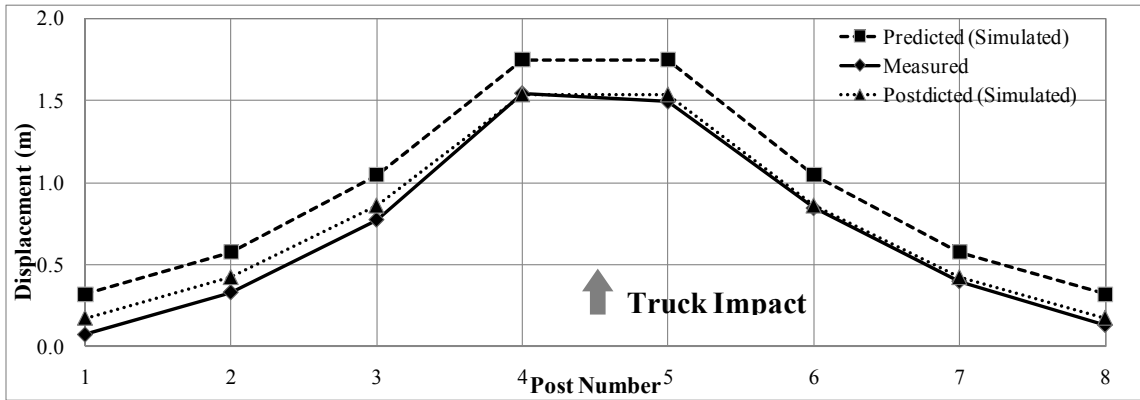
Figure 4.69. Comparison of permanent displacement of posts (M50 Group of posts system)
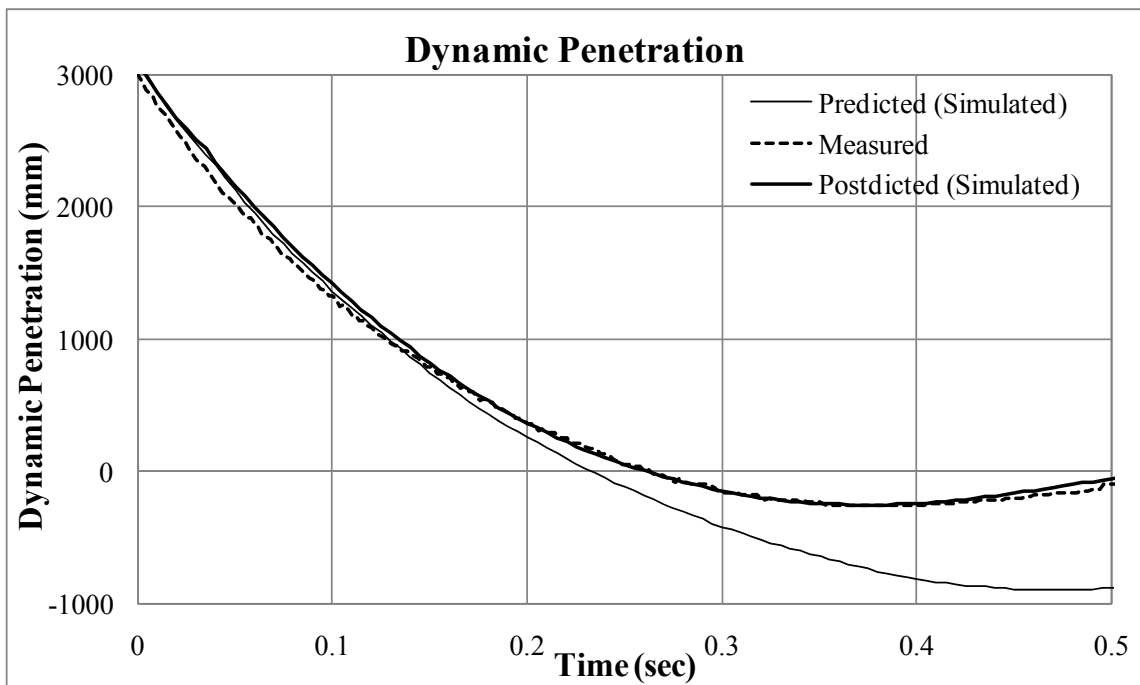

Figure 4.70. Simulated dynamic penetration (M50 group of posts)

The displacements of the simulation for design chart and the best estimated simulation using measured soil properties were compared with the measured post

displacements. Since the soil properties for simulation of design chart were underestimated, the behaviors of all post were overestimated. Measured and simulated permanent displacements of all posts at the ground level can be found in Figure 4.69.

The post displacements at 1.5 m above the ground level were measured using film analysis. The comparisons of these displacements for each post are shown in Figure 4.71, Figure 4.72, Figure 4.73 and Figure 4.74. Due to the failure of connection bolts between the posts and beams, the impact force could not be well transferred as simulation results. Thus the simulated displacements were underestimated except the center posts.
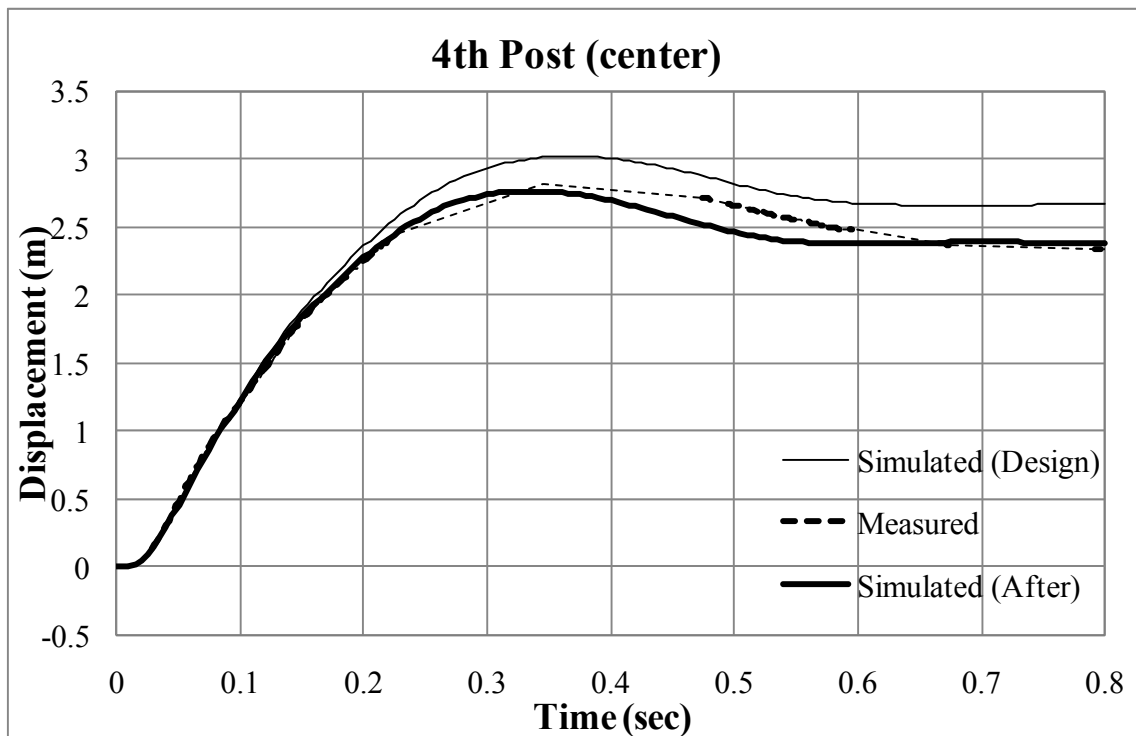

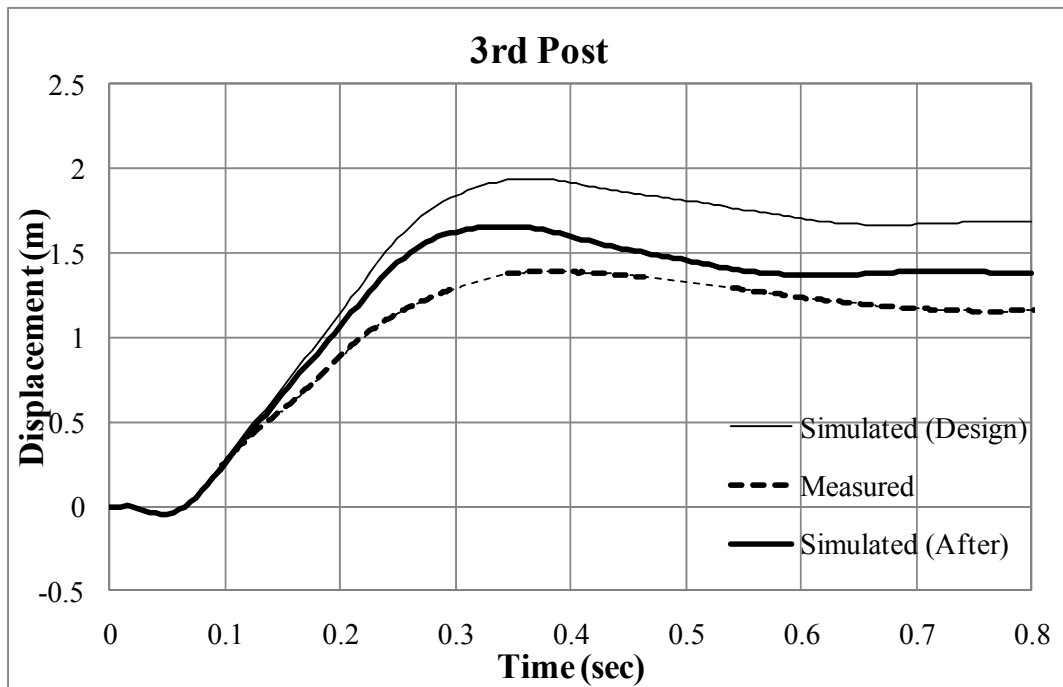Figure 4.71. Comparison of displacement of post 4 (M50 Group of posts system)

Figure 4.72. Comparison of displacement of post 3 (M50 Group of posts system)
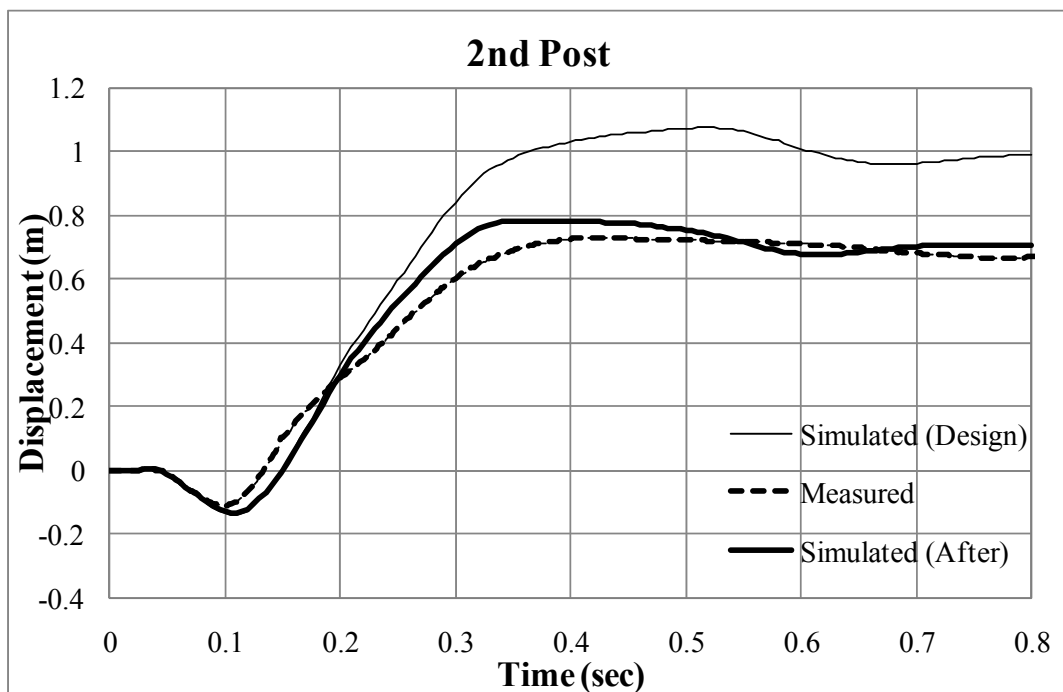

Figure 4.73. Comparison of displacement of post 2 (M50 Group of posts system)
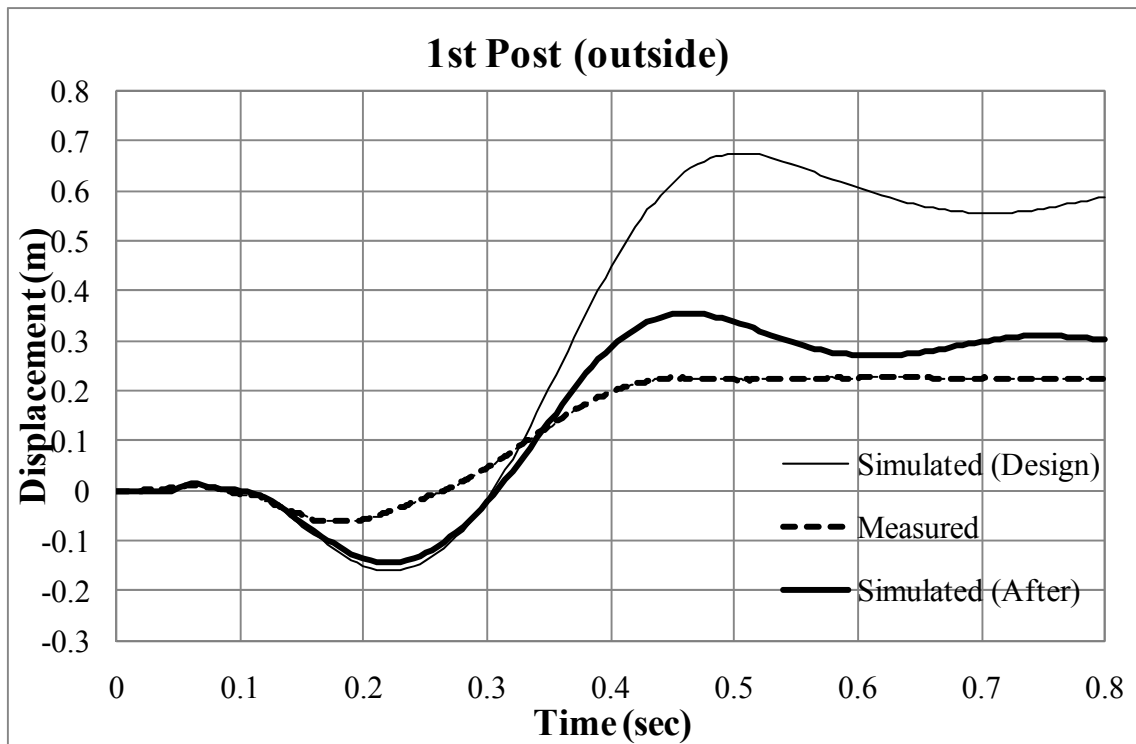
Figure 4.74. Comparison of displacement of post 1 (M50 Group of posts system)

The bending strains of each post were measured using strain gages as stated in Section 3.5. The measured and simulated strains of each post are shown in Figure 4.75, Figure 4.76 and Figure 4.77. Since strain of Post 3 could not be obtained from the experiments, the data was omitted. Measured strains were higher than simulated strains. It is largely due to the failure of connection bolts of the center posts. The bolts failed around at 0.1 sec and the strain signals of Post 3 and Post 4 were fluctuated compare to the simulated results. Simulated permanent displacement of the end posts, Post 1 was underestimated as shown in Figure 4.77. The permanent displacement of post 8 caused residual strain that was higher than the simulated strain of the post.
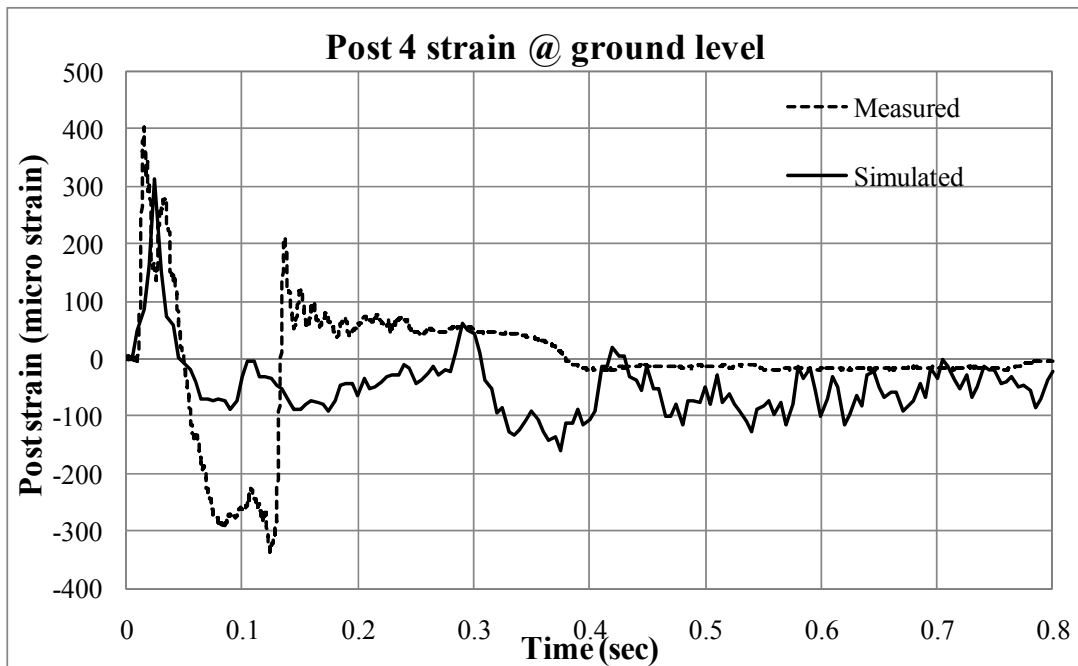
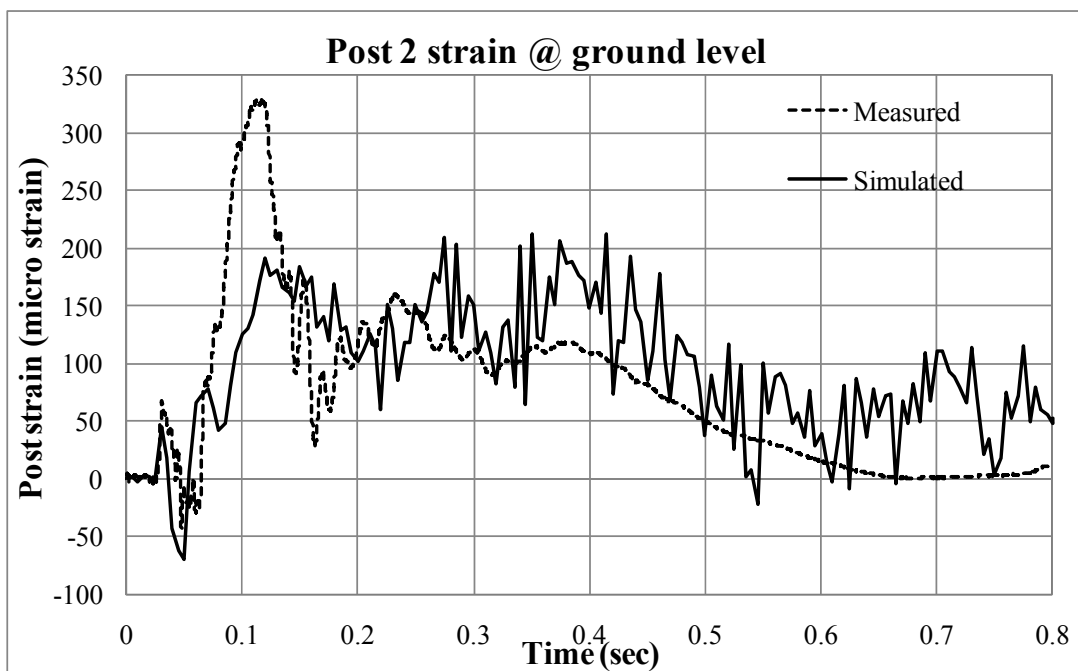**Figure 4.75. Comparison of strain of post 4 (M50 Group of posts system)**

Figure 4.76. Comparison of strain of post 2 (M50 Group of posts system)
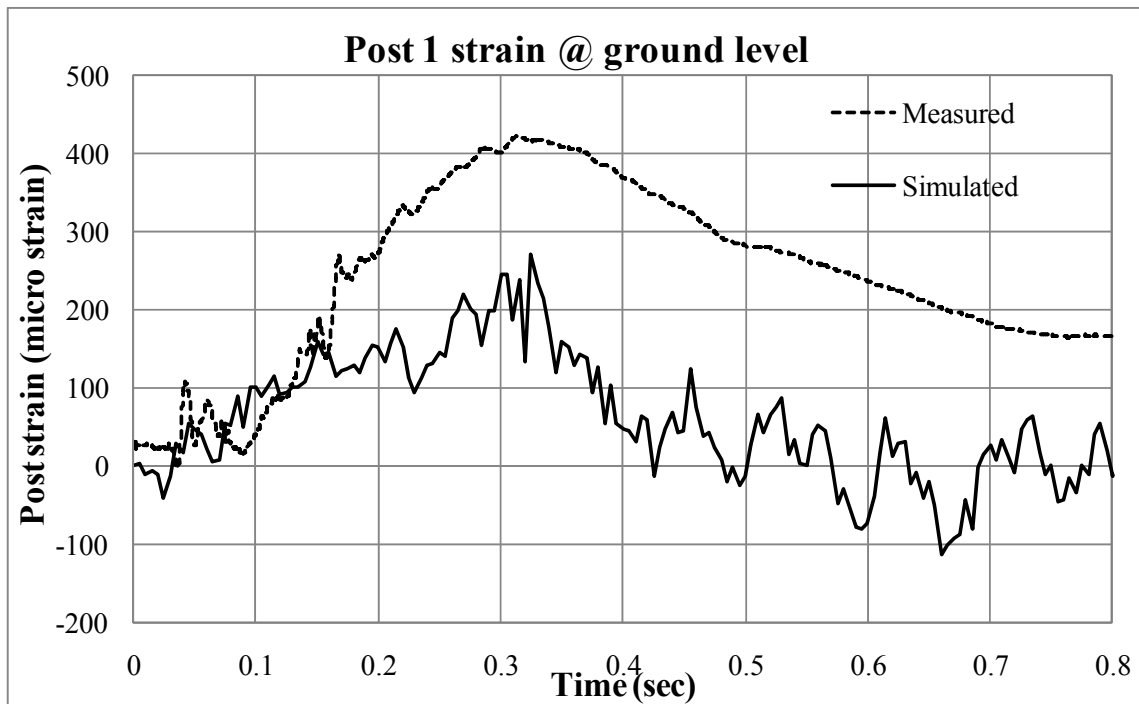
Figure 4.77. Comparison of strain of post 1 (M50 Group of posts system)

The reason that the strain of each post was measured was to calculate the force applying on each post at the ground level. Due to the torsion from the connection between the posts and the horizontal beams, the force could not be obtained. The simulated strain and bending moment at the ground level of each post have similar trends as shown in Figure 4.78 and Figure 4.79. However, the forces of each post could not be calculated, since the magnitude of the torsion acting on each post could not be estimated from the experiments.
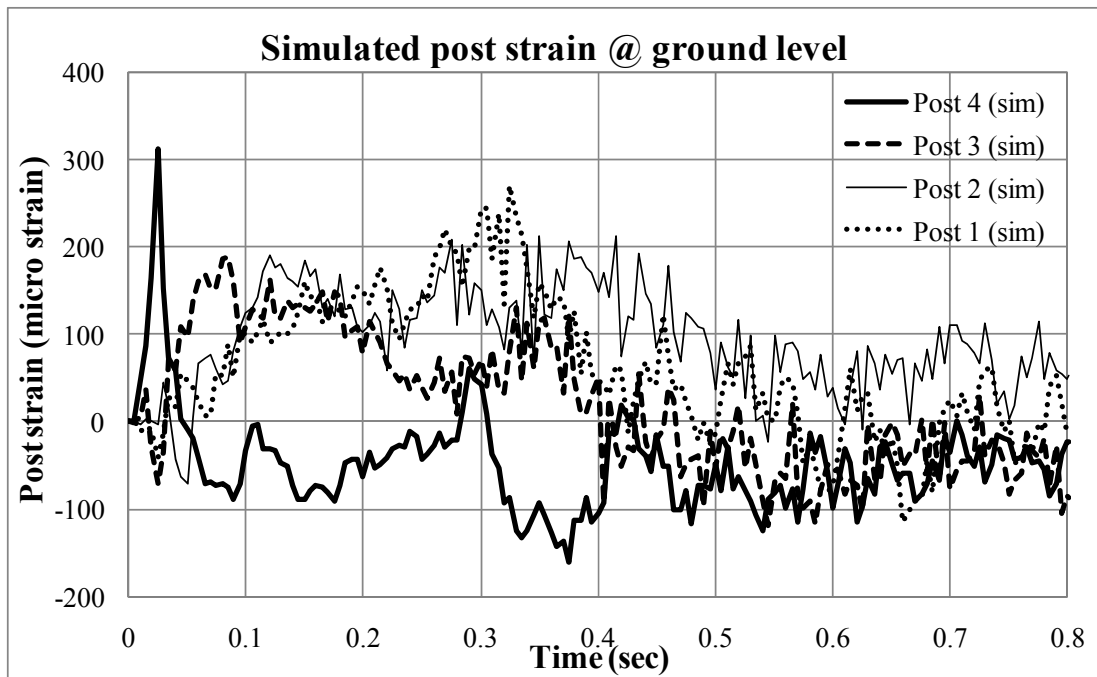
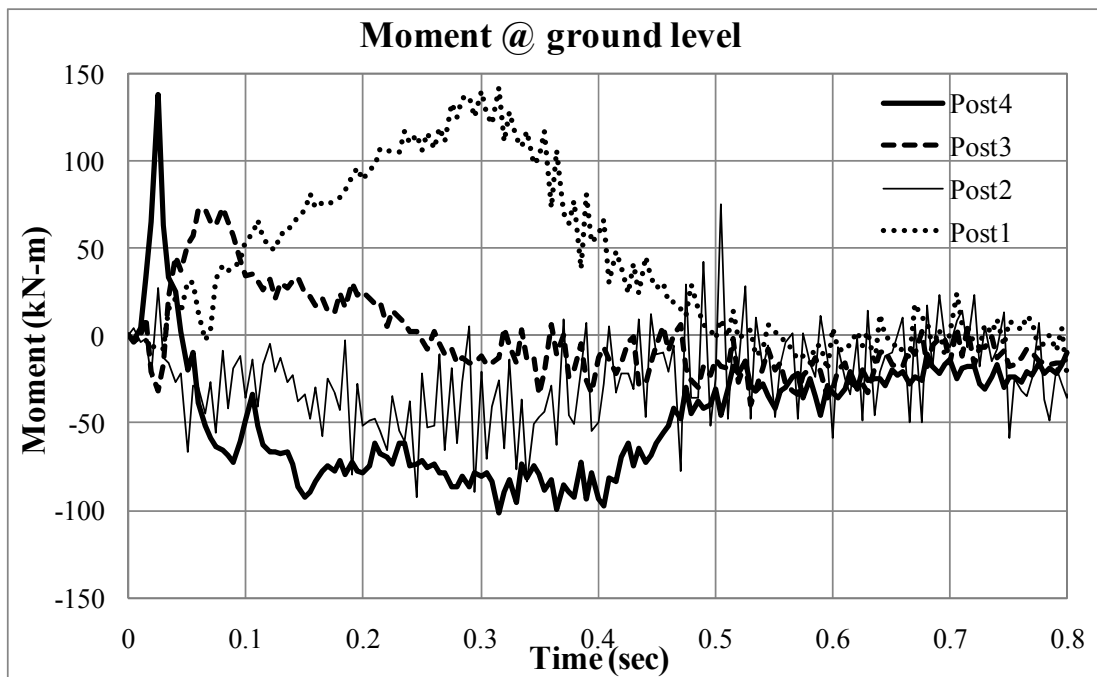**Figure 4.78. Simulated strains of posts (M50 Group of posts system)**

Figure 4.79. Simulated bending moment of posts (M50 Group of posts system)

The simulated 50ms average bending moments and forces of each post are shown in Figure 4.80 and Figure 4.81. In those figures, the force acting on Post 4 was converging to zero whereas the bending moment of the post was still applying due to the residual strain. Since the horizontal beams began bending toward the impact direction just after the impact, all posts experienced the opposite directional force at the beginning. Peak forces acting on each post were 185 kN, 83 kN, -45 kN and -65 kN. Post 1 that located further from the impact mainly experienced force acting on the opposite direction to the impact. The force acting on Post 3 was balanced.
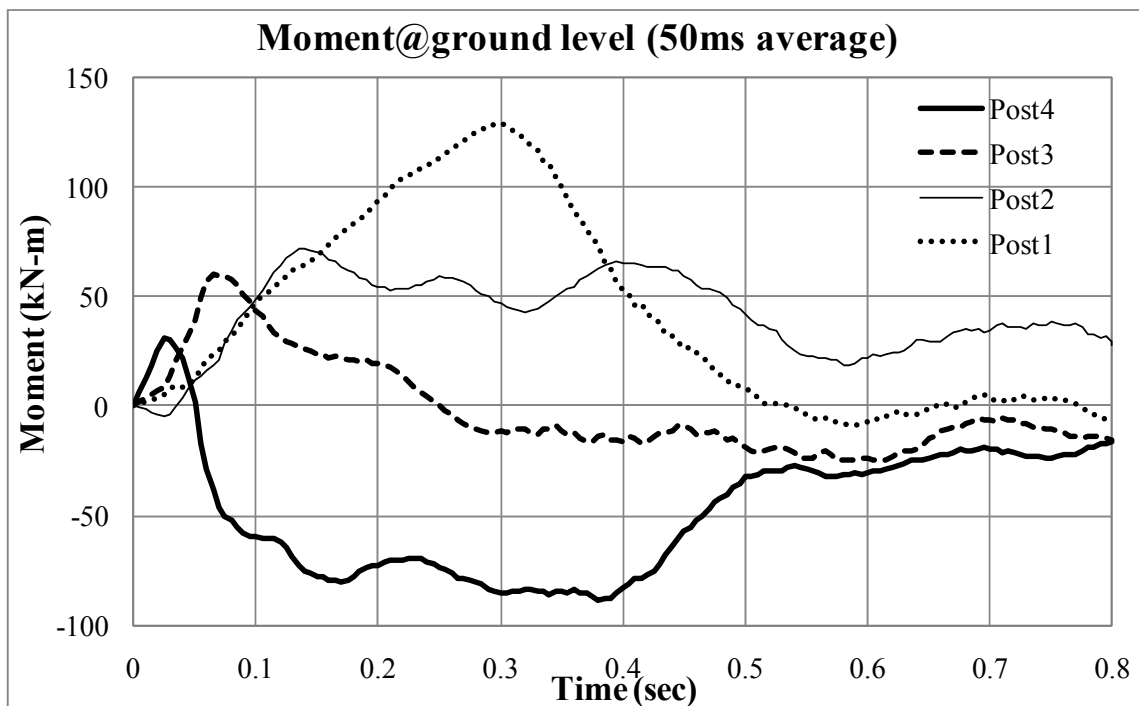

Figure 4.80. Simulated 50ms average bending moment of posts (M50 Group system)
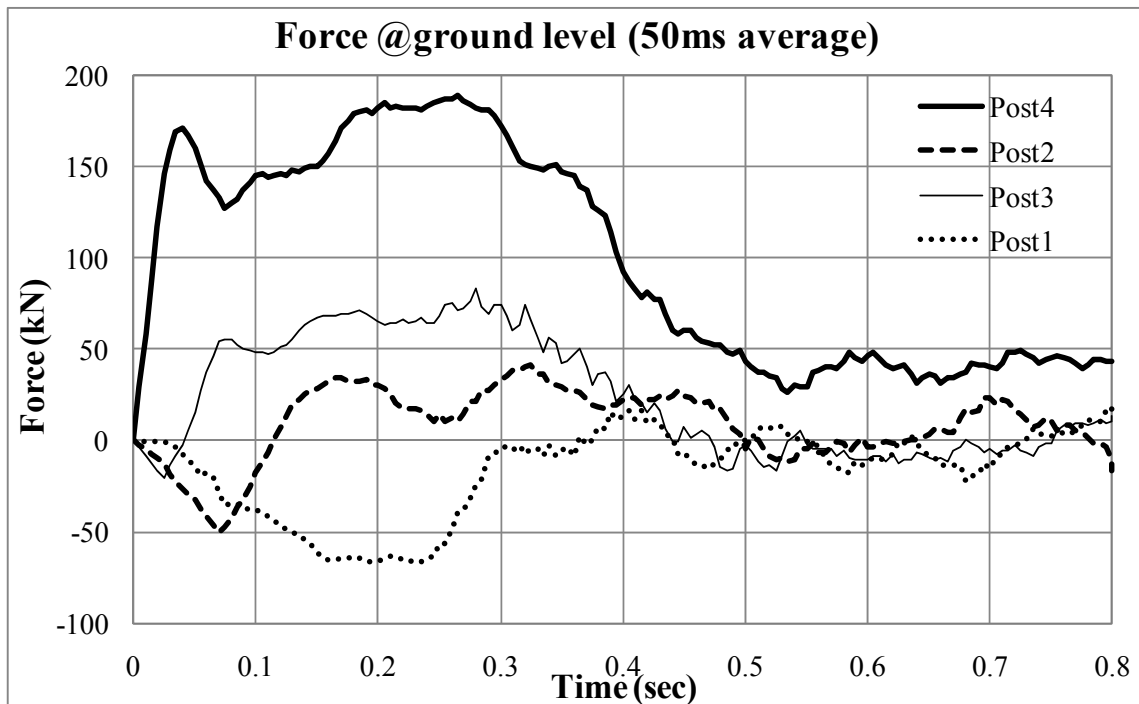
Figure 4.81. Simulated 50ms average forces of posts (M50 Group of posts system)

The sum of simulated force acting on each post is shown in Figure 4.82 along with the measured and simulated impact forces. Peak of impact force was 825 kN at 0.04 sec whereas peak of summated force on each post was 550 kN at 0.3 sec. The reason is that the impact force acting on the center of post system was transferred to all eight posts with some delay in time. Also the interaction between beams and each post including inertia effect, and force transferring distributed the force. The peak force of summated force on each post was reduced but the duration was increased.
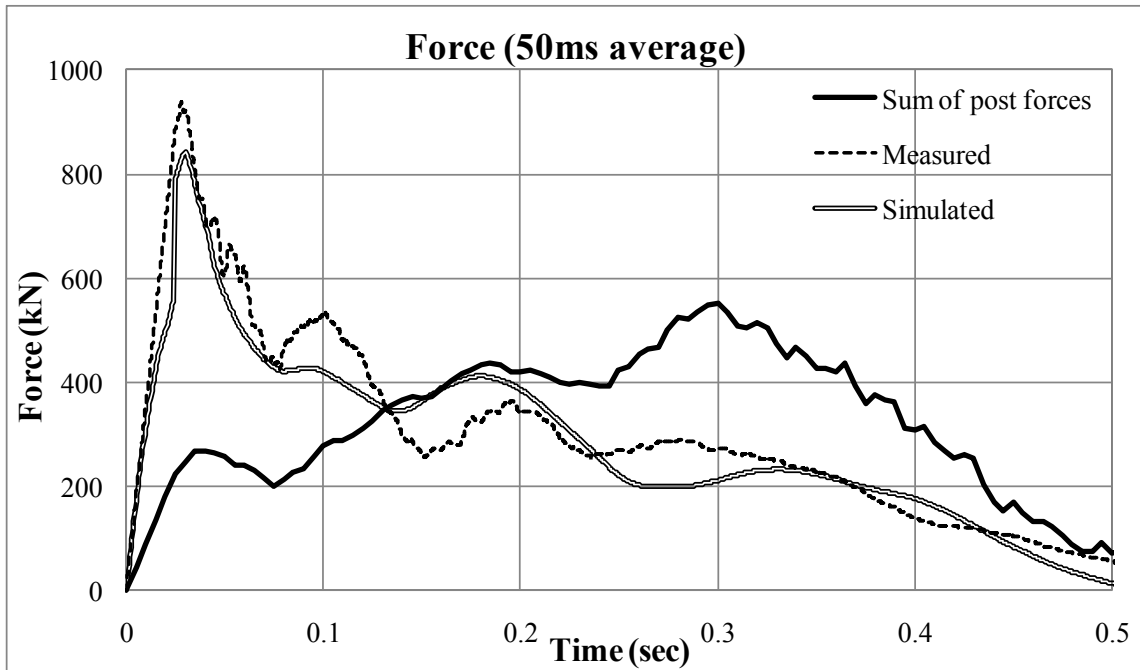
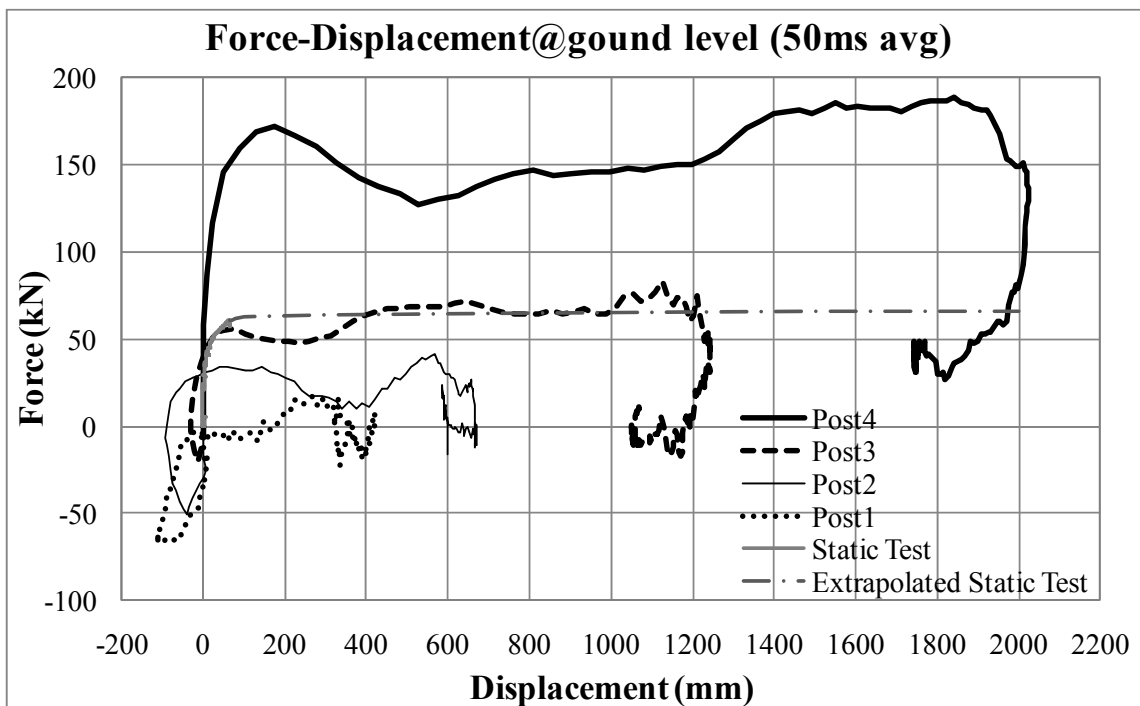**Figure 4.82. Summated forces acting on each post from simulation**

Figure 4.83. Simulated forces-displacement of posts (M50 Group of posts system)

The dynamic amplification factors of each post were 2.64, 1.20, 0.64 and 0.93 from the center of system. Since not all of posts fully engaged to the impact force, Dynamic factor of single post in loose sand can be considered as 2.64 and the critical dynamic factor obtained from pendulum test was 3.8. The reason can be that the post system and vehicle was more flexible than the rigid pendulum and the post for pendulum test. Also the inertia effect of mass of 8,300 kg for the post system above the ground level can be the other reason.

4.3.5 Conclusions

The calibration of the experiments consisted of comparing the predicted response with the measured response in the pendulum tests, the bogie tests, the full scale test on the single post in the very dense crushed rock, and the full scale test on the group of posts in the loose sand. These comparisons included deceleration of the truck, acceleration of the barrier, impact force history, velocity history, and displacement history.

The design charts are based on the results of ten medium scale pendulum impact tests, two medium scale bogie impact tests, one full scale impact test on a single post, one full scale impact test on a group of 8 side by side posts with a 5.2 m spacing and connected with two beams, approximately 150 four dimensional numerical simulations of full scale impact tests using LS-DYNA, as well as fundamental theoretical concepts. The best verifications are the two full scale tests with the 6800 kg truck going 80 km/h. In the case of the single post the test was done before the simulation. In the case of the group of posts the simulation was done prior to the test and the group system was

selected on the basis of the simulation results. The fact that the test essentially happened as predicted gives a good level of confidence in the design charts.

For the full-scale test on a single post, the force time graph shows that the measured peak force is higher than the predicted peak force; this is due to the fact that the predicted peak force is the actual contact force between the truck and the barrier while the measured force is the truck mass times the deceleration of the truck bed. The measured force ignores the crushing of the front of the truck. The accelerometer at the C.G. of the vehicle was not the same with the actual impact force since the longitudinal force measured at the C.G of the vehicle separated in longitudinal and vertical forces. Due to these two reasons, the measured impact force was higher by 30 % than the simulated impact force.

During the simulations for the pendulum tests, the force-time graph shows a loss of contact for the simulation which is not observed in the measurements; this may be due to the fact that the nose of the simulated pendulum was too rigid and created a bouncing effect at the contact.

After the full-scale experiment, the group of posts models was modified with the measured soil properties and checked with different soil boundary conditions including the configuration of the sand ditch. The size of soil boundary for design chart was spacious enough according to the numerical simulation result.

Due to the failure of connection bolts between the posts and beams, the impact force could not be well transferred. Thus the simulated rotation and displacement were underestimated except the center posts.

Peak forces acting on each post were 185 kN, 83 kN, -45 kN and -65 kN. Peak of impact force was 825 kN at 0.04 sec whereas peak of summated force on each post was 550 kN at 0.3 sec. Due to inertia effect and delay on force transferring to each post, The peak summated force on each post was smaller than the impact force but the duration was increased. Also the modeled vehicle can be deformed but not allow the failure of connections of vehicle parts that causes change in mass.

Dynamic amplification factors of each post were ranging from 2.64 to 0.64. Dynamic amplification factor of single W14X90 post in loose sand can be considered as 2.64 that is less than the critical dynamic factor obtained from pendulum test. The reason can be that the post system and vehicle was more flexible than the rigid pendulum and the post for pendulum test. Also the distributed forces on each post were mitigated by the inertia effect of mass of 8,300 kg for the post system above the ground level.

4.4 Development of design guidelines

Design guideline for post system directly embedded in soil to contain the vehicle impact of designation M50, M40 and M30 with P1 penetration rating from ASTM F2656-07was developed. To develop the proposed design guideline, a set of numerical simulations using LS-DYNA was performed based on the soil strength category. The initial finite element model was developed based on the full-scale impact test on single post, July 2007. The initial model was refined by using the model test results. After completion of the design chart, the method was partially verified by the full-scale impact test on group of posts system, May 2010.

The proposed design guideline was prepared for single post and group of posts system embedded in sand and clay. Drucker-Prager model that is a general constitutive model was used as a material model for sand. Isotropic elastic plastic with failure model, one of the simplest models for clay was used as a material model for clay. Though there are lots of constitutive models for clay, Isotropic elastic plastic with failure model will be used for this task due to the lack of supported model of LS-DYNA for clay.

Design method was developed to design not only single post but also group of posts system. Single post cannot meet the design criteria for all the impact condition designations in all soil conditions. For instance, a single post embedded in very dense crushed limestone or bedrock can meet the requirement of P1 penetration against M50 condition designation. Whereas the same post embedded in relatively weak soil such as loose sand or soft clay cannot arrest vehicle impact with M50 energy level. Also special needs for continuous barrier system can exist. Thus a design method for group of posts systems is required.

The design guideline was developed using a certain post configuration. The design chart for single post was developed using a wide flange beam, W14X109. Thus single post system should be installed using a post with equivalent to W14-109 Post or even stronger post in terms of post width and bending stiffness. In addition to the embedment depth, at least 1.5 m of post length above the ground level is required. In the same manner, the group of posts system needs at least eight of W14-90 post, four posts on each side of the impact location with a horizontal beam with hollow section HSS 10X10X1/2. Also at least 1.5m of post length above the ground level is needed. The post

and beam member having equivalent or stiffer bending stiffness can be used with cautious calculations.

4.4.1 Numerical simulation matrices

The proposed design guideline largely consists of four parts: single post in sand, single post in clay, group of posts in sand and group of posts in clay. The design guideline was developed based on a series of finite element analysis using LS-DYNA.

The design chart for single post embedded in sand was completed the numerical simulation matrix as shown in Table 4.14. The second column of the matrix represents the impact level or designation condition of ASTM F2656-07. From the third to ninth column include input soil properties from the proposed soil strength category. The last two columns include post embedment and the result according to the dynamic penetration rating P1 of the standard. If post system arrest the vehicle and dynamic penetration was less than 1 m, result is noted as OK. Numerical simulation matrix for single post embedded in clay is shown in Table 4.15. Post section was wide flange W14X109 for all single post simulations.

Table 4.14. Numerical simulation matrix for single post embedded in sand

Num	Energy level	Soil Strength	E (Mpa)	γ (kN/m3)	φ (deg)	ψ (deg)	c (kPa)	Depth (m)	Results
1	M50	V.Dense+	50	21.0	40	20	15.0	3.0	OK
2	M50	V.Dense	32	22.0	40	10	4.0	3.0	NG
3	M50	V.Dense	32	22.0	40	10	4.0	4.0	OK
4	M50	V.Dense/Dense	20	20.6	37	6	3.3	3.0	NG
5	M50	V.Dense/Dense	20	20.6	37	6	3.3	4.0	NG
6	M50	V.Dense/Dense	20	20.6	37	6	3.3	5.0	OK
7	M50	V.Dense/Dense	20	20.6	37	6	3.3	6.0	OK
8	M50	Dense	16	20.0	36	5	3.0	5.0	NG
9	M50	Dense	16	20.0	36	5	3.0	6.0	NG
10	M40	V.Dense	32	22.0	40	10	4.0	2.0	OK
11	M40	V.Dense/Dense	20	20.6	37	6	3.3	2.0	NG
12	M40	Dense	16	20.0	36	5	3.0	2.0	NG
13	M40	Dense	16	20.0	36	5	3.0	3.0	Ok
14	M40	Dense/Medium	12	19.1	35	0	2.5	3.0	OK
15	M40	Medium	8	18.0	33	-5	2.0	3.0	NG
16	M40	Medium	8	18.0	33	-5	2.0	4.0	NG
17	M40	Medium	8	18.0	33	-5	2.0	5.0	OK
18	M40	Medium	8	18.0	33	-5	2.0	6.0	OK
19	M40	Medium/Loose	4	17.3	29	-8	1.3	6.0	NG
20	M30	V.Dense/Dense	20	20.6	37	6	3.3	2.0	OK
21	M30	Dense	16	20.0	36	5	3.0	2.0	NG
22	M30	Dense/Medium	12	19.1	35	0	2.5	2.0	NG
23	M30	Medium	8	18.0	33	-5	2.0	3.0	OK
24	M30	Medium/Loose	4	17.3	29	-8	1.3	3.0	NG
25	M30	Medium/Loose	4	17.3	29	-8	1.3	4.0	NG
26	M30	Medium/Loose	4	17.3	29	-8	1.3	4.5	OK
27	M30	Medium/Loose	4	17.3	29	-8	1.3	5.0	OK
28	M30	Loose	2	17.0	27	-10	1.0	4.0	NG
29	M30	Loose	2	17.0	27	-10	1.0	5.0	NG
30	M30	Loose	2	17.0	27	-10	1.0	6.0	OK

Table 4.15. Numerical simulation matrix for single post embedded in clay

Num	Energy level	Soil Strength	E (Mpa)	γ (kN/m3)	σ_y (kPa)	c (kPa)	Depth (m)	Results
1	M50	Very Hard	34.0	22.0	500	250	6.0	NG
2	M40	Very Hard	34.0	22.0	500	250	2.0	NG
3	M40	V.Hard/Hard	25.5	21.1	390	195	3.0	OK
4	M40	Hard	18.0	20.0	280	140	5.0	OK
5	M40	Hard	18.0	20.0	280	140	4.0	OK
6	M40	Hard	18.0	20.0	280	140	3.0	NG
7	M40	Hard/Medium	10.0	19.0	170	85	6.0	OK
8	M40	Hard/Medium	10.0	19.0	170	85	5.0	OK
9	M40	Hard/Medium	10.0	19.0	170	85	4.0	OK
10	M40	Medium	6.0	18.0	100	50	6.0	OK
11	M40	Medium	6.0	18.0	100	50	5.0	NG
12	M40	Medum/Soft	3.5	17.5	60	30	6.0	NG
13	M30	Hard	18.0	20.0	280	140	3.0	OK
14	M30	Hard	18.0	20.0	280	140	2.0	NG
15	M30	Hard/Medium	10.0	19.0	170	85	4.0	OK
16	M30	Hard/Medium	10.0	19.0	170	85	3.0	OK
17	M30	Medium	6.0	18.0	100	50	4.0	OK
18	M30	Medum/Soft	3.5	17.5	60	30	5.0	OK
19	M30	Medum/Soft	3.5	17.5	60	30	4.0	NG
20	M30	Soft	2.0	17.0	28	14	6.0	OK
21	M30	Soft	1.5	17.0	22	11	6.0	NG

Design chart for group of posts system in sand and clay developed in the same manner with the design chart for single post. Posts and beam members have wide flange W14X90 and hollow section HSS 10X10X1/2 section, respectively. Eight posts embedded in homogeneous soil connected with a horizontal beam. Test vehicle impact along with the centerline of post system. Clearances between each post were limited for three cases: 2.44 m, 4.88 m and 7.32 m. Hence there are three design charts for each soil condition. For instance, design chart for group of posts in sand consists of M50, M40

and M30. Each design chart has three components for post spacing. The design charts

for group of posts in sand and clay are shown in Table 4.16 and Table 4.17, respectively.

Table 4.16. Numerical simulation matrix for group of posts embedded in sand

Num	Energy level	Soil Strength	E (MPa)	γ (kN/m3)	φ (deg)	ψ (deg)	c (kPa)	Depth (m)	Spacing (m)	Results
1	M50	V.Dense/Dense	20	20.6	37	6	3.3	1.0	7.32	OK
2	M50	Dense	16	20.0	36	5	3.0	1.5	7.32	OK
3	M50	Dense	16	20.0	36	5	3.0	1.0	7.32	NG
4	M50	Dense/Medium	12	19.1	35	0	2.5	1.5	7.32	OK
5	M50	Medium	8	18.0	33	-5	2.0	2.5	7.32	OK
6	M50	Medium	8	18.0	33	-5	2.0	2.0	7.32	OK
7	M50	Medium/Loose	4	17.3	29	-8	1.3	3.0	7.32	OK
8	M50	Medium/Loose	4	17.3	29	-8	1.3	2.5	7.32	NG
9	M50	Loose	2	17.0	27	-10	1.0	3.5	7.32	OK
10	M50	Loose	2	17.0	27	-10	1.0	3.0	7.32	OK
11	M50	Dense	16	20.0	36	5	3.0	1.0	4.88	OK
12	M50	Dense/Medium	12	19.1	35	0	2.5	1.0	4.88	NG
13	M50	Medium	8	18.0	33	-5	2.0	1.5	4.88	OK
14	M50	Medium/Loose	4	17.3	29	-8	1.3	2.0	4.88	OK
15	M50	Medium/Loose	4	17.3	29	-8	1.3	1.5	4.88	NG
16	M50	Loose	2	17.0	27	-10	1.0	4.0	4.88	OK
17	M50	Loose	2	17.0	27	-10	1.0	3.0	4.88	OK
18	M50	Loose	2	17.0	27	-10	1.0	2.5	4.88	OK
19	M50	Loose	2	17.0	27	-10	1.0	2.0	4.88	NG
20	M50	Loose	2	17.0	27	-10	1.0	1.0	4.88	NG
21	M50	Dense/Medium	12	19.1	35	0	2.5	1.0	2.44	OK
22	M50	Medium	8	18.0	33	-5	2.0	1.0	2.44	NG
23	M50	Medium/Loose	4	17.3	29	-8	1.3	1.5	2.44	OK
24	M50	Loose	2	17.0	27	-10	1.0	3.0	2.44	OK
25	M50	Loose	2	17.0	27	-10	1.0	2.0	2.44	OK
26	M40	Medium	8	18.0	33	-5	2.0	1.0	7.32	OK
27	M40	Medium	8	18.0	33	-5	2.0	1.0	4.88	OK
28	M40	Medium/Loose	4	17.3	29	-8	1.3	1.5	4.88	OK
29	M40	Medium/Loose	4	17.3	29	-8	1.3	1.0	4.88	NG
30	M40	Medium/Loose	4	17.3	29	-8	1.3	1.0	2.44	OK
31	M40	Loose	2	17.0	27	-10	1.0	2.0	7.32	OK
32	M40	Loose	2	17.0	27	-10	1.0	2.0	4.88	OK
33	M40	Loose	2	17.0	27	-10	1.0	1.5	7.32	NG
34	M40	Loose	2	17.0	27	-10	1.0	1.5	4.88	OK
35	M40	Loose	2	17.0	27	-10	1.0	1.0	4.88	NG
36	M40	Loose	2	17.0	27	-10	1.0	1.0	2.44	NG
37	M30	Loose	2	17.0	27	-10	1.0	1.0	7.32	OK
38	M30	Loose	2	17.0	27	-10	1.0	1.0	4.88	OK

Table 4.17. Numerical simulation matrix for group of posts embedded in clay

Num	Energy level	Soil Strength	E (Mpa)	γ (kN/m3)	σ_y (kPa)	c (kPa)	Depth (m)	Spacing (m)	Results
1	M50	V.Hard/Hard	25.5	21.1	390	195	1.0	7.32	OK
2	M50	Hard	18.0	20.0	280	140	1.0	4.88	OK
3	M50	Hard/Medium	11.5	19.1	190	95	1.0	7.32	OK
4	M50	Hard/Medium	11.5	19.1	190	95	1.0	4.88	OK
5	M50	Hard/Medium	10.0	19.0	170	85	2.0	7.32	OK
6	M50	Hard/Medium	10.0	19.0	170	85	1.5	7.32	OK
7	M50	Hard/Medium	10.0	19.0	170	85	1.0	2.44	OK
8	M50	Medium	6.0	18.0	100	50	1.5	7.32	OK
9	M50	Medium	6.0	18.0	100	50	1.0	7.32	NG
10	M50	Medium	6.0	18.0	100	50	1.0	4.88	OK
11	M50	Medium	6.0	18.0	100	50	1.0	2.44	OK
12	M50	Medium/Soft	3.5	17.5	60	30	3.0	7.32	OK
13	M50	Medium/Soft	3.5	17.5	60	30	2.5	7.32	OK
14	M50	Medium/Soft	3.5	17.5	60	30	2.0	7.32	OK
15	M50	Medium/Soft	3.5	17.5	60	30	2.0	4.88	OK
16	M50	Medium/Soft	3.5	17.5	60	30	1.5	7.32	NG
17	M50	Medium/Soft	3.5	17.5	60	30	1.5	4.88	OK
18	M50	Medium/Soft	3.5	17.5	60	30	1.0	4.88	NG
19	M50	Medium/Soft	3.5	17.5	60	30	1.0	2.44	OK
20	M50	Soft	2.0	17.0	28	14	3.0	7.32	NG
21	M50	Soft	2.0	17.0	28	14	2.5	4.88	OK
22	M50	Soft	2.0	17.0	28	14	2.0	2.44	OK
23	M50	Soft	1.5	17.0	22	11	4.0	7.32	OK
24	M50	Soft	1.5	17.0	22	11	3.5	7.32	NG
25	M50	Soft	1.5	17.0	22	11	2.5	4.88	OK
26	M50	Soft	1.5	17.0	22	11	2.0	2.44	OK
27	M50	Soft	1.5	17.0	22	11	1.5	2.44	NG
28	M40	Hard/Medium	10.0	19.0	170	85	1.0	7.32	OK
29	M40	Medium	6.0	18.0	100	50	1.0	7.32	OK
30	M40	Medium/Soft	3.5	17.5	60	30	1.0	7.32	OK
31	M40	Medium/Soft	3.5	17.5	60	30	1.0	4.88	OK
32	M40	Soft	2.0	17.0	28	14	1.5	7.32	OK
33	M40	Soft	2.0	17.0	28	14	1.5	4.88	OK
34	M40	Soft	2.0	17.0	28	14	1.0	4.88	NG
35	M40	Soft	2.0	17.0	28	14	1.0	2.44	OK
36	M40	Soft	1.5	17.0	22	11	1.5	7.32	OK
37	M40	Soft	1.5	17.0	22	11	1.0	2.44	OK
38	M30	Soft	2.0	17.0	28	14	1.0	7.32	OK
39	M30	Soft	1.5	17.0	22	11	1.0	7.32	OK

4.4.2 Single post results

Design method for single post consists of two charts: one for sand and the other for clay. Horizontal and vertical axes of the chart represent soil strength from the proposed soil strength category and post embedment, respectively.

The parameters influencing the design are the soil behavior, the post behavior, the type of post system, the truck mass, and the truck speed. The design charts were developed for a single post system and then for a group of post system. For the single post system, the following parameters were used:

1. different soil categories (soft to very hard and loose to very dense)

2. same post cross section (W14x109, 14 inches wide and weighing 109 lbs/ft of length)

3. different post embedment (2m to 6m)

4. same truck mass of 6800kg

5. different truck velocities (80km/h or M50, 65km/h or M40, 50km/h or M30)

Each result of numerical simulations was indicated as a circle or cross on design chart. If result of numerical simulation met the test criterion, the point is shown as a circle at the corresponding coordinates. Cross means that result of numerical simulation corresponding soil strength and post embedment could not meet the requirement. The lines connecting circles with same condition designation on chart are the design line of each condition designation: In each case the simulation result consisted of a movie simulating the truck impact against the post and all associated quantities as a function of

time. If the truck reached a velocity of zero (complete stop and possible rebound) and if the dynamic penetration of the truck was less than 1m (the dynamic penetration is defined as the distance between the initial position of the post and the maximum penetration of the leading edge of the flat bed of the truck during the impact), then the post system was deemed acceptable and an circle was placed on the design chart. If these two conditions were not met, then a cross was placed on the design chart. M50, M40 and M30. Prototype of design charts for single post in sand and clay are shown in Figure 4.84 and Figure 4.85. For each chart, the design curve for a given truck velocity was the one that connected the Os for the posts with the least embedment depth.
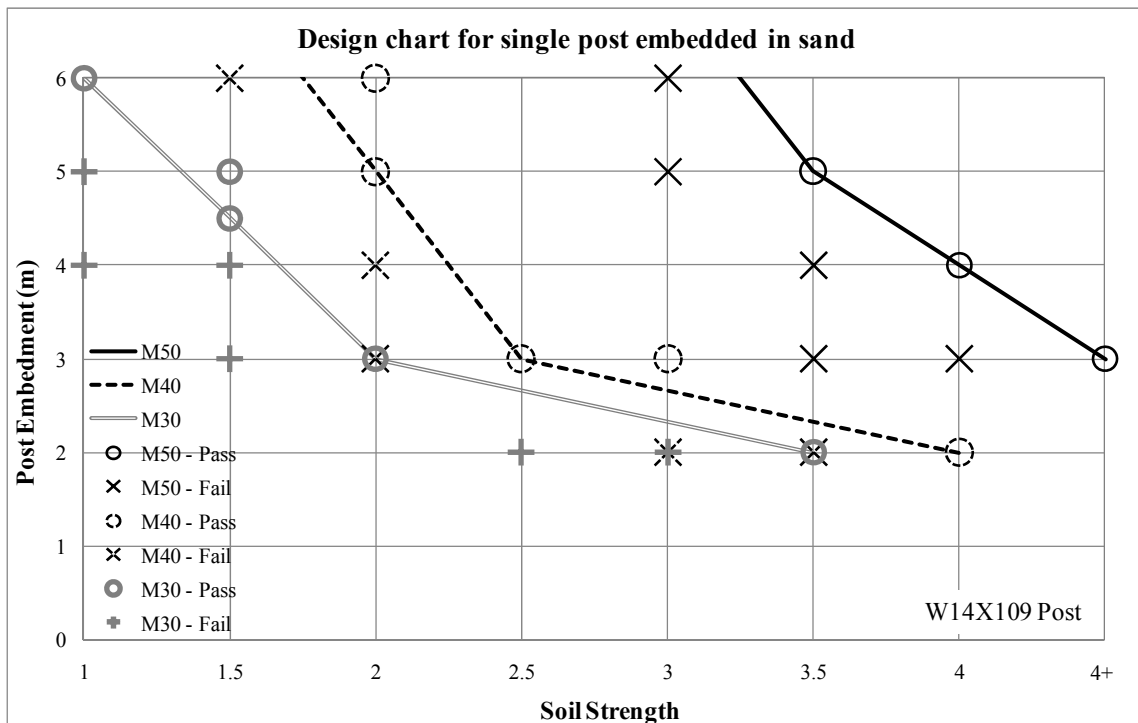
Figure 4.84. Result of numerical simulation for single post embedded in sand
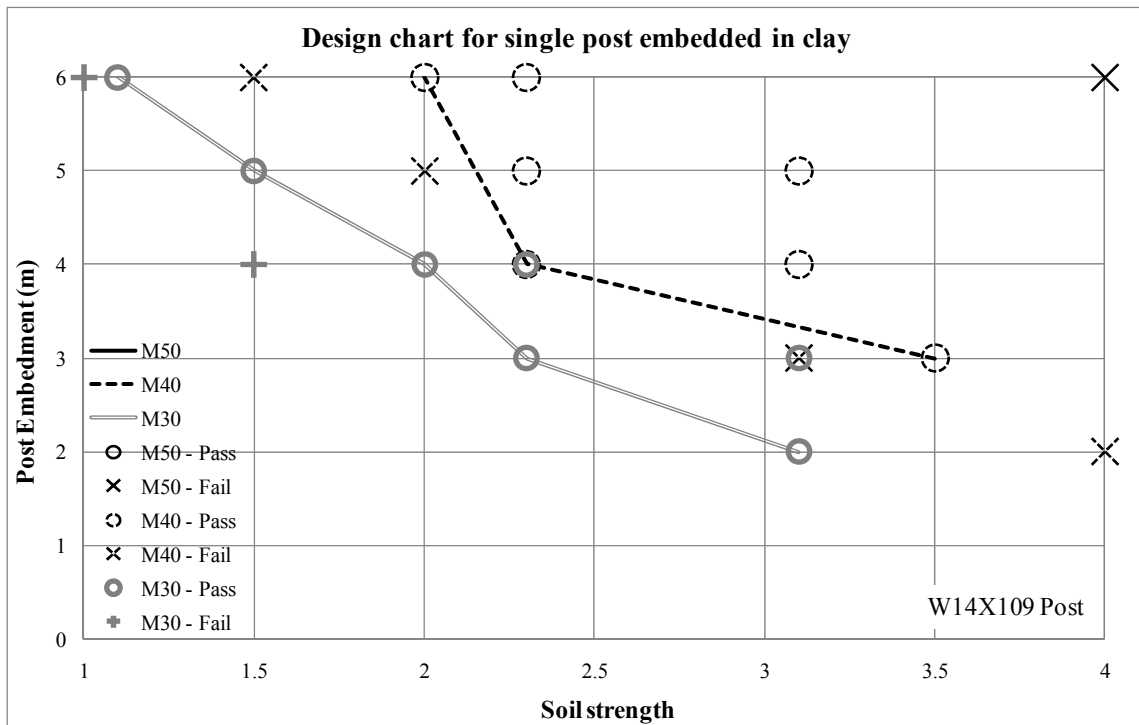
Figure 4.85. Result of numerical simulation for single post embedded in clay

4.4.3 Group of posts results

The group of posts system consisted of eight side by side posts with the impact taking place between the two center posts. The design charts were developed for the following parameters:

1. different soil categories (soft to very hard and loose to very dense)

2. same post cross section made of a wide flange steel I-beam(W14x90, 14 inches wide and weighing 90 lbs/ft of length)

3. same single beam made of a hollow steel square section (HSS10x10x1/2, 10 inches wide, 10 inches high, and ½ inches wall thickness)

4. different post clear spacing (2.44m, 4.88m, 7.32m)

5. different post embedment (1m to 6m)

6. same truck mass of 6800kg

7. different truck velocities (80km/h or M50, 65km/h or M40, 50km/h or M30)

Design method for group of posts consists of six charts: M50-sand, M40-sand, M30-sand, M50-clay, M40-clay and M30-caly. Horizontal and vertical axes of the chart represent soil strength from the proposed soil strength category and post embedment, respectively. Each design chart has three group of posts design according to three post clearances, 2.44 m, 4.88 m and 7.32 m. Post clearance is the distance measured form the end of one post to the end of the other post.

Design charts for group of posts in sand are shown in Figure 4.86, Figure 4.87 and Figure 4.88 for impact condition M50, M40 and M30, respectively. Circles and crosses on design chart represent each simulation result of pass to fail to meet the design requirements. Each design line for post spacing was drawn by connecting circles with minimum post embedment depth.

Design charts for group of posts in clay were developed in the same manner with the sand charts. Design charts for group of posts in clay are shown in Figure 4.89, Figure 4.90 and Figure 4.91 for impact condition M50, M40 and M30, respectively.
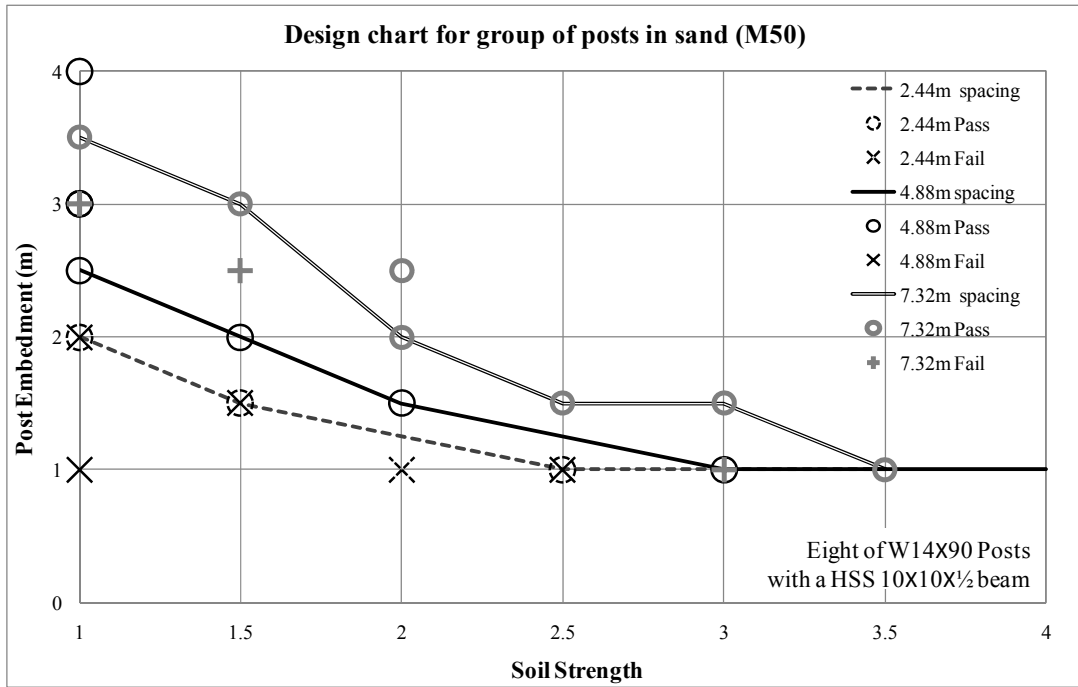
Figure 4.86. Result of numerical simulation for group of posts in sand (M50)
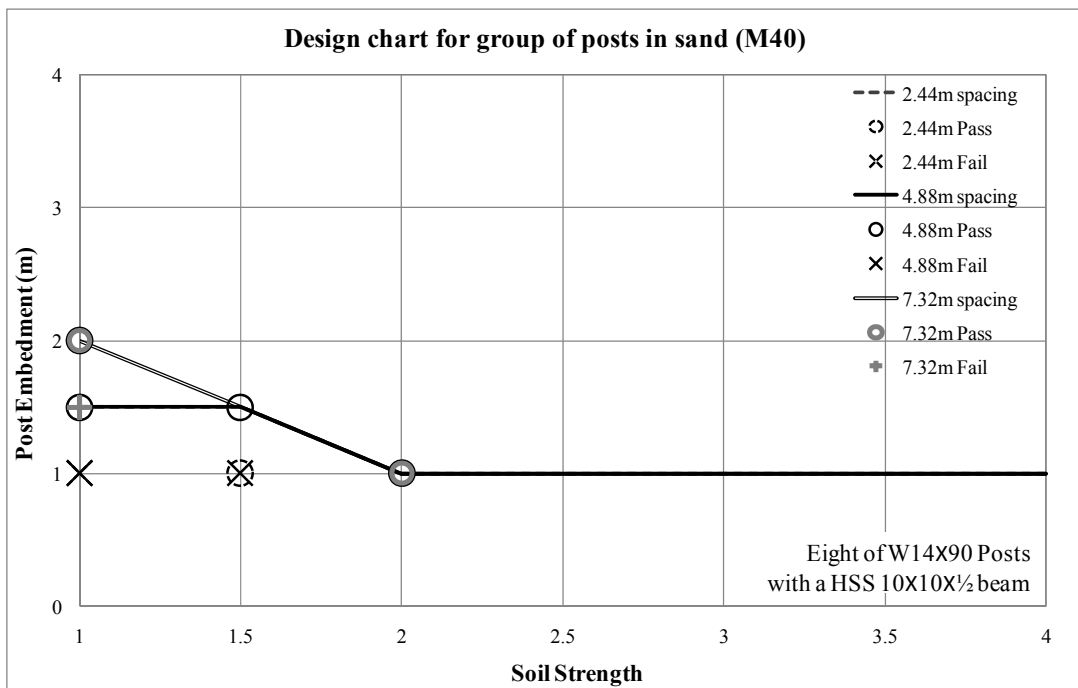
Figure 4.87. Result of numerical simulation for group of posts in sand (M40)
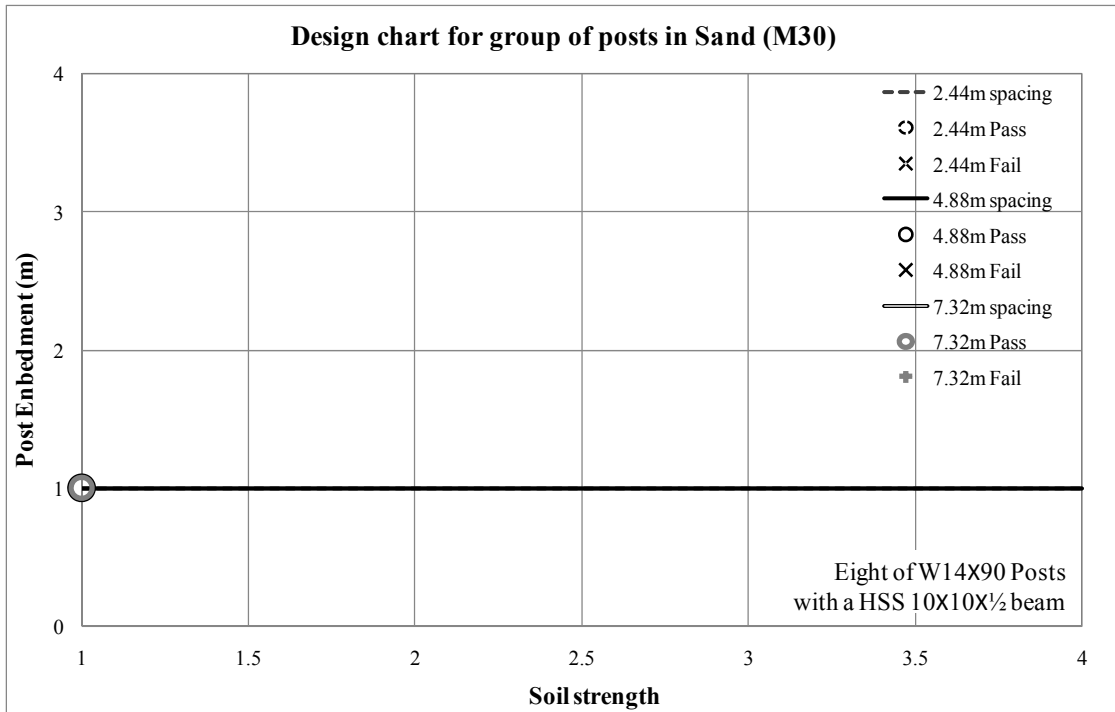
Figure 4.88. Result of numerical simulation for group of posts in sand (M30)
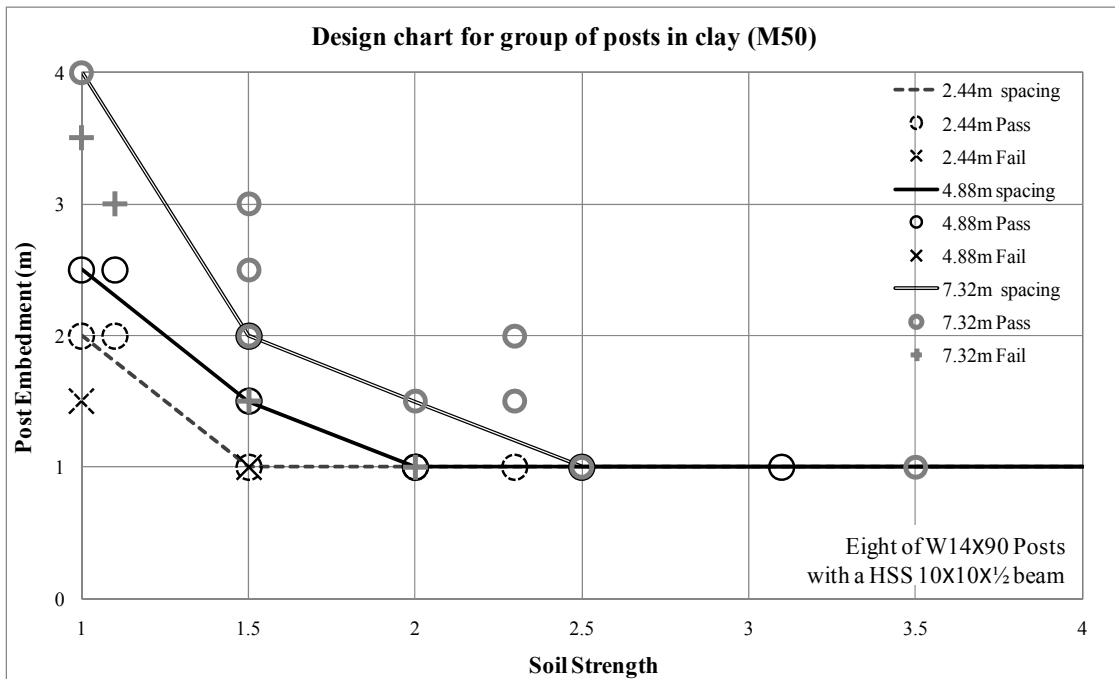
Figure 4.89. Result of numerical simulation for group of posts in clay (M50)

Design chart for group of posts in clay (M40)
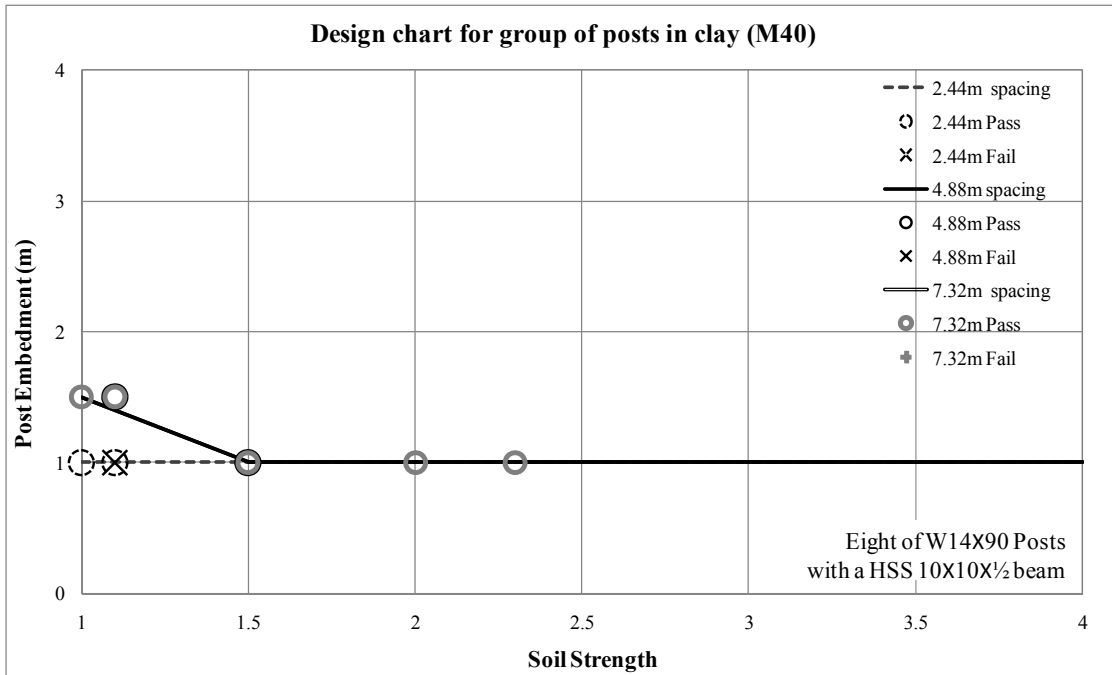
Figure 4.90. Result of numerical simulation for group of posts in clay (M40)

Design chart for group of posts in clay (M30)
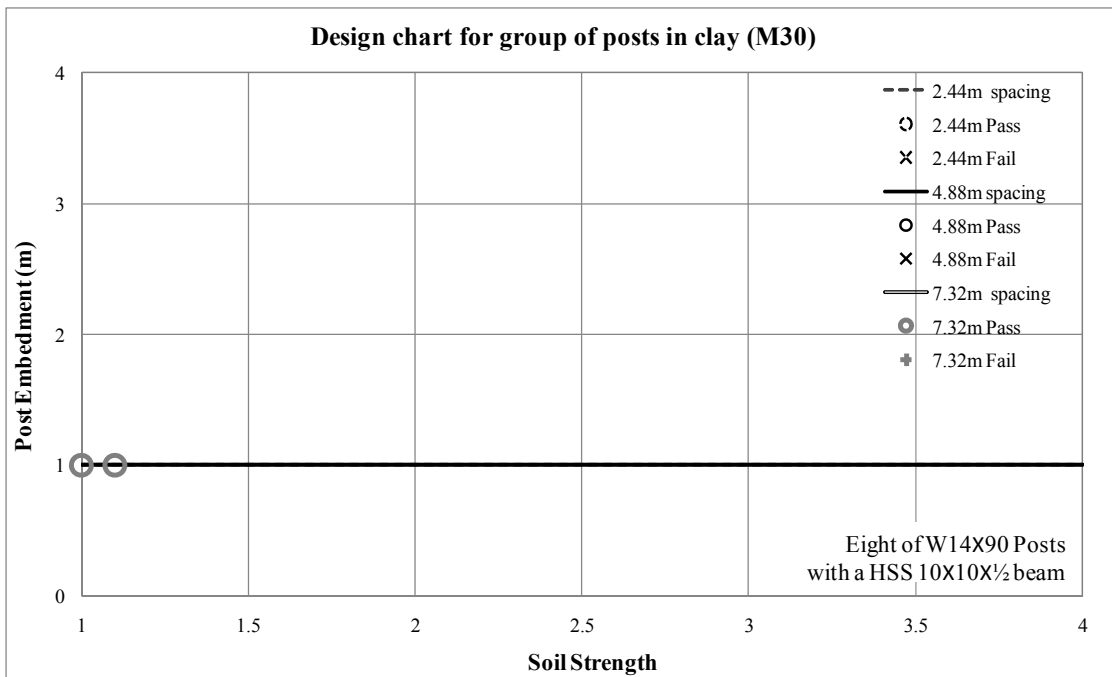
Figure 4.91. Result of numerical simulation for group of posts in clay (M30)

4.4.4 Conclusions

Design guideline for post system directly embedded in soil was developed using a set of numerical simulations using LS-DYNA based on the soil strength category. The developed design guideline is capable of designing single or group of posts system that can meet the requirements of the vehicle impact of designation M50, M40 and M30 with P1 penetration rating from ASTM F2656-07.

The proposed design guideline largely consists of four parts: single post in sand, single post in clay, group of posts in sand and group of posts in clay. For Group of posts system, clearances between each post were limited for three cases: 2.44 m, 4.88 m and 7.32 m. Each result of numerical simulations was indicated as a circle or cross on design chart. Circle means that result of numerical simulation corresponding soil strength and post embedment could meet the requirement. Each design line for impact condition designation or post spacing was drawn by simply connecting circles having minimum post embedment depth.

The design guideline was developed using a certain post configuration. The design chart for single post was developed using a wide flange beam, W14X109. Thus single post system should be installed using a post with equivalent to W14-109 Post or even stronger post in terms of post width and bending stiffness. In addition to the embedment depth, at least 1.5 m of post length above the ground level is required. In the same manner, the group of posts system needs at least eight of W14-90 post, four posts on each side of the impact location with a horizontal beam with hollow section HSS 10X10X1/2. Also at least 1.5m of post length above the ground level is needed. The post

and beam member having equivalent or stiffer bending stiffness can be used with cautious calculations.

It is recommended however that the cases with shallow embedment be verified at full scale because it is not clear that the simulation properly account the soil behavior at shallow depths including post pull-out. Thus the minimum post embedment depth is recommended as 2 m.

5. DESIGN GUIDELINES

Design guideline for post systems directly embedded in soil to arrest vehicle impact was developed and verified using the finite element analysis and the full-scale experiments. The designed post system using this method is capable of fulfilling the requirements of condition designations, M50, M40 and M30 with penetration rating P1 of ASTM F2656-07.
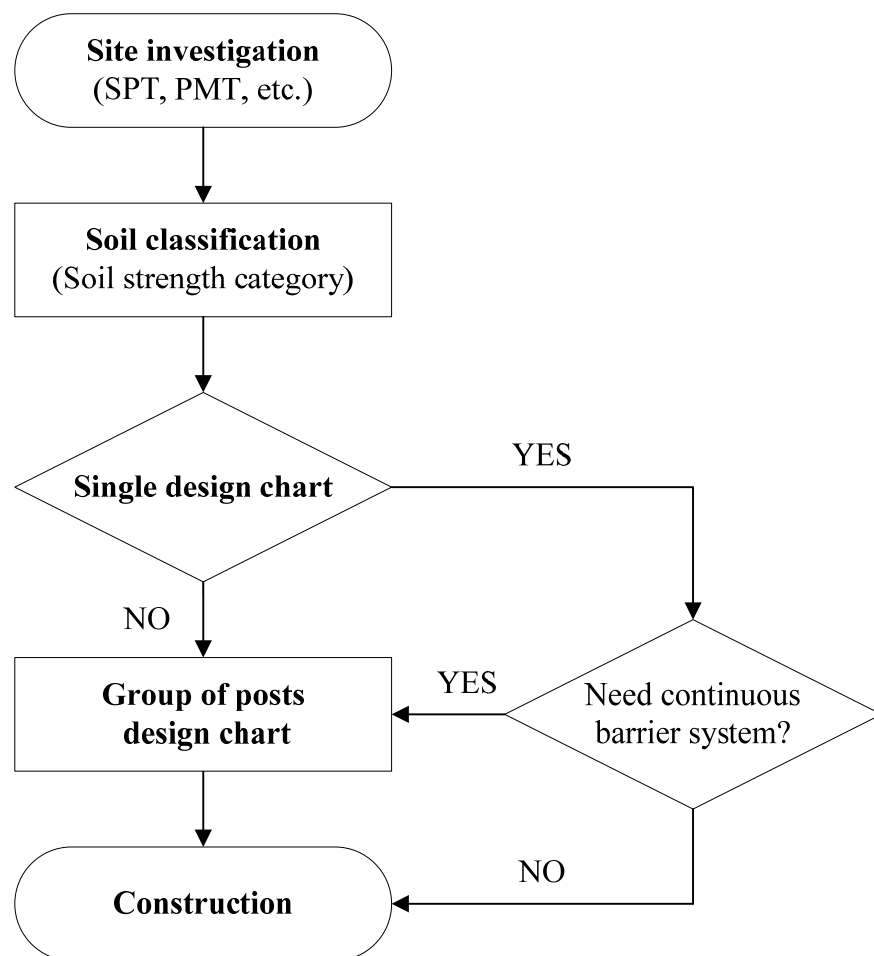
Figure 5.1. Recommended design procedure

Limitation on the design method is that member of post system cannot be changed besides the members used on the finite element analysis. W14X109 beam was used as a post member in developing single post design chart. W14X90 beams and HSS10X10X1/2 tube were used as posts and horizontal beam members, respectively. Each member of post system can be substituted by beams or tubes having same or larger width and bending stiffness. Also 1.5 m or more of post length above the ground level is required in addition to post embedment.

The first step of design procedure is subsurface exploration including either standard penetration test or pressuremeter test. The second step is classifying soil using the result of soil testing and the proposed soil strength classification and Unified Soil Classification System (USCS). Then, post system can be determined by using the proposed design chart as shown in Figure 5.1.

Design chart for single post embedded in sand are shown in Figure 5.2. Soil strength number on horizontal axis of the chart can be replaced with blow count of standard penetration test and pressuremeter limit pressure as shown in Figure 5.3 and Figure 5.4. In the same manner, design charts for single post embedded in clay are shown in Figure 5.5, Figure 5.6 and Figure 5.7. There are three design lines representing each impact condition designation on each chart. Design post embedment can be determined by reading coordinate of vertical axis corresponding soil strength and impact condition designation. If there is no corresponding post embedment on the single post chart, the solution will be either using design chart for group of posts system or ground modification to increase soil strength.
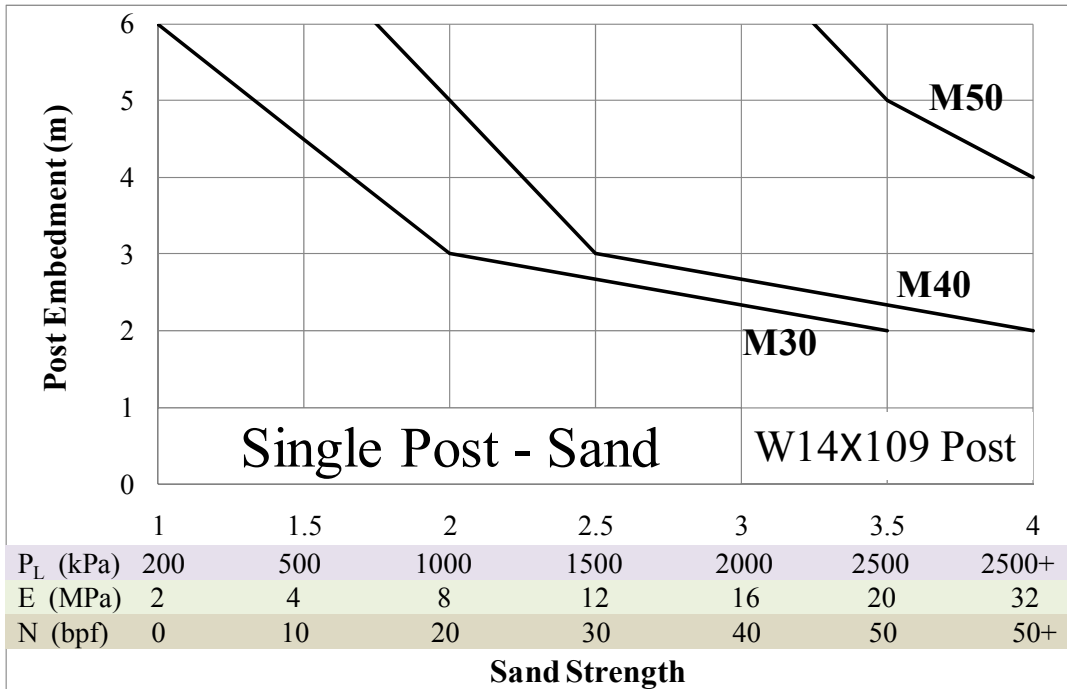
Figure 5.2. Design chart for single post in sand
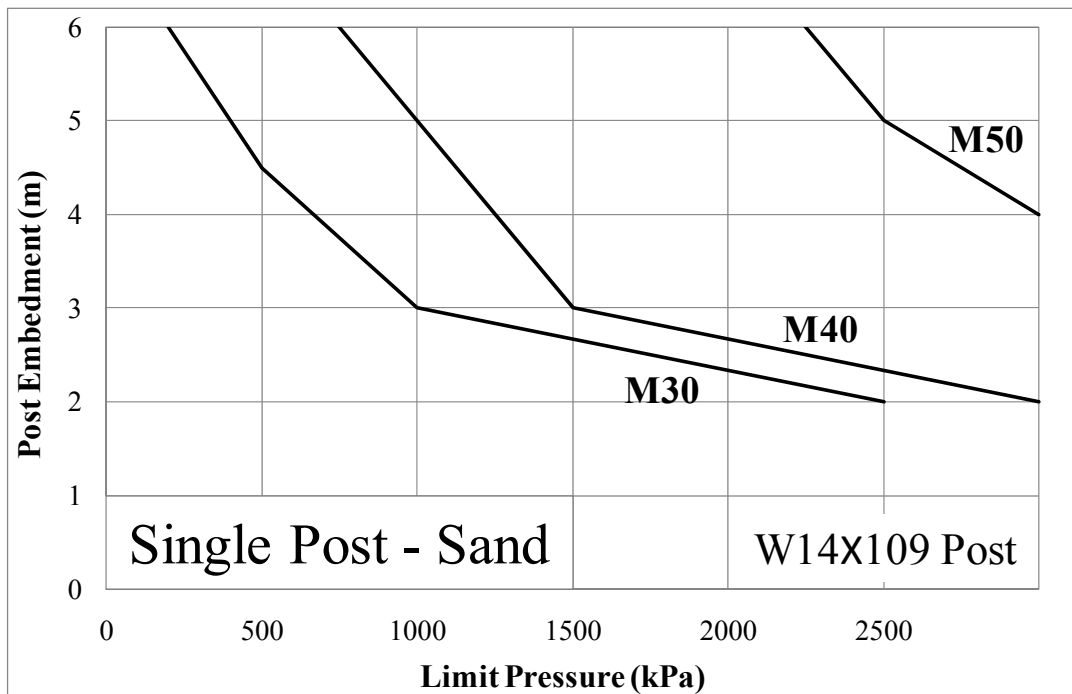
Figure 5.3. Design chart for single post in sand (PMT limit pressure)
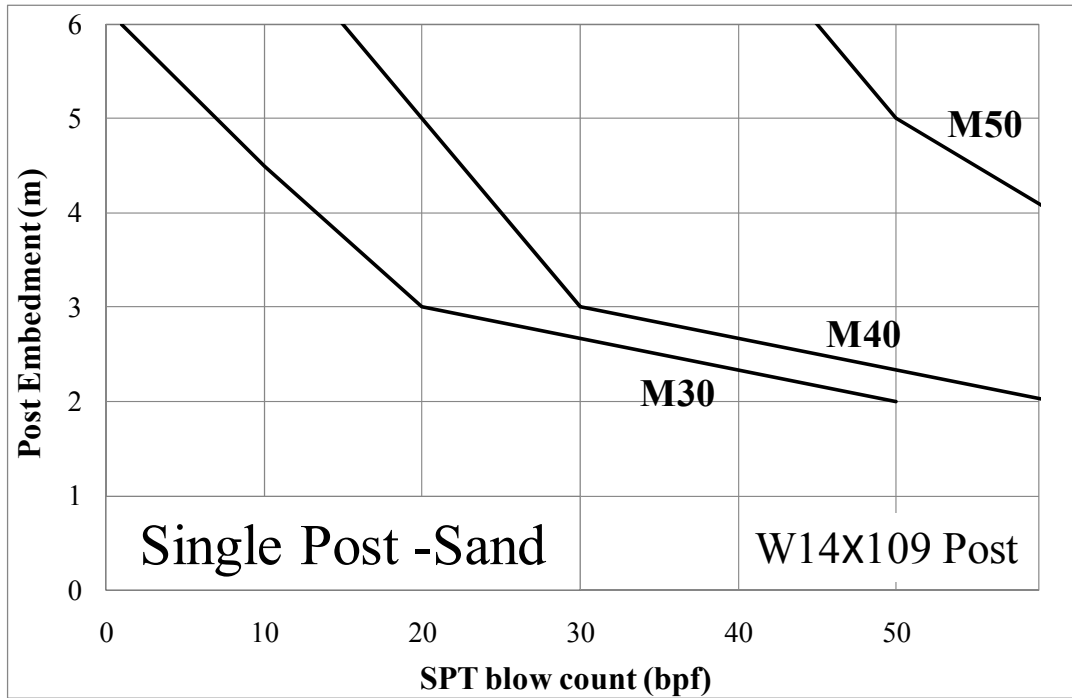
Figure 5.4. Design chart for single post in sand (SPT blow count)
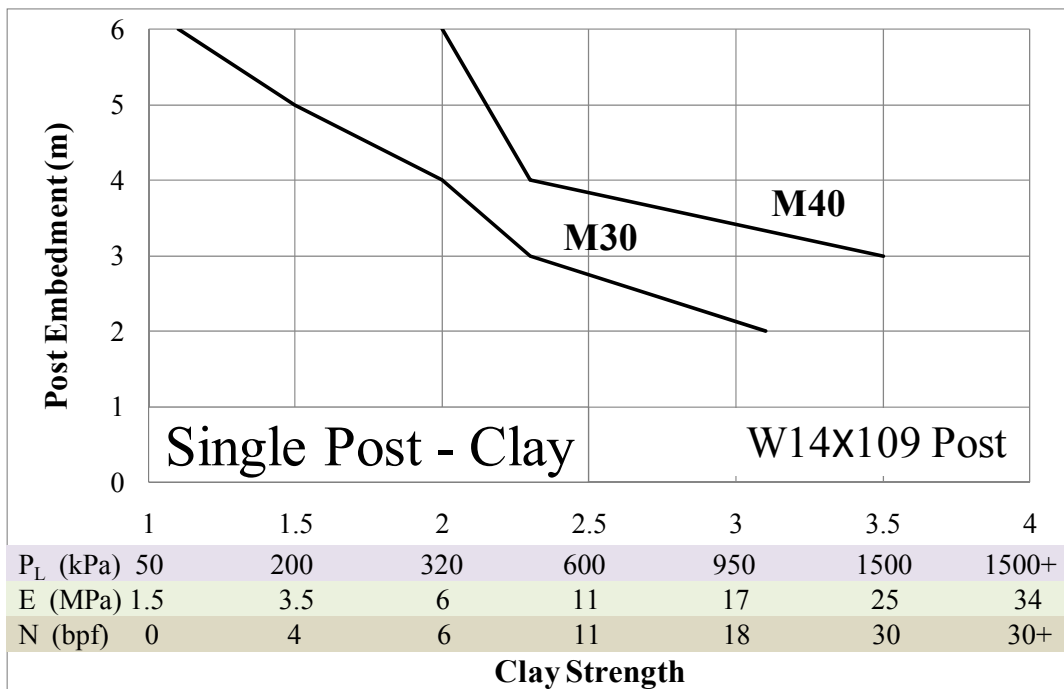

Figure 5.5. Design chart for single post in clay
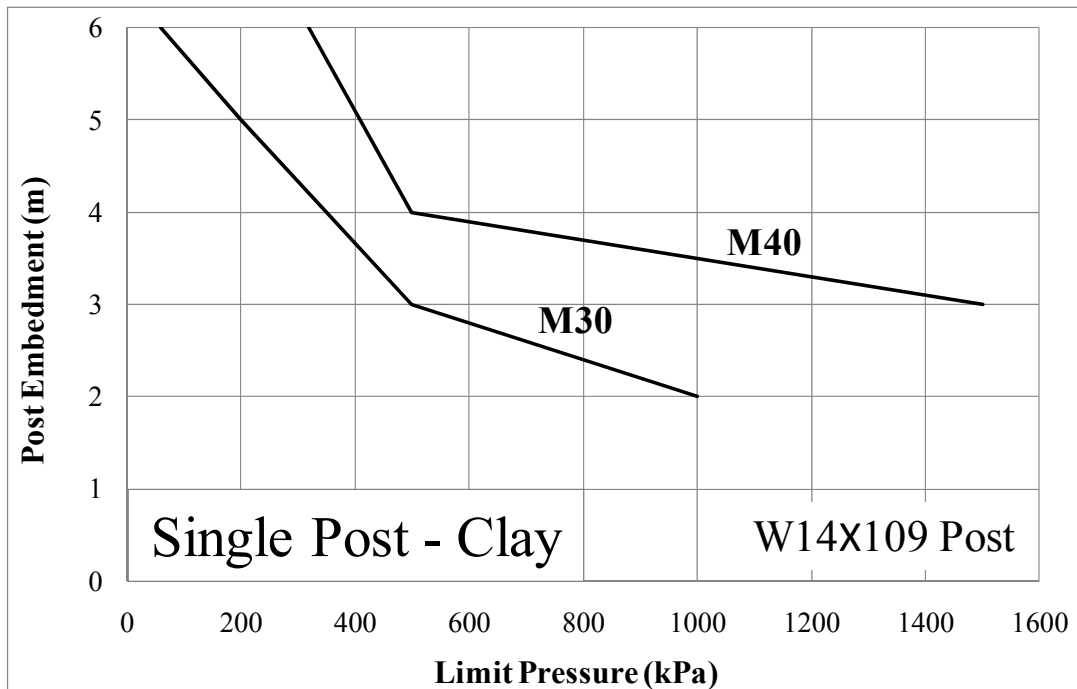
Figure 5.6. Design chart for single post in clay (PMT limit pressure)
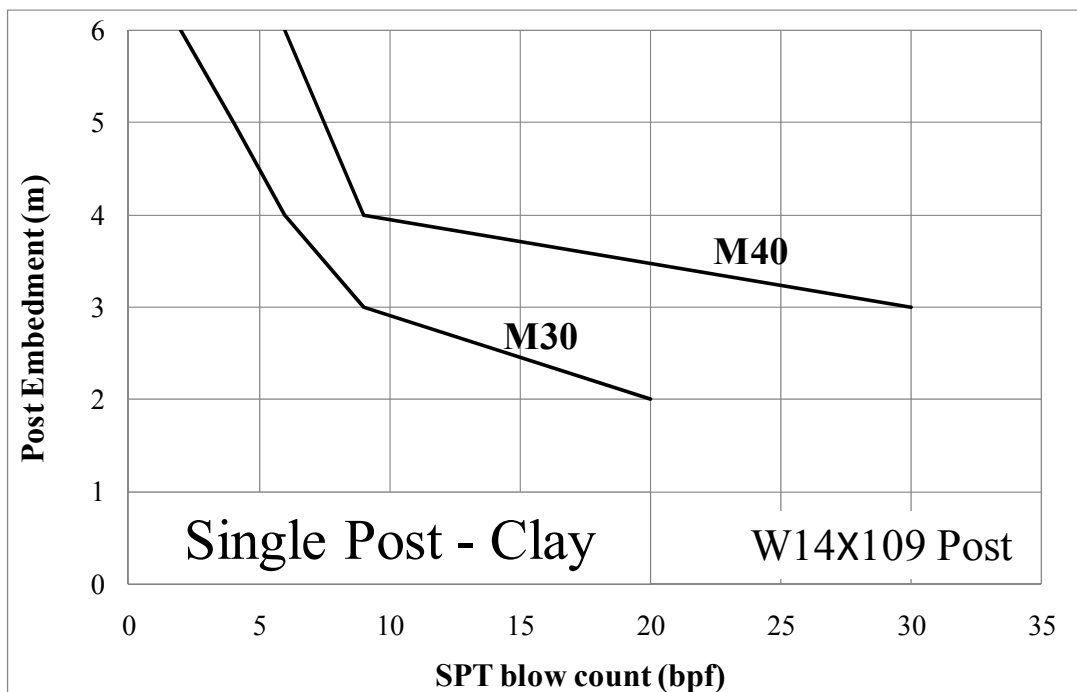
Figure 5.7. Design chart for single post in clay (SPT blow count)

Design charts for group of posts are needed when single post cannot arrest vehicle impact or continuous barrier system is required. There is an addition variable, post spacing or post clearance on designing group of posts system. Thus design chart for group of posts consists of six charts: M50-sand, M40-sand, M30-sand, M50-caly, M40-clay and M30-clay. Three design lines on each chart represent three.post clearance: 2.44 m 4.88 m and 7.32 m. Soil strength number on horizontal axis of the chart was replaced with blow count of standard penetration test and pressuremeter limit pressure for all six of design charts. Design post embedment can be determined by reading coordinate of vertical axis corresponding soil strength and impact condition designation. Design charts for group of posts in sand are shown in Figure 5.8 through Figure 5.16. Those of clay are shown in Figure 5.17 through Figure 5.25.

It is recommended however that the cases with shallow embedment be verified at full scale because it is not clear that the simulation properly account the soil behavior at shallow depths including post pull-out. Thus the minimum post embedment depth is recommended as 2 m.
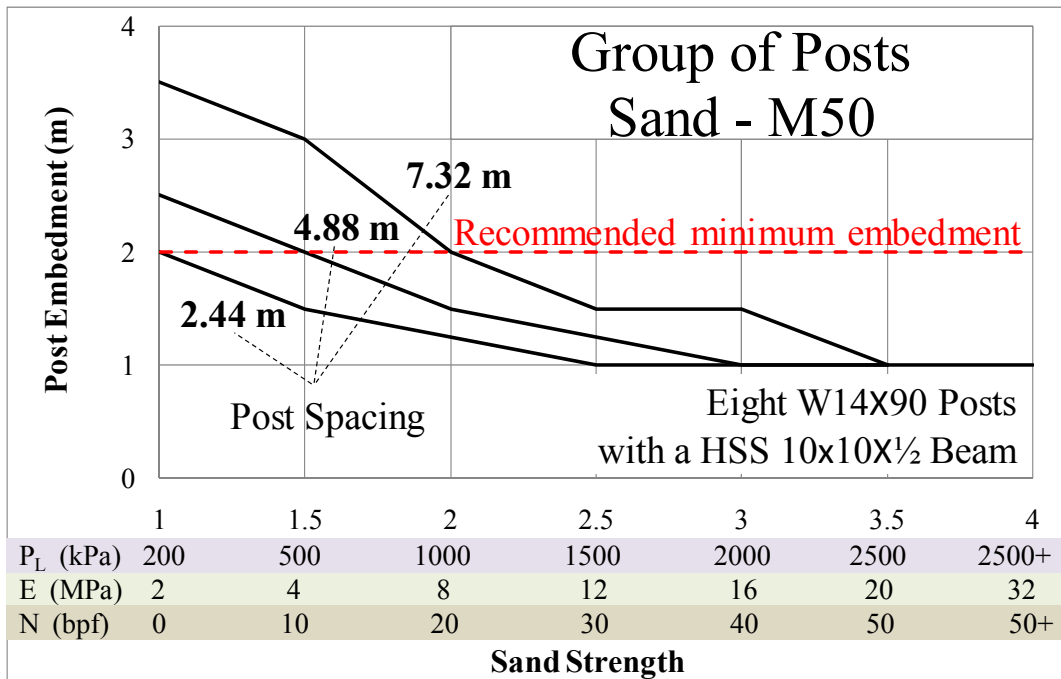
Figure 5.8. Design chart for M50 group of posts in sand
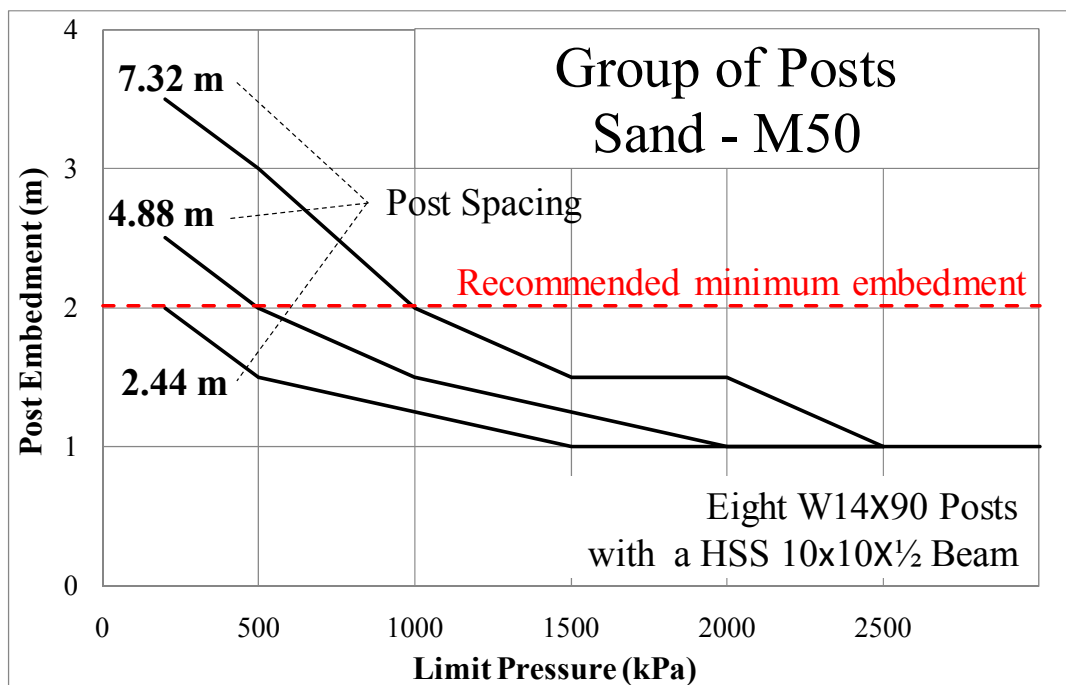
Figure 5.9. Design chart for M50 group of posts in sand (PMT limit pressure)
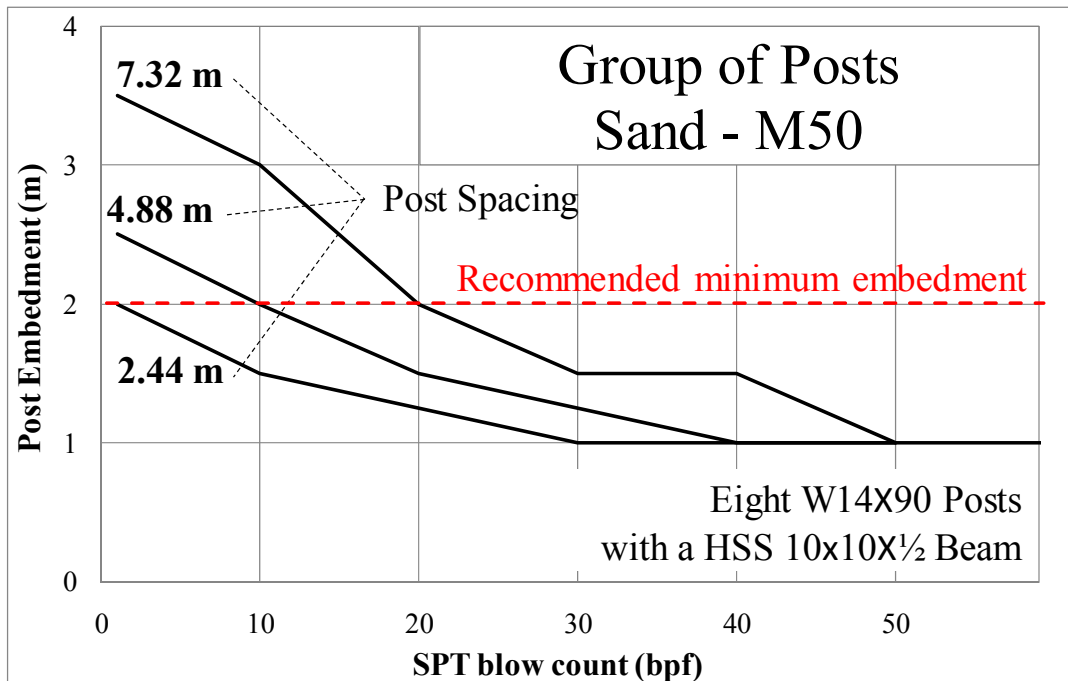
Figure 5.10. Design chart for M50 group of posts in sand (SPT blow count)
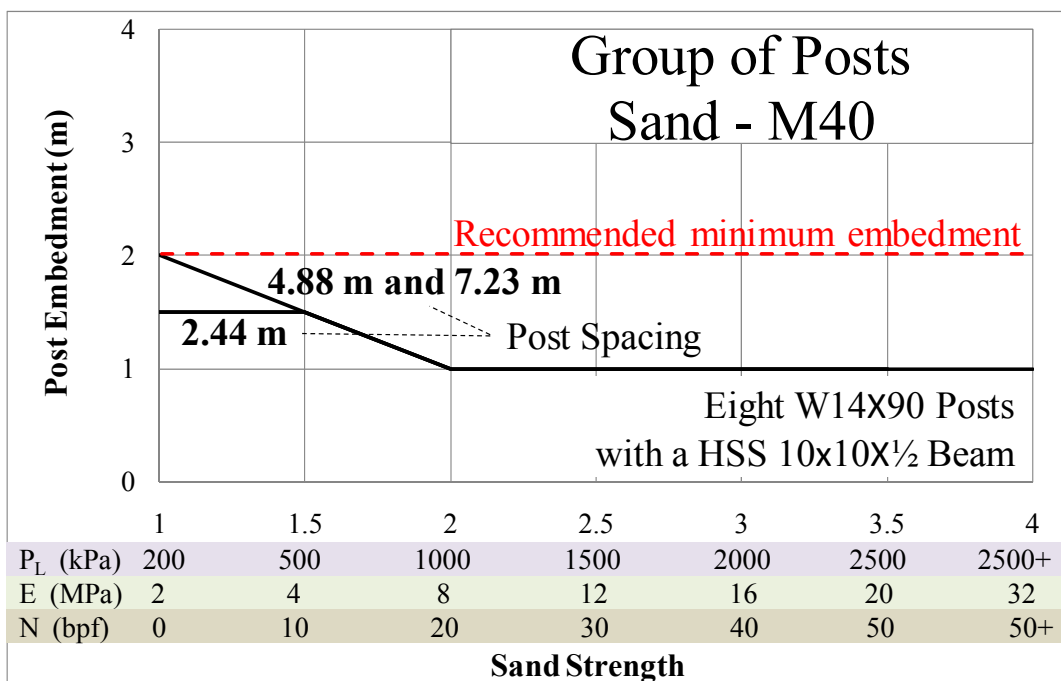
Figure 5.11. Design chart for M40 group of posts in sand
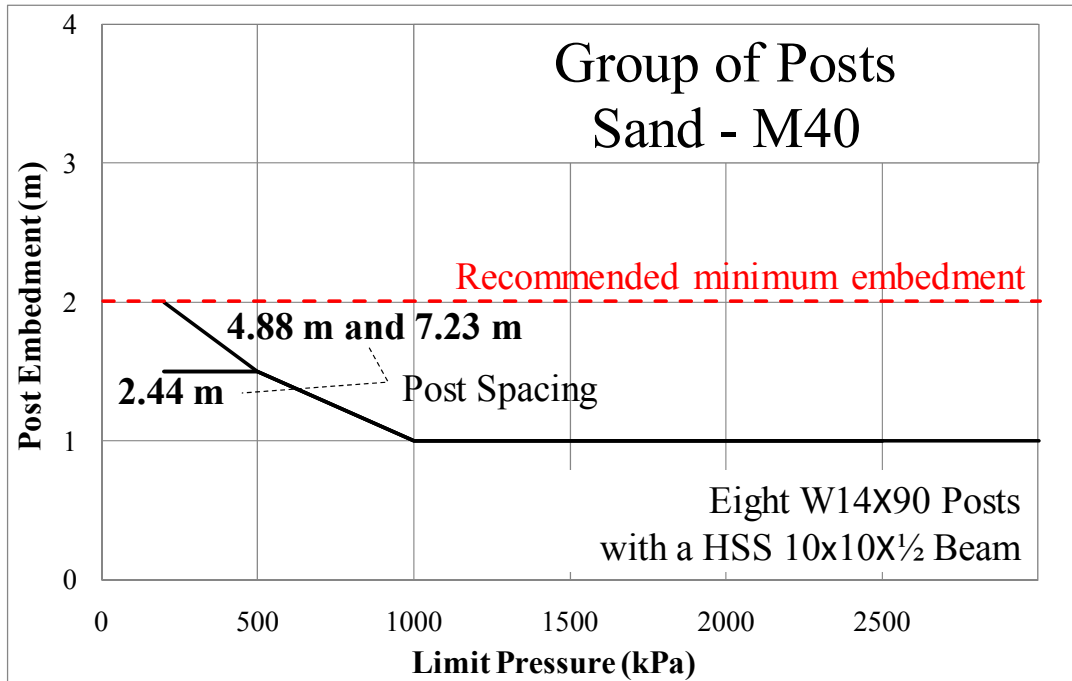
Figure 5.12. Design chart for M40 group of posts in sand (PMT limit pressure)
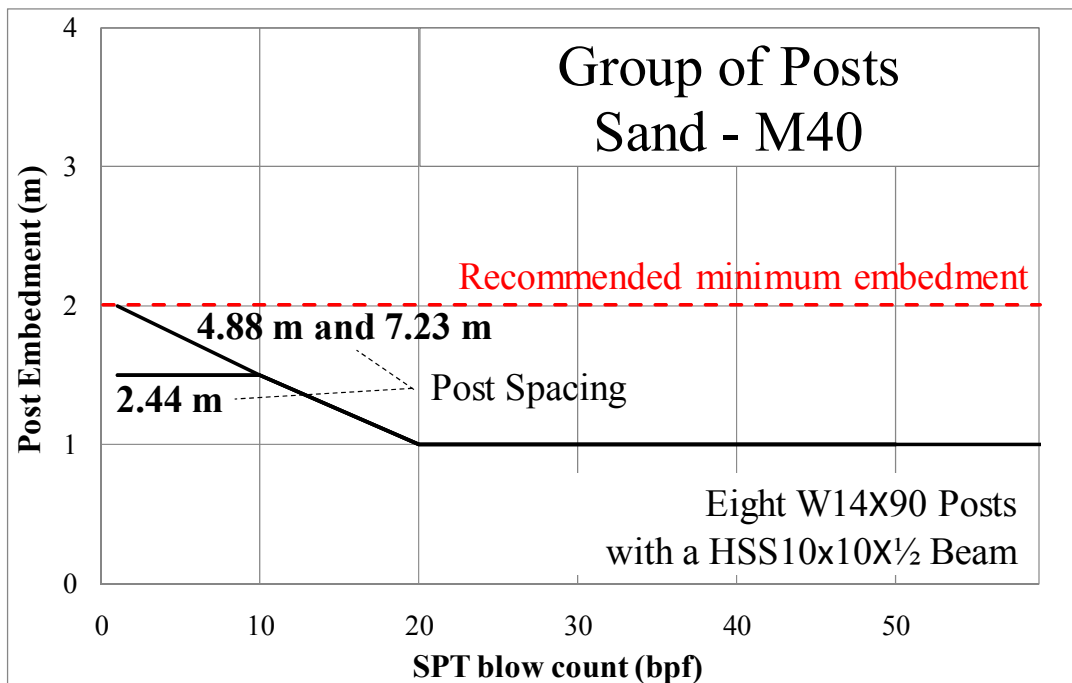
Figure 5.13. Design chart for M40 group of posts in sand (SPT blow count)

308
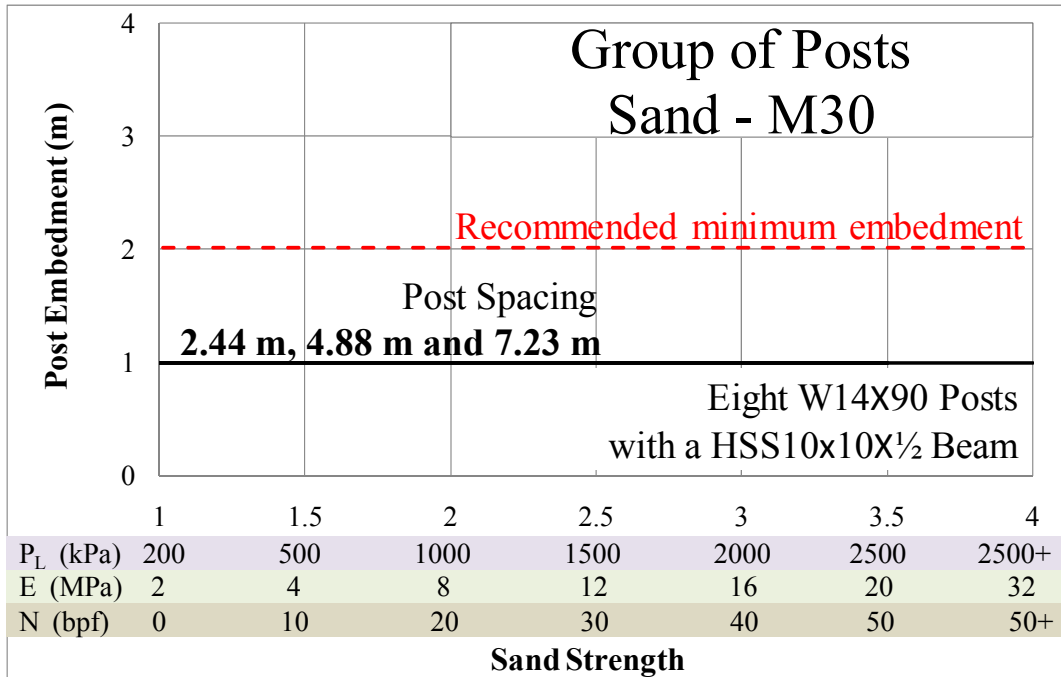
Figure 5.14. Design chart for M30 group of posts in sand
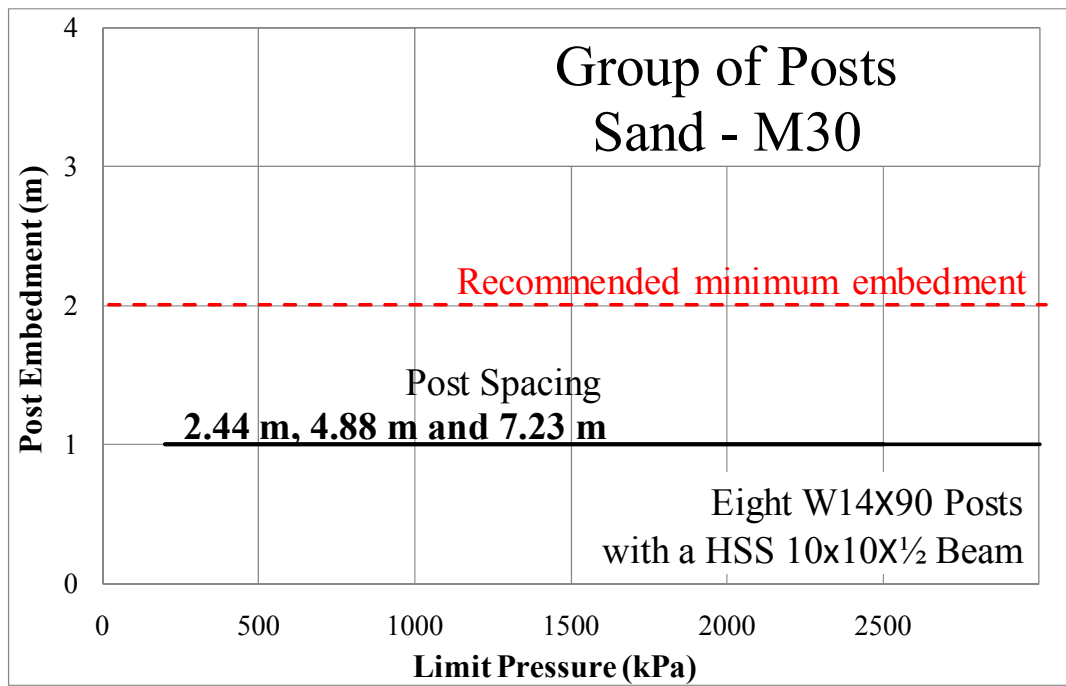
Figure 5.15. Design chart for M30 group of posts in sand (PMT limit pressure)
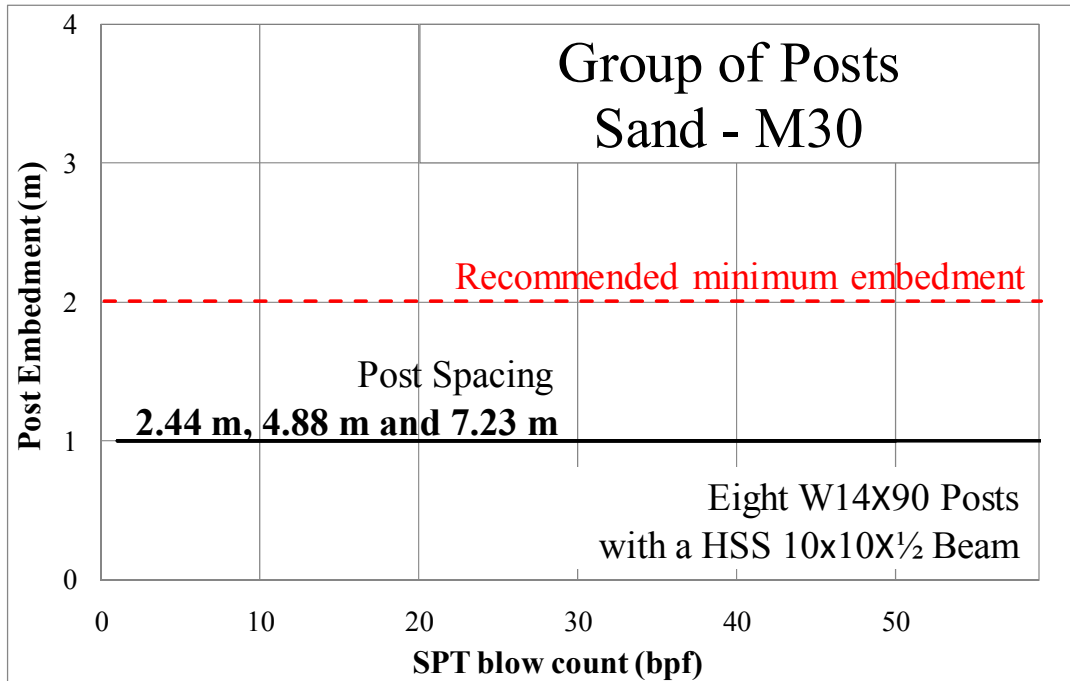
Figure 5.16. Design chart for M30 group of posts in sand (SPT blow count)
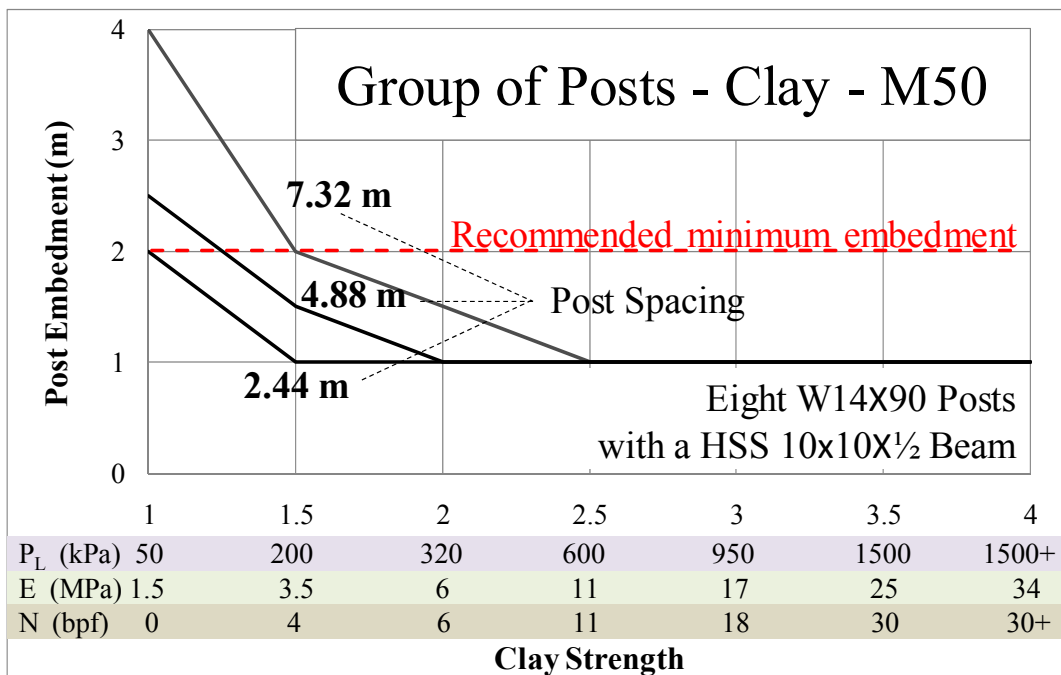
Figure 5.17. Design chart for M50 group of posts in clay
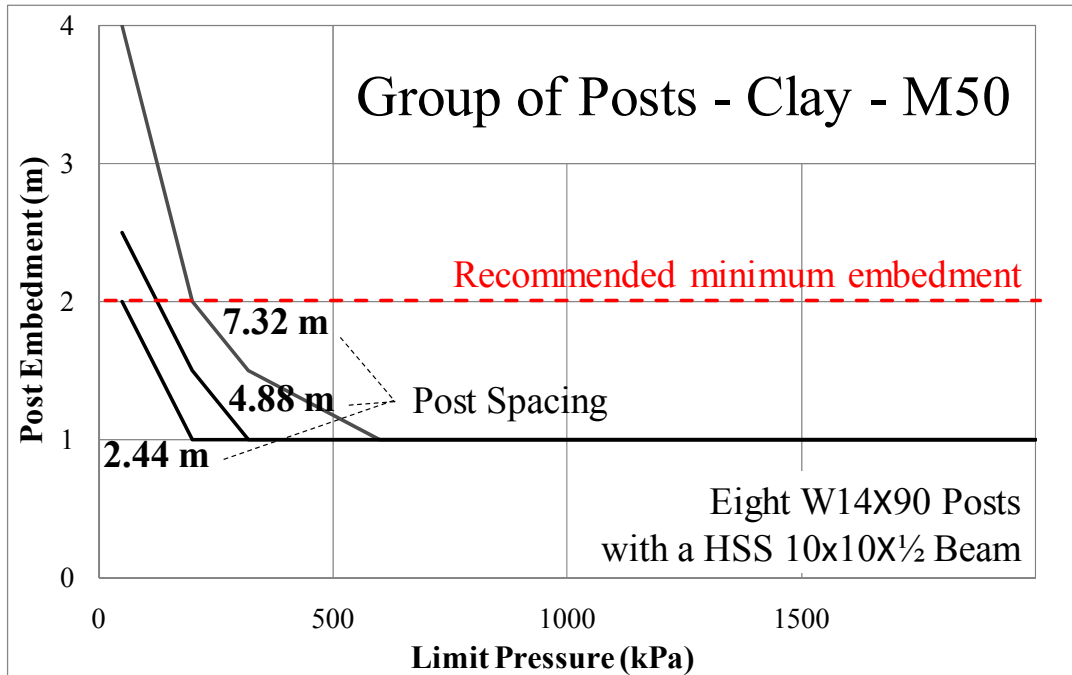
Figure 5.18. Design chart for M50 group of posts in clay (PMT limit pressure)
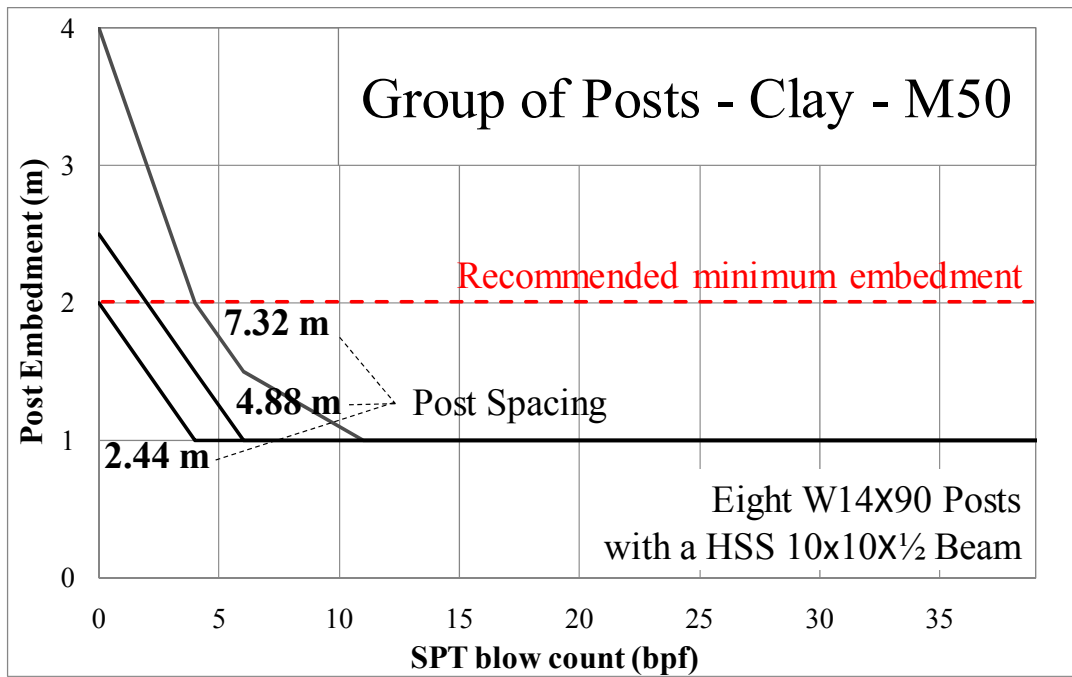
Figure 5.19. Design chart for M50 group of posts in clay (SPT blow count)
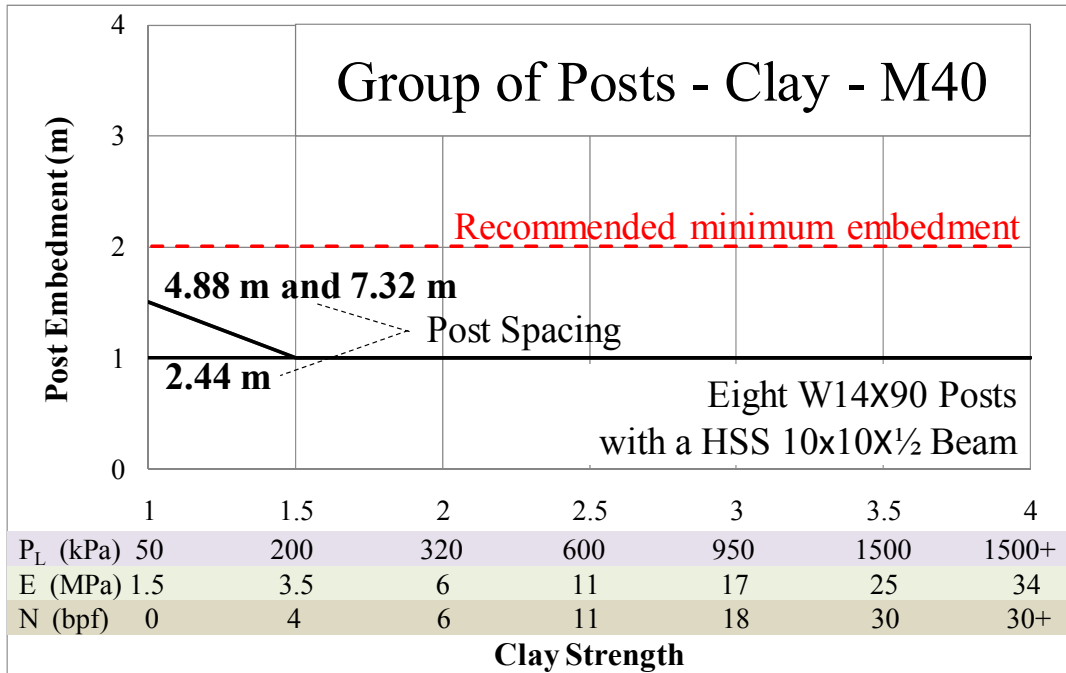
Figure 5.20. Design chart for M40 group of posts in clay
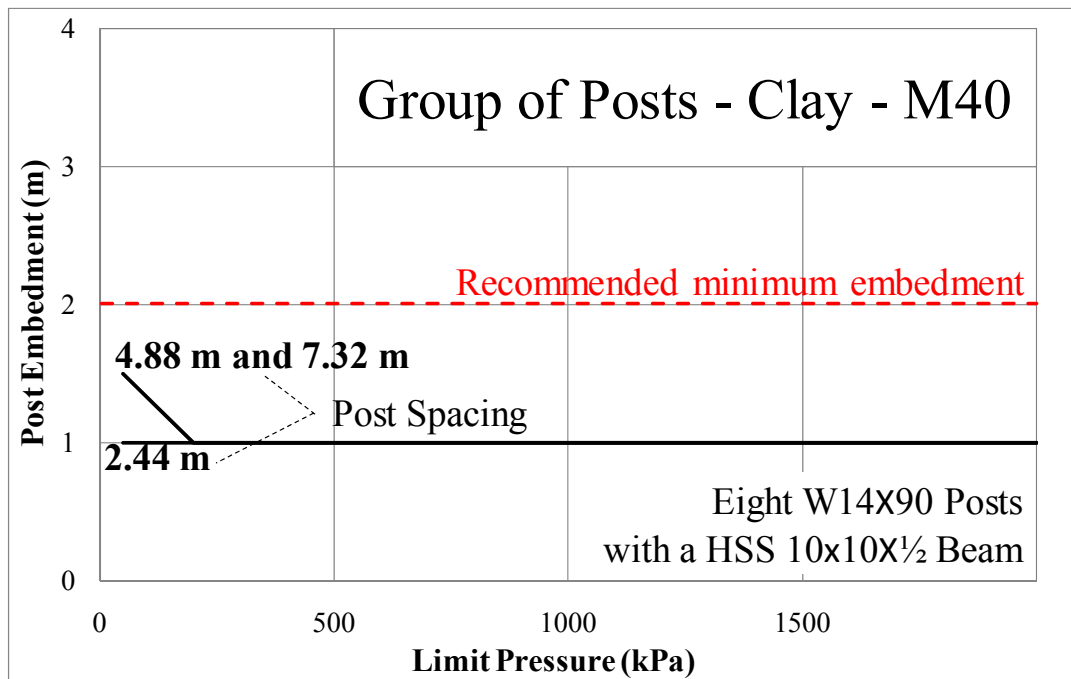
Figure 5.21. Design chart for M40 group of posts in clay (PMT limit pressure)
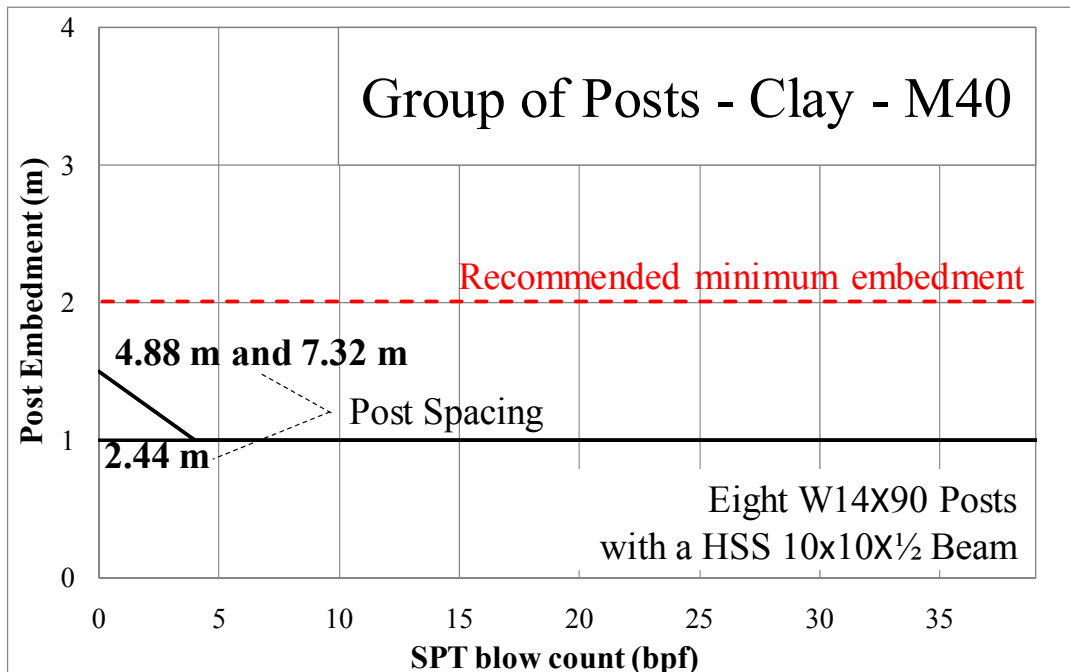
Figure 5.22. Design chart for M40 group of posts in clay (SPT blow count)
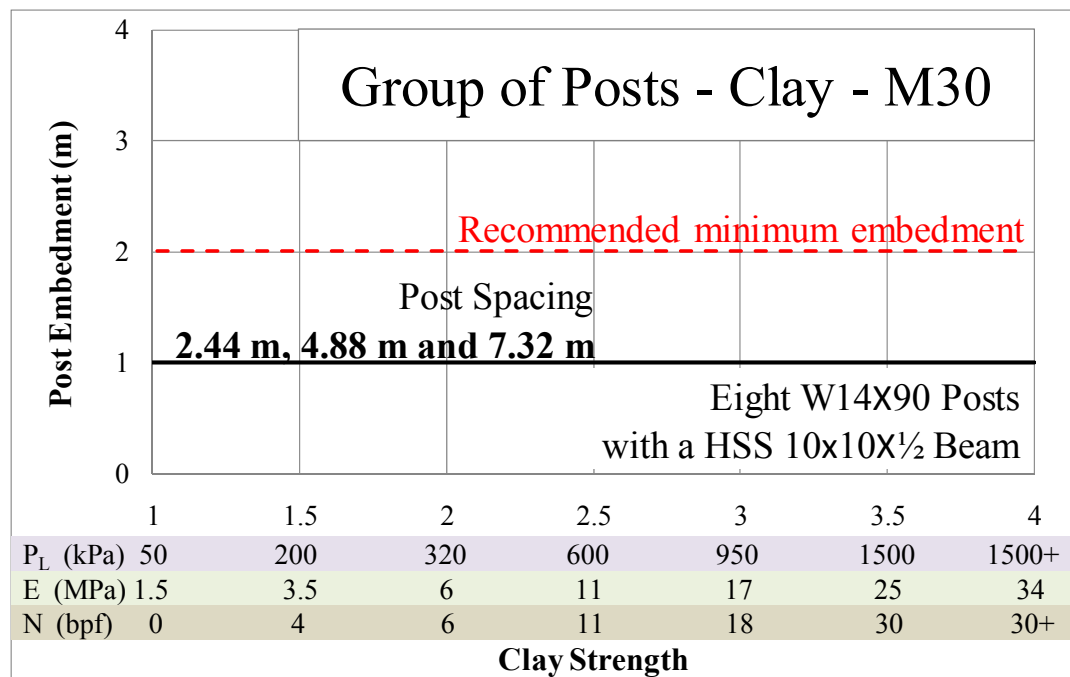
Figure 5.23. Design chart for M30 group of posts in clay
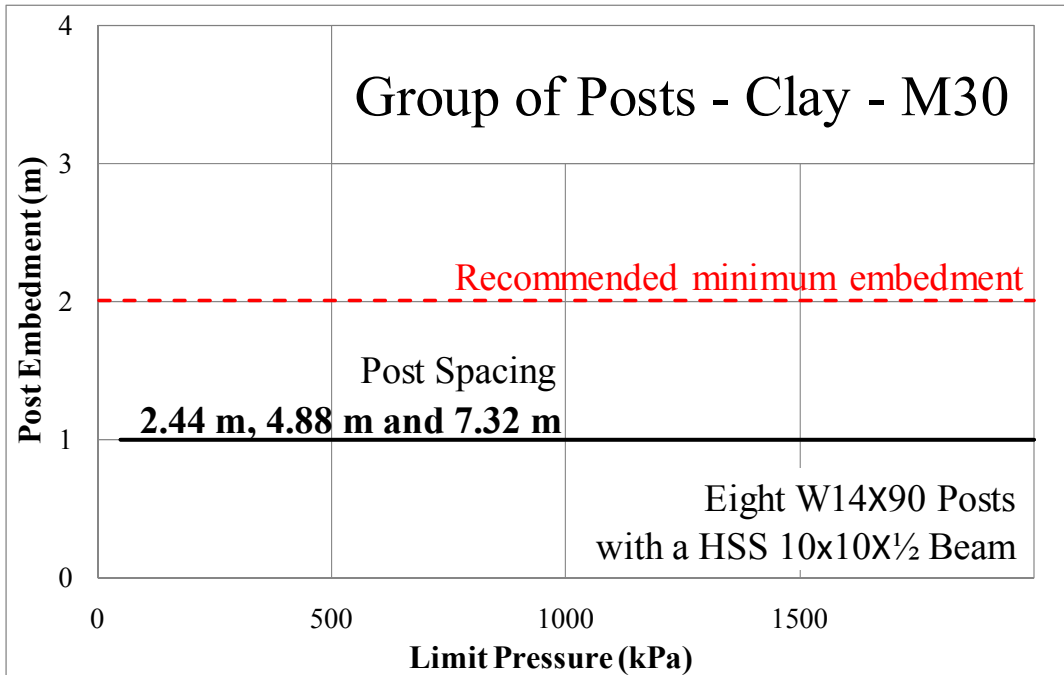
Figure 5.24. Design chart for M30 group of posts in clay (PMT limit pressure)
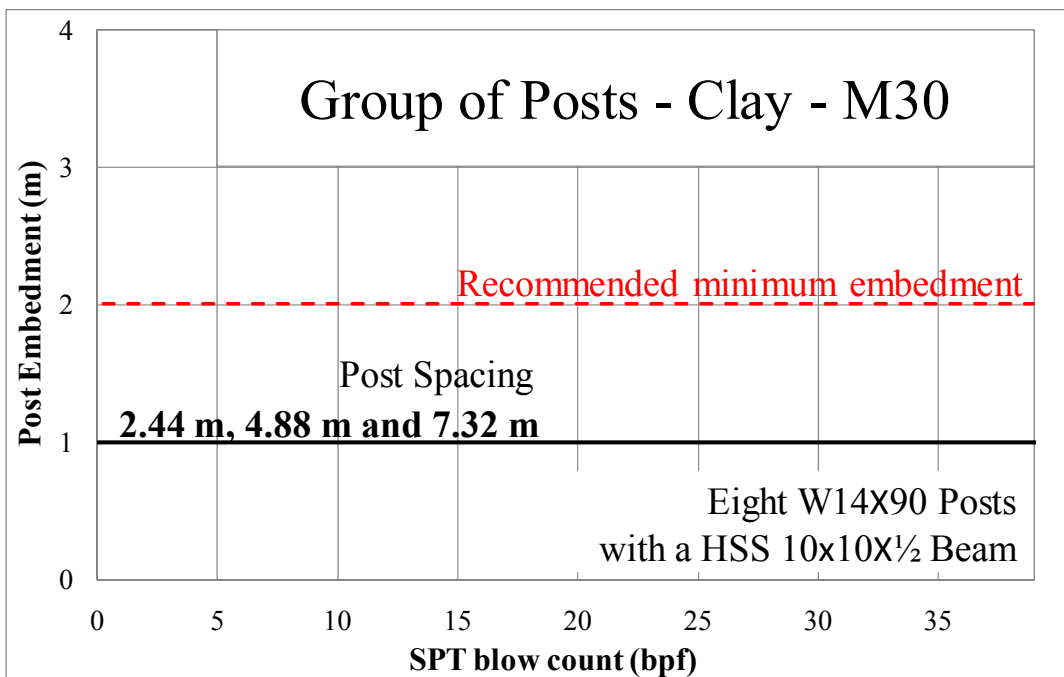
Figure 5.25. Design chart for M30 group of posts in clay (PMT limit pressure)

The design using these design charts should proceed:

1. Perform a site investigation including as a minimum SPT samples and blow count. Mini-pressuremeter tests are highly recommended in addition to SPT tests.

2. Classify the soil according to the Unified Soil Classification System. If the soil is found to be coarse grained according to the USCS, then the sand charts should be used. If the soil is found to be fine grained then the clay charts should be used.

3. Try first the single post design chart corresponding to the right soil and the right truck speed. Enter the soil strength on the horizontal axis and find out the necessary post embedment on the vertical axis. Note that the single posts design charts are for a W14x109 wide flange I beam. Any post which has at least this frontal width, bending stiffness and bending moment capacity is acceptable.

4. If a continuous barrier is desired, the single posts can be joined by a HSS10x10x1/2 beam provided the post spacing is less than or equal to 7.32m.

5. If no single post can be found to satisfy the design criteria, use the group of posts charts. Choose the one which corresponds to the right soil, and the right truck speed. Enter the soil strength on the horizontal axis and find out the necessary post embedment on the vertical axis for a given post spacing.

Note that the group of posts design charts are for a W14x90 posts connected by a HSS10x10x1/2 beam. Any post which has at least this frontal width, bending stiffness and bending moment capacity is acceptable. Any beam which has at least this bending stiffness, this bending moment capacity, and this tensile capacity is acceptable.

The following is an example (example. 1). A new anti-ram barrier needs to be designed to resist the penetration of a 6800 kg truck going 80 km/h (M50). The soil has an SPT blow count of 50 (blow/ft), a pressuremeter limit pressure of 2500 kPa, and a pressuremeter modulus of 23 MPa. The samples collected from the SPT are used to classify the soil according to the USCS which turns out to be SP (sand). The design chart for single post in sand (Figure 5.2) can be used in this case. As shown in Figure 5.26, W14-109 single posts with 5m of embedment can meet the requirements of M50 and P1.

The following is another example (example. 2). A new anti-ram barrier needs to be designed to resist the penetration of a 6800 kg truck going 80 km/h (M50) around an embassy. The soil has an SPT blow count of 10 (blow/ft), a pressuremeter limit pressure of 500 kPa, and a pressuremeter modulus of 4 MPa. The samples collected from the SPT are used to classify the soil according to the USCS which turns out to be SP (sand). According to the design chart for single post in sand (Figure 5.2), no single post can be found (Figure 5.27). A group of post is necessary and the design chart for M50 group of posts in sand (Figure 5.8) is selected as being the right one for this case (sand and M50). A spacing of 4.88 m is desirable and a post embedment of 2 m is found (Figure 5.28).
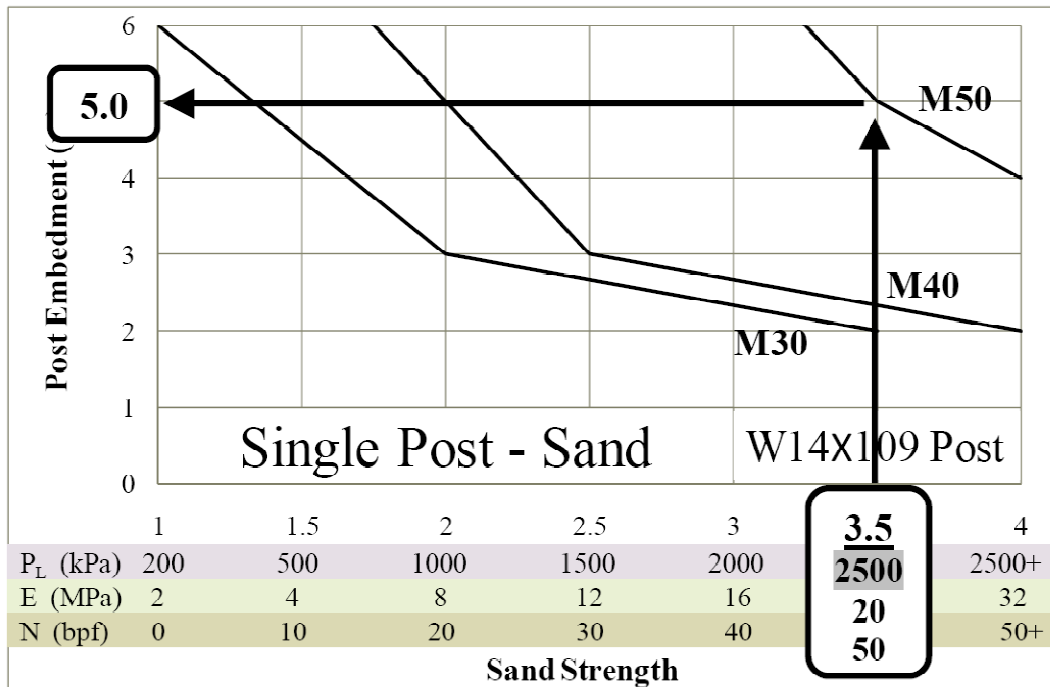
Figure 5.26. Design chart for single post in sand (Example. 1)
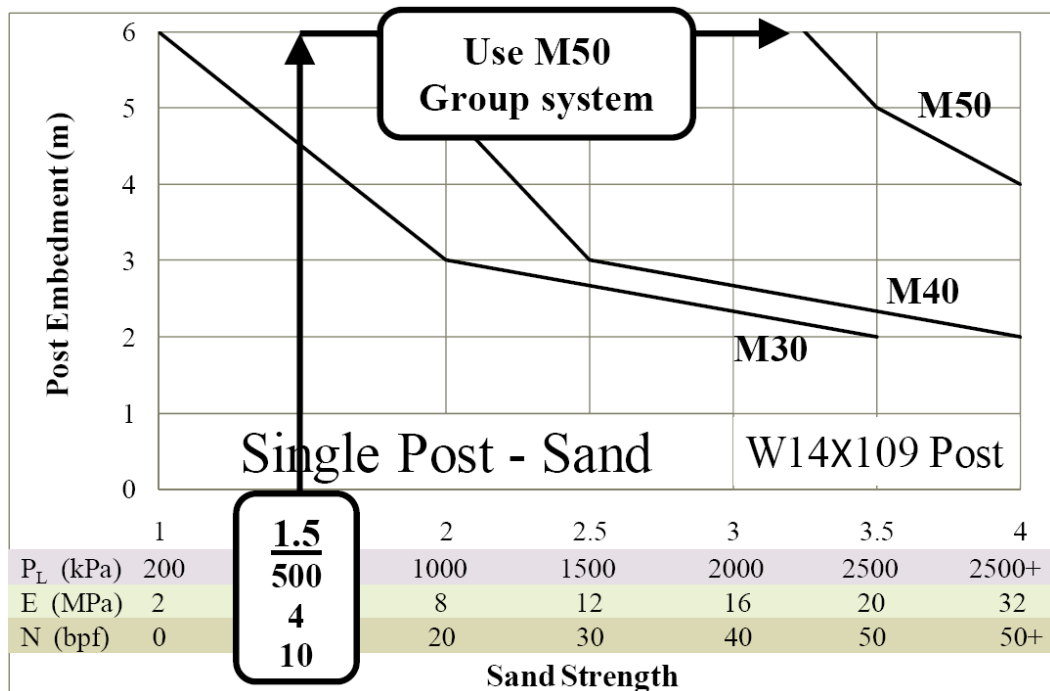
Figure 5.27. Design chart for single post in sand (Example. 2)
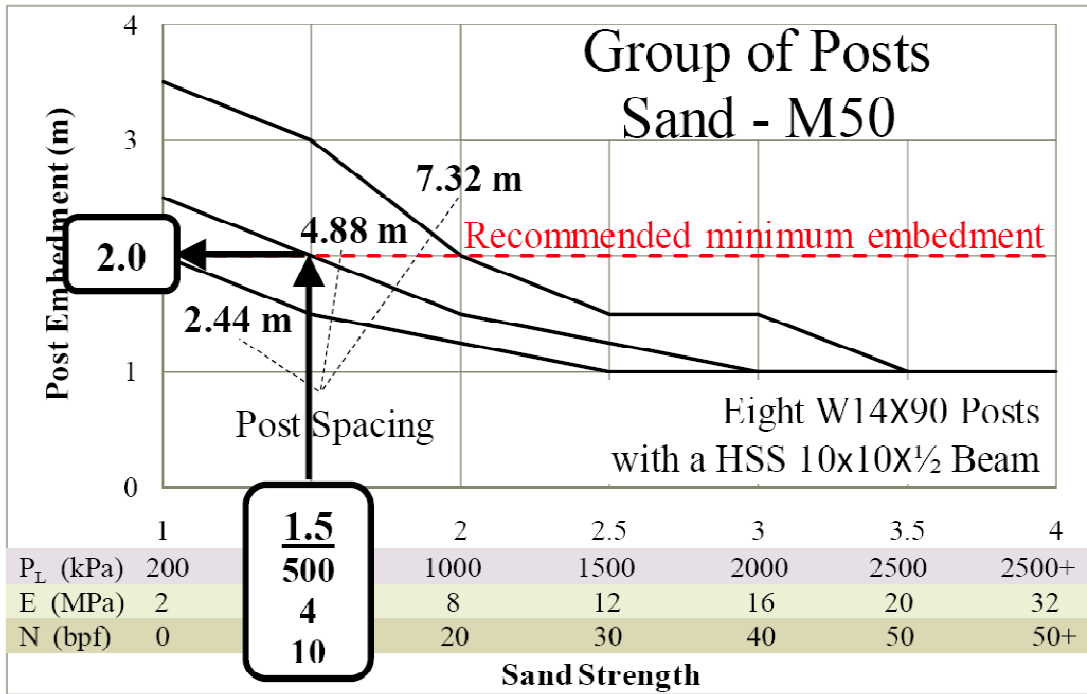
Figure 5.28. Design chart for M50 group of posts in sand (Example. 2)

6. CONCLUSIONS AND RECOMMENDATIONS

The main goal of this research is to develop design guidelines for single post and group of posts systems using wide-flange I-beam directly embedded in soil to contain truck impact in accordance with ASTM F2656-07, In order to fulfill the objective, a soil strength matrix was proposed, full-scale and model experiments were conducted to verify and develop the proposed design guideline and the design guideline was completed by using numerical simulations.

6.1 Soil strength category matrix

To develop the proposed design guideline, a soil strength category and the typical physical and engineering properties of each strength category were required for the numerical simulation purpose. The proposed soil strength categories allow classifying a soil in terms of soil strength. The category consists of seven strength classes with the range of physical and engineering soil properties for each sand and clay. The mean values of the range of each category were determined as the typical values of the each strength class. The proposed soil strength category matrix is shown in Table 3.7.

A preliminary soil strength category was developed by using literature reviews and soil tests. The preliminary one covered most of soil properties except dilation angle of sandy soil. For numerical modeling purpose, dilation angles of sand were needed. Since dilation angle of soil can be changed by soil density, stress state, and so on,

dilation angles of each soil were obtained by back calculation from numerical simulation of Pendulum test and full-scale test and the direct shear tests.

The proposed soil strength category was used as a mean of developing the design guidelines for the anti-ram post system directly embedded in soil. The soil strength category is not only a important means of achieving the object of this work but also a simple soil strength classification method using the results of either SPT or pressuremeter test. In addition, this work may be a helpful method to give an idea about general soil strength properties to the engineers and contractors who may work in unfavorable conditions including the use of unsophisticated equipment.

6.2 Model experiments

A series of static and pendulum or bogie tests in medium dense crushed limestone, loose sand or hard clay was conducted at TTI Proving Ground in June, 2008. Post systems including single post, group of post system were designed using the result of the dimensional analysis.

Single post directly embedded in soil may have a certain limit dynamic amplification factor. There is a limit dynamic amplification factor for a single post pendulum test embedded in the loose sand. Also the dynamic amplification factor of single post in the medium dense crushed limestone has a trend converging to a certain value. Limit amplification dynamic factor can be determined by the strength and stiffness of soil. The dynamic amplification factor increases as the strength of soil increases, since the dynamic amplification factor of the full-scale impact test in 2007

was 5.4 and the limit amplification dynamic factor of the single post in loose sand was 3.8. Limit impact velocity corresponding to limit dynamic amplification factor also increase as strength of soil increase. The limit impact velocity of the single post tests in loose sand was 16 km/h, whereas the limit impact velocity of the single post tests may be higher than 35 km/h.

Dynamic group efficient was ranging from approximately 70 % to 78% of the static group efficient for the impact tests. Group efficient of posts system under static and impact load decreases as number of posts increases.

According to the simple single degree of freedom analysis, the dynamic effect was largely from the inertia effect. Also the size of mobilized soil mass increases, as the soil strength increases.

6.3 Full-scale experiments

The single post system, July 2007 met the requirements for condition designation M50 and penetration rating P1 in accordance ASTM F2656-07. The 4m-long W14X109 post 3m embedded in the very dense crushed limestone brought the vehicle to a complete stop with 0.04m of dynamic penetration. The actual impact speed was 78.5 km/h and the mass of vehicle was 6813 kg. The peak impact force from the acceleration data was 1,350 kN. Dynamic factor was 5.4. The accelerations of the soil behind the post decreased to zero at the 2,500 mm of distance from the post. However, dynamic factor and size of mobilized soil wedge may be changed as a functions of impact velocity, mass of truck, soil strength, post strength, post depth, post shape, etc.

The group of posts system, May 2010 met the requirements for condition designation M50 and penetration rating P1 in accordance ASTM F2656-07. The eight 4.5 m long W14X90 posts 3m embedded in the loose sand with two HSS 8X8X1/2 horizontal beams brought the vehicle to a complete stop with 0.274 m of dynamic penetration. The actual impact speed was 80.3 km/h and the mass of vehicle was 6,835 kg. The peak impact force from the acceleration data was 925 kN. As flexibility of system increases, degree of damage of vehicle and impact force decreases, deformation of post system increases, according to the comparison with the M50 test on single post embedded in very dense crushed limestone.

The force acting on each post could not be calculated from the strain data. However, the strain history was used as a mean of validating the result of finite element analysis described. Also dynamic factor could not be obtained from the test data due to lack of data. Dynamic factor was estimated using both the result of experiment data and numerical simulation.

6.4 Numerical simulations

After the full-scale experiments, both the single post and group of posts models was modeled or modified with the measured soil properties and checked with different soil boundary conditions including the sand ditch. The size of soil boundary for design chart was spacious enough according to the numerical simulation result. The results from the finite element analysis using LS-DYNA were well matched with the actual measurements.

The simulated rotation and displacement were underestimated except the center posts in simulated group of posts model. Due to the failure of connection bolts between the posts and beams, the impact force could not be well transferred. Peak forces acting on each post were 185 kN, 83 kN, -45 kN and -65 kN. Peak of impact force was 825 kN at 0.04 sec whereas peak of summated force on each post was 550 kN at 0.3 sec. Due to inertia effect and delay on force transferring to each post, The peak summated force on each post was smaller than the impact force but the duration was increased. Also the modeled vehicle can be deformed but not allow the failure of connections of vehicle parts that causes change in mass.

The dynamic amplification factors of each post were ranging from 2.64 to 0.64. The dynamic amplification factor of single W14X90 post in loose sand can be considered as 2.64 that is less than the critical dynamic amplification factor obtained from pendulum test. The reason can be that the post system and vehicle was more flexible than the rigid pendulum and the post for pendulum test. Also the distributed forces on each post were mitigated by the inertia effect of mass of 8,300 kg for the post system above the ground level.

6.5 Design guidelines

Design guideline for post system directly embedded in soil was developed using a set of numerical simulations using LS-DYNA based on the soil strength category and results of experiments. The developed design guideline is capable of designing single or group of

posts system that can meet the requirements of the vehicle impact of designation M50, M40 and M30 with P1 penetration rating in accordance with ASTM F2656-07.

The initial finite element model was developed based on the full-scale impact test on single post, July 2007. The initial model was refined by using the model test results. After completion of the design chart, the method was partially verified by the full-scale impact test on group of posts system, May 2010. The proposed design guideline largely consists of four parts: single post in sand, single post in clay, group of posts in sand and group of posts in clay. For Group of posts system, clearances between each post were limited for three cases: 2.44 m, 4.88 m and 7.32 m.

The design guideline was developed using a certain post configuration. The design chart for single post was developed using a wide flange beam, W14X109. Thus single post system should be installed using a post with equivalent to W14-109 Post or even stronger post in terms of post width and bending stiffness. In addition to the embedment depth, at least 1.5 m of post length above the ground level is required. In the same manner, the group of posts system needs at least eight of W14-90 post, four posts on each side of the impact location with a horizontal beam with hollow section HSS 10X10X1/2. Also at least 1.5m of post length above the ground level is needed. The post and beam member having equivalent or stiffer bending stiffness can be used with cautious calculations. The minimum post embedment depth is recommended as 2 m since it is not clear that the simulation properly account the soil behavior at shallow depths including post pull-out.

6.6 Recommendations and future task

Precise analytical solution is required regarding interaction between soil and post system during vehicle impact including dynamic factor and inertia effect of soil. Throughout this study, there were some findings on relationship between dynamic factor and impact conditions including characteristics of impact, post system and soil. Analytical or empirical solution to quantify soil-post system interaction is required through theoretical or experimental efforts.

Design method without restriction on selecting post and beam sections is needed. The design charts developed in this project are for any soil, for three impact cases, and for the use of a post with a given cross section. There is a need to develop a simple methodology to solve the problem for any truck, any post, and any soil. Due to the lack of knowledge on interaction between post system and soil, the proposed design method was developed by using the series of finite element analysis. Major drawback of the method can be the restriction on selecting post and beam sections. Though the proposed method can design a barrier system capable to arrest vehicle impact, design method without restriction on selecting post and beam section is required in order to design more efficiently and economically.

Further verification on the proposed design guidelines is needed, especially the post system embedded in clay. The proposed design guideline was verified only two points in sand with two full-scale impact tests. The design charts for sand was modified or verified with experiments, whereas that for clay was modified using the bogie tests.

Thus further verification and modification on the proposed design charts for clay is recommended.

There is also a need for further verification of the design charts presented here especially in the case of shallow embedment. Since the post and the soil around the post were numerically merged during the finite element analysis, the verification of the pull-out capacity of the post systems with shallow embedment is needed. In addition to the further verifications, the probabilistic approach for the proposed design guidelines is recommended.

REFERENCES

Alberson, D. C., Buth, C. E., Briaud, J.-L., and Menhes, W. L. (2007). *DOS K12 Testing and Evaluation of Direct Embedded Pier*. Texas Transportation Institute, College Staion, TX.

Applied Foundation Tesing, Inc (2010). *Statnamic Load Testing Overview*, <http://www.testpile.com/PDF/Statnamic%20Testing%20Brief%20Overview%20for%20Web%20Site.pdf>, 2010.

Arrington, D. R., Alberson, D. C., and Menhes, W. L. (2010). *ASTM F2656-07 Test M50 on the Post and Beam Security Barrier in Sand* Texas Transportation Institute, College Staion, TX.

ASTM F 2656-07 (2007). *Standard Test Method for Vehicle Crash Testing of Perimeter Barriers,* ASTM International, West Conshohocken, PA.

Beason, W. L., and Hirsch, T. J. (1989). *Measurement of Heavy Vehicle Impact Forces and Inertia Properties*. Texas Transportation Institute, College Staion, TX.

Bolton, M. D. (1986). "The strength and dilatancy of sand." *Geotechnique*, 36(1), 65-78.

Bravo de los Rios, O. (2010). *Impact Test of 15,000 lb Truck at 50 mi/h Against Driven Post and Beam System in Loose Sand*, Texas A&M University, College Station, TX.

Briaud, J.-L. (1992). *The Pressuremeter*, A.A Balkema, Rotterdam, The Netherlands.

Briaud, J.-L. (1997). "SALLOP: Simple approach for lateral loads on piles." *Journal of Geotechnical and Geoenvironmental Engineering*, 123(10), 958-964.

Brinch Hansen, J. (1961). "The ultimate resistance of rigid piles against transversal forces." Geoteknisk Institu. Bull., Copenhagen.

Broms, B. B. (1964a). "Lateral resistance of piles in cohesionless soils." *Journal of the soil mechanics and foundations division*, 90(3), 123-156.

Broms, B. B. (1964b). "Lateral resistance of piles in cohesive soils." *Journal of the soil mechanics and foundations division*, 90(2), 27-63.

Brown, D. A. (2007). "Rapid lateral load testing of deep foundations." *DFI Journal*, Volume 1(1), 54-62.

Das, B. M. (1998). *Principles of Geotechnical Engineering*, PWS Publishing Company, Boston, MA.

Dewey Jr., J. F., Jayapalan, J. K., Hirsch, T. J., and Ross Jr., H. E. (1983). *A Study of the Soil-Structure Interaction Behavior of Highway Guardrail Posts*. Texas Transportation Institute, College Staion, TX.

Drucker, D. C., and Prager, W. (1952). "Soil mechanics and plastic analysis or limit design." *Quarterly of Applied*, 10(2), 157-165.

Eggers, D. W., and Hirsch, T. J. (1986). *The Effect of Embedment Depth, Soil Properties, and Post Type on the Performance of Highway Guardrail Post*. Texas Transportation Institute, College Staion, TX.

El Naggar, M. H. (1998). "Interpretationof lateral statnamic load test results." *Geotechnical Testing Journal*, 21(3), 169-179.

FEMA. (2003). *Reference Manual to Mitigate Potential Terrorist Attacks Against Buildings*, Risk management series, FEMA, Washington, DC.

KNR. (1999). *Design Criteria for Railroad Bridges*. Korean National Railroad (KNR), Republic of Korea.

LS-DYNA Theory Manual (2006). Livermore Software Technology Corporation, Livermore, CA.

LS-DYNA Keyword User's Manual Verosion 971 (2007). Livermore Software Technology Corporation, Livermore, CA.

Matlock, H., and Reese, L. C. (1960). "Generalized solutions for laterally loaded piles." *Journal of the Soil Mechanics and Foundations Division*, 86(5), 63-91.

Munson, B. R., Ypung, D. F., and Okiishi, T. H. (1998). *Fundamentals of Fluid Mechanics*, John Wiley & Sons, Inc., Ames, IA.

Novak, M. (1974). "Dynamic stiffness and damping of piles." *Canadian Geotechnical Journal*, 11(4), 574-598.

PLAXIS Version 8 Reference Manual (2002). PLAXIS b.v., Delft, The Netherlands.

Potts, D. M., and Zdravkovic, L. (1999). *Finite Element Analysis in Geotechnical Engineering: Theory*, Thomas Telford, London.

Poulos, H. G. (1971a). "Behavior of laterally loaded piles: I-single piles." *Journal of the Soil Mechanics and Foundations Division*, 97(5), 711-731.

Poulos, H. G. (1971b). "Behavior of laterally loaded piles: II-pile groups." *Journal of the Soil Mechanics and Foundations Division*, 97(5), 733-751.

Prakash, S., and Chandrasekaran, V. (1973). "Pile foundations under dynamic lateral loads." *Proc. of the 8th International Conference on Soil Mechanics and Foundation Engineering*, Moscow, 199-203.

Reid, J. D., Hascall, J. A., Sicking, D. L., and Faller, R. K. (2009). "Inertial effects during impact testing " *Transportation Research Record: Journal of the Transportation Research Board*, 2120, 39-46.

Rollins, K. M., and Sparks, A. (2002). "Lateral statnamic load testing & analysis of a pile group." *Journal of Geotechnical Engineering, ASCE*, 128(9), 711-723.

Rowe, P. W. (1962). "Stress-dilatancy relation for static equilibrium of assembly of particles in contact." *Proc. of the Royal Society of London. Series A, Mathmatical and Physical Science*, London, 500-527.

Saez Barrios, D. O. (2010). *Determination of Soil Properties for Sandy Soils and Road Base at Riverside Campus Using Laboratory Testing and Numerical Simulation*, Texas A&M University, College Station, TX.

SD-STD-02.01, Revision A. (2003). *Test Method for Vehicle Crash Testing of Perimeter Barriers and Gates,* Physical Security Division, U.S. Department of State, Washington, DC.

Terzaghi, K., Peck, R. B., and Mesri, G. (1996). *Soil Mechanics in Engineering Practice*, John Wiley & Sons, New York, NY.

Texas Transportation Institute (TTI) (2010). *Facilities: Crash testing*, <http://tti.tamu.edu/facilities/index.htm?cat_id=3219>, 2010.

Tucker, R. L. (1964). "Lateral analysis of piles with dynamic behaviour." *Proc. of the Conference on Deep Foundations*, Mexico City, 1, 157-171.

U.S. Department of State (2008). *DS certified anti-ram vehicle barriers*, Protective Design Center, United States Army Corps of Engineering, <https://pdc.usace.army.mil/library/BarrierCertification>, 2010.

Wood, D. M. (2001). *Geotechnical Modelling*, Spon Press, New York, NY.

APPENDIX A

SOIL TESTING

Figure A. 1 Standard Penetration Test (SPT)

Table A.1. Standard Penetration Test blow count of the very dense crushed rock (Impact test on the single post-crushed rock)

Depth (m)	1	2	3	N
0.60 - 0.74		50 for 0.13 m		50
1.22 – 1.52	33	52 for 0.15 m		50
1.83 – 2.30	33	25	13	38

Figure A. 2. Preparing a borehole and lowering the probe by driving
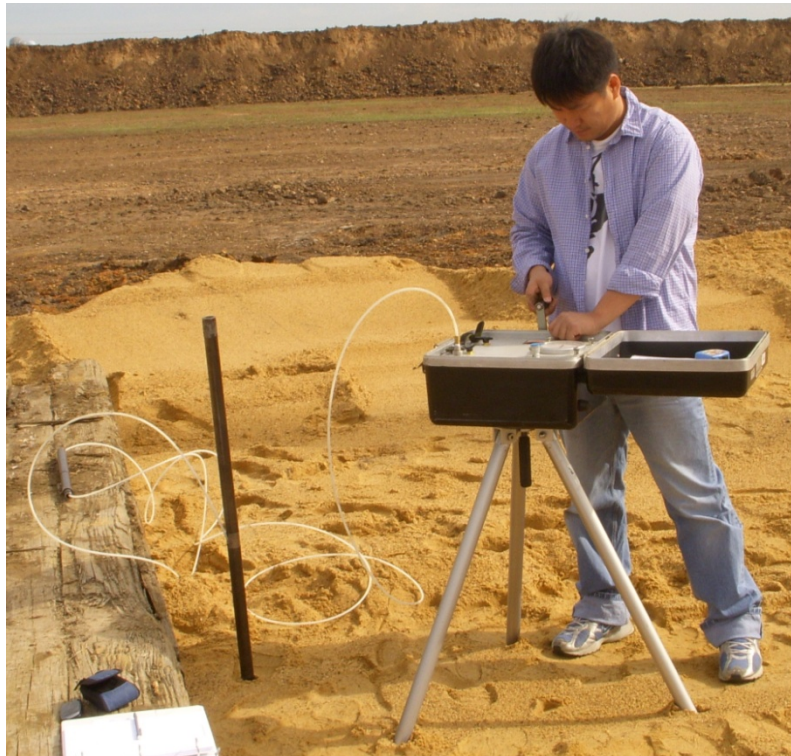
Figure A. 3. The PENCEL pressuremeter test

LOG OF BORING

PROJECT:	Briaud Drilling	BORING NO.	B-1
	Riverside Campus	PROJECT NO.	A1085033
	Bryan, Texas	DATE	5-29-08
CLIENT:	Texas A&M University	SURFACE ELEVATION	Existing Grade
	College Station, Texas		PAGE 1 of 1

DRILLING METHOD(S): Dry Augered 0 to 6 feet

GROUNDWATER INFORMATION:
Seepage was not observed while drilling.

Boring was dry and open to approximately 6 feet upon completion.

DEPTH (FT)	SOIL SYMBOL	SAMPLES	N: BLOWS/FT T: INCHES/100 BLOWS P: TONS/SQ FT R: PERCENT RQD: PERCENT	MOISTURE CONTENT (%)	DRY DENSITY POUNDS/CU. FT	ATTERBERG LIMITS (%)			MINUS NO. 200 SIEVE (%)	COMPRESSIVE STRENGTH (TONS/SQ. FT)	FAILURE STRAIN (%)	CONFINING PRESSURE (POUNDS/SQ. IN)	DESCRIPTION OF STRATUM
						LL	PL	PI					
1			P=1.5	18	105	44	15	29	72	2.0	7	0	Stiff brown and gray **LEAN CLAY (CL)**, with sand
2													
3			P=4.5+	18	106	52	13	39	83	5.1	8	0	Hard dark gray **FAT CLAY (CH)**, with sand
4													
5			P=4.5+	17	107	51	15	36	82	5.4	7	0	
6													Boring Terminated at 6 feet
7													
8													
9													
10													

N - STANDARD PENETRATION TEST RESISTANCE
T - TXDOT CONE PENETRATION RESISTANCE
P - POCKET PENETROMETER RESISTANCE
R - PERCENTAGE OF ROCK CORE RECOVERY
RQD - ROCK QUALITY DESIGNATION

REMARKS:

1Terracon

Figure A. 4. Soil test result from the Shelby tube sample (Bogie-clay B-1)

LOG OF BORING

PROJECT: Briaud Drilling
Riverside Campus
Bryan, Texas

CLIENT: Texas A&M University
College Station, Texas

BORING NO. B 2
PROJECT NO. A1085033
DATE 5-29-08
SURFACE ELEVATION Existing Grade

PAGE 1 of 1

DRILLING METHOD(S):
Dry Augered 0 to 4 feet

GROUNDWATER INFORMATION:
Seepage was not observed while drilling.

Boring was dry and open to approximately 4 feet upon completion.

FIELD DATA			LABORATORY DATA										
			MOISTURE CONTENT (%)	DRY DENSITY POUNDS/CU.FT	ATTERBERG LIMITS (%)			MINUS NO. 200 SIEVE (%)	COMPRESSIVE STRENGTH (TONS/SQ.FT)	FAILURE STRAIN (%)	CONFINING PRESSURE (POUNDS/SQ.IN)	
DEPTH (FT)	SOIL SYMBOL	SAMPLES / N-BLOWS/FT T-INCHES/100 BLOWS P-TONS/SQ.FT R-PERCENT RQD-PERCENT			LL	PL	PI					DESCRIPTION OF STRATUM

Field/Strata descriptions:

- N=9 — Stiff brown and gray **LEAN CLAY (CL)**, with sand
- N=17 — Very stiff dark gray **FAT CLAY (CH)**
- Boring Terminated at 4 feet

N - STANDARD PENETRATION TEST RESISTANCE
T - TXDOT CONE PENETRATION RESISTANCE
P - POCKET PENETROMETER RESISTANCE
R - PERCENTAGE OF ROCK CORE RECOVERY
RQD - ROCK QUALITY DESIGNATION

REMARKS:
Soil classifications are based on visual descriptions.

Terracon

Figure A. 5. Standard Penetration Test result (Bogie-clay B-2)

LOG OF BORING

PROJECT:	Briaud Drilling Riverside Campus Bryan, Texas	BORING NO.	B-3
		PROJECT NO.	A1065033
		DATE	5-29-08
CLIENT:	Texas A&M University College Station, Texas	SURFACE ELEVATION	Existing Grade
			PAGE 1 of 1

DRILLING METHOD(S):
Dry Augered 0 to 4 feet

GROUNDWATER INFORMATION:
Seepage was not observed while drilling.

Boring was dry and open to approximately 4 feet upon completion.

FIELD DATA			LABORATORY DATA								DESCRIPTION OF STRATUM

Field data columns: DEPTH (FT), SOIL SYMBOL, SAMPLES, N: BLOWS/FT T: INCHES/100 BLOWS P: TONS/SQ FT R: PERCENT RQD: PERCENT

Laboratory data columns: MOISTURE CONTENT (%), DRY DENSITY POUNDS/CU.FT, ATTERBERG LIMITS (%) [LIQUID LIMIT LL, PLASTIC LIMIT PL, PLASTICITY INDEX PI], MINUS NO. 200 SIEVE (%), COMPRESSIVE STRENGTH (TONS/SQ.FT), FAILURE STRAIN (%), CONFINING PRESSURE (POUNDS/SQ IN)

At depth ~1 ft: N=6 — Medium stiff brown and gray **LEAN CLAY (CL)**, with sand

At depth ~3 ft: N=10 — Stiff dark gray **FAT CLAY (CH)**, with sand

Boring Terminated at 4 feet

N - STANDARD PENETRATION TEST RESISTANCE
T - TXDOT CONE PENETRATION RESISTANCE
P - POCKET PENETROMETER RESISTANCE
R - PERCENTAGE OF ROCK CORE RECOVERY
RQD - ROCK QUALITY DESIGNATION

REMARKS:
Soil classifications are based on visual descriptions.

Terracon

Figure A. 6. Standard Penetration Test result (Bogie-clay B-3)

LOG OF BORING

PROJECT: Briaud Drilling
Riverside Campus
Bryan, Texas
CLIENT: Texas A&M University
College Station, Texas

BORING NO. B-4
PROJECT NO. A1085033
DATE 5-29-08
SURFACE ELEVATION Existing Grade

PAGE 1 of 1

DRILLING METHOD(S):
Dry Augered 0 to 6 feet

GROUNDWATER INFORMATION:
Seepage was not observed while drilling.
Boring was dry and open to approximately 6 feet upon completion.

FIELD DATA			LABORATORY DATA										DESCRIPTION OF STRATUM
DEPTH (FT)	SOIL SYMBOL	SAMPLES	N: BLOWS/FT T: INCHES/100 BLOWS P: TONS/SQ FT R: PERCENT RQD: PERCENT	MOISTURE CONTENT (%)	DRY DENSITY POUNDS/CU.FT	LL	PL	PI	MINUS NO. 200 SIEVE (%)	COMPRESSIVE STRENGTH (TONS/SQ FT)	FAILURE STRAIN (%)	CONFINING PRESSURE (POUNDS/SQ IN)	
1			P=2.5	13	109	33	16	17	67	2.2	6	0	Very Stiff brown and gray **SANDY LEAN CLAY (CL)**
2-3			P=4.0	21	96	51	17	34	81	1.6	10	0	Very stiff dark gray **FAT CLAY (CH)**, with sand
5			P=4.5+	18	104	51	16	35	78	4.0	7	0	-becomes hard
6													Boring Terminated at 6 feet

N - STANDARD PENETRATION TEST RESISTANCE
T - TXDOT CONE PENETRATION RESISTANCE
P - POCKET PENETROMETER RESISTANCE
R - PERCENTAGE OF ROCK CORE RECOVERY
RQD - ROCK QUALITY DESIGNATION

REMARKS:

Terracon

Figure A. 7. Soil test result from the Shelby tube sample (Bogie-clay B-4)

LOG OF BORING

PROJECT: Briaud Drilling
Riverside Campus
Bryan, Texas

CLIENT: Texas A&M University
College Station, Texas

BORING NO. B-5
PROJECT NO. A1005033
DATE 5-29-08
SURFACE ELEVATION Existing Grade

PAGE 1 of 1

FIELD DATA | **LABORATORY DATA**

Columns: DEPTH (FT), SOIL SYMBOL, SAMPLES, N: BLOWS/FT / T: INCHES/100 BLOWS / P: TONS/SQ FT / R: PERCENT / RQD PERCENT, MOISTURE CONTENT (%), DRY DENSITY POUNDS/CU.FT, ATTERBERG LIMITS (%) [LIQUID LIMIT (LL), PLASTIC LIMIT (PL), PLASTICITY INDEX (PI)], MINUS NO. 200 SIEVE (%), COMPRESSIVE STRENGTH (TONS/SQ FT), FAILURE STRAIN (%), CONFINING PRESSURE (POUNDS/SQ IN)

DRILLING METHOD(S):
Dry Augered 0 to 4 feet

GROUNDWATER INFORMATION:
Seepage was not observed while drilling.

Boring was dry and open to approximately 4 feet upon completion.

DESCRIPTION OF STRATUM

Loose **CRUSHED STONE**, with dark brown clay

N=9

N=8

Boring Terminated at 4 feet

N - STANDARD PENETRATION TEST RESISTANCE
T - TXDOT CONE PENETRATION RESISTANCE
P - POCKET PENETROMETER RESISTANCE
R - PERCENTAGE OF ROCK CORE RECOVERY
RQD - ROCK QUALITY DESIGNATION

REMARKS:
Soil classifications are based on visual descriptions.

Terracon

Figure A. 8. Standard Penetration Test result (Pendulum-crushed rock B-5)

LOG OF BORING

PROJECT: Briaud Drilling
Riverside Campus
Bryan, Texas
CLIENT: Texas A&M University
College Station, Texas

BORING NO. B-6
PROJECT NO. A1095033
DATE 5-29-08
SURFACE ELEVATION Existing Grade

PAGE 1 of 1

DRILLING METHOD(S):
Dry Augered 0 to 4 feet

GROUNDWATER INFORMATION:
Seepage was not observed while drilling.

Boring was dry and open to approximately 4 feet upon completion.

DESCRIPTION OF STRATUM

Medium dense CRUSHED STONE

N=14

N=7

-becomes loose, with dark gray clay

Boring Terminated at 4 feet

N - STANDARD PENETRATION TEST RESISTANCE
T - TXDOT CONE PENETRATION RESISTANCE
P - POCKET PENETROMETER RESISTANCE
R - PERCENTAGE OF ROCK CORE RECOVERY
RQD - ROCK QUALITY DESIGNATION

REMARKS:
Soil classifications are based on visual descriptions.

Terracon

Figure A. 9. Standard Penetration Test result (Pendulum-crushed rock B-6)

LOG OF BORING

PROJECT: Briaud Drilling
Riverside Campus
Bryan, Texas
CLIENT: Texas A&M University
College Station, Texas

BORING NO. B-7
PROJECT NO. A1085033
DATE 5-29-08
SURFACE ELEVATION Existing Grade

PAGE 1 of 1

DRILLING METHOD(S):
Dry Augered 0 to 4 feet

GROUNDWATER INFORMATION:
Seepage was not observed while drilling.

Boring was dry and open to approximately 4 feet upon completion.

DESCRIPTION OF STRATUM

Very loose pale brown **SAND**

N=1

N=WOH*

Boring Terminated at 4 feet

N - STANDARD PENETRATION TEST RESISTANCE
T - TXDOT CONE PENETRATION RESISTANCE
P - POCKET PENETROMETER RESISTANCE
R - PERCENTAGE OF ROCK CORE RECOVERY
RQD - ROCK QUALITY DESIGNATION

REMARKS.
*WOH: Weight of Hammer

Soil classifications are based on visual descriptions.

Terracon

Figure A. 10. Standard Penetration Test result (Pendulum-loose sand B-7)

LOG OF BORING

PROJECT:	Briaud Drilling
	Riverside Campus
	Bryan, Texas
CLIENT:	Texas A&M University
	College Station, Texas

BORING NO.	B-8
PROJECT NO.	A1085033
DATE	5-29-08
SURFACE ELEVATION	Existing Grade
	PAGE 1 of 1

DRILLING METHOD(S):
Dry Augered 0 to 4 feet

GROUNDWATER INFORMATION:
Seepage was not observed while drilling.

Boring was dry and open to approximately 4 feet upon completion.

FIELD DATA			LABORATORY DATA									
DEPTH (FT)	SOIL SYMBOL	SAMPLES	N: BLOWS/FT T: INCHES/100 BLOWS P: TONS/SQ.FT R: PERCENT RQD: PERCENT	MOISTURE CONTENT (%)	DRY DENSITY POUNDS/CU.FT	ATTERBERG LIMITS (%) LIQUID LIMIT (LL)	PLASTIC LIMIT (PL)	PLASTICITY INDEX (PI)	MINUS NO. 200 SIEVE (%)	COMPRESSIVE STRENGTH (TONS/SQ FT)	FAILURE STRAIN (%)	CONFINING PRESSURE (POUNDS/SQ IN)

DESCRIPTION OF STRATUM

Very loose pale brown **SAND**

N=WOH*

N=2

Boring Terminated at 4 feet

N - STANDARD PENETRATION TEST RESISTANCE	**REMARKS:**
T - TXDOT CONE PENETRATION RESISTANCE	*WOH: Weight of Hammer
P - POCKET PENETROMETER RESISTANCE	
R - PERCENTAGE OF ROCK CORE RECOVERY	Soil classifications are based on visual
RQD - ROCK QUALITY DESIGNATION	descriptions.

Terracon

Figure A. 11. Standard Penetration Test result (Pendulum-loose sand B-8)

LOG OF BORING NO. B-1

CLIENT:	Texas A&M	PROJECT:	Dr. Briaud Drilling
BORING LOCATION:	See Plan of Borings	SITE:	Texas A&M Riverside Campus Bryan, Texas

Graphic Log	DESCRIPTION Approx. Surface Elevation: Existing Grade	DEPTH, FEET	USCS SYMBOL	TYPE	SPT., BLOWS/FT	CALIBRATED HAND PENETROM., TSF	MOISTURE CONTENT, %	DRY DENSITY, PCF	LIQUID LIMIT, %	PLASTIC LIMIT, %	PLASTICITY INDEX	MINUS #200 SIEVE, %	COMPRESSIVE STRENGTH, TSF	FAILURE STRAIN, %	CONFINING PRESSURE, PSI
	FILL - SAND; tan, very loose			SS	woh										
				SS	2										
		5		SS	woh										
				SS	woh										
	10.0	10		SS	woh										
	Boring terminated at 10 feet.														

STRATIFICATION LINES REPRESENT APPROXIMATE BOUNDARIES BETWEEN SOIL TYPES. IN SITU, THE TRANSITION BETWEEN STRATA MAY BE MORE GRADUAL.	REMARKS:	Dry auger to 10 feet. Groundwater seepage was not observed during drilling.

WATER LEVEL OBSERVATIONS		Terracon	DATE DRILLED	Page 1 of 1
▽	▼		5/19/2010	FIGURE
▼	▼		PROJECT NUMBER	
FREE WATER WAS NOT OBSERVED DURING DRILLING OPERATIONS			93106033	A-1

Figure A. 12. Standard Penetration Test result (Group of posts-loose sand B-1)

LOG OF BORING NO. B-2

CLIENT:	Texas A&M	PROJECT:	Dr. Briaud Drilling
BORING LOCATION:	See Plan of Borings	SITE:	Texas A&M Riverside Campus Bryan, Texas

Graphic Log	DESCRIPTION Approx. Surface Elevation: Existing Grade	DEPTH, FEET	USCS SYMBOL	TYPE	SPT, BLOWS/FT	CALIBRATED HAND PENETROM., TSF	MOISTURE CONTENT, %	DRY DENSITY, PCF	LIQUID LIMIT, %	PLASTIC LIMIT, %	PLASTICITY INDEX	MINUS #200 SIEVE, %	COMPRESSIVE STRENGTH, TSF	FAILURE STRAIN, %	CONFINING PRESSURE, PSI
	FILL - SAND; tan, very loose			SS	3										
				SS	2										
		5		SS	woh										
				SS	woh										
	10.0			SS	1										
	Boring terminated at 10 feet.	10													

STRATIFICATION LINES REPRESENT APPROXIMATE BOUNDARIES BETWEEN SOIL TYPES. IN SITU, THE TRANSITION BETWEEN STRATA MAY BE MORE GRADUAL.

REMARKS: Dry auger to 10 feet.
Groundwater seepage was not observed during drilling.

WATER LEVEL OBSERVATIONS		**Terracon**	DATE DRILLED 5/19/2010	Page 1 of 1
⟍	⟍		PROJECT NUMBER 93105033	**FIGURE** A-2
⟍	⟍			
FREE WATER WAS NOT OBSERVED DURING DRILLING OPERATIONS				

Figure A. 13. Standard Penetration Test result (Group of posts-loose sand B-2)

Figure A. 14. Standard Penetration Test result (Group of posts-loose sand B-3)

APPENDIX B

FULL-SCALE IMPACT TEST – JULY 2007

Calculation using SALLOP: for design of the single post for the full-scale impact test
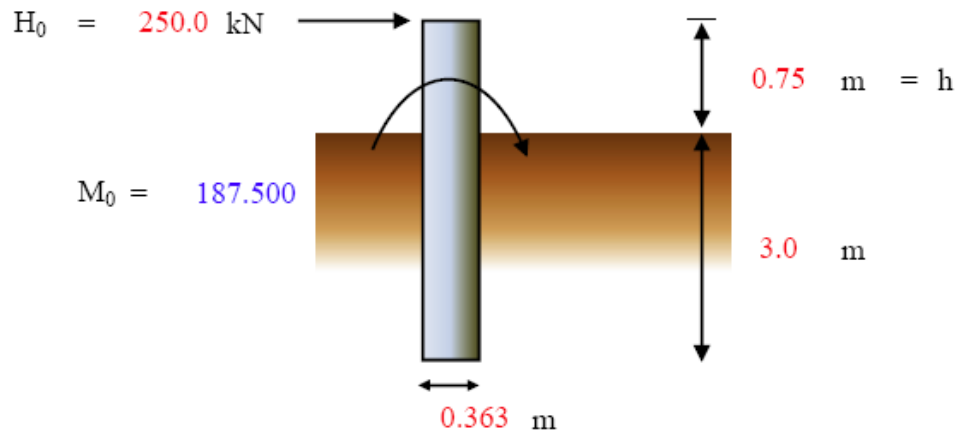
Pile	=	W14X109			
M_p	=	720	kips-ft	=	976.8	kN-m
Area	=	40	in2	=	0.0258	m2
Flange depth	=	14.3	in	=	0.3632	m
I_{steel}	=	1240	in4	=	0.0005161	m4
E_0	=		45000.0	kPa	
E_{steel}	=		2E+08	kPa	

$K \;=\; 2.3 \cdot E_0 \;=\; 2.3 \;\times\; 45000.000 \qquad\qquad\qquad\qquad =\; 103500.0 \;\; kPa$

$EI \;=\; E_{steel} \cdot I_{steel} \qquad\qquad =\; 103225.39 \;=\; 1.03E{+}05$

$l_0 \;=\; (4EI/K)^{1/4} \;=\; (\,4 \;\times\; 103225 \;/\; 103500\,)^{1/4} \qquad =\; 1.413 \;\; m$

where, E_0 = pressuremeter load modulus

    K = soil spring constant

    E = modulus of elasticity for the pile material

    I   = moment of inertia for the pile , H_0 = horizontal load

    l_0 = transfer length   , M_0 = applied moment at the ground surface

Embedded pile length, L =   3.0 m   m   **Check the interpolation!**

1. Lateral Pile Capacity

The zero-shear depth D_v is obtained by setting V (shear force) = 0;

$D_v = l_0 \cdot \tan^{-1}\{1/(1+2M_0/l_0H_0)\}$ =   0.458   m

P_L =   2500.000   kPa

$H_{ou} = 0.75 \cdot P_L \cdot B \cdot D_v$ =   0.75   ×   2500.000   ×   0.363   ×   0.458   =   311.915   kN

φ_1 =   1.00

φ_2 =   1

φ_3 =   1

$\varphi \cdot H_{ou}$ =   1.000   ×   1   ×   1   ×   311.915

       =   311.915   kN   > H_0 =   250.000   kN   **∴ O.K!**

where, D_v =   zero-shear depth

       φ_1 =   resistance factor

       φ_2 =   dynamic effect factor

       φ_3 =   group effect factor

       P_L =   preboring pressuremeter limit pressure within D_v

       H_{ou} =   lateral capacity of pile

2. Lateral Movement at The Ground Surface

$y_0 = \{(1+h/l_0) \cdot H_0 \cdot l_0^3 / (2EI)\}/(\varphi_2 \cdot \varphi_3)$ =   0.008   m   =   8.320   mm

3. Maximum Bending Moment

Maximum bending moment can be found by finding the value of Z_{max} which satisfied V = 0.

$Z_{max} = D_v$ =   0.458   m

M_{max} = $[0.5 \cdot H_0 l_0 \cdot \exp\text{-}(Z_{max}/l_0) \cdot \sqrt{\{(1+2h/l_0)^2 + 1\}}]/(\varphi_2 \cdot \varphi_3)$

       =   238.744   kN·m

4. Slope at The Ground Surface

$y'_0 = \{(1+h/l_0)^2 \cdot H_0 \cdot l_0^2 / (2EI)\}/(\varphi_2 \cdot \varphi_3)$ =   0.009742   radians

                                 =   0.558   degrees

5. Deflection and Slope of Cantilever Beam

Δ_{CANT} = $(H_{dynamic} \cdot h^3)/(3EI)$ =   0.001703   m   =   1.70   mm

y'_{CANT} = $(H_{dynamic} \cdot h^2)/(2EI)$ =   0.003406   radians

                                 =   0.195   degrees

y_h = $y_0 + y'_0 \cdot h + \Delta_{CANT}$ =   0.017330   m   =   17.33   mm   <   25.000   mm **∴ O.K!**

y'_h = $y'_c + y'_{CANT}$ = 0.013148 radians

= 0.753 degrees < 5 ° ∴ **O.K!**

5. Moment Check

$M_{dynamic}$ = $M_{max} \cdot DynamicFactor$

= 937.5 < Maximum available flexural strength (LRFD 977 kN-m ∴ **O.K!**
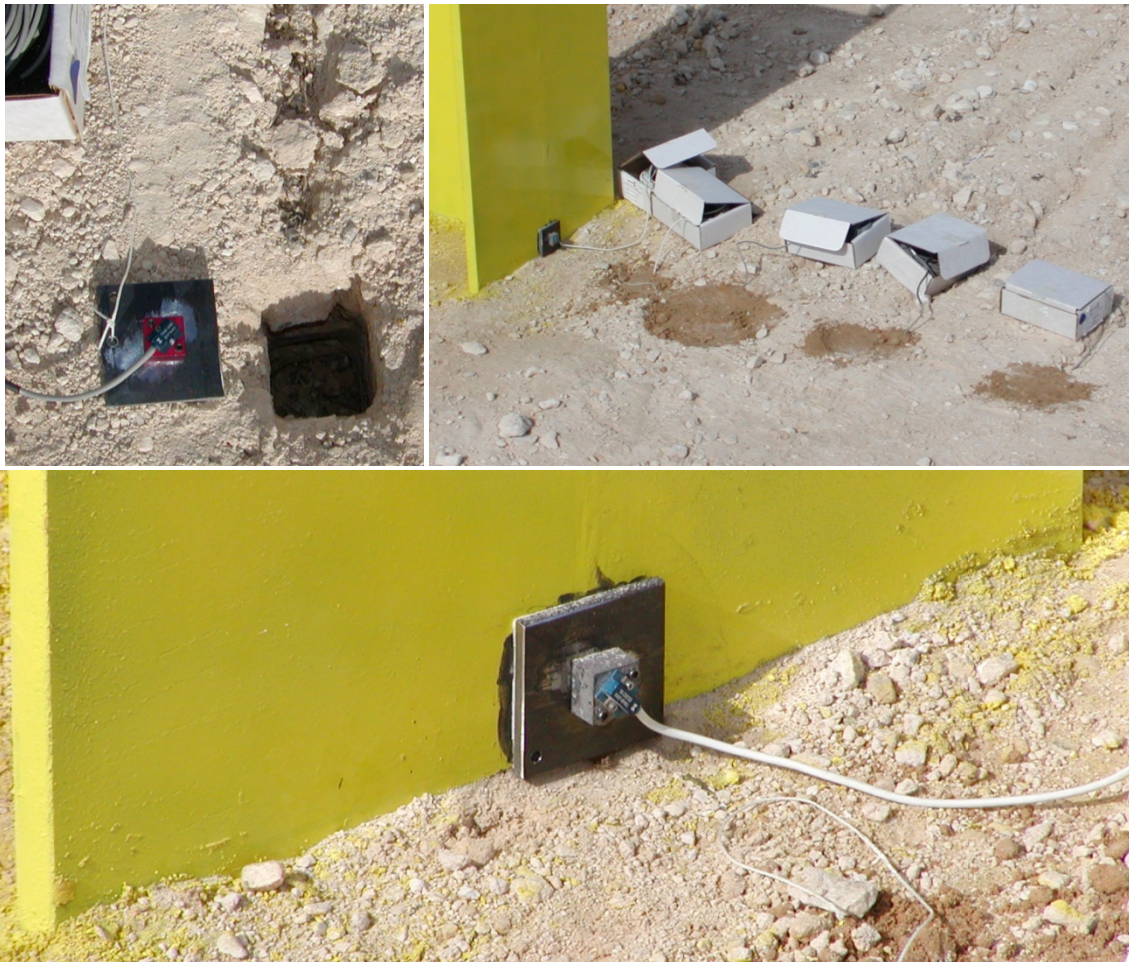
Figure B. 1. Accelerometers installed on the post and in the soil

DATE: 07-18-2007   TEST NO.: 400951-SNL7   VIN NO.: 1HTSCAAM5WH519789

YEAR: 1998   MAKE: NaviStar   MODEL: 4700

TIRE SIZE: 10R22.5   ODOMETER: Exempt
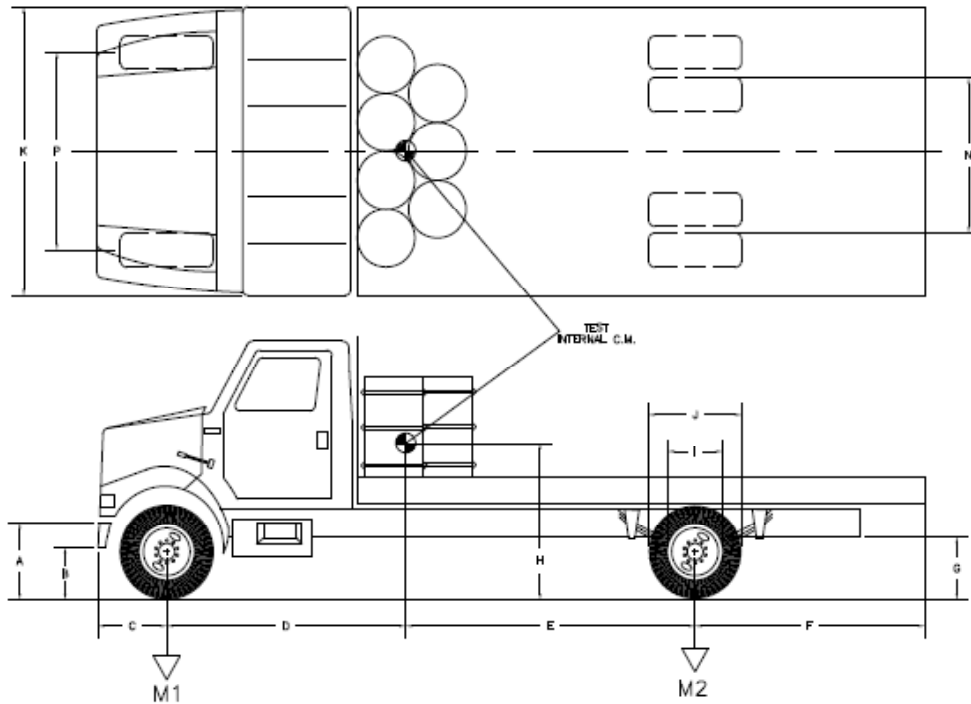
GEOMETRY (cm)

A 80   B 51   C 77   D 268.38   E 285.34   F 254   G 74

H ____   I 60   J 100   K 244   L 205   N 185

MASS DISTRIBUTION (kg)

LF 1764   RF 1746   LR 1610   RR 1692

MASS (kg)	CURB	TEST INERTIAL
M_1	2930	3511
M_2	2826	3302
M_{Total}	5756	6813

Figure B. 2. Vehicle properties (Alberson et al. 2007)

0.000 s

0.196 s

0.049 s

0.245 s

0.098 s

0.294 s

0.147 s
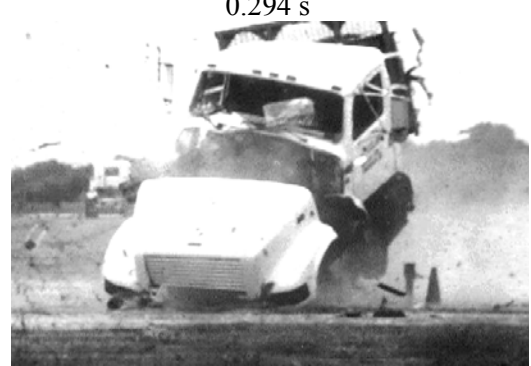
0.343 s

Figure B. 3. Sequential photographs - frontal view (Alberson et al. 2007)
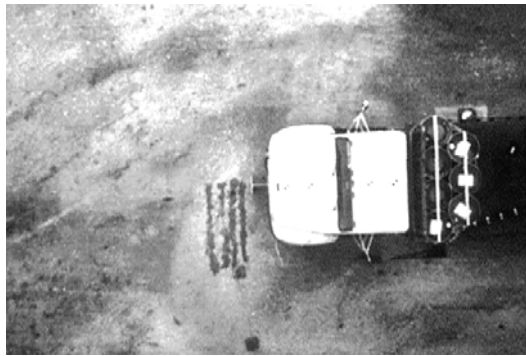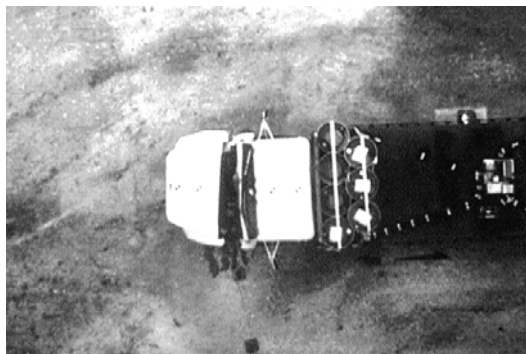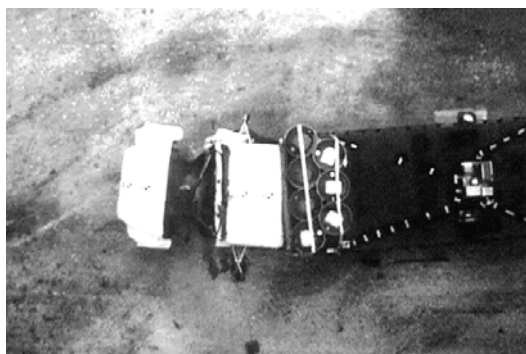
Figure B. 4. Sequential photographs - overhead and perpendicular views (Alberson et al. 2007)

0.196 s
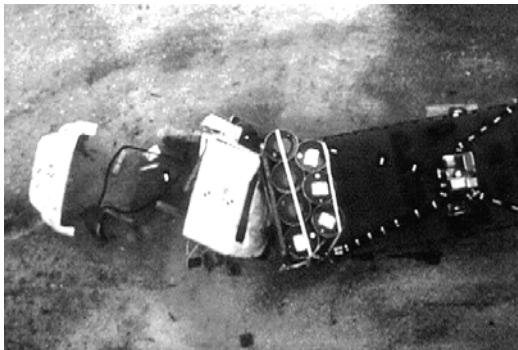
0.245 s
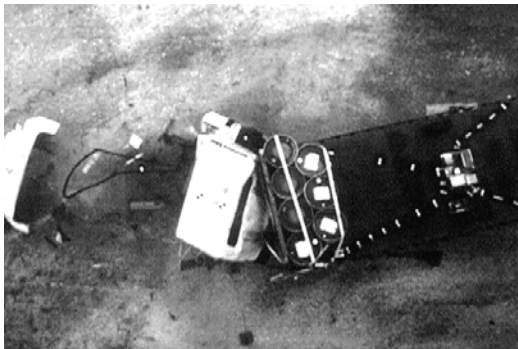
0.294 s
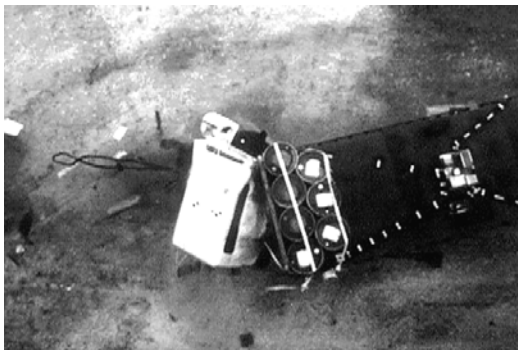
0.343 s

Figure B. 4. Continued

Figure B. 5. Soil deformation behind the post after the impact test
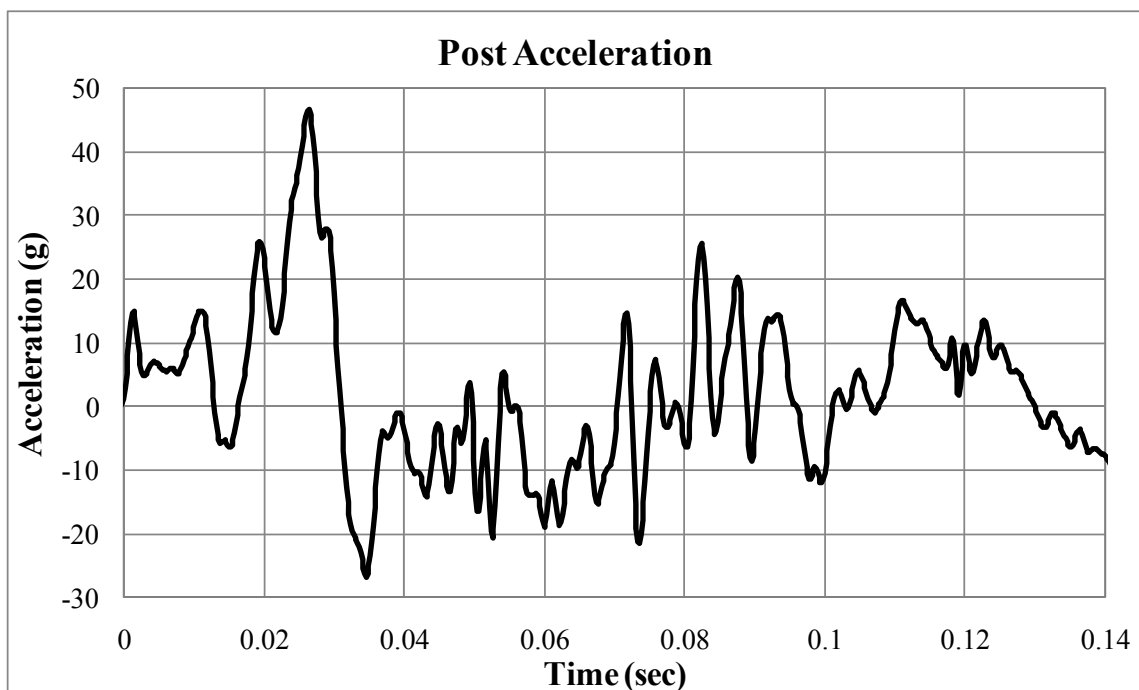
Figure B. 6. Post acceleration history (Raw)
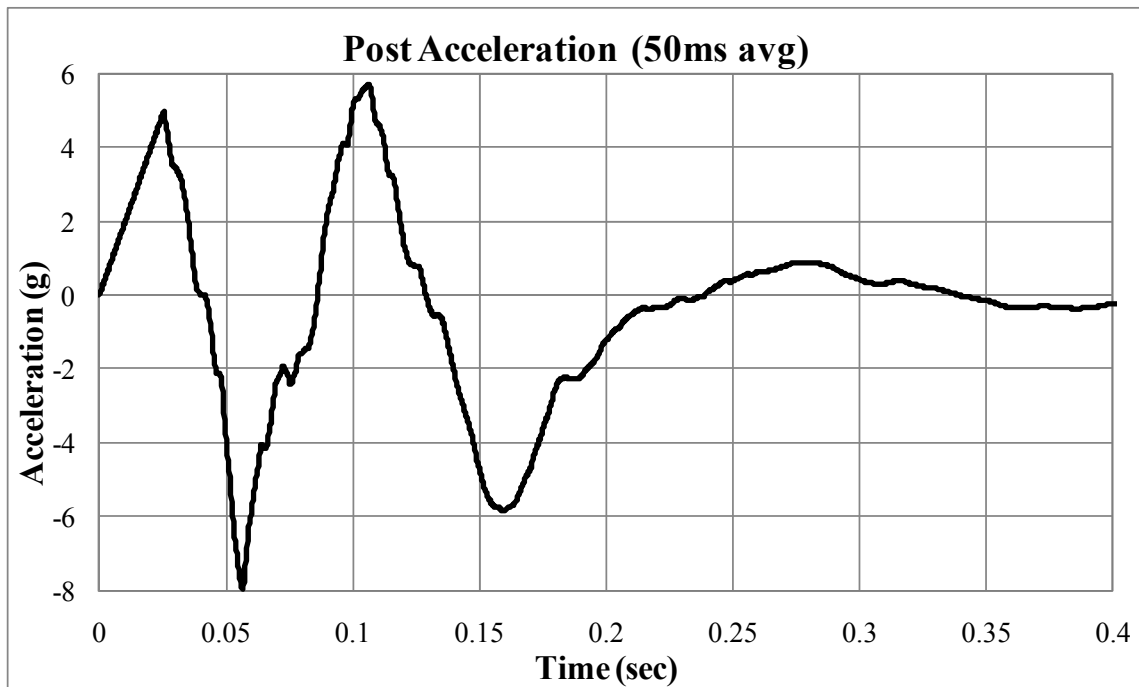
Figure B. 7. Post acceleration history (50ms average)
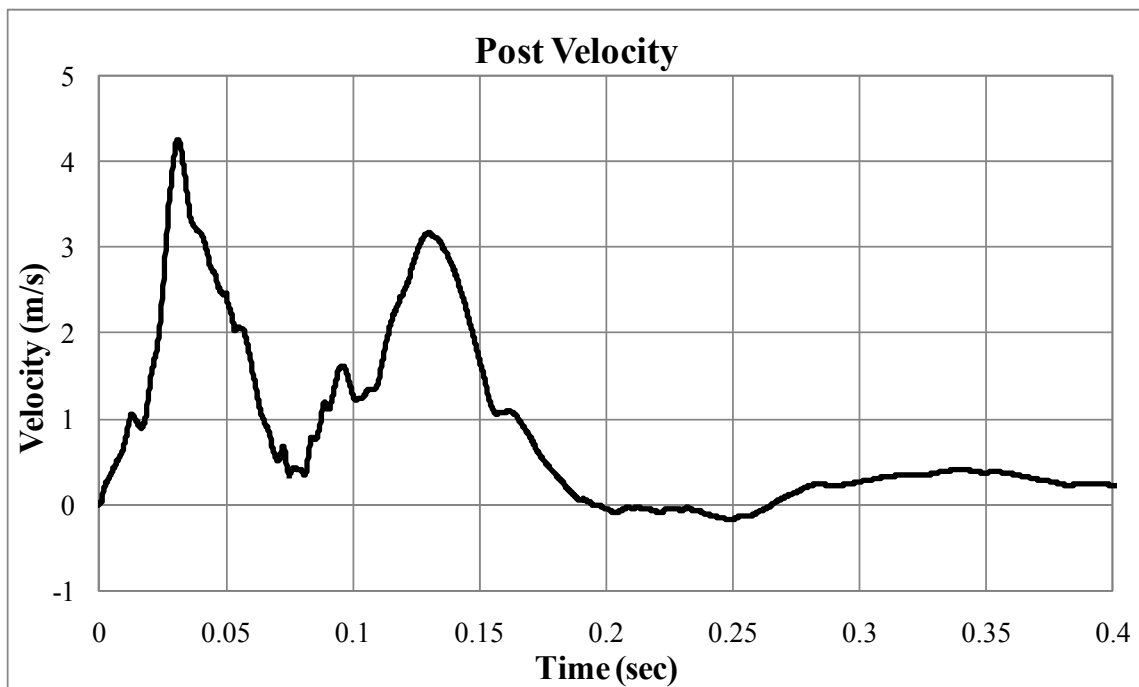
Figure B. 8. Post velocity history
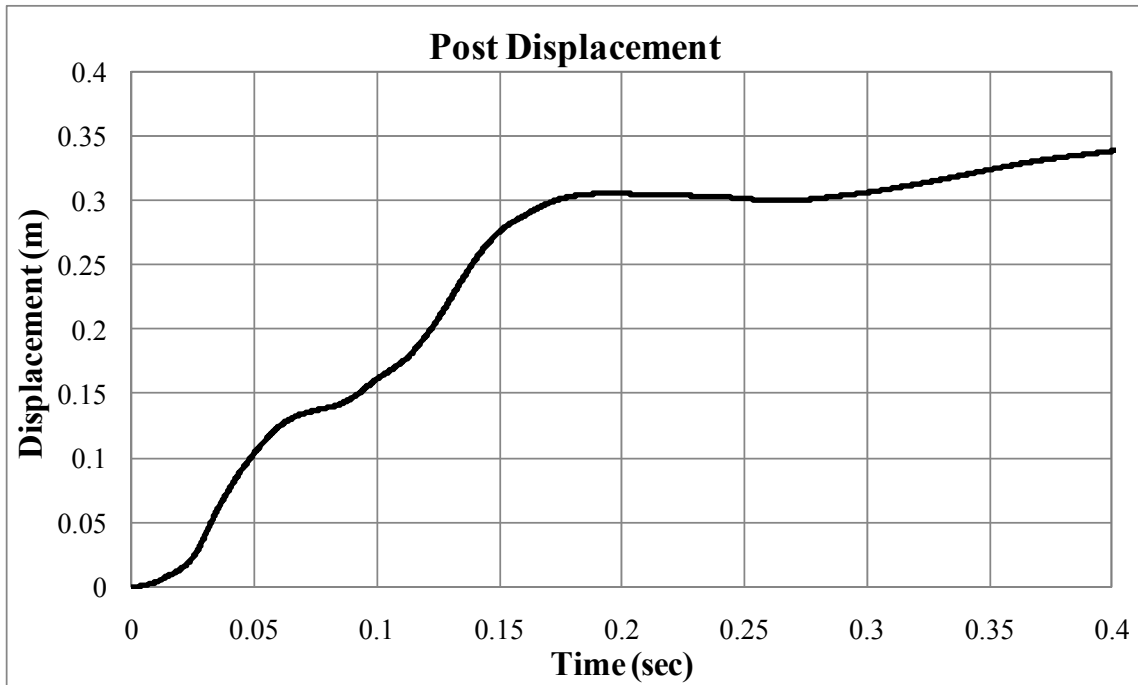
Figure B. 9 Post displacement history
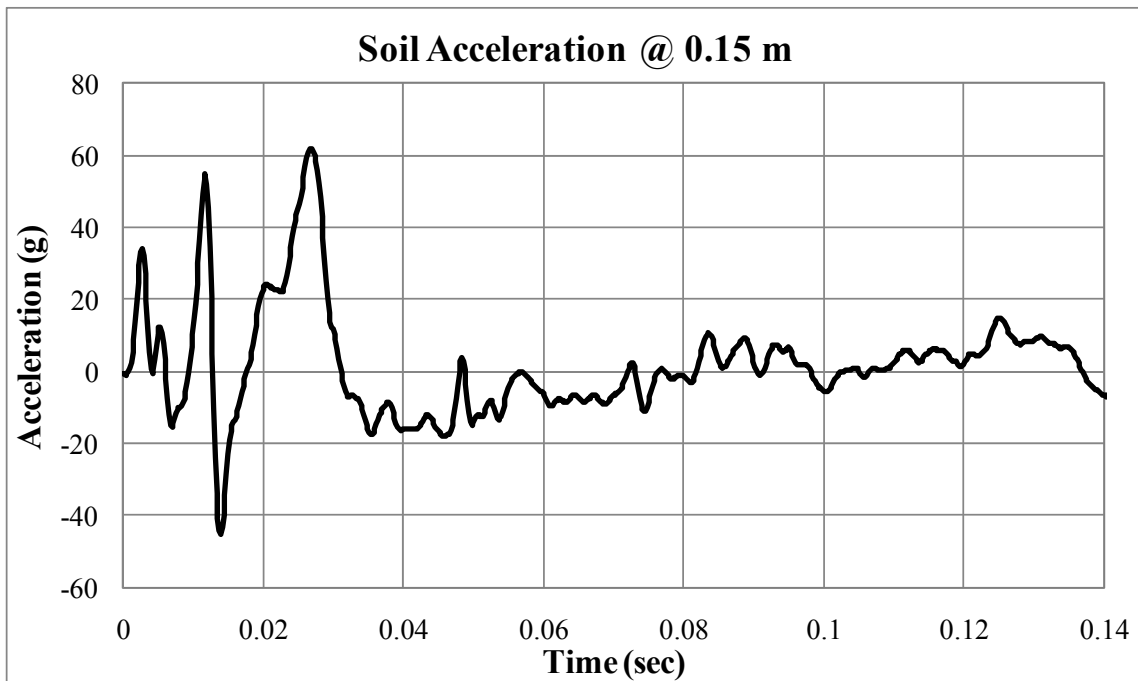
Figure B. 10. Soil acceleration history at 0.15 behind the post (Raw)
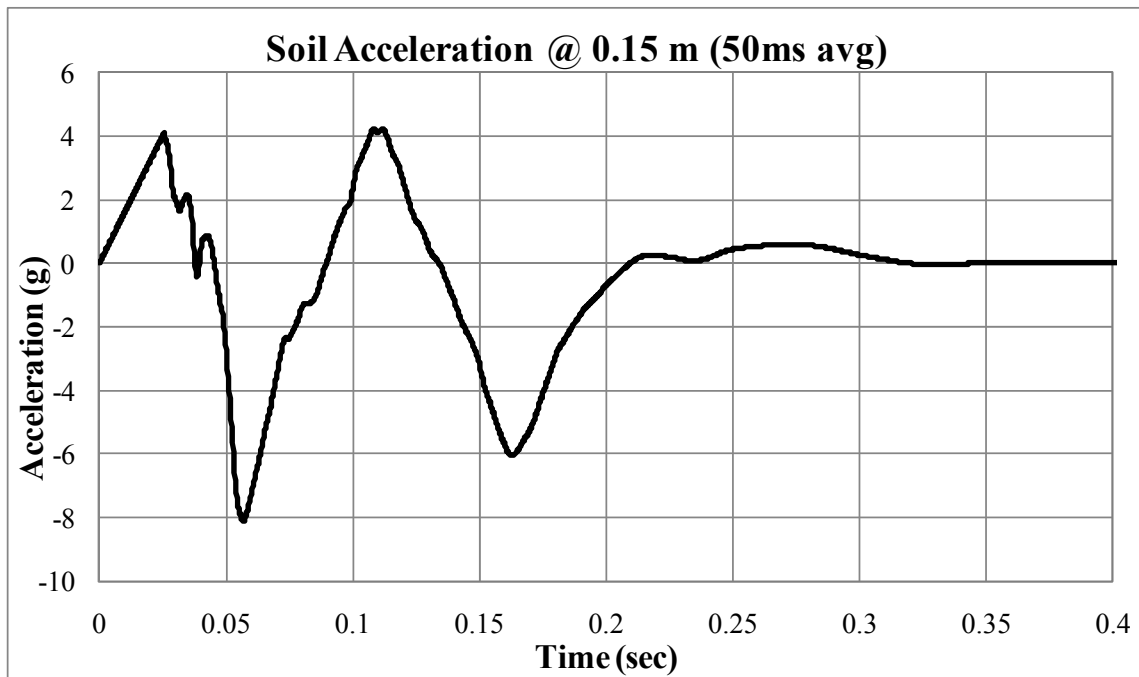
Figure B. 11. Soil acceleration history at 0.15 behind the post (50ms average)
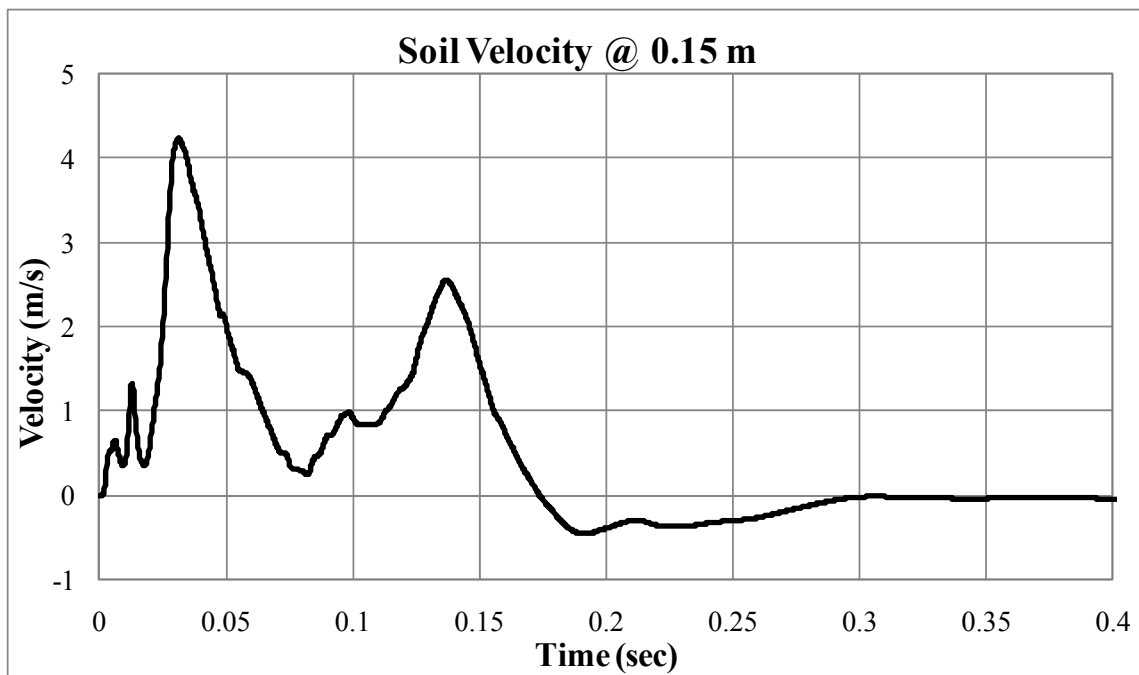
Figure B. 12. Soil velocity history at 0.15 behind the post
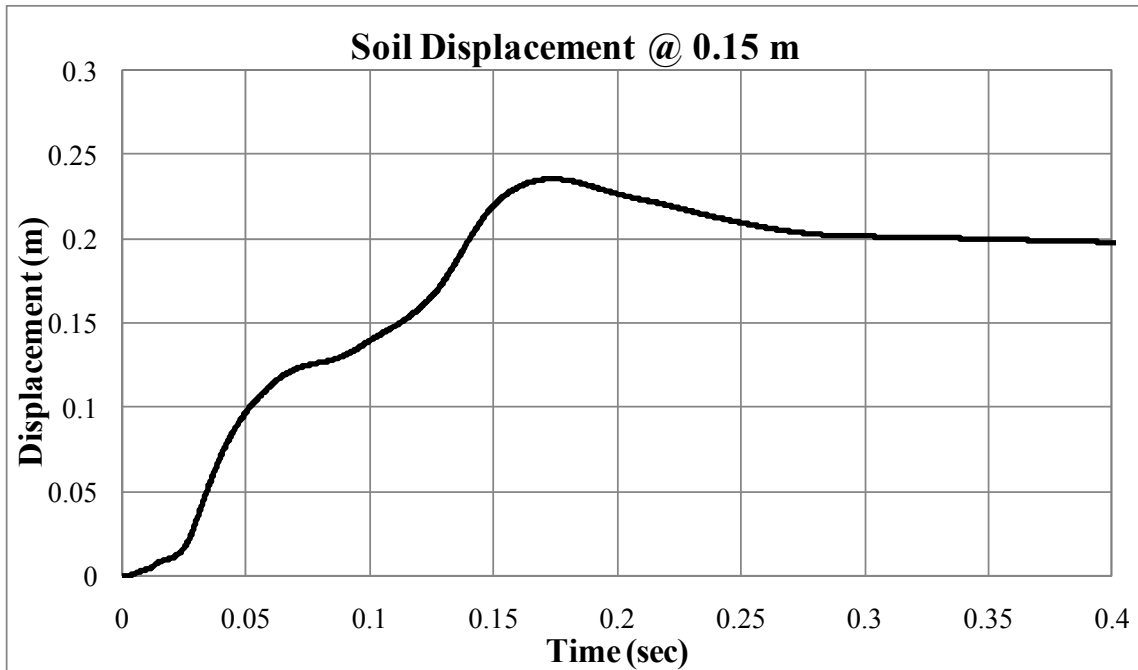
Figure B. 13. Soil displacement history at 0.15 behind the post
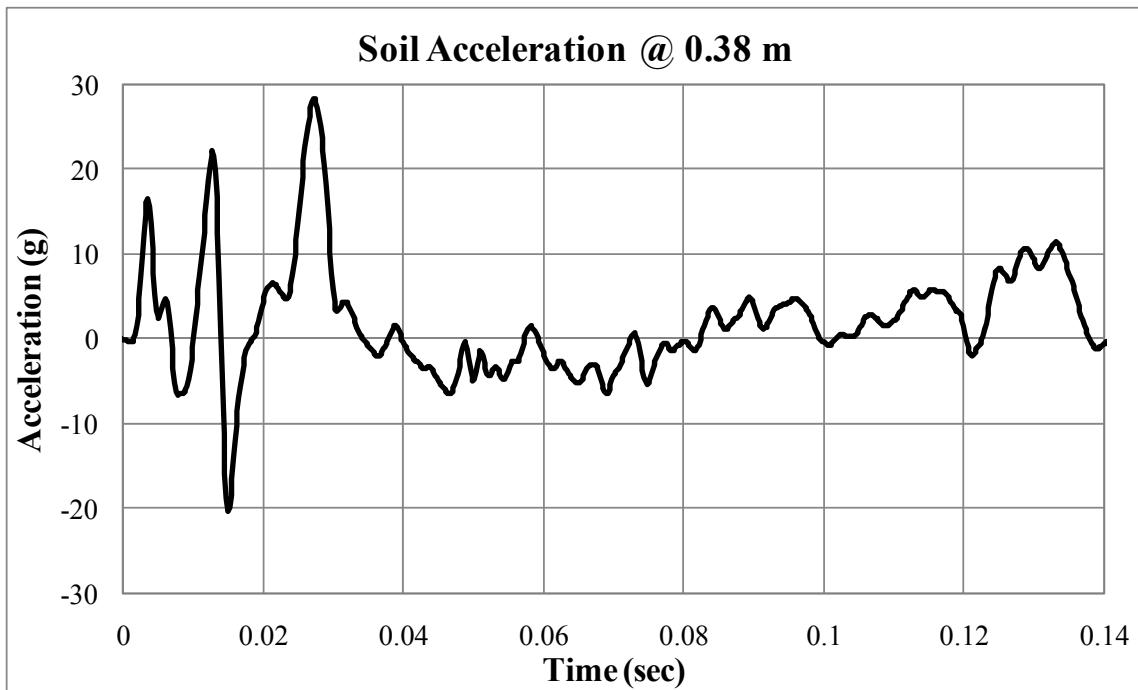
Figure B. 14. Soil acceleration history at 0.38 behind the post (Raw)
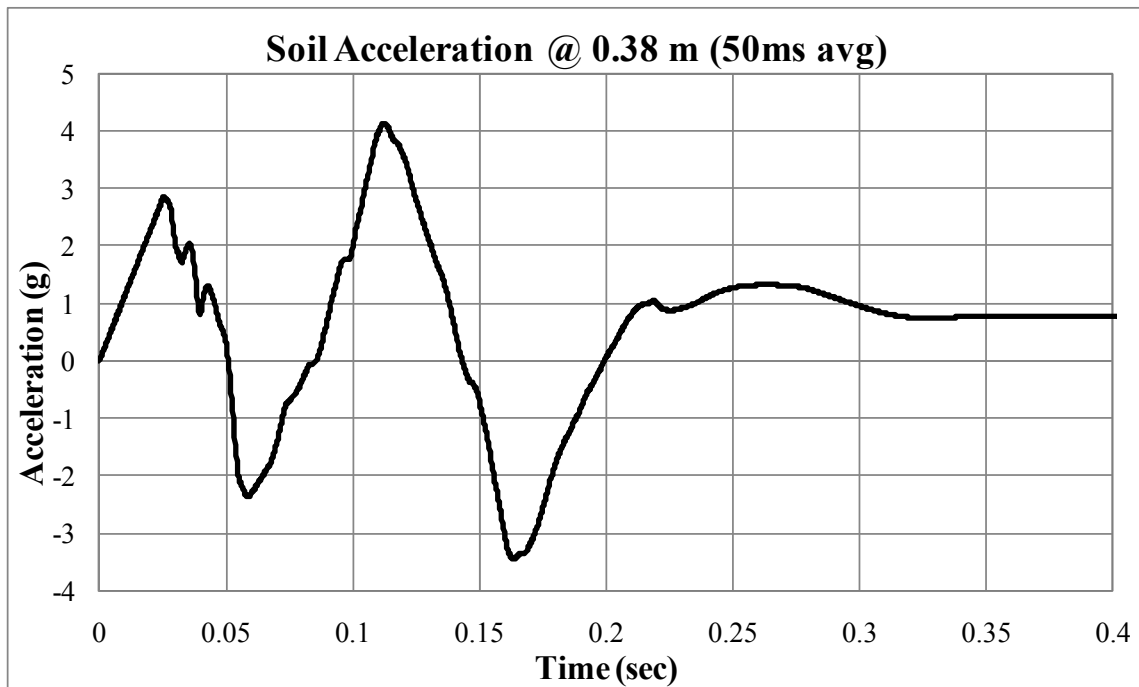
Figure B. 15. Soil acceleration history at 0.38 behind the post (50ms average)
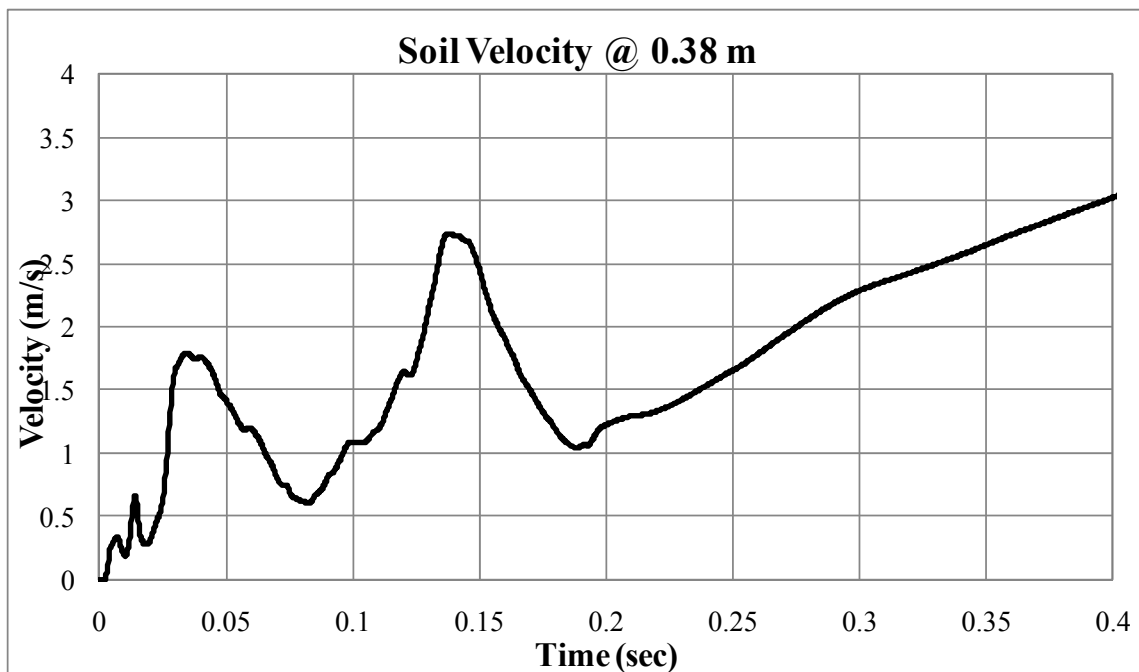
Figure B. 16. Soil velocity history at 0.38 behind the post
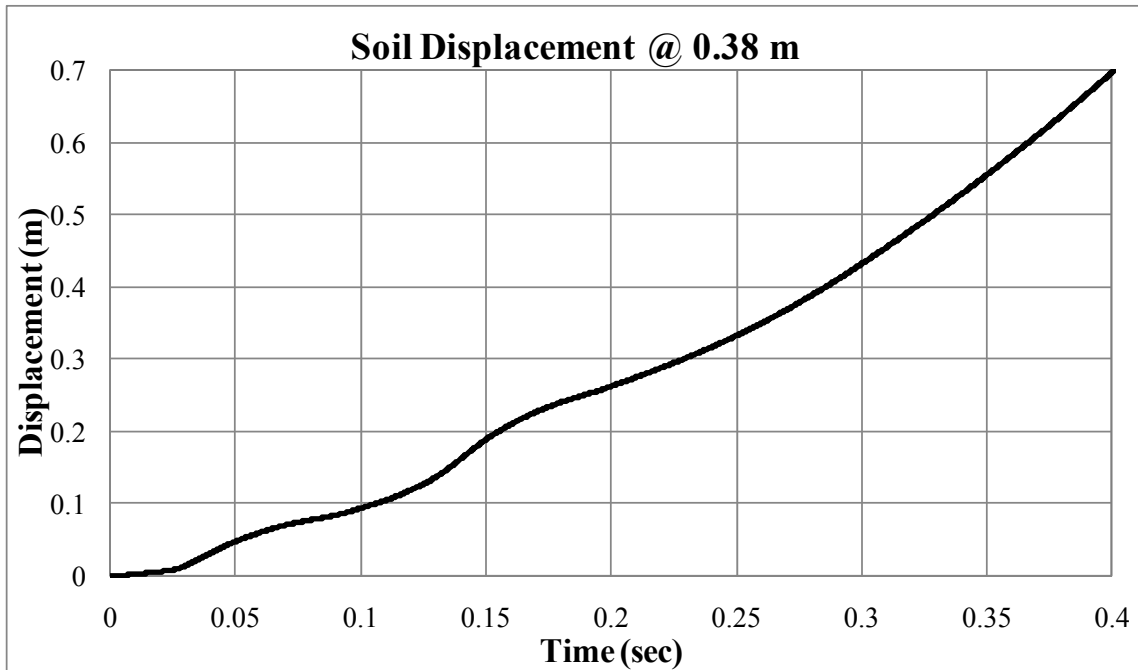
Figure B. 17. Soil displacement history at 0.38 behind the post
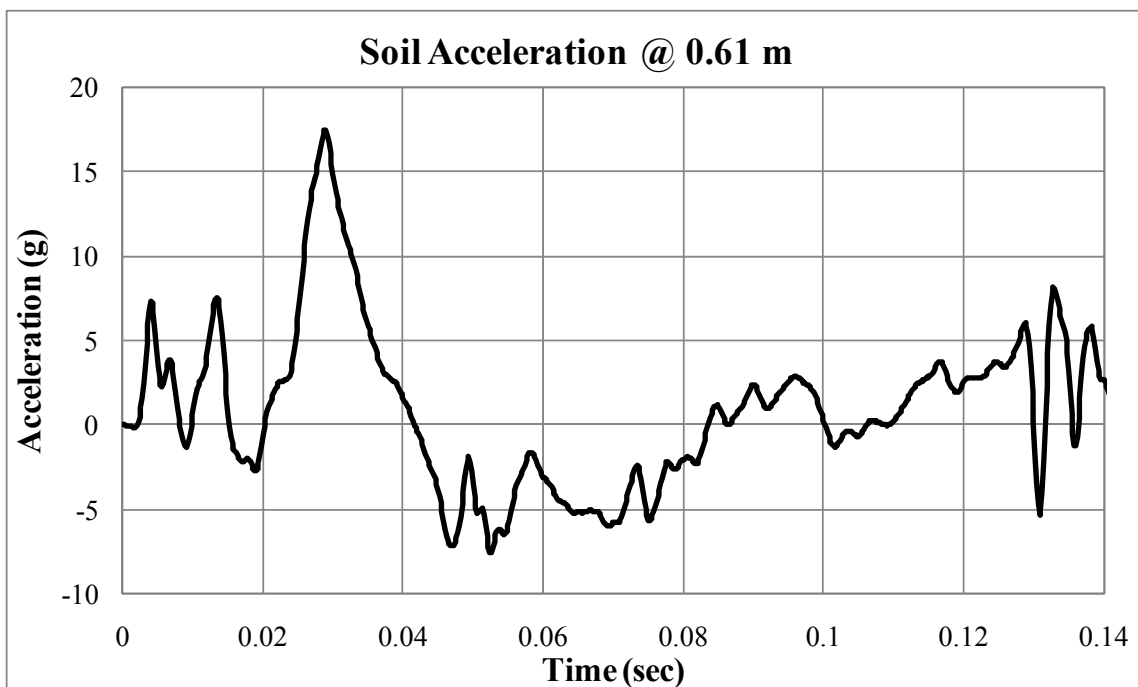
Figure B. 18. Soil acceleration history at 0.61 behind the post (Raw)
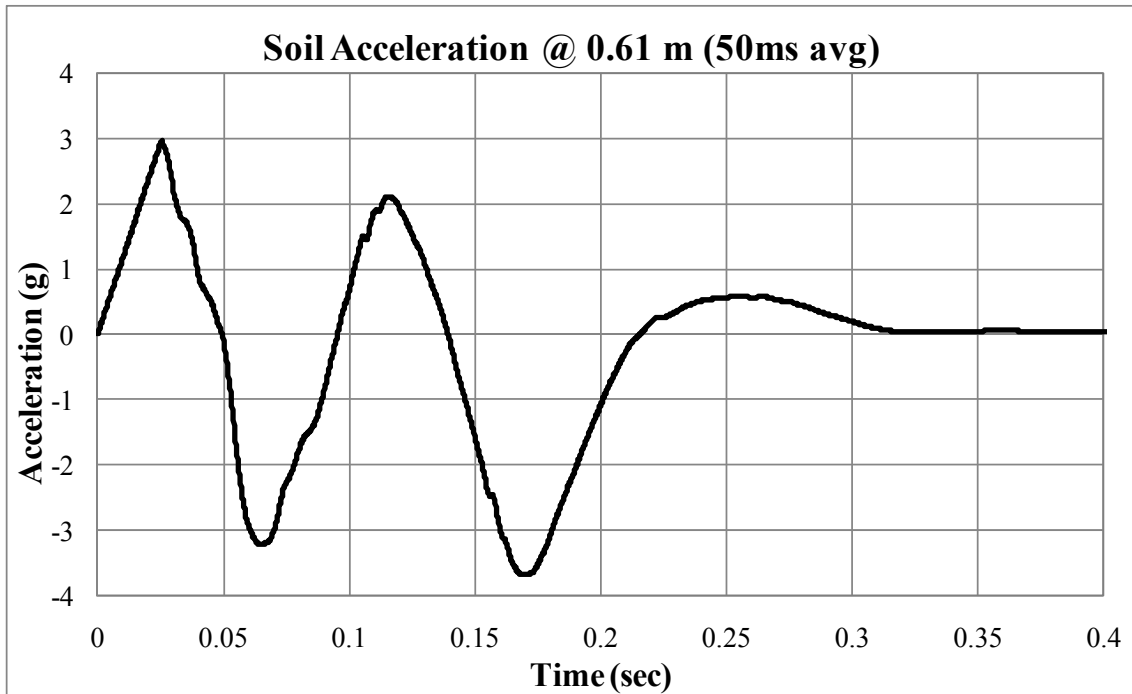
Figure B. 19. Soil acceleration history at 0.61 behind the post (50ms average)
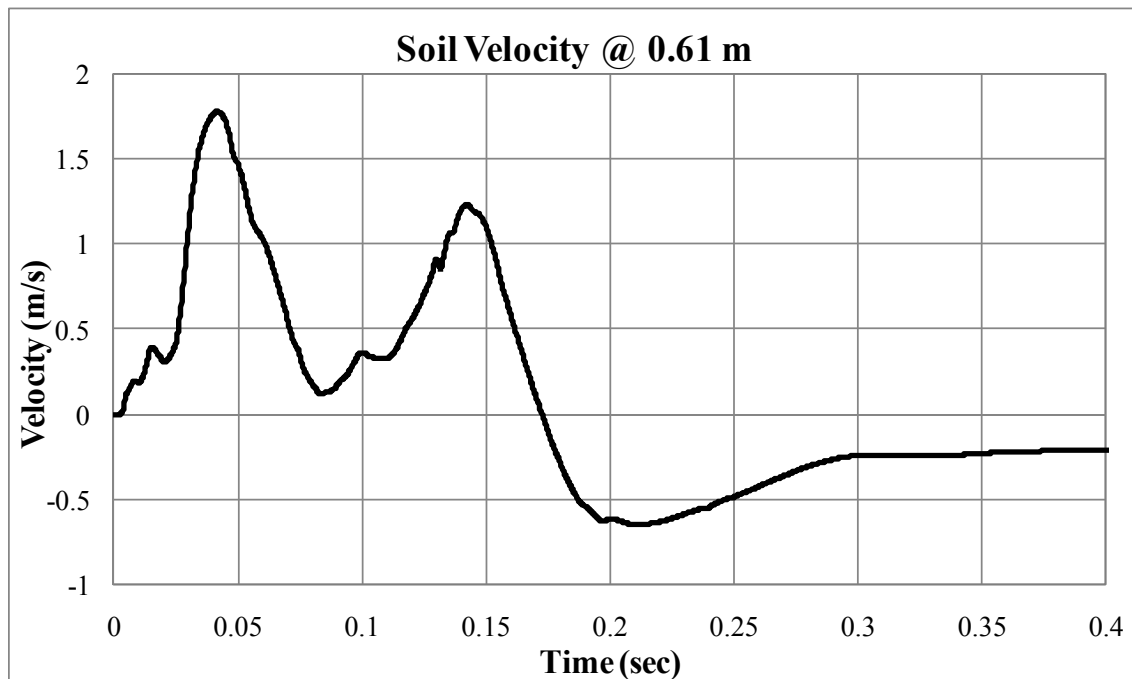
Figure B. 20. Soil velocity history at 0.61 behind the post
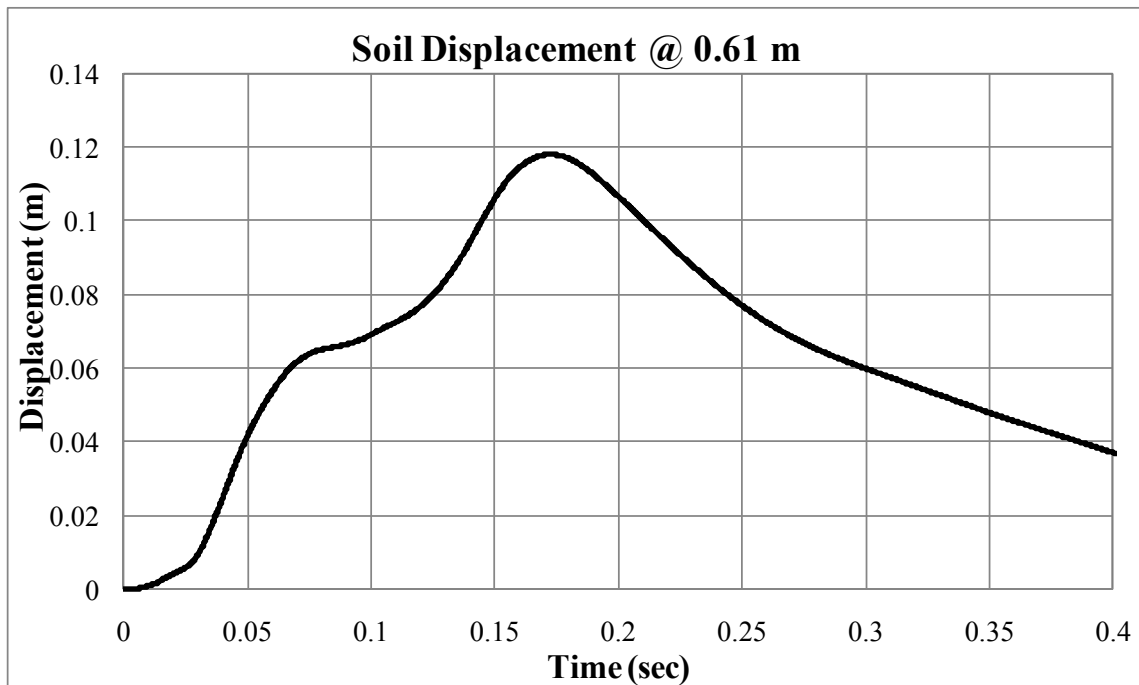
Figure B. 21. Soil displacement history at 0.61 behind the post
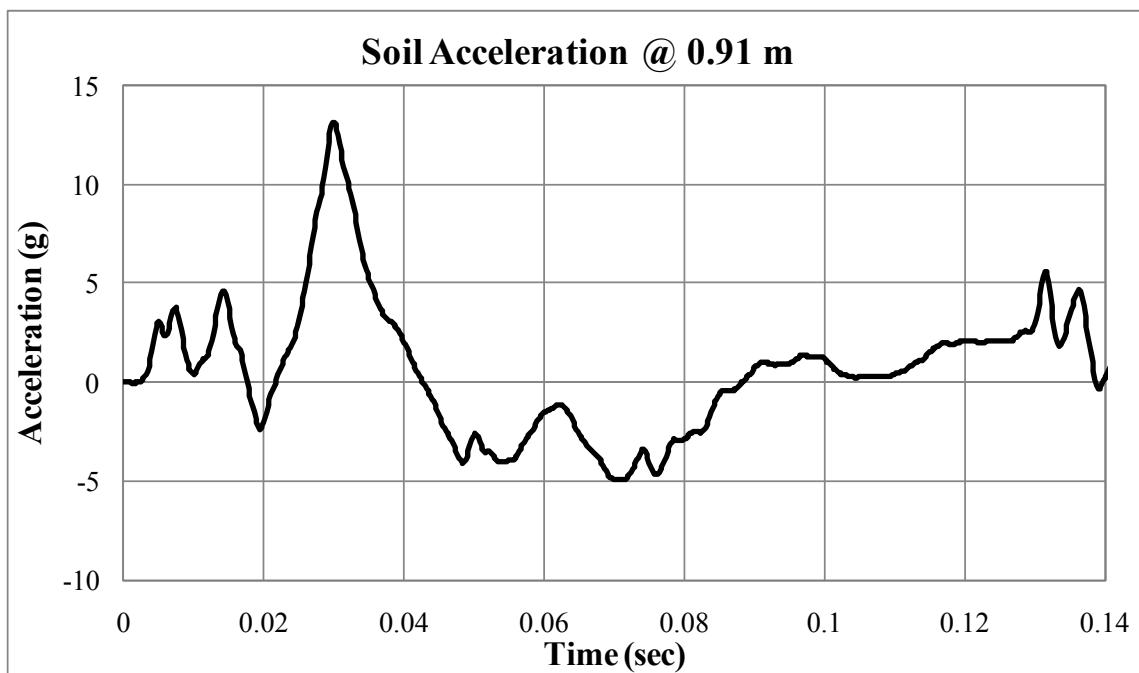
Figure B. 22. Soil acceleration history at 0.91 behind the post (Raw)
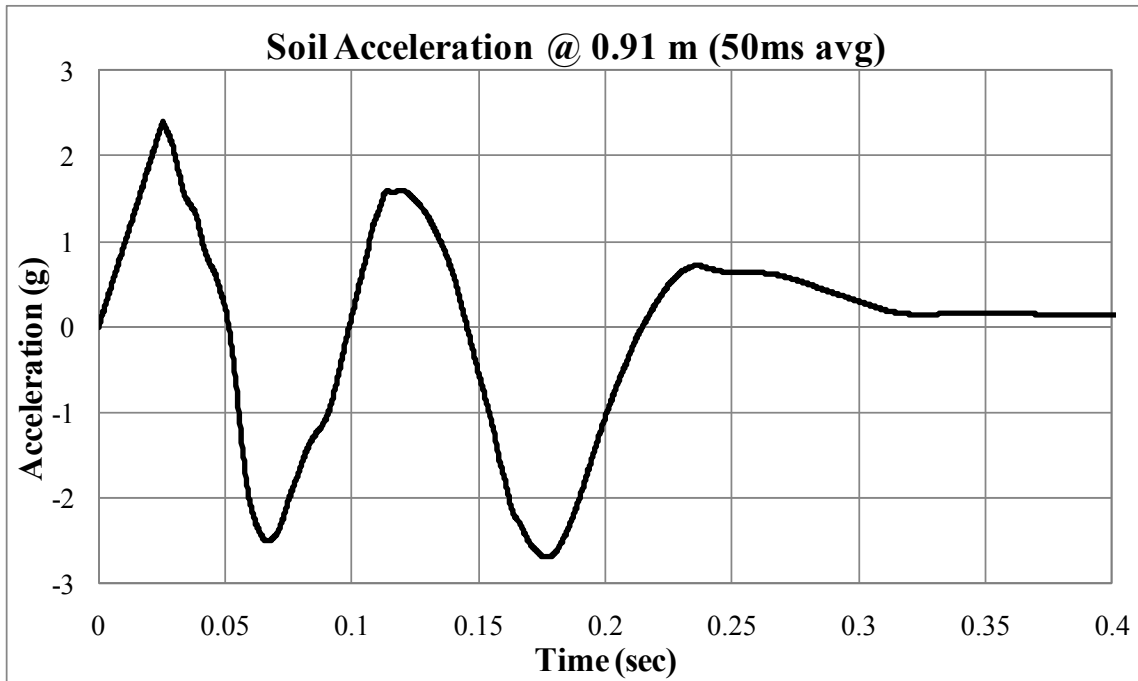
Figure B. 23. Soil acceleration history at 0.91 behind the post (50ms average)
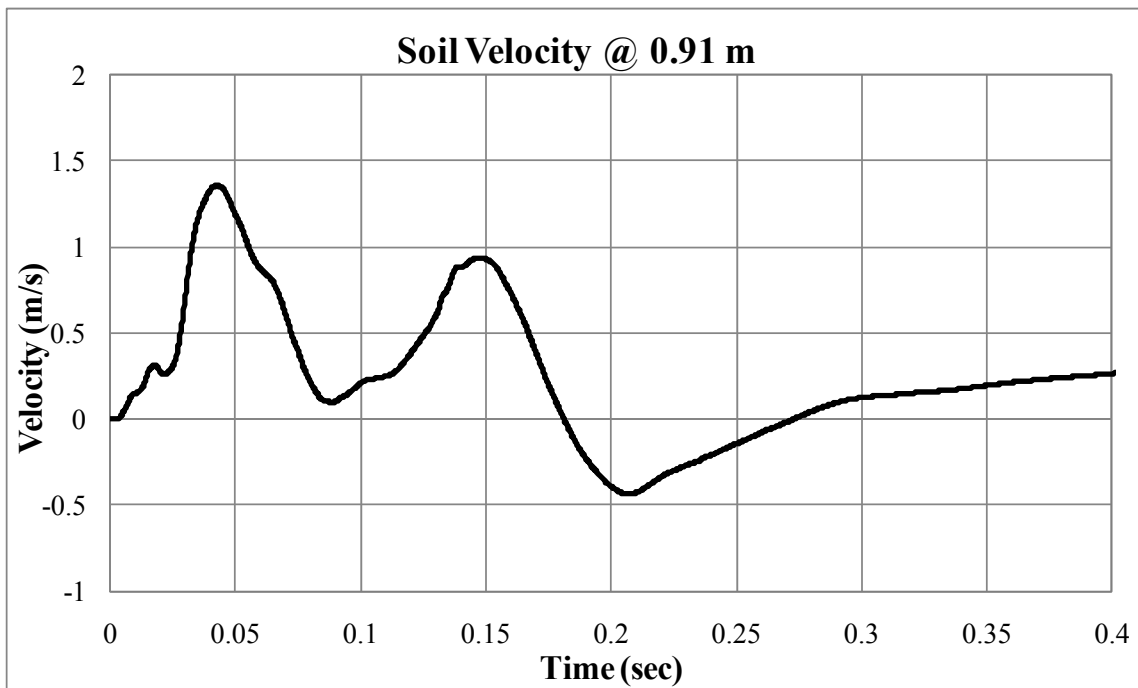
Figure B. 24. Soil velocity history at 0.91 behind the post
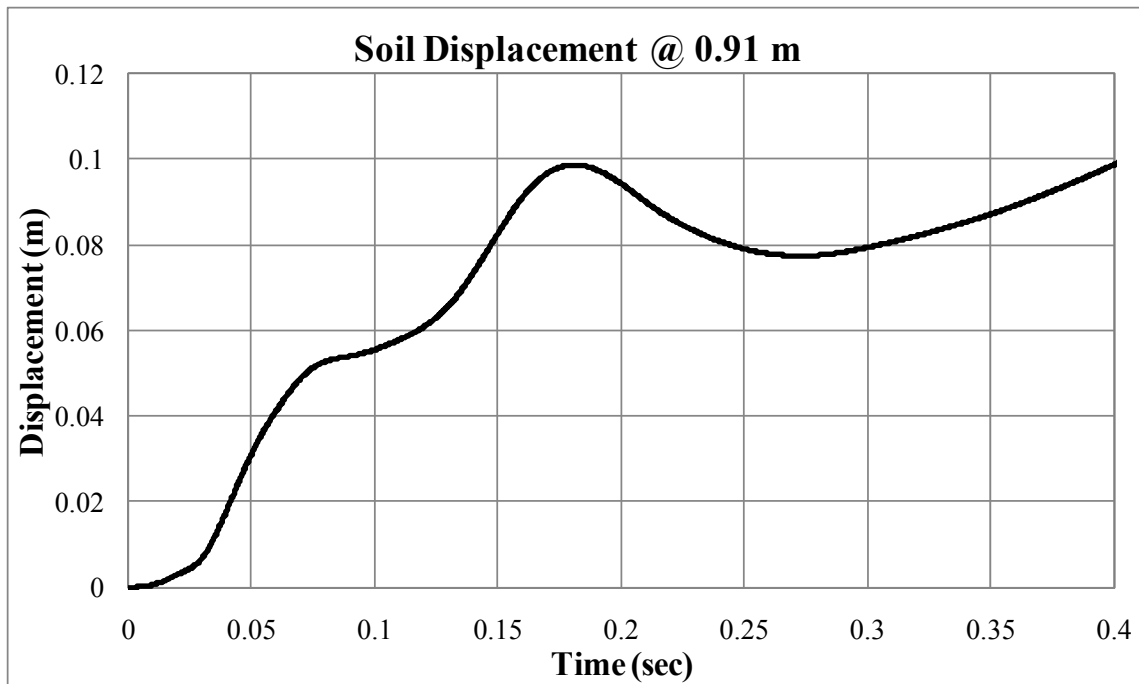
Figure B. 25. Soil displacement history at 0.91 behind the post

APPENDIX C

PENDULUM AND BOGIE TEST – JUNE 2008

Figure C. 1. Hydro Jack for static load test on posts for the model test

Figure C. 2. Displacement measurement of static load test on posts for the model test

Figure C. 3. Pendulum test on a single post embedded in loose sand (P6)

Figure C. 4. Group of posts systems for pendulum test

Figure C. 5. Accelerometer attached on a post system during pendulum test
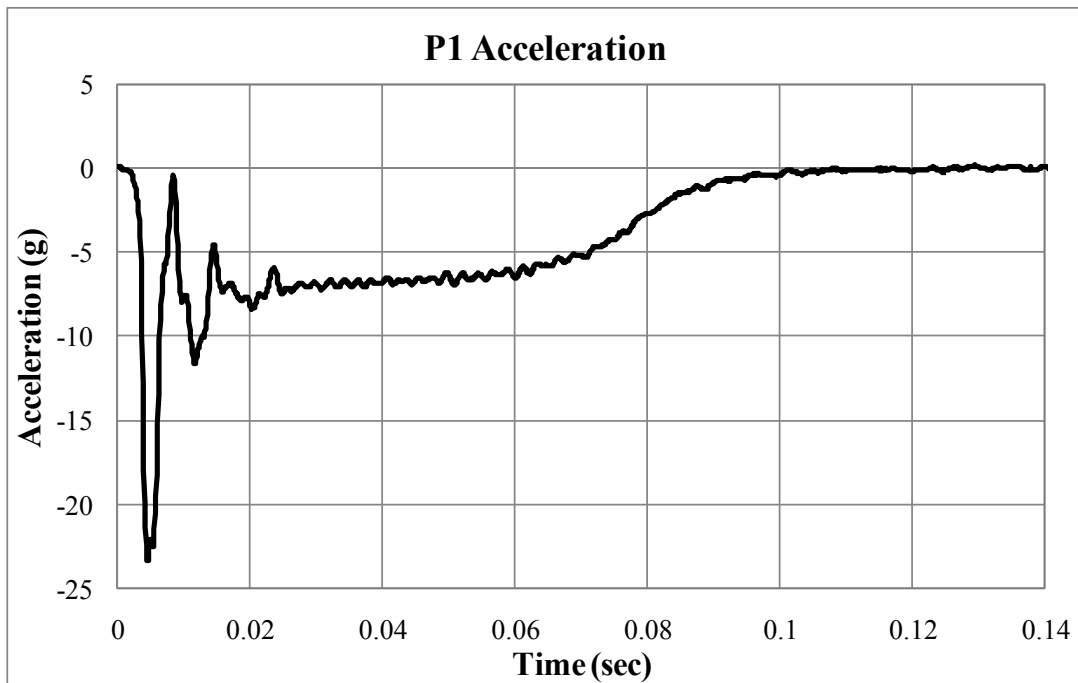
Figure C. 6. Raw pendulum deceleration history (P1)
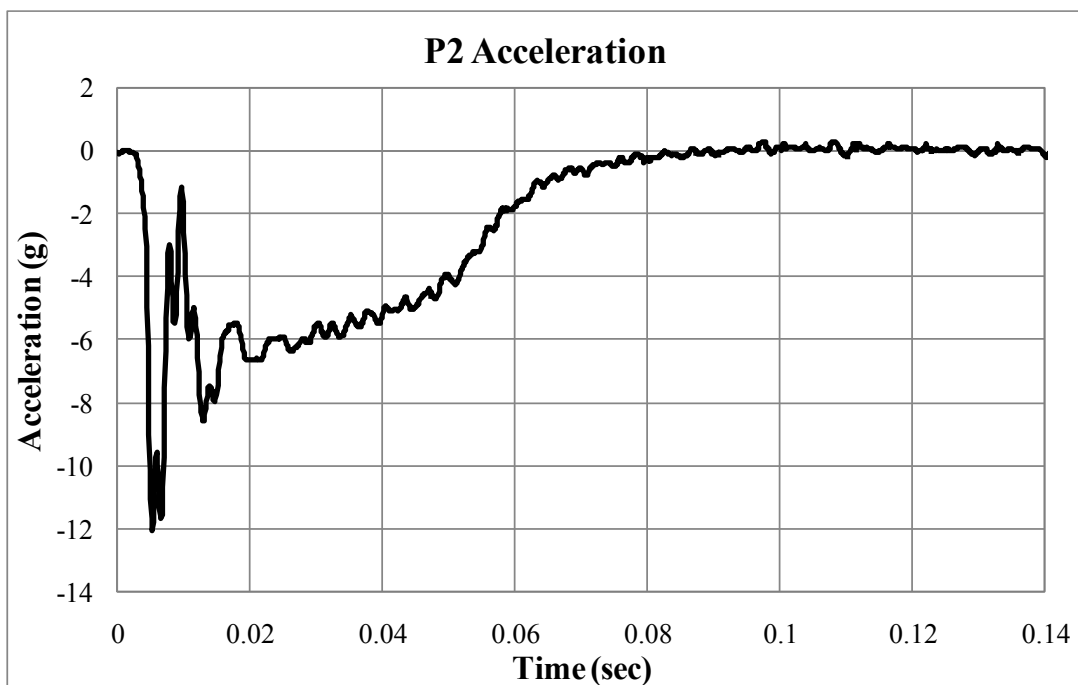
Figure C. 7. Raw pendulum deceleration history (P2)
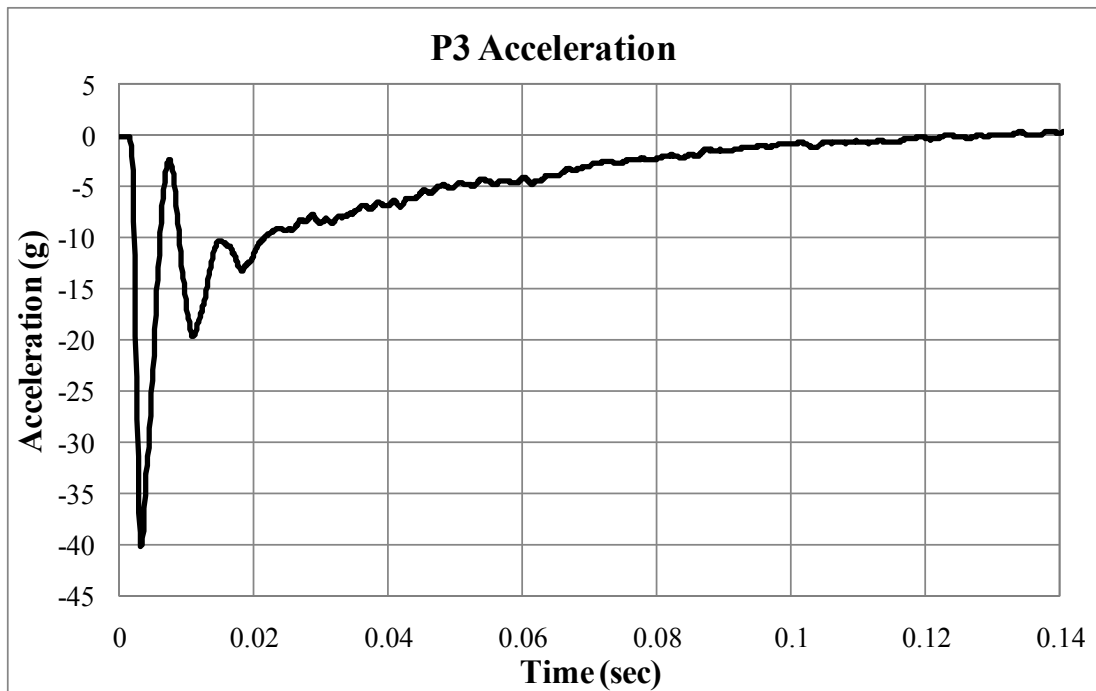
Figure C. 8. Raw pendulum deceleration history (P3)
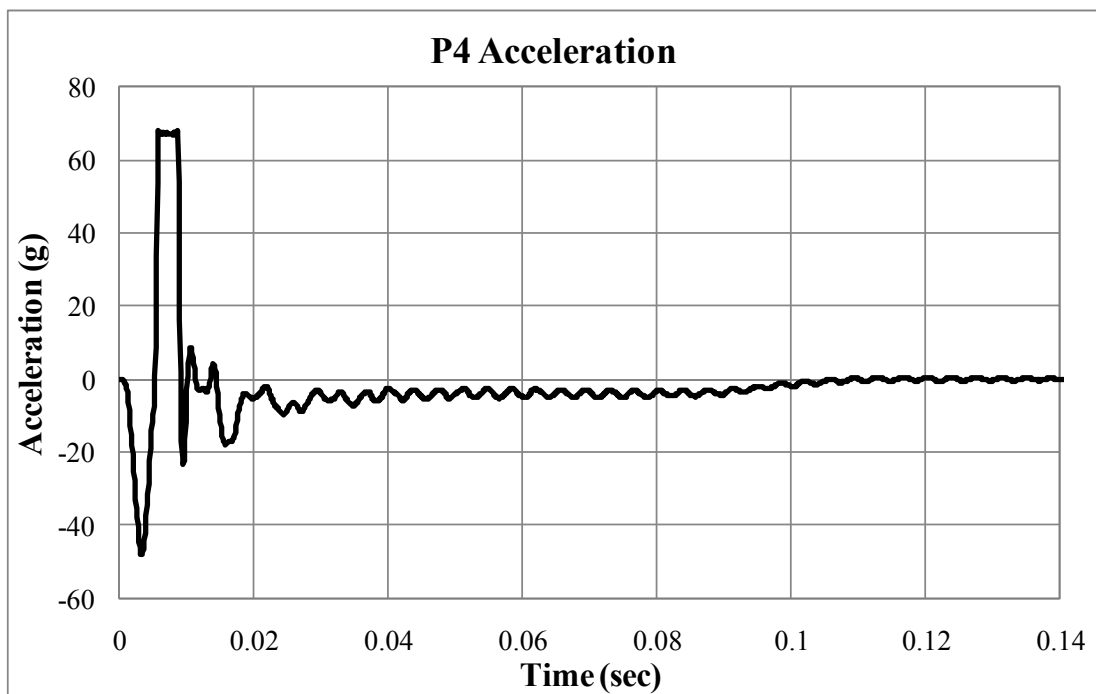
Figure C. 9. Raw pendulum deceleration history (P4)
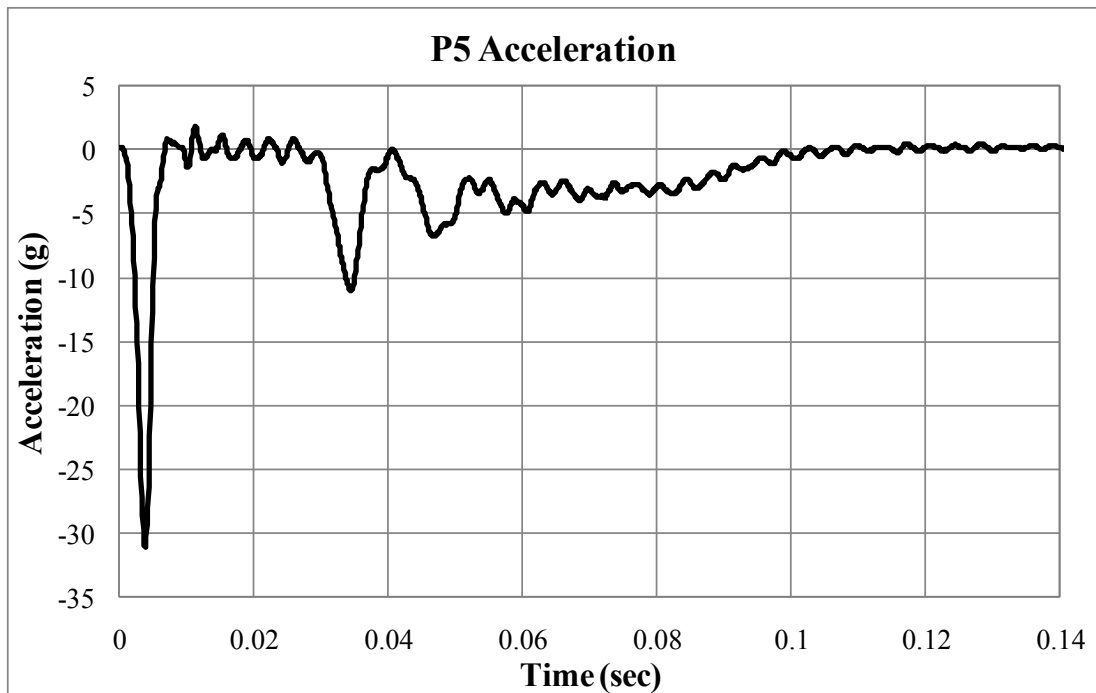
Figure C. 10. Raw pendulum deceleration history (P5)
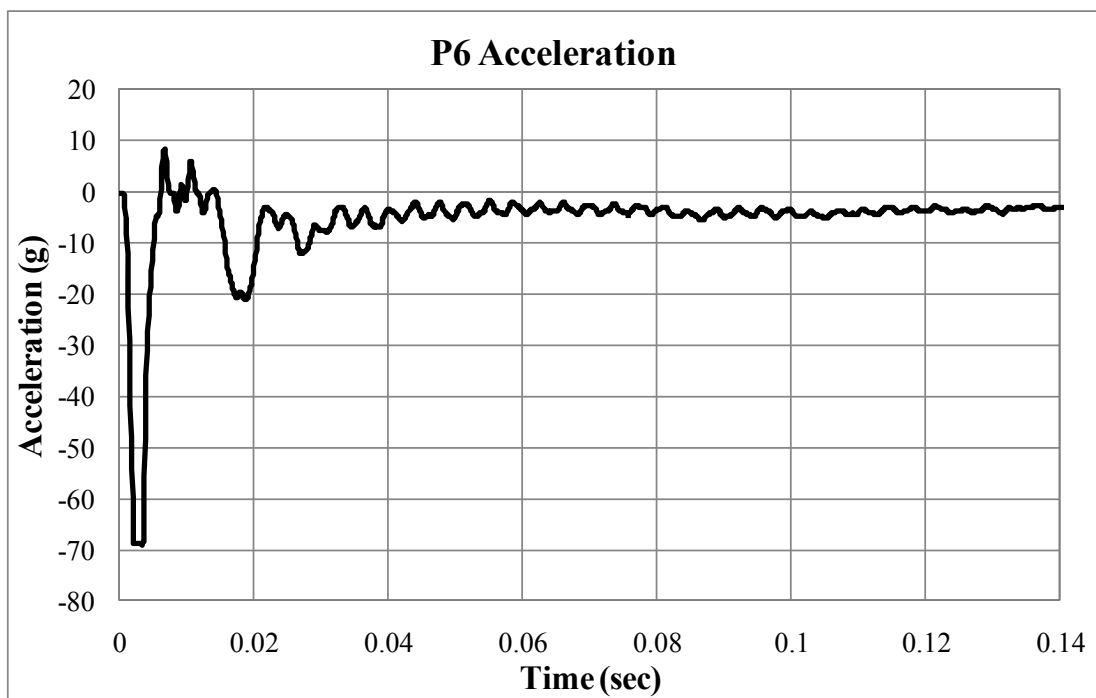
Figure C. 11. Raw pendulum deceleration history (P6)
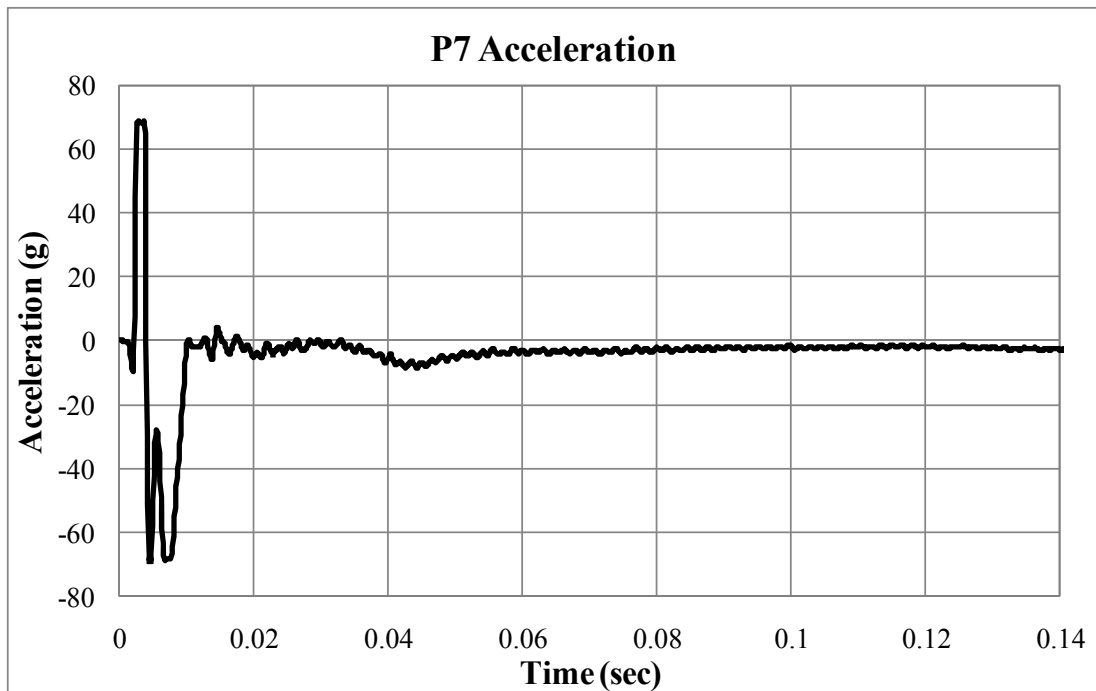
Figure C. 12. Raw pendulum deceleration history (P7)
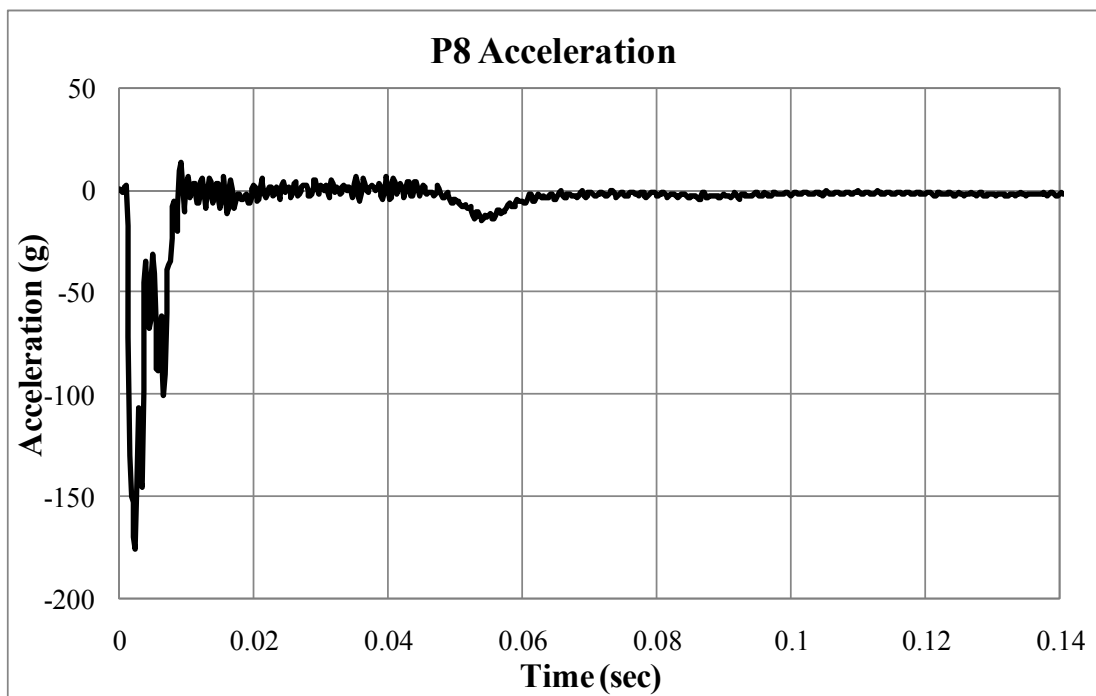
Figure C. 13. Raw pendulum deceleration history (P8)
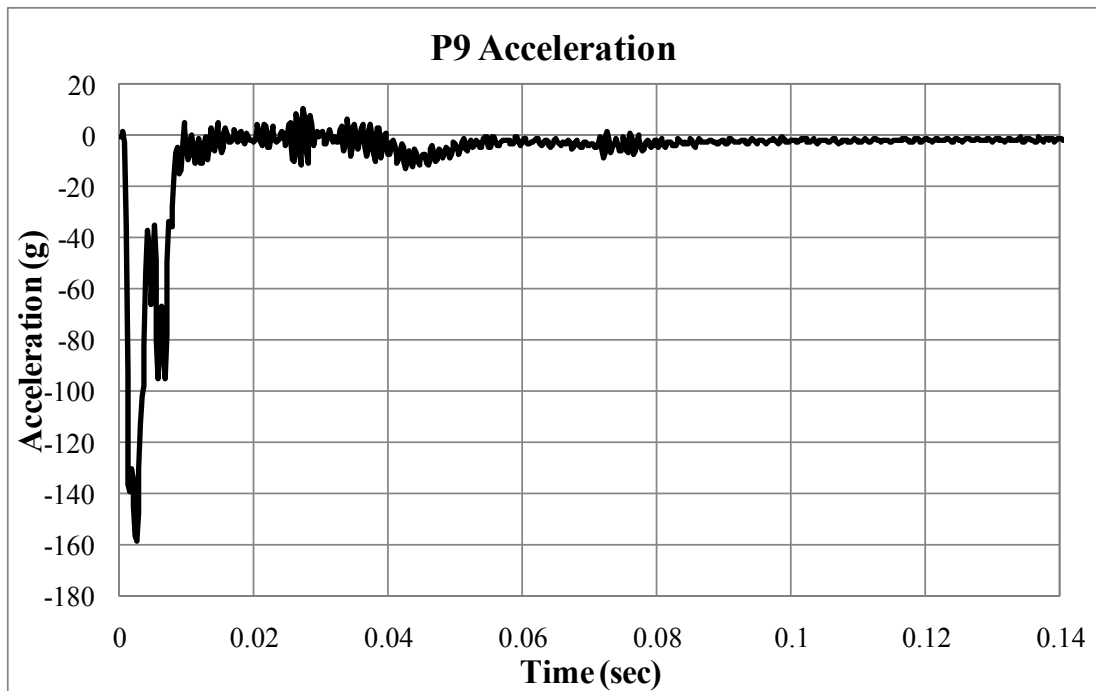
Figure C. 14. Raw pendulum deceleration history (P9)
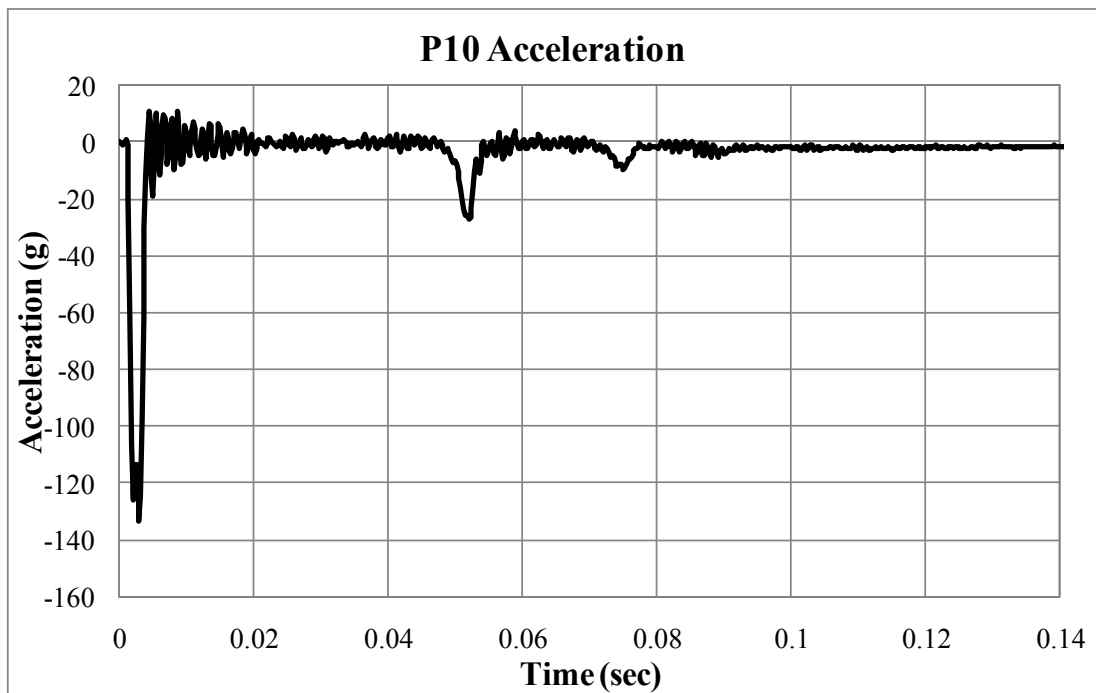
Figure C. 15. Raw pendulum deceleration history (P10)
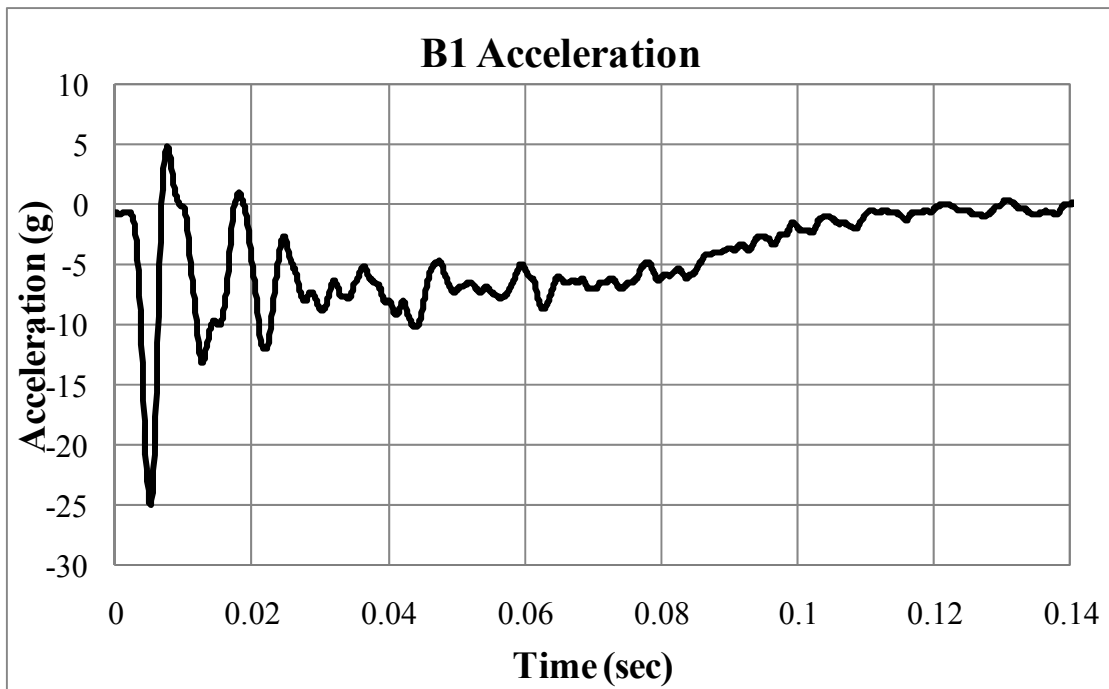
Figure C. 16. Raw bogie deceleration history (B1)
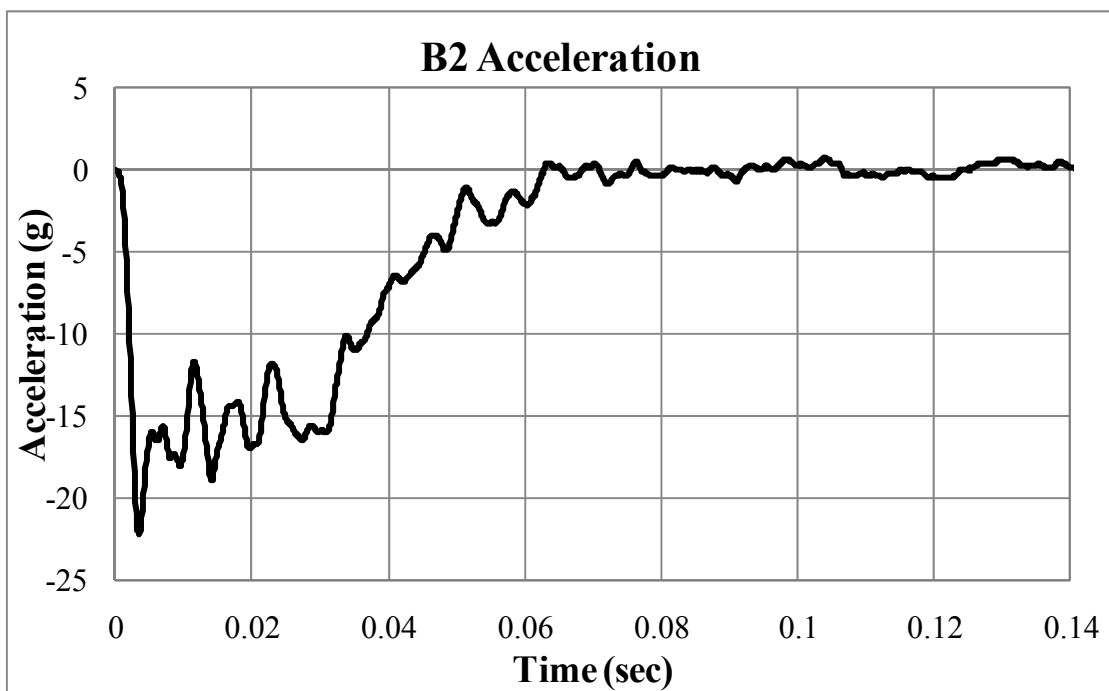
Figure C. 17. Raw bogie deceleration history (B1)

APPENDIX D

FULL-SCALE IMPACT TEST – MAY 2010

DATE: 2010-05-27   TEST NO.: 400951-SNL24   VIN NO.: 1HTSCABN41H369576

YEAR: 2001   MAKE: International   MODEL: 4700

TIRE SIZE: 275/80R22.5   ODOMETER: 145741
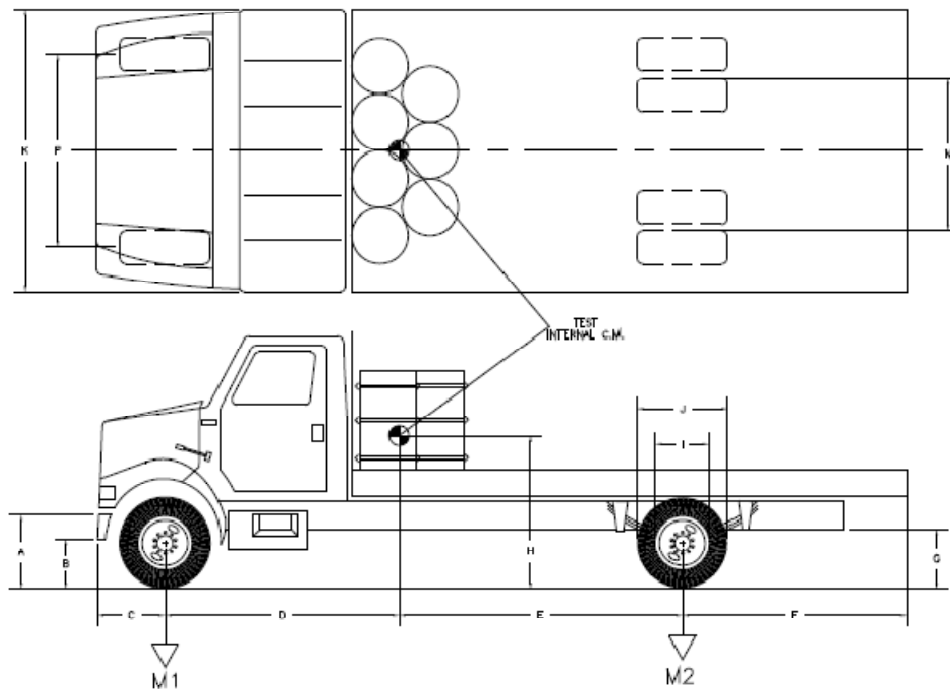
GEOMETRY (inches)

A 31.5   B 20.5   C 30.5   D 103.5   E 102.5   F 111.5   G 29.0
80.5

H _____   I 23.5   J 39.5   K 94.0   L 80.5   N _____   D+E = 206

Allowed Range for Wheelbase (D+E) = 208 ± 20 inches

MASS DISTRIBUTION (lb)

LF 3770   RF 3730   LR 3910   RR 3660

MASS (kg)	CURB	TEST INERTIAL	
M_1	6340	7500	
M_2	5800	7570	Allowed Range for Inertial Wt.=
M_{Total}	12,140	15,070	15000 ± 309 lb

Figure D.1. Test vehicle properties (Arrington et al. 2010)

Figure D.2.Dumping clean sand into the excavated ditch for the impact test

Figure D.3. Installation of horizontal beams of the group of posts system

Figure D.4. Hydro Jack for static load test on a post for the impact test on a group of posts system in loose sand

Figure D.5. Displacement measurement of static load test on a post for the impact test on a group of posts system in loose sand

0.000 s

0.196 s

0.049 s
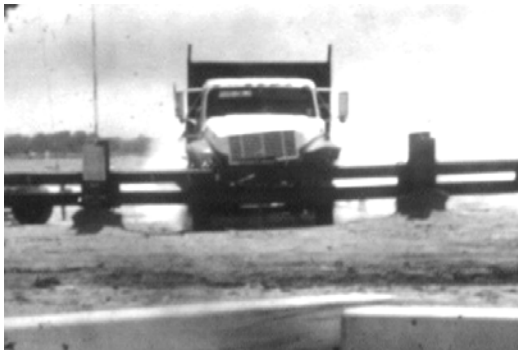
0.245 s

0.098 s

0.341 s

0.147 s

0.537 s

Figure D.6. Sequential photographs - frontal view (Arrington et al. 2010)
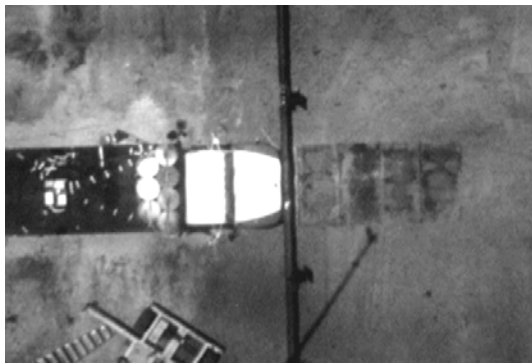
0.000 s
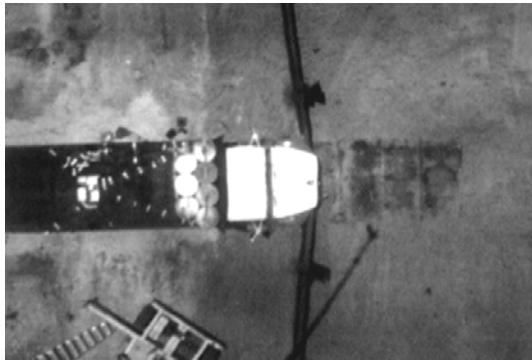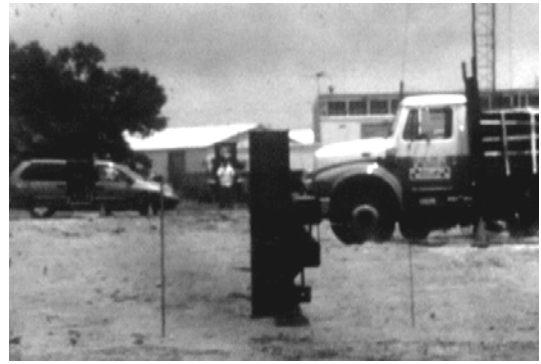
0.049 s
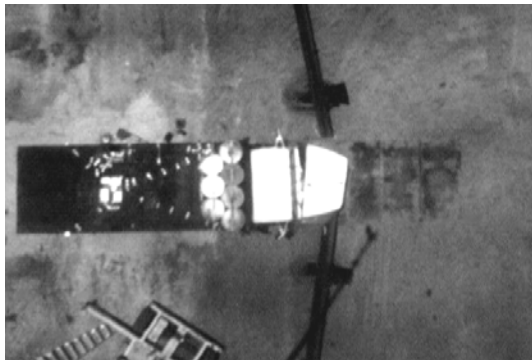
0.098 s
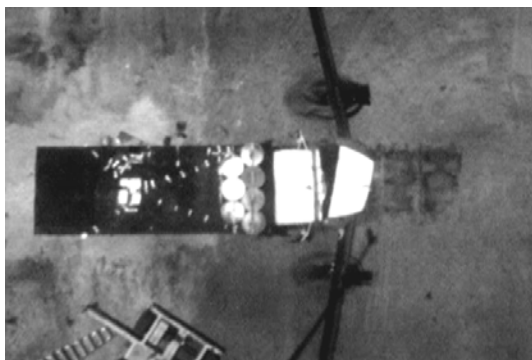
0.147 s

Figure D.7. Sequential photographs - overhead and perpendicular views (Arrington et al. 2010)
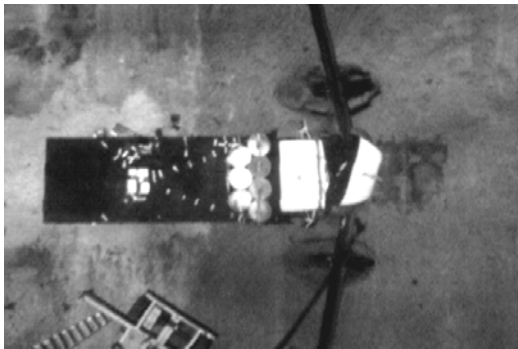
0.196 s
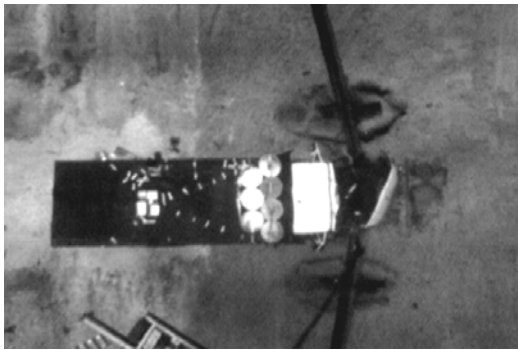
0.245 s
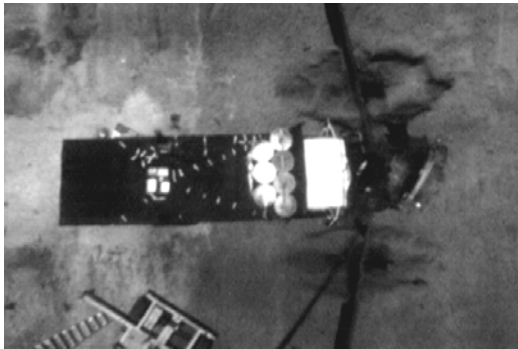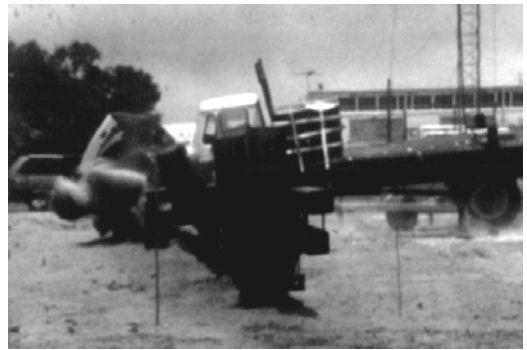
0.341 s
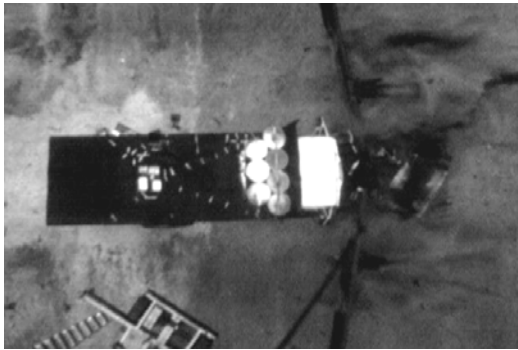
0.537 s

Figure D.7. Continued

Figure D.8. Sequential photographs for the impact test on group of posts system

APPENDIX E

NUMERICAL SIMULATIONS
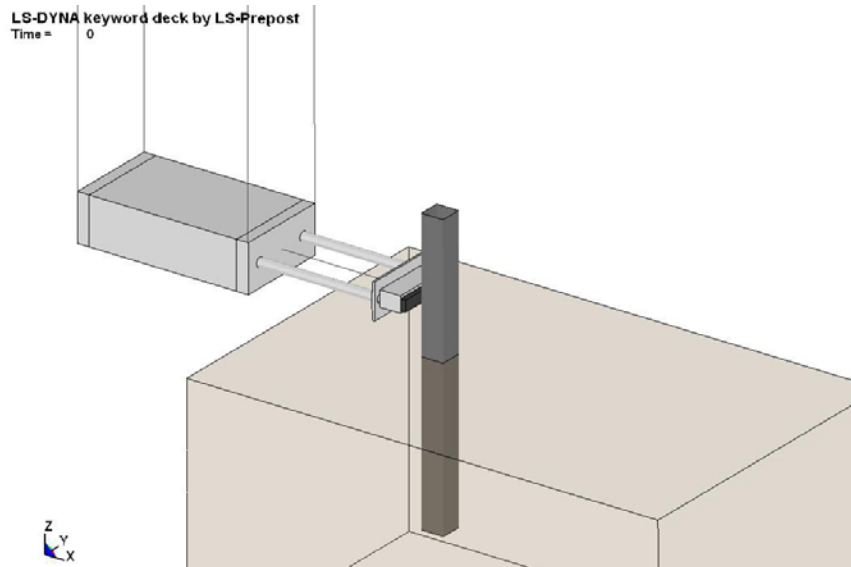
Figure E. 1. Numerical simulation of Pendulum test (P3) at 0.00 sec
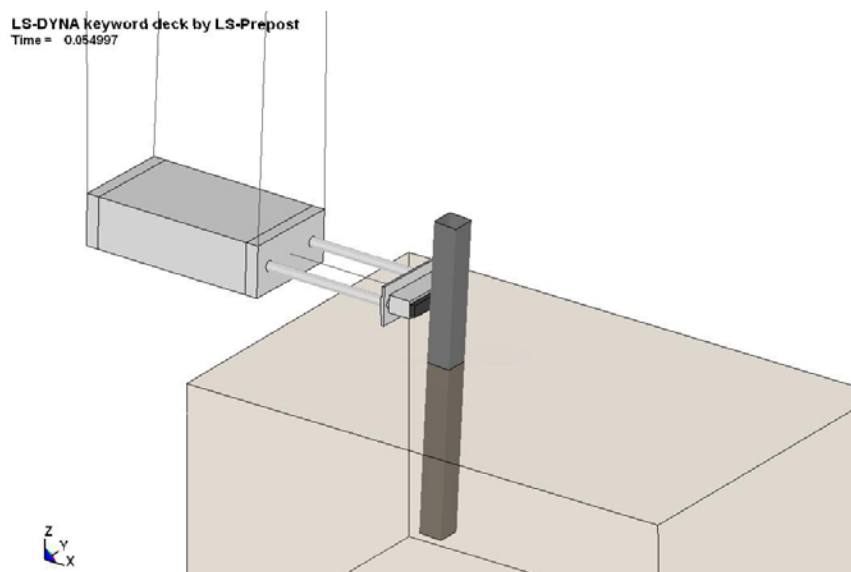
Figure E. 2. Numerical simulation of Pendulum test (P3) at 0.55 sec
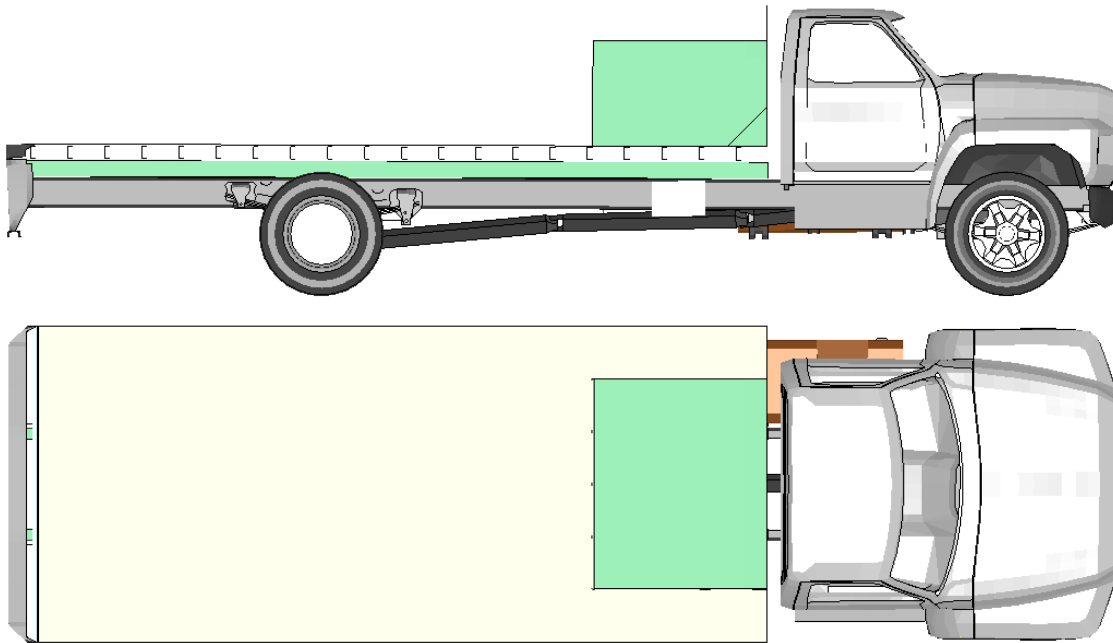
Figure E. 3. Finite element model of the test vehicle (side elevation and plan view)
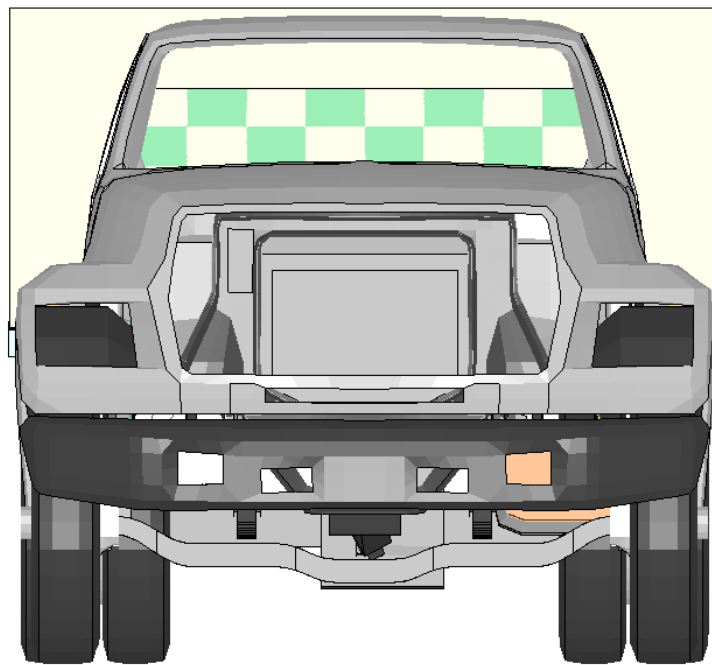
Figure E. 4. Finite element model of the test vehicle (front elevation view)
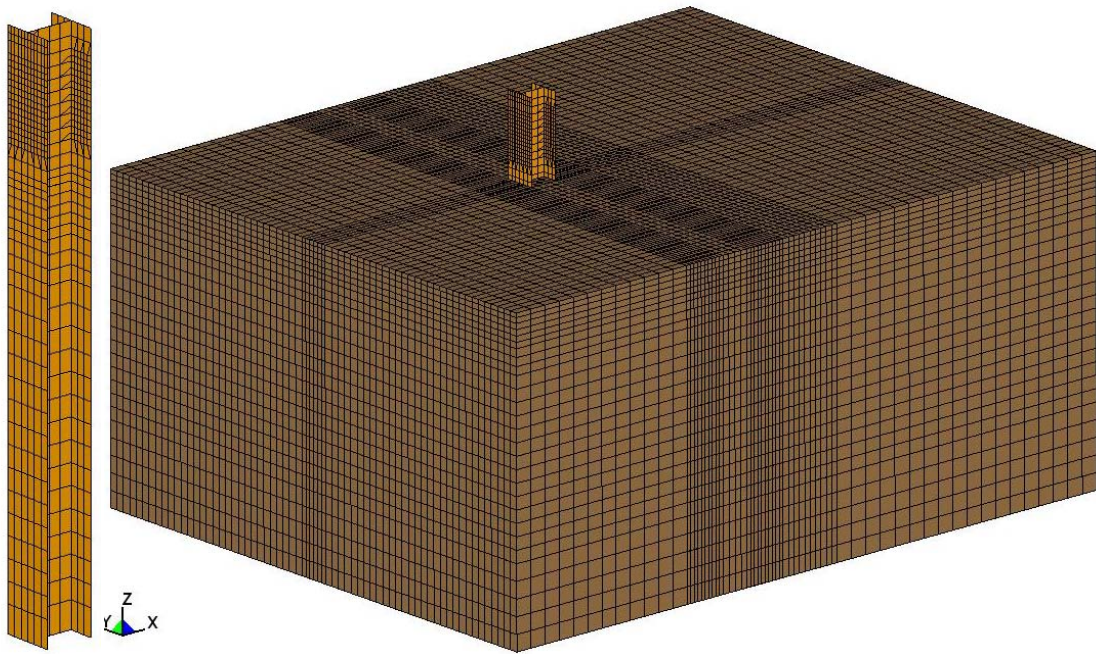
Figure E. 5. Finite element model of a single post and soil
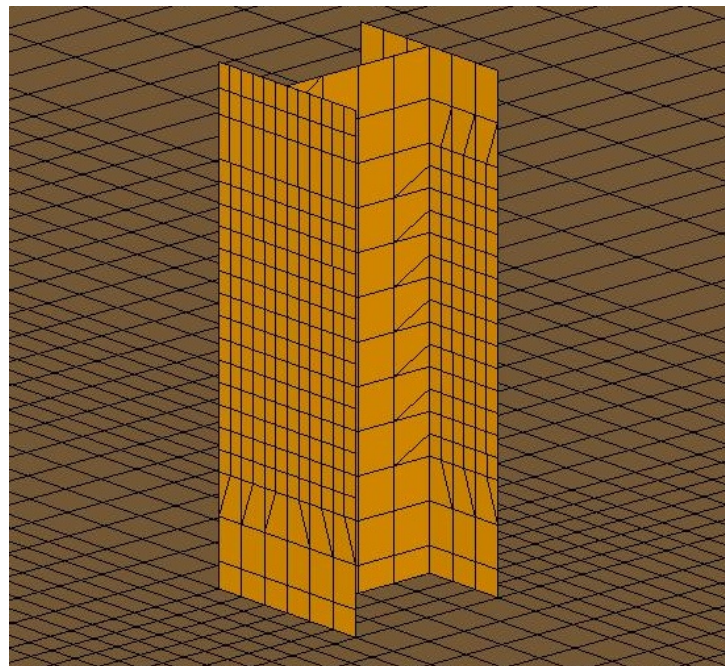
Figure E. 6. Fine post mesh to avoid the element tangling
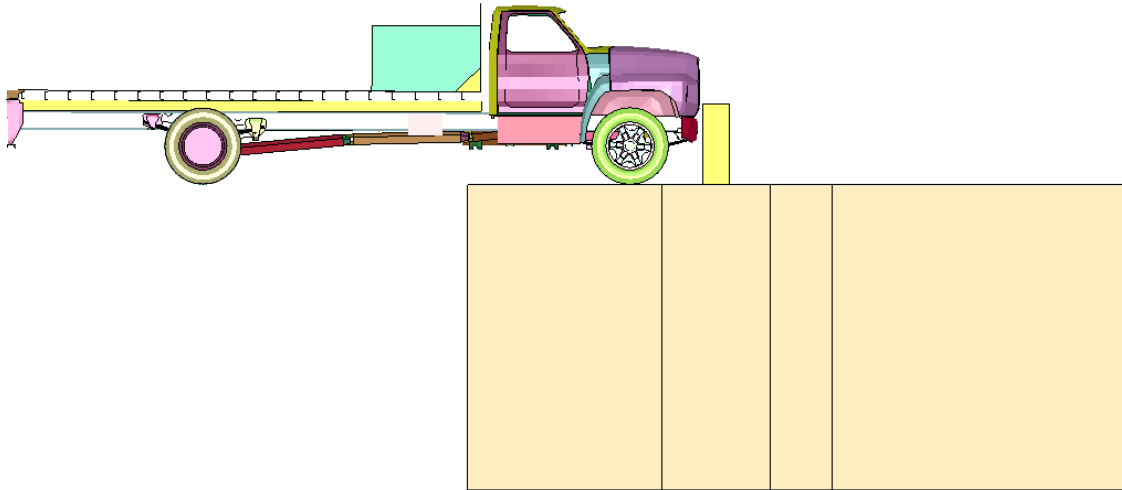
Figure E. 7. Finite element model of the impact test on a single post (side elevation)
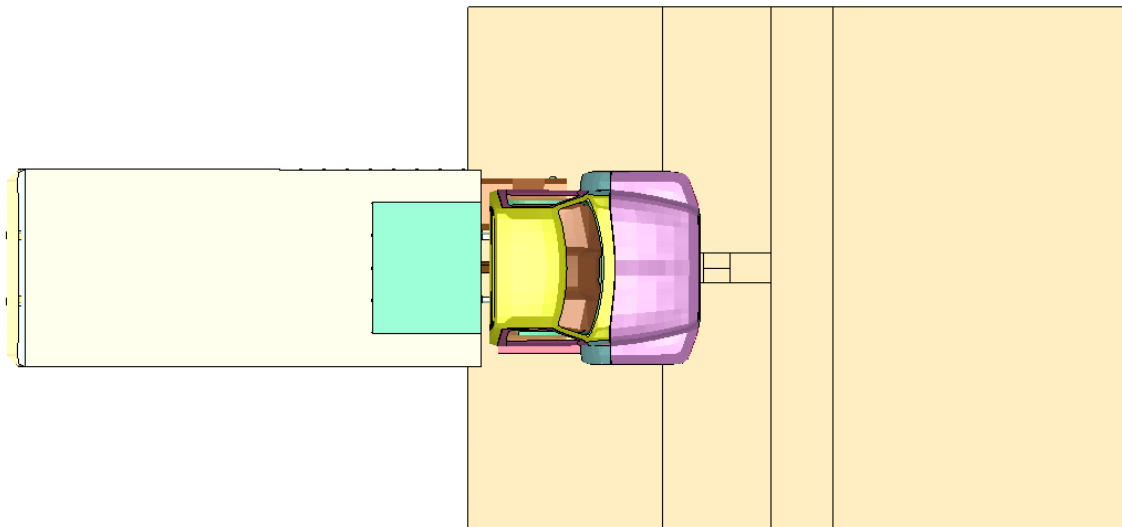
Figure E. 8. Finite element model of the impact test on a single post (plan view)
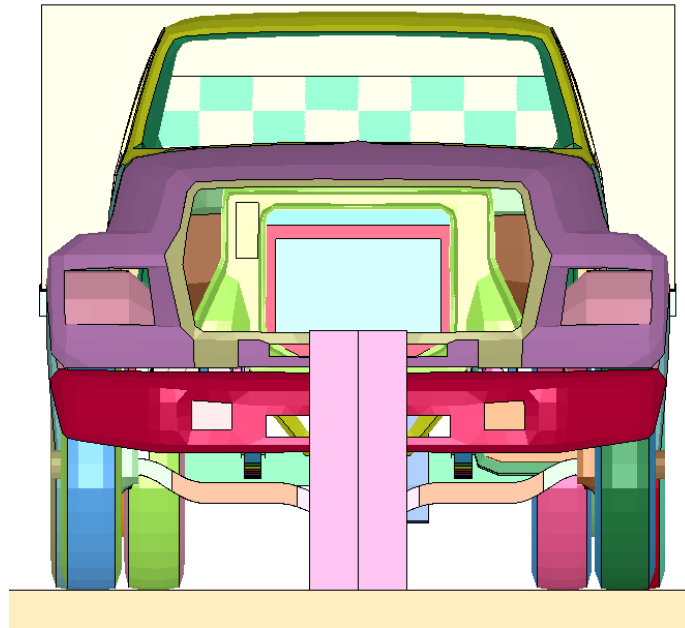
Figure E. 9. Finite element model of the impact test on a single post (front elevation)
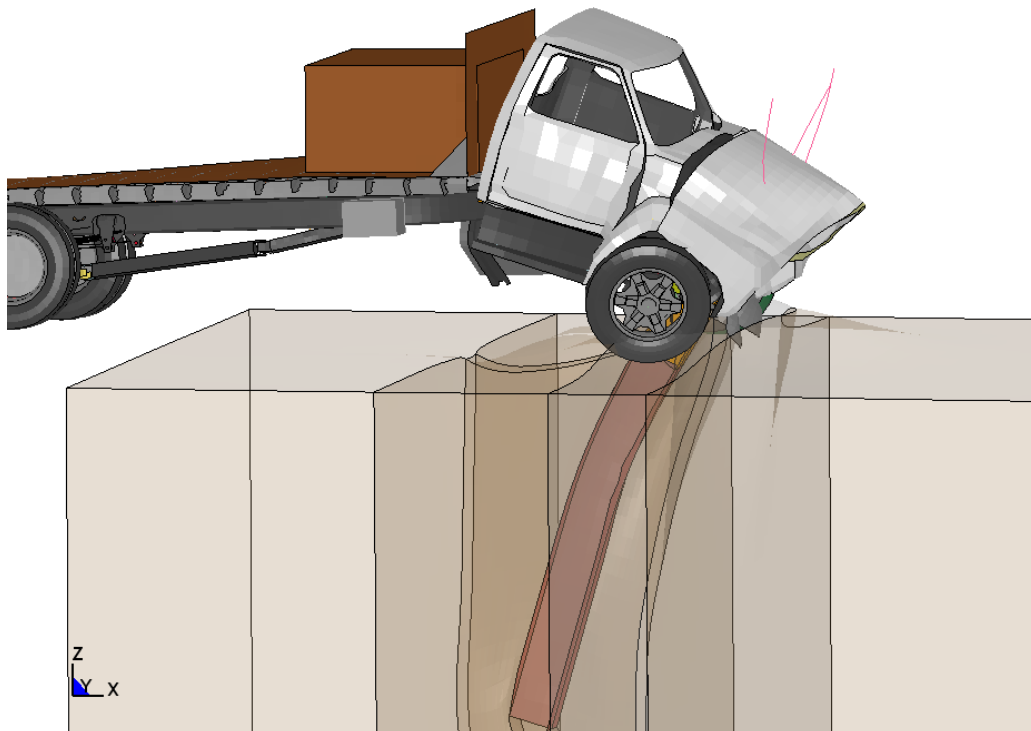
Figure E. 10. Numerical simulation of the full-scale impact test on a single post
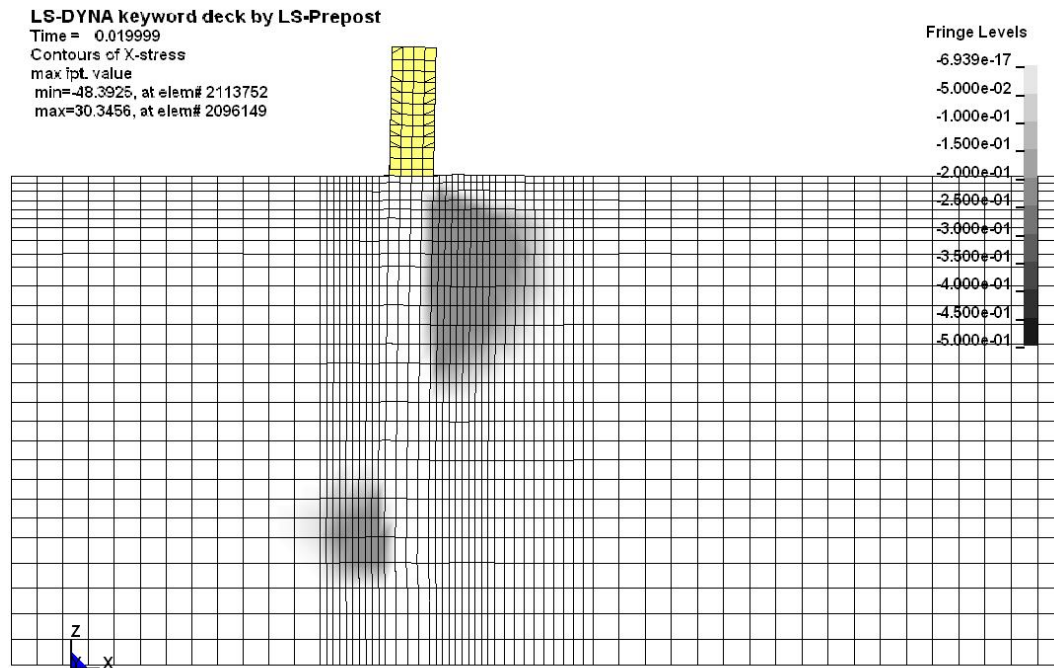
Figure E. 11. Simulated soil pressure of the impact test on a single post at 0.020 sec
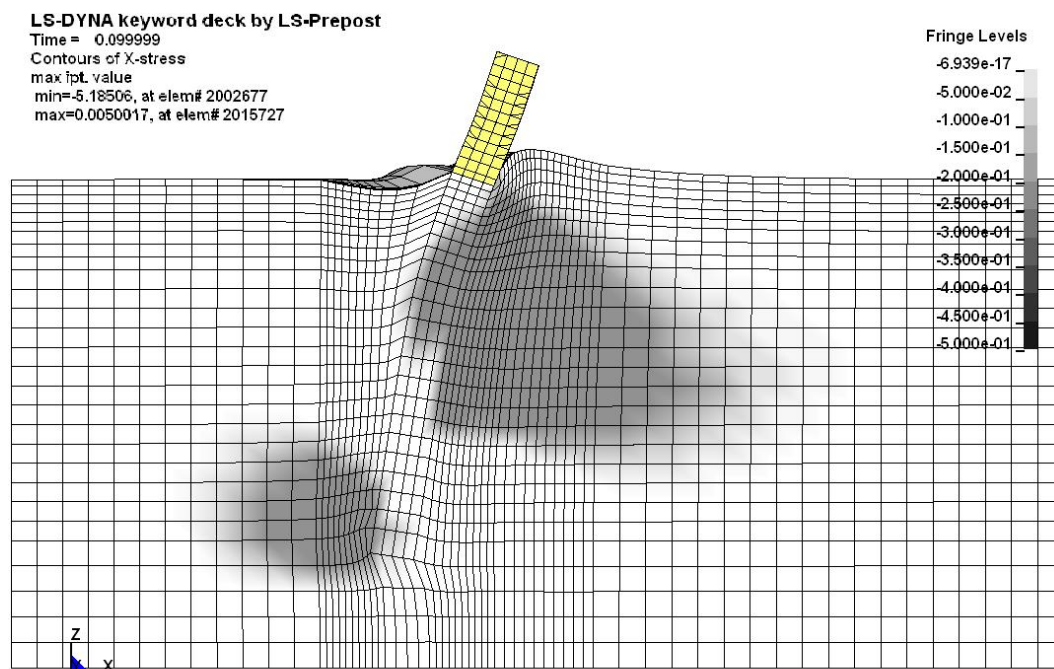
Figure E. 12. Simulated soil pressure of the impact test on a single post at 0.100 sec
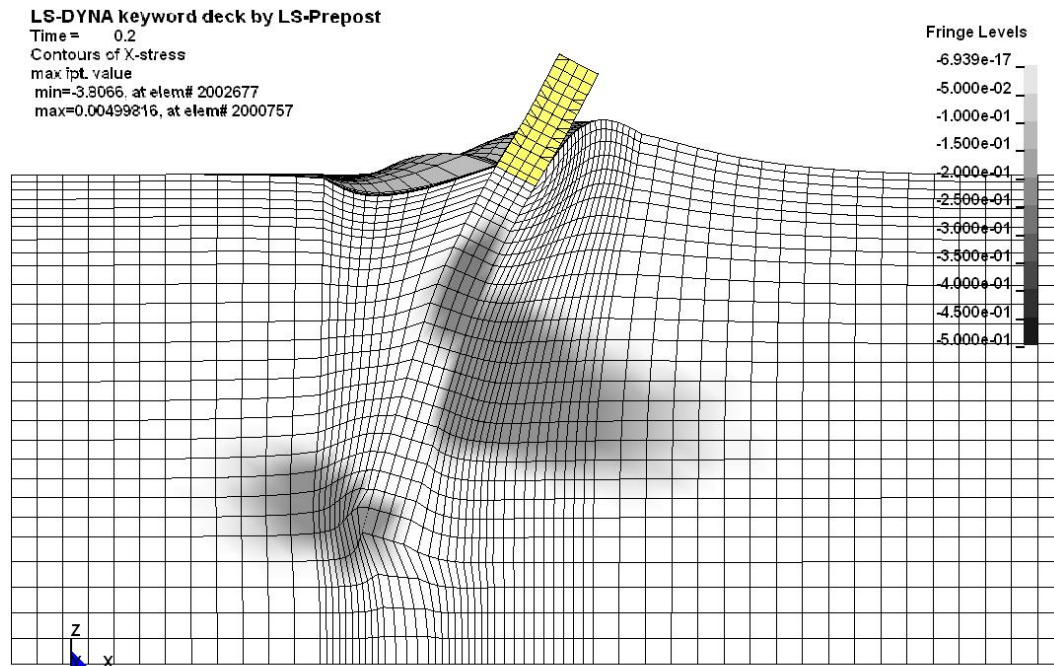
Figure E. 13. Simulated soil pressure of the impact test on a single post at 0.200 sec
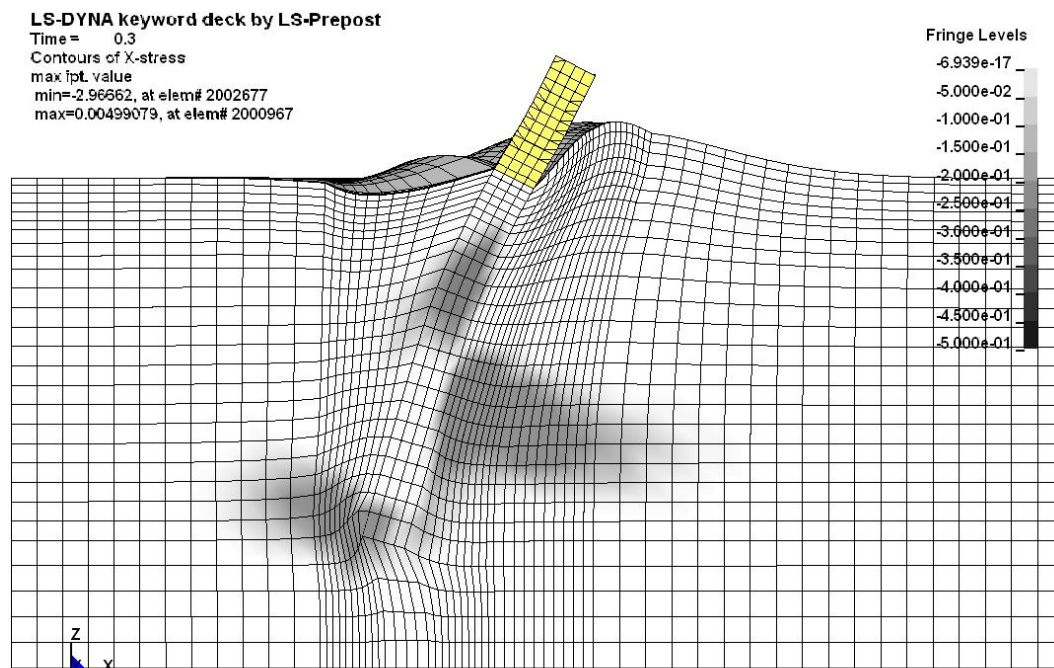
Figure E. 14. Simulated soil pressure of the impact test on a single post at 0.300 sec
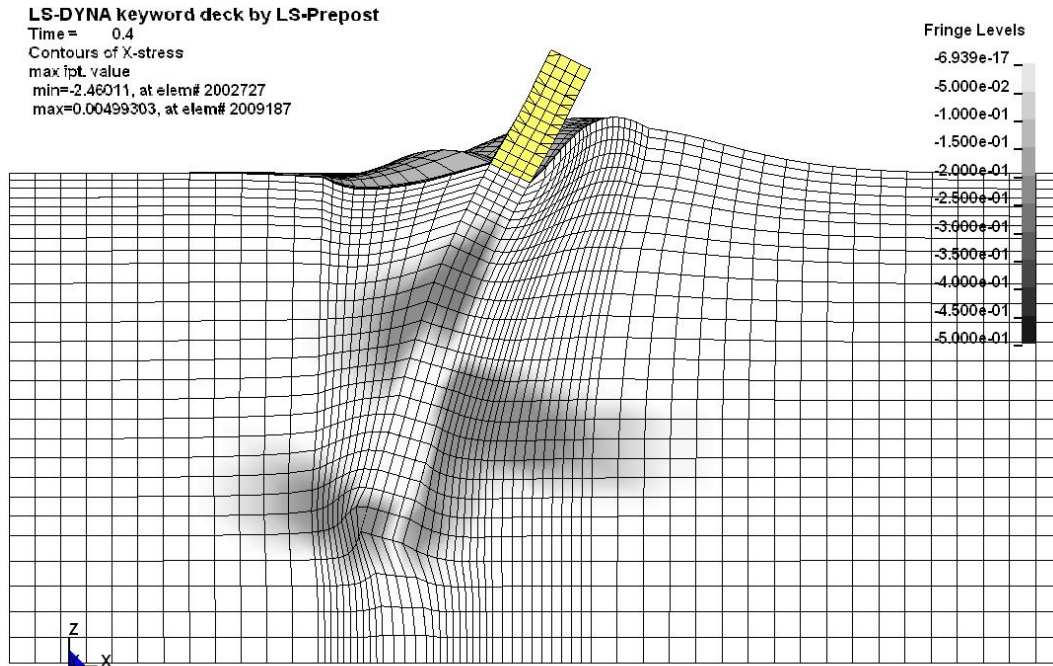
Figure E. 15. Simulated soil pressure of the impact test on a single post at 0.400 sec
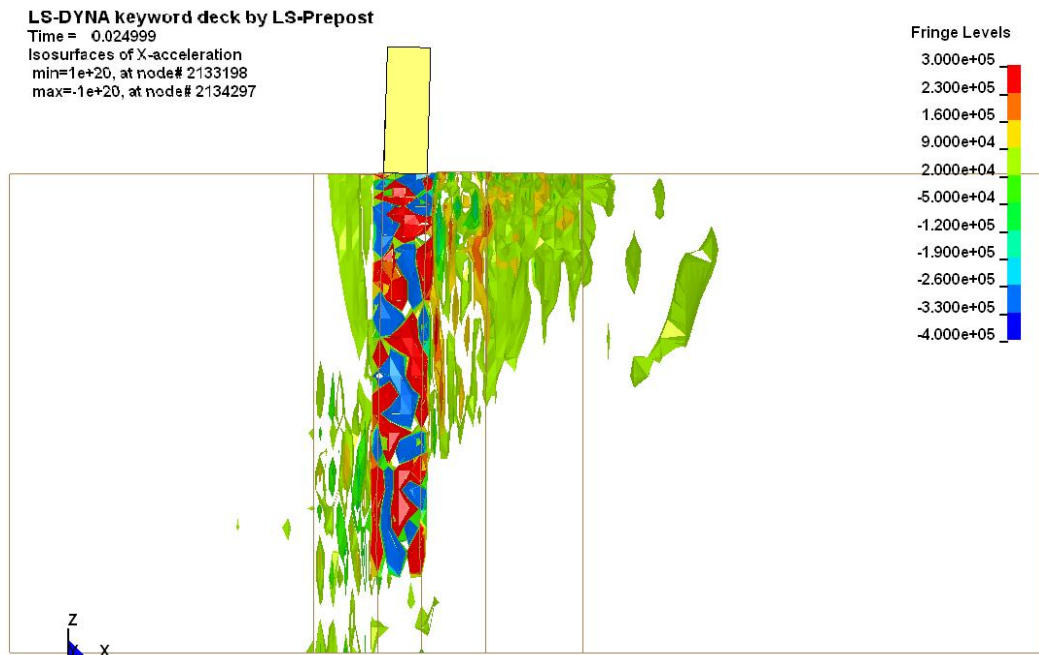
Figure E. 16. Simulated soil acceleration of the impact test on a single post at 0.025 sec
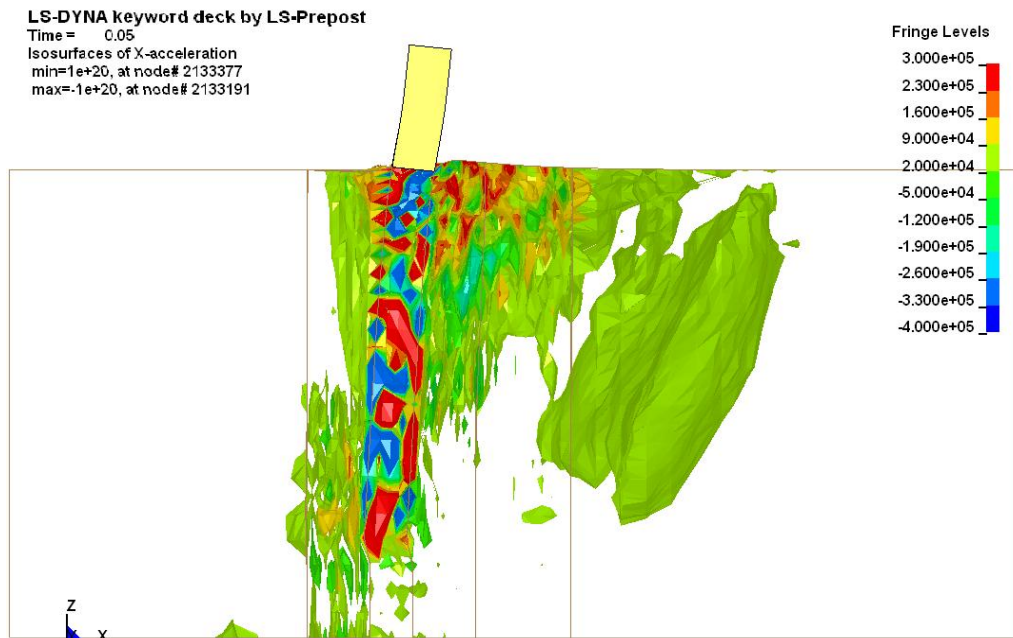
Figure E. 17. Simulated soil acceleration of the impact test on a single post at 0.050 sec
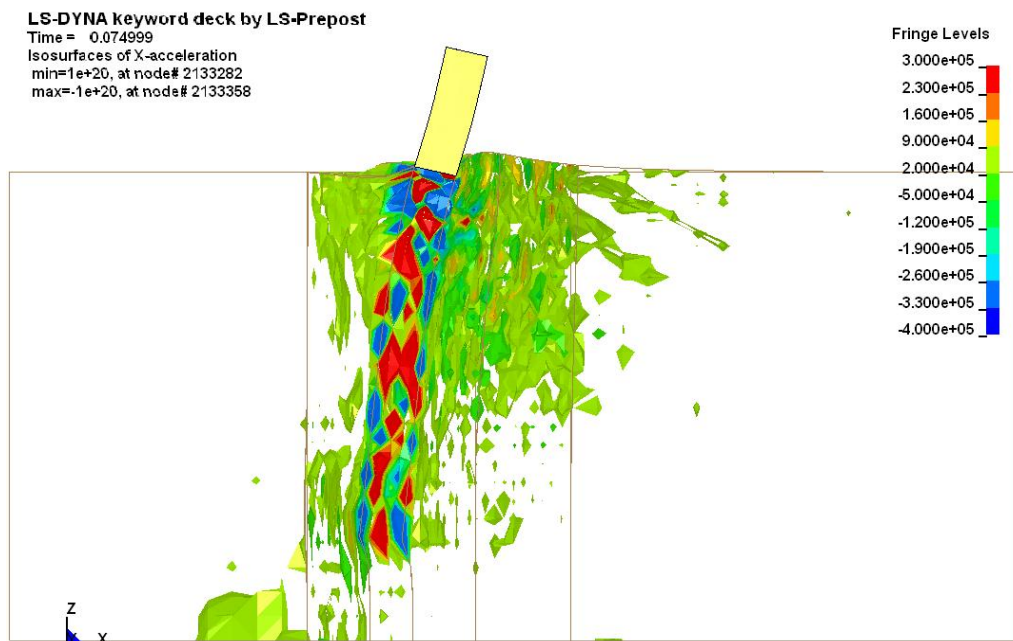
Figure E. 18. Simulated soil acceleration of the impact test on a single post at 0.075 sec
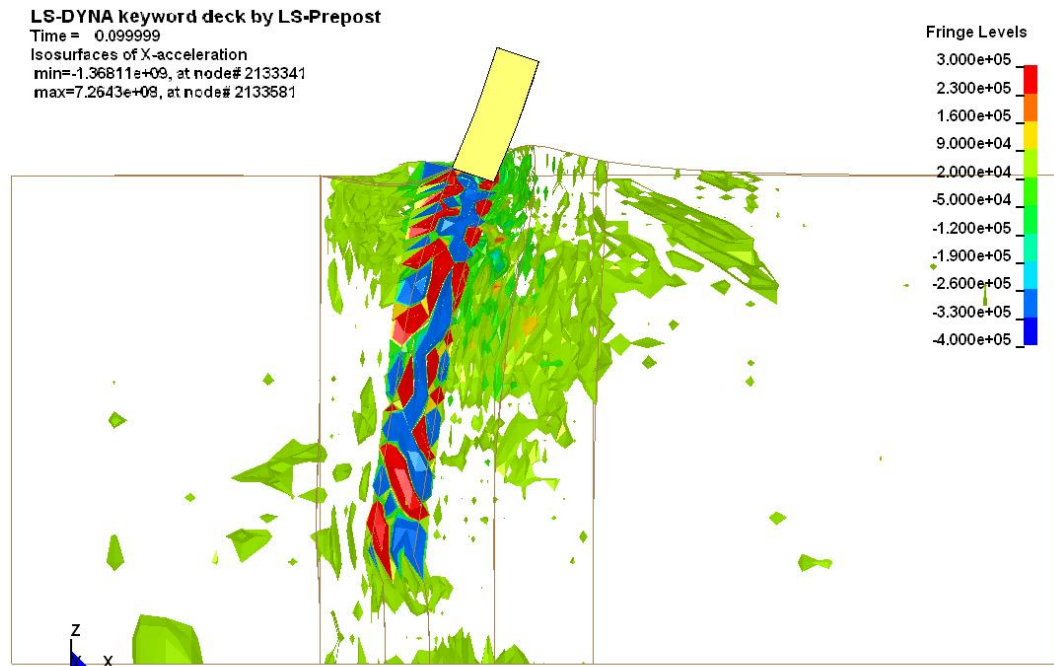
Figure E. 19. Simulated soil acceleration of the impact test on a single post at 0.100 sec
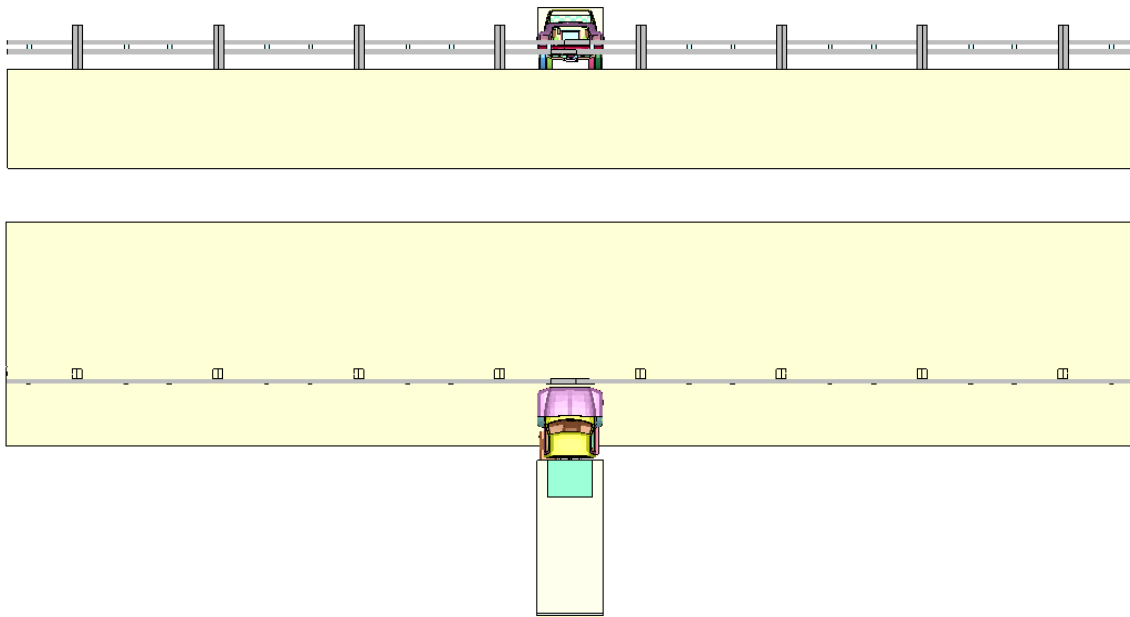
Figure E. 20. Finite element model of the impact test on a group of posts
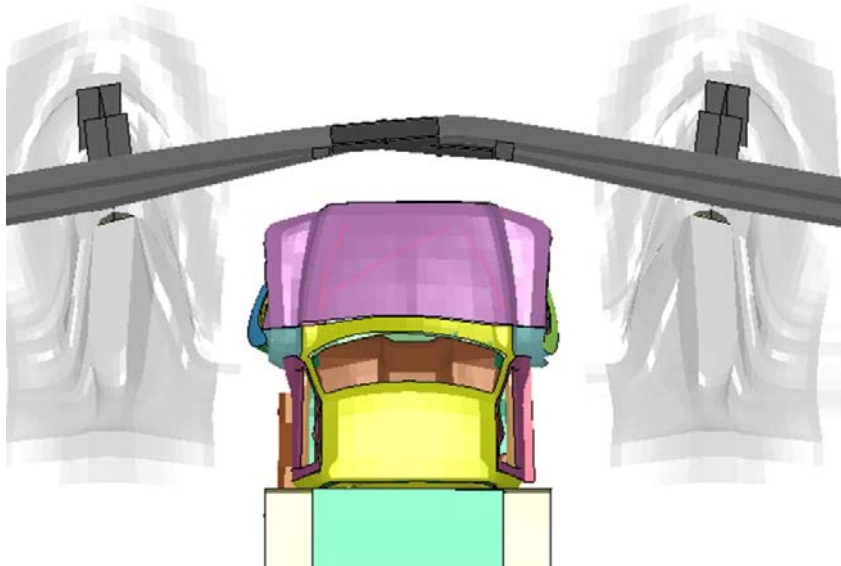
Figure E. 21. Numerical simulation of the impact test on a group of posts (plan view)
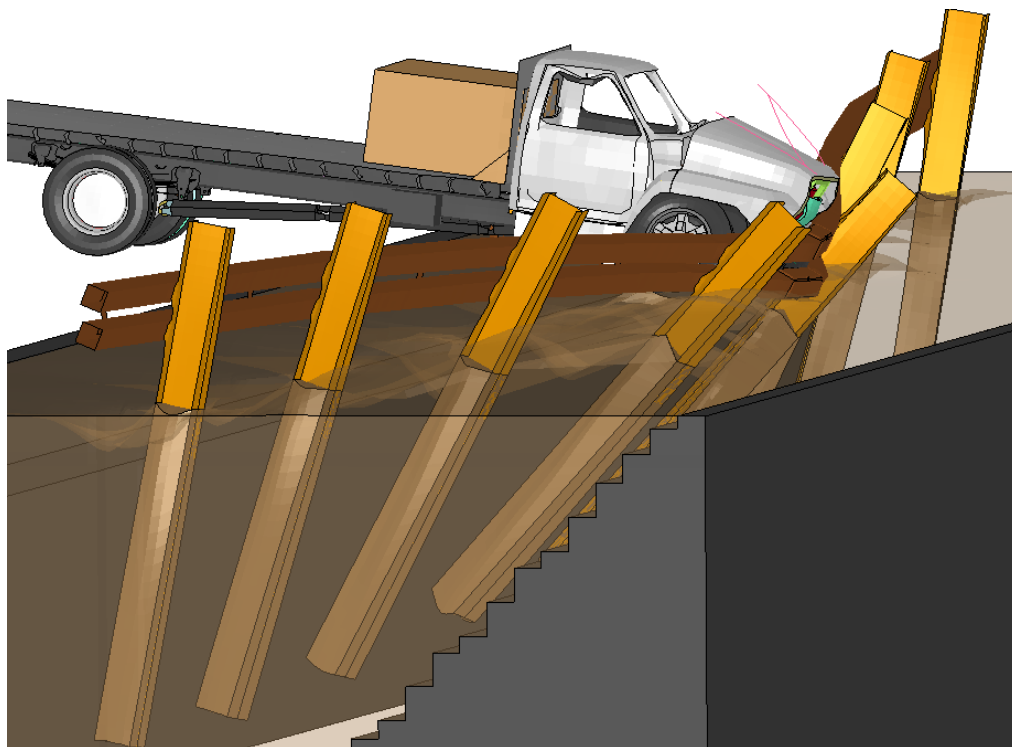
Figure E. 22. Numerical simulation of the impact test on a group of posts
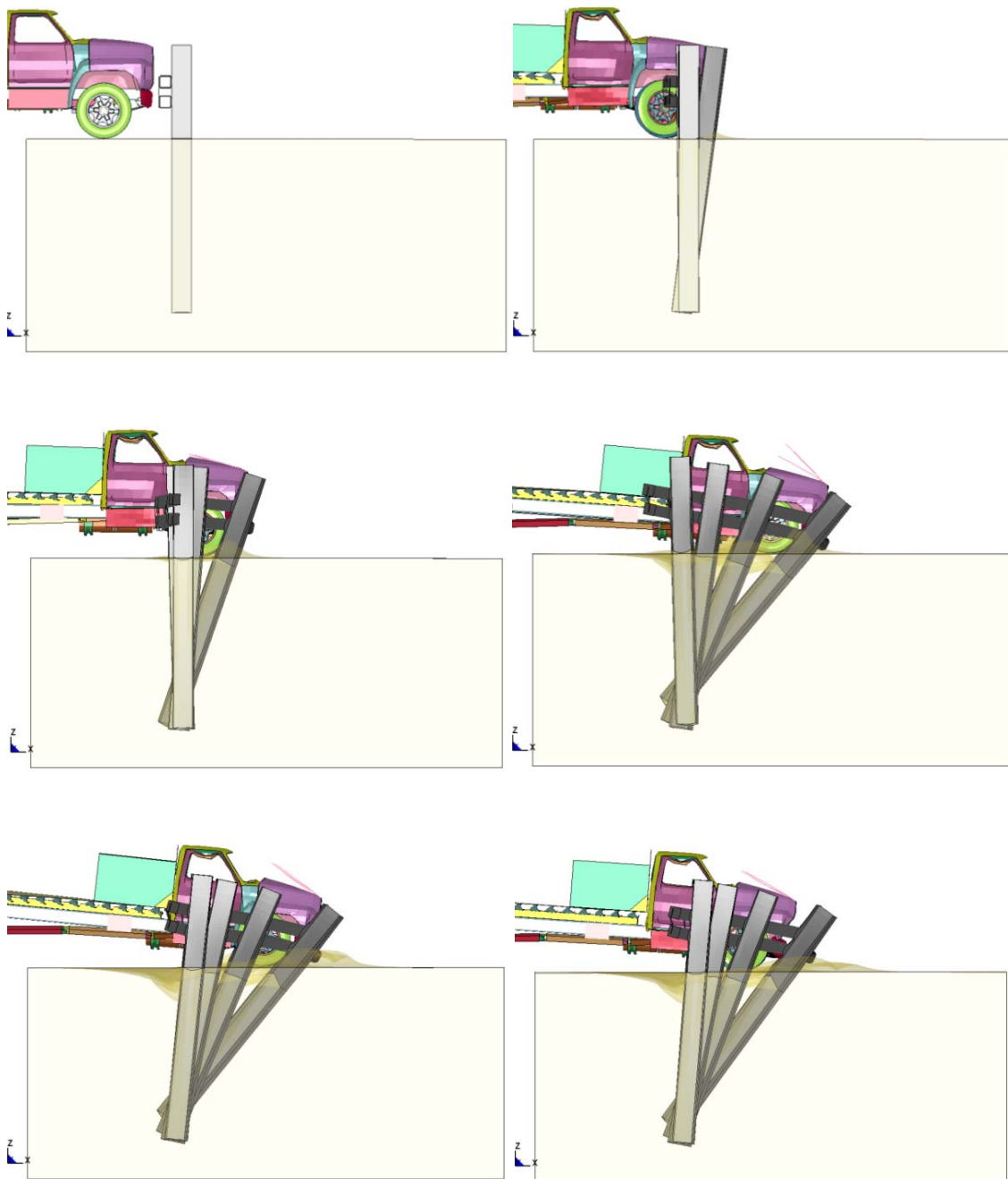
Figure E. 23. Simulated sequential figures of the full-scale impact test on group of posts
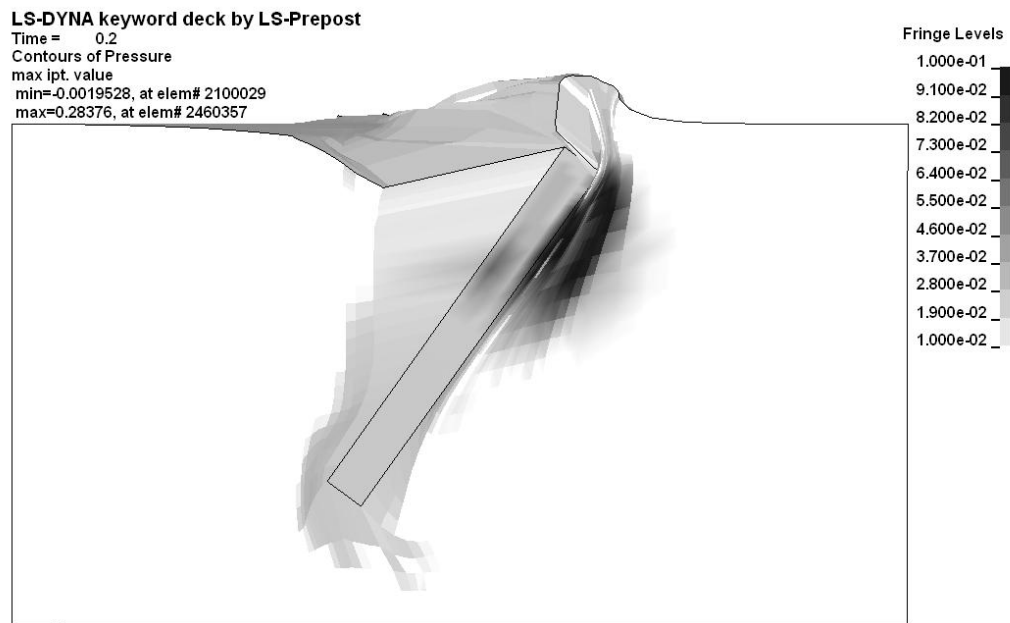
Figure E. 24. Simulated soil pressure at the two center posts of the group of posts at 0.200 sec
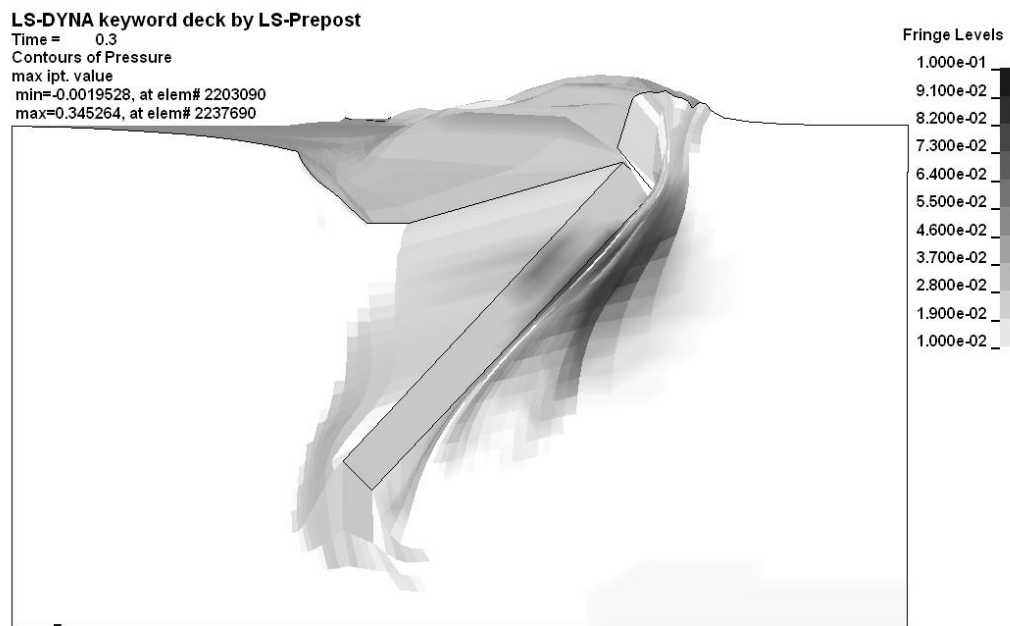
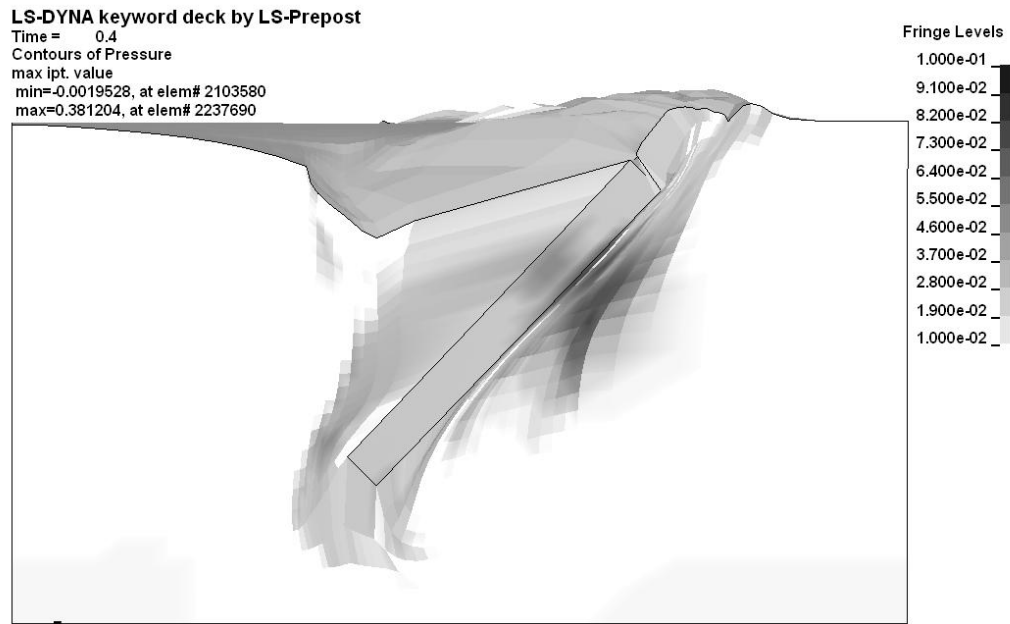**Figure E. 25. Simulated soil pressure at the two center posts of the group of posts at 0.300 sec**

Figure E. 26. Simulated soil pressure at the two center posts of the group of posts at 0.400 sec
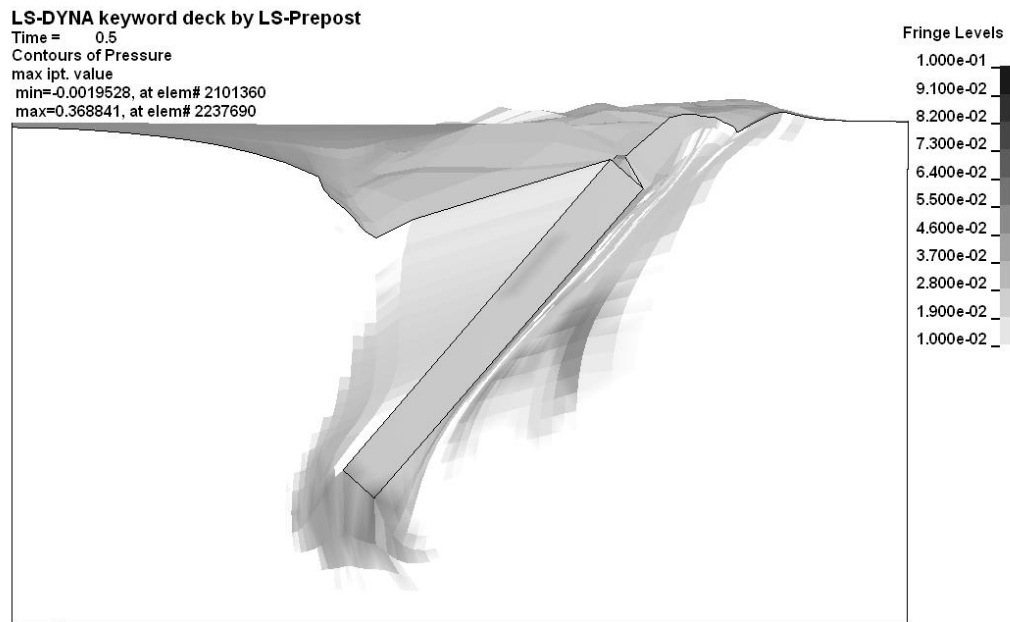

Figure E. 27. Simulated soil pressure at the two center posts of the group of posts at 0.500 sec
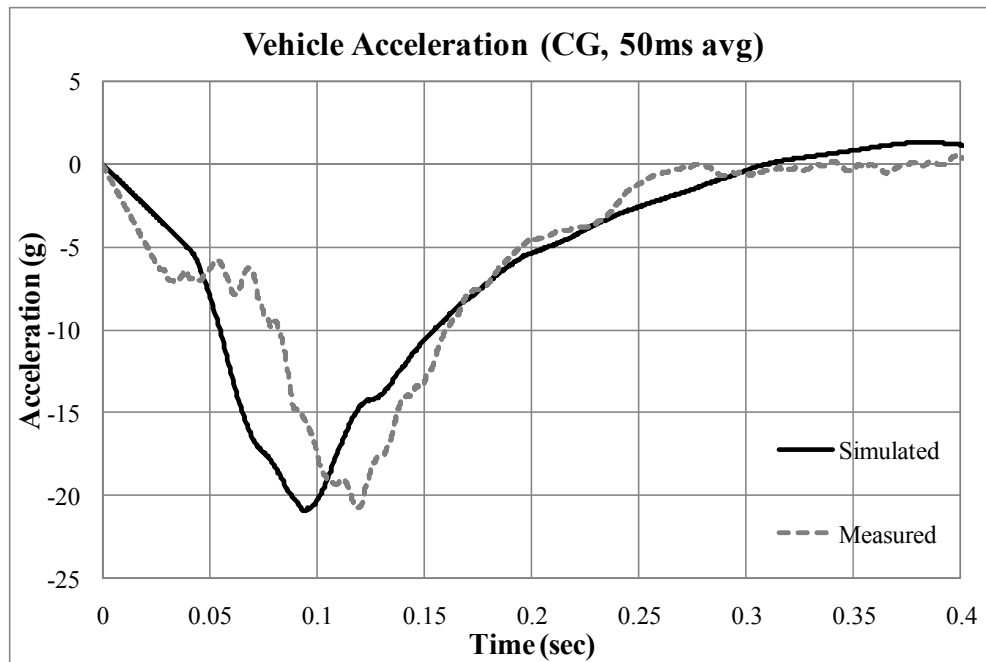
Figure E. 28. Simulated vehicle deceleration at the CG (the impact test on single post)
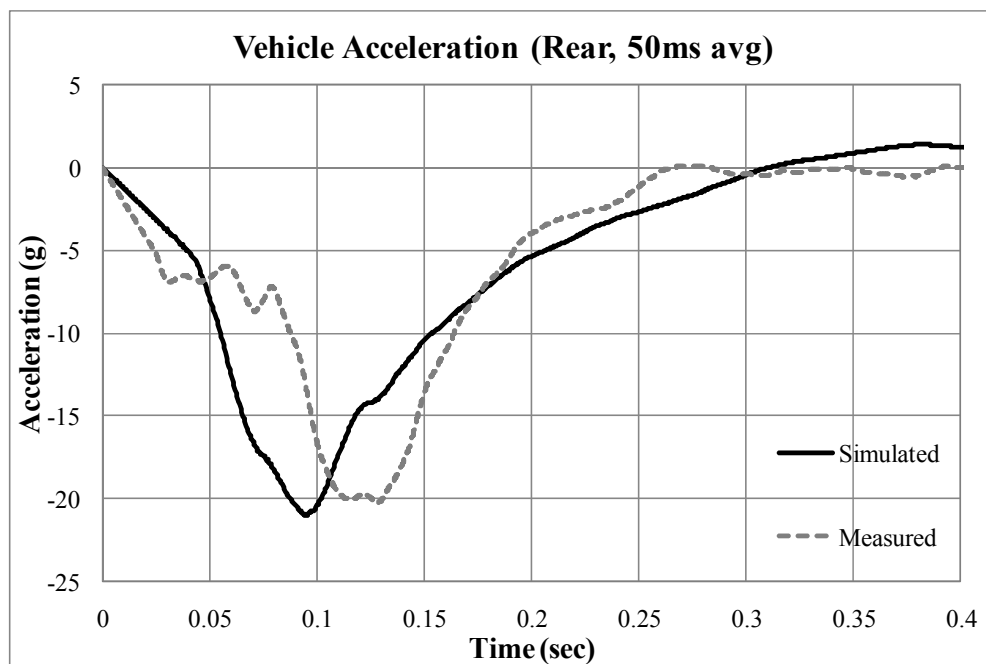

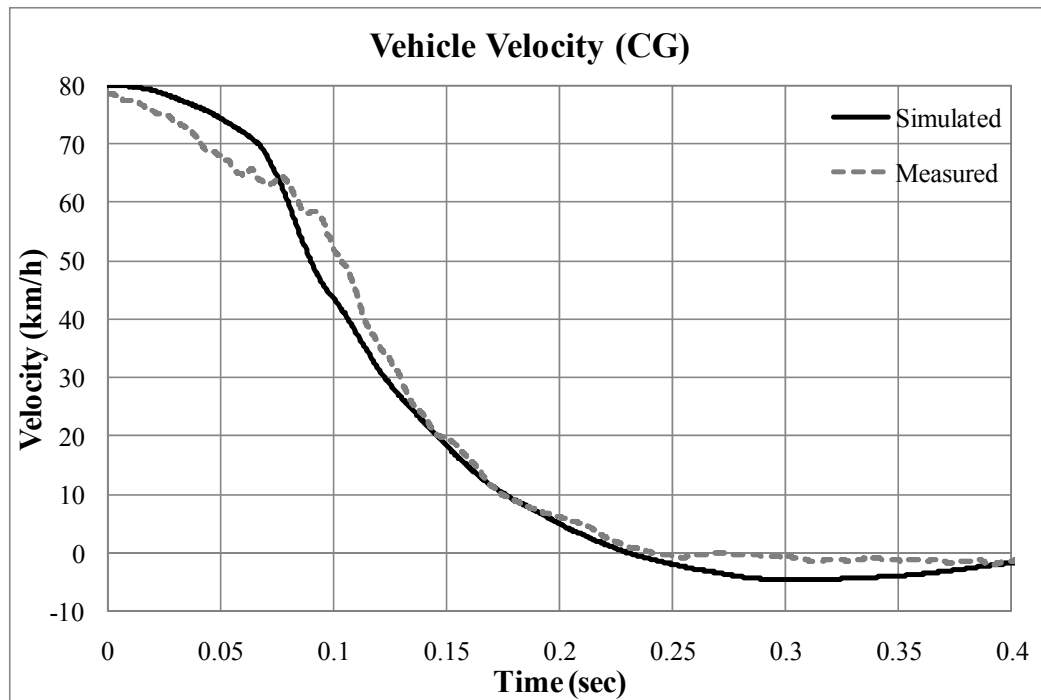**Figure E. 29. Simulated vehicle deceleration at the rear (the impact test on single post)**

Figure E. 30. Simulated vehicle velocity at the C.G (the impact test on single post)
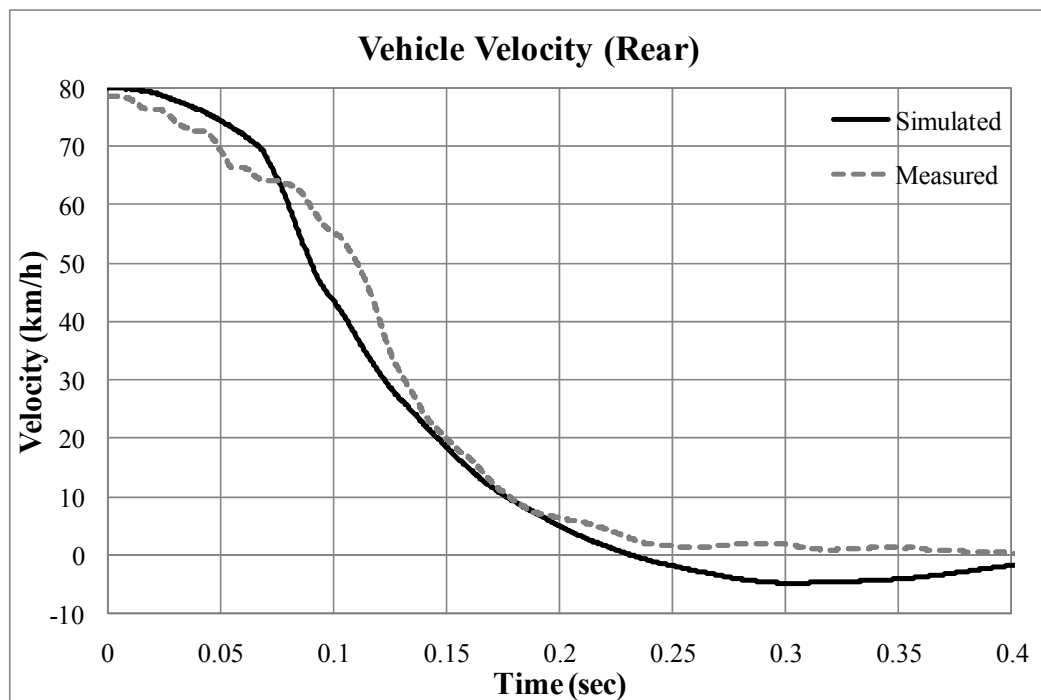

Figure E. 31. Simulated vehicle velocity at the rear (the impact test on single post)
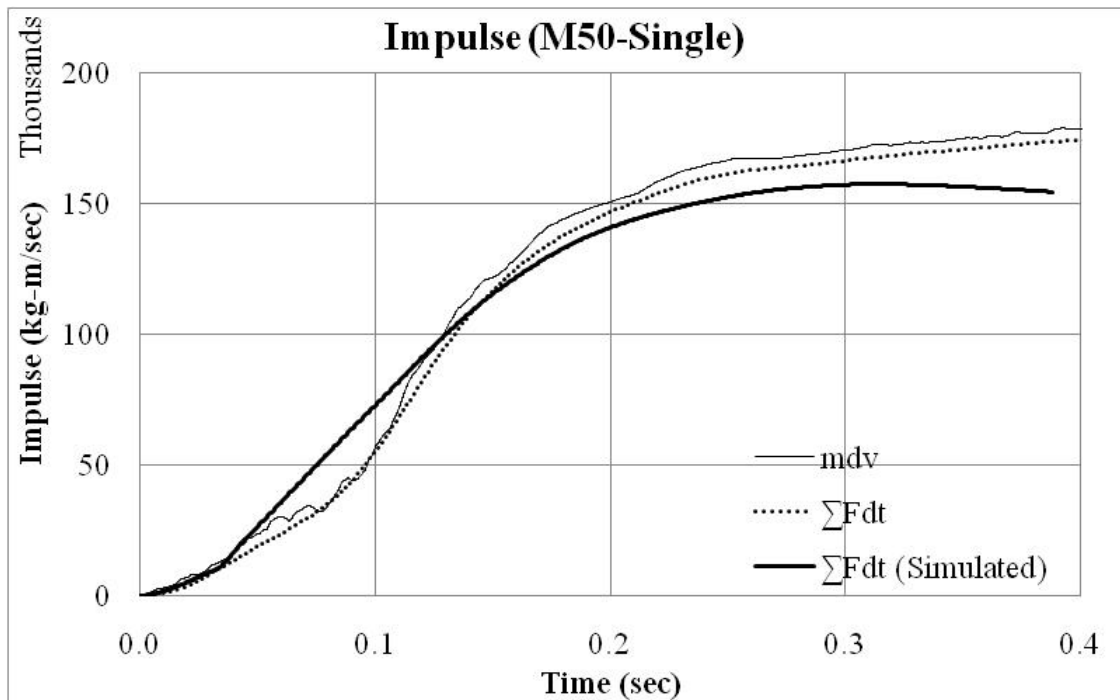
Figure E. 32. Measure and simulated impulse (the impact test on the single post)
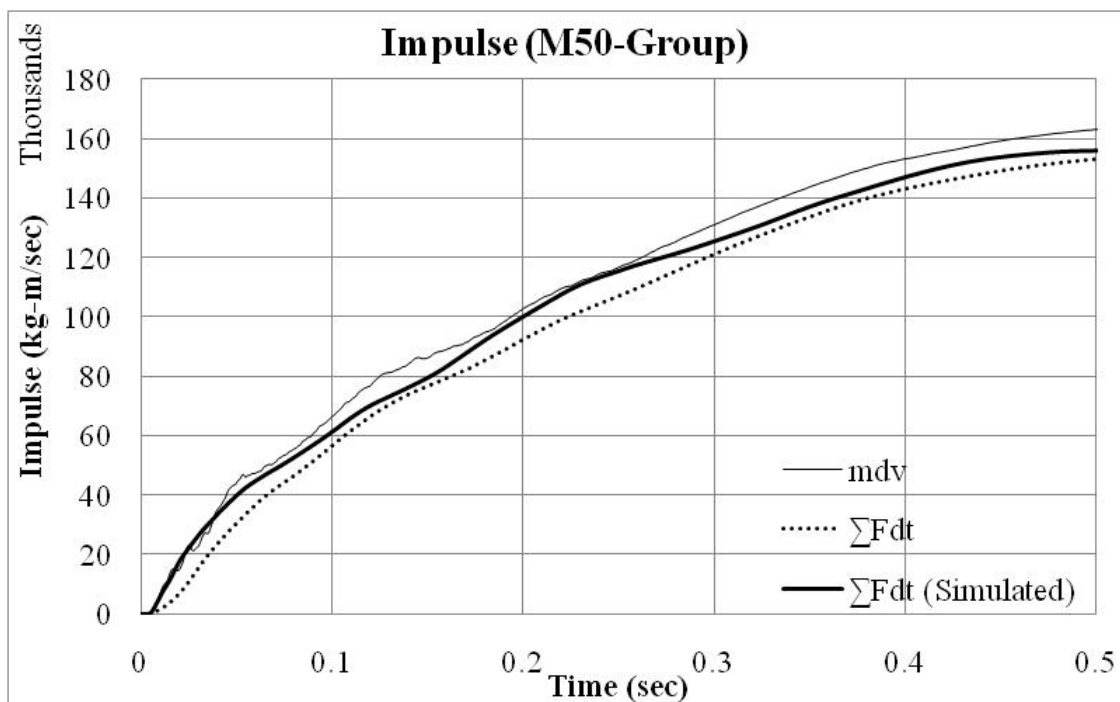

Figure E. 33. Measure and simulated impulse (the impact test on the group of posts)

Conservation of Energy

The conservation of energy equation can be expressed:

$$\Delta E_{Kinetic} = \int F_{(t)} dx + U \qquad \text{(E-1)}$$

Where, $\Delta E_{Kinetic}$ = change in kinetic energy $= \dfrac{1}{2}(mv_0{}^2 - mv_{(t)}{}^2)$

$\int F_{(t)} dx$ = mechanical work

m = mass of vehicle

v_0 = initial velocity of vehicle at the impact

$v_{(t)}$ = vehicle velocity at the time, t

$F_{(t)}$ = force acting on the post at the time, t

dx = displacement of the post at the impact level

U = strain energy

The strain energy of the vehicle during the impact can be obtained by using equation (E-2) as shown in Figure E. 34. All the quantities used for Figure E. 34 are obtained from the numerical simulation.
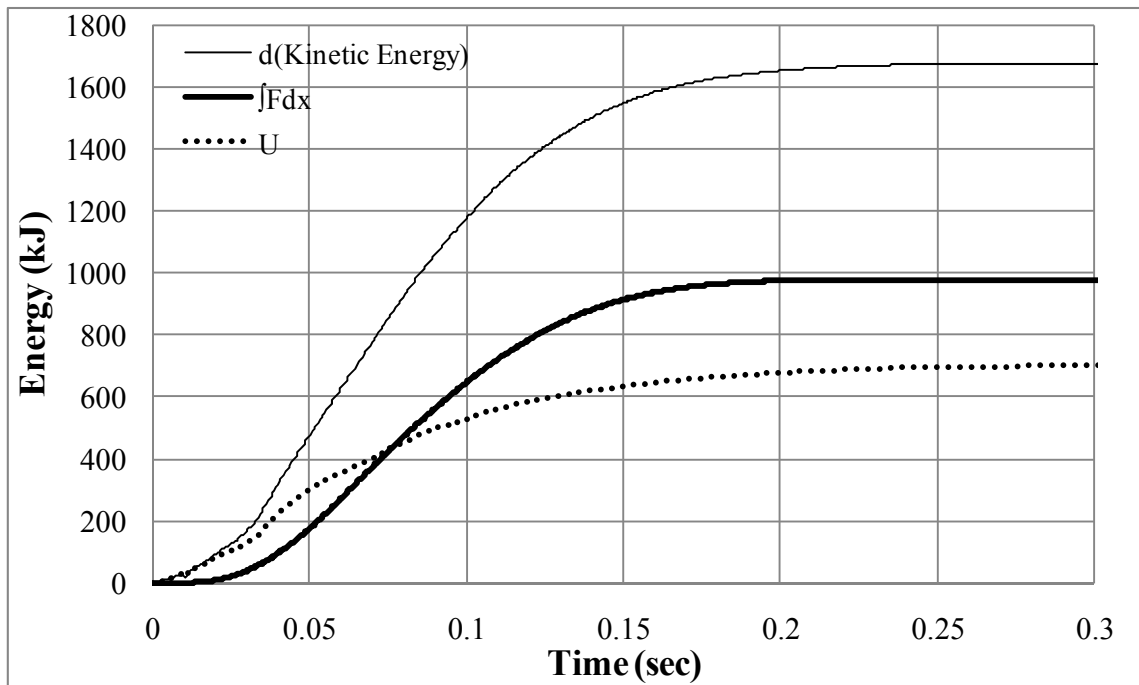
$$U = \Delta E_{Kinetic} - \int F dx \qquad \text{(E-2)}$$

Figure E. 34. Measure and simulated impulse (the impact test on the single post)

VITA

Seok Gyu Lim received his Bachelor of Engineering degree in civil engineering from Chung-Ang University, Seoul, Korea in February 2002. He continued at Chung-Ang University and received his Master of Engineering degree in civil engineering in February 2004. His thesis was titled "Evaluation of slope stability on the basis of neural network theory." He enrolled in the geotechnical engineering doctoral program at Zachry Department of Civil Engineering, Texas A&M University in September 2006 and received his Ph.D. in civil engineering in May 2011. He served as a Graduate Research Assistant for his committee chair, Dr. Jean-Louis Briaud investigating the topics of soil sampling, pressuremeter test, finite element analysis and lateral impact on soil embedded posts system. His research interests are foundation engineering, soil excavation, experimental methods for characterization of soil behavior, finite element analysis and dynamic soil-structure interaction.

Mr. Lim may be reached at 3136 TAMU, College Station, TX 77843-3136. His email is limsg0129@tamu.edu.